

---

---

EXPLORING THE ROLES  
OF MYELOID CELLS IN KIDNEY  
INJURY AND REPAIR

---

---

Timothy Michael Williams

Bachelor of Biomedical Science (Honours)

December 2014

Department of Anatomy and Developmental Biology  
Monash University,  
Melbourne, Australia

Submitted to Monash University in total fulfilment  
of the requirements for the degree of Doctor of Philosophy

### **Notice 1**

*Under the Copyright Act 1968, this thesis must be used only under the normal conditions of scholarly fair dealing. In particular no results or conclusions should be extracted from it, nor should it be copied or closely paraphrased in whole or in part without the written consent of the author. Proper written acknowledgement should be made for any assistance obtained from this thesis.*

### **Notice 2**

*I certify that I have made all reasonable efforts to secure copyright permissions for third-party content included in this thesis and have not knowingly added copyright content to my work without the owner's permission.*

---

**TABLE OF CONTENTS**

<b>List of Figures</b> .....	I
<b>List of Tables</b> .....	II
<b>Summary</b> .....	III
<b>General Declaration</b> .....	V
<b>Acknowledgments</b> .....	VI
<b>Research Output</b> .....	VIII
<b>Abbreviations</b> .....	XII

**Chapter 1: Literature Review**

<b>1.1 Introduction</b> .....	1
<b>1.2 The Kidney</b> .....	3
1.2.1 Kidney Disease in Society.....	5
1.2.2 Acute Kidney Injury .....	7
1.2.3 Ischaemia/Reperfusion Injury .....	8
<b>1.3 Macrophages in Renal Development, Injury, and Repair</b> .....	14
1.3.1 Classical versus Alternative Activation States .....	15
1.3.2 Tumor-associated Macrophages: Analogies with Embryonic Macrophages ....	20
1.3.3 The Role of Tissue Macrophages in Kidney Development .....	21
1.3.4 Macrophages in Kidney Disease .....	22
1.3.4.1 Suppression of Macrophage Activities in Chronic Kidney Disease .....	22
1.3.4.2 Positive Modulation of Macrophages in Acute Kidney Injury .....	25
1.3.5 Harnessing Macrophage Biology for Therapy .....	28
<b>1.4 CSF Signalling to Myeloid Cells in Inflammation</b> .....	30
<b>1.5 Hypothesis and Aims</b> .....	32

**Chapter 2: Establishing the Flow Cytometric Assessment of Myeloid Cells  
in Kidney Ischemia/Reperfusion Injury**

<b>2.1 Introduction</b> .....	33
<b>2.2 Materials and Methods</b> .....	35
2.2.1 Animals and Surgery .....	35
2.2.2 Digestion and Preparation of the Kidney and Spleen for Flow Cytometry .....	35

2.2.3 Cell Counts and Viability .....	36
2.2.4 Antibody Labeling .....	36
2.2.5 Flow Cytometric Acquisition and Analysis .....	37
2.2.6 Statistical Analysis .....	37
<b>2.3 Results</b> .....	<b>38</b>
2.3.1 Using Enzymes to Aid in the Digestion of the Kidney is more Suitable than MD Alone .....	38
2.3.2 Gating Strategy for Myeloid Cells in the Kidney .....	41
2.3.3 Gating Strategy for Myeloid Cell Subpopulations in the Kidney .....	43
2.3.4 Kidney and Spleen Ly6C <sup>+</sup> , Ly6G <sup>+</sup> , and MHCII <sup>+</sup> Cell Population Comparison	46
2.3.5 Assessing Epithelial Cells and Autofluorescence in the Post-Ischemic Kidney	48
<b>2.4 Discussion</b> .....	<b>50</b>
<b>Chapter 3: Phenotype and Influx Kinetics of Leukocytes and Inflammatory Cytokine Production in Ischaemia/Reperfusion Injury</b>	
<b>3.1 Introduction</b> .....	<b>54</b>
<b>3.2 Materials and Methods</b> .....	<b>57</b>
3.2.1 Animals and Surgery .....	57
3.2.2 Histopathology and Immunostaining .....	57
3.2.3 Digestion and Preparation of Kidneys for Flow Cytometry .....	58
3.2.4 Antibody Labelling .....	58
3.2.5 Flow Cytometric Acquisition and Analysis .....	58
3.2.6 Cytokine Bead Array .....	59
3.2.7 Statistical Analysis .....	59
<b>3.3 Results</b> .....	<b>60</b>
3.3.1 Histopathology .....	60
3.3.2 Kidney IR Injury Results in the Loss of EpCAM <sup>+</sup> Epithelial Cells and a Rise in Autofluorescence .....	60
3.3.3 Cellular Changes in the Kidney over a 7 Day Time-course of IR Injury: CD45 <sup>+</sup> Cells, Total Myeloid Cells and Granulocytes .....	64
3.3.4 Proportional and Numerical Changes in Monocyte and Macrophage Subpopulations in Response to IR Injury .....	67

---

3.3.5 Changes in the Flow Cytometric Profile of Kidney Monocytes and Macrophages following IR Injury .....	70
3.3.6 Analysis of Kidney Macrophage Subpopulations based on F4/80 and MHC Class II Expression .....	72
3.3.7 Changes in the Inflammatory Cytokine Profile over the Time-course of IR Injury .....	76
<b>3.4 Discussion .....</b>	<b>78</b>
 <b>Chapter 4: The Impact of GM-CSF and CSF-1R Blockade on Inflammation, Tissue Damage and Repair in Kidney Ischaemia/Reperfusion Injury</b>	
<b>4.1 Introduction .....</b>	<b>82</b>
<b>4.2 Materials and Methods .....</b>	<b>85</b>
4.2.1 Animals and Surgery .....	85
4.2.2 Antibody Administration .....	85
4.2.3 Digestion and Preparation of Kidney and Spleen for Flow Cytometry .....	87
4.2.4 Antibody Labelling .....	87
4.2.5 Flow Cytometric Acquisition and Analysis .....	88
4.2.6 Histology .....	88
4.2.7 Hydroxyproline and SDS-PAGE Analysis .....	88
4.2.8 Serum Cytokine Analysis .....	89
4.2.9 Kidney Function Assessment .....	89
4.2.10 Statistical Analysis .....	89
<b>4.3 Results .....</b>	<b>90</b>
4.3.1 The Effect of Short-term GM-CSF and CSF-1R Blockade on Total Cellularity, CD45 <sup>+</sup> Cells, CD11b <sup>+</sup> Cells and Granulocytes in the Spleen .....	90
4.3.2 The Effect of Short-term GM-CSF and CSF-1R Blockade on Cell Populations in the Injured Kidney .....	96
4.3.3 Changes in Macrophage Populations in the Kidney Following Short-term GM-CSF and CSF-1R Blockade .....	100
4.3.4 The Effect of Short-term GM-CSF and CSF-1R Blockade on EpCAM <sup>+</sup> Cells and Total Collagen in the Kidney Following IR Injury .....	104
4.3.5 Effects of Long-term GM-CSF and CSF-1R Blockade on Serum Cytokines .....	106

4.3.6 The Effect of Long-term GM-CSF and CSF-1R Blockade on Cell Populations in the Spleen .....	109
4.3.7 The Effect of Long-term GM-CSF and CSF-1R Blockade on Cells in the Injured Kidney .....	111
4.3.8 Histological Changes Following IR injury with the Long-term Blockade of GM-CSF and CSF-1R and the Quantification of EpCAM <sup>+</sup> epithelial cells .....	114
4.3.9 Assessment of Total Collagen in the Injured Kidney Following Long-term GM-CSF and CSF-1R Blockade .....	116
4.3.10 Changes in Renal Function Following IR Injury with Long-term GM-CSF and CSF-1R Blockade .....	118
<b>4.4 Discussion .....</b>	<b>120</b>
<b>Chapter 5: General Discussion .....</b>	<b>124</b>
<b>References .....</b>	<b>129</b>
<b>Appendices .....</b>	<b>148</b>

## List of Figures

### CHAPTER 1:

<b>Figure 1.1</b>	Schematic of the kidney and nephron .....	4
<b>Figure 1.2</b>	The defining chemokine and receptor profiles of classically and alternatively activated macrophages .....	17
<b>Figure 1.3</b>	Different types of macrophages can contribute to both damage and tissue repair processes following kidney injury .....	27

### CHAPTER 2:

<b>Figure 2.1</b>	Using enzymes to aid in the digestion of the kidney is more suitable than mechanical digestion alone .....	40
<b>Figure 2.2</b>	Gating strategy for assessing myeloid cells in the kidney .....	42
<b>Figure 2.3</b>	Gating strategy for CD11b <sup>+</sup> cell subpopulations in the kidney .....	45
<b>Figure 2.4</b>	Kidney and spleen Ly6C <sup>+</sup> , Ly6G <sup>+</sup> and MHCII <sup>+</sup> cell population comparison .....	47
<b>Figure 2.5</b>	Assessing epithelial cells and autofluorescence in the post-ischemic kidney .....	49

### CHAPTER 3:

<b>Figure 3.1</b>	Histopathology over the time-course of IR injury .....	62
<b>Figure 3.2</b>	IR injury results in the loss of EpCAM <sup>+</sup> epithelial cells and a rise in autofluorescence .....	63
<b>Figure 3.3</b>	Cellular changes in the kidney over a 7 day time-course in response to IR injury: CD45 <sup>+</sup> cells, myeloid cells and granulocytes .....	66
<b>Figure 3.4</b>	Proportional and numerical changes in monocyte and macrophage subpopulations in response to IR injury .....	69
<b>Figure 3.5</b>	Changes in the flow cytometric profile of kidney monocytes and macrophages in response to IR injury.....	71
<b>Figure 3.6</b>	Analysis of kidney macrophage subpopulations based on F4/80 and MHCII expression .....	74
<b>Figure 3.7</b>	Visualisation of MR <sup>+</sup> macrophages at day 1 and day 7 post-IR injury	75
<b>Figure 3.8</b>	Changes in the inflammatory cytokine profile over the time-course of IR injury .....	77

### CHAPTER 4:

<b>Figure 4.1</b>	The effect of short-term GM-CSF and CSF-1R blockade on cell populations in the spleen following kidney IR injury .....	91
<b>Figure 4.2</b>	The effect of short-term GM-CSF and CSF-1R blockade on monocyte and macrophage populations in the spleen following kidney IR injury	93
<b>Figure 4.3</b>	The effect of short-term GM-CSF and CSF-1R blockade on CSF-1R <sup>+</sup> cells in the spleen following kidney IR injury .....	95

<b>Figure 4.4</b>	The effect of short-term GM-CSF and CSF-1R blockade on cell populations in the injured kidney .....	97
<b>Figure 4.5</b>	The effect of short-term GM-CSF and CSF-1R blockade on monocytes and macrophages in the injured kidney .....	99
<b>Figure 4.6</b>	The effect of short-term GM-CSF and CSF-1R blockade on macrophage subsets in the injured kidney .....	101
<b>Figure 4.7</b>	The effect of short-term GM-CSF and CSF-1R blockade on alternatively activated macrophages in the injured kidney .....	103
<b>Figure 4.8</b>	The effect of short-term GM-CSF and CSF-1R blockade on EpCAM <sup>+</sup> cells and total collagen in the injured kidney .....	105
<b>Figure 4.9</b>	Effects of long-term GM-CSF and CSF-1R blockade on serum cytokine levels following kidney IR injury .....	108
<b>Figure 4.10</b>	The effect of long-term GM-CSF and CSF-1R blockade on CSF-1R <sup>+</sup> cells in the spleen following kidney IR injury .....	110
<b>Figure 4.11</b>	The effect of long-term GM-CSF and CSF-1R blockade on monocytes and macrophages in the injured kidney .....	112
<b>Figure 4.12</b>	The effect of long-term GM-CSF and CSF-1R blockade on macrophage subsets in the injured kidney .....	113
<b>Figure 4.13</b>	Histological changes in the kidney following IR injury with the long-term blockade of GM-CSF and CSF-1R .....	115
<b>Figure 4.14</b>	Assessment of collagen in the injured kidney following the long-term blockade of GM-CSF and CSF-1R .....	117
<b>Figure 4.15</b>	Changes in kidney function following IR injury with the long-term blockade of GM-CSF and CSF-1R .....	119

## List of Tables

### CHAPTER 1:

<b>Table 1.1</b>	The 5 stages of chronic kidney disease .....	6
------------------	--	---

## Summary

Kidney disease is a major health concern, affecting a growing number of people and placing an enormous burden on health care systems worldwide. There is no cure for kidney disease and the current treatments heavily impact patient quality of life. However, the kidneys possess a limited capacity to regenerate, which provides hope for the future development of treatments aimed at promoting endogenous repair. This approach, however, will not be without challenges, due to the broad range of kidney diseases arising from different aetiologies.

The macrophage is a myeloid cell type recognised for its roles in both inflammation and tissue repair. Originally identified as a contributor to innate host defence, these cells are now known to also possess immunomodulatory and wound healing capabilities. For these reasons, manipulating macrophage function may help promote endogenous repair in damaged kidneys. Recent attempts to define macrophage activation states as either classical (M1) or alternative (M2) have been useful, although this classification system appears too simplistic, due in part to the complexity of the *in vivo* environment during injury and disease, where macrophages receive a broad and changing range of stimuli. Therefore, this thesis presents a series of studies that examine the contribution of myeloid cells to the initial inflammatory phase and subsequent resolution/remodelling phase of experimental ischaemia/reperfusion (IR) injury, a model of acute kidney injury (AKI).

Chapter Two describes the establishment of a flow cytometry protocol for detecting and analysing myeloid cells in injured and non-injured kidneys. This involved optimising enzymatic digestion methods and identifying important monocyte and macrophage subpopulations, in addition to neutrophils and epithelial cells in the context of IR injury. Chapter Three utilised these methods to comprehensively characterise myeloid populations, inflammatory cytokines and epithelial cell loss throughout the initiation and resolution phases of kidney IR injury. The histopathology corresponding to each of the time-points was also examined. Finally, Chapter Four explored and compared the effects of granulocyte-macrophage-colony stimulating factor (GM-CSF) and colony stimulating factor-1 receptor (CSF-1R) blockade, using neutralising antibodies, on IR-mediated damage and repair. GM-CSF and CSF-1 are principal myeloid growth factors linked to pathogenesis and repair in a range of diseases. The effects on different cell types, serum cytokines, collagen content and renal function were assessed. While GM-CSF and CSF-1R blockade were able to reduce a

number of inflammatory mediators, the benefits were outweighed by impacts on reparative subpopulations of myeloid cells. In particular, CSF-1R blockade substantially reduced infiltrating inflammatory monocytes shortly following injury but also depleted mannose receptor (MR) expressing M2 macrophages. The prolonged administration of this antibody also resulted in a significant increase in the total collagen content at 14 days post-IR injury.

Monocyte-derived macrophages contribute to the pathogenesis of IR injury but are also crucial mediators of kidney remodelling. Therefore, selective/targeted depletion or manipulation of specific myeloid populations may be beneficial in reducing inflammation-mediated damage, whilst still allowing reparative subpopulations to resolve tissue damage, promote tubular regeneration and mediate tissue remodelling.

## General Declaration

In accordance with Monash University Doctorate Regulation 17.2 Doctor of Philosophy and Research Master's regulations the following declarations are made:

I hereby declare that this thesis contains no material which has been accepted for the award of any other degree or diploma at any university or equivalent institution and that, to the best of my knowledge and belief, this thesis contains no material previously published or written by another person, except where due reference is made in the text of the thesis.

This thesis includes 2 original papers, 1 published and 1 under consideration in a peer reviewed journal and 1 unpublished publication. In addition, a published invited review constitutes part of the literature review. The core theme of the thesis is exploring the role of myeloid cells in kidney injury and repair. The ideas, development and writing up of all the papers in the thesis were the principal responsibility of myself, the candidate, working within The Department of Anatomy and Developmental Biology, Faculty of Medicine, Nursing and Health Sciences, under the supervision of Associate Professor Sharon Ricardo. The inclusion of co-authors reflects the fact that the work came from active collaboration between researchers and acknowledges input into team-based research.

In the case of chapters 1, 2 and 3 my contribution to the work involved the following:

Thesis chapter	Publication title	Publication status	Nature and extent of candidate's contribution
1	Macrophages in Renal Development, Injury, and Repair	Published	90%
2	Establishing the Flow Cytometric Assessment of Myeloid Cells in Kidney Ischemia/Reperfusion Injury	Published	85%
3	Phenotype and Influx Kinetics of Leukocytes and Inflammatory Cytokine Production in Kidney Ischaemia/Reperfusion Injury	Submitted	85%

I have renumbered sections of submitted or published papers in order to generate a consistent presentation within the thesis.

Signed:



*Timothy Michael Williams*

Date: .....19/12/14.....

## Acknowledgments

I'm sitting in here in a bit of disbelief that this day is here. The last few years have been a big challenge and I could not have made it to this point without a wonderful group of people in my life.

Firstly, I want to thank my supervisor, Associate Professor Sharon Ricardo. I am so grateful for all of the support and opportunities that you have given me. You have created such a fantastic, productive and fun environment, and taught me so much. I'll take away so many great memories from my time in your lab.

To my co-supervisor, Dr Daniel Layton, it is hard to believe we haven't known each other our whole lives! Thank you so much for all of your help along the way and for being a great friend. I did love the early morning 'supervisor meetings' on the golf course, where we would legitimately discuss science, in and around everything else in life.

I am also indebted to those who collaborated with me throughout my studies. Thank you especially to Professor John Hamilton, Associate Professor Chrisan Samuels, Monash Micro Imaging and Monash Histology.

To everyone over the years who have made the Kidney Regeneration and Stem Cell Laboratory the place it is, thank you. I am fortunate to have seen it evolve over the years and have so many fond memories. I'd especially like to thank Liz, Mali and Tina for sorting me out when I joined the lab. Liz, I'll never forget your kindness in sharing your desk with me. To Mali, thank you for your friendship and being a constant source of entertainment. Why are kidneys so mean? Tina, there have been so many good times! I loved our chats about everything from politics to cycling. Thank you for always being there for me. To the current lab members, Vingo, Sheetal, Bo, Brooke, Ali, Kevin and Felicity, you have all made it such a great place to work. Thank you.

I also want to thank the rest of the MISCL crew, Robi, Jonny, Jen, Marco, Jade, Leona, Chris, Sara, Mark, Renae and everyone else who has been there along the way. Special thanks also to Shri for the awesome Pilates classes and for treating all my aches and pains.

To the best couple in the world, Clari and Trént. You are the best friends anyone could hope for. There have been so many hilarious times that it's almost unnatural. You have both kept me sane through my PhD and I'll be forever thankful. BJ, you have always been there for me, too. Thanks for being such a great mate.

Andrea, you have changed my life in so many ways. I have loved working with you and I am so proud of what you have achieved. Your support in my toughest times has meant so much to me. Thank you for your help with every aspect of my thesis, especially proof reading, formatting and printing! I know that thesis pain will soon fade and we will be left with so many great memories.

To Aloma, Edward and Jo, I'll never be able to repay you for everything you have done for me. Your kindness is simply amazing. I honestly couldn't have made it to this point without your help. I am really looking forward to all the fun things I know we will do in the years to come.

Dots and Clive, your love and support over the years have meant so much to me. You have always been there for me when I needed you and your love for each other has changed the way I view the world.

Mum, Dad and Marcus, you have always supported me in everything I have done. The last few years haven't been easy but I always feel like you are with me. This thesis and all the effort that went into it is for you.

## Research Output

### Published manuscripts included in this PhD thesis

*Invited Review: Williams TM, Little MH and Ricardo SD (2010). "Macrophages in Renal Development, Injury, and Repair." Semin Nephrol. 30(3): 255-67. Review. (Appendix)*

Impact factor: 2.942

Times cited: 16

JCR Category	Rank in category	Quartile in category
Urology & Nephrology	18 of 77	Q1

**Williams TM, Wise AF, Alikhan MA, Layton DS and Ricardo SD (2014). "Establishing the Flow Cytometric Assessment of Myeloid Cells in Kidney Ischemia/Reperfusion Injury."**

*Cytometry A. 85(3): 256-67. (Appendix)*

Impact Factor: 3.066

Times cited: 0

JCR Category	Rank in category	Quartile in category
Biochemical Research Methods	22 of 81	Q2
Cell Biology	15 of 75	Q3

**Williams TM, Wise AF, Layton DS and Ricardo SD. "Phenotype and Influx Kinetics of Leukocytes and Inflammatory Cytokine Production in Kidney Ischaemia/Reperfusion Injury."**

Submitted to *Am J Pathol*.

### Additional publications

Alikhan MA, Jones CV, **Williams TM**, Beckhouse AG, Fletcher AL, Kett MM, Sakkal S, Samuel CS, Ramsay RG, Deane JA, Wells CA, Little MH, Hume DA and Ricardo SD (2011).

"Colony-stimulating factor-1 promotes kidney growth and repair via alteration of macrophage responses." *Am J Pathol. 179(3): 1243-1256*

Impact Factor: 4.602

Times cited: 30

JCR Category	Rank in category	Quartile in category
Pathology	8 of 76	Q1

Jones CV, **Williams TM**, Walker KA, Dickinson H, Sakkal S, Rumnalle BA, Little MH, Jenkin G and Ricardo SD (2013). "M2 macrophage polarisation is associated with alveolar formation during postnatal lung development." *Respir Res. 14(41): 1-14.*

Impact factor: 3.382

Times cited: 7

JCR Category	Rank in category	Quartile in category
Respiratory System	16 of 54	Q2

Wise AF, **Williams TM**, Kiewiet MB, Payne NL, Siatskas C, Samuel CS, Ricardo SD (2014). “Human mesenchymal stem cells alter macrophage phenotype and promote regeneration via homing to the kidney following ischemia-reperfusion injury.” *Am J Physiol Renal Physiol*. 306(10): F1222-F1235.

Impact Factor: 3.300

Times Cited: 0

JCR Category	Rank in category	Quartile in category
Physiology	22 of 81	Q2
Urology & Nephrology	15 of 75	Q1

Jones CV, Alikhan MA, O'Reilly M, Sozo F, **Williams TM**, Harding R, Jenkin G and Ricardo SD (2014). “The effect of CSF-1 administration on lung maturation in a mouse model of neonatal hyperoxia exposure.” *Respir Res*. 15(110): 1-14.

Impact factor: 3.382

Times cited: 0

JCR Category	Rank in category	Quartile in category
Respiratory System	16 of 54	Q2

## Conference abstracts and presentations

### International

**Williams TM**, Alikhan TM, Sakkal S, Layton DS and Ricardo SD (2009). “CSF-1 mediated immune modulation enhances endogenous tissue repair in ischemia/reperfusion kidney injury.” *American Society of Nephrology Annual Meeting*, San Diego, USA

Alikhan MA, **Williams TM**, Sakkal S, Zhuang J, Deane JA and Ricardo SD (2011). “Colony-stimulating factor (CSF)-1 accelerates renal repair following ischemia-reperfusion (IR) injury via M2 macrophage-derived insulin-like growth factor (IGF)-1 signalling.” *World Congress of Nephrology*, Vancouver, Canada

Jones CV, **Williams TM**, Ramsay RG, Little MH, Hume DA and Ricardo SD (2011). “Colony stimulating factor-1 in the promotion of postnatal growth and kidney development in the mouse.” *World Congress of Nephrology*, Vancouver, Canada

Ricardo SD, Alikhan MA, Layton DS and **Williams TM** (2011). “Understanding endogenous repair following acute kidney injury using macrophage profiling and phenotypic analysis.” *American Society of Nephrology Annual Meeting*, Philadelphia, USA

Wise AF, **Williams TM**, Zhuang J, Samuel CS, Ricardo SD (2012). “Mesenchymal stem cells promote renal regeneration via alteration of macrophage phenotype.” *American Society of Nephrology Annual Meeting*, San Diego, USA

**Williams TM**, Wise AF, Barbuto J, Samuel CS, Layton DS, Hamilton JA, Ricardo SD (2014). “Blocking myeloid growth factors to protect against ischemia/reperfusion injury.” *American Society of Nephrology Annual Meeting*, Philadelphia, USA

Wise AF, **Williams TM**, Rudd S, Wells CA, Kerr PG, Ricardo SD (2014). "Human mesenchymal stem cells promote alternative activation of monocytes isolated from healthy and type 2 diabetic subjects." *American Society of Nephrology Annual Meeting*, Philadelphia, USA

### **National**

Alikhan MA, Fletcher AL, **Williams TM**, Samuel CS, Deane DA, Little MH and Ricardo SD (2008). "Characterisation of myeloid cell profile in endogenous renal repair following ischemia-reperfusion injury." *The 44<sup>th</sup> Annual Scientific Meeting of the Australia and New Zealand Society of Nephrology*, Newcastle, NSW  
Abstract published in: *Nephrology* 13 (Supp. S3); A155

Jones CV, Sakkal S, **Williams TW**, Little MH, Hume DA and Ricardo SD (2008). "Postnatal nephrogenesis and organ growth is enhanced in newborn mice treated with colony stimulating factor (CSF)-1." *A Healthy Start to Life conference*, Melbourne, VIC

**Williams TM**, Alikhan MA, Sakkal S, Layton DS and Ricardo SD (2009). "The role of M-CSF in modulating the innate immune response to ischemia/reperfusion injury allowing for tissue repair and regeneration." *Infection and Immunity*, Gold Coast, QLD  
**Invited Oral Presentation**

Jones CV, **Williams TM**, Sakkal S and Ricardo SD (2009). "Macrophages in postnatal kidney development." *The 45<sup>th</sup> Annual Scientific Meeting of the Australia and New Zealand Society of Nephrology*, Hobart, TAS  
Abstract published in: *Nephrology* 14(Supp. S1); A15

Alikhan MA, Fletcher AL, **Williams TM**, Sakkal S, Deane JA and Ricardo SD (2009). "The diversity of macrophage phenotype during the injury and remodeling phases of ischemia-reperfusion injury." *The 45<sup>th</sup> Annual Scientific Meeting of the Australia and New Zealand Society of Nephrology*, Hobart, TAS  
Abstract published in: *Nephrology* 14(Supp. S1); A38

**Williams TM**, Layton DS, Alikhan MA and Ricardo SD (2010). "The characterisation of myeloid cells, inflammatory cytokines and CSF-1 in acute kidney injury." *The 46<sup>th</sup> Annual Scientific Meeting of the Australia and New Zealand Society of Nephrology*, Perth, WA  
Abstract published in: *Nephrology* 15(Supp. S4); A90

**Williams TM**, Alikhan MA and Ricardo SD (2011). "The identification of therapeutic targets in CSF-1 mediated kidney repair." *The 47<sup>th</sup> Annual Scientific Meeting of the Australia and New Zealand Society of Nephrology*, Adelaide, SA  
Abstract published in: *Nephrology* 16(Supp. S1); A50

**Williams TM**, Layton DS, Samuel CS, Hamilton JA and Ricardo SD (2012). "Tissue inflammation: a hallmark of kidney repair?" *Translational Nephrology: from mechanisms to therapeutics*, Queenstown, New Zealand  
**Oral Presentation**

**Williams TM**, Layton DS, Samuel CS, Hamilton JA and Ricardo SD (2012). “The use of anti-CSF1R and anti-GM-CSF antibodies to modulate inflammation in ischemia/reperfusion injury.” *The 48<sup>th</sup> Annual Scientific Meeting of the Australia and New Zealand Society of Nephrology*, Auckland, New Zealand

Abstract published in: *Nephrology* 17(Supp. S2); A065.

Wise AF, **Williams TM**, Zhuang J, Samuel CS, Ricardo SD (2012). “The regenerative potential of mesenchymal stem cells following ischemia-reperfusion injury.” *The 48<sup>th</sup> Annual Scientific Meeting of the Australia and New Zealand Society of Nephrology*, Auckland, New Zealand

Abstract published in: *Nephrology* 17(Supp. S2); A064

**Williams TM**, Wise AF, Barbuto J, Samuel CS, Layton DS, Hamilton JA, Ricardo SD (2014). “Comparing the effects of short-term and prolonged administration of antibodies against GM-CSF and CSF-1R in ischemia/reperfusion injury.” *The 50<sup>th</sup> Annual Scientific Meeting of the Australia and New Zealand Society of Nephrology*, Melbourne, Victoria

Abstract published in: *Nephrology* 19(Supp. S4)

Wise AF, **Williams TM**, Wells CA, Kerr PG, Ricardo SD (2014). “Human bone marrow-derived mesenchymal stem cells alter the phenotype and gene profile of monocytes from type 2 diabetic patients.” *The 50<sup>th</sup> Annual Scientific Meeting of the Australia and New Zealand Society of Nephrology*, Melbourne, Victoria

Abstract published in: *Nephrology* 19(Supp. S4)

## Awards

Australia and New Zealand Society of Nephrology Travel Award to attend the ANZSN Annual Scientific Meeting Perth, WA – 2010

Australia and New Zealand Society of Nephrology Travel Award to attend the ANZSN Annual Scientific Meeting Adelaide, SA – 2011

Australia and New Zealand Society of Nephrology Travel Award to attend the ANZSN Annual Scientific Meeting Auckland, New Zealand – 2012

Australia and New Zealand Society of Nephrology Travel Award to attend the ASN Annual Scientific Meeting Philadelphia, USA – 2014

## Abbreviations

βig-H3	Transforming growth factor-β-induced matrix associated protein	ICAM	Intracellular adhesion molecule
A <sub>2A</sub> R	Adenosine 2A receptor	IF	Immunofluorescence
AKI	Acute kidney injury	IFN	Interferon
ANOVA	Analysis of variance	IGF	Insulin-like growth factor
ATN	Acute tubular necrosis	Ig	Immunoglobulin
ATP	Adenosine triphosphate	IHC	Immunohistochemistry
BSA	Bovine serum albumin	IL	Interleukin
BrdU	Bromodeoxyuridine	IP-10	Interferon gamma-induced protein 10
CBA	Cytokine bead array	IR	Ischaemia/reperfusion
LIF	Leukaemia inhibitory factor	i.p.	intraperitoneal
CCL	Chemokine (C-C motif) ligand	LEC	Liposome-encapsulated clodronate
CCR	Chemokine (C-C motif) receptor	LIF	Leukaemia inhibitory factor
CKD	Chronic kidney disease	LIX	LPS-induced CXC chemokine
CSF-1	Colony stimulating factor-1	LPS	Lipopolysaccharide
CSF-1R	Colony stimulating factor-1 receptor	M1	Classically activated macrophage
CXCL	Chemokine (C-X-C motif) ligand	M2	Alternatively activated macrophage
CVD	Cardiovascular disease	mAbs	Monoclonal antibodies
DAMPs	Danger-associated molecular patterns	MBL	Mannose-binding lectin
DCs	Dendritic cells	MCP	Monocyte chemoattractant protein
DMEM	Dulbecco's modified Eagle medium	M-CSF	Macrophage-colony stimulating factor
DT	Diphtheria toxin	MD	Mechanical digestion
DTR	Diphtheria toxin receptor	MDSCs	Myeloid-derived suppressor cells
ECM	Extracellular matrix	MFI	Mean fluorescence intensity
ED	Enzymatic digestion	MHCII	Major histocompatibility complex class II
EDTA	Ethylenediaminetetraacetic acid	MIF	Migration inhibitory factor
eGFR	estimated glomerular filtration rate	MIG	Monokine induced by gamma interferon
EpCAM	epithelial cell adhesion molecule	min	Minutes
ESRD	end-stage renal disease	MIP	Monocyte inflammatory protein
FBS	foetal bovine serum	MIP	Monocyte inflammatory protein
FMO	Fluorescence minus one	MMP	Matrix metalloproteinase
FSC-A	Forward scatter-area	MR	Mannose receptor
FSC-H	Forward scatter-height	MSR	Macrophage scavenger receptor
GBM	Glomerular basement membrane	MyD88	Myeloid differentiation factor 88
G-CSF	Granulocyte-colony stimulating factor	NADPH	Nicotinamide adenine dinucleotide phosphate
GFP	Green fluorescent protein	NEM	N-ethylmaleimide
GM-CSF	Granulocyte macrophage-colony stimulating factor	NF-κB	Nuclear factor kappa-light-chain enhancer of activated B-cells
h	Hours	NK	Natural killer
H&E	Haematoxylin and eosin		

		<b>Symbols</b>	
NKT	Natural killer T		
OCT	Optimum cutting temperature	$\alpha$	alpha
OPN	Osteopontin	$\beta$	beta
PBS	Phosphate buffered saline	$\gamma$	gamma
PFA	Paraformaldehyde	+	positive
PI	Propidium iodide	-	negative
PMSF	Phenylmethylsulfonyl	$^{\circ}\text{C}$	degrees Celsius
PT	Proximal tubule	$\mu\text{l}$	microliter
RANTES	Regulated on activation, normal T cell expressed and secreted	$\mu\text{m}$	micrometre
		mg	milligram
RT-PCR	Real-time polymerase chain reaction	ml	millilitre
ROS	Reactive oxygen species	mM	millimolar
RRTs	Renal replacement therapies	ng	nanogram
SDS-PAGE	Sodium dodecyl sulphate polyacrylamide gel electrophoresis	g/l	gram pre litre
		w/v	weight per volume
SLAM	Signalling lymphocyte-activating molecule		
SSC-A	Side scatter-area		
STAT	Signal transducers of transcription		
TAMs	Tumour-associated macrophages		
TEC	Tubular epithelial cell		
TGF	Transforming growth factor		
THP	Tamm-Horsfall protein		
TLRs	Toll-like receptors		
TNF	Tumour necrosis factor		
Treg	Regulatory T cell		
UUO	Unilateral ureteral obstruction		
VCAM	Vascular cell adhesion molecule		
VEGF	Vascular endothelial growth factor		

# CHAPTER 1

---

*Literature Review*

## Declaration for Thesis Chapter 1

### Declaration by candidate

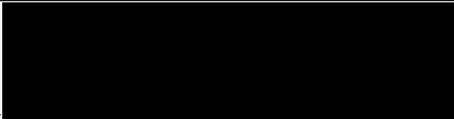
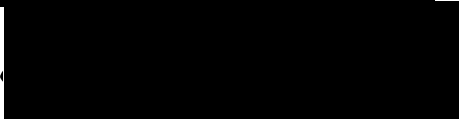
Part of this chapter was published in *Seminars in Nephrology*:

**Williams TM**, Little MH and Ricardo SD (2010). “Macrophages in Renal Development, Injury, and Repair” *Semin Nephrol* 30(3): 255-267. (Appendix)

In the case of Chapter 1, the nature and extent of my contribution to the work was the following:

Nature of contribution	Extent of contribution (%)
Design, preparation of manuscript	90%

The undersigned hereby certify that the above declaration correctly reflects the nature and extent of the candidate’s and co-authors’ contributions to this work.

<b>Candidate’s Signature</b>		<b>Date:</b> 19/12/14
<b>Main Supervisor’s Signature</b>		<b>Date:</b> 19/12/14

## 1.1 Introduction

Kidney disease is a major global health problem, and with no cure the prevalence continues to rise. Due to the progressive nature of chronic kidney disease (CKD), patients commonly develop end-stage renal disease (ESRD), which requires renal replacement therapies (RRTs) in the form of organ transplantation or dialysis. These treatments dramatically reduce quality of life and place a huge burden on health care resources. Therefore, there is a huge need for novel therapies, particularly those aimed at promoting endogenous repair.

Acute kidney injury (AKI) is defined as a sudden reduction in kidney function, which can result in renal failure (1). While the aetiology for AKI is broad, ischaemia/reperfusion (IR) injury often plays a central role (2). IR injury results from an interrupted or reduced blood supply to the kidney, causing tubular epithelial cell (TEC) death through apoptosis and necrosis, inflammatory cell infiltration and reduced renal function. The period of ischaemic insult determines the extent of IR injury and with less severe damage the kidney can repair and regenerate to varying degrees. These endogenous repair processes involve resolution of inflammation, TEC proliferation and collagen matrix remodelling. However, the capacity for the kidney to self-repair appears limited and there is still much to learn about the process. A full understanding of the cell types and molecular pathways involved in tissue repair will enable the development of new therapies to reduce the progression of kidney disease and promote endogenous regeneration.

One cell type known to mediate repair is the macrophage. Traditionally recognised as a pro-inflammatory cell type involved in innate immunity, more recent work has shown that these cells can acquire different activation or polarisation states. The classically activated (M1) macrophage is the inflammatory cell type originally identified, while the alternatively activated (M2) macrophage has anti-inflammatory and wound healing capabilities. These apparently opposing states allude to the high plasticity of this myeloid cell. However, this M1/M2 categorisation (see Section 1.3.1) is most likely too simplistic, as macrophages with a range of

functional capabilities are needed at different stages of repair following IR injury. Therefore, translating the reparative potential of macrophages into a cell-based therapy will require a detailed knowledge of their functions in different settings.

Flow cytometry is one technology capable of providing great insight into the cells involved at different stages of IR injury. This includes the numbers of different cell types and the changes in expression of particular receptors or other surface and intracellular molecules on specific populations. Using flow cytometry to assess cellular changes in murine models of IR injury, which closely represent the changes that occur in the clinical setting of hypoxia-induced kidney disease, has been and will continue to be very useful in identifying the main contributors to disease, identifying therapeutic targets and testing the effects of novel therapies.

This literature review will discuss the immune response to AKI, focusing on the contribution of macrophages to the initial inflammatory insult and their subsequent role in the resolution of inflammation and tissue repair. These diverse roles are possible due to the plasticity of this myeloid cell type and the diverse activation/polarisation states that they can acquire. Two principal myeloid growth factors, colony stimulating factor (CSF)-1 and granulocyte macrophage-colony stimulating factor (GM-CSF), are also discussed. Due to the important roles of these growth factors in development, homeostasis and inflammation, they each present as potential therapeutic targets in injury and disease.

Macrophage biology is an evolving field and through increased knowledge of their broad range of functions, manipulation of these cells may help deliver effective cell-based therapies to treat acute and chronic kidney diseases.

## 1.2 The Kidney

The kidneys are complex organs made up of many different cell types, which allude to their varied functions. Their primary role is to filter the blood, retaining important molecules while removing waste products and excess fluid as urine. This process regulates the body's fluid and electrolyte levels. In addition, the kidneys also produce renin, erythropoietin and calcitriol (active vitamin D), which control blood pressure, stimulate red blood cell production and mediate calcium absorption in bones, respectively. In general, the kidneys are responsible for maintaining a state of homeostasis.

Anatomically, the kidneys are divided into two main sections, being the outer cortex and the inner medulla. Spanning the cortex and medulla is the nephron, the functional unit of the kidney responsible for blood filtration and the subsequent reabsorption of vital molecules. In humans, nephrogenesis occurs entirely *in utero*, resulting in an endowment at birth of approximately one million nephrons per kidney. However, this number can vary widely, and is influenced by birth weight, gender, age, ethnicity and disease (3).

Each nephron is composed of a corpuscle and tubule. The corpuscle is comprised of a glomerulus, being a cluster of fine capillaries, surrounded by the Bowman's capsule. Blood from the renal artery enters the glomerulus via the afferent arteriole, where water and other solutes are passed from the arteries into the Bowman's space, mediated by high arterial pressure and a variety of highly specialised cells. This filtrate contains water and small molecules, such as sodium and potassium ions, calcium, glucose and amino acids, along with waste products. From the Bowman's space, the filtrate enters the renal tubule, which is divided into the proximal convoluted tubule, descending and ascending limbs of the loop of Henle, and a distal convoluted tubule. As the filtrate passes through the tubules, important molecules and water are reabsorbed and returned to the circulatory system. The remaining filtrate is passed to the collecting ducts and further concentrated before eventually passing as urine to the bladder via the ureters (Figure 1.1).

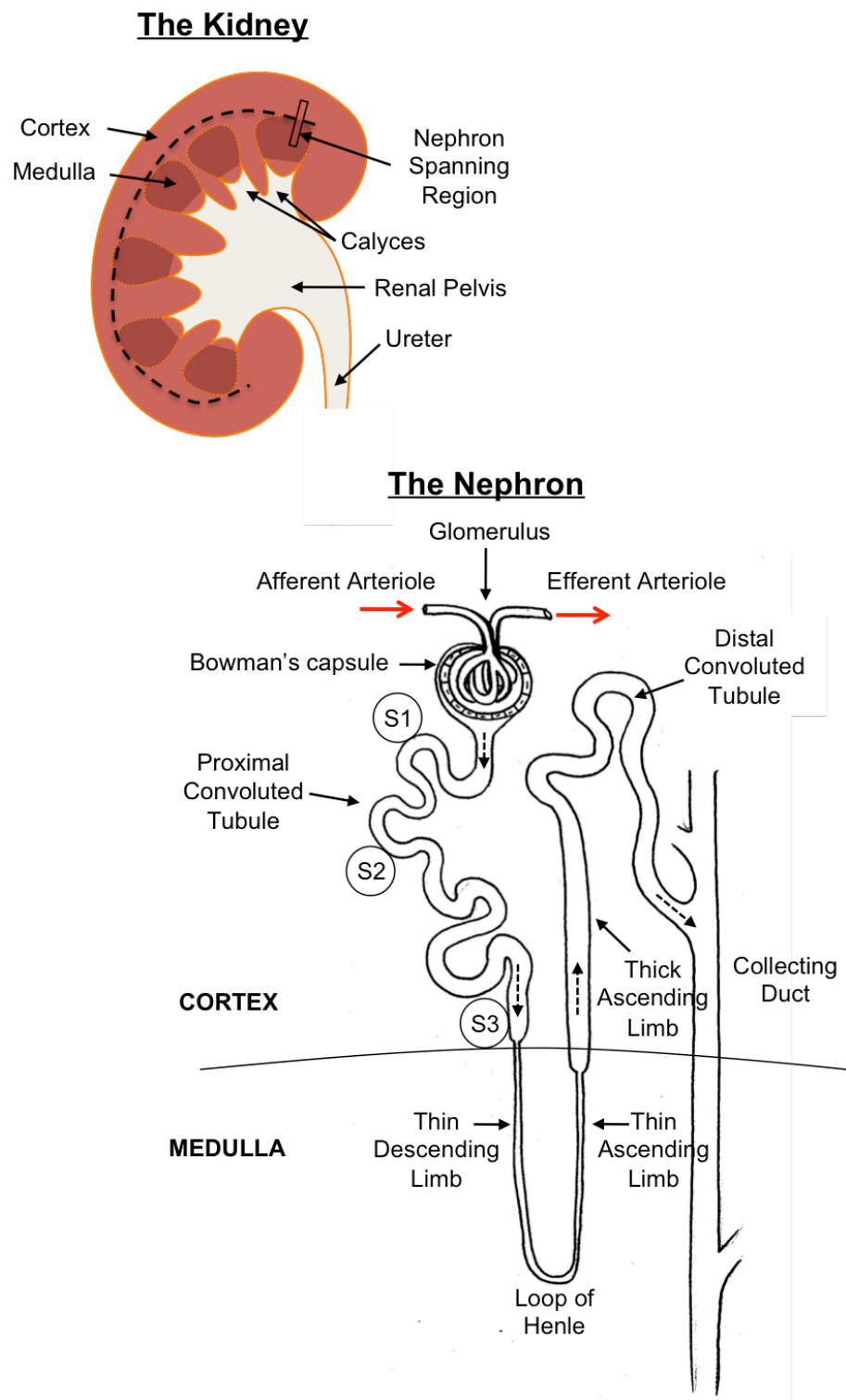


**Figure 1.1 Schematic of the kidney and nephron.** The kidney is divided into two compartments: the outer cortex and inner medulla. Spanning these compartments is the nephron, the functional unit of the kidney. The nephron is composed of a glomerulus and renal tubule. The tubule consists of a proximal convoluted tubule (S1, S2 and S3 segments), the loop of Henle and the distal convoluted tubule.

Renal function is commonly defined by the estimated glomerular filtration rate (eGFR), with a normal GFR being approximately 100mls/min/1.73m<sup>2</sup> (4). A slow decline in kidney function with age is normal. However, kidney diseases can rapidly decrease renal function in a relatively short period of time. Kidney disease can present as acute or chronic and with varied aetiology. Fortunately, the kidneys have a great capacity to compensate for reduced functionality and it appears that there is an inherent redundancy, as evidenced by the fact that people can be considered perfectly healthy even following a unilateral nephrectomy. However, this can be a double-edged sword, as declining kidney function can remain unnoticed, until a point where RRT is required.

### **1.2.1 Kidney Disease in Society**

CKD has become a major global health problem, affecting both developed and developing countries (5). It is estimated that 10% of people worldwide have some form of CKD, although the prevalence is significantly higher in particular populations (6, 7). Due to a sharp rise in the incidence and prevalence of CKD over recent years, a five-stage classification system was designed to aid in earlier and more accurate diagnosis, and to better track disease progression in order to improve outcomes (4, 8) (Table 1). Using this scale, stage 3 CKD with a GFR of less than 60 mL/min/1.73m<sup>2</sup> for 3 months or more is often considered to be moderate or clinically relevant CKD, although there are still significant risks associated with stages 1 and 2 (5). Subsequent reviews have led to the division of stage 3 into 3a and 3b, as different risks and clinical patterns exist for patients with early or late stage 3 CKD (9, 10). More recently, the addition of albuminuria measurements have been included in the CKD classification (10).

**Table 1.1 The 5 stages of chronic kidney disease (4, 9, 10)**

Stage	Description	GFR mL/min/1.73m <sup>2</sup>	Related Terms
1	Kidney damage with normal or ↑ GFR	≥90	Albuminuria, proteinuria, hematuria
2	Kidney damage with mild ↓ GFR	60-89	Albuminuria, proteinuria, hematuria
3a 3b	Moderate ↓ GFR	45-59 30-44	Chronic renal insufficiency, early renal insufficiency
4	Severe ↓ GFR	15-29	Chronic renal insufficiency, late renal insufficiency, pre-ESRD
5	Kidney failure	<15 (or dialysis)	Renal failure, uremia, ESRD

CKD encompasses many types of kidney diseases arising from diverse aetiologies, including both communicable and non-communicable diseases (11). Unfortunately, its progressive nature means that without appropriate intervention, CKD patients often develop ESRD, requiring RRT (12). Over the last few decades, the incidence of ESRD has been increasing dramatically but in more recent times the rate of new cases appears to be stabilising. However, while the incidence has stabilised, the number of new patients requiring RRT each year is at historic highs. This increase is driven by ageing populations and the rapid growth in associated diseases, including obesity, type 2 diabetes and cardiovascular disease (CVD) (7, 13, 14).

In the most recent data from Australia, the leading causes of new cases of ESRD were diabetic nephropathy (35%), glomerulonephritis (23%) and hypertension (15%) (15). In the USA, diabetes accounts for 44% of new ESRD patients with 28% attributed to hypertension (16). ESRD patient care also places an enormous burden on the health care system. In 2011, the annual cost in the USA per individual for haemodialysis, peritoneal dialysis and transplantation were \$87,954, \$71,630 and \$32,922, respectively. This equates to a total cost of \$49.3 billion or 7.2% of the Medicare budget to treat 1.4% of the total number of patients (16). The figures are similar in Australia, with the 2009 cost per patient for in centre haemodialysis, peritoneal dialysis and first year transplant being \$79,072, \$53,112 and \$81,549 (\$11,770 in year two),

respectively (17). In 2009, the expenditure in Australia on RRTs was approximately 1 billion dollars, with the cumulative cost between 2009-2020 predicted to reach 12 billion dollars (17).

While RRTs are effective in prolonging ESRD patient survival, they heavily impact quality of life (18). Many factors contribute to this, including the burden of attending centres for dialysis, modification to diet, dependence on medication, increased surgical procedures and an increase in infections. Transplant recipients generally have a better quality of life compared to dialysis patients, however, donor kidney demand far exceeds supply. Solid organ grafts also have a relatively limited survival time. For USA patients listed on the transplant list in 2007, the median waiting time was 4.3 years and 10% of newly listed patients died within 3 years of listing without receiving a transplant (16). The ten-year probability of graft failure is 54% for deceased donors and 38% for living donors, meaning that a large number of transplant recipients will be listed for re-transplantation, contributing to the over demand problem (16). An extra complication is the 20- to 30-fold increase in CVD for ESRD patients (5). Given the enormous burden that CKD, in particular ESRD, imposes on individuals and health care systems, there is a growing need to develop novel therapies to halt disease progression.

### **1.2.2 Acute Kidney Injury**

AKI, formerly termed acute renal failure, is defined as an abrupt loss of renal function, involving an increase in serum creatinine, often with a reduction in urine output (1). The incidence of AKI has been steadily increasing in recent times in both low- and high-income countries, although the cause and presentation differ substantially. For example, AKI can result from a lack of basic medical support, common in low income countries, or from advanced medical procedures, such as cardiac surgery, more widely available in high-income countries (19, 20). AKI is especially common in the intensive care unit, affecting up to two thirds of patients. Approximately 5% of these require RRT, which carries extremely high mortality rates of 50-60% (21).

The causes of AKI can be categorised as pre-renal, renal (intrinsic) and post-renal. However, different causes can be related, such is the case for pre-renal hypoperfusion leading to intrinsic acute tubular necrosis (ATN) (19). Other types of AKI include post-renal obstruction and various forms of inflammatory diseases, such as glomerulonephritis, interstitial nephritis, vasculitis and pyelonephritis (20). Sepsis and nephrotoxic drugs can also result in AKI, although tubular damage is not always associated with these forms of kidney disease (22-25).

The original notion that AKI fully resolves has been replaced with the understanding that partial or non-recovery are common outcomes, particularly for patients with existing kidney disease (19). A great deal of knowledge gained about AKI is from experimental models, particularly those involving mice and rats. These have been instrumental in understanding the roles of immune cells, cytokines and signalling pathways involved in AKI, allowing for the development of targeted therapies.

### **1.2.3 Ischaemia/Reperfusion Injury**

The kidney has a very high demand for oxygen to facilitate blood filtration and to meet cellular metabolic demand (26). This makes the kidneys susceptible to ischaemic insult, which can be caused by renal vascular disease, sepsis, nephrotoxins, transplantation and forms of vascular surgery (27). The pathophysiology of IR injury is characterised by inflammation, altered haemodynamics, and TEC damage. Hypoxia and reperfusion mediate cell activation and death, in turn promoting a complex inflammatory cascade that results in additional inflammation and the recruitment of a variety of leukocytes, including neutrophils, monocytes/macrophages, dendritic cells (DCs), T and B lymphocytes, natural killer (NK) cells and natural killer T (NKT) cells (28).

The initial ischaemic phase results in microvasculature endothelial activation and damage, which is in part mediated by the production of vasoactive mediators, such as endothelin (29, 30), and inflammatory cytokines. One such cytokine, tumour necrosis factor (TNF)- $\alpha$ , also elicits alterations to the glycocalyx that lines the endothelial luminal surface (31, 32). This enables rolling adhesion of leukocytes and their subsequent extravasation into the interstitium, a process that is mediated by increased expression of L-selectin on leukocytes, and P-selectin, E-selectin and intercellular adhesion molecule (ICAM)-1 on the endothelium (33-36). The vasoconstriction of the arterioles that results from IR injury contributes to a prolongation of hypoxia, which particularly affects TECs (37). Vasoconstriction also results in the reduction of glomerular filtration pressure and therefore GFR (38).

IR injury is also characterised by increased endothelial permeability and subsequent interstitial oedema, which further restricts blood flow, impedes tubular function and causes structural damage (39). This increased permeability is mediated by adenosine triphosphate (ATP) depletion and the production of inflammatory cytokines. The result is the disorganisation of the endothelial actin cytoskeleton and loss of vascular endothelial cadherin, disrupting the endothelial cell-cell junctions (38). There is also evidence to suggest that matrix metalloproteinase (MMP)-2 and MMP-9, which are up-regulated in the post-ischemic kidney, also contribute to endothelial permeability following IR injury (40).

Along with the infiltration of cells from both the innate and adaptive immune systems, the rapid immune response to kidney IR injury is characterised by a predominantly pro-inflammatory cytokine milieu. This includes TNF- $\alpha$ , interferon (INF)- $\gamma$ , interleukin (IL)-1, IL-6, monocyte chemoattractant protein (MCP)-1, transforming growth factor (TGF)- $\beta$ , regulated on activation, normal T cell expressed and secreted (RANTES) and IL-8 (41). Other inflammatory mediators, such as reactive oxygen species (ROS), Toll-like receptors (TLRs) and complement molecules also play a central role in the initiation and perpetuation of the inflammatory response. ROS generated by endothelial cells during hypoxia and reoxygenation have also been shown to

contribute to neutrophil adhesion and recruitment (42). ROS production can also damage cellular components, such as membranes and DNA, inhibit TEC proliferation and mediate expansion of the interstitium (43).

TLRs, a family of transmembrane pattern recognition receptors, can be expressed on both leukocytes and parenchymal kidney cells (44). Contributing to the innate immune response, TLRs are designed to recognise microbial products as well as endogenous molecules offered by damaged cells or cell fragments, known as damage-associated molecular pattern (DAMP) molecules (45). TLRs respond to ligand binding by recruiting adaptor proteins, of which 5 have been identified, in order to activate transcription factors. TLR-2 and TLR-4 have both been implicated in IR injury through myeloid differentiation factor 88 (MyD88)-dependent and independent activation of the nuclear factor kappa-light-chain-enhancer of activated B-cells (NF- $\kappa$ B), resulting in the production of pro-inflammatory cytokines and chemokines (46-48).

The complement system has also been implicated in the pathophysiology of IR injury. It involves a set of serum proteins that, upon binding to membrane bound receptors, initiate a cascading sequence of effector molecule production. A number of studies have implicated the alternative and mannose-binding lectin (MBL) complement pathways in the generation of pro-inflammatory cytokines and chemokines, the recruitment of leukocytes and the promotion of TEC death (49-51).

Following IR injury, TECs are shown to be highly susceptible to damage, particularly those of the S3 segment of the proximal tubules (PT), located in the outer stripe of the outer medulla. Damage to the medullary thick ascending limb of the distal tubule also develops with extended periods of ischaemia or if appropriate reoxygenation of this kidney compartment fails. The varied damage, both in degree and type, to cells at different parts of the nephron relates to the energy requirements of particular cells. Different genes are activated in the distal tubule

compared to the PT. The result is a propensity for apoptosis in the distal tubule following IR injury compared to necrosis of proximal TECs (52).

Following an ischaemic insult, there is shedding of the TEC brush border, a reduction in cytoskeletal integrity and lost cellular polarity. This involves a reorganisation and mislocation of membrane proteins, such as Na<sup>+</sup>K<sup>+</sup>-ATPase and  $\beta$ -integrin adhesion molecules (53), that in turn disrupts cell-cell interactions at adherent and tight junctions, resulting in the detachment and desquamation of TECs from the basement membrane. Longer ischaemic duration also promotes TEC apoptosis and necrosis. Within the tubular lumen, detached cells, cellular debris and other proteins, such as fibronectin and Tamm-Horsfall protein (THP), coalesce to form protein casts (53-55). This leads to tubular obstruction and an increase in the tubular pressure causing a back leak of filtrate across damaged cells. Impaired sodium reabsorption in the PTs can also lead to further reductions in GFR via the tubuloglomerular feedback system. In this case, the macula densa in the distal tubule responds to an increase in sodium concentration by promoting vasoconstriction of the afferent arterioles (56).

A number of leukocyte populations are known to contribute to the pathogenesis of IR injury. However, others have divergent roles that are linked to disease resolution. Targeting these different cell types may form the basis of future therapies by way of halting disease progression or promoting repair.

Neutrophils are among the earliest leukocytes to infiltrate the post-ischaemic kidney where they promote inflammation and contribute to the pathogenesis of IR injury (57, 58). These processes begin with the adherence of neutrophils to the activated endothelium, which precedes transmigration into the interstitium (59). Evidence suggests that neutrophils exacerbate hypoxia and promote IR injury through capillary plugging and the production of ROS, proteases and a range of cytokines and chemokines, including INF- $\gamma$ , IL-4, IL-6, IL-10 and TNF- $\alpha$  (59).

Neutrophils have also been shown to produce IL-17 in response to IR injury, which in turn stimulates IFN- $\gamma$ -mediated neutrophil infiltration and NKT cell activation (60).

NK cells play a role in the regulation of a variety of leukocytes through the production of cytokines, such as IFN- $\gamma$  and TNF- $\alpha$  (61). NK cells have also been shown to be an early contributor to kidney IR damage, mediated by osteopontin (OPN) and TLR-2 ligands expressed by TECs (62). OPN acts in NK cell recruitment where the NK cells provide apoptotic signals to the TECs (63, 64). In addition, NK cell binding to CD137L on TECs promotes chemokine (C-X-C motif) ligand (CXCL)1 and CXCL2 chemokine production and the subsequent recruitment of neutrophils (65). In the mouse, depletion of NK cells prior to IR injury conveyed protection in terms of reduced tissue pathology and serum creatinine (63).

Lymphocytes, particularly CD4<sup>+</sup> T cells, have been implicated in kidney IR injury to various degrees. T cell deficient *nu/nu* mice are protected from IR injury and reconstitution of CD4<sup>+</sup> T cells, but not CD8<sup>+</sup> T cells, re-establishes injury (66). Further, reconstitution with CD4<sup>+</sup> T cells that are unable to produce IFN- $\gamma$  fails to re-establish IR injury, signifying a pathological mechanism of CD4<sup>+</sup> T cell-mediated damage (66). In addition, mice deficient in the enzyme signal transducers of transcription (STAT)4, required for the differentiation of Th1 IFN- $\gamma$ -producing CD4<sup>+</sup> T cells, show modest protection from IR injury (67). Interestingly, STAT6<sup>-/-</sup> mice, deficient in Th2 CD4<sup>+</sup> T cells, develop more severe damage, due in part to an inherent lack of IL-4 (67). IL-16, a T cell chemoattractant produced by TECs has also been implicated to CD4<sup>+</sup> T cell-mediated IR injury (68).

Another T lymphocyte subset, the TCR $\beta$ <sup>+</sup>CD4<sup>+</sup>CD25<sup>+</sup>Foxp3<sup>+</sup> regulatory T cell (Treg) has been implicated in repair following kidney IR injury. In a study by Gandolfo *et al.*, Treg depletion with anti-CD25 monoclonal antibodies (mAbs) delivered 1 day after IR injury lead to worsened tubular damage and reduced TEC proliferation (69). Conversely, infusion with additional Tregs 1 day after injury reduced IFN- $\gamma$  production and enhanced kidney repair (69). Additional

evidence supports the notion that Tregs promote repair through IL-10-mediated innate immune system suppression (70).

NKT cells are a subpopulation of T lymphocytes that share surface receptors and functions with conventional T cells and NK cells. The CD1d restricted, invariant NKT cells are capable of producing a rapid burst of both Th1 and Th2 related cytokines upon interaction with glycolipids, which can activate other leukocytes (58). A small increase in the proportion of NKT cells has been observed in IR-injured kidneys within 24hrs of reperfusion (71). The severity of IR injury in NKT deficient mice and in mice following NKT cell neutralisation and depletion is also reduced, mediated by a reduction in IFN- $\gamma$ -producing neutrophils (72). These data from animal studies highlight the complexities involved in the lymphocyte response to IR injury.

Resident kidney DCs, which reside in the interstitium (73), form a heterogeneous population of professional antigen presenting cells that are suspected to contribute to the initial inflammatory response to kidney IR injury, in part through the activation of NKT cells. In the IR setting, resident DCs may also respond to the endogenous molecules released from damaged or dying cells (DAMPs) (74). However, they also possess the potential to induce tolerance (75). Li *et al.*, demonstrated that activation of adenosine 2A receptor ( $A_{2A}R$ ) signalling on DCs inhibits NKT cell activation, in turn reducing IFN- $\gamma$  production, limiting neutrophil infiltration and tissue damage in kidney IR injury (76). As proof of concept, mice with  $A_{2A}R$ -deficient DCs developed more severe injury, while administration of DCs activated and tolerised *ex vivo* with an  $A_{2A}R$  agonist and an NKT cell antigen were able to provide protection from IR injury, even when administered shortly after reperfusion (76). Another study proposed that resident kidney DCs are largely responsible for the TNF production in the early stages of IR injury, along with IL-6, MCP-1 and RANTES (77). In light of these studies, there is conjecture regarding the identity of DCs and the distinction from macrophages due to the heterogeneity of these cells and the overlap of surface receptors and functional capabilities (78-83).

The focus of this thesis is on macrophages in AKI. These myeloid cells form a heterogeneous population that are implicated in the initiation of IR injury but have also been shown to govern tissue repair and remodelling in inflammatory disease settings, including kidney injury. Harnessing the reparative capabilities of macrophages may form the basis of future therapies for both acute and chronic kidney diseases. The following is a detailed review of macrophages in development, injury and repair.

### **1.3 Macrophages in Renal Development, Injury, and Repair<sup>1</sup>**

In all vertebrates, macrophages are the first leukocytes to appear in the embryo. During postnatal and adult life they differentiate from haematopoietic precursor cells, a process that occurs exclusively in the bone marrow (84). In contrast, during early mammalian development primitive fetal macrophages appear to differentiate from a different cell origin independent of the blood monocyte (85-87). Macrophages in the embryo serve as specialized phagocytic cells (88). They are formed in the yolk sac and then migrate through the mesenchyme to invade the tissues of the embryo proper. With formation of the primitive vasculature, fetal macrophages migrate from the yolk sac into the liver. Fetal macrophages also proliferate and differentiate locally within tissues before forming tissue-specific macrophages (89, 90). Macrophages are essential during embryogenesis and play an important role in programmed cell death and tissue remodeling during organogenesis (88, 91). The production of both liver and bone marrow-derived macrophages is controlled by the growth factor colony stimulating factor (CSF)-1, also termed macrophage colony stimulating factor (M-CSF). CSF-1 binds to the CSF-1 receptor (CSF-1R) and genetic deletion of either of these genes in mice results in marked depletion of tissue macrophages (92, 93). The CSF-1 deficient *op/op* mouse (CSF-1<sup>op</sup>/CSF-1<sup>op</sup>) has revealed the importance of macrophages in the development of many organs especially the bone, brain and endocrine systems. In the brain, neuroepithelial cell growth requires macrophages (94). Macrophages are also required for the normal development of the pancreas and mammary gland (95, 96). Indeed, embryonic macrophage populations exist within almost all developing

---

<sup>1</sup>Pages 14-30 have been published in: Williams *et al.*, *Semin Nephrol*, 2010

organs and adopt highly specific locations, phenotypes and functions. In developed organs, the Kupffer cells of the liver, Langerhans cells of the skin, osteoclasts in the bone and microglia in the brain all represent highly specialized resident macrophage populations (86).

Once permanent or definitive hematopoiesis is established with increased gestation, the proliferative capacity of the macrophage declines and a distinct set of phagocytes, the monocyte–macrophages are formed (87, 97, 98). In the adult, macrophages are involved in inflammation and immune surveillance. However, the heterogeneity and cellular plasticity of macrophage populations with their ability to change phenotype in response to local stimuli, allows these cells to be highly specialized and display a wide and apparently opposing range of functions. Indeed, there is strong evidence that subpopulations of macrophages directly contribute to wound healing and tissue repair, supporting the concept that some macrophage phenotypes can promote organ regeneration following injury. However, this ability to change phenotype and function makes categorizing macrophage populations relatively difficult.

### **1.3.1 Classical versus Alternative Activation States**

Evidence supports the notion of two key macrophage polarization states described as M1 ‘classically activated’ pro-inflammatory macrophages and M2 ‘alternatively activated’ immune regulatory macrophages (99, 100) (Figure 1.2). In general, these two phenotypic states are somewhat comparable to the opposing Th1 and Th2 cells. A key factor driving M1 polarization and activation is interferon- $\gamma$  (IFN- $\gamma$ ), derived from CD4<sup>+</sup> Th1 cells, CD8<sup>+</sup> cytotoxic T cells and natural killer (NK) cells, either working alone or in conjunction with lipopolysaccharides (LPS), tumor necrosis factor- $\alpha$  (TNF- $\alpha$ ) and other microbial products (101). Culture of human CD14<sup>+</sup> monocytes in the presence of granulocyte macrophage CSF (GM-CSF) also induces M1 polarization. M1 macrophages produce pro-inflammatory cytokines, in particular interleukin (IL)-12 and IL-23, are phagocytic, present antigen via major histocompatibility complex (MHC) class II molecules (102) and generate toxic nitrogen and oxygen intermediates (103). This equips M1 macrophages to effectively eliminate intracellular pathogens and even some tumors

(104, 105). The IL-12 produced by M1 macrophages drives further Th1 polarization and stimulates additional IFN- $\gamma$  production from T cells and NK cells thereby perpetuating the inflammatory response. In kidney disease a predominantly M1 macrophage infiltrate results in tissue damage and cell loss followed by the accumulation of extracellular matrix (ECM) proteins. The downstream effect of the pro-inflammatory cascade is the development of renal interstitial fibrosis and impaired organ function. Thus, macrophage phenotype and the corresponding polarization state ultimately determine the outcome of acute inflammation and the progression to irreversible chronic scarring (106).

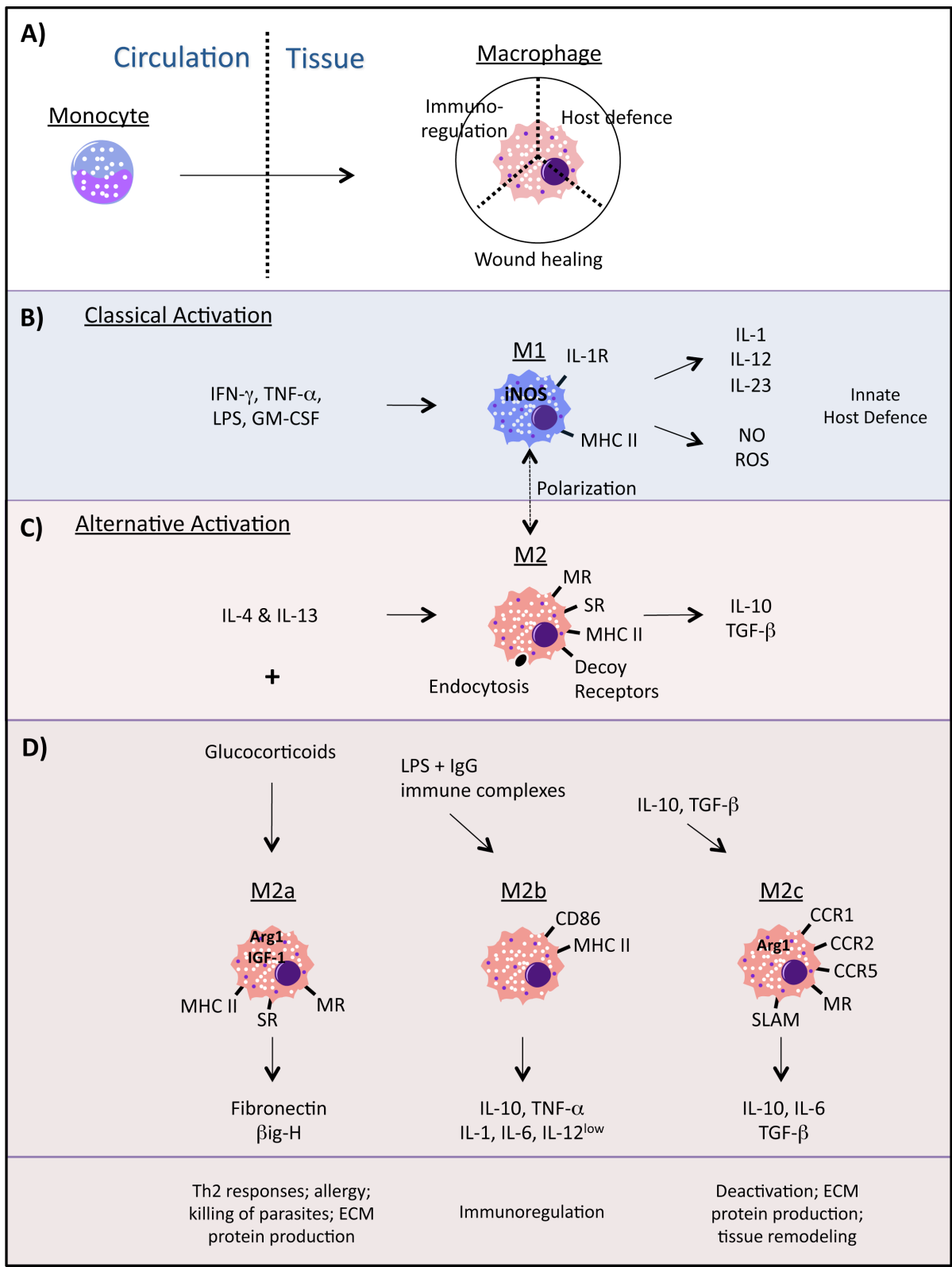


**Figure 1.2. The defining chemokine and receptor profiles of classically and alternatively activated macrophages.** Two proposed concepts for macrophage polarization are depicted. (A) Three groups of mature macrophages derived from blood monocytes that are specialized for host defence, immunoregulation or wound healing. The putative macrophage phenotypes from one category can share a range of features from the other two categories. The second model (B and C) suggests the existence of two polarization states, involving M1 or classically activated macrophages and M2 or alternatively activated macrophages. (B) Classically activated or M1 macrophages are defined based on the mode of activation and the subsequent receptor expression and production of pro-inflammatory cytokines, NO and ROS. (C) Activation typically occurs in response to IFN- $\gamma$  in conjunction with LPS or GM-CSF. Alternatively activated or M2 macrophages are broadly defined as being those activated in response to IL-4 and IL-13, resulting in the expression of mannose and scavenger receptors along with increased endocytosis abilities and the production of IL-10 and TGF- $\beta$ . Shifts in the polarization state between differentiated M1 and M2 macrophages may also occur. (D) Within the M2 group there are apparent differences in receptor expression, cytokine production and function resulting from activation in response to glucocorticoids (M2a), LPS and immune complexes (M2b) and IL-10 and TGF- $\beta$  (M2c).

Given a favourable microenvironment, M2 macrophages counteract progressive damaging inflammation and contribute to ECM remodelling and tissue repair. However, the exact definition of M2 'alternatively activated' macrophages is still under debate. Martinez *et al.* have classified M2 macrophages into three subsets, namely M2a, M2b and M2c macrophages, which differ in their mode of activation, cytokine profile and function (107).

M2a macrophage polarization following exposure to IL-4 and IL-13 or glucocorticoids results in increased expression of pattern recognition receptors including the mannose receptor (CD206) and scavenger receptor (CD163) together with up-regulation of MHC class II molecules and production of the chemokines CCL17, CCL22 and CCL24 (99, 108). M2a macrophages exhibit an enhanced capability for endocytosis, pinocytosis and antigen presentation. There is also increased production of the prototype ECM protein fibronectin, transforming growth factor- $\beta$  (TGF- $\beta$ ) induced matrix associated protein MP78/70 ( $\beta$ ig-H3) (109, 110) and insulin-like growth factor (IGF)-1, which has been shown to stimulate re-epithelialization in dermal wound healing (111, 112). Furthermore, IL-4 induced arginase production facilitates the conversion of arginine to ornithine, an intermediate in the synthesis of polyamines and collagen. These characteristics suggest an important role for M2a macrophages in tissue regeneration. However, these cells are more commonly associated with the encapsulation and killing of parasites, for perpetuating Th2 immunity and for being involved in allergic responses due to the expression of CCR3 ligands, which are involved in the attraction of eosinophils and basophils (113).

M2b macrophages characteristically produce high levels of IL-10 but differ from other alternatively activated cells in that they concomitantly produce pro-inflammatory cytokines, including TNF- $\alpha$ , IL-1 and IL-6 but low levels of IL-12. These cells become activated in response to classical activation stimuli (LPS) in the presence of immunoglobulin G (IgG) immune complexes and typically elicit an immunoregulatory response (114). This is due mainly to the high production of IL-10, capable of deactivating pro-inflammatory cytokines, especially TNF- $\alpha$ ,

whilst mediating an IL-4 dominant Th2 response (115) and inducing IgG class switching of B cells (116).

M2c macrophages, also termed deactivated, are induced by high levels of IL-10 and TGF- $\beta$  and have vital immunosuppressive roles whilst contributing to matrix remodeling and tissue repair. Interestingly, IL-10 induces the expression of pro-inflammatory chemokine receptors such as CCR1, CCR2 and CCR5 (117), which bind the ligands monocyte inflammatory proteins-1 $\alpha$  (MIP-1 $\alpha$ ) and MIP-1 $\beta$ , monocyte chemoattractant protein (MCP)-1 and CCL5. However, these receptors become uncoupled, interrupting signal transduction such that IL-10 inhibits cell migration in the presence of these pro-inflammatory chemokines resulting in macrophage deactivation. The positive role of M2c macrophages in tissue regeneration is not, however, the result of restricted migration but from the deactivation event that allows the chemokine receptors to function as decoy receptors. This contributes to M2c governed immunosuppression through the clearance of pro-inflammatory mediators. IL-10 also up-regulates cell surface expression of CD150, or signalling lymphocyte-activating molecule (SLAM), which appears uniquely on this subset of macrophages but is also an indicator of dendritic cell maturation (118). SLAM is known to activate T cells but due to its expression by M2c macrophages and its regulation by the immunoregulatory cytokine IL-10, it may play an important role in the induction of T regulatory cells and driving Th2 polarization. In support of this notion, SLAM is also linked to B cell stimulation and proliferation and subsequent immunoglobulin (Ig) production (119).

Regarding alternative macrophage activation, there is debate over the classification. The effects governed by IL-10 and IL-12 may not be sufficient to warrant the classification of different subsets, with the only true M2 macrophage being that which is activated with IL-4 and IL-13 (100). It has been proposed that the M1/M2 nomenclature be used as a guide when discussing specific cell subsets based on the precise ligands and chemokines associated with that cell. More recently, Mosser and Edwards suggested that three macrophage activation states exist, being

specialized for host defence, wound healing or immune regulation (120). Depending on the specific inflammatory and microenvironmental cues, macrophages can adopt particular phenotypic and functional characteristics, giving the impression of a range of subsets. Whichever classification system proves to be most accurate, the ability of macrophages to mediate renal repair most likely depends on the interplay of a number of different subsets that function to suppress Th1 (M1) induced inflammation, promote Th2 (M2) recruitment and/or polarization, clear cellular debris and promote tissue regeneration and reorganization through appropriate ECM production/degradation and angiogenesis.

### **1.3.2 Tumor-associated Macrophages: Analogies with Embryonic Macrophages**

The importance of macrophage phenotype in controlling immune responses is highlighted in malignancy. Macrophages in the fetal kidney, lung and brain share a characteristic gene expression profile comprising a variety of anti-inflammatory and pro-proliferative factors (121) but with a distinct genetic profile compared to the adult (87, 98, 122, 123). Macrophages in the embryonic kidney express a repertoire of markers suggestive of an M2 phenotype (121) and a number of the M2-associated genes identified in embryonic macrophages are shared by tumor-associated macrophages (TAMs) (124-126), including the mannose receptor, macrophage scavenger receptors (Msr1 and Msr2), CCL24, C1q, CD163 and TREM2 (121).

There is growing evidence that the tumor microenvironment influences M2 macrophages to produce a variety of pro-tumor growth and angiogenic factors as well as immunosuppressive molecules (124). Stemming from a common myeloid precursor, there are distinct subpopulations of myelomonocytic cells with different differentiation phenotypes, dependent on the site of tumor origin and progression of disease. Myeloid-derived suppressor cells (MDSCs; CD11b<sup>+</sup>Gr-1<sup>+</sup>F4/80<sup>-</sup>IL-4Ra<sup>+</sup>) of granulocyte origin are recruited to the tumor microenvironment where they become F4/80<sup>+</sup> (124, 126, 127). In addition, TAMs are derived from circulating monocytes and influence tumor growth. Both MDSCs and TAMs have a phenotype similar to M2 macrophages and may well represent a unique myeloid cell

differentiation program (124). Tumor-conditioned granulocytes may play a role in priming macrophages towards either an M1 or M2 phenotype (128). However, as in inflammation, it is unclear if macrophages remain committed to a single phenotype or whether they regress to a resting state that can be reactivated another way (129). Tumor progression and metastasis depends upon constant macrophage influx to assist tumor growth, angiogenesis and stromal remodeling. Macrophages may be either anti- or pro-angiogenic depending on their microenvironment. Recently, Kelly *et al.* reported that somatic cell senescence genes, Fas ligand and IL-10 are key regulators of macrophage polarization and determine their ability to regulate angiogenesis (130). Thus, targeting specific macrophage populations or immunotherapies designed to exploit the ability of macrophages to adopt an anti-angiogenic phenotype may effectively remodel the tumor microenvironment in order to suppress tumor cell proliferation and metastasis (131).

### **1.3.3 The Role of Tissue Macrophages in Kidney Development**

Macrophages play various roles in both kidney development and disease. Macrophages originating from the liver infiltrate the renal mesenchyme of the developing metanephros via the circulation prior to nephron formation (121). As the tubules of the developing nephrons are formed, the interstitial macrophages become intimately associated with the cortical nephron segments and with the loop of Henle in the medulla. The macrophages assemble in the interstitium adjacent to the basement membrane underlying the tubular epithelium and wrap cellular processes around the epithelium. It is in this location that a resident population of tissue macrophages persists within the kidney into adult life (121). Although we have documented the timing of the arrival of such macrophages, it is unclear whether their residence is permanent with such cells representing long-term residents or whether there is ongoing recruitment and turnover of this population, potentially but not necessarily from the circulating monocytic/macrophage population. We have examined the expression profile of such resident macrophages but have not found markers that would definitively distinguish between tissue and circulating monocyte-derived macrophages or from resident macrophages located in other

organs. However, the presence of macrophages from early kidney development and their intimate relationship with the forming tubules of the nephrons suggests that, as for organs such as the breast and the brain (94, 95, 132), macrophages are critical for kidney development. We have also demonstrated that the addition of CSF-1 to a developing murine kidney significantly promotes growth and differentiation and that this is accompanied by an increase in the number of macrophages present in the cultures (121). CSF-1 itself does not appear to be essential for kidney development as mice deficient in CSF-1 have kidneys (102). However, these mice are not completely devoid of macrophages and do access some CSF-1 from their mothers (133). However, it is possible that manipulation of the trophic role of macrophages within developing kidneys may be used to induce compensatory nephron production in fetuses suffering from intrauterine growth retardation.

#### **1.3.4 Macrophages in Kidney Disease**

Although the pathogenesis of renal disease is multi-factorial, the ideal therapy would both address causative factors and promote optimal cellular replacement following injury. Importantly, damaged kidneys can undergo endogenous repair of the nephron renal epithelia via cell proliferation (134). However, the capacity of the kidney and especially the glomerulus to undergo endogenous repair following injury is limited and typically insufficient.

##### **1.3.4.1 Suppression of Macrophage Activities in Chronic Kidney Disease**

The role of the macrophage in response to kidney injury has been traditionally regarded as inflammatory and detrimental. Although the nature of the damage would potentially result in a variable role for macrophages in disease onset and progression, glomerular and tubulointerstitial macrophage accumulation occurs in response to almost all insults. Both immune and non-immune injury results in macrophage infiltration leading to increased ECM accumulation and tubulointerstitial inflammation and fibrosis. Evidence suggests that glomerular macrophage accumulation makes an important contribution to diabetic nephropathy (135) as depletion or disruption of macrophage function limits disease severity. Macrophage

depletion using liposomal clodronate reduced mesangial ECM accumulation in a rat model of nephrotoxic nephritis (136) whilst gene deletion of MCP-1 reduced tubular injury and death in murine nephrotoxic nephritis (137). Mice lacking either L-selectin alone or all three selectins (E-, P- and L-selectin) exhibited reduced macrophage recruitment and less tubulointerstitial fibrosis and tubular apoptosis in experimental hydronephrosis implicating macrophages in tubular cell death (138). The induction of apoptosis by macrophages due to nitric oxide and TNF- $\alpha$  production results in direct cell death but macrophages may also reduce tubular expression of vascular endothelial growth factor (VEGF), leading to the disruption of the peritubular capillary network and resultant tissue ischemia (139, 140).

The growth factor CSF-1 is pivotal to the macrophage response in the adult kidney due to its role in macrophage differentiation and proliferation. In a chronic setting, CSF-1 is produced by the kidney in response to renal injury whilst cultured mesangial cells produce CSF-1, along with its receptor, CSF-1R (141). CSF-1 is also expressed by most renal carcinoma cell lines (142), potentially inducing a response in TAMs. The cortical and medullary tubular epithelium is a major site of CSF-1 production during anti-glomerular basement membrane (GBM) induced glomerulonephritis in rats (143) and is accompanied by considerable interstitial macrophage accumulation. In glomerulonephritis in humans, there is also increased CSF-1 production by both the tubular epithelium and glomerular cells (144). This results in glomerular accumulation and proliferation of macrophages. Although CSF-1 mediates macrophage recruitment and proliferation, it may also promote classical M1 macrophage activation in renal disease. Lenda *et al.* reported fewer interstitial macrophages and reduced tubular cell death in the obstructed kidneys of CSF-1<sup>op</sup>/CSF-1<sup>op</sup> mice with bone marrow-derived macrophages exhibiting resistance to LPS and IFN- $\gamma$ -induced classical activation following pre-incubation with anti-CSF-1R antibody (145). It is thus of interest that serum levels of CSF-1 are associated with acute allograft rejection (146). The delivery of an anti-CSF-1R antibody to mice post allograft transplantation reduced macrophage proliferation and accumulation within the allograft and

tubulointerstitial rejection, suggesting that signalling between CSF-1 and CSF-1R is critically important in acute rejection (147).

Somewhat paradoxically, CSF-1 treatment effectively promotes repair in a model of acute kidney damage (148), a finding that is almost completely opposite to the chronic setting. For example, although diabetic nephropathy is associated with interstitial macrophage recruitment (149), greatly increased levels of endogenous CSF-1 produced by glomerular podocytes and the damaged tubules fail to drive the renal repair observed in the acute models (143, 150). Furthermore, the inhibition of CSF-1 signaling with CSF-1R antibodies reduces the severity of chronic disease in obese diabetic mice (db/db) that exhibit a 36-fold increase in CSF-1 levels and increased CD68<sup>+</sup> glomerular macrophage numbers (150). Administration of anti-CSF-1R antibodies results in a 60% decrease in macrophage infiltration with decreased macrophage proliferation, suppression of diabetic glomerular hyperfiltration, reduced accumulation of glomerular type IV collagen and reduced tubular injury. In this chronic setting, CSF-1 is an important contributor to disease progression with endogenous CSF-1 driving the proliferation and recruitment of a pro-inflammatory or M1-like macrophage population.

Expression of CSF-1 occurs before the onset of injury in MRL-lpr autoimmune mice whilst C3H-lpr mice do not express CSF-1 and do not show autoimmune renal injury. However, targeted CSF-1 over-expression by the tubular epithelial cells of wildtype MRL and C3H mice does not result in the development of spontaneous renal injury (151). This indicates the importance of biological context and that mechanisms downstream of simple macrophage recruitment and proliferation determine outcome. Indeed, context is key as macrophage activity is a requirement for epithelial regeneration in other organs such as the injured colon (152) with data suggesting a role for macrophages in renal repair. Also, the nature of the disease model and the mediator under study is also important. For example, although macrophage migration inhibitory factor (MIF) induced leukocyte accumulation is detrimental in immune-initiated renal injury, MIF-deficient and wild-type mice exhibit comparable interstitial macrophage accumulation and

fibrosis in obstructive nephropathy (153). In the same model, osteopontin knockout mice exhibit reduced macrophage numbers but increased tubular cell apoptosis (154) whilst inhibition of CSF-1 failed to attenuate established albuminuria in db/db mice (150). Thus, the balance between cell death and ECM protein accumulation in fibrosis or epithelial regeneration and remodeling of collagen during kidney repair is likely to be governed by many environmental factors capable of shifting the balance between inflammatory M1 and wound healing M2 macrophage responses.

#### 1.3.4.2 Positive Modulation of Macrophages in Acute Kidney Injury

AKI has myriad causes including acute ischemia due to blood loss or chemical/toxic insults resulting in proximal tubular cell injury and rapid loss of renal function. When AKI results in acute renal failure, almost half the patients die as a result, while the remainder follow a natural course of self-mediated tissue repair (155). Evidence suggests that macrophages contribute to AKI such as ischemic damage. For example, reduced tubular necrosis and tubular apoptosis was observed in mice depleted of monocyte-macrophage populations by administration of liposomal clodronate (156). Although potential therapies to enhance recovery from AKI might logically aim to reduce inflammation to facilitate repair, another strategy is to direct macrophages to perform an anti-inflammatory and pro-reparative role. It is thus of interest that, in addition to regulating the growth, differentiation and survival of macrophages, CSF-1 appears to promote the anti-inflammatory and wound healing capabilities of macrophages in mice and humans (102, 157). CSF-1 has been linked to angiogenesis *in vivo* (158) with these effects likely to result from the production of vascular endothelial growth factor (VEGF) and matrix metalloproteinases (MMP) from CSF-1 activated macrophages (159, 160). Tumor studies demonstrate that increased CSF-1 levels correspond with angiogenesis and subsequent tumor growth and metastasis (161). The role of CSF-1 in these models has been demonstrated via the use of blocking antibodies, antisense oligonucleotides or small interfering RNAs, which reduces human mammary tumor xenografts in mice (162, 163). The depletion of phagocytic macrophages using liposomal clodronate also inhibits tumor development (164). A further

study compared CSF-1 inhibition with VEGF inhibition, another proposed method to block pathogenic angiogenesis associated with tumor development and retinal neovascular disease (165). Interestingly, the macrophages associated with retinal neovascular development did not express VEGF but had high levels of the collagenases MMP-2 and MMP-9 that contributed to vascular remodeling as a result of ECM degradation (166, 167). Although CSF-1 deficient CSF-1<sup>op</sup>/CSF-1<sup>op</sup> mice develop a normal vasculature, CSF-1 and macrophages are involved in the retinal neovascularization present in a mouse model of diabetic retinopathy in which hyperoxia results in ischemic vascular damage (165). Also, tumors in MMP-9 knockout mice exhibit disorganized and irregular ECM deposits similar to inhibition of CSF-1 in wild-type mice suggesting an important role for macrophage-derived MMPs in ECM remodeling (165). MMPs are also involved in chemokine and growth factor production, cell receptor expression and cell migration such that targeting MMPs may also aid the wound repair process (168, 169) (Figure 1.3). CSF-1 has also been shown to elicit a direct autocrine/paracrine effect on renal tubular epithelial cells following ischemic injury, where they transiently express the CSF-1R in conjunction with the endogenous production of CSF-1 (148). However, a macrophage-dependent repair process was also demonstrated following depletion of CD11b expressing cells although the impairment of repair was less than that evident following antibody-mediated blocking of CSF-1R on both epithelial cells and macrophages.

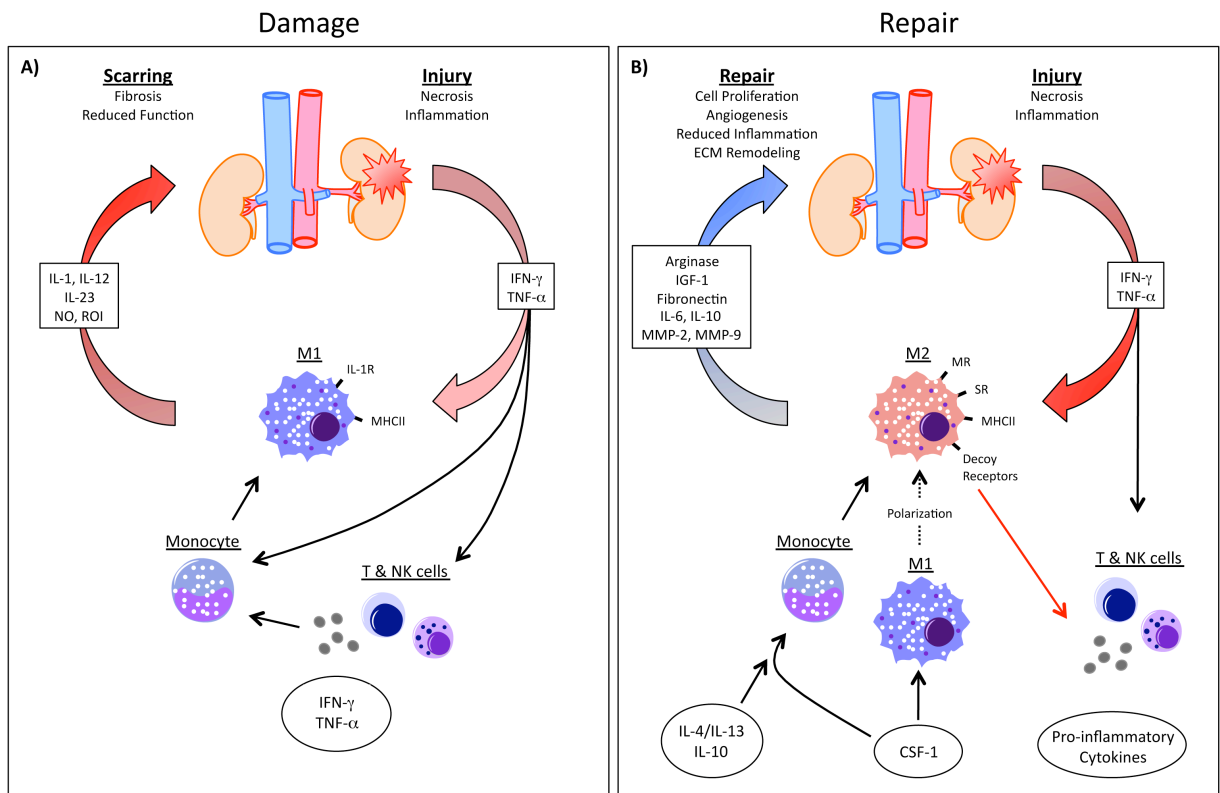


**Figure 1.3. Different types of macrophages can contribute to both damage and tissue repair processes following kidney injury.** (A) After damage, necrosis and apoptosis result in Th1-type inflammatory responses, primarily mediated by IFN- $\gamma$  and TNF- $\alpha$ . This recruits M1 or classically activated macrophages and Th1 associated T and NK cells, which produce additional pro-inflammatory cytokines to enhance the inflammatory response but which also perpetuate damage, resulting in fibrosis, scarring and reduced organ function. Pro-inflammatory factors act on both resident macrophages and circulating peripheral monocytes and macrophages, driving M1 polarization. (B) M2, or alternatively activated macrophages, can mediate cellular repair processes by clearing cellular debris, reducing inflammation, promoting angiogenesis, stimulating cellular proliferation and contributing to matrix remodeling. Targeting specific macrophage-related receptors or cell products may rapidly accelerate tissue repair and organ regeneration. The production of cytokines IL-4, IL-13 and IL-10 can facilitate M2 polarization and growth factors including CSF-1, arginase, IGF-1, fibronectin, certain interleukins and MMPs may further contribute to accelerated renal repair. In Panel B, the descending red arrow from the M2 macrophage indicates that decoupled pro-inflammatory chemokine receptors act as decoy receptors, eliminating particular pro-inflammatory mediators. IL-4, IL-13, IL-10 and CSF-1 may produce alternatively activated macrophages from monocytes as well as drive polarization of M2 from M1 macrophages.

### 1.3.5 Harnessing Macrophage Biology for Therapy

Although macrophages are recruited to the injured kidney, they can be alternatively activated to play a pro-reparative role via the production of anti-inflammatory cytokines (IL-4, IL-10) and this raises the possibility of therapeutically enhancing this reparative capacity *in vivo*. Potential therapeutic approaches include reducing macrophage infiltration, altering the response of the tissue to the presence of macrophages, delivering reparative factors directly to the kidney via genetic manipulation of macrophages or the induction of a M2 alternative activation phenotype *in situ* to directly promote repair.

Modulation of macrophage infiltration via the delivery of decoy receptors or antibodies has been discussed previously. For example, deficiency of selectins reduced macrophage infiltration and fibrosis in obstructive nephropathy (138). In contrast, blockade of either ICAM-1 or VCAM did not reduce macrophage numbers in nephrotoxic nephritis though disease was still less severe (170). Manipulation of a wide variety of chemoattractants, including MCP-1, MIP-1a, CCL5 and fractalkine, also reduce glomerular macrophage accumulation (171). Inhibition of classical activating cytokines including TNF- $\alpha$  or IL-1 $\beta$  is anti-inflammatory whilst the genetic deletion of anti-inflammatory cytokines such as IL-4, IL-10 and IL-13 that induce M2 macrophage activation result in more severe macrophage infiltration of glomeruli. In Alport syndrome, where there is a genetic defect in the gene for type IV collagen, the GBM irregularities are mediated, at least in part, by glomerular macrophage production of MMP-12 as specific inhibition of MMP-12 greatly improves GBM ultrastructure (172). This study implicates macrophages in the GBM damage of a genetic disease and indicates that modification of macrophage activity can improve outcome. Various methods of suppressing macrophage function have been reported to attenuate injury and fibrosis in experimental models of renal disease, including glomerulonephritis (173), allograft rejection (174) and obstructive nephropathy (175).

Modification of the response of the tissue itself to macrophage accumulation has been attempted via the delivery of specific genes directly into the kidney itself. For example, the gene for 15-lipoxygenase, the enzyme responsible for the production of lipoxins which reduce macrophage activation, was virally delivered into the glomeruli in a rat model of experimental glomerulonephritis via viral injection into the renal artery (176). Interestingly, this manipulation reduced proteinuria without reducing macrophage accumulation. An alternative strategy has been to utilize the efficient macrophage homing mechanism to deliver the gene product to the inflamed kidney. In these studies, macrophages that have been virally transduced to over-express anti-inflammatory mediators such as IL-1ra, IL-4 and IL-10 were administered with a beneficial effect on outcome evident (173, 177, 178). Also, the administration of macrophages transduced with a dominant-negative inhibitor of nuclear factor (NF)- $\kappa$ B reduced glomerular expression of inducible nitric oxide synthase and MHC class II expression in rats with nephrotoxic nephritis (179). Advances in this area have focussed on longer term gene expression using lentiviruses and the modification of the bone marrow to produce a continuous supply of anti-inflammatory cells; an approach successfully used in a model of Goodpasture syndrome (180).

An extension of the approach of genetic manipulation of macrophages to over-express a single anti-inflammatory molecule is to capitalize on our increasing understanding of macrophage heterogeneity in order to stimulate the appropriate alternative activation response. Such a manipulation would involve shifting the balance between M1 and M2 activation with this tipping of the M1/M2 balance predicted to bias the macrophage response to repair rather than inflammation. Direct evidence that this approach can be effective was shown following the adoptive transfer of murine splenic macrophages programmed *ex vivo* with IL-4/IL-13 to adopt an alternative activation state prior to systemic administration to a mouse model of chronic inflammatory renal disease. The macrophages trafficked to the inflamed kidneys and maintained their phenotype for up to 4 weeks (181). Furthermore, the adoptively transferred

macrophages modulated the host macrophages towards an M2 phenotype as has been suggested to occur in models of glomerular inflammation (178, 179).

#### 1.4 CSF Signalling to Myeloid Cells in Inflammation

The importance of CSF-1 signalling on macrophage development, survival and activation has been discussed, along with the varied effects on kidney disease pathogenesis when comparing the chronic and acute settings. More recently, work from our laboratory has shown that administration of recombinant CSF-1 protein to mice with established IR injury resulted in accelerated structural and functional recovery through the promotion of an anti-inflammatory macrophage response (182).

Another important myeloid growth factor, GM-CSF also has important roles in providing survival and proliferative signals to cells of the myeloid lineage, particularly during times of inflammation. GM-CSF has been implicated in the progression of a number of inflammatory disease models, including experimental rheumatoid arthritis, osteoarthritis and inflammatory lung disease (183-185). GM-CSF and CSF-1 have also been shown to induce M1-like and M2-like activation states *in vitro*, respectively (102, 186, 187). However, experiments examining *in vivo* CSF signalling suggest that the roles of these two growth factors are much more complex. Targeting CSF-1 and GM-CSF to manipulate inflammation and myeloid cell function does offer a realistic potential to successfully halt inflammation-mediated damage and enhance repair. To optimise CSF-related therapies by delivering protein, altering *in vivo* CSF expression or by neutralising these growth factors, timing the therapies to the specific phases of the disease will be vital. This itself requires a detailed knowledge of the events occurring at all stages of each disease.

In conclusion, there is considerable renewed interest in macrophages in both kidney development and disease with a focus upon their reparative functions. However, given the clear capacity for macrophages to play distinct roles at different times of the disease process, it will be important to better understand the nature of the inter-relationships between the various states of macrophage activation. It will also be critical to gain a better understanding of the distinction between embryonic and postnatal resident tissue macrophages and the kinetics of turnover of resident macrophages. It is likely that future insights into the complexity of macrophage biology will lead to novel therapies to promote renal development, diminish injury and promote repair of the diseased kidney.

## 1.5 Hypothesis and Aims

The preceding introduction has reviewed the pathophysiology of AKI, focusing on the response of immune cells and the effects of cytokines and chemokines. A particular emphasis was placed on macrophages due to their role in kidney disease pathogenesis and their ability to mediate tissue repair. This thesis assesses the contribution of different subpopulations of monocytes/macrophages and associated cytokines to IR injury and resolution.

Flow cytometry was used in this PhD to investigate the contributions of particular immune cells to the initial inflammatory phase and subsequent resolution phase of kidney IR injury. An advantage of flow cytometry is that it can identify and assess functionally important cell subpopulations and quantify subtle phenotypic changes in response to injury, disease and therapeutic intervention. As a range of parameters can be analysed together, these subpopulations can be assessed in the context of the entire organ, including other haematopoietic cells and non-haematopoietic cells. This is particularly important in inflammatory settings, where it is becoming more apparent that there are constant changes in the microenvironment and a dynamic interplay between the different cell types.

The overall hypothesis of this PhD is that a thorough understanding of the contribution of myeloid cells to IR injury will enable the fine manipulation of these cells to enhance repair mechanisms. Further, neutralising myeloid growth factors at the time of IR injury will provide protection against inflammation-mediated damage.

The aims of the studies described in this thesis are:

1. To optimise a digestion protocol for the flow cytometric assessment of kidneys. To develop a flow cytometric gating strategy to identify key myeloid subpopulations in the kidney following IR injury.
2. To perform a comprehensive characterisation of the kidney IR injury model of AKI using flow cytometry, specifically focusing on epithelial cells and subpopulations of myeloid cells throughout the inflammatory and remodelling phases of disease.
3. To determine the prophylactic effects of GM-CSF and CSF-1R blockade on kidney damage and repair following IR injury. To gain further insight into CSF signalling with the use of neutralising anti-GM-CSF and anti-CSF-1R monoclonal antibodies.

# CHAPTER 2

---

*Establishing the Flow Cytometric  
Assessment of Myeloid Cells in Kidney  
Ischemia/Reperfusion Injury*

## Declaration for Thesis Chapter 2

### Declaration by candidate

This chapter was published as is, in the *Cytometry A*:

**Williams TM**, Wise AF, Alikhan MA, Layton DS and Ricardo SD (2014). "Establishing the Flow Cytometric Assessment of Myeloid Cells in Kidney Ischemia/Reperfusion Injury" *Cytometry A*. 85(3): 256-267. (Appendix)

In the case of Chapter 3, the nature and extent of my contribution to the work was the following:

Nature of contribution	Extent of contribution (%)
Study design, execution of experiments, data analysis, interpretation of results, preparation of manuscript	85%

The following co-authors are students at Monash University and the extent of their contribution in percentage terms are stated below.

Name	Nature of contribution	Extent of contribution (%) for student co-authors only
Andrea Wise	Technical assistance and intellectual input	3%

The undersigned hereby certify that the above declaration correctly reflects the nature and extent of the candidate's and co-authors' contributions to this work.

<b>Candidate's Signature</b>		<b>Date:</b> 19/12/14
<b>Main Supervisor's Signature</b>		<b>Date:</b> 19/12/14

## 2.1 Introduction

A common feature of the progression of immune and non-immune kidney diseases of diverse aetiology is the infiltration of inflammatory macrophages (188). Macrophage numbers have shown to correlate with disease progression, making them a useful tool in predicting disease outcome (149, 188, 189). More recently, macrophage heterogeneity has been shown to correspond to the diverse roles that these cells play in both the initiation of tissue fibrosis and the positive role in wound healing and tissue remodeling (190, 191). Monocytes recruited in response to inflammatory cues can undergo differentiation into two broad macrophage subsets based on phenotype, function and polarization state. The classically activated or M1 macrophage is the pro-inflammatory cell type closely associated with the innate immune response, while the alternatively activated or M2 macrophage possesses a range of anti-inflammatory and wound healing capabilities (99, 100, 120). In part, achieving wound repair and tissue remodeling requires an appropriate balance between the M1 and M2 polarization states.

Traditionally, studies investigating the number of infiltrating macrophages in damaged kidneys have relied on immunohistochemistry (IHC) and immunofluorescence (IF) techniques to assess kidney histopathology, cell morphology and receptor expression. However, flow cytometry is becoming an increasingly important tool, particularly due to the ability to evaluate a panel of cell surface and intracellular markers on individual cells at a rate of over 10000 cells/second. Eight-color polychromatic flow cytometry in conjunction with two non-fluorescent parameters, forward and side light scattering, is now common and with the latest flow cytometers measuring up to twenty parameters, the information obtainable from each experiment is destined to grow, and with it the need for more rigorous methods of data analysis (192). However, even with improving technology, there remain a number of key challenges related to the preparation of kidney samples for flow cytometry, the selection of appropriate target markers and the informative analysis of the resulting data, which need to be addressed.

The aim of this study was to assess the impact of enzymes (used to produce a kidney single cell suspension) and ischemia/reperfusion (IR) injury on cell yield, viability, surface marker expression and autofluorescence. Gating strategies were created that best characterize various myeloid cell types, especially where particular receptors were expressed at low levels. The panel of monocyte-, macrophage-, dendritic cell (DC)- and granulocyte-associated markers used included CD11b, CD11c, Ly6C, Ly6G, major histocompatibility complex class II (MHCII), colony stimulating factor-1 receptor (CSF-1R or CD115), mannose receptor (MR or CD206) and F4/80. Particular emphasis of the study was on the assessment of kidney myeloid cell analysis in the inflammatory phase of IR injury, which is characterized by widespread epithelial cell death, an influx of pro-inflammatory cells and heightened inflammatory cytokine production.

In addition, the apoptotic and necrotic epithelial cells of the damaged kidney tubular epithelium, related to the reduced glomerular filtration that follows injury, leads to the accumulation of tubular casts (53). This hallmark of AKI results in autofluorescence and non-specific background signals, which leads to difficulties in interpretation of flow cytometric data that are unique to the kidney. Unless corrected, this can lead to erroneous analysis. The intrinsic autofluorescent properties of kidney cells also apply to macrophages due to their propensity to phagocytose cellular debris.

Finally, backgating analysis was used to define and extend the knowledge of myeloid subpopulations in terms of their co-expression of multiple markers and for their spatial location on parent dot plots. This study clarifies and addresses the anomalies encountered when assessing myeloid cells in the kidney, as compared to the more commonly assessed primary and secondary lymphoid organs, while forming a comparative base for which various therapies aimed at manipulating cell numbers and function can be referenced.

## 2.2 Materials and Methods

### 2.2.1 Animals and Surgery

Male 6-8 week old (20–25g) C57BL/6J mice obtained from Monash Animal Services (Melbourne, Australia) were used. All studies were approved by the Monash University Animal Ethics Committee and were performed in accordance with the *Australian Code of Practice for the Care and Use of Animals for Scientific Purposes*. Mice were anesthetized with 2.0% inhaled isoflurane (Abbott Australasia, Sydney, Australia) before the left renal pedicle was occluded using a vascular clamp (0.4-1.0mm; Fine Science Tools, Heidelberg, Germany) for 40min via a flank incision to induce unilateral IR injury (n=5 mice/group/time-point). Following removal of the clamp, reperfusion was visually confirmed prior to wound closure using silk suture (size 5-0, Ethicon, New Jersey, USA). An additional group of mice served as a sham-operated control group where the animals were anaesthetized and a flank incision was performed without renal pedicle clamping.

### 2.2.2 Digestion and Preparation of the Kidney and Spleen for Flow Cytometry

Mice were culled using a CO<sub>2</sub> cull chamber at 6 hours, 1 day or 7 days after IR injury. The spleen and left kidney were removed and placed in cold FACS buffer (PBS supplemented with 0.2% BSA, 0.02% NaN<sub>3</sub> and 5mM EDTA). Spleens were cleaned of any connective tissue and mechanically digested in cold FACS buffer to produce a single cell suspension. Mechanical digestion (MD) was achieved by making small incisions in the side of the spleen before gently pressing the organ between two frosted glass slides. Kidneys were decapsulated and finely chopped with surgical scissors before enzymatic digestion (ED) in 1mL of dissociation media consisting of HBSS (Sigma-Aldrich, St. Louis, USA) supplemented with 3mg/mL collagenase/dispase (Roche Applied Science, Penzberg, Germany), 0.2mg/mL DNase type 1 (Roche Applied Science), 50μM CaCl<sub>2</sub>, preheated to 37°C. The samples were mixed on a rotary tube suspension mixer (20 RPM; Ratek Instruments, Melbourne, Australia) at 37°C for 20min and then mechanically digested using a 1000μL pipette tip. The samples were mixed for two

further 5min periods (20 RPM) with mechanical dissociation in between. After 30min, mechanical dissociation with an 18-gauge needle resulted in a single cell suspension. 9mL of cold FACS buffer was added in order to inhibit enzyme activity.

ED for kidneys and MD for spleens were used for all aspects of this study except for the comparison between ED and MD (Section Results 2.3.1 and Figure 2.1) where both ED and MD were performed on each of the organs.

All single cell suspensions were incubated for 1min with 1mL of red blood cell lysis buffer (8.3g/L Na<sub>4</sub>Cl, 10mM Tris-HCl, pH7.5) to remove red blood cells. All samples were filtered with a 40µm nylon cell strainer (BD Bioscience, San Jose, USA) prior to antibody labeling.

### **2.2.3 Cell Counts and Viability**

For flow cytometry cell preparation, cell counts and viability determination were performed using a Z2 Coulter Counter (Beckman Coulter, USA). In addition, for the ED versus MD study, propidium iodide (PI) was also used to determine cell viability.

### **2.2.4 Antibody Labeling**

Three million cells from kidney or spleen single cell suspensions were incubated for 20min at 4°C in the dark with the following fluorochrome-conjugated anti-mouse antibodies: anti-CD45 APC-Cy7 (clone 30-F11; Biolegend, San Diego, USA) and PE-Cy5 (clone 30-F11; BD Biosciences), anti-CD11b PE-Cy7 (clone M1/70; BD Biosciences), anti-CD11c Pacific Blue (clone N418; Biolegend), anti-I-A/I-E (MHCII) PE-Cy5 (clone M5/114.15.2; Biolegend), anti-CSF-1R (CD115) PE (clone AFS98; eBioscience, San Diego, USA), anti-F4/80 APC (clone BM8; eBioscience), anti-Ly6G Alexa Fluor 647 (clone 1A8; Biolegend), anti-Ly6C FITC (clone HK1.4; Biolegend), anti-CD206 (mannose receptor) Alexa Fluor 488 (clone C068C2; Biolegend) and anti-epithelial cell adhesion molecule (EpCAM or CD326) PE-Cy7 (clone G8.8; Biolegend). Fc receptor block (anti-CD16/32 antibody) was added to all antibody cocktails. Intracellular MR

labeling involved the use of a CytoFix/CytoPerm kit (BD Biosciences). Following surface receptor labeling, cells were permeabilized and incubated with antibody for 30min at 4°C in the dark before being washed twice in 1x Perm/Wash buffer (BD Biosciences) and resuspend in FACS buffer. Isotype matched controls were used for each antibody in a fluorescence minus one (FMO) manner.

### **2.2.5 Flow Cytometric Acquisition and Analysis**

Data were acquired on a BD FACS Canto II flow cytometer (BD Biosciences) equipped with 405nm, 488nm and 633nm excitation lasers in conjunction with FACS Diva acquisition software (BD Biosciences). Compensation was performed with single color controls for each organ using the same conjugated antibodies used in the study. Data analysis was performed using FlowLogic FCS analysis software (Inivai Technologies, Melbourne, Australia).

### **2.2.6 Statistical analysis**

Statistical analysis was performed using GraphPad Prism software version 6.0c (GraphPad Software Inc., San Diego, USA). A Student's *t*-test (unpaired, two-tailed, with Welch's correction) was used to analyze data between two groups. A one-way analysis of variance with a Tukey's multiple comparisons test was used to analyze data contained in three groups. Data are displayed as means  $\pm$  SEM.  $P < 0.05$  was considered statistically significant.

## 2.3 Results

### 2.3.1 Using Enzymes to Aid in the Digestion of the Kidney is more Suitable than MD Alone

Using enzymes (collagenase/dispase, DNase type I) to aid in the digestion of kidney tissue risks cleaving particular cell surface receptors. In addition, optimal primary and secondary lymphoid organ cell preparations are often achieved with MD alone. It was therefore necessary to test whether ED is indeed required for kidney dissociation. Ten mice received 40min unilateral IR injury and 24hrs later the spleen and injured kidney were removed. One group of 5 mice had both organs digested with the aid of enzymes while the remaining mice had their organs digested purely by mechanical means. Once digested, cells from each organ were labeled with antibodies against CD45, CD11b, CD11c, Ly6C, Ly6G, MHCII, F4/80 and CSF-1R, and assessed using flow cytometry. Our data shows that in both the spleen and the kidney, ED yielded a higher viable cell count compared to MD (spleen MD:  $5.54 \times 10^7$ , spleen ED:  $1.49 \times 10^8$ ,  $P < 0.0001$ ; kidney MD:  $2.56 \times 10^7$ , kidney ED:  $4.40 \times 10^7$ ,  $P = 0.0025$ ) (Figure 2.1a). Furthermore, propidium iodide staining revealed that ED yielded greater viability for both spleen and kidney cells (spleen MD: 74.2%, spleen ED: 86.1%,  $P < 0.0001$ ; kidney MD: 67.7%, kidney ED: 77.3%,  $P = 0.0153$ ) (Figure 2.1b). In assessing hematopoietic cells (as per the gating hierarchy described in Figure 2.1c), we found no difference in the proportion of CD45<sup>+</sup> leukocytes in the spleen with the different digestion methods (MD: 98.8%, ED: 98.3%). However, ED of the kidney resulted in a significantly greater proportion of CD45<sup>+</sup> cells compared to MD (MD: 6.1%, ED: 13.9%,  $P = 0.0003$ ) (Figure 2.1d). Within the CD45<sup>+</sup> cell pool in the kidney, the digestion method caused no difference in the proportion of Ly6G<sup>+</sup> granulocytes (MD: 28.6%, ED: 26.0%). However, in the spleen, ED significantly reduced the proportion of this cell type (MD: 4.8%, ED: 1.8%,  $P = 0.0241$ ) (Figure 2.1e). In both organs, ED significantly increased the expression (mean fluorescence intensity) of both Ly6G and CD11b on this population, as seen in the dot plots (Figure 2.1e) (data not shown).

After excluding the granulocytes, three populations of CD11b<sup>+</sup> cells were assessed in conjunction with CD11c expression (Figure 2.1f). In the spleen, ED resulted in a greater proportion of CD11b<sup>+</sup>CD11c<sup>high</sup> DCs (MD: 0.9%, ED: 1.4%,  $P=0.0034$ ), although the populations were less well defined compared to those acquired following MD (Figure 2.1f). There were very few cells that shared this phenotype in the kidney, regardless of the digestion method. The proportion of a second population, which expressed low levels of CD11c, was statistically higher following ED in both the kidney (MD: 4.2%, ED: 13.5%,  $P=0.0003$ ) and spleen (MD: 1.6%, ED: 2.1%,  $P=0.0084$ ) (Figure 2.1f). There was no significant difference in the proportion of CD11b<sup>+</sup>CD11c<sup>-</sup>(Ly6G<sup>-</sup>) cells between the two groups in either the kidney (MD: 50.7%, ED: 56.4%) or spleen (MD: 4.0%, ED: 3.2%) (Figure 2.1f).

F4/80 expression was assessed on the same CD11b<sup>+</sup>Ly6G<sup>-</sup> population with a notable difference identified between the two digestion methods in the kidney. With MD, the F4/80<sup>+</sup> cells were barely detectable but made up over 9% of CD11b<sup>+</sup>Ly6G<sup>-</sup> cells following ED (MD: 2.8%, ED: 9.1%,  $P<0.0001$ ) (Figure 2.1g). In the spleen there was no difference in the proportion of F4/80<sup>+</sup> cells (MD: 1.4%, ED: 1.3%) although the population appeared more dispersed following ED (Figure 2.1g). In addition, the two digestion methods resulted in substantial differences in the CD11b<sup>+</sup>F4/80<sup>low/-</sup> populations in the kidney. Once gated, the MFI for the F4/80-APC parameter was assessed and shown to be significantly greater following ED (MD: 505 MFI, ED: 1070 MFI,  $P<0.0001$ ) (Figure 2.1g).

In the spleen, ED reduced the expression of two CSF-1R<sup>+</sup> populations: a Ly6C<sup>high</sup>CSF-1R<sup>+</sup> (MD: 1.38%, ED: 0.03%,  $P=0.0073$ ) and a Ly6C<sup>-</sup>CSF-1R<sup>+</sup> population (MD: 1.0%, ED: 0.2%,  $P<0.0001$ ) (Figure 2.1h). Very few CSF-1R<sup>+</sup> cells were detected in either group in the kidney (data not shown). It must be noted that a change in the proportion of one population can affect the proportion of other populations. However, ED does appear important for assessing F4/80 expression in the kidney, while dramatically reducing surface CSF-1R expression, as demonstrated in the spleen. With this knowledge, a suitable gating strategy was created to clearly identify subpopulations of CD11b<sup>+</sup> cells in the kidney, both in the steady state and in the inflammatory phase following IR injury.

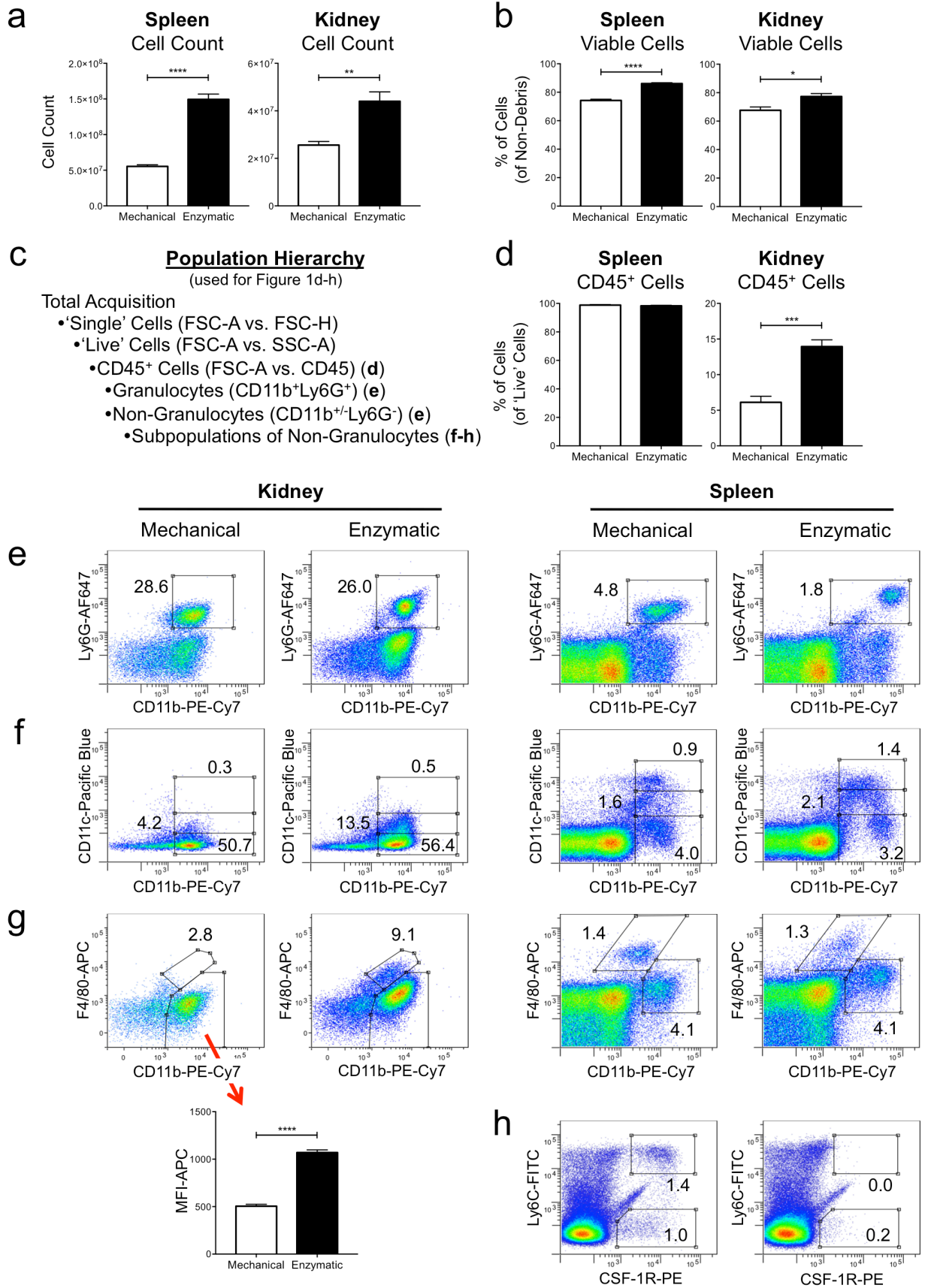


**Figure 2.1. Using enzymes to aid in the digestion of the kidney is more suitable than mechanical digestion alone.**

To compare the effects of two different organ digestion methods, spleens and kidneys from mice at 24hrs post-IR injury were subjected to either mechanical digestion (MD) or enzymatic digestion (ED). For both organs, ED yielded a higher cell count (a). ED also resulted in a greater proportion of viable cells as assessed using propidium iodide (b). The gating hierarchy used to assess viable cells, CD45<sup>+</sup> cells, Ly6G<sup>+</sup> granulocytes and subpopulations of CD11b<sup>+</sup>Ly6G<sup>-</sup> cells is shown (c). There was no difference in the proportion of CD45<sup>+</sup> cells in the spleen between ED and MD. However, ED yielded a greater proportion of CD45<sup>+</sup> cells in the kidney compared to MD (d). The digestion method had no impact on the proportion of CD11b<sup>+</sup>Ly6G<sup>+</sup> granulocytes in the kidney but significantly reduced the proportion of granulocytes in the spleen (e). In the spleen ED resulted in a greater proportion of CD11b<sup>+</sup>CD11c<sup>high</sup> and CD11b<sup>+</sup>CD11c<sup>low</sup> cells compared to MD (f). However, ED increased CD11b expression and resulted in less well-defined CD11c populations (f). The CD11b<sup>+</sup>CD11c<sup>high</sup> group was largely absent in the kidney, while ED greatly increased the proportion of the CD11b<sup>+</sup>CD11c<sup>low</sup> population (f). There was no significant difference in the proportions between the CD11b<sup>+</sup>CD11c<sup>-</sup> populations in either organ with regards to the digestion method (f). The proportion of F4/80<sup>+</sup> cells was significantly greater in the kidney following ED compared to MD (g). No difference was observed in this population in the spleen between MD and ED (g). The MFI of the CD11b<sup>+</sup>F4/80<sup>low/-</sup> population in the kidney (depicted graphically) was significantly increased following ED compared to MD (g). CSF-1R expression was dramatically reduced in the spleen following ED compared to MD for both Ly6C<sup>high</sup> and Ly6C<sup>-</sup> populations (h). Numbers on dot plots represent proportions of parent populations. Statistical analysis was performed using a Student's *t*-test (unpaired, two-tailed, with Welch's correction); \*\**P*<0.01, \*\*\**P*<0.001, \*\*\*\**P*<0.0001. Data are displayed as means ± SEM (*n*=5/group).

### 2.3.2 Gating Strategy for Myeloid Cells in the Kidney

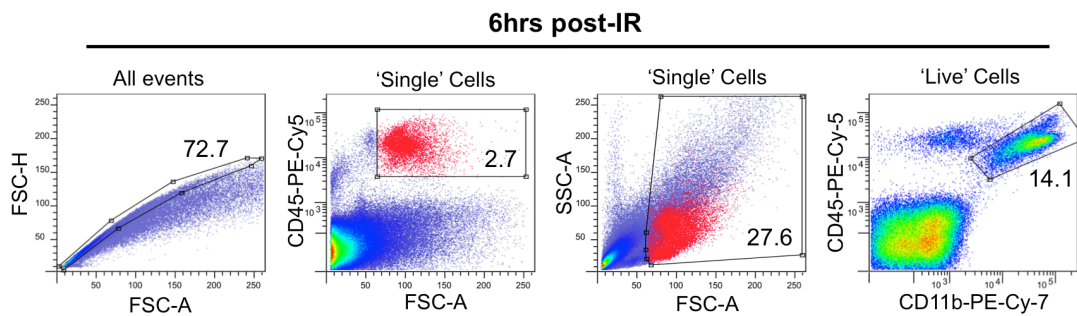
With up to eight-color flow cytometry commonly employed to assess cell phenotypes, there are inevitably many different theoretical subsets that can be defined in any experiment. Here we describe a gating procedure designed to clearly identify important myeloid cell populations in the kidney, accounting for the high potential for autofluorescence, particularly following injury. Figure 2.2a outlines the population hierarchy used to distinguish between CD11b<sup>+</sup>Ly6G<sup>+</sup> granulocytes and CD11b<sup>+</sup>Ly6G<sup>-</sup> non-granulocytes. Initially, a polygon gate was created on the FSC-A vs. FSC-H plot to select the ‘Single’ cells that passed by the lasers individually (Figure 2.2b). CD45<sup>+</sup> cells from the resulting daughter population were subsequently viewed against FSC-A. These cells represent a viable CD45<sup>+</sup> population as compared with a similar population identified using propidium iodide to exclude dead cells (data not shown). These CD45<sup>+</sup> cells were colored red and viewed on a FSC-A vs. SSC-A plot. The coloring of this population enabled a ‘Live’ gate to be drawn on the FSC-A vs. SSC-A plot, to select viable hematopoietic cells and exclude debris (Figure 2.2b). This is otherwise difficult to achieve when assessing cells in the kidney as compared to those from lymphoid organs due to the low proportion of CD45<sup>+</sup> cells. This same technique can also be employed to aid in the creation of the initial ‘Single’ cells gate. A population of CD45<sup>+</sup>CD11b<sup>+</sup> cells (encompassing resident and infiltrating myeloid cells) was selected from the ‘Live’ cell pool (Figure 2.2b). The plots in Figure 2.2b represent the cells in the kidney 6hrs post-IR surgery, which is characterized by an influx of CD45<sup>+</sup> cells. Granulocytes were identified in the resulting daughter population based on the positive expression of Ly6G (also Ly6C<sup>low</sup>) (Figure 2.2c) with their proportion being significantly higher at 6hrs post-IR injury (sham-IR: 23.0%, IR: 28.3%,  $P=0.0222$ ). An inverse gate effectively excluded the granulocytes for further analysis of myeloid cell subpopulations. Examples from sham-IR and IR kidney at 6hrs post-surgery are shown (Figure 2.2c).

**a** Population Hierarchy

Total Acquisition

- 'Single' Cells (FSC-A vs. FSC-H) (b)
- 'Live' Cells (FSC-A vs. SSC-A) (b)
- CD45<sup>+</sup>CD11b<sup>+</sup> Cells (CD11b vs. CD45) (b)
  - Granulocytes (Ly6C<sup>low</sup>Ly6G<sup>+</sup>) (c)
  - Non-Granulocytes (Ly6C<sup>+</sup>Ly6G<sup>-</sup>) (c)

**b**



**C**

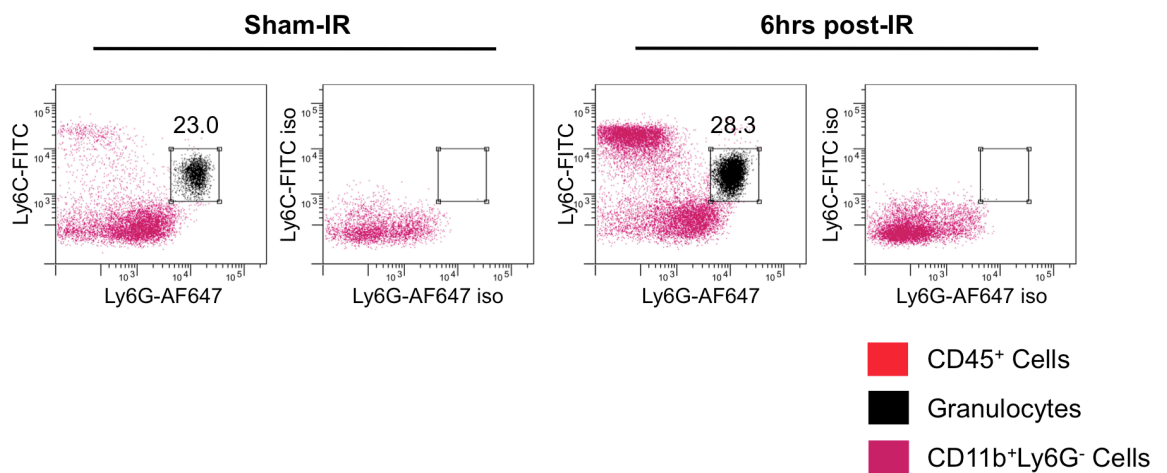


**Figure 2.2. Gating strategy for assessing myeloid cells in the kidney.**

The population hierarchy shows the CD11b<sup>+</sup> gating strategy (a). 'Single' cells (excluding doublets and triplets) were selected with a polygon gate on a FSC-A vs. FSC-H dot plot (b). CD45<sup>+</sup> cells were gated on the resulting daughter population on a FSC-A vs. CD45 dot plot. These cells were colored (red) and viewed on a FSC-A vs. SSC-A dot plot (b). A 'Live' cell gate (which excludes debris) was created with the aid of the colored CD45<sup>+</sup> cells (b). CD45<sup>+</sup>CD11b<sup>+</sup> cells were selected with a polygon gate (b). Granulocytes were selected by gating on Ly6C<sup>low</sup>Ly6G<sup>+</sup> cells (c). An inverse gate to select CD11b<sup>+</sup>Ly6C<sup>+/</sup>Ly6G<sup>-</sup> cells (pink) was used to gate out granulocytes (black) for further analysis of myeloid cell subsets (c). Plots in b are from a kidney taken 6hrs post-IR injury. Plots in c are from kidneys taken 6hrs post-IR surgery from IR and sham-IR animals. Numbers on dot plots represent proportions of parent populations.

### 2.3.3 Gating Strategy for Myeloid Cell Subpopulations in the Kidney

The gating strategy used to interrogate CD11b<sup>+</sup>Ly6G<sup>-</sup> subsets shown in Figure 2.3a extends from the gating procedure described in Results 2.3.2. Expression of the antigen-presenting molecule MHCII was compared to other markers to identify subpopulations of monocytes and macrophages. An intracellular antibody against MR was used to identify M2 macrophages (Figure 2.3b). A quadrant gate was used to identify two MR<sup>+</sup> populations based on a combination of MR and MHCII expression. While most mature M2 macrophages co-express MHCII (16.9% of CD45<sup>+</sup>CD11b<sup>+</sup>Ly6G<sup>-</sup> cells at 24hrs post-IR injury), there was a population of MHCII<sup>-</sup> cells in which MR was detected (8.5%). The example shown is from a kidney assessed 24hrs following IR injury, prior to the recognized tissue remodeling phase, where M2 macrophages are the predominant macrophage population (193).

CD11b<sup>+</sup>Ly6G<sup>-</sup> cells were also examined for their expression of the monocyte-associated marker Ly6C (Figure 2.3c), the historical mature macrophage marker F4/80 (Figure 2.3d) and the DC-associated marker CD11c (Figure 2.3e). These markers were all compared to the expression of MHCII. Both a Ly6C<sup>high</sup> (sham-IR: 3.8%, IR: 27.9%,  $P=0.0004$ ) and a Ly6C<sup>low</sup> (sham-IR: 1.4%, IR: 4.5%,  $P=0.0257$ ) population not expressing MHCII were identified with a much greater proportion in the IR injured kidney. Ly6C is a marker of monocyte immaturity and expression is lost as monocytes transition into macrophages. A general population of Ly6C<sup>+</sup> cells expressing MHCII was seen (sham-IR: 3.3%, IR: 11.0%,  $P=0.0066$ ), indicating a population of maturing monocytes, which appear to down-regulate their expression of Ly6C and up-regulate MHCII concomitantly (Figure 2.3c). F4/80 has historically been regarded as a mature macrophage marker (194). However, more recent reports have shown that it is not expressed on all macrophage populations and has been identified on some Ly6C<sup>+</sup> monocytes along with a range of other myeloid cells, revoking its status as a sole identifier of macrophages (195-198). When viewed against MHCII, three F4/80<sup>+</sup> populations were identified (Figure 2.3d). The classical F4/80<sup>+</sup>MHCII<sup>high</sup> mature macrophage was prominent in both sham-IR and IR groups (gated population) (sham-IR: 59.0%, IR: 30.5%,  $P=0.0001$ ). When viewed as an overlay containing

F4/80 stained cells and an isotype control antibody, an F4/80<sup>+</sup>MHCII<sup>low</sup> and an F4/80<sup>+</sup>MHCII<sup>high</sup> population were made evident, particularly following IR-injury (Figure 2.3d). The latter population also corresponded with the Ly6C<sup>high</sup> monocyte population when these cells were gated on a MHCII vs. Ly6C plot and colored (green) (Figure 2.3d).

There is much discussion surrounding the similarities and differences between macrophages and DCs. In this model, a clearly defined CD11b<sup>+</sup>CD11c<sup>high</sup> population, generally recognized as DCs, was not observed in the kidney (Figure 2.3e). There were cells that expressed a low level of CD11c but this population differs from the distinct CD11c<sup>high</sup> DCs seen in other organs, such as the spleen. For this reason, CD11c expression was viewed on the CD45<sup>+</sup>CD11b<sup>+</sup> population, rather than as an initial differentiating marker for macrophages and DCs. To further investigate the changes to these cells following IR injury, the entire MHCII<sup>high</sup> population was gated and the change in the MFI for the anti-CD11c antibody analyzed. As seen in the overlay plots for both the sham-IR and the IR groups at 6hrs post-surgery, antibody labeling exists at levels above the isotype control. There is also a significant increase in the MFI of this parameter following IR injury (sham-IR: 570 MFI, IR: 770 MFI,  $P=0.031$ ) (Figure 2.3e).

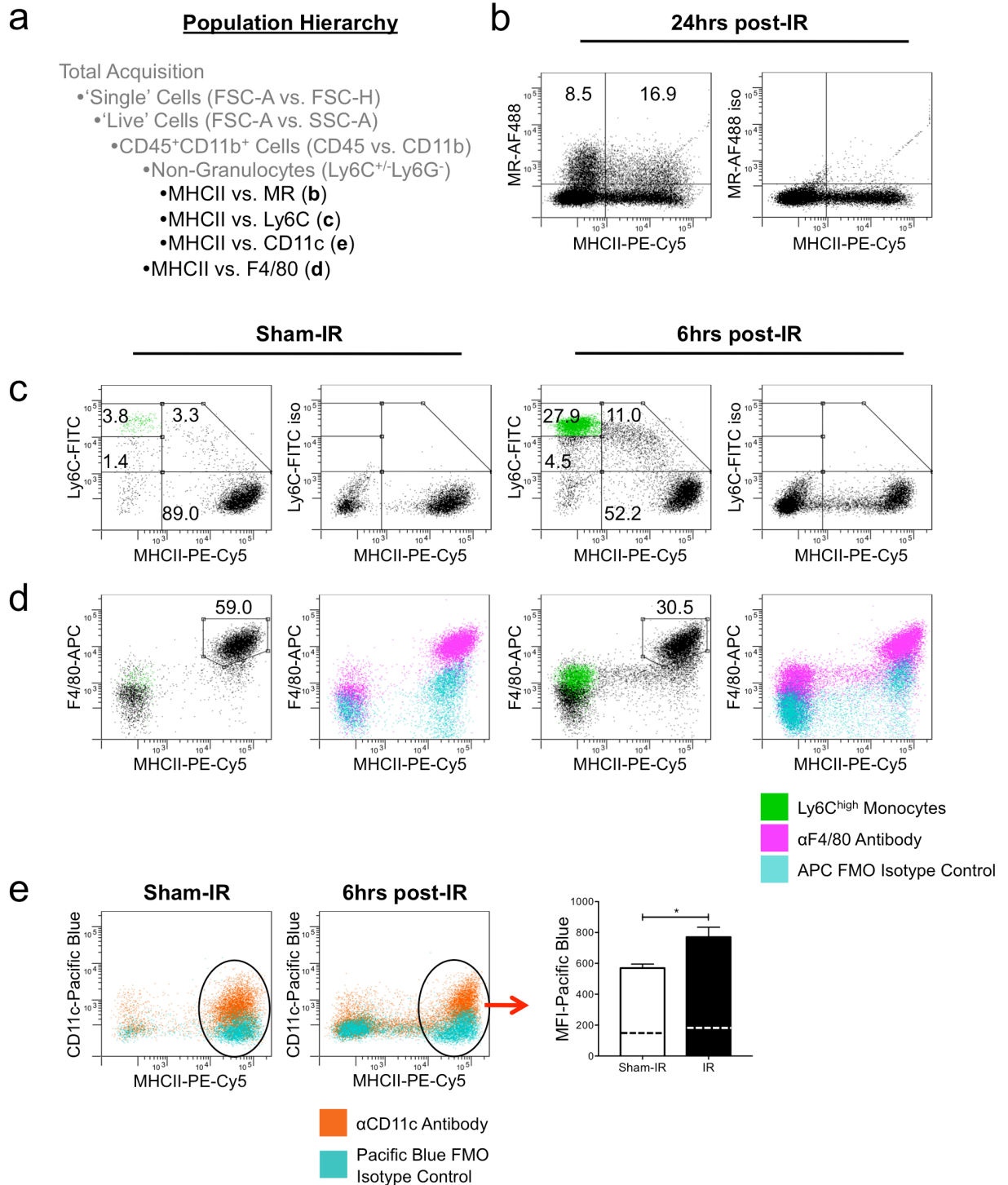


**Figure 2.3. Gating strategy for CD11b<sup>+</sup> cell subpopulations in the kidney.**

The gating hierarchy (continued from Figure 2) shows the procedure used to assess CD11b<sup>+</sup> cells following the exclusion of Ly6G<sup>+</sup> granulocytes (a). M2 macrophages, defined as being MR<sup>+</sup>, were assessed in conjunction with the expression of MHCII (b). Subsequent monocyte/macrophage subsets were defined based on the cellular expression of MHCII, Ly6C, F4/80 and CD11c (c-e). Ly6C was used to distinguish monocytes at various maturation stages. Ly6C<sup>high</sup> cells (MHCII<sup>-</sup>) are immature monocytes. The marker is down regulated as the cells mature. A prominent Ly6C<sup>high</sup> (MHCII<sup>-</sup>) population is present at 6hrs post IR-injury (green) (c), along with a smaller Ly6C<sup>low</sup>MHCII<sup>-</sup> population (c). A maturing or transitioning population of MHCII<sup>low</sup>Ly6C<sup>+</sup> cells exist, particularly following IR-injury (c). A prominent Ly6C<sup>+</sup>MHCII<sup>high</sup> population exists in kidneys following both sham-IR and IR-surgery (c). MHCII can also be used to distinguish between three F4/80<sup>+</sup> populations. A prominent F4/80<sup>+</sup>MHCII<sup>high</sup> population was identified (gated cells) (d). The dot plot overlay shows this population (pink) compared with an isotype control antibody (light blue) (d). The overlay also helped identify populations of F4/80<sup>+</sup>MHCII<sup>low</sup> and F4/80<sup>+</sup>MHCII<sup>-</sup> cells. The latter corresponds to the Ly6C<sup>high</sup> population (green) (d). Low levels of CD11c expression can make it difficult to distinctly categorize CD11c<sup>+</sup> cells in the kidney, as opposed to its expression when examined in lymphoid organs or the blood. Here the CD11c labeled cells (orange) were overlaid with an isotype control (light blue) (e). In addition, the MFI of the CD11c-Pacific Blue antibody was assessed for the MHCII<sup>high</sup> population. This data is displayed graphically with the MFI for the isotype controls indicated using a broken line (e). Appropriate isotype controls (iso) are displayed. Numbers on dot plots represent proportions of parent populations. Statistical analysis was performed using a Student's *t*-test (unpaired, two-tailed, with Welch's correction); \**P*<0.05. Data are displayed as means ± SEM (*n*=5/group).

### 2.3.4 Kidney and Spleen Ly6C<sup>+</sup>, Ly6G<sup>+</sup>, and MHCII<sup>+</sup> Cell Population Comparison

Backgating analysis was used to further characterize various myeloid subpopulations in the kidney. Comparisons were also made between these cells and their counterparts in the spleen. Figure 2.4a shows Ly6G<sup>+</sup>(Ly6C<sup>low</sup>) granulocytes (blue). These cells are also displayed on the grandparent FSC-A vs. SSC-A plot (Figure 2.4b). Granulocytes in the spleen appear similar to those in the sham-IR and IR kidney 6hrs post-surgery. However, they compose a greater proportion of the CD45<sup>+</sup>CD11b<sup>+</sup> pool (spleen: 72.5%, sham-IR kidney: 23.0%, IR kidney: 28.3%).

In a similar fashion, MHCII<sup>+</sup>Ly6C<sup>-</sup> cells (red) (Figure 2.4a) were backgated and overlaid onto the same FSC-A vs. SSC-A plots (Figure 2.4b) (spleen: 34.2%, sham-IR kidney: 89.0%, IR kidney: 52.2% of the CD45<sup>+</sup>CD11b<sup>+</sup>Ly6G<sup>-</sup> pool). A far greater proportion and number of Ly6C<sup>high</sup> cells (green) were present in the IR kidney compared to the sham-IR kidneys (spleen: 31.2%, sham-IR kidney: 3.8%, IR kidney: 27.9% of the CD45<sup>+</sup>CD11b<sup>+</sup>Ly6G<sup>-</sup> pool) (Figure 2.4a). There were distinctly fewer MHCII<sup>-</sup>Ly6C<sup>low</sup> cells (purple) compared to the Ly6C<sup>high</sup> population (spleen: 9.2%, sham-IR kidney: 1.4%, IR kidney: 4.5% of the CD45<sup>+</sup>CD11b<sup>+</sup>Ly6G<sup>-</sup> pool) (Figure 2.4a). The maturing or transitioning monocytes (MHCII<sup>low</sup>Ly6C<sup>+</sup>, light blue) are also most prevalent in the IR compared to the sham-IR kidneys (spleen: 12.4%, sham-IR kidney: 3.3%, IR kidney: 11.0% of the CD45<sup>+</sup>CD11b<sup>+</sup>Ly6G<sup>-</sup> pool) (Figure 2.4a). All of the Ly6C expressing cells from both organs present in a similar fashion on the FSC-A vs. SSC-A plots, as do the MHCII<sup>+</sup> populations. The granulocyte population in the spleen appears to be composed of cells with a greater range of size and granularity compared to that in the kidney (Figure 2.4b).

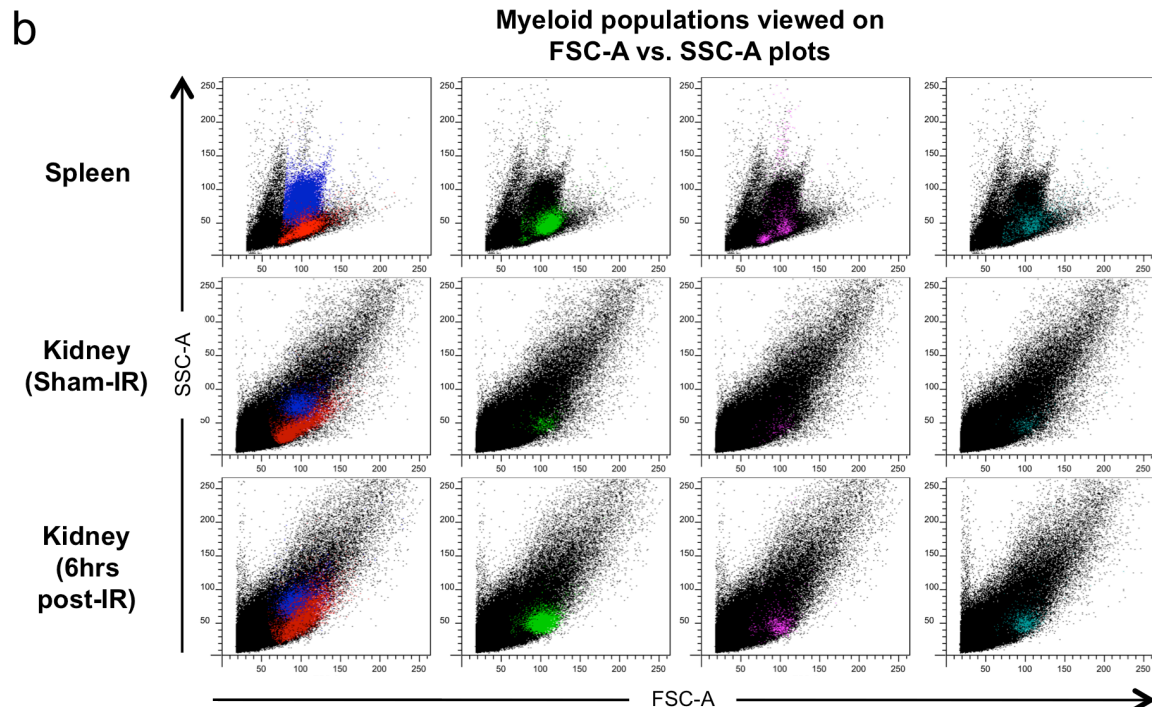
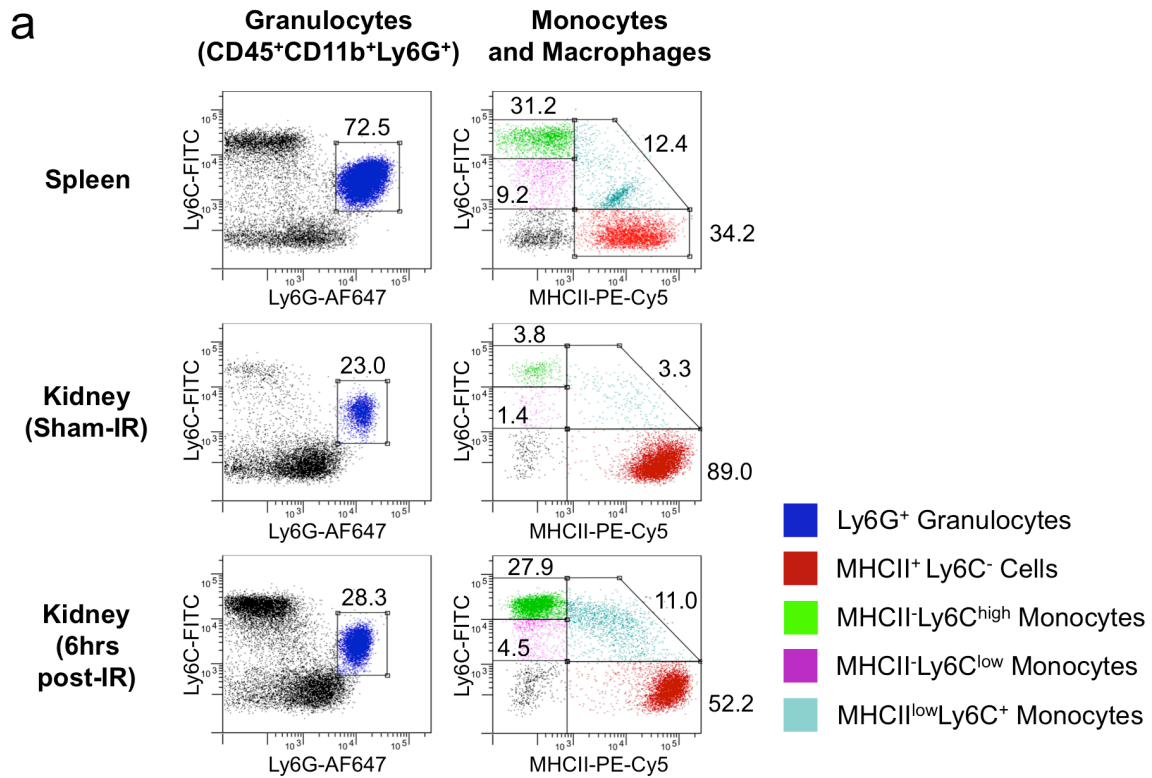


**Figure 2.4. Kidney and spleen Ly6C<sup>+</sup>, Ly6G<sup>+</sup> and MHCII<sup>+</sup> cell population comparison.**

Backgating analysis of flow cytometry data was used to compare the relative positioning of Ly6G<sup>+</sup> granulocytes (dark blue), MHCII<sup>+</sup>Ly6C<sup>-</sup> cells (red), MHCII<sup>-</sup>Ly6C<sup>high</sup> cells (green), MHCII<sup>-</sup>Ly6C<sup>low</sup> cells (purple) and maturing or transitioning monocytes (MHCII<sup>low</sup>Ly6C<sup>+</sup>) (light blue) (a). Backgating analysis of these populations shows their profiles on FSC-A vs. SSC-A dot plots (b). Examples from spleen and kidneys at 6hrs post sham-IR and IR surgery. Numbers on dot plots represent proportions of parent populations.

### 2.3.5 Assessing Epithelial Cells and Autofluorescence in the Post-Ischemic Kidney

Epithelial proliferation leading to regeneration and repair is central to processes of healing following various forms of kidney disease, including IR injury (182). As such, the pan epithelial marker EpCAM was used to assess the impact of IR injury on epithelial cell populations. To assess EpCAM<sup>+</sup> cells, 'Single' cells were gated, followed by 'Live' cells (to exclude debris), as depicted in the population hierarchy (Figure 2.5a). EpCAM expression was then compared to CD45 expression, with a gate placed around the CD45<sup>+</sup>EpCAM<sup>+</sup> population (Figure 2.5b). The proportion of EpCAM<sup>+</sup> cells had already significantly decreased at 6hrs post-IR injury (sham-IR: 16.3%, IR: 9.6%,  $P=0.0001$ ) and fell further as seen at day 7 post-injury (sham-IR: 14.3%, IR: 5.9%,  $P=0.0001$ ). Autofluorescence can pose a problem, as is evident when the kidneys taken 6hrs post-IR are displayed alongside those taken 7 days post-injury, where prominent autofluorescence is visible in the IR anti-EpCAM antibody and isotype control groups (Figure 2.5b). The autofluorescence was not present in the IR group 6hrs post-injury. For the day 7 time-point, a modified EpCAM<sup>+</sup> gate was created in order to exclude the autofluorescence from the EpCAM<sup>+</sup> population. This method can also be employed for clearly distinguishing CD45<sup>+</sup> cells from the rest of the kidney cells. Backgating analysis of the EpCAM<sup>+</sup>, autofluorescent and CD45<sup>+</sup> cells was performed to view their location on the parent FSC-A vs. SSC-A dot plot (Figure 2.5c). The difference between the different cell types is clear, with the CD45<sup>+</sup> cells forming a tighter group further along the forward scatter axis compared to the EpCAM<sup>+</sup> cells and autofluorescent events.

Autofluorescence increases progressively with time after IR injury. Figure 2.5d shows autofluorescent cells, after gating on CD45<sup>+</sup>CD11b<sup>+</sup> cells, on a Ly6C vs. MHCII plot from a sham-IR kidney along with injured kidneys at 24hrs and 7 days post-IR. The autofluorescent populations were backgated and shown in pink on the CD11b vs. CD45 parent plot. At 7 days post-IR the autofluorescence is very difficult to distinguish from non-autofluorescent CD11b<sup>+</sup> cells. Empty channels may be useful for gating out autofluorescence that is associated with IR-induced damage. The increase in the autofluorescence increased almost threefold between 24hrs and 7 days post-IR injury (sham-IR: 1.3%, 24hrs post-IR: 7.8%, 7 days post-IR: 21.2%) (Figure 2.5e).

**a**

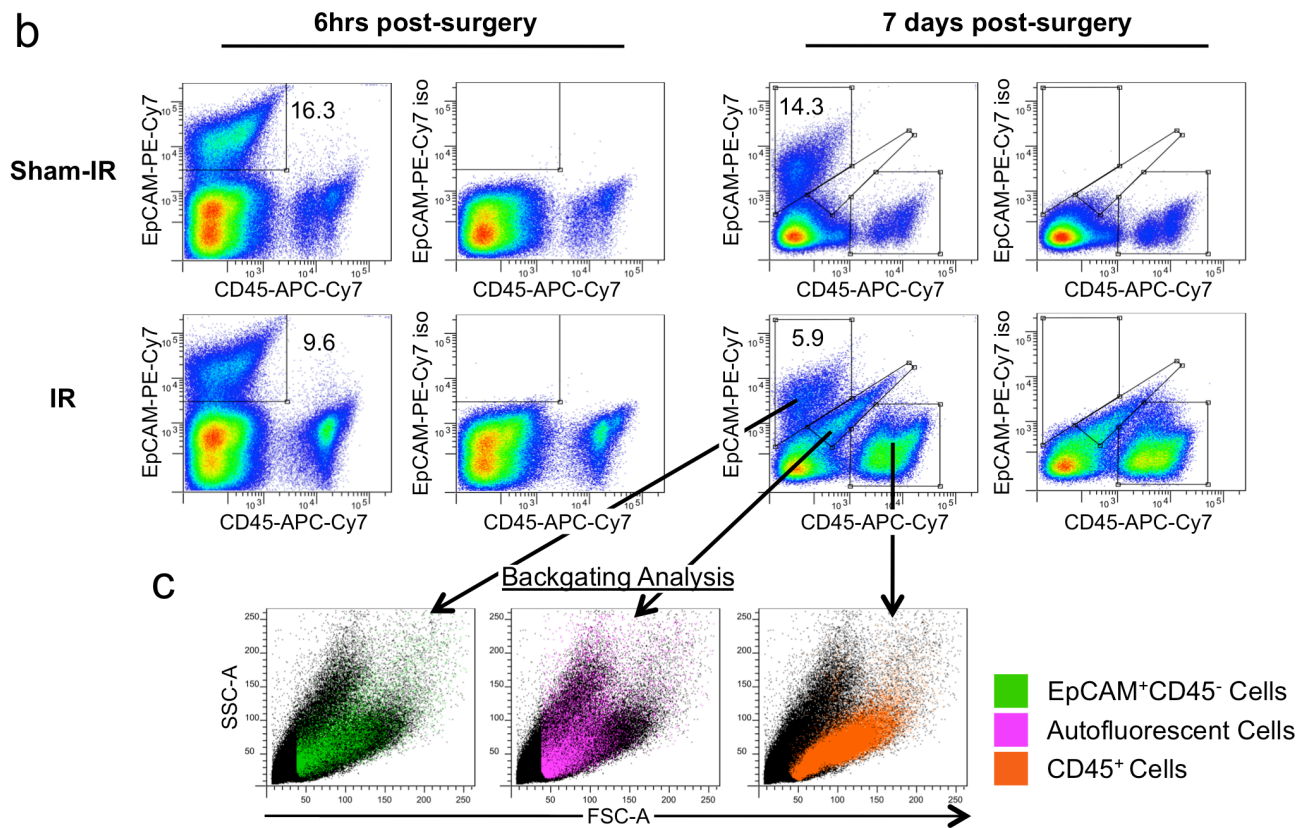
**Population Hierarchy**

(EpCAM/CD45 analysis)

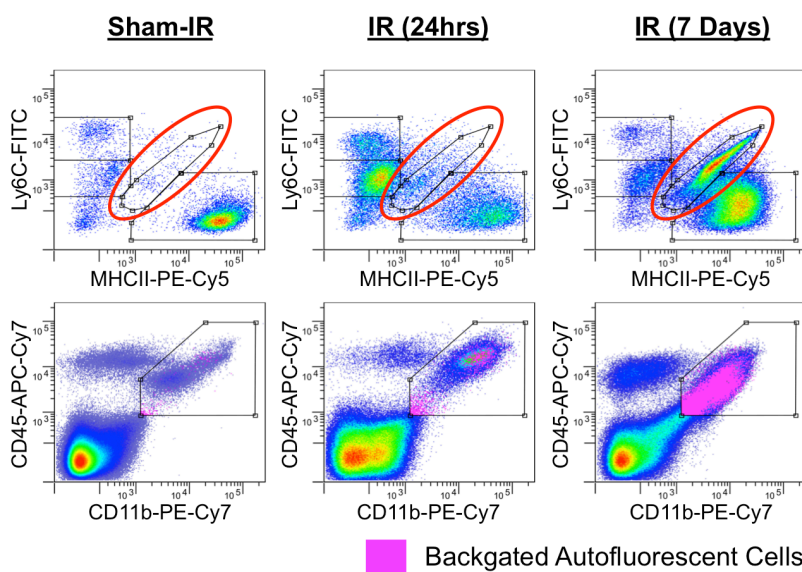
Total Acquisition

- 'Single' Cells (FSC-A vs. FSC-H)
- 'Live' Cells (FSC-A vs. SSC-A)
  - EpCAM<sup>+</sup>CD45<sup>-</sup> Cells (CD45 vs. EpCAM) (b)
  - Autofluorescent Cells (CD45 vs. EpCAM) (b)
  - CD45<sup>+</sup> Cells (CD45 vs. EpCAM) (b)

**b**



**d**



**e**

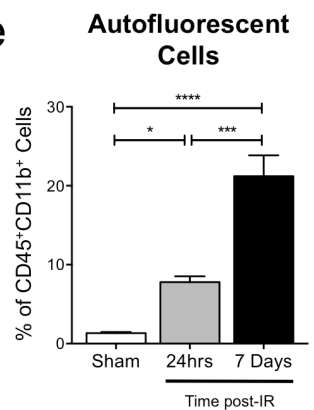


**Figure 2.5. Assessing epithelial cells and autofluorescence in the post-ischemic kidney.**

The population hierarchy resulting from the EpCAM<sup>+</sup> epithelial gating analysis is shown (a). Following the gating of 'Single' cells (FSC-A vs. FSC-H) and 'Live' cells (FSC-A vs. SSC-A) (data not shown), EpCAM<sup>+</sup> epithelial cells were selected for their expression of EpCAM and for a lack of expression of the hematopoietic marker CD45 (b). With the progression of time in the IR model, autofluorescence becomes increasingly prominent. In this example, at 7 days post-IR, the EpCAM<sup>+</sup> gate was altered so as not to include autofluorescent cells (b). Backgating analysis shows the difference in the FSC-A vs. SSC-A profile of CD45<sup>-</sup>EpCAM<sup>+</sup>, autofluorescent and CD45<sup>+</sup> populations (c). An autofluorescent population appeared when examining the CD45<sup>+</sup>CD11b<sup>+</sup> cell pool in the kidney following IR injury (d). On the MHCII vs. Ly6C dot plots, autofluorescence became more prominent with time after injury (d). This autofluorescent population was backgated and displayed in pink on the parent CD11b vs. CD45 plot (d). The increase in the proportion of this autofluorescent population with time (after injury) is shown graphically (e). Numbers on dot plots represent proportions of parent populations. Statistical analysis was performed using a one-way analysis of variance with a Tukey's multiple comparisons test; \*\* $P < 0.01$ , \*\*\* $P < 0.001$ , \*\*\*\* $P < 0.0001$ . Data are displayed as means  $\pm$  SEM ( $n = 5$ /group).

## 2.4 Discussion

Identifying and characterizing macrophage functional/polarization states is necessary to understand processes of disease progression and healing. Here, we have described a polychromatic flow cytometry analysis strategy, taking into account light scattering and autofluorescent characteristics, to assess infiltrating and resident cells in the uninjured kidney and in the inflammatory phase following IR injury. Performing backgating analysis along with coloring populations and viewing them against multiple parameters will lead to more detailed phenotypic and functional descriptions. This includes information regarding the maturation state of the cell, its autofluorescent properties and functional capacity, which can be linked to other data, such as cytokine production and enzyme activity. This is particularly relevant to tissue macrophages due to their heterogeneity, especially in the disease setting where they play central roles in inflammation and tissue remodeling.

One marker that we focused on was Ly6C, as its expression can be used to define monocyte maturation and function, with Ly6C<sup>high</sup> pro-inflammatory cells down regulating the marker as they mature into Ly6C<sup>low</sup> macrophages (199). In addition, the activation of monocytes at various maturation stages leads to mature macrophages of distinct functional states (199). Following unilateral ureteral obstruction, Ly6C<sup>high</sup> cells have been shown to home to kidneys where they differentiate into monocytes/macrophages of distinct functional states, indeed identified by the level of Ly6C expression (200). Our data showed that the initial inflammatory phase of the IR model involves a dramatic increase in the proportion and number of Ly6C<sup>high</sup> monocytes. As such, assessing changes in this population with various treatments or in fact targeting this cell type directly may impact the degree of injury or provide increased potential for regeneration. A number of studies have used antibodies against Gr-1, a complex formed by both Ly6C and Ly6G, to separate monocytes from granulocytes (201). Confirmed here in the kidney, using separate antibodies against Ly6C and Ly6G allows for an easier delineation of monocytes and granulocytes, and where applicable allows for further separation of the granulocyte pool into

neutrophils and eosinophils (202). Monocyte populations have also been defined by their expression of the chemokine receptors, CX<sub>3</sub>CR1 and CCR2 (203, 204). CD11b<sup>+</sup>CCR2<sup>low</sup>GR1<sup>-</sup>Ly6C<sup>-</sup>CX<sub>3</sub>CR1<sup>high</sup> monocytes migrate to normal tissues while inflammatory monocytes with a CD11b<sup>+</sup>CCR2<sup>high</sup>GR1<sup>int</sup>Ly6C<sup>high</sup>CX<sub>3</sub>CR1<sup>low</sup> phenotype home to injured tissues (205).

We also chose to assess MR expression as it is a useful identifier of M2 macrophages (190, 206). Indeed, mannose receptor 2 has been shown to be upregulated on macrophages following unilateral ureteral obstruction and is believed to play a role in modulating fibrosis through binding and internalizing collagen via an extracellular fibronectin type II domain (207, 208). Interestingly, this study showed that two populations of MR<sup>+</sup> cells (MHCII<sup>-</sup> and MHCII<sup>+</sup>) exist in the kidney at 24hrs post IR injury. Again, targeting or manipulating this cell type may help promote kidney remodeling and regeneration. When considering assessing MR expression with flow cytometry, it should be noted that MR is expressed weakly on the cell surface (209). Membrane permeabilization may result in more effective labeling, although this does not allow for isolation of a potential viable M2 population via FACS.

Autofluorescence is another characteristic of kidney IR injury that needs to be considered carefully. Myeloid cells, particularly those expressing CD11b, CD11c and high levels of F4/80, exhibit autofluorescence at a range of excitation and emission wavelengths (196). Certain myeloid populations can even be defined based on their autofluorescence signature. However, if a full panel of fluorochromes is being used then there is a risk of erroneous emission signals. Using an FMO approach for antibody controls is useful for identifying and minimizing the effects of autofluorescence (210). This study showed that autofluorescence increases over time in kidney IR injury and can be potentially problematic when assessing both hematopoietic and non-hematopoietic populations. Measuring autofluorescence may also prove to be a useful indicator of injury and repair, especially if assessed over a longer time-course and correlated with other injury biomarkers.

The subtle differential expression of markers such as MHCII may also prove to be important in characterizing macrophage subsets and determining functional capabilities. Even the notion of a DC has been challenged in recent times with some evidence suggesting that they might be more closely associated with macrophages than previously thought. This study highlights the difference in the expression of the classical DC marker, CD11c, between the spleen and the kidney, and that the lack of a clear CD11c population may mean that examining CD11c on subpopulations may be more useful than trying to, for example, separate the CD45<sup>+</sup> population into macrophages and DCs. The assessment of CD11c expression in this study also demonstrates the usefulness of measuring MFI for a particular antibody in lieu of, or in addition to, population proportions, especially when the expression is low or when shifts in expression levels are subtle.

Part of the challenge in using flow cytometry to assess subpopulations of cells in the kidney is choosing an appropriate panel of markers to investigate. This is further complicated knowing that different digestion methods may enhance detection of a particular cell type or negatively impact individual markers or receptors. The enzymatic digestion protocol described in this paper was optimized for the combination of enzymes used (collagenase/dispase, DNase type 1). The enzyme concentrations and incubation times, along with the method of mechanical dissociation (size of pipette tip and timing of the dissociations), were all methodically tested to achieve an optimal digestion as determined by cell counts, viability and flow cytometric profiles. This study demonstrated that enzymatic digestion is indeed required to achieve greater viable and CD45<sup>+</sup> cell yields and to most effectively study cells expressing markers such as F4/80. However, variations in dissociation media may be required for different disease models, as some are characterized by inflammation, cell infiltrate and cell death, whilst others may centre on fibrosis and collagen deposition. The combination of collagenase/dispase and DNase type 1 appeared to impact negatively on CSF-1R expression, as seen on Ly6C<sup>high</sup> and Ly6C<sup>-</sup> cells in the spleen, again highlighting the need to optimize digestion methods for each specific study.

Equally as rapid as the advancements in flow cytometer technology, is the development of new fluorochromes and viability dyes. These are providing narrower emission spectra allowing for greater clarity in population identification. There is also now a range of viability dyes available for a large variety of excitation and emission wavelengths. The interactive tools available online, such as spectra viewers and panel builders are also very useful in creating optimal antibody cocktails.

### **Conclusion**

This study has highlighted some of the advantages and limitations associated with assessing kidney cells using flow cytometry, particularly in the IR injury model. This can be an incredibly powerful tool but requires a tested and systematic approach, including the method for organ digestion, antibody selection (target antigen and fluorochrome) and specific gating strategies. Other analytical techniques, including IHC, IF and PCR should be used in conjunction with flow cytometry data to provide a complete depiction of cell types present together with localization in the tissue in which they reside. The obvious extension of the use of flow cytometry to analyze cell populations is the sorting of live populations for further investigations *in vitro* or in adoptive transfer experiments.

# CHAPTER 3

---

*Phenotype and Influx Kinetics of Leukocytes  
and Inflammatory Cytokine Production in  
Kidney Ischaemia/Reperfusion Injury*

## Declaration for Thesis Chapter 3

### Declaration by candidate

This chapter has been submitted to *The American Journal of Pathology*:

**Williams TM, Wise AF, Layton SD and Ricardo SD (2014).** “Phenotype and Influx Kinetics of Leukocytes and Inflammatory Cytokine Production in Kidney Ischaemia/Reperfusion Injury”.

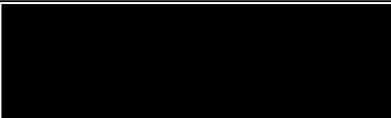
In the case of Chapter 3, the nature and extent of my contribution to the work was the following:

Nature of contribution	Extent of contribution (%)
Study design, execution of experiments, data analysis, interpretation of results, preparation of manuscript	85%

The following co-authors are students at Monash University and the extent of their contribution in percentage terms have been stated below.

Name	Nature of contribution	Extent of contribution (%) for student co-authors only
Andrea Wise	Technical assistance and intellectual input	3%

The undersigned hereby certify that the above declaration correctly reflects the nature and extent of the candidate’s and co-authors’ contributions to this work.

<b>Candidate’s Signature</b>		<b>Date:</b> 19/12/14
<b>Main Supervisor’s Signature</b>		<b>Date:</b> 19/12/14

### 3.1 Introduction

IR injury is one of the leading causes of AKI. In a clinical context, various forms of cardiac and vascular surgery, kidney transplantation, sepsis, radiocontrast agents and other nephrotoxins have been implicated in ischaemic kidney damage (211-218). These acute insults to the kidney trigger inflammation and cause TEC death, resulting in reduced renal function (27). Fortunately, the kidney has a capacity to undergo endogenous repair, although this appears limited. These repair processes revolve around reducing the initial inflammatory response, TEC replacement and remodelling of the extracellular matrix.

Macrophages form a heterogeneous population implicated in both IR-induced inflammation and tissue repair. This is made possible by the varied activation states that they can acquire and a high cellular plasticity. While the M1/M2 paradigm describing macrophage polarisation as either pro-inflammatory (M1) or anti-inflammatory/immunomodulatory/reparative (M2) is useful, it cannot fully describe the complexity of macrophage activation in the setting of kidney IR injury. For example, the high plasticity of macrophages has been demonstrated extensively *in vitro* (101, 219-222), however, the propensity to switch polarisation state in the kidney *in vivo* is poorly understood.

Conceivably, distinct subpopulations of monocytes may give rise to macrophages of a specific activation state. In a study using a murine unilateral ureteral obstruction (UUO) model of kidney disease, different bone marrow-derived monocytes, defined by the level of Ly6C expression, were reported to differentiate into phenotypically different mature macrophages (200). In particular, Ly6C<sup>low</sup> monocytes were found to transition into profibrotic, M2 macrophages (200). The temporal down-regulation of Ly6C also provides a marker of murine monocyte maturation (199). Among the first to characterise these monocytes, Sunderkotter *et al.* demonstrated that following diphtheria toxin (DT)-mediated depletion of CD11b<sup>+</sup> cells in CD11bDTR mice, bone marrow-derived Ly6C<sup>high</sup> cells were the first monocytes to repopulate the

blood and their maturation resulted in the progressive emergence of Ly6C<sup>low</sup> and finally Ly6C<sup>high</sup> monocytes and macrophages. In addition, the immature Ly6C<sup>high</sup> monocytes preferentially homed to sites of both acute and chronic inflammation (199). These findings suggest that macrophages are derived from monocytes following a steady and predictable maturation process but that the timing of the activation cues can affect homing patterns and functional outcomes.

Insight into the nature of macrophage activation and the mechanisms by which they modulate the immune response to IR injury can be gained through examining their interplay with neutrophils. Neutrophils are early responders to IR injury where they promote inflammation and contribute to tissue damage through the production of ROS, proteases and cytokines, including IFN- $\gamma$ , TNF- $\alpha$ , IL-6, IL-4 and IL-10 (59, 60, 72). Macrophages are known to recruit neutrophils to sites of inflammation, which in turn recruit inflammatory monocytes (223). However, mechanisms exist to regulate neutrophil recruitment and survival in order to actively reduce inflammation (223). For example, macrophage-derived MMP-12 is involved in the proteolytic processing of MIP-2 (CXCL2), thereby disrupting its ability to mediate neutrophil chemotaxis (224). Heightened production of TNF by macrophages also promotes neutrophil apoptosis (225) and macrophage phagocytosis of apoptotic neutrophils stimulates the production of anti-inflammatory mediators, such as TGF- $\beta$  (226).

Kidney IR injury can be described in terms of an initial inflammatory phase followed by a resolution phase. However, rather than two distinct series of events, dynamic changes to the microenvironment most likely cause shifts in the balance between inflammation and immunomodulation. Assessing cells through both phases will help place them in the context of kidney inflammation and repair.

Harnessing specialised macrophage functions by manipulating macrophage activation may lead to novel therapies to treat kidney disease. However, a thorough understanding of the cell types involved at various stages of experimental kidney disease is required to target the correct cell subpopulation. This study is the first to perform a comprehensive characterisation of the IR injury model of AKI, specifically focusing on epithelial cells and subpopulations of myeloid cells throughout the inflammatory and remodelling phases of the disease. Flow cytometry was predominantly used to characterise the loss, infiltration and maturation of specific cell types in conjunction with cytokine production. This characterisation will provide a reference point for future studies designed to manipulate cell function in order to promote endogenous repair of damaged kidneys.

## 3.2 Materials and Methods

### 3.2.1 Animals and Surgery

Male 6-8 week old (20–25g) C57BL/6J mice were anaesthetised with 2.0% inhaled isoflurane (Abbott Australasia, Sydney, Australia) before the left renal pedicle was occluded using a vascular clamp (0.4-1.0mm; Fine Science Tools, Heidelberg, Germany) for 40 min via a flank incision to induce unilateral IR injury (n=5 mice/group/time-point). Following removal of the clamp, reperfusion was visually confirmed prior to wound closure using silk suture (size 5-0, Ethicon, New Jersey, USA). An additional group of mice served as a sham-operated control group where the animals were anaesthetised and a flank incision was performed without kidney pedicle clamping. IR injury was assessed at 0.25 (6 h), 1, 3, 5 and 7 days post-surgery.

### 3.2.2 Histopathology and Immunostaining

Mid-coronal kidney sections from mice at 0.25 (6 h), 1, 3, 5 and 7 days post-IR or sham surgery were immersion-fixed in 4% paraformaldehyde (PFA) and embedded in paraffin for haematoxylin and eosin (H&E) staining. Additional kidney tissue was transferred into 30% sucrose post-PFA fixation and frozen in optimum cutting temperature (OCT) medium (Tissue-Tek, PELCO International, USA). Kidneys were sectioned at 4 $\mu$ m for immunohistological staining using a cryostat (Leica, Nussloch Germany). For the visualisation of MR, kidney sections were stained with a rat anti-mouse MR primary antibody (AbD Serotec, Kidlington, UK) followed by an Alexa Fluor 555 goat anti-rat secondary antibody (Molecular Probes, Eugene, USA) and then counterstained with DAPI (Molecular Probes). Sections were viewed with a Provis AX70 microscope (Olympus, Tokyo, Japan). Bright field images were captured using an Olympus DP70 colour camera. Fluorescence images were captured with an F-view II digital camera (Soft Imaging System, Munster, Germany).

### 3.2.3 Digestion and Preparation of Kidneys for Flow Cytometry

Mice were culled at 0.25 (6 h), 1, 3, 5 and 7 days after IR injury. At each time-point the left kidney was removed and placed in cold FACS buffer (PBS supplemented with 0.2% BSA, 0.02% NaN<sub>3</sub> and 5mM EDTA) and were enzymatically digested as we have previously described (227). Single cell suspensions were incubated with red blood cell lysis buffer (8.3g/L Na<sub>4</sub>Cl, 10mM Tris-HCl, pH7.5) and samples filtered with a 40µm nylon cell strainer (BD Bioscience, San Jose, USA) prior to antibody labelling. For flow cytometry cell preparation, cell counts and viability determination were performed using a Z2 Coulter counter (Beckman Coulter, USA).

### 3.2.4 Antibody Labelling

Antibody labelling was performed as previously described (227). Three million cells from each kidney single cell suspension were incubated for 20min at 4°C in the dark with the following fluorochrome-conjugated anti-mouse antibodies: anti-CD45 APC-Cy7 (clone 30-F11; Biolegend, San Diego, USA) and PE-Cy5 (clone 30-F11; BD Biosciences), anti-CD11b PE-Cy7 (clone M1/70; BD Biosciences), anti-CD11c Pacific Blue (clone N418; Biolegend), anti-I-A/I-E (MHCII) PE-Cy5 (clone M5/114.15.2; Biolegend), anti-CSF-1R (CD115) PE (clone AFS98; eBioscience, San Diego, USA), anti-F4/80 APC (clone BM8; eBioscience), anti-Ly6G Alexa Fluor 647 (clone 1A8; Biolegend), anti-Ly6C FITC (clone HK1.4; Biolegend), and anti-EpCAM (CD326) PE-Cy7 (clone G8.8; Biolegend). Fc receptor block (anti-CD16/32 antibody) was added to all antibody cocktails. Isotype matched controls were used for each antibody in FMO manner.

### 3.2.5 Flow Cytometric Acquisition and Analysis

Data were acquired on a FACS Canto II flow cytometer (BD Biosciences) equipped with 405nm, 488nm and 633nm excitation lasers in conjunction with FACS Diva acquisition software (BD Biosciences). Compensation was performed with single colour controls for each organ using the same conjugated antibodies used in the study. Data analysis was performed using FlowLogic FCS analysis software (Inivai Technologies, Melbourne, Australia).

### 3.2.6 Cytokine Bead Array

The production of the pro-inflammatory cytokines TNF, IL-6, MCP-1 and IL-10 by kidney cells following IR injury at 0.25 (6 h), 1, 3, 5 and 7 days post-IR was assessed using a mouse inflammation cytometric bead array (CBA) kit (BD Biosciences, USA). Briefly, following the digestion of the kidneys into single cell suspensions,  $2 \times 10^6$  cells were incubated in media (DMEM with 5% FBS, L-glutamine and penicillin/streptomycin) at 37°C, 5% CO<sub>2</sub> in a final volume of 200µL for 24 h. Following incubation, the cells were centrifuged at 470g for 5min to form a pellet. The supernatant containing the cytokines was collected and stored at -20°C. To quantify cytokine production, supernatants were thawed and stained with antibodies provided in the CBA kit. The amount of cytokine produced was determined by correlating the result with the standard curve created using supplied cytokine standards. The capture bead-cytokine-detection antibody complexes were detected on a FACS Canto II and data analysed using FCAP Array software (Soft Flow, Inc. USA). Final quantitative results for each cytokine were expressed in pg/ml.

### 3.2.7 Statistical analysis

Statistical analysis was performed using GraphPad Prism software version 6.0c (GraphPad Software Inc., San Diego, USA). A Student's *t*-test (unpaired, two-tailed) was used to analyse data between two groups. Data are displayed as mean  $\pm$  SEM.  $P < 0.05$  was considered statistically significant.

### 3.3 Results

#### 3.3.1 Histopathology

As shown in Figure 3.1, H&E staining of kidneys isolated from sham-IR mice demonstrated normal kidney histoarchitecture, with intact tubules and glomeruli. As early as 6 h following IR injury, widespread structural damage was evident within the kidney. This included the loss of tubular epithelium, formation of protein casts, and an inflammatory cell infiltrate. Over the 7 day time-course, the infiltrate steadily increased. Kidney sections at day 7 post-IR displayed the most prominent damage, with protein casts still present, vast interstitial matrix expansion, tubular dilation and the greatest amount of inflammatory cells.

#### 3.3.2 Kidney IR Injury Results in the Loss of EpCAM<sup>+</sup> Epithelial Cells and a Rise in Autofluorescence

Throughout the time-course of IR injury, the total kidney cellularity was assessed to determine the balance between cell infiltration and proliferation, and cell death. No difference was observed between IR and sham-IR kidneys until day 3 post-IR, where there were significantly fewer cells in IR kidneys (IR:  $3.10 \times 10^7$ , sham:  $4.67 \times 10^7$ ,  $P < 0.05$ ). Total cellularity progressively decreased in injured kidneys, as observed at 5 and 7 days post-IR (day 5, IR:  $2.42 \times 10^7$ , sham:  $4.14 \times 10^7$ ,  $P < 0.001$ ; day 7, IR:  $1.67 \times 10^7$ , sham:  $4.25 \times 10^7$ ,  $P < 0.001$ ) (Figure 3.2a).

The characteristic loss of epithelial cells following ischaemic injury was also assessed using flow cytometry (Figures 3.2b and 3.2c). Pseudocolour dot plots show the changes in EpCAM<sup>+</sup> epithelial cells compared to CD45<sup>+</sup> haematopoietic cells (Figure 3.2b). As early as 6 h post-IR injury, the proportion of EpCAM<sup>+</sup> cells was significantly lower in IR kidneys (IR: 9.0%, sham: 16.1%,  $P < 0.001$ ) while the proportion of CD45<sup>+</sup> cells had increased, predominantly from cell infiltration (IR: 27.3%, sham: 16.3%,  $P < 0.001$ ). There was also a rapid 35% reduction in the number of EpCAM<sup>+</sup> cells at this 6 h time-point (IR:  $5.7 \times 10^5$ , sham:  $3.7 \times 10^5$ ,  $P < 0.01$ ). There were fewer EpCAM<sup>+</sup> cells in the IR kidneys at all time-points, although the difference was not

statistically significant at 1 day post-injury (Figure 3.2c). The large proportional decreases were a combination of epithelial cell loss and infiltrating CD45<sup>+</sup> cells (Figure 3.2b). These results reflect the visual changes observed in the kidney histopathology shown in Figure 3.1.

Interestingly, we observed a change in autofluorescence as a result of IR injury (coloured pink in Figure 3.2b, displayed graphically in Figure 3.2d). In sham mice and at 6 h and 1 day post-injury in IR kidneys, autofluorescence was negligible. However, autofluorescence became increasingly prominent in IR kidneys from 3 days post-IR onwards (day 3, IR: 2.1%/1.05x10<sup>5</sup>; day 5, IR: 3.7%/2.91x10<sup>5</sup>; day 7, IR: 7.9%/3.80x10<sup>5</sup>; Figure 3.2d). The presence of autofluorescence reflects the type of damage and response to it by particular immune cells and must be taken into consideration when assessing cells by flow cytometry, particularly in the later stages of the IR injury model.

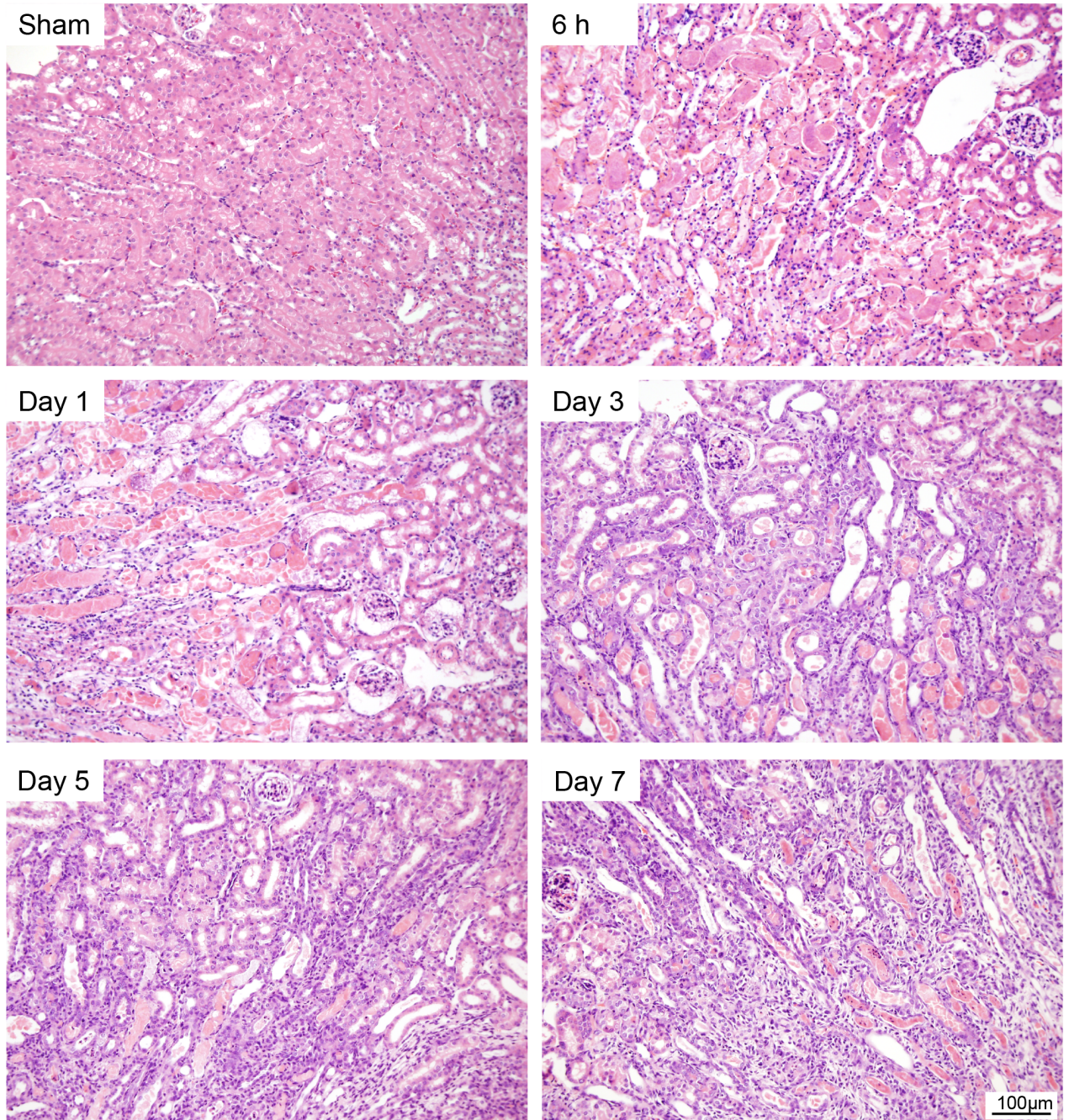


**Figure 3.1. Histopathology over the time-course of IR injury**

Representative photomicrographs of H&E staining in sham, 6 h, 1 day, 3 day, 5 day and 7 day post-IR kidneys. Sham kidneys show normal morphology. IR injury resulted in TEC loss, protein cast formation extracellular matrix expansion and inflammatory cell infiltration. Magnification x200. TEC, tubular epithelial cell.

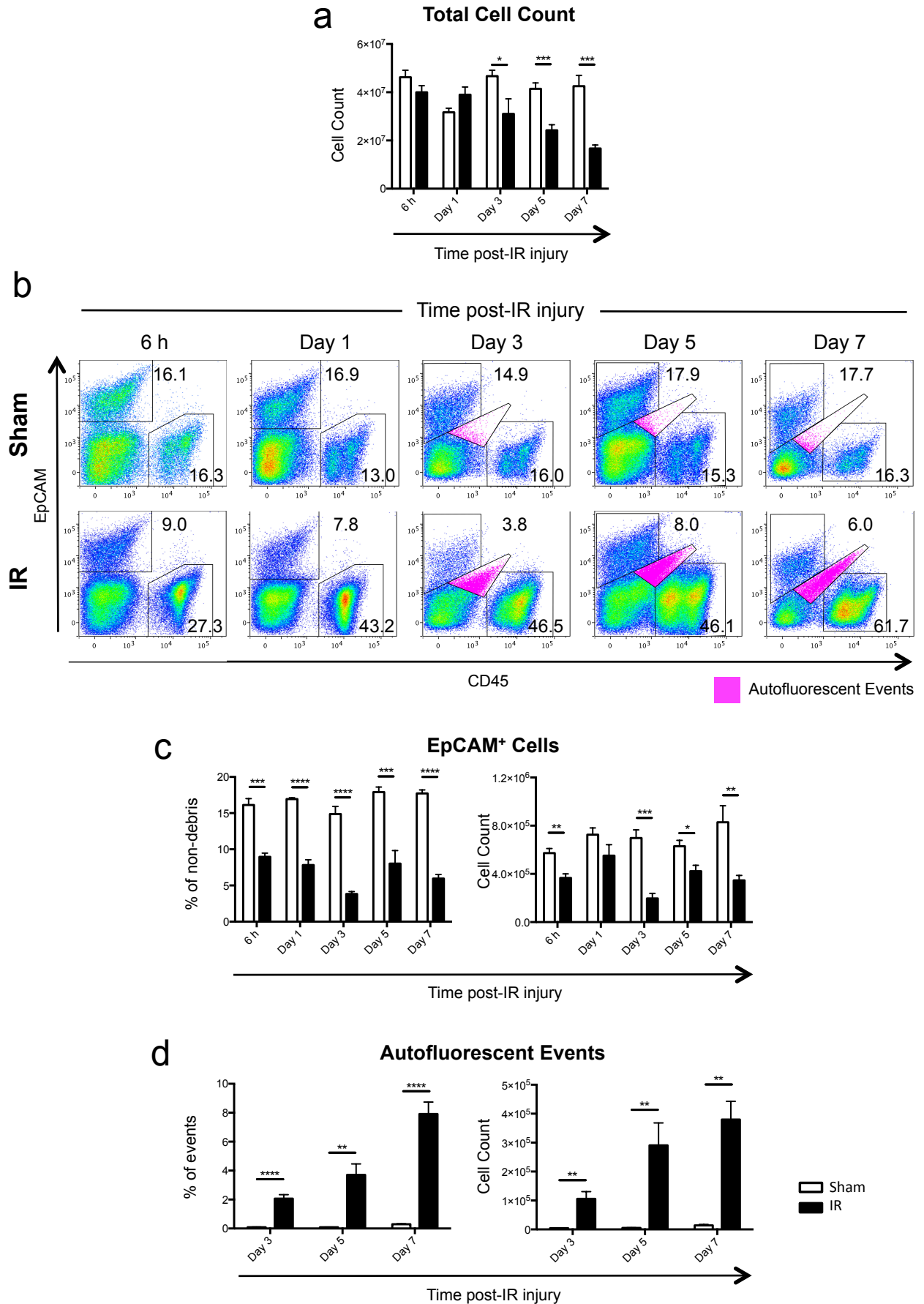


**Figure 3.2. IR injury results in the loss of EpCAM<sup>+</sup> epithelial cells and a rise in autofluorescence**

The impact of IR injury on the total kidney cell count (**a**), epithelial cells (**b** and **c**) and autofluorescence (**b** and **d**) were assessed throughout a time-course of IR injury using flow cytometry. Dot plots display EpCAM<sup>+</sup> epithelial cells, viewed against CD45<sup>+</sup> haematopoietic cells (**b**). At 3, 5 and 7 days post-IR, autofluorescent events were gated and coloured pink (**b**). Numbers on dot plots represent proportions of total viable cells. Data are displayed as mean  $\pm$  SEM ( $n=5$ /group). \*  $P<0.05$ , \*\*  $P<0.01$ , \*\*\*  $P<0.001$ , \*\*\*\*  $P<0.0001$ .

### 3.3.3 Cellular Changes in the Kidney over a 7 day Time-course of IR Injury: CD45<sup>+</sup> Cells, Total Myeloid Cells and Granulocytes

Flow cytometry was used to assess the CD45<sup>+</sup> population throughout the time-course of kidney IR injury. In sham animals, these cells did not form more than 11% of viable cells/non-debris (Figure 3.3a). With injury, the proportion increased progressively from 17.2% at 6 h post-IR to 57.5% of viable cells/non-debris at day 7 post-IR (Figure 3.3a). The number of CD45<sup>+</sup> cells followed a similar trend. At 6 h post-IR, there were  $7.8 \times 10^5$  cells in IR kidneys compared with  $4.3 \times 10^5$  in sham kidneys ( $P < 0.01$ ) (Figure 3.3a). The total number of CD45<sup>+</sup> cells also progressively increased over the time-course to  $2.6 \times 10^6$  at day 7 post-IR (Figure 3.3a).

Total myeloid cells, defined here as CD45<sup>+</sup>CD11b<sup>+</sup>, were assessed due to their diverse roles in inflammation and repair. At all time-points following IR injury, these cells comprised a greater proportion of viable cells/non-debris in the damaged kidneys compared to those in sham controls (Figure 3.3b). At 6 h post-IR, myeloid cells comprised 14.1% of viable cells/non-debris in the IR group, compared to 7.5% in the sham ( $P < 0.001$ ) (Figure 3.3b). The greatest proportional increase in these cells occurred between 6 h and day 1, where 30.0% of viable cells/non-debris were CD45<sup>+</sup>CD11b<sup>+</sup> (sham: 5.4%;  $P < 0.0001$ ). The proportion in injured kidneys continued to increase gradually with time, reaching 47.8% at day 7 (sham: 6.2%,  $P < 0.0001$ ) (Figure 3.3b). A similar pattern was observed with the total numbers of myeloid cells (Figure 3.3b). Six hours after injury there were almost double the number of myeloid cells in the injured kidney compared to sham (IR:  $6.42 \times 10^5$ , sham:  $3.34 \times 10^5$ ,  $P < 0.001$ ). One day post-IR, there were more than twice as many myeloid cells in the damaged kidney compared to that at 6 h (day 1, IR:  $1.48 \times 10^6$ , sham:  $2.17 \times 10^5$ ,  $P < 0.0001$ ). From day 1 onwards, the numbers in the injured kidneys progressively increased, reaching  $2.13 \times 10^6$  at day 7 (sham:  $2.81 \times 10^5$ ,  $P < 0.001$ ) (Figure 3.3b).

Within the myeloid population, granulocytes were positively identified by the expression of Ly6G, in conjunction with low levels of Ly6C. Granulocytes are polymorphonuclear cells of

which the vast majority are neutrophils. Six hours post-IR in this study, granulocytes constituted over a fifth of all myeloid cells in both the sham and IR groups but with a higher proportion in the injured kidney (IR: 28.3%, sham: 23.0%,  $P < 0.05$ ) (Figure 3.3c). At day 1, levels in the sham group had decreased to 6.1% compared to 36.7% in injured kidneys ( $P < 0.0001$ ). From this time-point onwards, the proportion of granulocytes dropped to less than 8% in the IR groups and approximately 4% in the sham groups. The elevated proportion in the sham group at 6 h is most likely explained by transient inflammation caused by the sham-IR surgery. There was no proportional difference observed at 5 days post-IR (day 3, IR: 7.5%, sham 3.2%,  $P < 0.0001$ ; day 5, IR: 3.8%, sham: 3.0%; day 7, IR: 6.4%, sham: 4.0%,  $P < 0.05$ ) (Figure 3.3c). The number of granulocytes was significantly greater at all time-points in injured kidneys compared to the sham controls (Figure 3.3c). However, the number dramatically peaked 1 day post-IR, at  $5.52 \times 10^5$  cells (sham:  $1.3 \times 10^4$ ,  $P < 0.0001$ ). At all other time-points, the number of granulocytes was less than  $2.0 \times 10^5$  (Figure 3.3c). Assessing CD45<sup>+</sup> cells, the total myeloid population and inflammatory granulocytes allow for a detailed account of the cellular response to IR injury. Monocytes and macrophages are also known to respond quickly to inflammatory cues and are involved in crosstalk with a variety of cells, including neutrophils. Their additional roles in tissue repair make them an important population to assess.

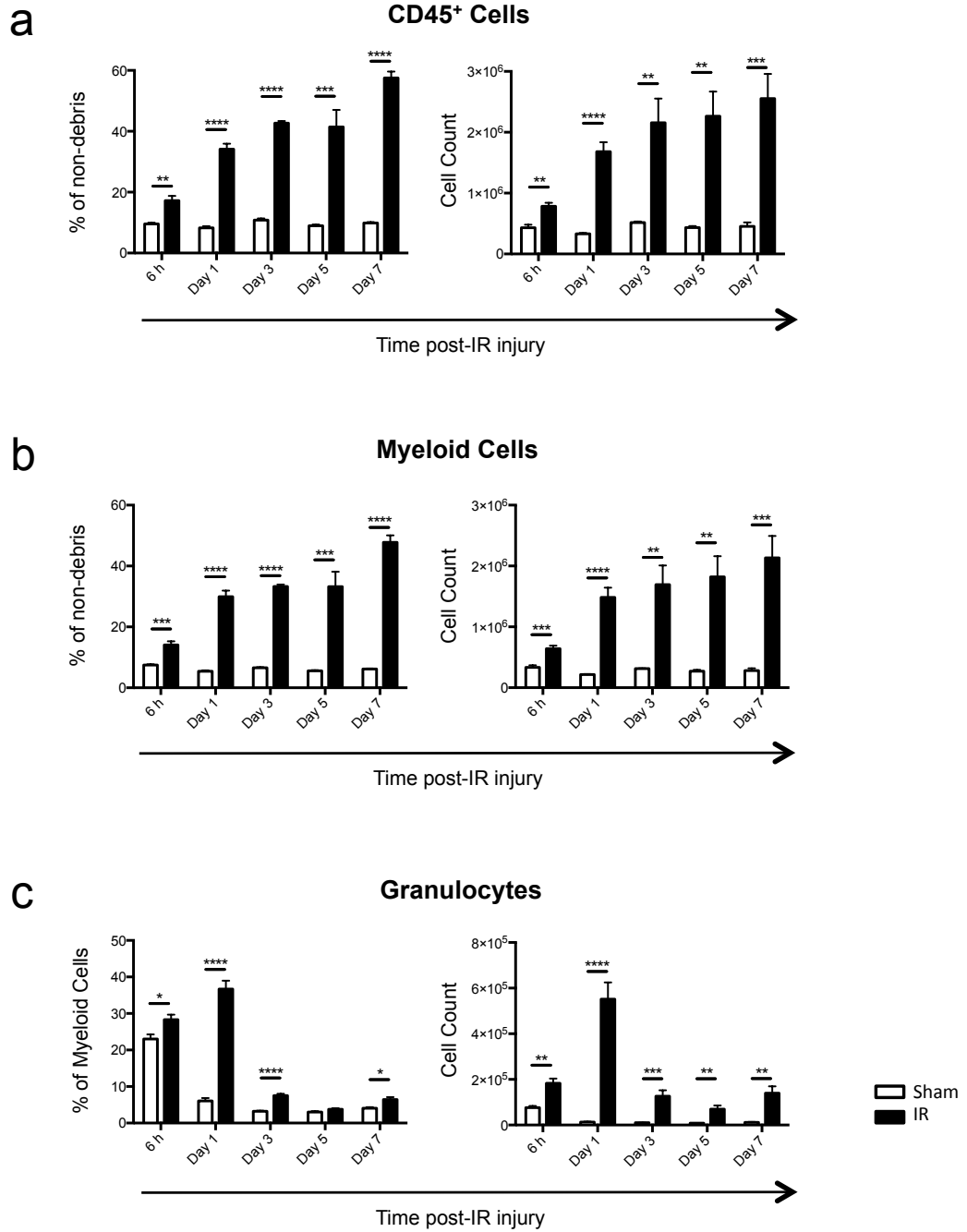


**Figure 3.3. Cellular changes in the kidney over a 7 day time-course in response to IR injury: CD45<sup>+</sup> cells, myeloid cells and granulocytes**

CD45<sup>+</sup> cells (a), CD45<sup>+</sup>CD11b<sup>+</sup> myeloid cells (b) and Ly6C<sup>low</sup>Ly6G<sup>+</sup> granulocytes (c) were assessed throughout a time-course of IR injury using flow cytometry. Data are displayed as mean  $\pm$  SEM ( $n=5$ /group). \*  $P<0.05$ , \*\*  $P<0.01$ , \*\*\*  $P<0.001$ , \*\*\*\*  $P<0.0001$ .

### 3.3.4 Proportional and Numerical Changes in Monocyte and Macrophage Subpopulations in Response to IR Injury

After excluding granulocytes from the CD45<sup>+</sup>CD11b<sup>+</sup> cell pool, four monocyte/macrophage populations were assessed for proportion and number (Figure 3.4a-d). These populations, as described previously (227), were defined by the differential expression of Ly6C and MHC class II: Ly6C<sup>high</sup>MHCII<sup>-</sup> monocytes, Ly6C<sup>low</sup>MHCII<sup>-</sup> monocytes, Ly6C<sup>+</sup>MHCII<sup>low</sup> monocytes and MHCII<sup>+</sup>Ly6C<sup>-</sup> macrophages.

Ly6C<sup>high</sup> inflammatory monocytes rapidly infiltrated the kidney following IR injury, comprising 28.7% of the monocyte/macrophage pool at 6 h post-IR compared to 3.8% in the sham ( $P<0.0001$ ). This dropped to 13.3% at 1 day post-IR before comprising a lower proportion than in sham kidneys at days 5 and 7 (Figure 3.4a). Ly6C<sup>high</sup> monocyte numbers were highest at 6 h post-IR (IR:  $1.3 \times 10^5$ , sham:  $9.8 \times 10^3$ ,  $P<0.0001$ ) and 1 day post-IR (IR:  $1.2 \times 10^5$ , sham:  $2.9 \times 10^3$ ,  $P<0.0001$ ). At day 3, the number of Ly6C<sup>high</sup> cells had fallen to  $4.5 \times 10^4$  and continued to gradually decrease through to day 7 but remained significantly higher than in the sham groups at all time-points (Figure 3.4a). Interestingly, similar numbers of Ly6C<sup>high</sup> monocytes and granulocytes were detected in kidneys at 6 h post-IR.

The Ly6C<sup>low</sup>MHCII<sup>-</sup> monocyte population is represented in a similar manner to the Ly6C<sup>high</sup> monocytes in both proportion and number but with the peak for each occurring at day 1 in the IR group (Figure 3.4b). The proportion of Ly6C<sup>low</sup>MHCII<sup>-</sup> cells in injured kidneys was greater than in the sham group at 6 h, day 1 and day 3 post-IR injury but lower than sham levels at days 5 and 7. At their peak, these cells comprised 14.0% of the monocyte/macrophage pool, compared to 0.6% in the sham ( $P<0.0001$ ). At all other time-points in IR kidneys, these cells formed less than 4% of the monocytes/macrophages (Figure 3.4b). Cell counts were very low for both groups at all time-points with the exception of those in the IR group at day 1, where there were  $1.3 \times 10^5$  cells.

More prominent than the Ly6C<sup>low</sup>MHCII<sup>-</sup> population are the maturing monocytes, described as Ly6C<sup>+</sup>MHCII<sup>low</sup>, although these cells form a heterogeneous population with varying expression levels of the two markers. In injured kidneys, these cells formed a greater proportion of the monocyte/macrophage pool at 6 h, 1 day and 3 days post-IR (6 h, IR: 10.9%, sham: 3.2%,  $P < 0.01$ ; day 1, IR: 16.5%, sham: 1.5%,  $P < 0.0001$ ; day 3, IR: 2.4%, sham: 1.2%,  $P < 0.01$ ) but resided at sham levels at 5 and 7 days post-IR (Figure 3.4c). In terms of number, fewer than  $1 \times 10^4$  cells were detected in the sham kidneys at any time-point. However, at 6 h post-IR, the cell count in injured kidneys reached  $5.0 \times 10^4$  (sham:  $8.2 \times 10^3$ ,  $P < 0.001$ ) before peaking at  $1.6 \times 10^5$  at day 1 (sham:  $3.1 \times 10^3$ ,  $P < 0.001$ ). After 3 days the cell count was still relatively high at  $1.3 \times 10^5$  (sham:  $3.6 \times 10^3$ ,  $P < 0.01$ ) before decreasing to  $3.0 \times 10^4$  at day 5 and  $2.4 \times 10^4$  at day 7 (Figure 3.4c).

Changes in the MHCII<sup>+</sup>Ly6C<sup>-</sup> mature macrophage population fit in with the observations of infiltrating immature monocytes transitioning into mature macrophages once in the injured kidney. The proportion of total MHCII<sup>+</sup> macrophages decreased dramatically in IR kidneys from sham levels of approximately 90% to 52.3% at 6 h, 42.4% at day 1 and 46.7% at day 3 (Figure 3.4d). No differences in the proportion of this population were detected between IR and sham groups at either day 5 or day 7 post-IR (Figure 3.4d). Even though there was a proportional difference after 6 h, there was no difference in the number of macrophages with injury at this early time-point (IR:  $2.4 \times 10^5$ , sham:  $2.3 \times 10^5$ ). However, at 1 day post-IR, there was double the number of cells in the IR kidneys compared to the shams (IR:  $3.9 \times 10^5$ , sham:  $1.9 \times 10^5$ ,  $P < 0.001$ ) (Figure 3.4d). The number of macrophages progressively increased throughout the time-course, reaching  $1.6 \times 10^6$  on day 7 (sham:  $2.3 \times 10^5$ ,  $P < 0.001$ ) (Figure 3.4d).

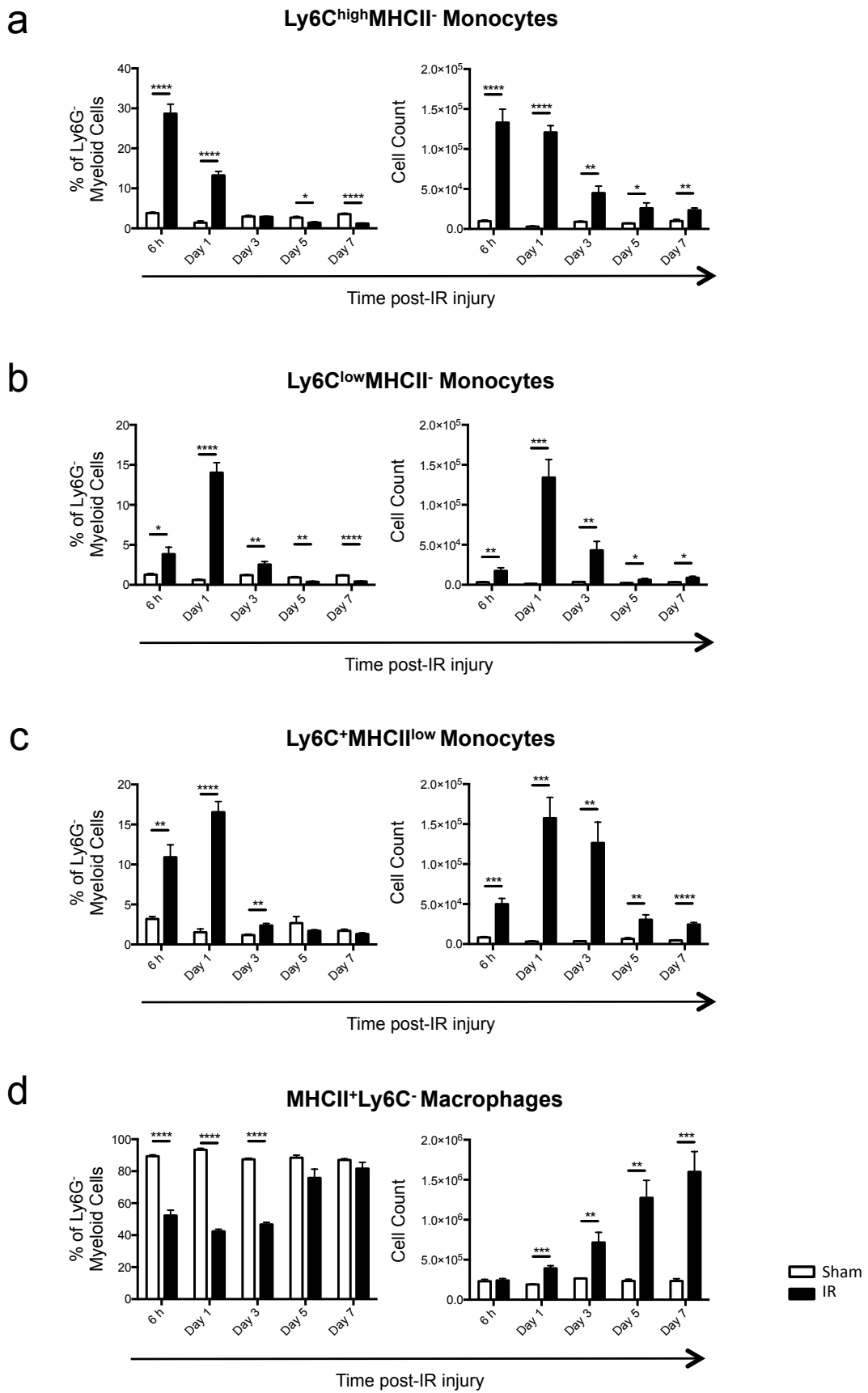


**Figure 3.4. Proportional and numerical changes in monocyte and macrophage subpopulations in response to IR injury**

Monocyte and macrophage populations were assessed throughout a time-course of IR injury using flow cytometry. Four populations were assessed based on the differential expression of Ly6C and MHC class II: Ly6C<sup>high</sup>MHCII<sup>-</sup> immature monocytes (**a**), Ly6C<sup>low</sup>MHCII<sup>-</sup> monocytes (**b**), Ly6C<sup>+</sup>MHCII<sup>low</sup> transitioning monocytes (**c**) and MHCII<sup>+</sup>Ly6C<sup>-</sup> macrophages (**c**). Percentages represent proportions of myeloid cells excluding granulocytes. Data are displayed as mean  $\pm$  SEM ( $n=5$ /group). \*  $P<0.05$ , \*\*  $P<0.01$ , \*\*\*  $P<0.001$ , \*\*\*\*  $P<0.0001$ .

### **3.3.5 Changes in the Flow Cytometric Profile of Kidney Monocytes and Macrophages following IR Injury**

Pseudocolour dot plots in Figure 3.5a show the effect of IR injury on the four monocyte/macrophage populations defined by Ly6C and MHC class II expression. In addition to the changes in cell proportion following injury, the dot plots reveal a noticeable decrease in the level of MHC class II expression on macrophages from IR kidneys. When MHC class II expression was quantified (represented by the MFI), a significant decrease was detected from 1 day post-IR onwards (Figure 3.5b).

Figure 3.5c shows the Ly6C and MHC class II isotype controls used to define the monocyte and macrophage subsets at day 7 post-IR. From 3 days post-injury onwards, the expression of the negative populations shifted from that observed at the earlier time-points. Even after selectively gating viable cells and excluding autofluorescent events, specific gates were required for the different phases of the injury model. As shown in this example, it was vital to have appropriate isotype controls set up in an FMO manner to accurately gate on true positive events.

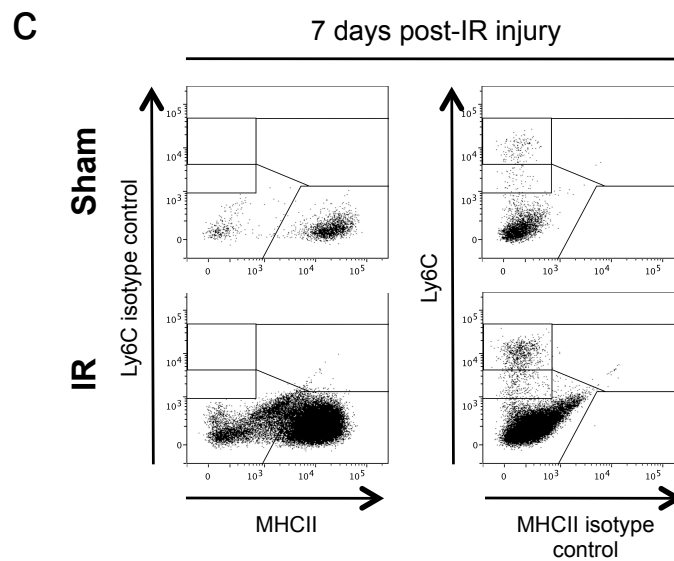
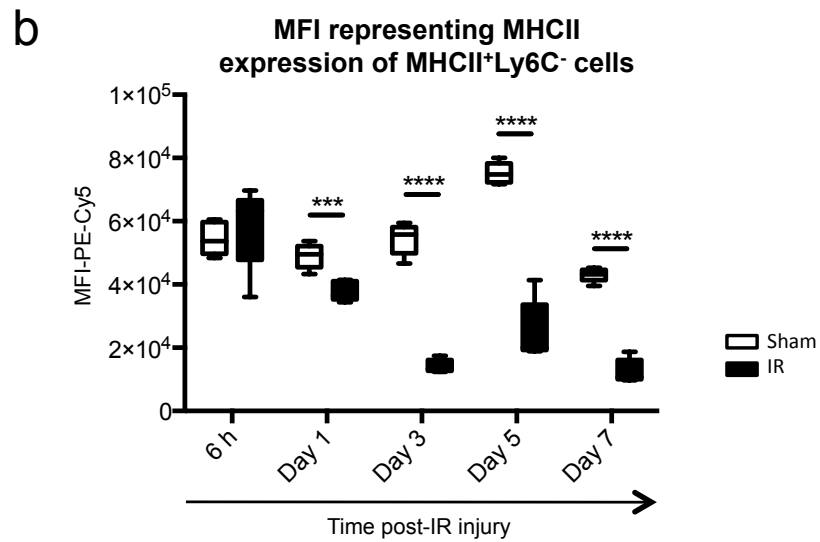
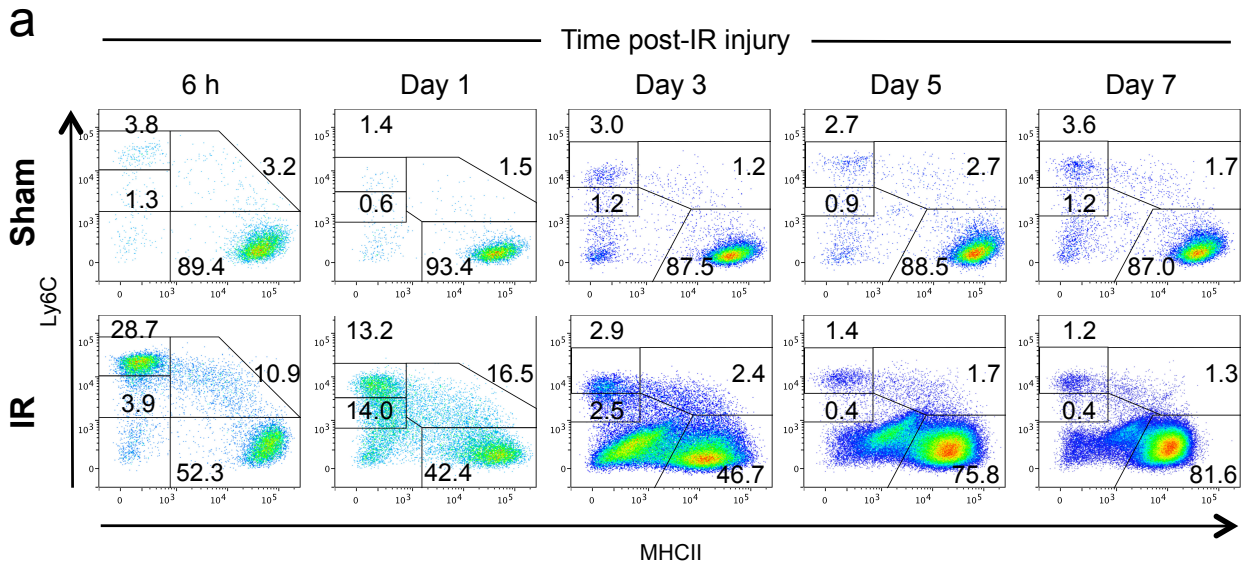


**Figure 3.5. Changes in the flow cytometric profile of kidney monocytes and macrophages in response to IR injury**

Pseudocolour dot plots show the flow cytometric profile of four monocyte/macrophage populations, throughout a time-course of IR injury, based on the differential expression of Ly6C and MHC class II (a). The MFIs representing MHC class II expression on MHCII<sup>+</sup>Ly6C<sup>-</sup> macrophages are displayed graphically (b). Examples of isotype controls (from day 7) are displayed for both groups (c). Numbers on the dot plots represent proportions of myeloid cells excluding granulocytes. Data are displayed as mean ± SEM (*n*=5/group). \* *P*<0.05, \*\* *P*<0.01, \*\*\* *P*<0.001, \*\*\*\* *P*<0.0001.

### 3.3.6 Analysis of Kidney Macrophage Subpopulations based on F4/80 and MHC Class II Expression

Further assessment of macrophages was performed based on the expression of the classical macrophage marker, F4/80. Figure 6a shows the expression of F4/80 and MHC class II on CD45<sup>+</sup>CD11b<sup>+</sup> cells at each time-point. In sham groups, the predominant population is F4/80<sup>high</sup>MHCII<sup>high</sup>, comprising approximately 70% of all CD11b<sup>+</sup> cells (Figure 3.6a and 3.6b). Following IR-injury, this population decreased to 31.4% at 6 h post-IR (sham: 58.6%;  $P < 0.0001$ ) and further to 16.6% at day 1 (sham: 72.6%,  $P < 0.0001$ ) before increasing to 33.6% at day 3 (sham: 73.1%,  $P < 0.0001$ ) (Figure 3.6a and 3.6b). As this population is composed of Ly6C<sup>-</sup> cells (data not shown), the decrease in proportion is explained by the infiltration of Ly6C<sup>high</sup> monocytes. By day 5, the proportion of F4/80<sup>high</sup>MHCII<sup>high</sup> macrophages in the IR group had returned to sham levels (Figure 3.6b). The numbers of F4/80<sup>high</sup>MHCII<sup>high</sup> macrophages increased over the time-course of injury in a similar fashion to the MHCII<sup>+</sup>Ly6C<sup>-</sup> cells. At day 1, there was a small increase in F4/80<sup>high</sup>MHCII<sup>high</sup> cells in the IR group compared to the sham (IR:  $2.3 \times 10^5$ , sham:  $1.5 \times 10^5$ ,  $P < 0.0001$ ) (Figure 3.6b). Three days post-IR, there were  $5.3 \times 10^5$  cells in IR kidneys (sham:  $2.2 \times 10^5$ ;  $P < 0.01$ ), which doubled to  $1.1 \times 10^6$  cells at day 5 (sham:  $2.0 \times 10^5$ ,  $P < 0.001$ ) and increased further to  $1.5 \times 10^6$  cells at day 7 (sham:  $2.0 \times 10^5$ ,  $P < 0.001$ ) (Figure 3.6b).

A second population, F4/80<sup>high</sup>MHCII<sup>low</sup> macrophages, emerged from 3 days post-IR onwards (Figure 3.6a). This population was practically nonexistent in the sham or early stage IR groups but represented 36.5% of all CD45<sup>+</sup>CD11b<sup>+</sup> cells at day 3 in IR kidneys (Figure 3.6a and 3.6c). Two days later, the proportion of these cells had decreased to 14.2% and by day 7 only represented 9.2% of the myeloid pool (Figure 3.6a and 3.6c). These cells appeared to mature into the F4/80<sup>high</sup>MHCII<sup>high</sup> population.

Ly6C<sup>high</sup> monocytes (coloured pink) were also displayed on the on the MHC class II versus F4/80 pseudocolour dot plots (Figure 3.6a). When assessed using FMO isotype controls, these cells

were shown to express low levels of F4/80 but were MHC class II<sup>+</sup> (Figure 3.6a). These F4/80<sup>low</sup>MHCII<sup>+</sup> cells (of which the majority are Ly6C<sup>high</sup>) represented on average 5.7% of myeloid cells in sham kidneys compared to 21.1% in IR kidneys at 6 h (sham: 5.3%,  $P < 0.0001$ ) and 20.2% at day 1 post-IR (sham: 3.6%,  $P < 0.0001$ ). The proportion decreased progressively to 1.9% at day 7 (sham: 4.7%,  $P < 0.0001$ ), significantly lower than the sham control (Figure 3.6a).

In addition to the previously described Ly6C<sup>high</sup>F4/80<sup>low</sup>MHCII<sup>+</sup> population, an F4/80<sup>low</sup>MHCII<sup>low</sup> population was also present after IR injury. In control animals, this population was negligible, making up less than 2% of the CD45<sup>+</sup>CD11b<sup>+</sup> cell pool. However, at 6 h and 1 day post-injury, these cells comprised 7.0% and 15.0% of the same population (Figure 3.6a). While 5% of the myeloid cells fell within the F4/80<sup>low</sup>MHCII<sup>low</sup> gate at 3 days after surgery, the population appeared to have changed phenotype to form the F4/80<sup>high</sup>MHCII<sup>low</sup> population described earlier.

By examining the five time-points throughout the early and late stages of the IR injury model, it appears that immature, Ly6C<sup>high</sup> monocytes infiltrate the kidney early after injury. These cells most likely express low levels of F4/80, which is up-regulated concurrently with MHC class II, while Ly6C expression is lost. The final stage in their maturation is the transition from MHCII<sup>low</sup> to MHCII<sup>high</sup> expression, although the level of MHC class II expression doesn't reach that found on resident macrophages in the steady state.

Immunofluorescence microscopy was also used to visualise the presence and localisation of macrophages expressing the M2 marker, MR (CD206). Very few MR<sup>+</sup> macrophages (green) were observed in sham control kidneys (Figure 3.7a). However, an increase in MR<sup>+</sup> cells were observed in the interstitium, lining the tubules at both early (day 1, Figure 3.7b) and late (day 7, Figure 3.7c) stages of the injury model, with a greater amount of staining at 7 days post-IR injury.

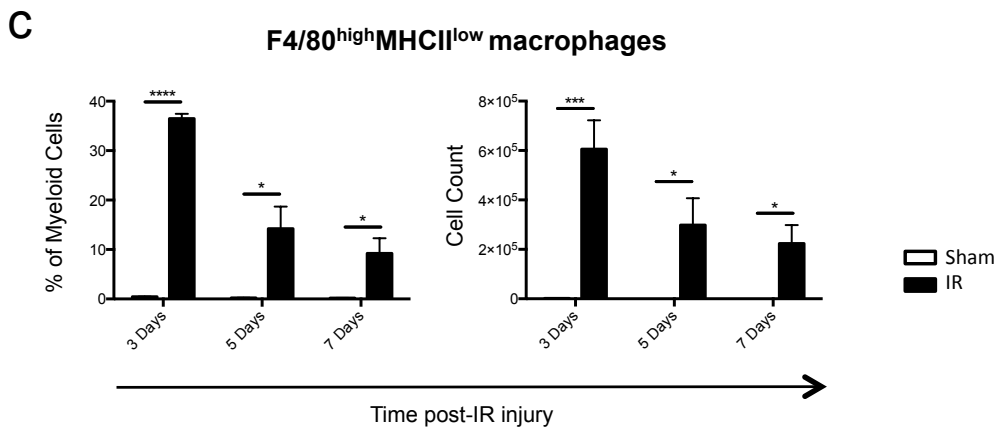
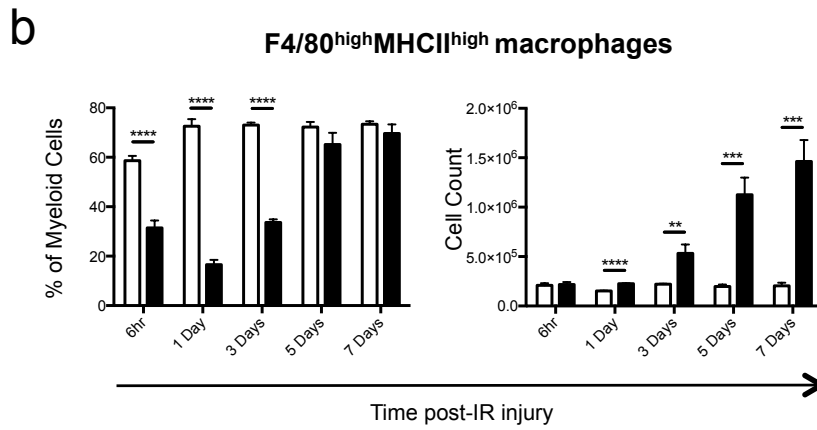
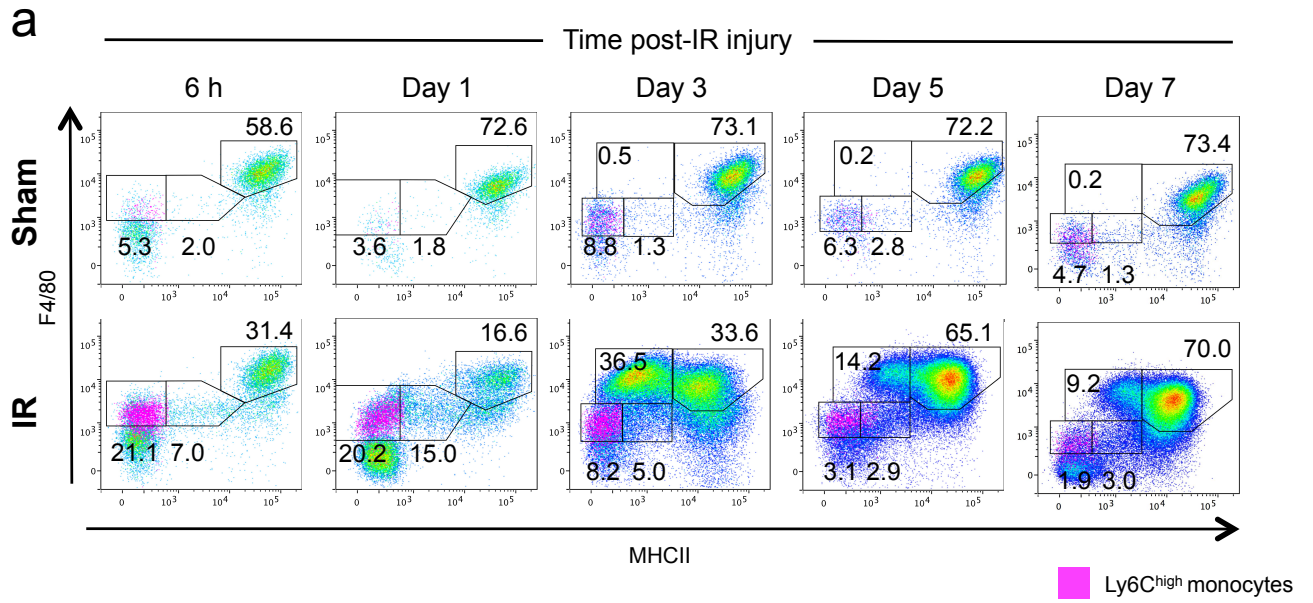


**Figure 3.6. Analysis of kidney macrophage subpopulations based on F4/80 and MHC class II expression**

Further phenotypic assessment of the monocyte/macrophage populations was performed based on F4/80, MHC class II and Ly6C expression. Pseudocolour dot plots compare F4/80 and MHC class II expression throughout a time-course of IR injury (a). Ly6C<sup>high</sup> monocytes (coloured pink) are displayed on the F4/80 versus MHC class II dot plots (a). The proportion and number of mature F4/80<sup>high</sup>MHCII<sup>high</sup> (b) and F4/80<sup>high</sup>MHCII<sup>low</sup> macrophages (c) are displayed graphically. Numbers on dot plots and percentages on graphs represent proportions of CD45<sup>+</sup>CD11b<sup>+</sup> cells. Data are displayed as mean ± SEM (n=5/group). \*  $P < 0.05$ , \*\*  $P < 0.01$ , \*\*\*  $P < 0.001$ , \*\*\*\*  $P < 0.0001$ .

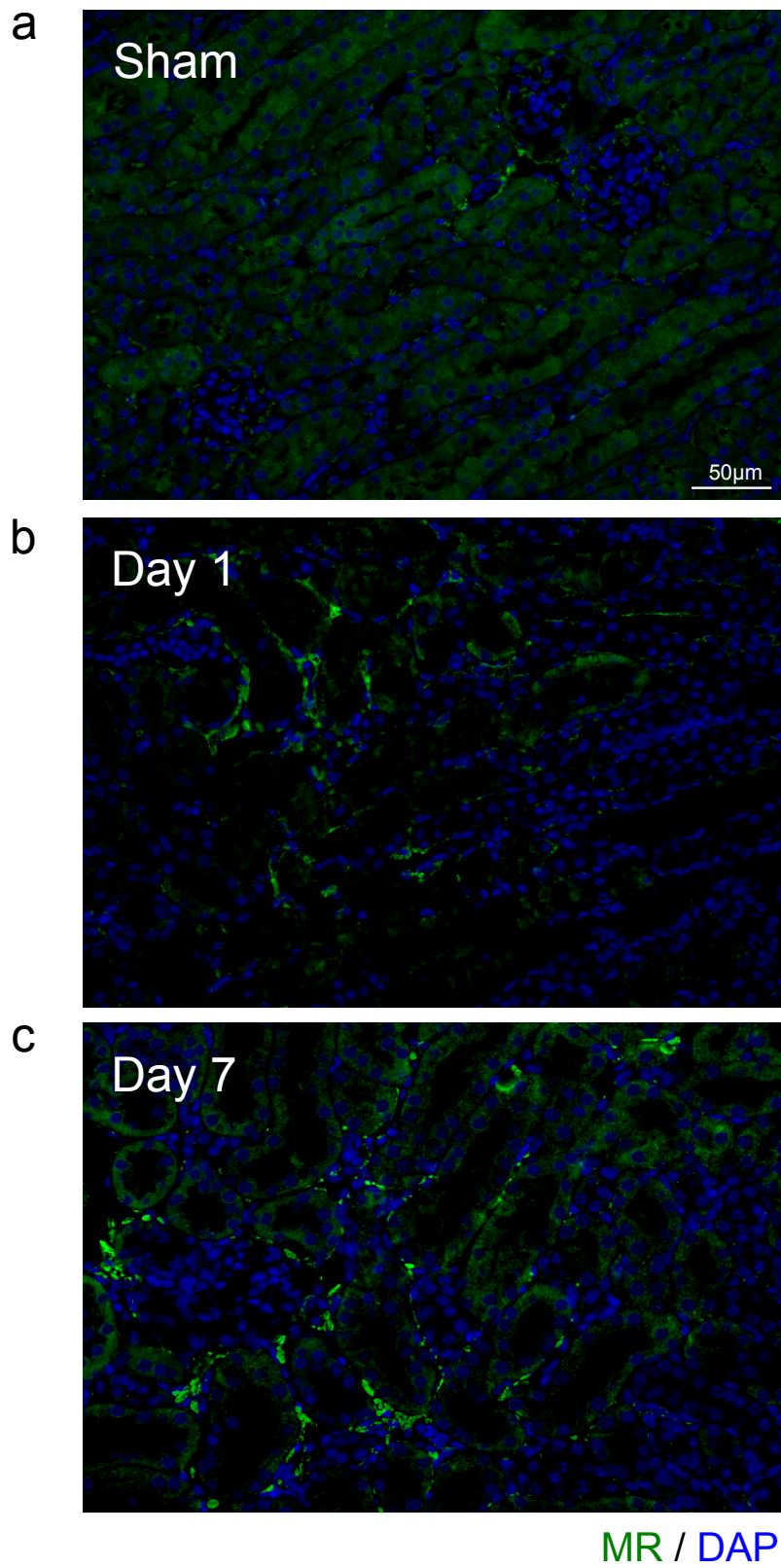


**Figure 3.7. Visualisation of MR<sup>+</sup> macrophages at day 1 and day 7 post-IR injury**

Representative fluorescence micrographs showing MR<sup>+</sup> macrophages (green) in sham kidneys (a) and IR injured kidneys at 1 (b) and 7 (c) days post-surgery. Magnification x200.

### 3.3.7 Changes in the Inflammatory Cytokine Profile over the Time-course of IR Injury

Four cytokines central to inflammation and myeloid cell activation (IL-6, MCP-1, TNF and IL-10) were measured to show the changes in the cytokine profile through the inflammatory and resolution phases of the IR-injury model (Figure 3.8).

IL-6 production was significantly higher following IR injury at all time-points and progressively increased from 751pg/ml at 6 h post-IR (sham: 450pg/ml,  $P<0.05$ ) through to 9011pg/ml at 7 days (402pg/ml,  $P<0.0001$ ) (Figure 3.8). MCP-1 production was also significantly increased in response to IR injury at all time-points, with levels progressively increasing from 6 h post-IR (IR: 172pg/ml, sham: 68pg/ml,  $P<0.01$ ) through to day 5 (IR: 1625pg/ml, sham: 123pg/ml,  $P<0.05$ ) before declining at day 7 (IR: 648pg/ml, sham: 61pg/ml,  $P<0.001$ ) (Figure 3.8). There were no differences in the levels of TNF between sham and IR groups for the first three days of the model. However, this was followed by significant increases in the IR groups at day 5 (IR: 508pg/ml, sham: 146pg/ml,  $P<0.01$ ) and day 7 (IR: 583pg/ml, sham: 129pg/ml,  $P<0.01$ ) (Figure 3.8). Interestingly, the levels of IL-10, an immunoregulatory cytokine involved in M2 activation, were significantly higher in response to IR at all time-points. This difference was only minor at 6 h post-IR (IR: 58pg/ml, sham: 28pg/ml,  $P<0.01$ ) but increased substantially through to day 3 (IR: 594pg/ml, sham: 23pg/ml,  $P<0.001$ ) where they remained for the remainder of the time-course (Figure 3.8).

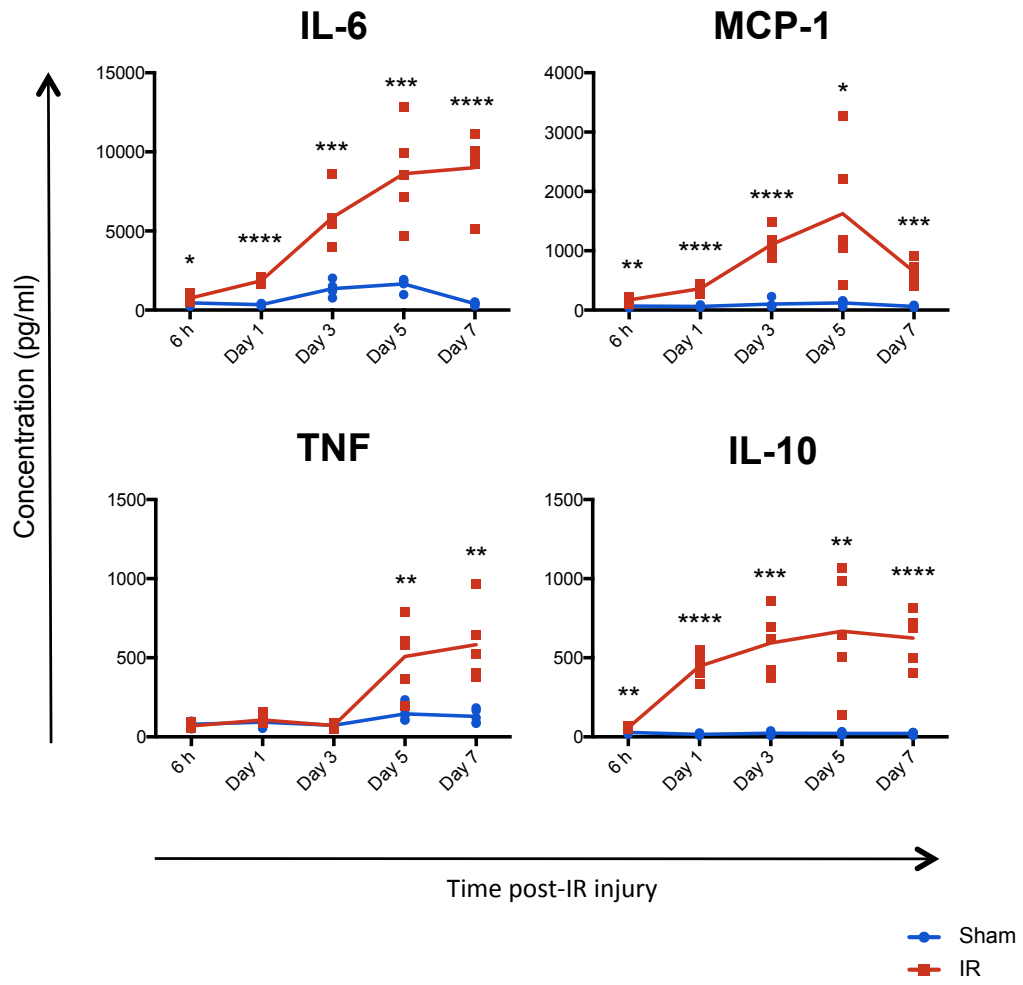


**Figure 3.8. Changes in the inflammatory cytokine profile over the time-course of IR injury**  
Cytokine production by cells from damaged kidneys was measured throughout a time-course of IR injury. Concentrations (pg/ml) for IL-6, MCP-1, TNF and IL-10 are displayed graphically, depicting the mean concentration along with individual data points. ( $n=5/\text{group}$ ). \*  $P<0.05$ , \*\*  $P<0.01$ , \*\*\*  $P<0.001$ , \*\*\*\*  $P<0.0001$ .

### 3.4 Discussion

This study has used flow cytometry with a comprehensive array of antibodies to identify major myeloid cell subpopulations and cytokines involved in kidney IR-injury. Assessing these cells at five time-points allowed for the mapping of cell loss, infiltration and maturation. This is the first study to comprehensively characterise the changes associated with IR injury throughout the damaging and remodelling phases of the model, focusing on different monocyte and macrophage populations based on the differential expression of Ly6C, F4/80 and MHC class II, along with cytokine production and changes in tissue histopathology. This information can be used as a baseline to test the effects of novel treatments while also identifying possible therapeutic targets.

Ly6C expression is not only a useful surface marker for defining monocyte maturation but has also been linked to the differentiation of functionally different macrophages (200). In murine UUO, it was shown that kidneys signal to the bone marrow to recruit Ly6C<sup>high</sup> monocytes, rather than monocytes already in the circulation. In a similar pattern, our study showed a rapid influx of Ly6C<sup>high</sup> monocytes into the injured kidney, along with Ly6G<sup>+</sup> neutrophils. This infiltration also corresponded to the increased production of the pro-inflammatory cytokines MCP-1 and IL-6, along with the immunoregulatory cytokine, IL-10. The systemic effects of IR injury were recently highlighted in a study by Brøchner *et al.*, which showed that at 24 h post-bilateral IR injury there were raised plasma levels of IL-6 and IL-10 along with increased neutrophil accumulation in the lungs and livers of mice compared to sham kidney IR injury and hind leg IR injury, which served as an additional control (228). TNF is another pro-inflammatory cytokine with divergent effects. At low concentrations TNF prolongs neutrophil survival, while at high concentrations, it induces neutrophil apoptosis (225). In our study, TNF production by kidney cells increased significantly at 5 and 7 days post-injury, signifying a concerted effort to reduce inflammation.

Whilst the down-regulation of Ly6C denotes the maturation of the infiltrating monocytes into tissue macrophages, what is more difficult to deduce is the relative contribution to the kidney myeloid cell pool of infiltrating versus proliferating cells. Only recently was it demonstrated that proliferation and differentiation of infiltrating bone marrow-derived cells contribute to kidney fibrosis following UUO (200, 229). In addition, Jang *et al.* used green fluorescent protein (GFP)<sup>+</sup> bone marrow chimeric mice and bromodeoxyuridine (BrdU) incorporation to show that infiltrated bone marrow-derived cells account for greater than 80% of proliferating cells in the post-ischemic kidney and contribute to fibrosis (230). In addition, the authors showed that after administering the antioxidant apocynin (a nicotinamide adenine dinucleotide phosphate (NADPH) oxidase inhibitor), ROS-mediated bone marrow-derived cell infiltration was reduced, which in turn resulted in fewer bone marrow-derived, proliferating interstitial cells. Surprisingly, this also caused an increase in TEC proliferation (230).

The expression of the monocyte marker, Ly6C, on cells in the kidney challenges the classical notion of blood monocytes differentiating into tissue macrophages upon extravasation. This is explained in other studies, which have shown cells can maintain a monocyte phenotype upon entering tissues without differentiating into macrophages or DCs (231, 232). Following on from this point, our study did not attempt to distinguish macrophages from DCs due to the debate that has surrounded the definition of these cells when considering their high plasticity, functions, molecular markers and response to certain growth factors (233). CD11c is one surface marker that has typically been used to identify DCs. However, recent work cautions against using this marker to distinguish DCs from macrophages (79, 81). For example, splenic monocytes have been shown to transiently express CD11c during inflammation (234). It is therefore prudent to define mature monocyte-derived cells based on cell functions and responses in specific settings.

Assessing EpCAM expression may prove to be even more important than for the simple evaluation of viable epithelial cell numbers. While most of the cellular responses to IR injury involve haematopoietic cells, reduced renal function relates directly to the changes in the kidney endothelial and epithelial cells (38). As demonstrated in this study, IR injury causes a large and rapid reduction in the number of EpCAM<sup>+</sup> cells and so replacement of the lost epithelial cells is one appropriate measurement of an effective therapy. Antibodies against EpCAM stain the basolateral cell membranes of the distal tubules and collecting ducts of normal kidney. However, a study by Trzpis *et al.* suggest that in addition, EpCAM expression is associated with epithelial morphogenesis and regeneration (235). More specifically, they showed by RT-PCR that EpCAM gene expression is up-regulated in the renal cortex following IR injury. In line with these findings, EpCAM is also used as a diagnostic marker and therapeutic target for a number of renal cell carcinomas (236). In the liver, the up-regulation of EpCAM denotes regeneration through re-epithelialisation (237). Further to this, EpCAM has been implicated in the processes of differentiation, migration and proliferation (238, 239). In this study, there was no indication by flow cytometry that EpCAM<sup>+</sup> cells were being replenished 7 days post-IR injury.

Neutrophils have been shown to infiltrate the kidney shortly following IR injury, where they promote inflammation and disease progression (60). A number of different techniques aimed at neutrophil depletion, inhibiting recruitment and targeting production of inflammatory mediators have also had prophylactic benefits in animal models of the disease (240-243). However, a greater understanding of their relationship with other cell types involved in IR injury, particularly macrophages, regarding the timing of infiltration and the length of time that they persist is important in the development of therapies to promote endogenous repair.

The immune response to IR injury is complex and involves many cells and mediators. Macrophages and neutrophils have been shown to be major contributors to many inflammatory diseases, including IR injury, but the contribution from cells including NK (63), NKT (72), DCs

(77), T cells (244) and B cells (245, 246) should not be ignored. A number of studies have shown that inhibiting specific functions relating to these leukocytes can provide protection from IR injury. However, developing therapies to promote healing following IR injury will require enhancing mechanisms of repair. While it is known that promoting M2 macrophage polarisation is able to promote kidney repair, the requirements for the initial inflammatory response is less understood. It may be that inflammation is required to recruit monocytes capable of becoming reparative cells, or perhaps the pro-inflammatory microenvironment is needed to trigger resident macrophages to take on an alternative activation state in order to reduce inflammation, which in turn enables cell-mediated repair processes to occur. One method for selectively reducing aspects of the immune response to injury is to use neutralising antibodies to inhibit the functions of cytokines or receptors. The benefit of using neutralising antibodies is that the effects are transient and so blocking particular molecules can be restricted to different stages of the disease. The challenge then becomes choosing the appropriate molecules to target.

This study has used flow cytometry in conjunction with histological assessment to comprehensively characterise the myeloid cell types involved in the early inflammatory and resolution phases of IR injury. The infiltration of myeloid cells was compared to the rapid loss of EpCAM<sup>+</sup> epithelial cells and the timing of pro-inflammatory cytokine production, along with the M2-associated cytokine, IL-10. A substantial decrease in the numbers of inflammatory monocytes and neutrophils at 3 days post-IR injury, highlights the brief window in which to target these cells for therapeutic benefit. The progressive increase in macrophage numbers appears linked to the initial monocyte infiltration. Future studies are required to determine the importance of the increased macrophage population regarding dampening of inflammation and mediating repair. The results provide a reference point for future studies aimed at manipulating the immune response to AKI through specific targeting of individual cell types and effector molecules.

# CHAPTER 4

---

*The Impact of GM-CSF and CSF-1R Blockade on  
Inflammation, Tissue Damage and Repair  
in Kidney Ischaemia/Reperfusion Injury*

## 4.1 Introduction

Renal IR injury in rodents provides a useful model for investigating the mechanisms of hypoxia-, inflammation- and cell-mediated kidney damage, along with tissue repair mechanisms. In addition to impact trauma and sudden restriction or occlusion of the renal blood supply, IR injury is associated with a number of common clinical procedures, such as kidney transplantation (247-249), partial nephrectomy (250-252), coronary bypass surgery (212, 253) and other abdominal, thoracic and vascular procedures (254-256). Chapter Two described a flow cytometry based method for assessing myeloid cells in murine kidney IR injury. Chapter Three provided insights into the inflammatory response to acute IR insult. This Chapter investigates the application of both prophylactic and therapeutic treatments targeting IR-mediated kidney damage through altering the myeloid response to injury.

Depletion of tissue macrophages can provide protection against kidney IR injury. However, this is dependent on the method of depletion (257, 258). Macrophage depletion using liposome-encapsulated clodronate (LEC) can reduce ATN and protect renal function in mice with IR injury. In comparison, targeted depletion of cells expressing CD11b and CD11c by injecting human DT to mice, which have the DT receptor (DTR) under the control of the CD11b or CD11c promoter, failed to provide any form of protection (257, 258). Examination of the differential production of cytokines with the two depletion methods showed that LEC depletion, but not DT-induced depletion, resulted in reduced levels of IL-1 $\beta$ , CXCL1, GM-CSF and MCP-1 (258).

Neutralising specific growth factors and cytokines to modulate the macrophage response may prove to be an effective and clinically feasible method of protecting against IR injury. Two prime candidates are CSF-1 and GM-CSF due to their roles as principal myeloid mediators. CSF-1 is widely expressed in the steady state and promotes monocyte and macrophage differentiation, survival, activation, proliferation and chemotaxis (259, 260). However, its

expression is often increased at sites of inflammation, causing increased monocyte/macrophage accumulation and exacerbation of a number of diseases (261, 262). In contrast, GM-CSF is readily detectible only in times of infection or inflammation, where it provides pro-survival and proliferative signals to cells of the myeloid lineage (263, 264). Considered a pro-inflammatory cytokine, GM-CSF has been identified as a mediator of a number of inflammatory diseases, as highlighted in models for multiple sclerosis, lung inflammation and rheumatoid arthritis (265-267). These CSFs have also been linked to macrophage polarisation *in vitro*, whereby culturing cells of the macrophage lineage with GM-CSF or CSF-1 results in macrophages that resemble pro-inflammatory M1 and anti-inflammatory M2 cells, respectively, based on their cytokine and gene expression profiles (102, 187, 268, 269). In a study by Fleetwood *et al.*, murine GM-CSF cultured macrophages differentially produced TNF- $\alpha$ , IL-6, IL-12p70 and IL-23 compared to IL-10 and MCP-1 from CSF-1 cultured macrophages upon stimulation with LPS (187). Similar effects have been observed with human monocytes/macrophages, although with some variation in the cytokines (222).

Using mAbs to neutralise the effects of GM-CSF and CSF-1 (by targeting the ligand or its receptor) conveys protection in a number of inflammatory disease settings, including models of arthritis and lung inflammation, predominantly through halting myeloid cell proliferation and inhibiting the release of pro-inflammatory mediators (184, 185). In the kidney, endogenous GM-CSF is a mediator of different forms of glomerular nephritis (270), while CSF-1R blockade targeting macrophage accumulation and inflammation successfully halted disease progression in early diabetic nephropathy (150) and crescentic anti-GBM glomerulonephritis (271), and reduced the severity of tubulointerstitial rejection in renal allografts (147). Contrary to this, administration of CSF-1 to mice with established IR injury can accelerate repair and improve renal function (148, 182). However, neutralising either of these CSFs *in vivo* is unlikely to produce the opposite result to administering additional GM-CSF or CSF-1, due to the complexity of the *in vivo* setting.

In this study, CSF-1 and GM-CSF signalling was blocked using mAbs in a mouse model of renal IR injury. Specifically, anti-GM-CSF and anti-CSF-1R mAbs were administered to mice beginning two days prior to injury. To investigate the importance of timing in CSF signalling, two mAb administration regimens were compared. These involved a short-term blockade, spanning the initial inflammatory phase of IR injury and a long-term blockade, continuing throughout both the inflammatory and reparative phases of the model.

## 4.2 Materials and Methods

### 4.2.1 Animals and Surgery

Male 6-8 week old (20–25g) C57BL/6J mice were anaesthetised with 2.0% inhaled isoflurane (Abbott Australasia, Sydney, Australia) before the left renal pedicle was occluded using a vascular clamp (0.4-1.0mm; Fine Science Tools, Heidelberg, Germany) for 40min via a flank incision to induce unilateral IR injury ( $n=5-6$  mice/group/time-point). Following removal of the clamp, reperfusion was visually confirmed prior to wound closure using silk suture (size 5-0, Ethicon, New Jersey, USA). In order to assess renal function, mice received 25min bilateral IR (or sham-IR) injury.

### 4.2.2 Antibody Administration

Mice were injected with anti-GM-CSF (clone 22E9, rat anti-mouse IgG2a), anti-CSF-1R (clone AFS98, rat anti-mouse IgG2a mAb) or isotype control (anti- $\beta$ -galactosidase) mAbs ( $n=5-6$ /group; 250 $\mu$ g/injection for short-term blockade or 100 $\mu$ g/injection for long-term blockade; i.p.; made up with PBS to a final volume of 200 $\mu$ l) on days -2, 0 and 2 post-IR injury for short-term blockade or days -2, 0, 2, 4, 7 and 10 post-IR injury for long-term blockade (mice culled at day 7 did not receive an injection on day 7).

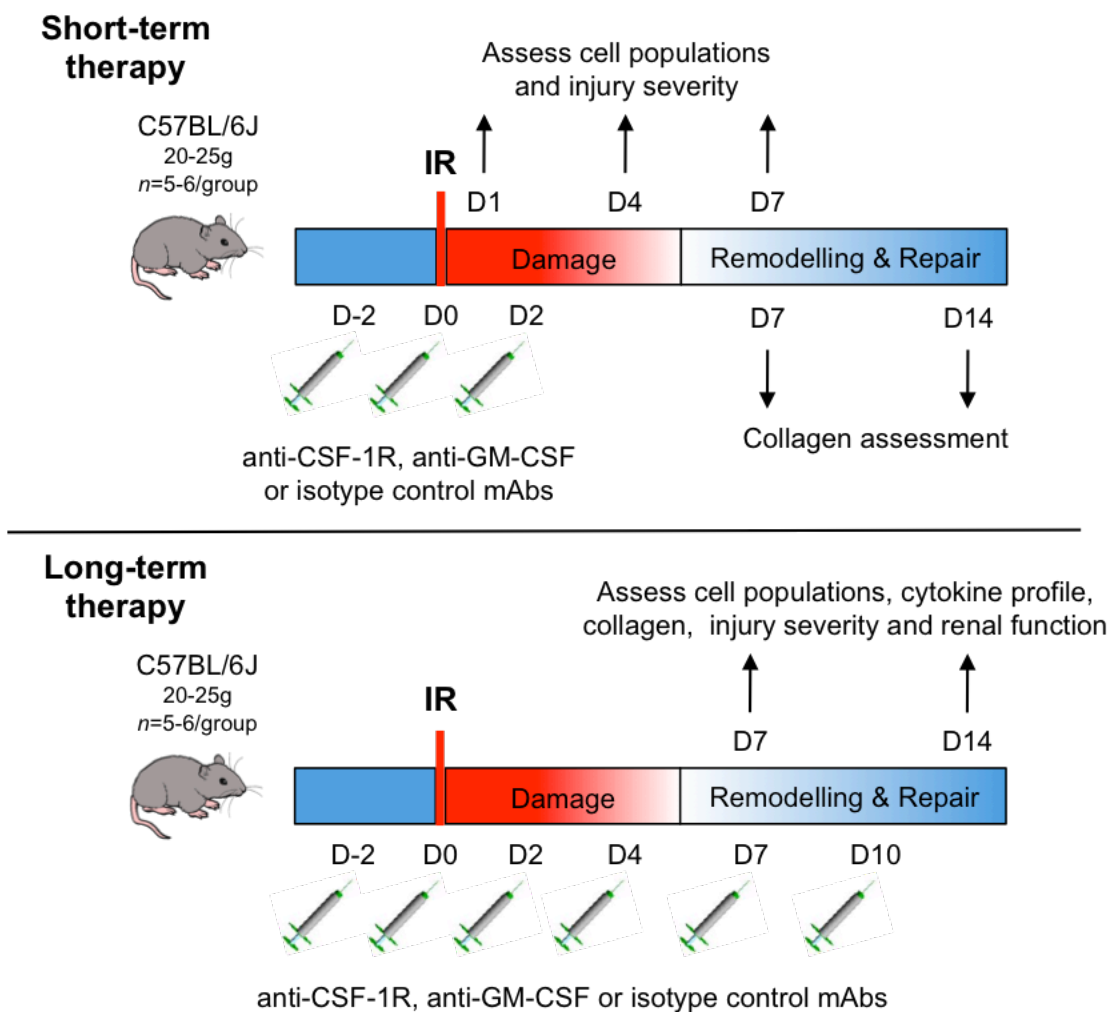


Figure: Schematic depicting the timing of neutralising antibody administration in the short-term and long-term regimens.

### 4.2.3 Digestion and Preparation of Kidney and Spleen for Flow Cytometry

Mice receiving short-term therapy were culled at 1, 4 and 7 days post-IR injury. The spleen and left kidney were removed and placed in cold FACS buffer (PBS supplemented with 0.2% BSA, 0.02% NaN<sub>3</sub> and 5mM EDTA). Splens were subjected to mechanical digestion and kidneys were digested enzymatically as previously described (227). Single cell suspensions were incubated with red blood cell lysis buffer (8.3g/L Na<sub>4</sub>Cl, 10mM Tris-HCl, pH7.5) and samples filtered with a 40µm nylon cell strainer (BD Bioscience, San Jose, USA) prior to antibody labelling. Cell counts and viability determination were performed using a Z2 Coulter counter (Beckman Coulter, USA).

### 4.2.4 Antibody Labelling

Antibody labelling was performed as previously described (227). Three million cells from kidney and spleen single cell suspensions were incubated for 20min at 4°C in the dark with the following fluorochrome-conjugated anti-mouse antibodies: anti-CD45 APC-Cy7 (clone 30-F11; Biolegend, San Diego, USA) and PE-Cy5 (clone 30-F11; BD Biosciences), anti-CD11b PE-Cy7 (clone M1/70; BD Biosciences), anti-CD11c Pacific Blue (clone N418; Biolegend), anti-I-A/I-E (MHCII) PE-Cy5 (clone M5/114.15.2; Biolegend), anti-CSF-1R (CD115) PE (clone AFS98; eBioscience, San Diego, USA), anti-F4/80 APC (clone BM8; eBioscience), anti-Ly6G Alexa Fluor 647 (clone 1A8; Biolegend), anti-Ly6C FITC (clone HK1.4; Biolegend), anti-EpCAM (CD326) PE-Cy7 (clone G8.8; Biolegend) and anti-CD206 (MR) Alexa Fluor 488 (clone MR5D3; Biolegend). For MR labelling, cells were fixed and permeabilised using Cytotfix/Cytoperm Fixation/Permeabilization Solution (BD Biosciences). Antibodies used for intracellular labelling were diluted in Perm/Wash Buffer (BD Biosciences) as per the manufacturer's instructions. Fc receptor block (anti-CD16/32 antibody) was added to all antibody cocktails. Isotype matched controls were used for each antibody in a FMO manner.

#### 4.2.5 Flow Cytometric Acquisition and Analysis

Data was acquired on a FACS Canto II flow cytometer (BD Biosciences) equipped with 405nm, 488nm and 633nm excitation lasers in conjunction with FACS Diva acquisition software (BD Biosciences). Compensation was performed with single colour controls for each organ using the same conjugated antibodies used in the study. Data analysis was performed using FlowLogic FCS analysis software (Inivai Technologies, Melbourne, Australia).

#### 4.2.6 Histology

To assess histopathology, mid-coronal kidney samples were immersion-fixed in 4% PFA and embedded in paraffin. Kidney sections were cut at a thickness of 4 $\mu$ m and stained with H&E to visualise kidney histopathology.

#### 4.2.7 Hydroxyproline and SDS-PAGE Analysis

Hydroxyproline was assessed to determine total kidney collagen (% collagen content/dry tissue weight) as previously described (272). In brief, snap frozen tissue samples, containing cortex and medulla, were lyophilised to measure dry weight before being re-hydrated in buffer containing 1.5M NaCl, 0.5M Tris/HCl pH7.5, 0.5ml of 100x proteinase inhibitors (10mM N-ethylmaleimide (NEM), 0.5M benzamide hydrochloride, 0.1M phenylmethylsulfonyl (PMSF), made up to a final volume with distilled water, at 4°C for 6 hours. Samples were then hydrolysed in 6M hydrochloric acid and hydroxyproline levels were determined by measuring the absorbance of the hydrolysed samples at 558nm with a Digital Spectrophotometer (Varian, Palo Alto, USA). Collagen content was calculated by multiplying hydroxyproline values by a factor of 6.94. Interstitial collagen subtypes were assessed using sodium dodecyl sulphate polyacrylamide gel electrophoresis (SDS-PAGE) as previously described (273). Kidney samples were pepsin digested and the supernatants collected for analysis on a 5% (wt/vol) acrylamide gel with a 3.5% (wt/vol) stacking gel.  $\alpha_1$ (III) and  $\alpha_1$ (I) collagen chains were separated with interrupted electrophoresis with delayed reduction of type III collagen. The gels were stained

with 0.1% Coomassie blue R-250 overnight at 4°C before being destained with 30% (vol/vol) methanol containing 7% (vol/vol) acetic acid.

#### 4.2.8 Serum Cytokine Analysis

Blood samples were taken at the time of death and centrifuged to allow serum to be collected. Serum samples were stored at -80°C prior to being screened for 32 mouse cytokines with a MILLIPLEX<sub>MAP</sub> Cytokine/Chemokine assay (MCYTMAG-70K-PX32, Merck Millipore, Billerica, USA).

#### 4.2.9 Kidney Function Assessment

Serum creatinine and urea was measured in mice that received bilateral IR injury at 14 days post-IR. Samples were analysed with i-STAT CHEM8+ cartridges with the i-STAT system ( $n=8$ ; Abbott, Ontario, Canada.)

#### 4.2.10 Statistical Analysis

Statistical analysis was performed using GraphPad Prism software version 6.0c (GraphPad Software Inc., San Diego, USA). A one-way analysis of variance (ANOVA) with a Tukey's multiple comparisons post-hoc test was used to analyse data from three or more groups. Data are displayed as mean  $\pm$  SEM unless otherwise stated.  $P<0.05$  was considered statistically significant.

## 4.3 Results

### 4.3.1 The Effect of Short-term GM-CSF and CSF-1R Blockade on Total Cellularity, CD45<sup>+</sup> Cells, CD11b<sup>+</sup> Cells and Granulocytes in the Spleen

Neutralising mAbs against GM-CSF or CSF-1R were administered to mice every 2 days, beginning in a prophylactic manner, 2 days before IR injury and continuing until 2 days post-injury. To test the systemic effect of the mAbs, cell populations in the spleen were examined at 1, 4 and 7 days post-injury. Flow cytometry was used to analyse various cell populations, employing a similar gating strategy to that described previously (227). To analyse haematopoietic cells, non-autofluorescent CD45<sup>+</sup> cells were selected from 'single cells' (FSC-A vs FSC-H). CD11b<sup>+</sup> cells were subsequently selected from the CD45<sup>+</sup> pool.

Neither GM-CSF or CSF-1R blockade altered the total spleen cellularity at any time-point (Figure 4.1a), nor was there any effect on the proportion or number of CD45<sup>+</sup> cells (Figure 4.1b). However, CSF-1R blockade reduced the proportion and number of CD11b<sup>+</sup> cells 1 day post-IR compared to the isotype control group (Figure 4.1c). The number of granulocytes (Ly6C<sup>low</sup>Ly6G<sup>+</sup>) was also significantly lower following both GM-CSF ( $P < 0.05$ ) and CSF-1R blockade ( $P < 0.05$ ) 1 day post-surgery compared to the isotype control group (Figure 4.1d).

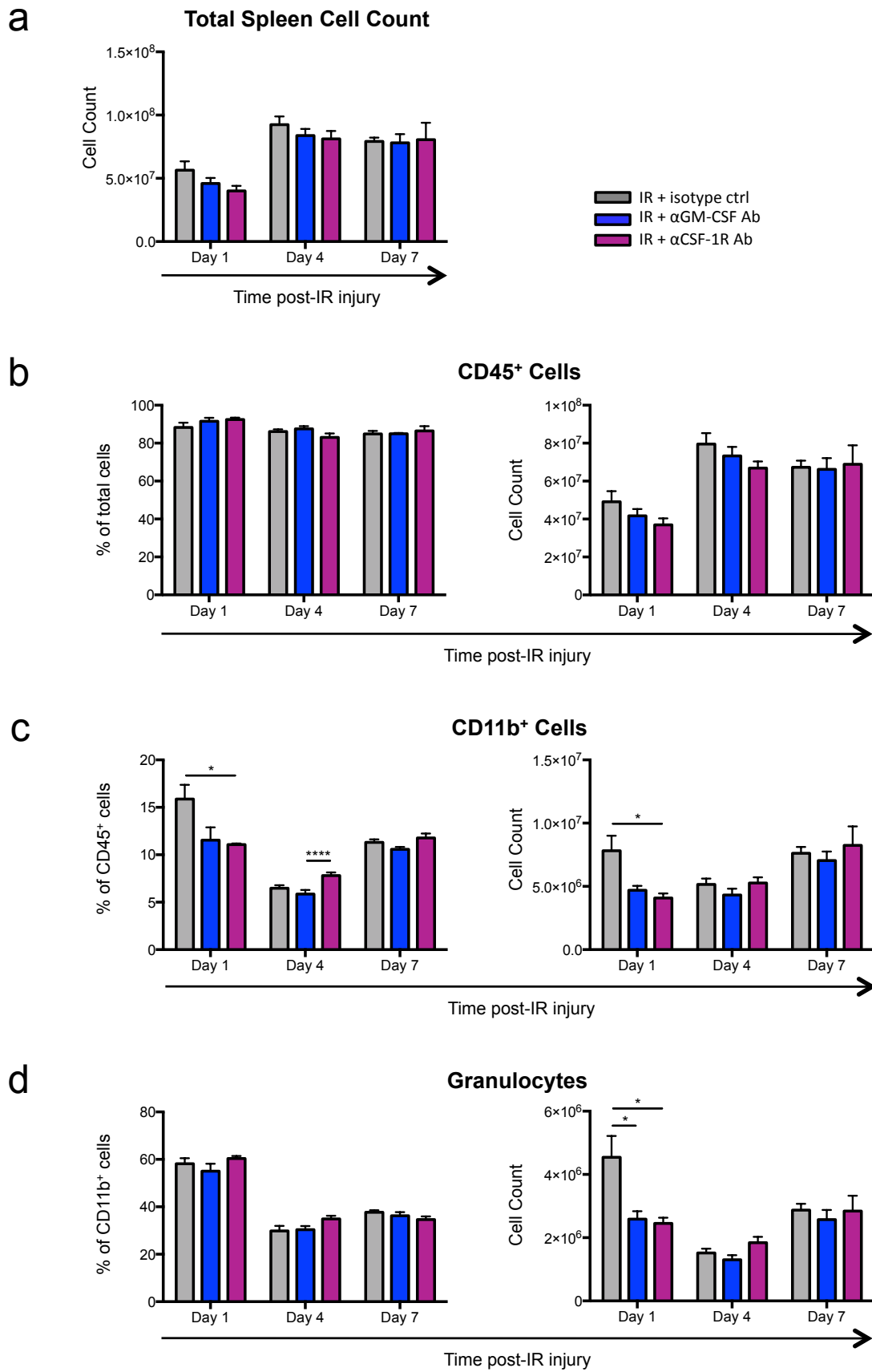


**Figure 4.1. The effect of short-term GM-CSF and CSF-1R blockade on cell populations in the spleen following kidney IR injury.**

Spleens were assessed at 1, 4 and 7 days after kidney IR injury using flow cytometry. Results displayed graphically show the total cellularity (**a**), proportion and number of CD45<sup>+</sup> cells (**b**), proportion and number of CD11b<sup>+</sup> cells (**c**) and the proportion and number of granulocytes (Ly6C<sup>low</sup>Ly6G<sup>+</sup>; **d**). Data are displayed as means  $\pm$  SEM.  $n=4-6$ /group. \*  $P<0.05$ , \*\*  $P<0.01$ , \*\*\*  $P<0.001$ , \*\*\*\*  $P<0.0001$ .

A number of myeloid populations were also examined, based on the differential expression of the markers Ly6C and MHC class II. Pro-inflammatory, immature Ly6C<sup>high</sup> monocytes (also MHCII<sup>+</sup>) existed in higher proportions following CSF-1R blockade at both day 4 and day 7 post-injury, compared to both other groups (Figure 4.2a). However, this is due to decreases in other CD11b<sup>+</sup> populations as there was no difference in the number of Ly6C<sup>high</sup> cells at any time-point. A maturing monocyte population, exhibiting decreasing Ly6C expression with a concomitant up-regulation of MHC class II (described here as Ly6C<sup>+</sup>MHCII<sup>low</sup>), was reduced in number 1 day after injury with both GM-CSF and CSF-1R blockade compared to the control mAb (Figure 4.2b). Very few changes were observed in the CD11b<sup>+</sup>MHCII<sup>+</sup>Ly6C<sup>-</sup> population, except for a higher proportion of these cells in the anti-CSF-1R mAb group at day 7 (Figure 4.2c). More noticeable differences were observed in a MR<sup>+</sup>F4/80<sup>+</sup> M2 macrophage subpopulation (Figure 4.2d). CSF-1R blockade resulted in a lower proportion of these macrophages compared to the anti-GM-CSF mAb group and the isotype control group, with the difference being statistically significant at both days 4 and 7 post-IR. This translated to a significant reduction in cell number following CSF-1R blockade at days 1 and 4. GM-CSF blockade also reduced the number of MR<sup>+</sup>F4/80<sup>+</sup> cells at day 4 compared to the control group (Figure 4.2d).

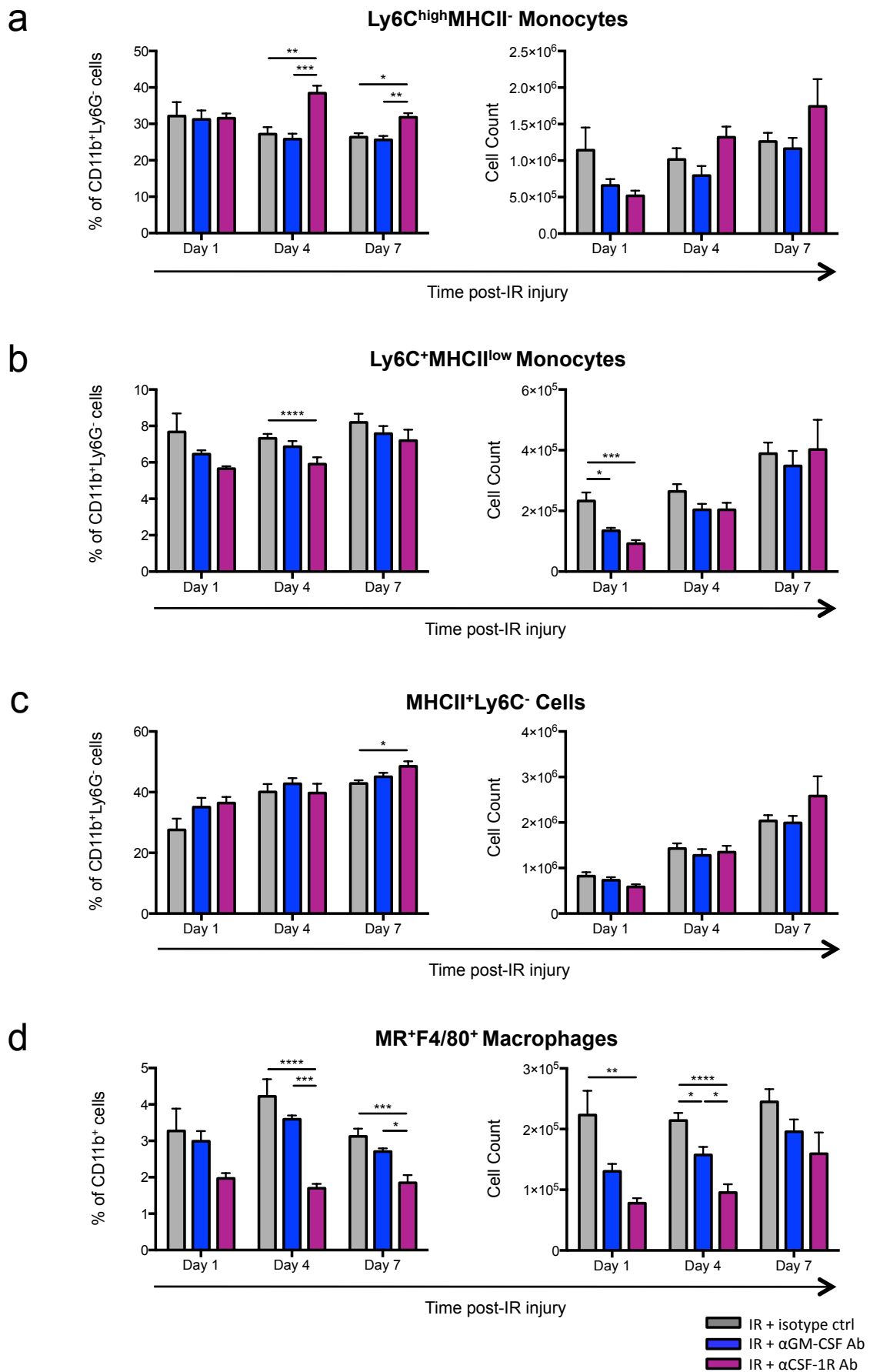


**Figure 4.2. The effect of short-term GM-CSF and CSF-1R blockade on monocyte and macrophage populations in the spleen following kidney IR injury.**

The effects of short-term GM-CSF and CSF-1R blockade on splenic monocyte and macrophage populations were assessed at 1, 4 and 7 days after kidney IR injury using flow cytometry. Results displayed graphically show the proportion and number of Ly6C<sup>high</sup> monocytes (a), proportion and number of Ly6C<sup>+</sup>MHCII<sup>low</sup> monocytes (b), proportion and number of MHCII<sup>+</sup>Ly6C<sup>-</sup> cells (c) and the proportion and number of MR<sup>+</sup>F4/80<sup>+</sup> M2 macrophages (d). Data are displayed as means  $\pm$  SEM.  $n=4-6/\text{group}$ . \*  $P<0.05$ , \*\*  $P<0.01$ , \*\*\*  $P<0.001$ , \*\*\*\*  $P<0.0001$ .

CSF-1R expression was detected on both a Ly6C<sup>high</sup> monocyte population and a Ly6C<sup>low</sup> cell type. Backgating analysis on the latter population revealed low to intermediate levels of CD11c expression (data not shown). No difference in the CSF-1R<sup>+</sup>Ly6C<sup>high</sup> population was observed at any time-point, with the exception of a lower proportion of cells following CSF-1R blockade at 7 days post-injury (Figure 4.3a). In contrast, anti-CSF-1R mAb administration dramatically reduced the proportion and number of CSF-1R<sup>+</sup>Ly6C<sup>low</sup> cells at all time-points compared to the isotype control (Figure 4.3b). There was also an increase in the proportion of these cells following GM-CSF neutralisation 1 and 4 days post-surgery compared to the isotype control (Figure 4.3b). Closer inspection of the CSF-1R versus Ly6C dot plots showed a dramatic decrease in the CSF-1R expression on the Ly6C<sup>high</sup> population with CSF-1R blockade (Figure 4.3c). In fact, this population only marginally remained within the CSF-1R<sup>+</sup> gate, which was established strictly using FMO controls. This change is also represented graphically by plotting the MFI, representing CSF-1R expression (Figure 4.3d). Regarding the Ly6C<sup>high</sup> population, CSF-1R blockade significantly reduced the CSF-1R MFI at all three time-points relative to the other groups. At days 1 and 4, GM-CSF blockade resulted in a slightly higher MFI compared to the isotype control. For the Ly6C<sup>low</sup> population, CSF-1R blockade again dramatically reduced the MFI of the CSF-1R parameter at all three time-points, while the slight increase in MFI with anti-GM-CSF mAb was only seen at day 4 post-injury (Figure 4.3d).

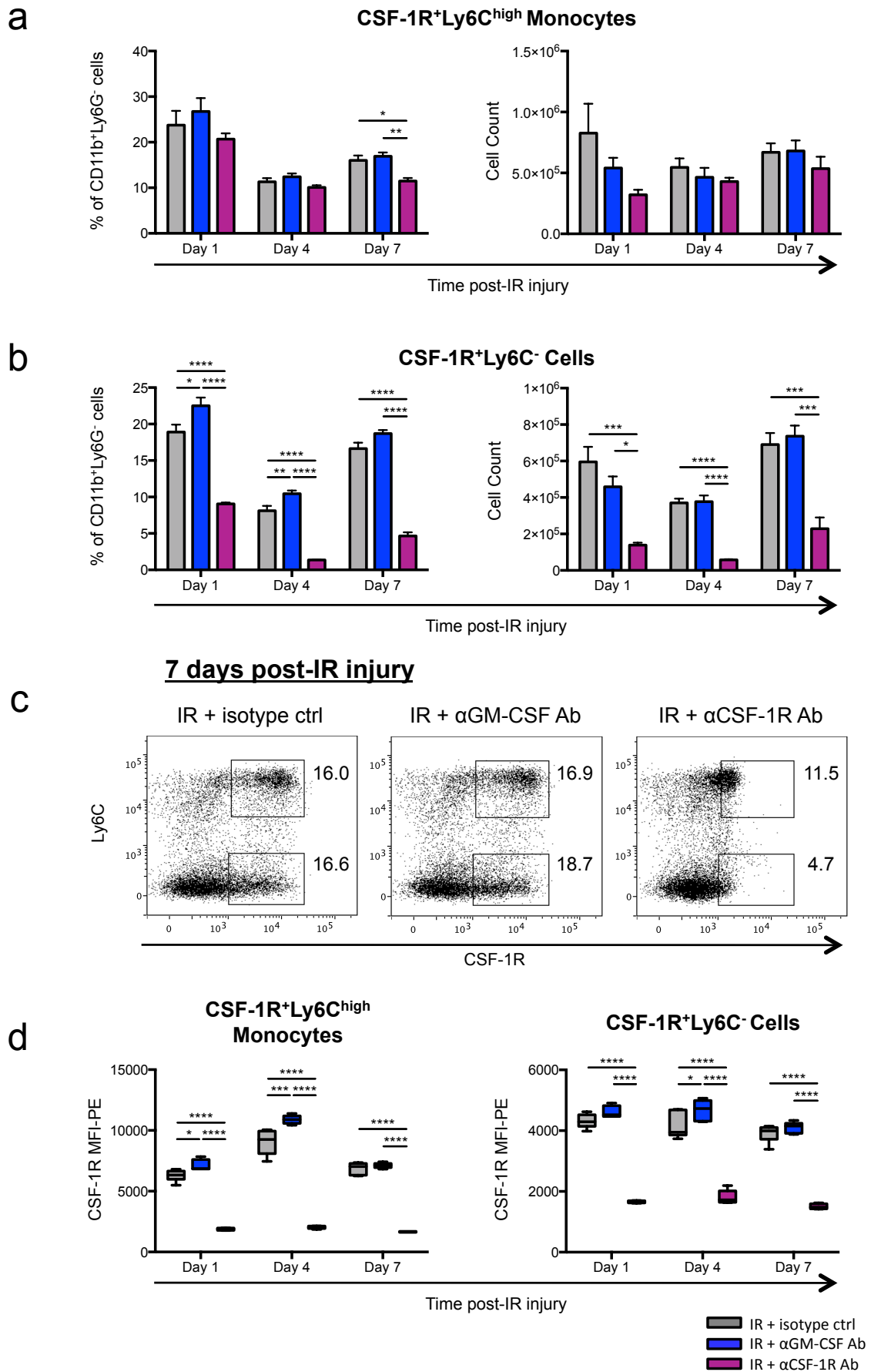


**Figure 4.3. The effect of short-term GM-CSF and CSF-1R blockade on CSF-1R<sup>+</sup> cells in the spleen following kidney IR injury.**

The effects of short-term GM-CSF and CSF-1R blockade on CSF-1R<sup>+</sup> cells in the spleen were examined at 1, 4 and 7 days after kidney IR injury using flow cytometry. Results displayed graphically show the proportion and number of CSF-1R<sup>+</sup>Ly6C<sup>high</sup> monocytes (**a**) and CSF-1R<sup>+</sup>Ly6C<sup>-</sup> macrophages (**b**). Representative dot plots from 7 days post-injury show the effect of the neutralising mAbs on these two populations (**c**). MFIs, representing the level of CSF-1R expression, was quantified for each population and displayed graphically (**d**). MFIs are displayed in box and whisker plots. Numbers on the dot plots represent proportions of Ly6C<sup>low</sup>Ly6G<sup>-</sup> cells. Data in bar graphs are displayed as means  $\pm$  SEM.  $n=4-6$ /group. \*  $P<0.05$ , \*\*  $P<0.01$ , \*\*\*  $P<0.001$ , \*\*\*\*  $P<0.0001$ . MFI, mean fluorescence intensity.

### 4.3.2 The Effect of Short-term GM-CSF and CSF-1R Blockade on Cell Populations in the Injured Kidney

In Chapter Three, characterisation of this IR injury model depicted a rapid loss in total kidney cellularity together with an influx of haematopoietic cells. The same progressive cell loss was observed in this study with no additional changes occurring with GM-CSF or CSF-1R blockade (Figure 4.4a). In contrast, CD45<sup>+</sup> cell proportions and numbers were reduced at all time-points following anti-CSF-1R mAb administration (Figure 4.4b). There were also significantly fewer CD45<sup>+</sup> cells 4 days post-IR following GM-CSF blockade (Figure 4b). Similar reductions were observed in the CD11b<sup>+</sup> population (Figure 4.4c). These similarities were due to CD11b<sup>+</sup> cells forming between 70% and 91% of CD45<sup>+</sup> cells in the isotype control group throughout the time-course (Figure 4.4c). Within the CD11b<sup>+</sup> population, Ly6C<sup>low</sup>Ly6G<sup>+</sup> granulocytes, predominantly neutrophils, were assessed. The proportion of these granulocytes was significantly greater at all time-points following CSF-1R blockade compared to the other groups (Figure 4.4d). However, this increase in proportion is largely due to a decrease in the proportions of other myeloid cell types. The only difference in cell number compared to the isotype control was a decrease at day 1. At 4 and 7 days post-IR, the anti-GM-CSF mAb group had fewer granulocytes than the anti-CSF-1R mAb group, although the granulocyte cell count was much smaller in all 3 groups at these time-points compared to that at day 1. An apparent reduction in granulocytes following GM-CSF blockade 1 day post-IR was not statistically significant (Figure 4.4d). This suggests that GM-CSF and CSF-1R neutralisation did have some subtle effects on the granulocyte population throughout the time-course.

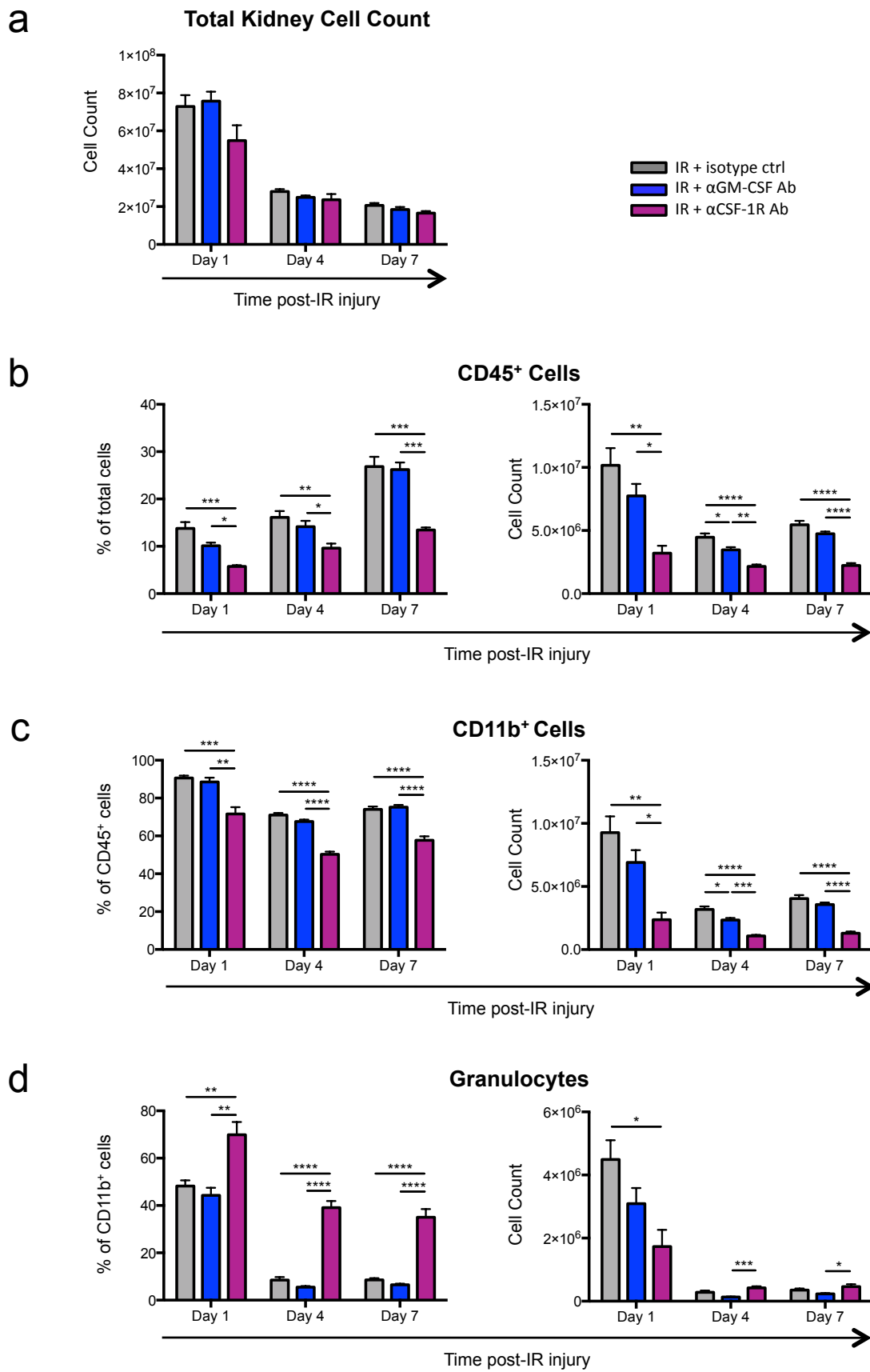


**Figure 4.4. The effect of short-term GM-CSF and CSF-1R blockade on cell populations in the injured kidney.**

The effects of short-term GM-CSF and CSF-1R blockade on kidney cell populations were assessed at 1, 4 and 7 days after IR injury using flow cytometry. Results displayed graphically show the total cellularity (**a**), proportion and number of non-autofluorescent, CD45<sup>+</sup> cells (**b**), proportion and number of CD11b<sup>+</sup> cells (**c**) and the proportion and number of granulocytes (Ly6C<sup>low</sup>Ly6G<sup>+</sup>, **d**). Data are displayed as means  $\pm$  SEM.  $n=4-6/\text{group}$ . \*  $P<0.05$ , \*\*  $P<0.01$ , \*\*\*  $P<0.001$ , \*\*\*\*  $P<0.0001$ .

To assess infiltrating monocytes and macrophages, the CD11b<sup>+</sup>Ly6G<sup>-</sup> cells were examined. The proportional changes for this population were the reflection of those seen for the granulocytes. That is, a decrease in the cell proportion following CSF-1R blockade compared to the other groups at all three time-points (Figure 4.5a). This equated to a greatly reduced number of CD11b<sup>+</sup>Ly6G<sup>-</sup> cells at all time-points compared to the isotype control and anti-GM-CSF mAb groups. There also appeared to be a slight decrease in cell number as a result of GM-CSF blockade, although it was only deemed statistically significant at day 4 (Figure 4.5a). In Chapter 3, Ly6C<sup>high</sup> monocytes were shown to infiltrate the injured kidney soon after injury, before maturing into MHCII<sup>+</sup>Ly6C<sup>-</sup> macrophages within the first three days of injury. In the current setting, CSF-1R blockade almost completely eliminated the initial Ly6C<sup>high</sup> monocyte influx (Figure 4.5b). At days 4 and 7 post-injury, these cells represented a greater proportion of the CD11b<sup>+</sup>Ly6G<sup>-</sup> population in the anti-CSF-1R mAb group. However, there was no difference in the Ly6C<sup>high</sup> cell numbers at these same time-points, which were all very low, consistent with previous findings in Chapter Three (Figure 4.5b). In effect, administering the anti-CSF-1R mAb two days prior to IR injury and again on the day of surgery eliminated an entire inflammatory mediator from the injured kidney. Similar effects were observed in the maturing Ly6C<sup>+</sup>MHCII<sup>low</sup> monocyte population (Figure 4.5c). These cells formed a lower proportion of the CD11b<sup>+</sup>Ly6G<sup>-</sup> cell pool at day 1 following CSF-1R blockade compared to the other groups but a higher proportion at days 4 and 7 post-IR. GM-CSF blockade did not impact the numbers of this cell type at any time-point (Figure 4.5c). In regards to the mature, MHCII<sup>+</sup>Ly6C<sup>-</sup> macrophages, CSF-1R blockade caused consistent depletion at all time-points. These cells formed a greater proportion of the CD11b<sup>+</sup>Ly6G<sup>-</sup> cells at day 1 but a lower proportion at day 7 compared to the other two groups (Figure 4.5d), although, these are proportions of an already vastly reduced cell population. Therefore, the absolute cell numbers provide the best insight into the effects of the neutralising antibodies. GM-CSF blockade also reduced the cell count at day 4 compared to the isotype control mAb but not to the same extent as with the CSF-1R blockade (Figure 4.5d). The decrease in this mature population accounts for the increased proportions of monocytes observed at days 4 and 7 post-IR.

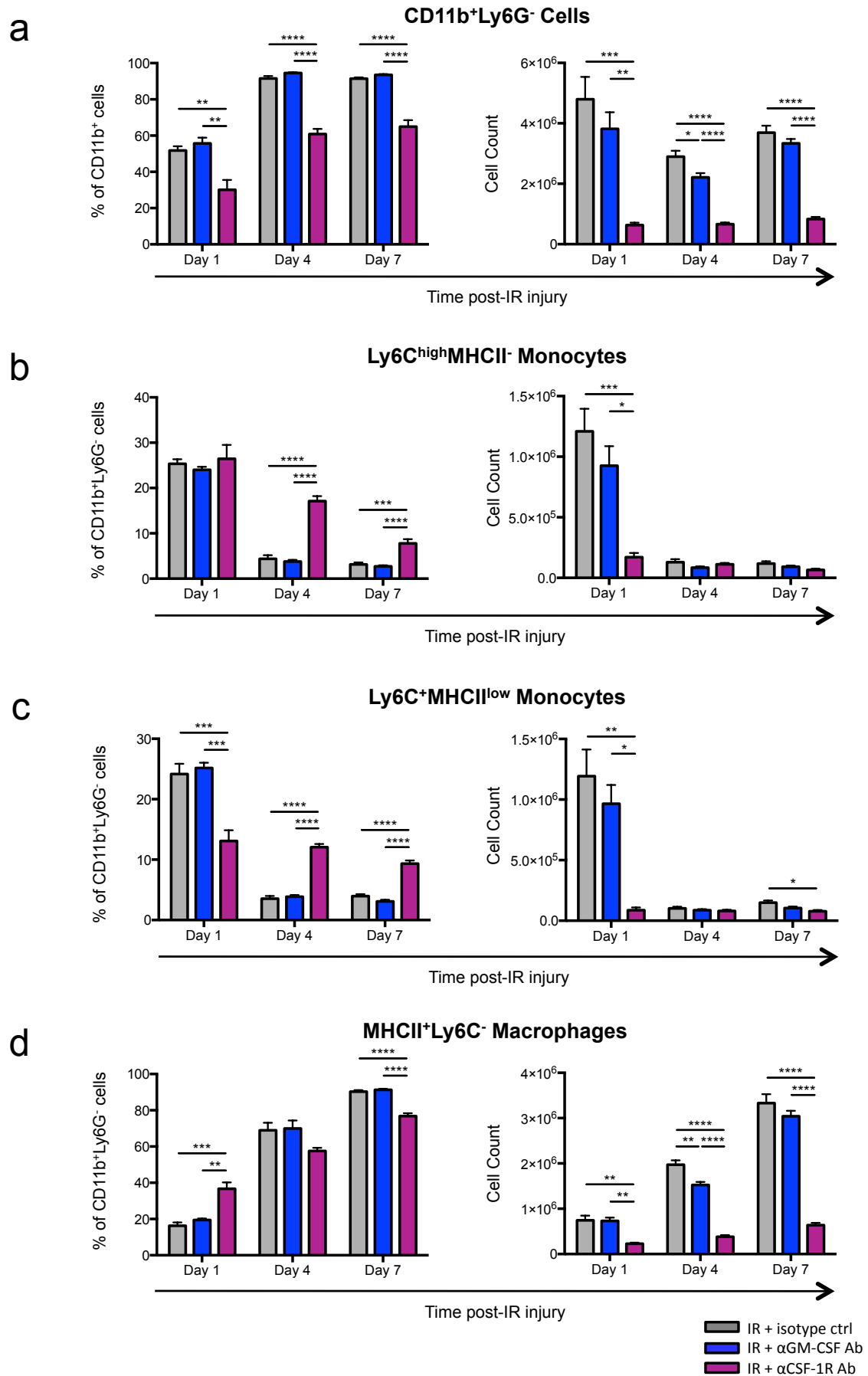


**Figure 4.5. The effect of short-term GM-CSF and CSF-1R blockade on monocytes and macrophages in the injured kidney.**

The effects of short-term GM-CSF and CSF-1R blockade on monocytes and macrophages in the kidney were examined at 1, 4 and 7 days after IR injury using flow cytometry. Results displayed graphically show the proportion and number of CD11b<sup>+</sup>Ly6G<sup>-</sup> cells (non-granulocytes myeloid cells) (a), proportion and number of Ly6C<sup>high</sup> monocytes (b), proportion and number of Ly6C<sup>+</sup>MHCII<sup>low</sup> monocytes (c) and the proportion and number of MHCII<sup>+</sup>Ly6C<sup>-</sup> macrophages (d). Data are displayed as means ± SEM. *n*=4-6/group. \* *P*<0.05, \*\* *P*<0.01, \*\*\* *P*<0.001, \*\*\*\* *P*<0.0001.

### 4.3.3 Changes in Macrophage Populations in the Kidney following Short-term GM-CSF and CSF-1R Blockade

To more thoroughly investigate the changes to mature macrophages, F4/80<sup>+</sup>MHCII<sup>+</sup> cells were assessed. This population formed less than 6.2% of all CD11b<sup>+</sup> cells following anti-CSF-1R mAb administration, compared to approximately 15%, 45% and 63% at days 1, 4 and 7, respectively, in the isotype control group (Figure 4.6a). The proportional changes were also represented in the absolute cell numbers, which showed the population was almost completely depleted following CSF-1R blockade. GM-CSF blockade also reduced the number of these cells compared to the isotype control group at day 4 but to a lesser extent (Figure 4.6a). Further assessment showed that MR<sup>+</sup>F4/80<sup>+</sup> M2 macrophages formed 11.7% of the CD11b<sup>+</sup> population 1 day after surgery and rose to over 60% at both days 4 and 7, as observed in the isotype control group (Figure 4.6b). These cells also progressively increased in abundance from 1.1x10<sup>6</sup> cells at day 1, to 2.0x10<sup>6</sup> at day 4 and 2.4x10<sup>6</sup> at day 7. No proportional or numerical differences were observed with GM-CSF blockade. However, anti-CSF-1R mAb administration depleted these cells throughout the time-course, with no more than 7.5x10<sup>4</sup> cells detected at any time-point (Figure 4.6b). To gain further insight into the phenotype of these MR<sup>+</sup>F4/80<sup>+</sup> cells, they were coloured pink and viewed on dot plots displaying MHC class II and Ly6C expression (Figure 4.6c). Interestingly, these cells did not form a uniform population but involved Ly6C<sup>-</sup> cells expressing MHC class II at low and high levels. With knowledge from previous studies investigating the pattern of MHC class II expression, it can be assumed that with increasing time post-IR injury, the MHCII<sup>low</sup>Ly6C<sup>-</sup> cells up-regulate the expression of MHC class II to form the MHCII<sup>high</sup> population. In this case, the MR<sup>+</sup> cells do not appear to be derived from the Ly6C<sup>high</sup> monocytes.

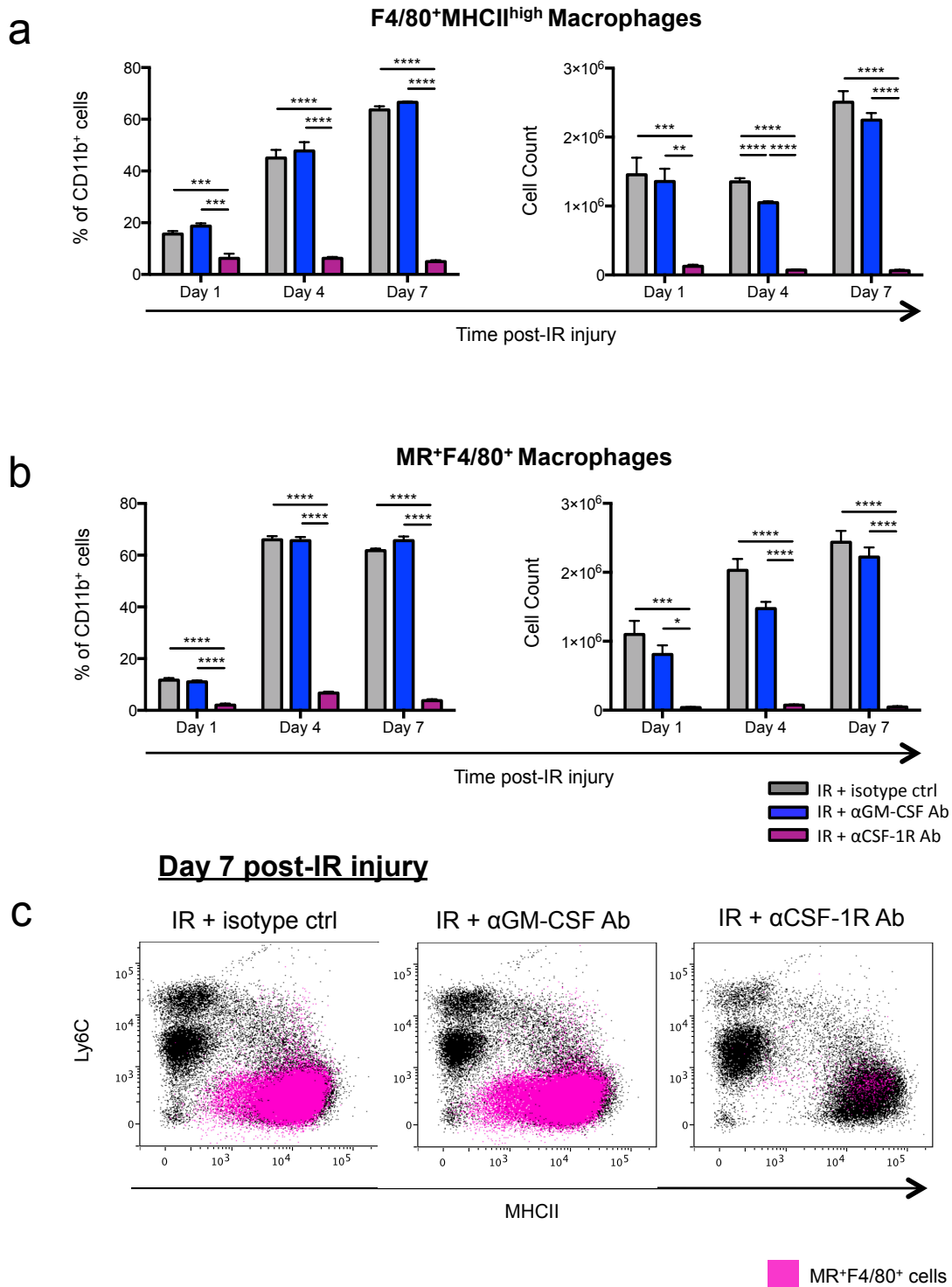


**Figure 4.6. The effect of short-term GM-CSF and CSF-1R blockade on macrophage subsets in the injured kidney.**

The effects of short-term GM-CSF and CSF-1R blockade on macrophage populations in the kidney were examined at 1, 4 and 7 days after IR injury using flow cytometry. Results displayed graphically show the proportion and number of F4/80<sup>+</sup>MHCII<sup>high</sup> macrophages (a) and MR<sup>+</sup>F4/80<sup>+</sup> M2 macrophages (b). Representative dot plots from 7 days post-IR injury show MR<sup>+</sup>F4/80<sup>+</sup> M2 macrophages (coloured pink) on MHC class II vs Ly6C plots (c). Data are displayed as means ± SEM. *n*=4-6/group. \* *P*<0.05, \*\* *P*<0.01, \*\*\* *P*<0.001, \*\*\*\* *P*<0.0001.

To investigate these subpopulations further, MHC class II expression was compared to that of MR (Figure 4.7a). For these parameters, four distinct populations were evident, including two MR<sup>+</sup> populations: MR<sup>+</sup>MHCII<sup>high</sup> cells and MR<sup>+</sup>MHCII<sup>low</sup> cells (Figure 4.7a). For the MR<sup>+</sup>MHCII<sup>high</sup> cells, CSF-1R blockade significantly reduced the proportion and cell number at all three time-points (Figure 4.7b). At days 4 and 7, GM-CSF blockade also reduced the number of these cells but not to the same extent (Figure 4.7b). CSF-1R blockade also significantly reduced the MR<sup>+</sup>MHCII<sup>low</sup> population at all time-points. However, GM-CSF blockade did not cause any significant changes (Figure 4.7c). These two MR<sup>+</sup> populations were also assessed for the expression of F4/80. The histograms in Figure 4.7d show that both of these cell types express high levels of F4/80 with the levels being slightly greater on the MR<sup>+</sup>MHCII<sup>low</sup> cells (blue histogram), compared to the MR<sup>+</sup>MHCII<sup>high</sup> cells (green histogram). Neutralising GM-CSF did not alter the level of F4/80 expression. No plot is shown for the anti-CSF-1R mAb group due to the low number of cells in the injured kidney (Figure 4.7d). Additional analysis confirmed that these MR<sup>+</sup> populations did not express Ly6C (data not shown).

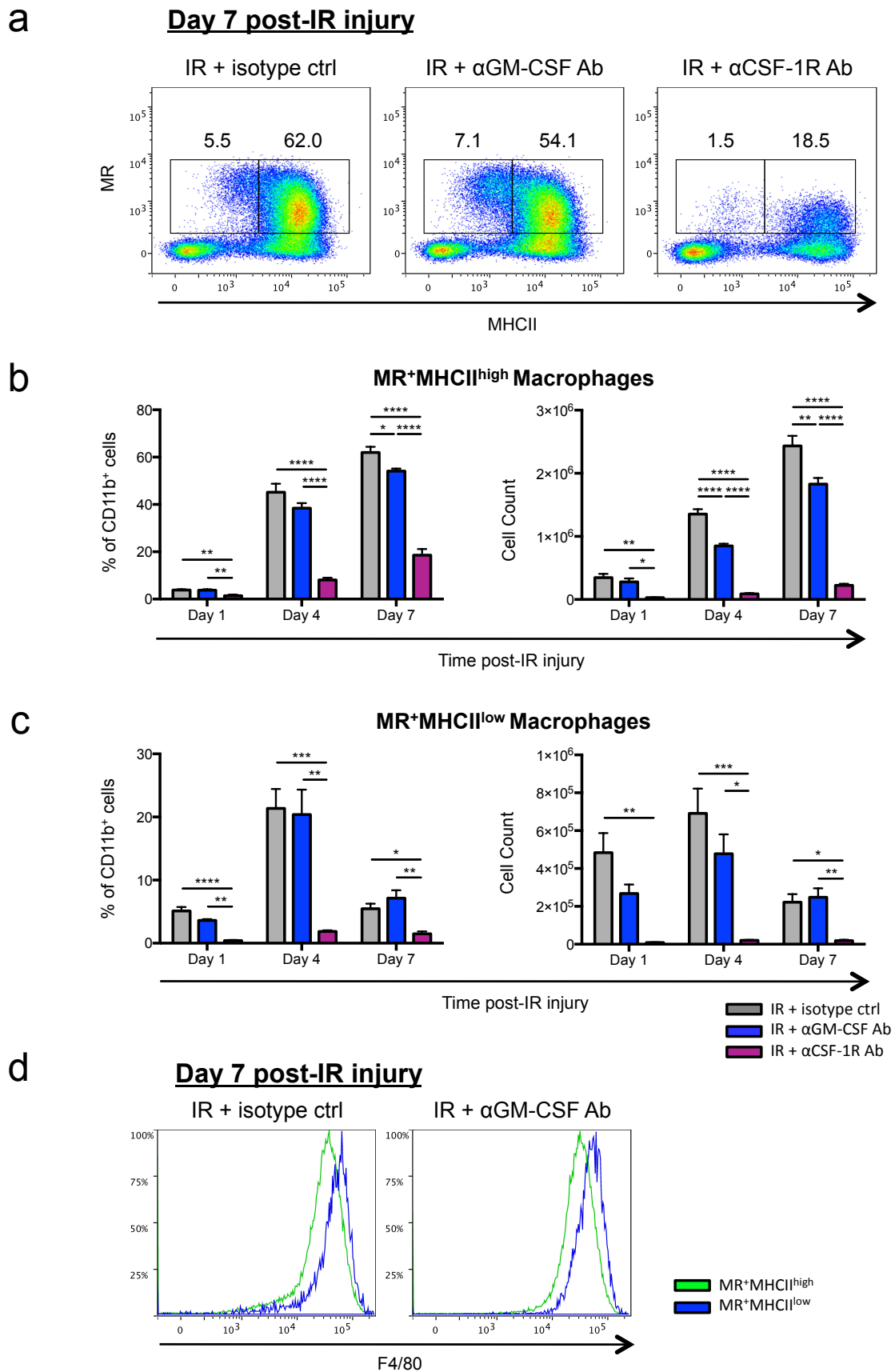


**Figure 4.7. The effect of short-term GM-CSF and CSF-1R blockade on alternatively activated macrophages in the injured kidney.**

The effects of short-term GM-CSF and CSF-1R blockade on alternatively activated macrophage populations in the kidney were examined at 1, 4 and 7 days after IR injury using flow cytometry. Representative pseudocolour dot plots from 7 days post-injury show the impact of the neutralising mAbs on macrophages (a). The proportion and number of MR<sup>+</sup>MHCII<sup>high</sup> (b) and MR<sup>+</sup>MHCII<sup>low</sup> macrophages (c) are displayed graphically. Representative histograms from 7 days post-IR injury show the F4/80 expression on these two MR<sup>+</sup> populations (d). Expression levels are overlaid on the same plot for the isotype control and anti-GM-CSF mAb groups. No histogram is shown for the anti-CSF-1R mAb group due to the very low number of macrophages in the kidney. Numbers on the dot plots represent proportions of CD11b<sup>+</sup> cells. Data are displayed as means ± SEM. *n*=4-6/group. \* *P*<0.05, \*\* *P*<0.01, \*\*\* *P*<0.001, \*\*\*\* *P*<0.0001.

#### 4.3.4 The Effect of Short-term GM-CSF and CSF-1R Blockade on EpCAM<sup>+</sup> Cells and Total Collagen in the Kidney following IR Injury

The effect of short-term GM-CSF and CSF-1R blockade on EpCAM<sup>+</sup> epithelial cells and total kidney collagen were assessed to determine any renoprotective effects. Chapter Three provides evidence that, in response to IR injury, the number of EpCAM<sup>+</sup> cells in the kidney decreases over the first 7 days but with the majority of cell loss occurring within the first three days. In this study, neither neutralising antibody reduced the amount of EpCAM<sup>+</sup> cell loss or promoted EpCAM<sup>+</sup> cell replacement within the 7 day investigation period (Figure 4.8a).

Hydroxyproline was measured and used to determine total collagen content as a proportion of dry tissue weight. Aberrant collagen deposition can be interpreted as fibrosis and can also negatively impact renal function. In this study, the collagen concentration increased from day 7 to 14 as a result of IR injury. However, there was no difference between the control and treatment groups at either 7 or 14 days post-IR injury (day 7, isotype control: 1.56%, anti-GMCSF: 1.58%, anti-CSF-1R: 1.81%; day 14, isotype control: 2.42%, anti-GMCSF: 2.08%, anti-CSF-1R: 2.42%) (Figure 4.8b).

Collectively, these results suggested that directly depleting monocytes and macrophages through the administration of an anti-CSF-1R mAb or by blocking the pro-inflammatory effects of GM-CSF from two days prior to IR injury through to 4 days post-injury has no clear benefits on EpCAM<sup>+</sup> cell number or the longer-term effects on collagen levels at days 7 and 14. A possibility is that the short-term regime only delayed the inflammation and cell loss that ensues from IR injury. Therefore, the long-term administration of the same antibodies was examined, again beginning two days prior to IR-surgery but continuing through until 10 days post-IR injury, assessing various parameters at days 7 and 14 post-surgery.

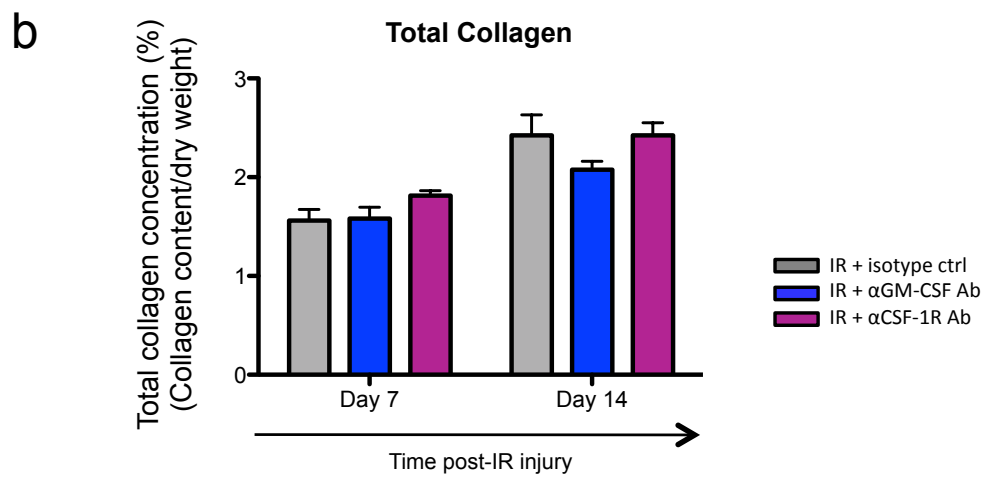
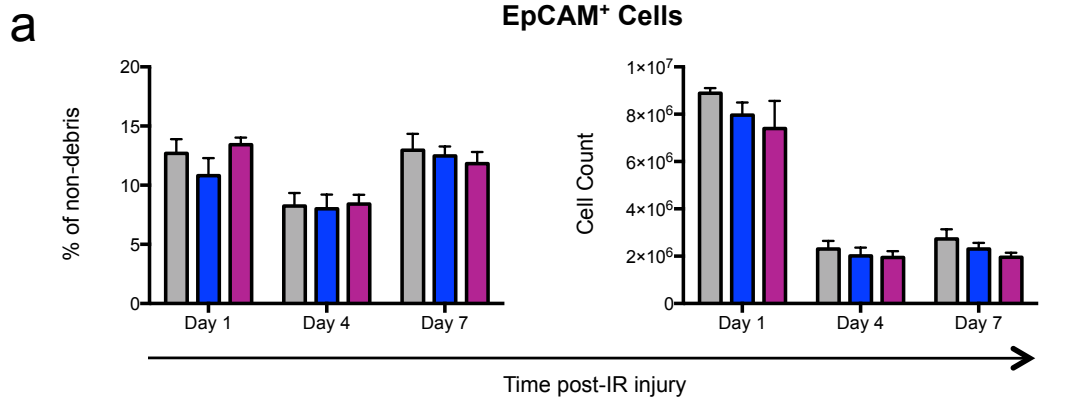


**Figure 4.8. The effect of short-term GM-CSF and CSF-1R blockade on EpCAM<sup>+</sup> cells and total collagen in the injured kidney.**

Displayed graphically are the proportion and number of EpCAM<sup>+</sup> epithelial cells as assessed at 1, 4 and 7 days post-IR injury (a) and the total collagen concentration as a proportion of dry tissue weight at 7 and 14 days post-IR injury (b). Data are displayed as means  $\pm$  SEM.  $n=4-6$ /group.

#### 4.3.5 Effects of Long-term GM-CSF and CSF-1R Blockade on Serum Cytokines

Blocking the CSF-1R had distinct effects on monocytes and macrophages due to their dependency on CSF-1 for survival. The effectiveness of the short-term administration of anti-GM-CSF mAb was more difficult to determine, as the changes to the cell numbers were more subtle. As the short-term blockade failed to impact collagen deposition or EpCAM<sup>+</sup> cell numbers, it was decided to test the long-term blockade of GM-CSF and CSF-1R, incorporating the quantification of 32 inflammation related serum cytokines by way of a multiplex protein array. The only change with the long-term regime was a dose of 100µg/injection, compared to 250µg/injection for the short-term blockade study. Additional testing showed that the reduced dose caused a very similar degree of cell depletion in the anti-CSF-1R mAb administered IR mice and the new dose remained inline with other investigations into inflammatory disorders using these mAbs (274).

Included in the panel of cytokines assessed were three colony-stimulating factors: CSF-1, GM-CSF and granulocyte-colony stimulating factor (G-CSF). Circulating CSF-1 levels were elevated at day 7 following CSF-1R blockade, most likely due to the lack of available receptors to bind to (CSF-1, day 7, iso ctrl: 21.88pg/ml, anti-GM-CSF: 16.86pg/ml, anti-CSF-1R: 385.78pg/ml,  $P < 0.05$  vs iso ctrl,  $P < 0.05$  vs anti-GM-CSF) (Figure 4.9). Blocking GM-CSF and CSF-1R both reduced circulating GM-CSF levels at 7 days post-injury (GM-CSF, day 7, iso ctrl: 220.52pg/ml, anti-GM-CSF: 23.14pg/ml,  $P < 0.01$  vs iso ctrl, anti-CSF-1R: 74.68pg/ml,  $P < 0.05$  vs iso ctrl). The concentration of G-CSF, which has roles in myelopoiesis (275, 276), was also lower at day 14 following CSF-1R blockade (G-CSF, day 14, iso ctrl: 235.52pg/ml, anti-GM-CSF: 152.54pg/ml, anti-CSF-1R: 133.78pg/ml,  $P < 0.05$  vs iso ctrl). These results indicate that the two neutralising antibodies were effectively binding to their target. Re-populating BM-derived Ly6C<sup>high</sup> monocytes at approximately 13 days post-IR (based on preliminary studies investigating the timing of re-population after a single anti-CSF-1R mAb injection) may account for the return to a normal circulating CSF-1 concentration at day 14.

Concentrations of a number of other cytokines were also altered with the administration of the two antibodies. The cytokines for which the levels were altered following CSF-1R blockade were generally different to those altered by neutralising GM-CSF. Changes were also most pronounced at the day 7 time-point. Among the effects caused by CSF-1R blockade was an increase at day 7 in the concentrations of IL-1 $\beta$ , IL-5, IL-12p70, IL-15, IL-17, leukaemia inhibitory factor (LIF) and MCP-1 (CCL2) (Figure 4.9). These changes occurred in conjunction with a decrease in IFN- $\gamma$ -induced protein 10 (IP-10 or CXCL10) and MIP-2 (CXCL2) at day 7 and monokine induced by IFN- $\gamma$  (MIG or CXCL9), MIP-1 $\alpha$  (CCL3), MIP-1 $\beta$  (CCL4), RANTES and VEGF at day 14. GM-CSF blockade caused a decrease in IL-2, IL-9, MIP-2 and an increase in MIG at day 7, along with a decrease in MIP-1 $\beta$ , MIP-2 and RANTES at day 14 (Figure 4.9). Of interest were the increased concentrations of IL-4 and IL-10 at day 7 with CSF-1R blockade. Both of these cytokines are associated with M2 macrophage polarisation. There were no significant alterations seen in the levels of eotaxin, IL-1 $\alpha$ , IL-3, IL-6, IL-7, IL-12p40, IL-13, CXCL1, LPS-induced CXC chemokine (LIX or CXCL5) or TNF- $\alpha$  following administration of either antibody (data not shown).

These data provides insight into the potential impact blocking GM-CSF and CSF-1R has on myeloid cell function. To link the changes observed in circulating cytokines with alterations in cell populations following long-term blockade, flow cytometry was again used to assess different cell types.

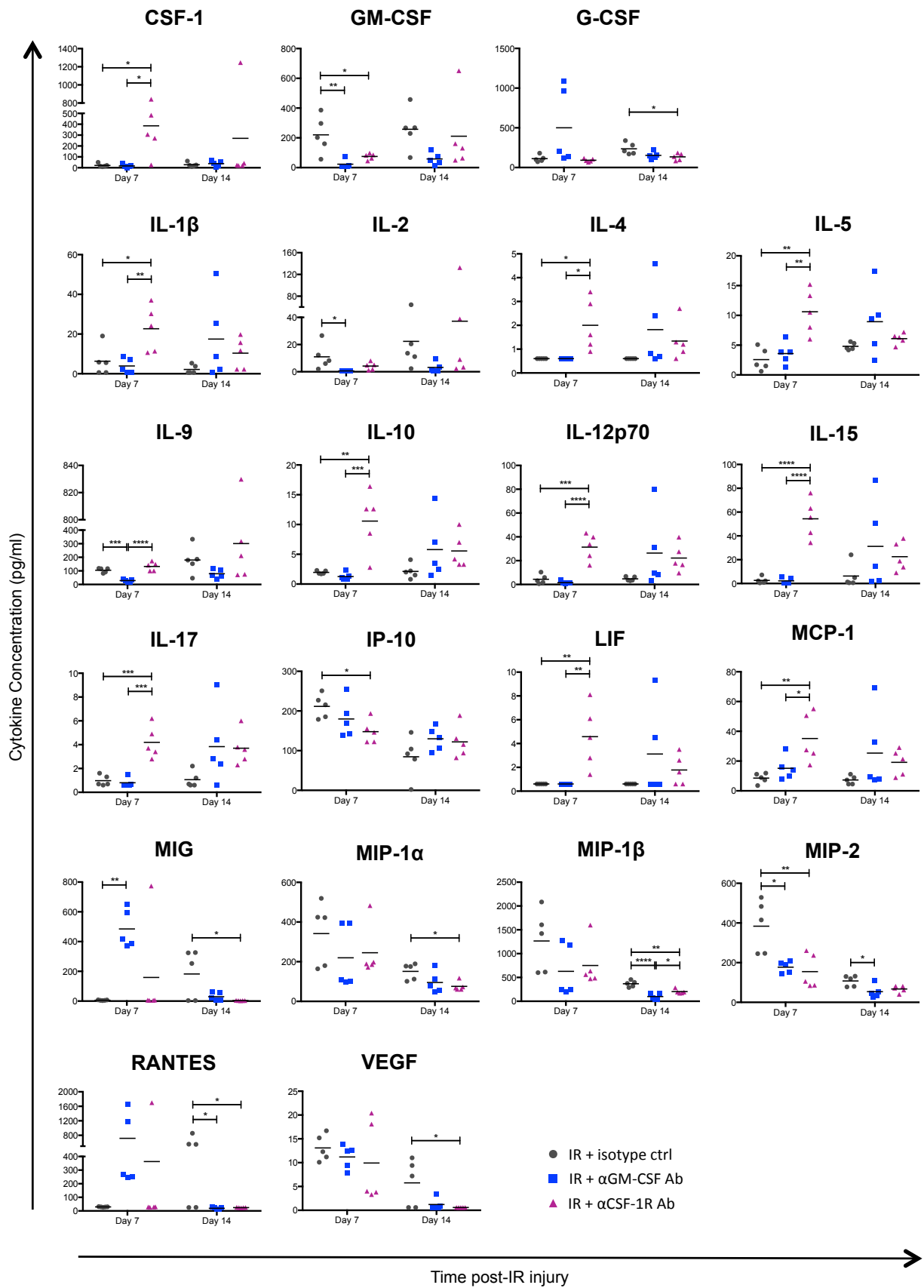


**Figure 4.9. Effects of long-term GM-CSF and CSF-1R blockade on serum cytokine levels following kidney IR injury.**

Serum cytokines were assessed with a multiplex protein array at 7 and 14 days post-IR following the long-term blockade of GM-CSF and CSF-1R. Scatter plots display all cytokines for which the concentrations were altered as a result of neutralising mAb administration. Individual data points and the mean concentration are plotted. Data are displayed as means  $\pm$  SEM.  $n=5$ /group. \*  $P<0.05$ , \*\*  $P<0.01$ , \*\*\*  $P<0.001$ , \*\*\*\*  $P<0.0001$ .

Abbreviations: CSF-1, colony stimulating factor-1; G-CSF, granulocyte colony-stimulating factor; GM-CSF, granulocyte macrophage colony-stimulating factor; IL, interleukin; IP-10, interferon gamma-induced protein; LIF, leukaemia inhibitory factor; MCP-1, monocyte chemotactic protein; MIG, monokine induced by gamma interferon; MIP, monocyte inflammatory protein; RANTES, regulated and normal T cell expressed and secreted; VEGF, vascular endothelial growth factor.

### 4.3.6 The Effect of Long-term GM-CSF and CSF-1R Blockade on Cell Populations in the Spleen

Similar to results from short-term blockade, no changes were observed in the total cellularity or number of CD45<sup>+</sup> cells with either neutralising antibody (data not shown). There were also no significant changes to the numbers of CD11b<sup>+</sup> cells, granulocytes or CD11b<sup>+</sup>Ly6G<sup>-</sup> cells compared to the isotype control group (data not shown). In addition, no differences were observed regarding the proportion and number of CSF-1R<sup>+</sup>Ly6C<sup>high</sup> cells (Figure 4.10a). For the CSF-1R<sup>+</sup>Ly6C<sup>-</sup> cells, however, administering anti-CSF-1R mAb dramatically reduced the proportion and cell count at the day 7 time-point (Figure 4.10b). Assessing the dot plots revealed that the CSF-1R expression level for the Ly6C<sup>high</sup> cells had again been greatly reduced but remained at levels slightly above that in the isotype control (Figure 4.10c).

The CSF-1R expression level (MFI) was again quantified for the Ly6C<sup>high</sup> and Ly6C<sup>-</sup> populations (Figure 4.10d). This revealed a large decrease in CSF-1R on the Ly6C<sup>high</sup> population at day 7 with CSF-1R blockade. At day 14, expression levels for all three groups had decreased greatly and no differences were observed between groups at this time-point. There was also a decrease in MFI for the CSF-1R<sup>+</sup>Ly6C<sup>-</sup> cells at day 7. At day 14, CSF-1R MFI was only lower in the anti-CSF-1R mAb group compared to the anti-GM-CSF mAb group (Figure 4.10d). These results, along with the serum cytokine data, confirm the effectiveness of the anti-CSF-1R mAb in the periphery, from where many inflammatory cells are recruited.

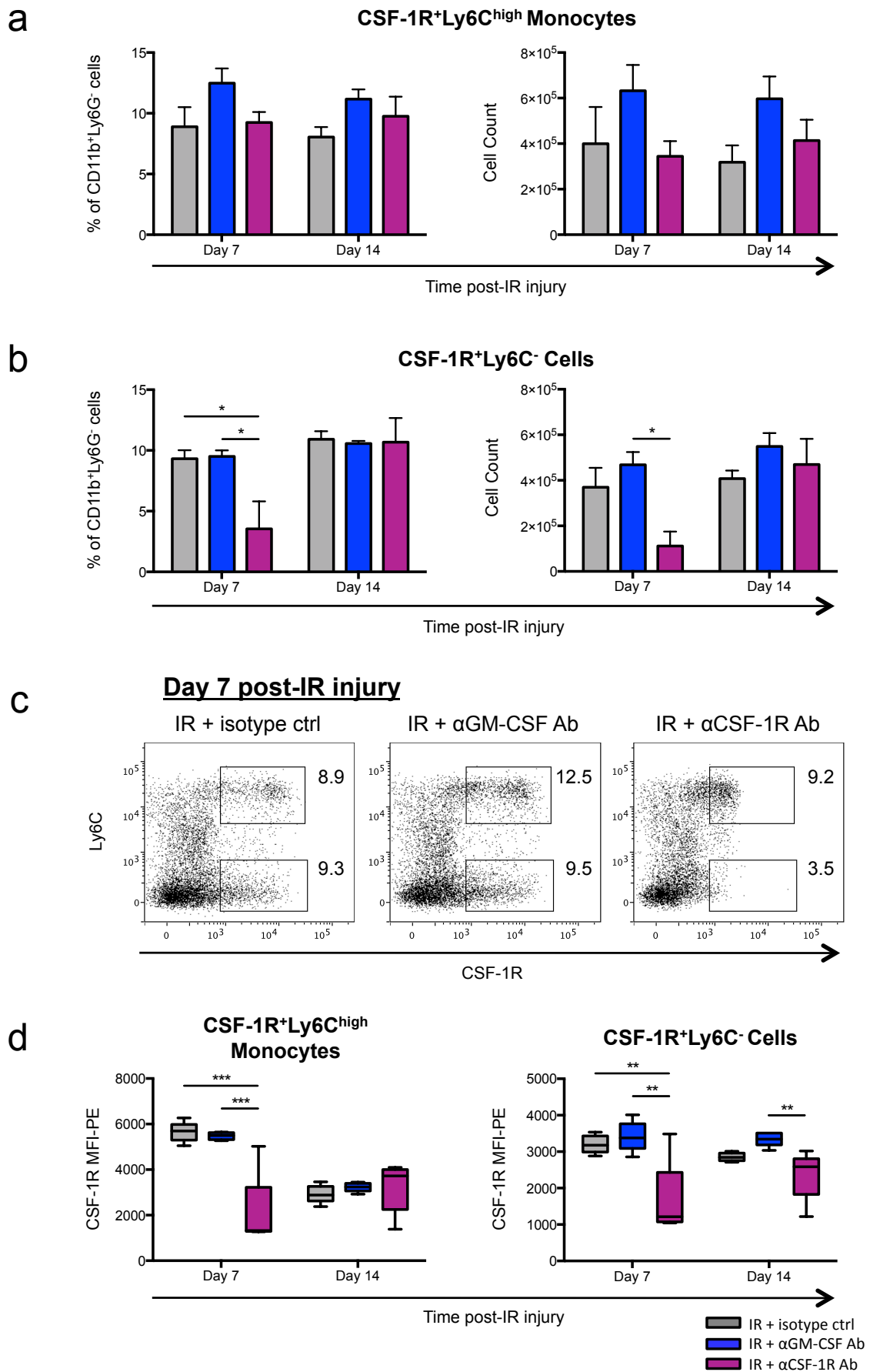


**Figure 4.10. The effect of long-term GM-CSF and CSF-1R blockade on CSF-1R<sup>+</sup> cells in the spleen following kidney IR injury.**

The effects of long-term GM-CSF and CSF-1R blockade on CSF-1R<sup>+</sup> cells in the spleen were examined at 7 and 14 days after kidney IR injury using flow cytometry. Results displayed graphically show the proportion and number of CSF-1R<sup>+</sup>Ly6C<sup>high</sup> monocytes (a) and CSF-1R<sup>+</sup>Ly6C<sup>-</sup> macrophages (b). Representative dot plots from 7 days post-injury show the effect of the neutralising mAbs on these two populations (c). MFI representing the level of CSF-1R expression was quantified for each population and displayed graphically (d). MFIs are displayed in box and whisker plots. Numbers on the dot plots represent proportions of Ly6C<sup>low</sup>Ly6G<sup>-</sup> cells. Data are displayed as means ± SEM for bar graphs. *n*=5/group. \* *P*<0.05, \*\* *P*<0.01, \*\*\* *P*<0.001, \*\*\*\* *P*<0.0001. MFI, mean fluorescence intensity.

#### 4.3.7 The Effect of Long-term GM-CSF and CSF-1R Blockade on Cells in the Injured Kidney

Changes were observed in a number of populations in the kidney following the long-term blockade of CSF-1R but not GM-CSF. There was no alteration to the total cellularity with administration of the neutralising antibodies. However, CSF-1R blockade did reduce the number of CD45<sup>+</sup> cells 7 days post-injury, most likely due to the reduction in the number of CD11b<sup>+</sup> cells at this time-point (data not shown). No change was observed in the numbers of granulocytes at either time-point with GM-CSF or CSF-1R blockade (data not shown). There was, however, a greater proportion and number of Ly6C<sup>high</sup> monocytes 7 days post-IR but no differences between groups at day 14 (Figure 4.11a). This increase in inflammatory monocytes appears to contradict the effect of short-term CSF-1R blockade at the same time-point. However, the proportion and cell count are relatively similar between the two regimes. There was also a higher proportion of maturing Ly6C<sup>+</sup>MHCII<sup>low</sup> cells at both day 7 and 14 post-injury, which translated to an increased cell count 7 days after surgery (Figure 4.11b). The altered inflammatory response following CSF-1R blockade may have resulted in a delayed increase in these monocyte populations. The reverse of this trend was evident for the mature, MHCII<sup>+</sup>Ly6C<sup>-</sup> population, with CSF-1R blockade lowering the cell proportion and number at day 7 (Figure 4.11c). There were no changes in this population at day 14.

A closer examination of the mature macrophage subsets revealed similar changes to those observed with the MHCII<sup>+</sup>Ly6C<sup>-</sup> population. The proportion and number of F4/80<sup>+</sup>MHCII<sup>high</sup> macrophages were decreased in mice administered anti-CSF-1R mAb compared to the other groups at day 7 but not at day 14 (Figure 4.12a). The alternatively activated MR<sup>+</sup>MHCII<sup>high</sup> macrophages were similarly reduced in proportion and number following CSF-1R blockade at day 7 with respect to the isotype control (Figure 4.12b). As initially described in Figure 4.7, all MR<sup>+</sup>MHCII<sup>high</sup> cells expressed high levels of F4/80 at both time-points. MR<sup>+</sup>F4/80<sup>+</sup> cells at day 14 post-injury were again coloured pink and displayed on MHC class II versus Ly6C dot plots (Figure 4.12c). The noted difference with the MR<sup>+</sup> cells at this time-point compared to those at day 7 shown in Figure 4.6c is the lack of the MHCII<sup>low</sup> population. This evidence shows that the shift towards an MHCII<sup>high</sup> phenotype is complete by 14 days post-IR injury.

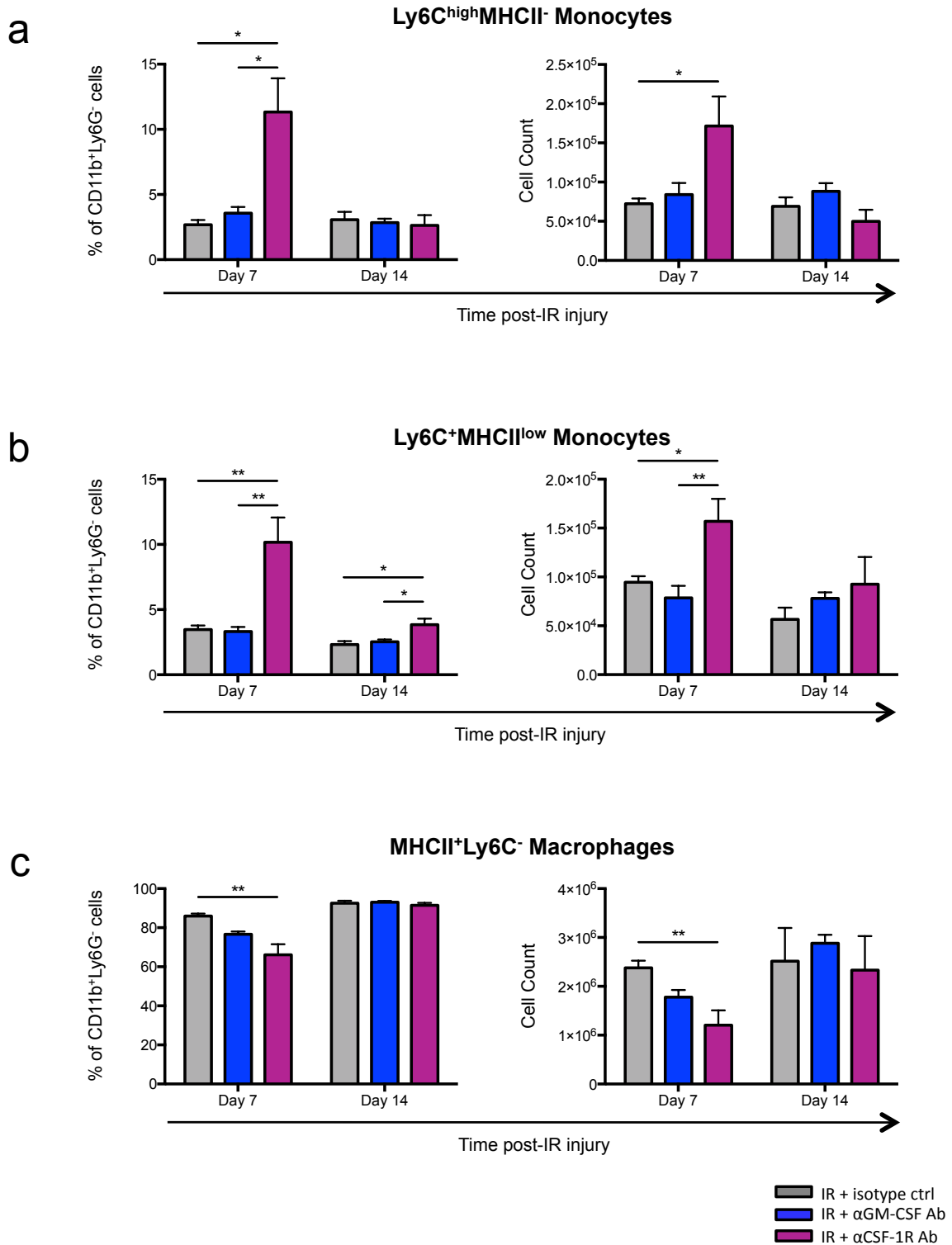


**Figure 4.11. The effect of long-term GM-CSF and CSF-1R blockade on monocytes and macrophages in the injured kidney.**

The effects of long-term GM-CSF and CSF-1R blockade on CSF-1R<sup>+</sup> cells in the kidney were examined at 7 and 14 days after IR injury using flow cytometry. Results displayed graphically show the proportion and number of Ly6C<sup>high</sup> monocytes (a), proportion and number of Ly6C<sup>+</sup>MHCII<sup>low</sup> monocytes (b) and the proportion and number of MHCII<sup>+</sup>Ly6C<sup>-</sup> macrophages (c). Data are displayed as means ± SEM. *n*=5/group. \* *P*<0.05, \*\* *P*<0.01, \*\*\* *P*<0.001, \*\*\*\* *P*<0.0001.

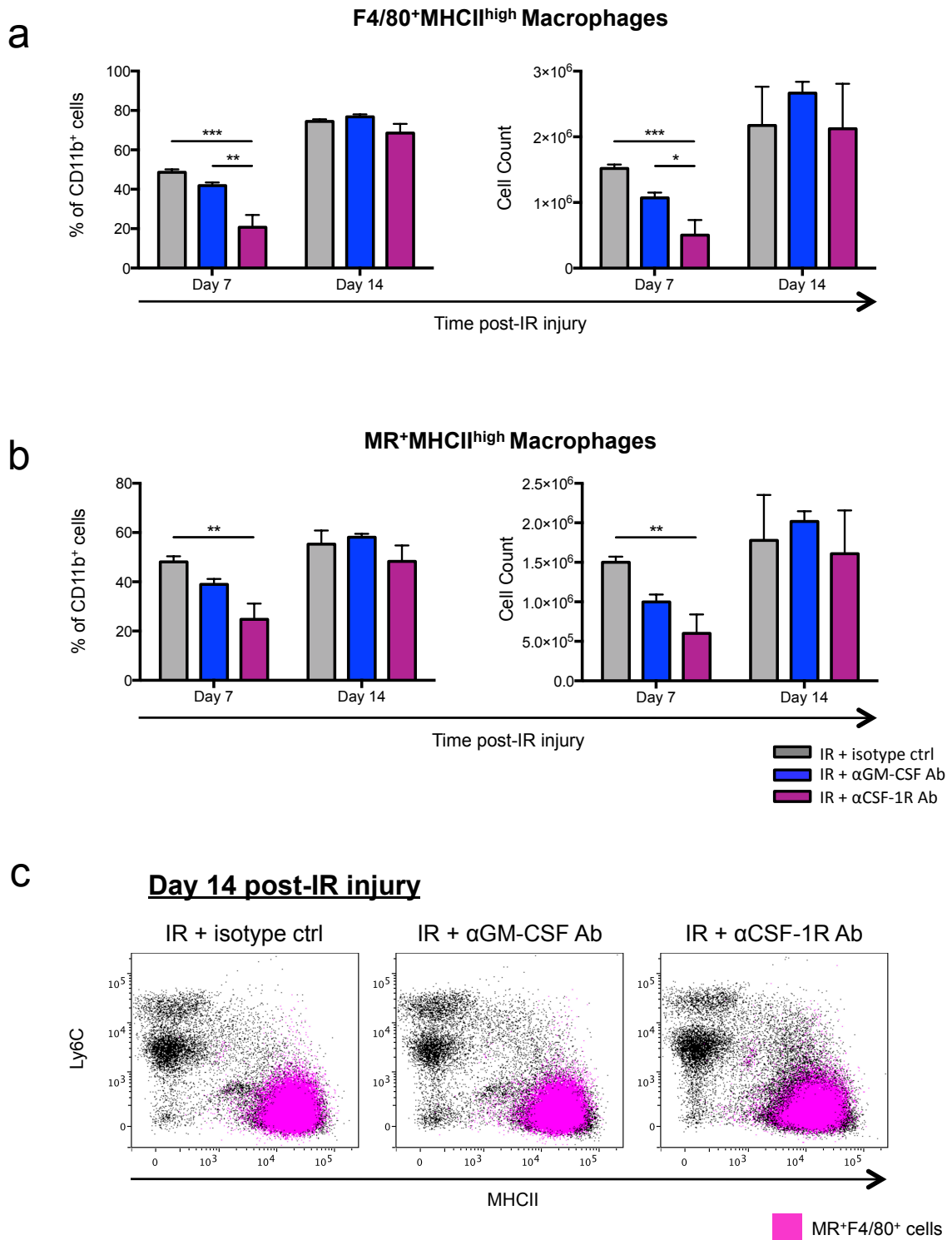


**Figure 4.12. The effect of long-term GM-CSF and CSF-1R blockade on macrophage subsets in the injured kidney.**

The effects of long-term GM-CSF and CSF-1R blockade on macrophage subsets in the kidney were examined at 7 and 14 days after IR injury using flow cytometry. Results displayed graphically show the proportion and number of F4/80<sup>+</sup>MHCII<sup>high</sup> macrophages (a) and MR<sup>+</sup>MHCII<sup>high</sup> M2 macrophages (b). Representative dot plots from 14 days post-injury show MR<sup>+</sup>F4/80<sup>+</sup> M2 macrophages (coloured pink) on MHC class II vs Ly6C plots (c). Data are displayed as means ± SEM. *n*=5/group. \* *P*<0.05, \*\* *P*<0.01, \*\*\* *P*<0.001, \*\*\*\* *P*<0.0001.

#### 4.3.8 Histological Changes following IR Injury with the Long-term Blockade of GM-CSF and CSF-1R and the Quantification of EpCAM<sup>+</sup> Epithelial Cells

Kidney histopathology was assessed at 7 and 14 days post-IR following the long-term GM-CSF and CSF-1R blockade to identify structural changes that cannot be observed with flow cytometry. At 7 days following IR injury and isotype control treatment, widespread TEC damage was evident in the kidney. Sloughing of TECs into the tubular lumen and the formation of proteinaceous casts were evident. In addition, there was expansion of the interstitial matrix that was filled with inflammatory cells (Figure 4.13a). By day 14 post-IR, re-epithelisation was evident with fewer protein casts present. However, there was still widespread loss of tissue architecture. Interestingly, neither mAb treatment appeared to alter the renal histoarchitecture at either day 7 and 14, in comparison to the isotype control group.

The visual assessment gained from studying the histopathology was compared to the flow cytometric quantification of EpCAM<sup>+</sup> epithelial cells. There were no differences caused by GM-CSF or CSF-1R blockade at day 7. However, there were significantly fewer EpCAM<sup>+</sup> cells at day 14 following CSF-1R blockade compared to the isotype control group (iso ctrl:  $1.46 \times 10^6$ , anti-GM-CSF:  $1.33 \times 10^6$ , anti-CSF-1R:  $8.71 \times 10^5$ ,  $P < 0.05$  for iso ctrl vs anti-CSF-1R) (Figure 4.13b). As the proportion and number of EpCAM<sup>+</sup> cells increased from day 7 to day 14 in the isotype control group, the results indicate that CSF-1R blockade limited the replacement/replenishment of these epithelial cells (Figure 4.13b). Longer time-points are required to determine the extent of CSF-1R blockade on the inhibition of EpCAM<sup>+</sup> cell replenishment. These results demonstrate that the potential anti-inflammatory effects from blocking GM-CSF or CSF-1R do not provide protection from EpCAM<sup>+</sup> cell loss. Further to this, the prolonged depletion of monocytes and macrophages is a likely contributor to the impaired replacement of these cells. To assess structural changes occurring at these time-points, collagen content and its distribution following GM-CSF and CSF-1R blockade were assessed.

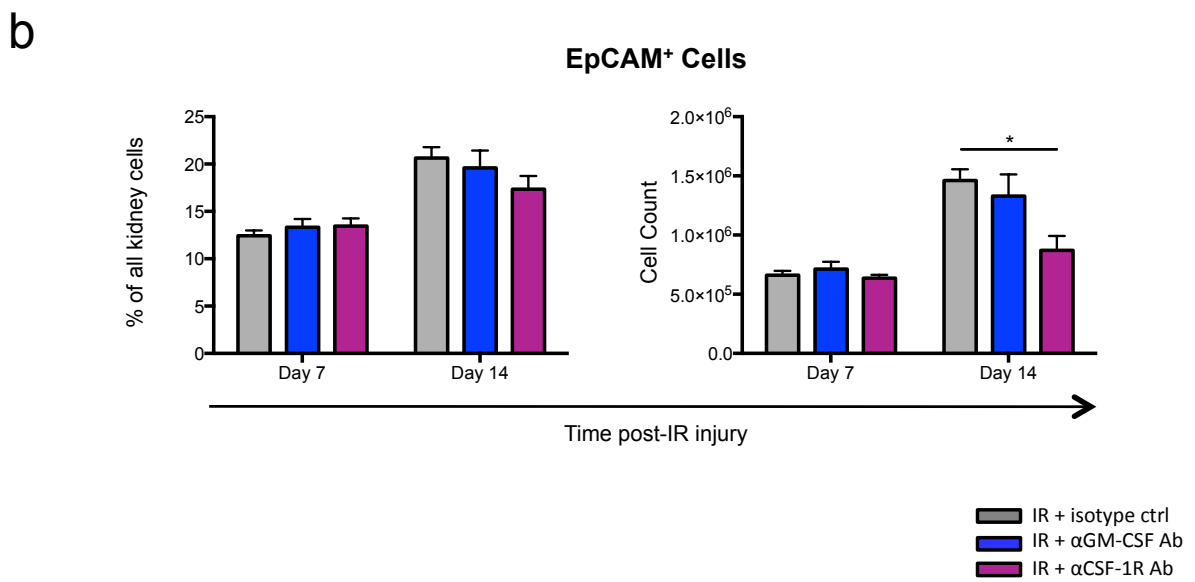
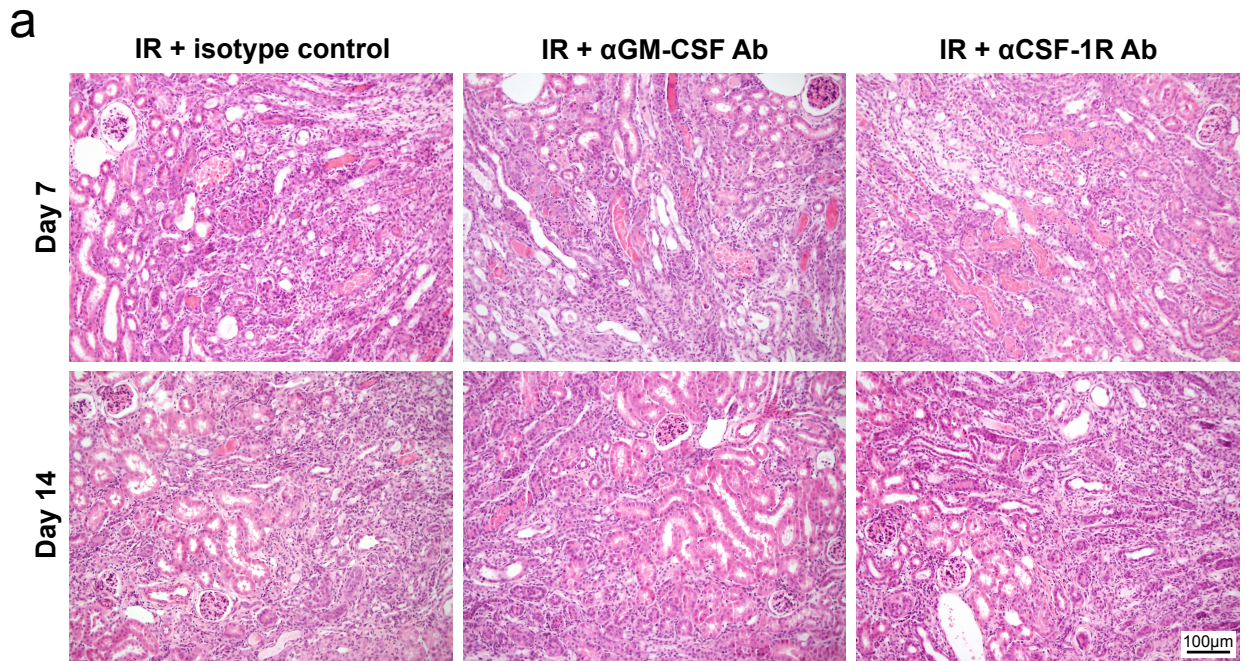


**Figure 4.13. Histological changes in the kidney following IR injury with the long-term blockade of GM-CSF and CSF-1R.**

Representative photomicrographs of H&E stained kidney sections from isotype control, anti-GM-CSF and anti-CSF-1R treated mice (a). The effects of long-term GM-CSF and CSF-1R blockade on EpCAM<sup>+</sup> cells in the kidney were quantified using flow cytometry. Displayed graphically are the proportion and number of EpCAM<sup>+</sup> epithelial cells as assessed at 7 and 14 days post-injury (b). Data are displayed as means  $\pm$  SEM.  $n=5$ /group. \*  $P<0.05$ , \*\*  $P<0.01$ , \*\*\*  $P<0.001$ , \*\*\*\*  $P<0.0001$ .

#### 4.3.9 Assessment of Total Collagen in the Injured Kidney following Long-term GM-CSF and CSF-1R Blockade

Hydroxyproline was measured in injured kidneys at days 7 and 14 post-injury following long-term GM-CSF and CSF-1R blockade to determine the total collagen content as a means of assessing fibrosis. As with the short-term antibody administration, there was no difference between the control and treatment groups at day 7 post-injury (isotype control: 1.73%, anti-GM-CSF: 1.93%, anti-CSF-1R: 1.75%; Figure 4.14a). However, CSF-1R blockade resulted in a significantly greater collagen concentration at day 14 compared to the other groups (isotype control: 2.82%, anti-GM-CSF: 2.48%, anti-CSF-1R: 5.38%,  $P < 0.05$  anti-CSF-1R vs isotype control,  $P < 0.01$  anti-CSF-1R vs anti-GM-CSF) (Figure 4.14a).

Further analysis of the collagen subtypes using SDS-PAGE revealed that the predominant subtypes that contributed to the increase in collagen were type I collagen [ $\alpha_1(I)$  and  $\alpha_2(I)$  monomers and dimers of two  $\alpha_1(I)$  chains ( $\beta_{11}$ ) or  $\alpha_1(I)$  and  $\alpha_2(I)$  monomers ( $\beta_{12}$ )] and a small amount of type V collagen (Figure 4.14b).

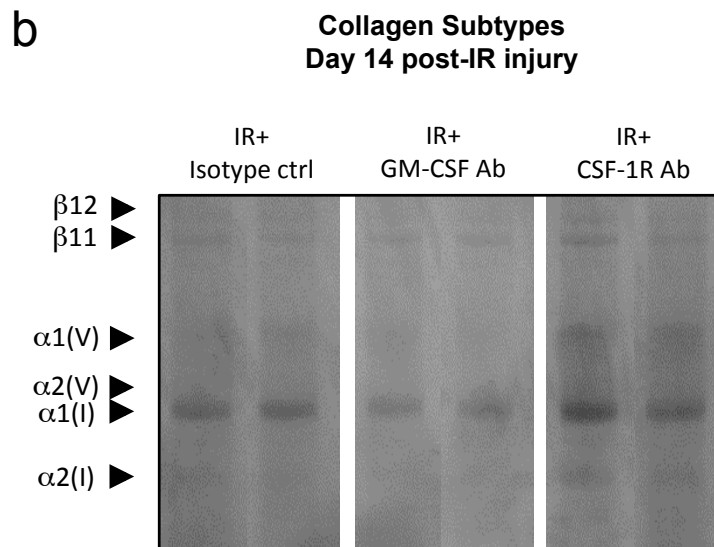
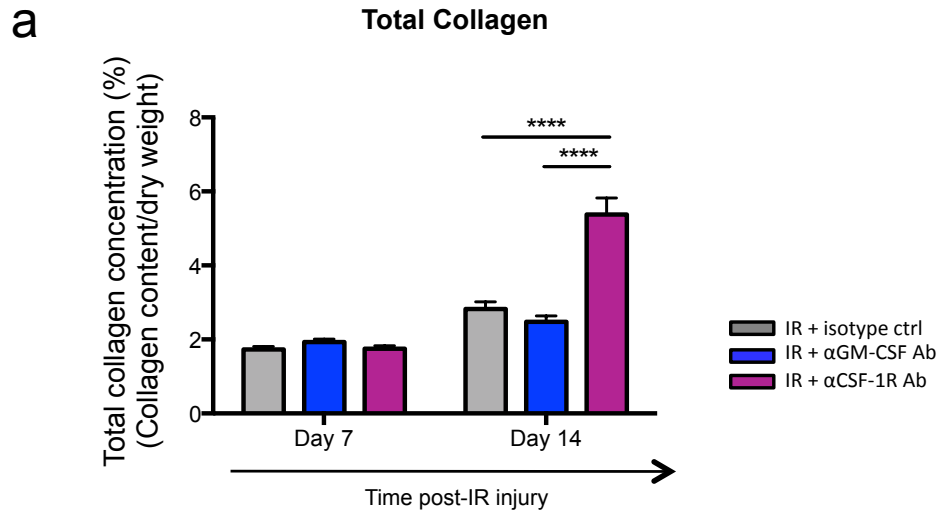


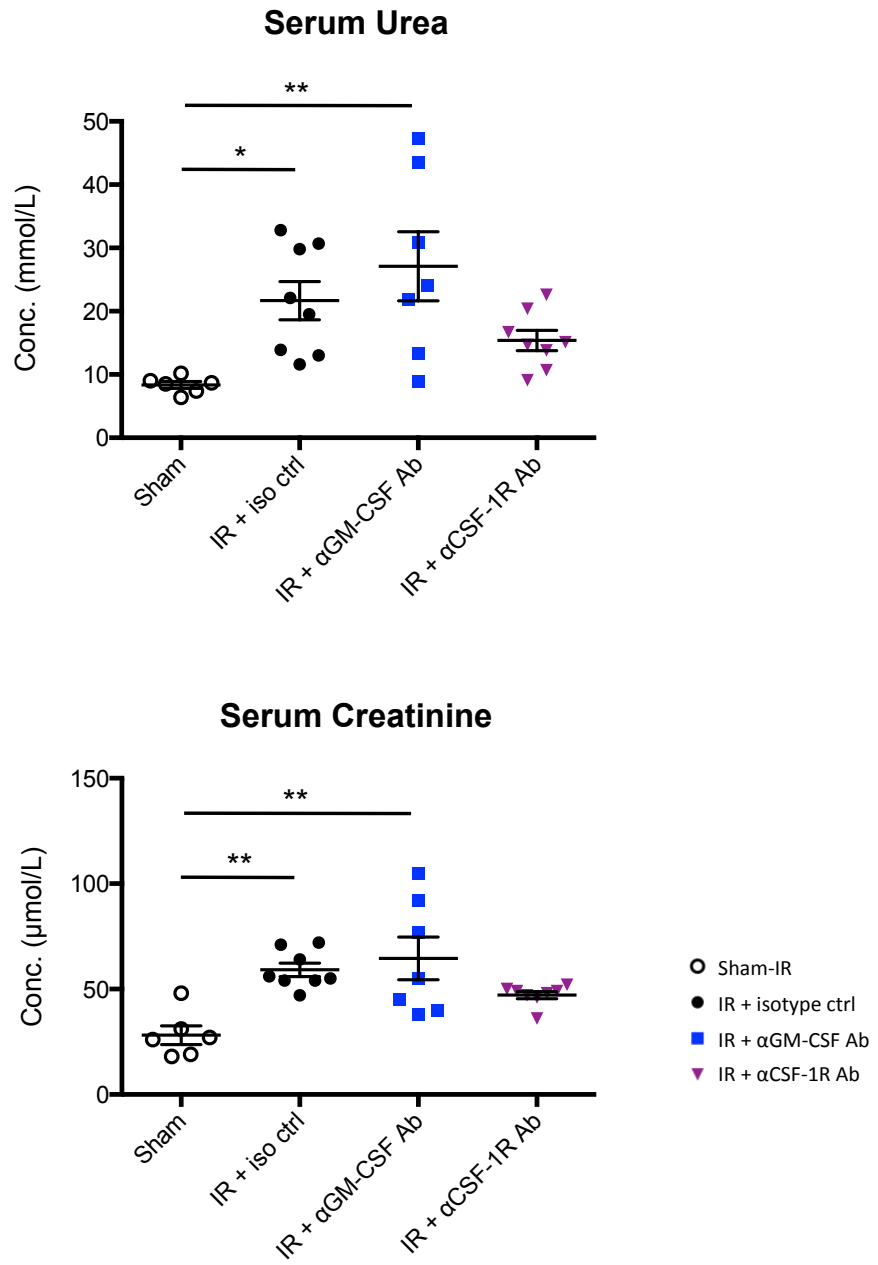
**Figure 4.14. Assessment of collagen in the injured kidney following the long-term blockade of GM-CSF and CSF-1R.**

Picrosirius red staining was used to visualise collagen deposition (red staining) within the kidney (a). A hydroxyproline assay was used to determine total collagen concentration as a proportion of dry tissue weight at 7 and 14 days post-injury (b). SDS-PAGE analysis shows the main collagen subtypes present at day 14 post-injury (c). Data are displayed as means  $\pm$  SEM.  $n=5-6/\text{group}$ . \*  $P<0.05$ , \*\*  $P<0.01$ , \*\*\*  $P<0.001$ , \*\*\*\*  $P<0.0001$ .

#### **4.3.10 Changes in Renal Function following IR Injury with Long-term GM-CSF and CSF-1R Blockade**

Renal function was assessed in a bilateral IR injury model (25 minutes of ischaemia) due to the compensatory capacity of individual kidneys. At day 14 post-IR following the long-term blockade of GM-CSF and CSF-1R, serum urea and serum creatinine levels were analysed as a measurement of renal function. A sham-injury group was included to define baseline levels of serum urea and creatinine.

Urea and creatinine levels were both significantly higher in the IR + isotype control group (urea; 21.7mmol/L,  $P<0.05$ ; creatinine; 59.1 $\mu$ mol/L,  $P<0.01$ ) and the IR + anti-GM-CSF mAb group (urea; 27.1mmol/L,  $P<0.01$ ; creatinine; 64.6 $\mu$ mol/L,  $P<0.01$ ) compared to the sham-IR control (urea; 8.4mmol/L; creatinine; 28.2 $\mu$ mol/L), indicating reduced renal function (Figure 4.15). The most promising results were for the mice that received the anti-CSF-1R mAb. The mean values for both serum urea (15.4mmol/L) and creatinine (47.1 $\mu$ mol/L) were higher than in the sham-IR group but lower than in the IR + isotype control group although not statistically significant (Figure 4.15).

**Day 14 post-IR injury**

**Figure 4.15. Changes in kidney function following IR injury with the long-term blockade of GM-CSF and CSF-1R.**

Urea and creatinine concentrations were measured in serum samples obtained from mice 14 days after bilateral IR injury (25min ischaemia) following long-term GM-CSF and CSF-1R blockade (or sham-IR injury with no mAb administration). Scatter plots display individual data points with means  $\pm$  SEM.  $n=6-8$ /group. \*  $P<0.05$ , \*\*  $P<0.01$ , \*\*\*  $P<0.001$ , \*\*\*\*  $P<0.0001$ .

## 4.4 Discussion

This study provides insights into the roles of GM-CSF and CSF-1, along with the cells that they govern, in kidney IR injury. More specifically, it appears that the damaging effects of ischaemia cannot be mitigated by a marked reduction in inflammatory myeloid cell infiltrate shortly after reperfusion. The results also point to the importance of CSF-1- and macrophage-mediated repair processes in the recovery from IR injury. The aim of this study was two fold: to determine if the blockade of the CSF-1R or GM-CSF could provide renoprotection by reducing the infiltration and function of pro-inflammatory cells into the injured kidney and to identify differences between short-term and long-term blockade.

Short-term CSF-1R blockade proved very effective in depleting monocytes and macrophages within the kidney at all stages within the first 7 days of injury. Even after two injections (days -2 and 0) there was a greatly reduced number of infiltrating Ly6C<sup>high</sup> inflammatory monocytes, far below control levels. This reduction also extended to the mature macrophage population (F4/80<sup>+</sup>MHCII<sup>+</sup>), where the additional injection (day 2) resulted in almost complete depletion throughout the time-course. Possibly more significant is that the MR<sup>+</sup> M2 macrophage population was also depleted throughout the 7 days. Interestingly, reductions in the same populations in the spleen were not as apparent. Possible explanations include a more acute requirement for CSF-1 in the pro-inflammatory kidney microenvironment or alternative survival mechanisms offered to the splenic monocytes and macrophages. Neutralising GM-CSF did not have a dramatic impact on monocyte numbers but did result in fewer kidney F4/80<sup>+</sup>MHCII<sup>+</sup> macrophages 4 days post-injury. Neutralising GM-CSF did, however, result in significantly fewer granulocytes, compared to the anti-CSF-1R mAb group at 4 and 7 post-IR. Consistent with findings in Chapter Three, the majority of epithelial reduction occurred shortly after IR injury. Epithelial cell preservation was one aspect that we were interested in assessing with the GM-CSF and CSF-1R blockade. Unfortunately, neither mAb reduced the amount of EpCAM<sup>+</sup>

epithelial cell loss. Another aspect is enhanced epithelial replacement, which requires the assessment at later time-points.

The development of fibrosis, assessed at 7 and 14 days post-injury, did not appear to be linked to the magnitude of the initial infiltration or presence of pro-inflammatory monocytes and macrophages. Previous studies have shown that depleting macrophages by other methods prior to IR injury can reduce damage and preserve renal function (277-279). However, the degree of protection in these studies may be influenced by the length of ischaemic time, which ranged from 22-32min, and may vary depending on the time post-surgery that kidney function was assessed. In this study, an ischaemic time of 40min was used, which is considered a severe form of acute injury but still within the range that allows for some degree of organ recovery and repair.

Having determined that the short-term neutralisation of GM-CSF and CSF-1R failed to alter the fibrotic outcome of this IR injury, additional mAb injections were performed at 4, 7 and 10 days post-surgery, with assessment at days 7 and 14. To gain insight into the systemic effects of GM-CSF and CSF-1R blockade, 32 serum cytokines were measured at 7 and 14 days post-IR. Notably, circulating CSF-1 levels were increased at day 7 with CSF-1R blockade, most likely due to the inability of CSF-1R<sup>+</sup> cells to bind the ligand. Also, the anti-GM-CSF mAb effectively decreased circulating GM-CSF levels at the same time-point. Generally speaking, the two different neutralising mAbs altered a different set of cytokines. In a previous study, “M2-like” macrophages primed with CSF-1 produced increased MCP-1 and IL-10 after stimulation *in vitro* (187). Here, CSF-1R blockade also led to increased levels of these two cytokines in the circulation at day 7. This may be due to the increased circulating CSF-1 levels or other compensatory mechanisms resulting from monocyte and macrophage depletion. IL-4, also related to M2 polarisation, was elevated at day 7. In addition, CSF-1R blockade led to increased levels of a number of pro-inflammatory cytokines (IL-1 $\beta$ , IL-2, IL-12p70, IL-15 and IL-17) compared to the control mAb. These results demonstrate that targeting the functions of this

one growth factor is not sufficient in causing a widespread reduction in inflammatory mediators. GM-CSF neutralisation, however, did have the intended effect of reducing a number of pro-inflammatory mediators, including IL-2 and IL-9 at day 7, and MIP-1 $\beta$  and RANTES at day 14 compared the control mAb. MIP-2 was also reduced at both time-points.

Interestingly, with the long-term CSF-1R blockade there was a slight but significant increase in the number of Ly6C<sup>high</sup> and Ly6C<sup>low</sup> monocytes at day 7 that was not detected following short-term blockade, although the cell counts were still comparable. This result indicates that even 7 days post-IR injury, there are still chemoattractant signals attracting inflammatory cells from the circulation. This is consistent with the elevated levels of serum MCP-1 detected at day 7.

Short-term CSF-1R blockade had no influence on EpCAM<sup>+</sup> epithelial cell protection or replacement. However, the lower EpCAM<sup>+</sup> cell count at day 14 following long-term CSF-1R blockade alludes to the importance of mature macrophages in TEC repair. Besides changes in cell numbers, the biggest effect from the mAb administration was a large proportional increase in the collagen content at day 14 with CSF-1R blockade. It is difficult to determine if this is aberrant collagen deposition or an indication of matrix replacement. The reduced serum urea and creatinine levels in this group at day 14 could support the latter, although as the differences in the functional data with CSF-1R blockade were not significant, it is difficult to form this conclusion.

Previous studies have shown the importance of CSF-1 in switching macrophage phenotype towards an M2 state to promote tissue repair (182). In the study by Alikhan *et al.*, CSF-1 protein was administered after the establishment of injury, which resulted in accelerated repair of kidney structure and function. More advanced tracing studies may be of use to establish the differentiation fate and contribution to repair of the infiltrating Ly6C<sup>high</sup> and Ly6C<sup>low</sup> monocytes in this setting and to help determine if and when the blockade of the CSF-1R may be advantageous in CSF-1-mediated repair. As the anti-CSF-1R mAb delivery depletes both the

immature, infiltrating monocytes and the mature macrophages indiscriminately, and given the importance of M2 macrophages in extracellular matrix remodelling, a more specifically targeted depletion method may be able to provide more useful anti-inflammatory effects or create an environment more favourable for repair. That said, the complex nature of the inflammatory cascade and the conditions required for M2 polarisation may be very closely associated and a fine manipulation of this balance may be all that is needed to switch on reparative functions slightly earlier.

GM-CSF and CSF-1R blockade has proven beneficial in a number of inflammation-mediated diseases. In these inflammatory disease settings, it may be that the immune driven aspect of the disease, as opposed to the ischaemic cell death and sterile inflammation that results from IR injury, is what allowed the therapy to be effective. In kidney IR injury, these therapies caused broad changes in circulating cytokines and kidney myeloid populations. In particular, CSF-1R blockade caused widespread depletion of pro-inflammatory monocytes and mature macrophages. While the anti-inflammatory effects of these mAb treatments were obvious, ablation of the M2 macrophages may have compromised some aspects of tissue repair. Altogether the results from this study demonstrate the complexity of the *in vivo* setting. Due to the broad range of inflammatory mediators and signalling pathways involved, coordinating the timing of the therapy to the evolving disease state is required for optimal results.

# CHAPTER 5

---

*General Discussion*

## General Discussion

The impact of kidney disease on individuals and health care systems worldwide is enormous. The number of people with kidney disease is also growing, largely due to the increased prevalence of type 2 diabetes and ageing populations. To date, conventional treatments for kidney disease have focused on delaying the progression towards ESRD and RRT. However, in recent times there has been a shift to develop novel therapies to promote endogenous kidney repair. Although a significant challenge remains in a setting of fibrosis and declining function, this outcome may be possible through harnessing the immunomodulatory and reparative capabilities of macrophages. Therefore, this thesis aimed to further the knowledge of myeloid cell biology in kidney IR injury, a model of AKI, with a particular focus on monocytes and macrophages. In Chapter Two, a flow cytometry protocol was established for detecting and analysing myeloid cells in injured and non-injured kidneys. Chapter Three utilised this methodology to characterise myeloid populations, inflammatory cytokines and epithelial cell loss throughout the initiation and resolution phases of kidney IR injury. Finally, Chapter Four explored and compared the effects of GM-CSF and CSF-1R blockade, thereby inhibiting principal mediators of myeloid cell functions, on IR-mediated damage and repair.

Inflammation undoubtedly can have deleterious effects in kidney disease and many studies have successfully achieved protection in experimental models through inhibiting or blocking inflammatory cells and mediators. Macrophages are known contributors to the inflammatory response in kidney IR injury, so it is surprising that in a study that tested two methods of macrophage ablation, clodronate-mediated depletion was protective while DT-mediated depletion was not (257). DT administration resulted in the near complete depletion of kidney macrophages (liver and splenic macrophages were unaffected), while MR<sup>+</sup> M2 renal macrophages were resistant to clodronate-mediated depletion. These results confirm the existence and functional importance of different macrophage populations within the kidney. However, the kidney microenvironment, which changes throughout the phases of IR injury, can

also influence macrophage activation. In a separate study involving clodronate depletion of macrophages prior to IR, adoptive transfer of resting RAW 264.7 cells (a murine macrophage cell line) re-instated injury when delivered at the time of injury and at 24 hours post-surgery. However, when delivered 48 hours post-IR, these cells promoted repair (280). In comparison, IFN- $\gamma$ -stimulated BM macrophages maintained their M1 phenotype when delivered to mice at the time of injury (during the inflammatory phase) but switched to an M2 state when administered 3 days post-IR (during the resolution phase) (193).

These results also provide insight into the nature of CSF-1 mediated kidney repair. In separate studies, administering CSF-1 to mice with established IR injury accelerated repair and remodelling through the promotion of a reparative macrophage activation state (148, 182). In these studies, CSF-1 was delivered throughout the resolution phase of the injury model, promoting TEC proliferation and improving renal function. Using DT-mediated macrophage depletion, Menke *et al.* reported that CSF-1-mediated repair involved both macrophage-dependent and -independent mechanisms, demonstrating that CSF-1 also signals directly to TECs (148). Alikhan *et al.* further demonstrated that CSF-1 mediates repair through the promotion of M2 macrophage activation (182). Conversely, in an experimental lupus nephritis model, circulating CSF-1 was implicated in the increased numbers of intrarenal macrophages mediating TEC apoptosis, while CSF-1 deficiency provided protection from kidney damage (281).

Taken together, these results highlight the dynamic interplay between macrophages and the microenvironment. In the present study, it is likely that CSF-1R blockade failed to provide protection from IR due to the depletion of MR<sup>+</sup> macrophage populations. This likely counteracted any protective effects from inhibiting inflammatory monocyte infiltration. Results from Chapter Three show that the majority of monocyte infiltration in kidney IR injury occurs within the first 24 hours of reperfusion. Therefore, there was most likely a lack of cells and time required to repopulate the mature MR<sup>+</sup> macrophages in order to promote tubular replacement

and repair. However, the results in Chapter Four pertaining to collagen levels at 7 and 14 days post-IR suggest that the impact on myeloid cells following short-term CSF-1R blockade was not extensive enough to promote excess fibrosis, as was the case with long-term CSF-1R blockade.

Relatively few studies have investigated the role of GM-CSF in kidney IR injury and repair. As GM-CSF has been identified as a mediator in other inflammatory diseases, and due to its role in the survival and activation of neutrophils and macrophages (260), neutralising GM-CSF was a legitimate approach to provide protection against IR injury. However, only modest reductions in some myeloid populations were observed, generally within 4 days post-injury, with no impact on epithelial cell numbers or collagen accumulation compared to control IR kidneys. Very recently, Huen *et al.* described a unique alternative activation state in macrophages following co-culture of pro-inflammatory macrophages with either mouse PT cells or primary TECs (282). The activation of these macrophages occurred via STAT5 signalling, as opposed to the canonical IL-4-stimulated STAT6 pathway, and while they shared *Arg1* and *Cd206* gene expression with IL-4-activated macrophages, they uniquely expressed *Msr1* but lacked *Fizz1*, *Ym1* and *Igf-1* gene expression. It was also shown that culturing naïve BM-derived macrophages in mouse PT cell conditioned media promoted the same activation state, which was inhibited with the addition of GM-CSF neutralising antibody. The authors also administered anti-GM-CSF antibodies to mice during the resolution phase of IR injury and observed reduced tubular proliferation but no impact on serum creatinine levels 5 days post-IR (282). Interestingly, as shown in Chapter Four of this thesis, neutralising GM-CSF prior to IR injury also did not impact renal function as assessed at 7 and 14 days post-IR.

Modulation of the inflammatory response to IR injury with neutralising antibodies nevertheless holds enormous potential for limiting damage caused by inflammation. The findings from this thesis suggest that future research in kidney regeneration should aim to target specific subpopulations of cells and focus on manipulating individual functions within these cells, such as the increased production or inhibition of specific cytokines. Further research is also required

to determine the importance of infiltrating cells, such as inflammatory neutrophils and monocytes, for subsequent repair mechanisms. Due to the apparent importance of timing therapies to specific disease phases, neutralising CSF-1 (or blocking CSF-1R) and GM-CSF may have benefits despite lack of efficacy extending into the resolution phase of IR injury. In this regard, one approach may be combination therapy using blockade during inflammation followed by injecting the growth factors during the resolution phase.

Epigenetic modification is another method that could be very useful in modulating macrophage function and their response to stimuli (283). Epigenetics involve post-translational chromatin modifications that confer functional changes in gene activity (284). A cell's epigenetic landscape is modified based on events that occur during development and from environmental signals. This in turn influences the manner that cells respond to new stimuli. Targeting chromatin regulators with synthetic compounds has already proven to be successful in inhibiting inflammatory responses by macrophages. The pre-treatment of BM-derived macrophages with one such compound, I-BET, prior to LPS stimulation, suppressed a range of LPS-inducible chemokines and cytokines (285). Administration of this compound to mice prior to the induction of endotoxic shock was also able to prevent death (285). Using such compounds to selectively suppress the pro-inflammatory functions of macrophages would most likely be a better-targeted approach than the depletion of entire macrophage populations.

Since Metchnikoff first identified and described macrophages as scavenging phagocytes, their identity has been constantly evolving, from pro-inflammatory cells of the innate immune system, to the recent classification of M1 and M2 polarisation states. As discussed by Martinez and Gordon (286), this classification system is simplistic, as the environment created for *in vitro* polarisation does not reflect the complexity of the *in vivo* setting. The *in vitro* conditions involving purely M1 or M2 stimuli do not translate to the *in vivo* setting and the M1/M2 model suggests that activated macrophages conform to stable activation states. The context of signalling also requires consideration, as a cell's response to a stimulus will be different in times

of cell maturation, pathogen clearance and resolution from inflammation and injury. There is also only a partial overlap of signalling pathways for each activation state due to the range of different M1 and M2 stimuli, adding to the heterogeneity of the activated populations. While the concept of macrophage activation states is useful, in reality, it may not be possible to fully classify macrophage activation. However, a thorough understanding of macrophage capabilities and specific disease environments will aid in the development of highly specific and effective therapies.

### **Conclusion**

Kidney disease represents a range of disorders arising from different aetiologies. The difficulty in developing new treatments is due to highly complex disease processes and immune responses. The ability to resolve kidney injury following damage rests on a fine balance regarding the initial inflammatory response and the replacement of damaged cells and structures. Macrophage plasticity and diversity offers the possibility of new therapies through modulating their phenotype and function. To achieve this, an intimate knowledge is needed of all cells involved in a specific disease or injury, along with safe and specific methods of targeting them.

# REFERENCES

---

## References

1. Mehta RL et al. Acute Kidney Injury Network: report of an initiative to improve outcomes in acute kidney injury. *Crit Care*. 2006;11(2):R31–R31.
2. Chatauret N, Badet L, Barrou B, Hauet T. Ischemia-reperfusion: From cell biology to acute kidney injury. *Prog Urol*. 2014;24 Suppl 1:S4–S12.
3. Puelles VG et al. Glomerular number and size variability and risk for kidney disease. *Curr Opin Nephrol Hypertens*. 2011;20(1):7–15.
4. Levey AS et al. Definition and classification of chronic kidney disease: a position statement from Kidney Disease: Improving Global Outcomes (KDIGO). *Kidney Int*. 2005;67(6):2089–2100.
5. Couser WG, Remuzzi G, Mendis S, Tonelli M. The contribution of chronic kidney disease to the global burden of major noncommunicable diseases. *Kidney Int*. 2011;80(12):1258–1270.
6. Levey AS, Coresh J. Chronic kidney disease. *Lancet*. 2012;379(9811):165–180.
7. Eckardt K-U et al. Evolving importance of kidney disease: from subspecialty to global health burden. *Lancet*. 2013;382(9887):158–169.
8. National Kidney Foundation. K/DOQI clinical practice guidelines for chronic kidney disease: evaluation, classification, and stratification. *Am J Kidney Dis*. 2002;39(2 Suppl 1):S1–266.
9. Kirsztajn GM, Suassuna JHR, Bastos MG. Dividing stage 3 of chronic kidney disease (CKD): 3A and 3B. *Kidney Int*. 2009;76(4):462–3– author reply 463–4.
10. Inker LA et al. KDOQI US commentary on the 2012 KDIGO clinical practice guideline for the evaluation and management of CKD. *Am J Kidney Dis*. 2014;63(5):713–735.
11. Nugent RA, Fathima SF, Feigl AB, Chyung D. The Burden of Chronic Kidney Disease on Developing Nations: A 21st Century Challenge in Global Health. *Nephron Clin Pract*. 2011;118(3):c269–c277.
12. Mazzuchi N, Fernandez-Cean JM, Carbonell E. Criteria for selection of ESRD treatment modalities. *Kidney Int*. 2000;57:S136–S143.
13. AIHW. Projections of the incidence of treated end-stage kidney disease in Australia 2011;1–72.
14. Codreanu I, Perico N, Sharma SK, Schieppati A, Remuzzi G. Prevention programmes of progressive renal disease in developing nations. *Nephrology (Carlton, Vic)*. 2006;11(4):321–328.
15. Registry A. Australia and New Zealand Dialysis and Transplant Registry 2013;1–235.
16. U.S. Renal Data System (USRDS). 2013 Annual Data Report: Atlas of End-Stage Renal Disease in the United States. *National Institutes of Health, National Institute of Diabetes and Kidney Diseases, Bethesda, MD*. 2013;1–326.

17. Cass A et al. *The Economic Impact of End-Stage Kidney Disease in Australia*. 2010.
18. Madhan K. Quality of life. *Nephrology*. 2010;15:S32–S34.
19. Lameire NH et al. Acute kidney injury: an increasing global concern. *Lancet*. 2013;382(9887):170–179.
20. Bellomo R, Kellum JA, Ronco C. Acute kidney injury. *Lancet*. 2012;380(9843):756–766.
21. Hoste EAJ, Schurgers M. Epidemiology of acute kidney injury: how big is the problem? *Crit Care Med*. 2008;36(4 Suppl):S146–51.
22. Bagshaw SM, George C, Bellomo R, Bellomo R. Early acute kidney injury and sepsis: a multicentre evaluation. *Crit Care*. 2008;12(2):R47–R47.
23. Vanmassenhove J et al. AKI in early sepsis is a continuum from transient AKI without tubular damage over transient AKI with minor tubular damage to intrinsic AKI with severe tubular damage. *Int Urol Nephrol*. 2014;46(10):2003–2008.
24. Pannu N, Nadim MK. An overview of drug-induced acute kidney injury. *Crit Care Med*. 2008;36(4 Suppl):S216–23.
25. Clec'h C, Razafimandimby D, Laouisset M, Chemouni F, Cohen Y. Incidence and outcome of contrast-associated acute kidney injury in a mixed medical-surgical ICU population: a retrospective study. *BMC Nephrol*. 2013;14(1):31–31.
26. Evans RG, Gardiner BS, Smith DW, O'Connor PM. Intrarenal oxygenation: unique challenges and the biophysical basis of homeostasis. *Am J Physiol Renal Physiol*. 2008;295(5):F1259–70.
27. Bonventre JVJ, Yang LL. Cellular pathophysiology of ischemic acute kidney injury. *J Clin Invest*. 2011;121(11):4210–4221.
28. Jang HR, Ko GJ, Wasowska BA, Rabb H. The interaction between ischemia-reperfusion and immune responses in the kidney. *J Mol Med*. 2009;87(9):859–864.
29. Wilhelm SMS, Simonson MSM, Robinson AVA, Stowe NTN, Schulak JAJ. Endothelin up-regulation and localization following renal ischemia and reperfusion. *Kidney Int*. 1999;55(3):1011–1018.
30. Knoll T et al. Therapeutic administration of an endothelin-A receptor antagonist after acute ischemic renal failure dose-dependently improves recovery of renal function. *J Cardiovasc Pharmacol*. 2001;37(4):483–488.
31. Henry CB, Duling BR. TNF-alpha increases entry of macromolecules into luminal endothelial cell glycocalyx. *Am J Physiol Heart Circ Physiol*. 2000;279(6):H2815–23.
32. Mulivor AW, Lipowsky HH. Inflammation- and ischemia-induced shedding of venular glycocalyx. *Am J Physiol Heart Circ Physiol*. 2004;286(5):H1672–H1680.
33. Suzuki J et al. Cytokine Secretion from Human Monocytes Potentiated by P-Selectin-Mediated Cell Adhesion. *Int Arch Allergy Immunol*. 2012;160(2):152–160.

34. Singbartl K, Green SA, Ley K. Blocking P-selectin protects from ischemia/reperfusion-induced acute renal failure. *FASEB J*. 1999;14(1):48–54.
35. Singbartl K, Ley K. Protection from ischemia-reperfusion induced severe acute renal failure by blocking E-selectin. *Crit Care Med*. 2000;28(7):2507–2514.
36. Karasawa K et al. Vascular-Resident CD169-Positive Monocytes and Macrophages Control Neutrophil Accumulation in the Kidney with Ischemia-Reperfusion Injury. *J Am Soc Nephrol*. 2015;26(4):896–906.
37. Sutton TA, Fisher CJ, Molitoris BA. Microvascular endothelial injury and dysfunction during ischemic acute renal failure. *Kidney Int*. 2002;62(5):1539–1549.
38. Sutton TA et al. Injury of the renal microvascular endothelium alters barrier function after ischemia. *Am J Physiol Renal Physiol*. 2003;285(2):F191–F198.
39. Herrler T et al. The intrinsic renal compartment syndrome: new perspectives in kidney transplantation. *Transplantation*. 2010;89(1):40–46.
40. Sutton TA et al. Minocycline reduces renal microvascular leakage in a rat model of ischemic renal injury. *Am J Physiol Renal Physiol*. 2005;288(1):F91–7.
41. Donnahoo KK et al. Early renal ischemia, with or without reperfusion, activates NFkappaB and increases TNF-alpha bioactivity in the kidney. *J Urol*. 2000;163(4):1328–1332.
42. Millar TM, Phan V, Tibbles LA. ROS generation in endothelial hypoxia and reoxygenation stimulates MAP kinase signaling and kinase-dependent neutrophil recruitment. *Free Radic Biol Med*. 2007;42(8):1165–1177.
43. Kim J, Jung KJ, Park KM. Reactive oxygen species differently regulate renal tubular epithelial and interstitial cell proliferation after ischemia and reperfusion injury. *Am J Physiol Renal Physiol*. 2010;298(5):F1118–F1129.
44. Anders H-J, Banas B, Schlöndorff D. Signaling danger: toll-like receptors and their potential roles in kidney disease. *J Am Soc Nephrol*. 2004;15(4):854–867.
45. Beg AA. Endogenous ligands of Toll-like receptors: implications for regulating inflammatory and immune responses. *Trends Immunol*. 2002;23(11):509–512.
46. Shigeoka AA et al. TLR2 is constitutively expressed within the kidney and participates in ischemic renal injury through both MyD88-dependent and -independent pathways. *J Immunol*. 2007;178(10):6252–6258.
47. Vallés PG, Lorenzo AG, Bocanegra V, Vallés R. Acute kidney injury: what part do toll-like receptors play? *Int J Nephrol Renovasc Dis*. 2014;7:241–251.
48. Wu H et al. TLR4 activation mediates kidney ischemia/reperfusion injury. *J Clin Invest*. 2007;117(10):2847–2859.
49. de Vries B et al. The mannose-binding lectin-pathway is involved in complement activation in the course of renal ischemia-reperfusion injury. *Am J Pathol*. 2004;165(5):1677–1688.

50. Thurman JM, Lucia MS, Ljubanovic D, Holers VM. Acute tubular necrosis is characterized by activation of the alternative pathway of complement. *Kidney Int.* 2005;67(2):524–530.
51. Peng Q et al. C3a and C5a promote renal ischemia-reperfusion injury. *J Am Soc Nephrol.* 2012;23(9):1474–1485.
52. Lieberthal W, Nigam SK. Acute renal failure. I. Relative importance of proximal vs. distal tubular injury. *Am J Physiol.* 1998;275(5 Pt 2):F623–31.
53. Zuk AA, Bonventre JVJ, Brown DD, Matlin KSK. Polarity, integrin, and extracellular matrix dynamics in the postischemic rat kidney. *Am J Physiol.* 1998;275(3):C711–C731.
54. Zuk A, Bonventre JV, Matlin KS. Expression of fibronectin splice variants in the postischemic rat kidney. *Am J Physiol Renal Physiol.* 2001;280(6):F1037–F1053.
55. Wangsiripaisan A, Gengaro PE, Edelstein CL, Schrier RW. Role of polymeric Tamm-Horsfall protein in cast formation: oligosaccharide and tubular fluid ions. *Kidney Int.* 2001;59(3):932–940.
56. Blantz RC, Deng A, Miracle CM, Thomson SC. Regulation of kidney function and metabolism: a question of supply and demand. *Trans Am Clin Climatol Assoc.* 2007;118:23–43.
57. Miura M, Fu X, Zhang QW, Remick DG, Fairchild RL. Neutralization of Gro alpha and macrophage inflammatory protein-2 attenuates renal ischemia/reperfusion injury. *Am J Pathol.* 2001;159(6):2137–2145.
58. Kinsey GR, Li L, Okusa MD. Inflammation in acute kidney injury. *Nephron Exp Nephrol.* 2007;109(4):e102–e107.
59. Awad AS et al. Compartmentalization of neutrophils in the kidney and lung following acute ischemic kidney injury. *Kidney Int.* 2009;75(7):689–698.
60. Li L et al. IL-17 produced by neutrophils regulates IFN-gamma-mediated neutrophil migration in mouse kidney ischemia-reperfusion injury. *J Clin Invest.* 2009;120(120(1)):331–342.
61. Vivier E, Tomasello E, Baratin M, Walzer T, Ugolini S. Functions of natural killer cells. *Nat Immunol.* 2008;9(5):503–510.
62. Kim HJ et al. TLR2 signaling in tubular epithelial cells regulates NK cell recruitment in kidney ischemia-reperfusion injury. *J Immunol.* 2013;191(5):2657–2664.
63. Zhang Z-X et al. NK cells induce apoptosis in tubular epithelial cells and contribute to renal ischemia-reperfusion injury. *J Immunol.* 2008;181(11):7489–7498.
64. Zhang Z-X et al. Osteopontin expressed in tubular epithelial cells regulates NK cell-mediated kidney ischemia reperfusion injury. *J Immunol.* 2010;185(2):967–973.
65. Kim HJ et al. Reverse signaling through the costimulatory ligand CD137L in epithelial cells is essential for natural killer cell-mediated acute tissue inflammation. *Proc Natl Acad Sci USA.* 2012;109(1):E13–E22.

66. Burne MJ et al. Identification of the CD4(+) T cell as a major pathogenic factor in ischemic acute renal failure. *J Clin Invest*. 2001;108(9):1283–1290.
67. Yokota N, Burne-Taney M, Racusen L, Rabb H. Contrasting roles for STAT4 and STAT6 signal transduction pathways in murine renal ischemia-reperfusion injury. *Am J Physiol Renal Physiol*. 2003;285(2):F319–F325.
68. Wang S et al. Decreased renal ischemia-reperfusion injury by IL-16 inactivation. *Kidney Int*. 2008;73(3):318–326.
69. Gandolfo MT et al. Foxp3+ regulatory T cells participate in repair of ischemic acute kidney injury. *Kidney Int*. 2009;76(7):717–729.
70. Kinsey GR et al. Regulatory T cells suppress innate immunity in kidney ischemia-reperfusion injury. *J Am Soc Nephrol*. 2009;20(8):1744–1753.
71. Ascon DBD et al. Phenotypic and functional characterization of kidney-infiltrating lymphocytes in renal ischemia reperfusion injury. *J Immunol*. 2006;177(5):3380–3387.
72. Li L et al. NKT cell activation mediates neutrophil IFN-gamma production and renal ischemia-reperfusion injury. *J Immunol*. 2007;178(9):5899–5911.
73. Soos TJ et al. CX3CR1+ interstitial dendritic cells form a contiguous network throughout the entire kidney. *Kidney Int*. 2006;70(3):591–596.
74. Rosin DL, Okusa MD. Dangers Within: DAMP Responses to Damage and Cell Death in Kidney Disease. *J Am Soc Nephrol*. 2011;22(3):416–425.
75. Coates PTH et al. In vivo-mobilized kidney dendritic cells are functionally immature, subvert alloreactive T-cell responses, and prolong organ allograft survival. *Transplantation*. 2004;77(7):1080–1089.
76. Li L et al. Dendritic cells tolerized with adenosine A2AR agonist attenuate acute kidney injury. *J Clin Invest*. 2012;122(11):3931–3942.
77. Dong X et al. Resident dendritic cells are the predominant TNF-secreting cell in early renal ischemia-reperfusion injury. *Kidney Int*. 2007;71(7):619–628.
78. Ferenbach D, Hughes J. Macrophages and dendritic cells: what is the difference? *Kidney Int*. 2008;74(1):5–7.
79. Hume DA. Macrophages as APC and the dendritic cell myth. *J Immunol*. 2008;181(9):5829–5835.
80. Geissmann F, Gordon S, Hume DA, Mowat AM, Randolph GJ. Unravelling mononuclear phagocyte heterogeneity. *Nat Rev Immunol*. 2010;10(6):453–460.
81. Bradford BM, Sester DP, Hume DA, Mabbott NA. Defining the anatomical localisation of subsets of the murine mononuclear phagocyte system using integrin alpha X (Itgax, CD11c) and colony stimulating factor 1 receptor (Csf1r, CD115) expression fails to discriminate dendritic cells from macrophages. *Immunobiology*. 2011;216(11):1228–1237.
82. Hume DA, Mabbott N, Raza S, Freeman TC. Can DCs be distinguished from macrophages

- by molecular signatures? *Nat Immunol*. 2013;14(3):187–189.
83. Rogers NM, Ferenbach DA, Isenberg JS, Thomson AW, Hughes J. Dendritic cells and macrophages in the kidney: a spectrum of good and evil. *Nat Rev Nephrol*. 2014;10(11):625–643.
84. van Furth R et al. The mononuclear phagocyte system: a new classification of macrophages, monocytes, and their precursor cells. *Bull World Health Organ*. 1972;46(6):845–852.
85. Takahashi K, Naito M. Development, differentiation, and proliferation of macrophages in the rat yolk sac. *Tissue Cell*. 1993;25(3):351–362.
86. Hume DA. The mononuclear phagocyte system. *Curr Opin Immunol*. 2006;18(1):49–53.
87. Lichanska AM et al. Differentiation of the mononuclear phagocyte system during mouse embryogenesis: the role of transcription factor PU.1. *Blood*. 1999;94(1):127–138.
88. Ovchinnikov DA. Macrophages in the embryo and beyond: Much more than just giant phagocytes. *Genesis*. 2008;46(9):447–462.
89. Takeya M, Takahashi K. Ontogenic development of macrophage subpopulations and Ia-positive dendritic cells in fetal and neonatal rat spleen. *J Leukoc Biol*. 1992;52(5):516–523.
90. Izumi S, Takeya M, Takagi K, Takahashi K. Ontogenetic development of synovial A cells in fetal and neonatal rat knee joints. *Cell Tissue Res*. 1990;262(1):1–8.
91. Henson PM, Hume DA. Apoptotic cell removal in development and tissue homeostasis. *Trends Immunol*. 2006;27(5):244–250.
92. Cohen PE, Chisholm O, Arceci RJ, Stanley ER, Pollard JW. Absence of colony-stimulating factor-1 in osteopetrotic (csfmop/csfmop) mice results in male fertility defects. *Biol Reprod*. 1996;55(2):310–317.
93. Dai X-M et al. Targeted disruption of the mouse colony-stimulating factor 1 receptor gene results in osteopetrosis, mononuclear phagocyte deficiency, increased primitive progenitor cell frequencies, and reproductive defects. *Blood*. 2002;99(1):111–120.
94. Michaelson MD et al. CSF-1 deficiency in mice results in abnormal brain development. *Development*. 1996;122(9):2661–2672.
95. van Nguyen A, Pollard JW. Colony stimulating factor-1 is required to recruit macrophages into the mammary gland to facilitate mammary ductal outgrowth. *Dev Biol*. 2002;247(1):11–25.
96. Banaei-Bouchareb L et al. Insulin cell mass is altered in Csf1op/Csf1op macrophage-deficient mice. *J Leukoc Biol*. 2004;76(2):359–367.
97. Shepard JL, Zon LI. Developmental derivation of embryonic and adult macrophages. *Curr Opin Hematol*. 2000;7(1):3–8.
98. Lichanska AM, Hume DA. Origins and functions of phagocytes in the embryo. *Exp Hematol*. 2000;28(6):601–611.

99. Mantovani A et al. The chemokine system in diverse forms of macrophage activation and polarization. *Trends Immunol.* 2004;25(12):677–686.
100. Martinez FO, Helming L, Gordon S. Alternative activation of macrophages: an immunologic functional perspective. *Annu Rev Immunol.* 2009;27:451–483.
101. Cassol E, Cassetta L, Rizzi C, Alfano M, Poli G. M1 and M2a polarization of human monocyte-derived macrophages inhibits HIV-1 replication by distinct mechanisms. *J Immunol.* 2009;182(10):6237–6246.
102. Verreck FAW et al. Human IL-23-producing type 1 macrophages promote but IL-10-producing type 2 macrophages subvert immunity to (myco)bacteria. *Proc Natl Acad Sci USA.* 2004;101(13):4560–4565.
103. MacMicking J, Xie QW, Nathan C. Nitric oxide and macrophage function. *Annu Rev Immunol.* 1997;15:323–350.
104. Nathan C, Shiloh MU. Reactive oxygen and nitrogen intermediates in the relationship between mammalian hosts and microbial pathogens. *Proc Natl Acad Sci USA.* 2000;97(16):8841–8848.
105. Kito T, Kuroda E, Yokota A, Yamashita U. Cytotoxicity in glioma cells due to interleukin-12 and interleukin-18-stimulated macrophages mediated by interferon-gamma-regulated nitric oxide. *J Neurosurg.* 2003;98(2):385–392.
106. Ricardo SD, van Goor H, Eddy AA. Macrophage diversity in renal injury and repair. *J Clin Invest.* 2008;118(11):3522–3530.
107. Martinez FO, Sica A, Mantovani A, Locati M. Macrophage activation and polarization. *Front Biosci.* 2008;13:453–461.
108. Watanabe K, Jose PJ, Rankin SM. Eotaxin-2 generation is differentially regulated by lipopolysaccharide and IL-4 in monocytes and macrophages. *J Immunol.* 2002;168(4):1911–1918.
109. Gratchev A et al. Alternatively activated macrophages differentially express fibronectin and its splice variants and the extracellular matrix protein beta1G-H3. *Scand J Immunol.* 2001;53(4):386–392.
110. Gibson MA, Kumaratilake JS, Cleary EG. Immunohistochemical and ultrastructural localization of MP78/70 (beta1g-h3) in extracellular matrix of developing and mature bovine tissues. *J Histochem Cytochem.* 1997;45(12):1683–1696.
111. Tsuboi R, Shi CM, Sato C, Cox GN, Ogawa H. Co-administration of insulin-like growth factor (IGF)-I and IGF-binding protein-1 stimulates wound healing in animal models. *J Invest Dermatol.* 1995;104(2):199–203.
112. Kratz G, Lake M, Gidlund M. Insulin like growth factor-1 and -2 and their role in the re-epithelialisation of wounds; interactions with insulin like growth factor binding protein type 1. *Scand J Plast Reconstr Surg Hand Surg.* 1994;28(2):107–112.
113. Elsner J, Escher SE, Forssmann U. Chemokine receptor antagonists: a novel therapeutic approach in allergic diseases. *Allergy.* 2004;59(12):1243–1258.

114. Gerber JS, Mosser DM. Reversing lipopolysaccharide toxicity by ligating the macrophage Fc gamma receptors. *J Immunol*. 2001;166(11):6861–6868.
115. Anderson CF, Mosser DM. Cutting edge: biasing immune responses by directing antigen to macrophage Fc gamma receptors. *J Immunol*. 2002;168(8):3697–3701.
116. Anderson CF, Mosser DM. A novel phenotype for an activated macrophage: the type 2 activated macrophage. *J Leukoc Biol*. 2002;72(1):101–106.
117. Sozzani S et al. Interleukin 10 increases CCR5 expression and HIV infection in human monocytes. *J Exp Med*. 1998;187(3):439–444.
118. Bleharski JR, Niazi KR, Sieling PA, Cheng G, Modlin RL. Signaling lymphocytic activation molecule is expressed on CD40 ligand-activated dendritic cells and directly augments production of inflammatory cytokines. *J Immunol*. 2001;167(6):3174–3181.
119. Punnonen J et al. Soluble and membrane-bound forms of signaling lymphocytic activation molecule (SLAM) induce proliferation and Ig synthesis by activated human B lymphocytes. *J Exp Med*. 1997;185(6):993–1004.
120. Mosser DM, Edwards JP. Exploring the full spectrum of macrophage activation. *Nat Rev Immunol*. 2008;8(12):958–969.
121. Rae F et al. Characterisation and trophic functions of murine embryonic macrophages based upon the use of a Csf1r-EGFP transgene reporter. *Dev Biol*. 2007;308(1):232–246.
122. Martinez FO, Gordon S, Locati M, Mantovani A. Transcriptional profiling of the human monocyte-to-macrophage differentiation and polarization: new molecules and patterns of gene expression. *J Immunol*. 2006;177(10):7303–7311.
123. Greaves DR, Gordon S. Macrophage-specific gene expression: current paradigms and future challenges. *Int J Hematol*. 2002;76(1):6–15.
124. Antonio Sica VB. Altered macrophage differentiation and immune dysfunction in tumor development. *J Clin Invest*. 2007;117(5):1155.
125. Lamagna C, Aurrand-Lions M, Imhof BA. Dual role of macrophages in tumor growth and angiogenesis. *J Leukoc Biol*. 2006;80(4):705–713.
126. Mantovani A, Sica A, Locati M. Macrophage polarization comes of age. *Immunity*. 2005;23(4):344–346.
127. Biswas SK et al. A distinct and unique transcriptional program expressed by tumor-associated macrophages (defective NF-kappaB and enhanced IRF-3/STAT1 activation). *Blood*. 2006;107(5):2112–2122.
128. Tsuda Y et al. Three Different Neutrophil Subsets Exhibited in Mice with Different Susceptibilities to Infection by Methicillin-Resistant Staphylococcus aureus. *Immunity*. 2004;21(2):215–226.
129. Gordon S, Taylor PR. Monocyte and macrophage heterogeneity. *Nat Rev Immunol*. 2005;5(12):953–964.

130. Kelly J, Khan AA, Yin J, Ferguson TA, Apte RS. Senescence regulates macrophage activation and angiogenic fate at sites of tissue injury in mice. *J Clin Invest*. 2007;117(11):3421–3426.
131. Luo Y et al. Targeting tumor-associated macrophages as a novel strategy against breast cancer. *J Clin Invest*. 2006;116(116(8)):2132–2141.
132. Gouon-Evans V, Lin EY, Pollard JW. Requirement of macrophages and eosinophils and their cytokines/chemokines for mammary gland development. *Breast Cancer Res*. 2002;4(4):155–164.
133. Roth P, Dominguez MG, Stanley ER. The effects of colony-stimulating factor-1 on the distribution of mononuclear phagocytes in the developing osteopetrotic mouse. *Blood*. 1998;91(10):3773–3783.
134. Humphreys BD, Bonventre JV. The contribution of adult stem cells to renal repair. *Nephrol Ther*. 2007;3(1):3–10.
135. Shikata K, Makino H. Role of macrophages in the pathogenesis of diabetic nephropathy. *Contributions to nephrology*. 2001;(134):46–54.
136. Huang XR et al. Mechanisms of T cell-induced glomerular injury in anti-glomerular basement membrane (GBM) glomerulonephritis in rats. *Clin Exp Immunol*. 1997;109(1):134–142.
137. Tesch GHG, Maifert SS, Schwarting AA, Rollins BJB, Kelley VRV. Monocyte chemoattractant protein 1-dependent leukocytic infiltrates are responsible for autoimmune disease in MRL-Fas(lpr) mice. *J Exp Med*. 1999;190(12):1813–1824.
138. Lange-Sperandio B, Cachat F, Thornhill BA, Chevalier RL. Selectins mediate macrophage infiltration in obstructive nephropathy in newborn mice. *Kidney Int*. 2002;61(2):516–524.
139. Khan S, Cleveland RP, Koch CJ, Schelling JR. Hypoxia induces renal tubular epithelial cell apoptosis in chronic renal disease. *Lab Invest*. 1999;79(9):1089–1099.
140. Kang DH et al. Impaired angiogenesis in the remnant kidney model: I. Potential role of vascular endothelial growth factor and thrombospondin-1. *J Am Soc Nephrol*. 2001;12(7):1434–1447.
141. Mori T et al. Mouse mesangial cells produce colony-stimulating factor-1 (CSF-1) and express the CSF-1 receptor. *J Immunol*. 1990;144(12):4697–4702.
142. Gerharz CD, Reinecke P, Schneider EM, Schmitz M. Secretion of GM-CSF and M-CSF by human renal cell carcinomas of different histologic types. *Urology*. 2001;
143. Isbel NM et al. Tubules are the major site of M-CSF production in experimental kidney disease: correlation with local macrophage proliferation. *Kidney Int*. 2001;60(2):614–625.
144. Isbel NM, Nikolic-Paterson DJ, Hill PA, Dowling J, Atkins RC. Local macrophage proliferation correlates with increased renal M-CSF expression in human glomerulonephritis. *Nephrol Dial Transplant*. 2001;16(8):1638–1647.

145. Lenda DM, Kikawada E, Stanley ER, Kelley VR. Reduced macrophage recruitment, proliferation, and activation in colony-stimulating factor-1-deficient mice results in decreased tubular apoptosis during renal inflammation. *J Immunol*. 2003;170(6):3254–3262.
146. Le Meur Y et al. Serum levels of macrophage-colony stimulating factor (M-CSF): a marker of kidney allograft rejection. *Nephrol Dial Transplant*. 2004;19(7):1862–1865.
147. Jose MD, Le Meur Y, Atkins RC, Chadban SJ. Blockade of macrophage colony-stimulating factor reduces macrophage proliferation and accumulation in renal allograft rejection. *Am J Transplant*. 2003;3(3):294–300.
148. Menke J et al. CSF-1 signals directly to renal tubular epithelial cells to mediate repair in mice. *J Clin Invest*. 2009;119(8):2330–2342.
149. Nguyen D et al. Macrophage accumulation in human progressive diabetic nephropathy. *Nephrology (Carlton, Vic)*. 2006;11(3):226–231.
150. Lim AKH et al. Antibody blockade of c-fms suppresses the progression of inflammation and injury in early diabetic nephropathy in obese db/db mice. *Diabetologia*. 2009;52(8):1669–1679.
151. Naito T et al. Macrophage growth factors introduced into the kidney initiate renal injury. *Mol Med*. 1996;2(3):297–312.
152. Pull SL, Doherty JM, Mills JC, Gordon JI, Stappenbeck TS. Activated macrophages are an adaptive element of the colonic epithelial progenitor niche necessary for regenerative responses to injury. *Proc Natl Acad Sci USA*. 2005;102(1):99–104.
153. Rice EK et al. Macrophage accumulation and renal fibrosis are independent of macrophage migration inhibitory factor in mouse obstructive nephropathy. *Nephrology (Carlton, Vic)*. 2004;9(5):278–287.
154. Ophascharoensuk V et al. Obstructive uropathy in the mouse: role of osteopontin in interstitial fibrosis and apoptosis. *Kidney Int*. 1999;56(2):571–580.
155. Nony PA, Schnellmann RG. Mechanisms of renal cell repair and regeneration after acute renal failure. *J Pharmacol Exp Ther*. 2003;304(3):905–912.
156. Jo S-K, Sung S-A, Cho W-Y, Go K-J, Kim H-K. Macrophages contribute to the initiation of ischaemic acute renal failure in rats. *Nephrol Dial Transplant*. 2006;21(5):1231–1239.
157. Otero K et al. Macrophage colony-stimulating factor induces the proliferation and survival of macrophages via a pathway involving DAP12 and beta-catenin. *Nat Immunol*. 2009;10(7):734–743.
158. Aharinejad S et al. CSF-1 treatment promotes angiogenesis in the metaphysis of osteopetrotic (toothless, tl) rats. *Bone*. 1995;16(3):315–324.
159. Eubank TD, Galloway M, Montague CM, Waldman WJ, Marsh CB. M-CSF induces vascular endothelial growth factor production and angiogenic activity from human monocytes. *J Immunol*. 2003;171(5):2637–2643.

160. Johnson C, Sung H-J, Lessner SM, Fini ME, Galis ZS. Matrix metalloproteinase-9 is required for adequate angiogenic revascularization of ischemic tissues: potential role in capillary branching. *Circ Res*. 2004;94(2):262–268.
161. Lin EY, Nguyen AV, Russell RG, Pollard JW. Colony-stimulating factor 1 promotes progression of mammary tumors to malignancy. *J Exp Med*. 2001;193(6):727–740.
162. Aharinejad S et al. Colony-stimulating factor-1 blockade by antisense oligonucleotides and small interfering RNAs suppresses growth of human mammary tumor xenografts in mice. *Cancer Res*. 2004;64(15):5378–5384.
163. Paulus P, Stanley ER, Schäfer R, Abraham D, Aharinejad S. Colony-stimulating factor-1 antibody reverses chemoresistance in human MCF-7 breast cancer xenografts. *Cancer Res*. 2006;66(8):4349–4356.
164. Zeisberger SM et al. Clodronate-liposome-mediated depletion of tumour-associated macrophages: a new and highly effective antiangiogenic therapy approach. *Br J Cancer*. 2006;95(3):272–281.
165. Kubota Y et al. M-CSF inhibition selectively targets pathological angiogenesis and lymphangiogenesis. *J Exp Med*. 2009;206(5):1089–1102.
166. Murphy G et al. Assessment of the role of the fibronectin-like domain of gelatinase A by analysis of a deletion mutant. *J Biol Chem*. 1994;269(9):6632–6636.
167. Ashworth JL et al. Fibrillin degradation by matrix metalloproteinases: implications for connective tissue remodelling. *Biochem J*. 1999;340 ( Pt 1):171–181.
168. Sternlicht MD, Werb Z. How matrix metalloproteinases regulate cell behavior. *Annu Rev Cell Dev Biol*. 2001;17:463–516.
169. Somerville RPT, Oblander SA, Apte SS. Matrix metalloproteinases: old dogs with new tricks. *Genome Biol*. 2003;4(6):216.
170. Allen AR et al. Endothelial expression of VCAM-1 in experimental crescentic nephritis and effect of antibodies to very late antigen-4 or VCAM-1 on glomerular injury. *J Immunol*. 1999;162(9):5519–5527.
171. Erwig L-P, Kluth DC, Rees AJ. Macrophages in renal inflammation. *Curr Opin Nephrol Hypertens*. 2001;10(3):341–347.
172. Rao VH et al. Role for macrophage metalloelastase in glomerular basement membrane damage associated with alport syndrome. *Am J Pathol*. 2006;169(1):32–46.
173. Yokoo T et al. Prophylaxis of antibody-induced acute glomerulonephritis with genetically modified bone marrow-derived vehicle cells. *Hum Gene Ther*. 1999;10(16):2673–2678.
174. Yang J et al. Targeting of macrophage activity by adenovirus-mediated intragraft overexpression of TNFRp55-Ig, IL-12p40, and vIL-10 ameliorates adenovirus-mediated chronic graft injury, whereas stimulation of macrophages by overexpression of IFN-gamma accelerates chronic graft injury in a rat renal allograft model. *J Am Soc Nephrol*. 2003;14(1):214–225.

175. Nishida M et al. Adoptive transfer of macrophages ameliorates renal fibrosis in mice. *Biochem Biophys Res Commun.* 2005;332(1):11–16.
176. Munger KA et al. Transfection of rat kidney with human 15-lipoxygenase suppresses inflammation and preserves function in experimental glomerulonephritis. *Proc Natl Acad Sci USA.* 1999;96(23):13375–13380.
177. Kluth DC et al. Macrophages transfected with adenovirus to express IL-4 reduce inflammation in experimental glomerulonephritis. *J Immunol.* 2001;166(7):4728–4736.
178. Wilson H. Bone-Marrow-Derived Macrophages Genetically Modified to Produce IL-10 Reduce Injury in Experimental Glomerulonephritis. *Mol Ther.* 2002;6(6):710–717.
179. Wilson HM et al. Inhibition of Macrophage Nuclear Factor- $\kappa$ B Leads to a Dominant Anti-Inflammatory Phenotype that Attenuates Glomerular Inflammation in Vivo. *Am J Pathol.* 2005;167(1):27–37.
180. Yokoo T et al. Genetically modified bone marrow continuously supplies anti-inflammatory cells and suppresses renal injury in mouse Goodpasture syndrome. *Blood.* 2001;98(1):57–64.
181. Wang Y et al. Ex vivo programmed macrophages ameliorate experimental chronic inflammatory renal disease. *Kidney Int.* 2007;72(3):290–299.
182. Alikhan MA et al. Colony-stimulating factor-1 promotes kidney growth and repair via alteration of macrophage responses. *Am J Pathol.* 2011;179(3):1243–1256.
183. Cook AD et al. Granulocyte-macrophage colony-stimulating factor is a key mediator in inflammatory and arthritic pain. *Ann Rheum Dis.* 2013;72(2):265–270.
184. Cook AD et al. Granulocyte-macrophage colony-stimulating factor is a key mediator in experimental osteoarthritis pain and disease development. *Arthritis Res Ther.* 2012;14(5):R199.
185. Vlahos R et al. Neutralizing granulocyte/macrophage colony-stimulating factor inhibits cigarette smoke-induced lung inflammation. *Am J Respir Crit Care Med.* 2010;182(1):34–40.
186. Verreck FAW, de Boer T, Langenberg DML, van der Zanden L, Ottenhoff THM. Phenotypic and functional profiling of human proinflammatory type-1 and anti-inflammatory type-2 macrophages in response to microbial antigens and IFN-gamma- and CD40L-mediated costimulation. *J Leukoc Biol.* 2006;79(2):285–293.
187. Fleetwood AJ, Lawrence T, Hamilton JA, Cook AD. Granulocyte-macrophage colony-stimulating factor (CSF) and macrophage CSF-dependent macrophage phenotypes display differences in cytokine profiles and transcription factor activities: implications for CSF blockade in inflammation. *J Immunol.* 2007;178(8):5245–5252.
188. Duffield JS. Macrophages and immunologic inflammation of the kidney. *Semin Nephrol.* 2010;30(3):234–254.
189. Chow F, Ozols E, Nikolic-Paterson DJ, Atkins RC, Tesch GH. Macrophages in mouse type 2 diabetic nephropathy: correlation with diabetic state and progressive renal injury. *Kidney Int.* 2004;65(1):116–128.

190. Ricardo SD, van Goor H, Eddy AA. Macrophage diversity in renal injury and repair. *J Clin Invest*. 2008;118(11):3522–3530.
191. Williams TM, Little MH, Ricardo SD. Macrophages in Renal Development, Injury, and Repair. *Semin Nephrol*. 2010;30(3):255–267.
192. Chattopadhyay PK, Roederer M. Cytometry: Today's technology and tomorrow's horizons. *Methods*. 2012;57(3):251–258.
193. Lee S et al. Distinct macrophage phenotypes contribute to kidney injury and repair. *J Am Soc Nephrol*. 2011;22(2):317–326.
194. Austyn JM, Gordon SS. F4/80, a monoclonal antibody directed specifically against the mouse macrophage. *Eur J Immunol*. 1981;11(10):805–815.
195. Taylor PRP, Brown GDG, Geldhof ABA, Martinez-Pomares LL, Gordon SS. Pattern recognition receptors and differentiation antigens define murine myeloid cell heterogeneity *ex vivo*. *Eur J Immunol*. 2003;33(8):2090–2097.
196. Mitchell AJ et al. Technical advance: autofluorescence as a tool for myeloid cell analysis. *J Leukoc Biol*. 2010;88(3):597–603.
197. Nonaka K et al. Skewing the Th cell phenotype toward Th1 alters the maturation of tumor-infiltrating mononuclear phagocytes. *J Leukoc Biol*. 2008;84(3):679–688.
198. Stables MJ et al. Transcriptomic analyses of murine resolution-phase macrophages. *Blood*. 2011;118(26):e192–208.
199. Sunderkötter C et al. Subpopulations of mouse blood monocytes differ in maturation stage and inflammatory response. *J Immunol*. 2004;172(7):4410–4417.
200. Lin SL, Castaño AP, Nowlin BT, Lupper ML, Duffield JS. Bone marrow Ly6Chigh monocytes are selectively recruited to injured kidney and differentiate into functionally distinct populations. *J Immunol*. 2009;183(10):6733–6743.
201. Fleming TJJ, Fleming MLM, Malek TRT. Selective expression of Ly-6G on myeloid lineage cells in mouse bone marrow. RB6-8C5 mAb to granulocyte-differentiation antigen (Gr-1) detects members of the Ly-6 family. *J Immunol*. 1993;151(5):2399–2408.
202. Rose S, Misharin A, Perlman H. A novel Ly6C/Ly6G-based strategy to analyze the mouse splenic myeloid compartment. *Cytometry A*. 2012;81(4):343–350.
203. Geissmann F, Jung S, Littman DR. Blood monocytes consist of two principal subsets with distinct migratory properties. *Immunity*. 2003;19(1):71–82.
204. Li L et al. The chemokine receptors CCR2 and CX3CR1 mediate monocyte/macrophage trafficking in kidney ischemia-reperfusion injury. *Kidney Int*. 2008;74(12):1526–1537.
205. Tacke F, Randolph GJ. Migratory fate and differentiation of blood monocyte subsets. *Immunobiology*. 2006;211(6-8):609–618.
206. Gordon S. Alternative activation of macrophages. *Nat Rev Immunol*. 2003;3(1):23–35.

207. Kushiya T et al. Alteration in the phenotype of macrophages in the repair of renal interstitial fibrosis in mice. *Nephrology (Carlton, Vic)*. 2011;16(5):522–535.
208. Lopez-Guisa JM et al. Mannose Receptor 2 Attenuates Renal Fibrosis. *J Am Soc Nephrol*. 2012;23(2):236–251.
209. Martinez-Pomares LL et al. Analysis of mannose receptor regulation by IL-4, IL-10, and proteolytic processing using novel monoclonal antibodies. *J Leukoc Biol*. 2003;73(5):604–613.
210. Perfetto SP, Chattopadhyay PK, Roederer M. Seventeen-colour flow cytometry: unravelling the immune system. *Nat Rev Immunol*. 2004;4(8):648–655.
211. Ryckwaert F, Boccara G, Frappier J-M, Colson PH. Incidence, risk factors, and prognosis of a moderate increase in plasma creatinine early after cardiac surgery. *Crit Care Med*. 2002;30(7):1495–1498.
212. Rosner MH, Okusa MD. Acute kidney injury associated with cardiac surgery. *Clin J Am Soc Nephrol*. 2006;1(1):19–32.
213. Yoo Y-C, Shim J-K, Song Y, Yang S-Y, Kwak Y-L. Anesthetics influence the incidence of acute kidney injury following valvular heart surgery. *Kidney Int*. 2014;86(2):414–422.
214. Ryckwaert F, Alric P, Picot M-C, Djoufelkit K, Colson P. Incidence and circumstances of serum creatinine increase after abdominal aortic surgery. *Intensive Care Med*. 2003;29(10):1821–1824.
215. Hattori R et al. Direct visualization of cortical peritubular capillary of transplanted human kidney with reperfusion injury using a magnifying endoscopy. *Transplantation*. 2005;79(9):1190–1194.
216. Schmitz V, Schaser KD, Olschewski P, Neuhaus P, Puhl G. In vivo Visualization of Early Microcirculatory Changes following Ischemia/Reperfusion Injury in Human Kidney Transplantation. *Eur Surg Res*. 2008;40(1):19–25.
217. Heyman SN, Rosen S, Rosenberger C. Renal parenchymal hypoxia, hypoxia adaptation, and the pathogenesis of radiocontrast nephropathy. *Clin J Am Soc Nephrol*. 2007;3(1):288–296.
218. Rosenberger C, Rosen S, Heyman SN. Renal parenchymal oxygenation and hypoxia adaptation in acute kidney injury. *Clin Exp Pharmacol Physiol*. 2006;33(10):980–988.
219. Xu W, Zhao X, Daha MR, van Kooten C. Reversible differentiation of pro- and anti-inflammatory macrophages. *Mol Immunol*. 2013;53(3):179–186.
220. Sierra-Filardi E, Vega MA, Sánchez-Mateos P, Corbí AL, Puig-Kröger A. Heme Oxygenase-1 expression in M-CSF-polarized M2 macrophages contributes to LPS-induced IL-10 release. *Immunobiology*. 2010;215(9-10):788–795.
221. Mia S, Warnecke A, Zhang X-M, Malmström V, Harris RA. An optimized protocol for human M2 macrophages using M-CSF and IL-4/IL-10/TGF- $\beta$  yields a dominant immunosuppressive phenotype. *Scand J Immunol*. 2014;79(5):305–314.

222. Jaguin M, Houlbert N, Fardel O, Lecreur V. Polarization profiles of human M-CSF-generated macrophages and comparison of M1-markers in classically activated macrophages from GM-CSF and M-CSF origin. *Cell Immunol.* 2013;281(1):51–61.
223. Soehnlein O, Lindbom L. Phagocyte partnership during the onset and resolution of inflammation. *Nat Rev Immunol.* 2010;10(6):427–439.
224. Dean RA et al. Macrophage-specific metalloelastase (MMP-12) truncates and inactivates ELR+ CXC chemokines and generates CCL2, -7, -8, and -13 antagonists: potential role of the macrophage in terminating polymorphonuclear leukocyte influx. *Blood.* 2008;112(8):3455–3464.
225. van den Berg JM, Weyer S, Weening JJ, Roos D, Kuijpers TW. Divergent effects of tumor necrosis factor alpha on apoptosis of human neutrophils. *J Leukoc Biol.* 2001;69(3):467–473.
226. Freire-de-Lima CG et al. Apoptotic cells, through transforming growth factor-beta, coordinately induce anti-inflammatory and suppress pro-inflammatory eicosanoid and NO synthesis in murine macrophages. *J Biol Chem.* 2006;281(50):38376–38384.
227. Williams TM, Wise AF, Alikhan MA, Layton DS, Ricardo SD. Establishing the flow cytometric assessment of myeloid cells in kidney ischemia/reperfusion injury. *Cytometry A.* 2014;85(3):256–267.
228. Brøchner AC, Dagnaes-Hansen F, Højberg-Holm J, Toft P. The inflammatory response in blood and in remote organs following acute kidney injury. *APMIS.* 2014;122(5):399–404.
229. Jang H-S et al. Bone marrow-derived cells play a major role in kidney fibrosis via proliferation and differentiation in the infiltrated site. *Biochim Biophys Acta.* 2013;1832(6):817–825.
230. Jang H-S, Kim JI, Han SJ, Park KM. Recruitment and subsequent proliferation of bone marrow-derived cells in the postischemic kidney are important to the progression of fibrosis. *Am J Physiol Renal Physiol.* 2014;306(12):F1451–61.
231. Crane MJ et al. The monocyte to macrophage transition in the murine sterile wound. *PLoS ONE.* 2013;9(1):e86660–e86660.
232. Jakubzick C et al. Minimal differentiation of classical monocytes as they survey steady-state tissues and transport antigen to lymph nodes. *Immunity.* 2013;39(3):599–610.
233. Jenkins SJ, Hume DA. Homeostasis in the mononuclear phagocyte system. *Trends Immunol.* 2014;35(8):358–367.
234. Drutman SB, Kendall JC, Trombetta ES. Inflammatory spleen monocytes can upregulate CD11c expression without converting into dendritic cells. *J Immunol.* 2012;188(8):3603–3610.
235. Trzpis M et al. Expression of EpCAM is up-regulated during regeneration of renal epithelia. *J Pathol.* 2008;216(2):201–208.
236. Liu L et al. Immunohistochemical analysis of chromophobe renal cell carcinoma, renal oncocytoma, and clear cell carcinoma: an optimal and practical panel for differential

- diagnosis. *Arch Pathol Lab Med*. 2007;131(8):1290–1297.
237. Breuhahn K et al. Expression of epithelial cellular adhesion molecule (Ep-CAM) in chronic (necro-)inflammatory liver diseases and hepatocellular carcinoma. *Hepatol Res*. 2005;34(1):7–7.
238. Münz M et al. The carcinoma-associated antigen EpCAM upregulates c-myc and induces cell proliferation. *Oncogene*. 2004;23(34):5748–5758.
239. Du W et al. EpCAM: a potential antimetastatic target for gastric cancer. *Dig Dis Sci*. 2010;55(8):2165–2171.
240. Ranganathan PV, Jayakumar C, Mohamed R, Dong Z, Ramesh G. Netrin-1 regulates the inflammatory response of neutrophils and macrophages, and suppresses ischemic acute kidney injury by inhibiting COX-2-mediated PGE2 production. *Kidney Int*. 2013;83(6):1087–1098.
241. Fukuzawa N et al. High renal ischemia temperature increases neutrophil chemoattractant production and tissue injury during reperfusion without an identifiable role for CD4 T cells in the injury. *Transpl Immunol*. 2009;22(1-2):62–71.
242. Garcia-Cenador MB et al. Cardiotrophin-1 administration protects from ischemia-reperfusion renal injury and inflammation. *Transplantation*. 2013;96(12):1034–1042.
243. Chaturvedi S et al. Slit2 prevents neutrophil recruitment and renal ischemia-reperfusion injury. *J Am Soc Nephrol*. 2013;24(8):1274–1287.
244. Ysebaert DKD et al. T cells as mediators in renal ischemia/reperfusion injury. *Kidney Int*. 2004;66(2):491–496.
245. Burne-Taney MJM et al. B cell deficiency confers protection from renal ischemia reperfusion injury. *J Immunol*. 2003;171(6):3210–3215.
246. Renner B et al. B cell subsets contribute to renal injury and renal protection after ischemia/reperfusion. *J Immunol*. 2010;185(7):4393–4400.
247. Ojo AO, Wolfe RA, Held PJ, Port FK, Schmouder RL. Delayed graft function: risk factors and implications for renal allograft survival. *Transplantation*. 1997;63(7):968–974.
248. Tullius SG et al. Contribution of prolonged ischemia and donor age to chronic renal allograft dysfunction. *J Am Soc Nephrol*. 2000;11(7):1317–1324.
249. Ponticelli C. Ischaemia-reperfusion injury: a major protagonist in kidney transplantation. *Nephrol Dial Transplant*. 2014;29(6):1134–1140.
250. Takagi T et al. Predictors for postoperative renal function after open partial nephrectomy: including postoperative biomarkers. *Int J Urol*. 2012;19(9):823–828.
251. Thompson RH et al. Every Minute Counts When the Renal Hilum Is Clamped During Partial Nephrectomy. *Eur Urol*. 2009;58(3):340–345.
252. Huang J et al. Effect of remote ischaemic preconditioning on renal protection in patients undergoing laparoscopic partial nephrectomy: a “blinded” randomised controlled

trial. *BJU Int.* 2013;112(1):74–80.

253. Ranucci M et al. Oxygen delivery during cardiopulmonary bypass and acute renal failure after coronary operations. *Ann Thorac Surg.* 2005;80(6):2213–2220.

254. Brunelli SM et al. Preoperative statin use and postoperative acute kidney injury. *Am J Med.* 2012;125(12):1195–1204.e3.

255. Macedo E, Castro I, Yu L, Abdulkader RRC, Vieira JM Jr. Impact of Mild Acute Kidney Injury (AKI) on Outcome after Open Repair of Aortic Aneurysms. *Ren Fail.* 2008;30(3):287–296.

256. Ellenberger C et al. Incidence, risk factors and prognosis of changes in serum creatinine early after aortic abdominal surgery. *Intensive Care Med.* 2006;32(11):1808–1816.

257. Ferenbach DA et al. Macrophage/monocyte depletion by clodronate, but not diphtheria toxin, improves renal ischemia/reperfusion injury in mice. *Kidney Int.* 2012;82(8):928–933.

258. Lu L et al. Depletion of Macrophages and Dendritic Cells in Ischemic Acute Kidney Injury. *Am J Nephrol.* 2012;35(2):181–190.

259. Stanley ER, Chitu V. CSF-1 receptor signaling in myeloid cells. *Cold Spring Harb Perspect Biol.* 2014;6(6):1–21.

260. Hamilton JA. Colony-stimulating factors in inflammation and autoimmunity. *Nat Rev Immunol.* 2008;8(7):533–544.

261. Paniagua RT et al. c-Fms-mediated differentiation and priming of monocyte lineage cells play a central role in autoimmune arthritis. *Arthritis Res Ther.* 2010;12(1):R32.

262. Menke J et al. Colony-stimulating factor-1: a potential biomarker for lupus nephritis. *J Am Soc Nephrol.* 2015;26(2):379–389.

263. Zhu S-NS, Chen MM, Jongstra-Bilen JJ, Cybulsky MIM. GM-CSF regulates intimal cell proliferation in nascent atherosclerotic lesions. *CORD Conference Proceedings.* 2009;206(10):2141–2149.

264. Zahran N et al. Neutrophil apoptosis: impact of granulocyte macrophage colony stimulating factor on cell survival and viability in chronic kidney disease and hemodialysis patients. *Arch Med Sci.* 2013;9(6):984–989.

265. McQualter JL et al. Granulocyte macrophage colony-stimulating factor: a new putative therapeutic target in multiple sclerosis. *J Exp Med.* 2001;194(7):873–882.

266. Puljic R et al. Lipopolysaccharide-induced lung inflammation is inhibited by neutralization of GM-CSF. *Eur J Pharmacol.* 2007;557(2-3):230–235.

267. Greven DEA et al. Preclinical characterisation of the GM-CSF receptor as a therapeutic target in rheumatoid arthritis. *Ann Rheum Dis.* [published online ahead of print: June 16, 2014]; doi:10.1136/annrheumdis-2014-205234

268. Dumont NA, Frenette J. Macrophage colony-stimulating factor-induced macrophage differentiation promotes regrowth in atrophied skeletal muscles and C2C12 myotubes. *Am J*

*Pathol.* 2013;182(2):505–515.

269. Lacey DCD et al. Defining GM-CSF- and Macrophage-CSF-Dependent Macrophage Responses by In Vitro Models. *J Immunol.* 2012;188(11):5752–5765.

270. Kitching AR et al. The requirement for granulocyte-macrophage colony-stimulating factor and granulocyte colony-stimulating factor in leukocyte-mediated immune glomerular injury. *J Am Soc Nephrol.* 2002;13(2):350–358.

271. Han Y, Ma FY, Tesch GH, Manthey CL, Nikolic-Paterson DJ. c-fms blockade reverses glomerular macrophage infiltration and halts development of crescentic anti-GBM glomerulonephritis in the rat. *Lab Invest.* 2011;91(7):978–991.

272. Samuel CS, Butkus A, Coghlan JP, Bateman JF. The effect of relaxin on collagen metabolism in the nonpregnant rat pubic symphysis: the influence of estrogen and progesterone in regulating relaxin activity. *Endocrinology.* 1996;137(9):3884–3890.

273. Samuel CS. Determination of collagen content, concentration, and sub-types in kidney tissue. *Methods Mol Biol.* 2008;466:223–235.

274. Lenzo JC et al. Control of macrophage lineage populations by CSF-1 receptor and GM-CSF in homeostasis and inflammation. *Immunol Cell Biol.* 2012;90(4):429–440.

275. Lieschke GJ et al. Mice lacking granulocyte colony-stimulating factor have chronic neutropenia, granulocyte and macrophage progenitor cell deficiency, and impaired neutrophil mobilization. *Blood.* 1994;84(6):1737–1746.

276. Jiang D, Schwarz H. Regulation of granulocyte and macrophage populations of murine bone marrow cells by G-CSF and CD137 protein. *PLoS ONE.* 2009;5(12):e15565.

277. Oh D-J et al. Fractalkine receptor (CX3CR1) inhibition is protective against ischemic acute renal failure in mice. *Am J Physiol Renal Physiol.* 2008;294(1):F264–71.

278. Day Y-J et al. Renal ischemia-reperfusion injury and adenosine 2A receptor-mediated tissue protection: the role of CD4+ T cells and IFN-gamma. *J Immunol.* 2006;176(5):3108–3114.

279. He Z et al. Macrophages are not the source of injurious interleukin-18 in ischemic acute kidney injury in mice. *Am J Physiol Renal Physiol.* 2009;296(3):F535–F542.

280. Vinuesa E et al. Macrophage involvement in the kidney repair phase after ischaemia/reperfusion injury. *J Pathol.* 2007;214(1):104–113.

281. Menke J et al. Circulating CSF-1 promotes monocyte and macrophage phenotypes that enhance lupus nephritis. *J Am Soc Nephrol.* 2009;20(12):2581–2592.

282. Huen SC et al. GM-CSF Promotes Macrophage Alternative Activation after Renal Ischemia/Reperfusion Injury. *J Am Soc Nephrol.* [published online ahead of print: November 11, 2014]; doi:10.1681/ASN.2014060612

283. Ivashkiv LB. Epigenetic regulation of macrophage polarization and function. *Trends Immunol.* 2013;34(5):216–223.

284. Natoli G. Maintaining Cell Identity through Global Control of Genomic Organization. *Immunity*. 2010;33(1):12–24.

285. Nicodeme E et al. Suppression of inflammation by a synthetic histone mimic. *Nature*. 2010;468(7327):1119–1123.

286. Martinez FO, Gordon S. The M1 and M2 paradigm of macrophage activation: time for reassessment. *F1000Prime Rep*. 2013;6:13.

# APPENDICES

---

# Macrophages in Renal Development, Injury, and Repair

Timothy M. Williams, BBiomed Sci (Hons),\* Melissa H. Little, PhD,<sup>†</sup> and Sharon D. Ricardo, PhD\*

---

**Summary:** Macrophages have long been regarded as classic mediators of innate immunity because of their production of proinflammatory cytokines and their ability to induce apoptotic cell death. As a result of such activities and the detrimental long-term effect of kidney inflammation, macrophages principally have been regarded as mediators of glomerular damage, tubular cell death, and the downstream fibrotic events leading to chronic kidney disease. Although this has been the accepted consequence of macrophage infiltration in kidney disease, macrophages also play a critical role in normal organ development, cell turnover, and recovery from injury in many organs, including the kidney. There is also a growing awareness that there is considerable heterogeneity of phenotype and function within the macrophage population and that a greater understanding of these different states of activation may result in the development of therapies specifically designed to capitalize on this variation in phenotype and cellular responses. In this review, we discuss the current understanding of induction and consequences of classic versus alternative macrophage activation and highlight what additional therapeutic options this may provide for the management of both acute and chronic kidney disease as well as renal cancer.

Semin Nephrol 30:255-267 © 2010 Elsevier Inc. All rights reserved.

**Keywords:** *Macrophage, kidney development, innate immunity, classic activation, alternative activation, chemokines, CSF-1*

---

In all vertebrates, macrophages are the first leukocytes to appear in the embryo. During postnatal and adult life they differentiate from hematopoietic precursor cells, a process that occurs exclusively in the bone marrow.<sup>1</sup> In contrast, during early mammalian development primitive fetal macrophages appear to differentiate from a different cell origin independent of the blood monocyte.<sup>2-4</sup> Macrophages in the embryo serve as specialized phagocytic cells.<sup>5</sup> They are formed in the yolk sac and then mi-

grate through the mesenchyme to invade the tissues of the embryo proper. With formation of the primitive vasculature, fetal macrophages migrate from the yolk sac into the liver. Fetal macrophages also proliferate and differentiate locally within tissues before forming tissue-specific macrophages.<sup>6,7</sup> Macrophages are essential during embryogenesis and play an important role in programmed cell death and tissue remodeling during organogenesis.<sup>5,8</sup> The production of both liver and bone marrow-derived macrophages is controlled by the growth factor colony stimulating factor (CSF)-1, also termed *macrophage colony stimulating factor*. CSF-1 binds to the CSF-1 receptor (CSF-1R) and genetic deletion of either of these genes in mice results in marked depletion of tissue macrophages.<sup>9,10</sup> The CSF-1-deficient *op/op* mouse (CSF-1<sup>op</sup>/CSF-1<sup>op</sup>) has revealed the importance of macrophages in the development of many organs, especially the bone, brain, and endocrine systems. In the brain, neuroepithelial cell

---

\*Monash Immunology and Stem Cell Laboratories, Monash University, Clayton, Victoria, Australia.

<sup>†</sup>Institute for Molecular Bioscience, The University of Queensland, St Lucia, Queensland, Australia.

This study was supported by an Australian Stem Cell Centre and Monash University Joint Scholarship Scheme (T.W.); Dr Little is a Principal Research Fellow of the National Health and Medical Research Council; the research of the authors was supported by the Australian Stem Cell Centre. Address reprint requests to Assistant Professor Sharon D. Ricardo, Monash Immunology and Stem Cell Laboratories, Monash University, Building 75, STRIP 1, Clayton, Victoria 3800, Australia. E: [REDACTED]

0270-9295/ - see front matter

© 2010 Elsevier Inc. All rights reserved. doi:10.1016/j.semnephrol.2010.03.011

growth requires macrophages.<sup>11</sup> Macrophages also are required for the normal development of the pancreas and mammary gland.<sup>12,13</sup> Indeed, embryonic macrophage populations exist within almost all developing organs and adopt highly specific locations, phenotypes, and functions. In developed organs, the Kupffer cells of the liver, Langerhans cells of the skin, osteoclasts in the bone, and microglia in the brain all represent highly specialized resident macrophage populations.<sup>3</sup>

Once permanent or definitive hematopoiesis is established with increased gestation, the proliferative capacity of the macrophage declines and a distinct set of phagocytes, the monocyte-macrophages, are formed.<sup>4,14,15</sup> In the adult, macrophages are involved in inflammation and immune surveillance. However, the heterogeneity and cellular plasticity of macrophage populations with their ability to change phenotype in response to local stimuli allows these cells to be highly specialized and display a wide and apparently opposing range of functions. Indeed, there is strong evidence that subpopulations of macrophages directly contribute to wound healing and tissue repair, supporting the concept that some macrophage phenotypes can promote organ regeneration after injury. However, this ability to change phenotype and function makes categorizing macrophage populations relatively difficult.

### CLASSIC VERSUS ALTERNATIVE ACTIVATION STATES

Evidence supports the notion of two key macrophage polarization states described as M1 “classically activated” proinflammatory macrophages, and M2 “alternatively activated” immune regulatory macrophages<sup>16,17</sup> (Fig. 1). In general, these two phenotypic states are somewhat comparable with the opposing Th1 and Th2 cells. A key factor driving M1 polarization and activation is interferon- $\gamma$  (IFN- $\gamma$ ), derived from CD4<sup>+</sup> Th1 cells, CD8<sup>+</sup> cytotoxic T cells, and natural killer cells, either working alone or in conjunction with lipopolysaccharides (LPS), tumor necrosis factor- $\alpha$  (TNF- $\alpha$ ), and other microbial products.<sup>18</sup> Culture of human CD14<sup>+</sup> monocytes in the presence of granulocyte macrophage CSF also induces M1 polarization. M1

macrophages produce proinflammatory cytokines, in particular interleukin (IL)-12 and IL-23, are phagocytic, present antigen via major histocompatibility complex (MHC) class II molecules,<sup>19</sup> and generate toxic nitrogen and oxygen intermediates.<sup>20</sup> This equips M1 macrophages to eliminate intracellular pathogens and even some tumors effectively.<sup>21,22</sup> The IL-12 produced by M1 macrophages drives further Th1 polarization and stimulates additional IFN- $\gamma$  production from T cells and natural killer cells, thereby perpetuating the inflammatory response. In kidney disease a predominantly M1 macrophage infiltrate results in tissue damage and cell loss followed by the accumulation of extracellular matrix (ECM) proteins. The downstream effect of the proinflammatory cascade is the development of renal interstitial fibrosis and impaired organ function. Thus, macrophage phenotype and the corresponding polarization state ultimately determines the outcome of acute inflammation and the progression to irreversible chronic scarring.<sup>23</sup>

Given a favorable microenvironment, M2 macrophages counteract progressive damaging inflammation and contribute to ECM remodeling and tissue repair. However, the exact definition of M2 alternatively activated macrophages is still under debate. Martinez et al<sup>24</sup> have classified M2 macrophages into three subsets, namely M2a, M2b, and M2c macrophages, which differ in their mode of activation, cytokine profile, and function.

M2a macrophage polarization after exposure to IL-4 and IL-13 or glucocorticoids results in increased expression of pattern recognition receptors including the mannose receptor (CD206) and scavenger receptor (CD163) together with up-regulation of MHC class II molecules and production of the chemokines CCL17, CCL22, and CCL24.<sup>16,25</sup> M2a macrophages show an enhanced capability for endocytosis, pinocytosis, and antigen presentation. There is also increased production of the prototype ECM protein fibronectin, transforming growth factor (TGF)- $\beta$ -induced matrix associated protein MP78/70 ( $\beta$ ig-H3),<sup>26,27</sup> and insulin-like growth factor, which has been shown to stimulate re-epithelialization in dermal wound healing.<sup>28,29</sup>

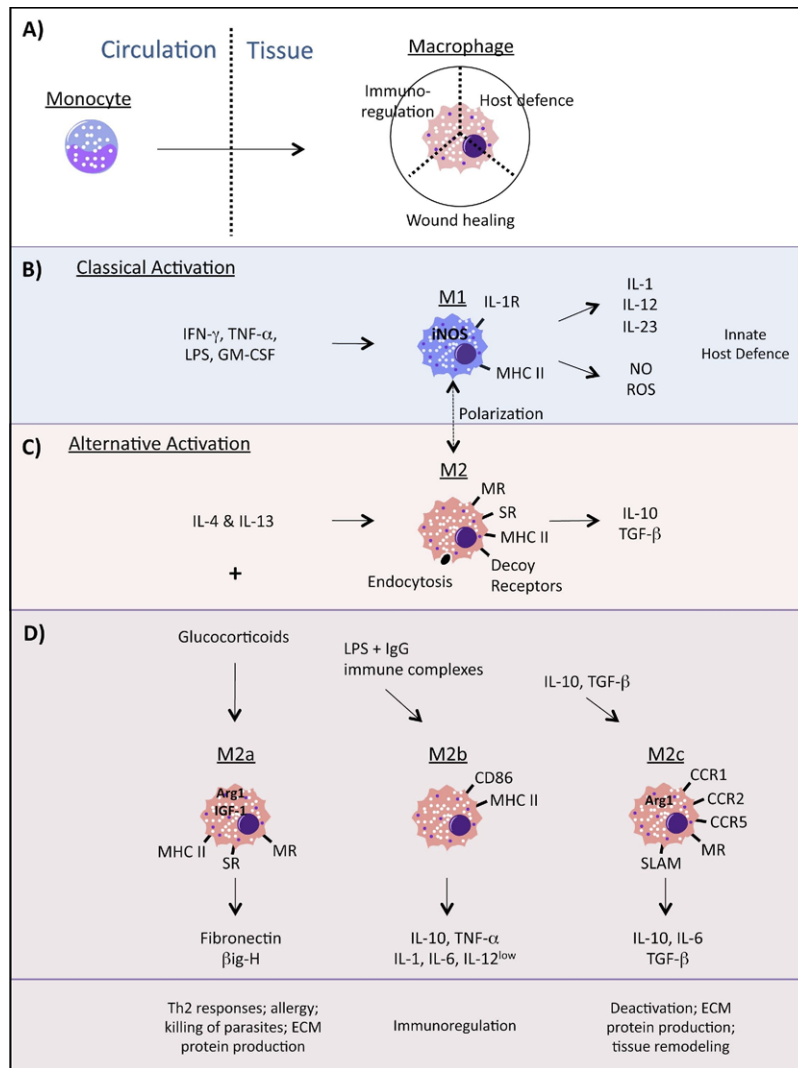


**Figure 1.** The defining chemokine and receptor profiles of classically and alternatively activated macrophages. Two proposed concepts for macrophage polarization are depicted. (A) Three groups of mature macrophages are derived from blood monocytes that are specialized for host defense, immunoregulation, or wound healing. The putative macrophage phenotypes from one category can share a range of features from the other two categories. (B and C) The possible existence of two polarization states, involving M1 (classically activated macrophages) and M2 (alternatively activated macrophages). (B) Classically activated or M1 macrophages are defined based on the mode of activation and the subsequent receptor expression and production of proinflammatory cytokines, nitric oxide (NO), and reactive oxygen species (ROS). Activation typically occurs in response to IFN- $\gamma$  in conjunction with LPS or granulocyte macrophage CSF (GM-CSF). (C) Alternatively activated or M2 macrophages are defined broadly as being those activated in response to IL-4 and IL-13, resulting in the expression of mannose and scavenger receptors along with increased endocytosis abilities and the production of IL-10 and transforming growth factor- $\beta$  (TGF- $\beta$ ). Shifts in the polarization state between differentiated M1 and M2 macrophages also may occur. (D) Within the M2 group there are apparent differences in receptor expression, cytokine production, and function resulting from activation in response to glucocorticoids (M2a), LPS and immune complexes (M2b), and IL-10 and TGF- $\beta$  (M2c).

Furthermore, IL-4-induced arginase production facilitates the conversion of arginine to ornithine, an intermediate in the synthesis of polyamines and collagen. These characteristics suggest an important role for M2a macrophages

in tissue regeneration. However, these cells are associated more commonly with the encapsulation and killing of parasites, for perpetuating Th2 immunity, and for being involved in allergic responses owing to the expression of CCR3

ligands, which are involved in the attraction of eosinophils and basophils.<sup>30</sup>

M2b macrophages characteristically produce high levels of IL-10 but differ from other alternatively activated cells in that they concomitantly produce proinflammatory cytokines, including TNF- $\alpha$ , IL-1, and IL-6, but low levels of IL-12. These cells become activated in response to classic activation stimuli (LPS) in the presence of IgG immune complexes and typically elicit an immunoregulatory response.<sup>31</sup> This mainly is owing to the high production of IL-10, capable of deactivating proinflammatory cytokines, especially TNF- $\alpha$ , while mediating an IL-4-dominant Th2 response<sup>32</sup> and inducing IgG class switching of B cells.<sup>33</sup>

M2c macrophages, also termed *deactivated*, are induced by high levels of IL-10 and transforming growth factor (TGF)- $\beta$  and have vital immunosuppressive roles while contributing to matrix remodeling and tissue repair. Interestingly, IL-10 induces the expression of proinflammatory chemokine receptors such as CCR1, CCR2, and CCR5,<sup>34</sup> which bind the ligands monocyte inflammatory proteins-1 $\alpha$  and monocyte inflammatory proteins-1 $\beta$ , monocyte chemoattractant protein-1, and CCL5. However, these receptors become uncoupled, interrupting signal transduction such that IL-10 inhibits cell migration in the presence of these proinflammatory chemokines, resulting in macrophage deactivation. The positive role of M2c macrophages in tissue regeneration, however, is not the result of restricted migration but from the deactivation event that allows the chemokine receptors to function as decoy receptors. This contributes to M2c governed immunosuppression through the clearance of proinflammatory mediators. IL-10 also up-regulates cell surface expression of CD150, or signaling lymphocyte-activating molecule, which appears uniquely on this subset of macrophages but is also an indicator of dendritic cell maturation.<sup>35</sup> Signaling lymphocyte-activating molecule is known to activate T cells, but because of its expression by M2c macrophages and its regulation by the immunoregulatory cytokine IL-10, it may play an important role in the induction of T-regulatory cells and driving Th2 polarization. In support of this notion, signaling lymphocyte-activating molecule

also is linked to B-cell stimulation and proliferation and subsequent immunoglobulin (Ig) production.<sup>36</sup>

Regarding alternative macrophage activation, there is debate over the classification. The effects governed by IL-10 and IL-12 may not be sufficient to warrant the classification of different subsets, with the only true M2 macrophage being that which is activated with IL-4 and IL-13.<sup>17</sup> It has been proposed that the M1/M2 nomenclature be used as a guide when discussing specific cell subsets based on the precise ligands and chemokines associated with that cell. More recently, Mosser and Edwards<sup>37</sup> suggested that three macrophage activation states exist, specializing in either host defense, wound healing, or immune regulation. Depending on the specific inflammatory and microenvironmental cues, macrophages can adopt particular phenotypic and functional characteristics, giving the impression of a range of subsets. Whichever classification system proves to be most accurate, the ability of macrophages to mediate renal repair most likely depends on the interplay of a number of different subsets that function to suppress Th1 (M1)-induced inflammation, promote Th2 (M2) recruitment and/or polarization, clear cellular debris, and promote tissue regeneration and reorganization through appropriate ECM production/degradation and angiogenesis.

### TUMOR-ASSOCIATED MACROPHAGES: ANALOGIES WITH EMBRYONIC MACROPHAGES

The importance of macrophage phenotype in controlling immune responses is highlighted in malignancy. Macrophages in the fetal kidney, lung, and brain share a characteristic gene expression profile comprising a variety of anti-inflammatory and pro-proliferative factors<sup>38</sup> but with a distinct genetic profile compared with the adult.<sup>4,15,39,40</sup> Macrophages in the embryonic kidney express a repertoire of markers suggestive of an M2 phenotype<sup>38</sup> and a number of the M2-associated genes identified in embryonic macrophages are shared by tumor-associated macrophages (TAMs),<sup>41-43</sup> including the mannose receptor, macrophage scavenger re-

ceptors 1 and 2, CCL24, C1q, CD163, and TREM2.<sup>38</sup>

There is growing evidence that the tumor microenvironment influences M2 macrophages to produce a variety of pro-tumor growth and angiogenic factors as well as immunosuppressive molecules.<sup>41</sup> Stemming from a common myeloid precursor, there are distinct subpopulations of myelomonocytic cells with different differentiation phenotypes, dependent on the site of tumor origin and progression of disease. Myeloid-derived suppressor cells (CD11b<sup>+</sup>Gr-1<sup>-</sup>F4/80<sup>-</sup>IL-4R $\alpha$ <sup>+</sup>) of granulocyte origin are recruited to the tumor microenvironment where they become F4/80<sup>+</sup>.<sup>41,43,44</sup> In addition, TAMs are derived from circulating monocytes and influence tumor growth. Both myeloid-derived suppressor cells and TAMs have a phenotype similar to M2 macrophages and may well represent a unique myeloid cell differentiation program.<sup>41</sup> Tumor-conditioned granulocytes may play a role in priming macrophages toward either a M1 or M2 phenotype.<sup>45</sup> However, as in inflammation, it is unclear if macrophages remain committed to a single phenotype or whether they regress to a resting state that can be reactivated another way.<sup>46</sup> Tumor progression and metastasis depends on constant macrophage influx to assist tumor growth, angiogenesis, and stromal remodeling. Macrophages may be either anti-angiogenic or pro-angiogenic depending on their microenvironment. Recently, Kelly et al<sup>47</sup> reported that somatic cell senescence genes, Fas ligand, and IL-10 are key regulators of macrophage polarization and determine their ability to regulate angiogenesis.<sup>47</sup> Thus, targeting specific macrophage populations or immunotherapies designed to exploit the ability of macrophages to adopt an anti-angiogenic phenotype may effectively remodel the tumor microenvironment to suppress tumor cell proliferation and metastasis.<sup>48</sup>

### THE ROLE OF TISSUE MACROPHAGES IN KIDNEY DEVELOPMENT

Macrophages play various roles in both kidney development and disease. Macrophages originating from the liver infiltrate the renal mesenchyme of the developing metanephros via the circulation before nephron formation.<sup>38</sup> As the

tubules of the developing nephrons are formed, the interstitial macrophages become associated intimately with the cortical nephron segments and with the loop of Henle in the medulla. The macrophages assemble in the interstitium adjacent to the basement membrane underlying the tubular epithelium and wrap cellular processes around the epithelium. It is in this location that a resident population of tissue macrophages persists within the kidney into adult life.<sup>38</sup> Although we have documented the timing of the arrival of such macrophages, it is unclear whether their residence is permanent with such cells representing long-term residents or whether there is ongoing recruitment and turnover of this population, potentially but not necessarily from the circulating monocytic/macrophage population. We have examined the expression profile of such resident macrophages but have not found markers that definitively would distinguish between tissue and circulating monocyte-derived macrophages or from resident macrophages located in other organs. However, the presence of macrophages from early kidney development and their intimate relationship with the forming tubules of the nephrons suggests that, as for organs such as the breast and the brain,<sup>11,12,49</sup> macrophages are critical for kidney development. We also have shown that the addition of CSF-1 to a developing murine kidney significantly promotes growth and differentiation and that this is accompanied by an increase in the number of macrophages present in the cultures.<sup>38</sup> CSF-1 itself does not appear to be essential for kidney development because mice deficient in CSF-1 have kidneys.<sup>9</sup> However, these mice are not completely devoid of macrophages and do access some CSF-1 from their mothers.<sup>50</sup> However, it is possible that manipulation of the trophic role of macrophages within developing kidneys may be used to induce compensatory nephron production in fetuses suffering from intrauterine growth retardation.

### MACROPHAGES IN KIDNEY DISEASE

Although the pathogenesis of renal disease is multifactorial, the ideal therapy would both address causative factors and promote optimal cellular replacement after injury. Importantly,

damaged kidneys can undergo endogenous repair of the nephron renal epithelia via cell proliferation.<sup>51</sup> However, the capacity of the kidney and especially the glomerulus to undergo endogenous repair after injury is limited and typically insufficient.

### Suppression of Macrophage Activities in Chronic Kidney Disease

The role of the macrophage in response to kidney injury traditionally has been regarded as inflammatory and detrimental. Although the nature of the damage potentially would result in a variable role for macrophages in disease onset and progression, glomerular and tubulointerstitial macrophage accumulation occurs in response to almost all insults. Both immune and nonimmune injury results in macrophage infiltration, leading to increased ECM accumulation and tubulointerstitial inflammation and fibrosis. Evidence suggests that glomerular macrophage accumulation makes an important contribution to diabetic nephropathy<sup>52</sup> because depletion or disruption of macrophage function limits disease severity. Macrophage depletion using liposomal clodronate reduced mesangial ECM accumulation in a rat model of nephrotoxic nephritis<sup>53</sup> whereas gene deletion of monocyte chemoattractant protein-1 reduced tubular injury and death in murine nephrotoxic nephritis.<sup>54</sup> Mice lacking either L-selectin alone or all three selectins (E-, P-, and L-selectin) showed reduced macrophage recruitment and less tubulointerstitial fibrosis and tubular apoptosis in experimental hydronephrosis implicating macrophages in tubular cell death.<sup>55</sup> The induction of apoptosis by macrophages owing to nitric oxide and TNF- $\alpha$  production results in direct cell death, but macrophages also may reduce tubular expression of vascular endothelial growth factor (VEGF), leading to the disruption of the peritubular capillary network and resultant tissue ischemia.<sup>56,57</sup>

The growth factor CSF-1 is pivotal to the macrophage response in the adult kidney because of its role in macrophage differentiation and proliferation. In a chronic setting, CSF-1 is produced by the kidney in response to renal injury whereas cultured mesangial cells produce CSF-1, along with its receptor, CSF-1R.<sup>58</sup>

CSF-1 also is expressed by most renal carcinoma cell lines,<sup>59</sup> potentially inducing a response in TAMs. The cortical and medullary tubular epithelium is a major site of CSF-1 production during anti-glomerular basement membrane (GBM)-induced glomerulonephritis in rats<sup>60</sup> and is accompanied by considerable interstitial macrophage accumulation. In glomerulonephritis in human beings, there also is increased CSF-1 production by both the tubular epithelium and glomerular cells.<sup>61</sup> This results in glomerular accumulation and proliferation of macrophages. Although CSF-1 mediates macrophage recruitment and proliferation, it also may promote classic M1 macrophage activation in renal disease. Lenda et al<sup>62</sup> reported fewer interstitial macrophages and reduced tubular cell death in the obstructed kidneys of CSF-1<sup>ob</sup>/CSF-1<sup>ob</sup> mice with bone marrow-derived macrophages showing resistance to LPS and IFN- $\gamma$ -induced classic activation after pre-incubation with anti-CSF-1R antibody. It is thus of interest that serum levels of CSF-1 are associated with acute allograft rejection.<sup>63</sup> The delivery of an anti-CSF-1R antibody to mice after allograft transplantation reduced macrophage proliferation and accumulation within the allograft and tubulointerstitial rejection, suggesting that signaling between CSF-1 and CSF-1R is critically important in acute rejection.<sup>64</sup>

Somewhat paradoxically, CSF-1 treatment effectively promotes repair in a model of acute kidney damage,<sup>65</sup> a finding that is almost completely opposite to the chronic setting. For example, although diabetic nephropathy is associated with interstitial macrophage recruitment,<sup>66</sup> greatly increased levels of endogenous CSF-1 produced by glomerular podocytes and the damaged tubules fail to drive the renal repair observed in the acute models.<sup>60,67</sup> Furthermore, the inhibition of CSF-1 signaling with CSF-1R antibodies reduces the severity of chronic disease in obese diabetic mice (*db/db*) that show a 36-fold increase in CSF-1 levels and increased CD68<sup>+</sup> glomerular macrophage numbers.<sup>67</sup> Administration of anti-CSF-1R antibodies results in a 60% decrease in macrophage infiltration with decreased macrophage proliferation, suppression of diabetic glomerular hyperfiltration, reduced accumulation of glomer-

ular type IV collagen, and reduced tubular injury. In this chronic setting, CSF-1 is an important contributor to disease progression, with endogenous CSF-1 driving the proliferation and recruitment of a proinflammatory or M1-like macrophage population.

Expression of CSF-1 occurs before the onset of injury in Fas deletion mutant gene, *Ipr* (MRL/*Ipr*) autoimmune mice whereas C3H-*Ipr* mice do not express CSF-1 and do not show autoimmune renal injury. However, targeted CSF-1 overexpression by the tubular epithelial cells of wild-type MRL and C3H mice does not result in the development of spontaneous renal injury.<sup>68</sup> This indicates the importance of biological context and that mechanisms downstream of simple macrophage recruitment and proliferation determine outcome. Indeed, context is key because macrophage activity is a requirement for epithelial regeneration in other organs such as the injured colon,<sup>69</sup> with data suggesting a role for macrophages in renal repair. Also, the nature of the disease model and the mediator under study also is important. For example, although macrophage migration inhibitory factor-induced leukocyte accumulation is detrimental in immune-initiated renal injury, migration inhibitory factor-deficient and wild-type mice show comparable interstitial macrophage accumulation and fibrosis in obstructive nephropathy.<sup>70</sup> In the same model, osteopontin knockout mice show reduced macrophage numbers but increased tubular cell apoptosis<sup>71</sup> whereas inhibition of CSF-1 failed to attenuate established albuminuria in *db/db* mice.<sup>67</sup> Thus, the balance between cell death and ECM protein accumulation in fibrosis or epithelial regeneration and remodeling of collagen during kidney repair is likely to be governed by many environmental factors capable of shifting the balance between inflammatory M1 and wound healing M2 macrophage responses.

### Positive Modulation of Macrophages in Acute Kidney Injury

Acute kidney injury has myriad causes including acute ischemia owing to blood loss or chemical/toxic insults resulting in proximal tubular cell injury and rapid loss of renal function. More than half of patients with acute kidney

injury die as a result, whereas the remainder follow a natural course of self-mediated tissue repair.<sup>72</sup> Evidence suggests that macrophages contribute to acute kidney injury such as ischemic damage. For example, reduced tubular necrosis and tubular apoptosis was observed in mice depleted of monocyte-macrophage populations by administration of liposomal clodronate.<sup>73</sup> Although potential therapies to enhance recovery from acute kidney injury might logically aim to reduce inflammation to facilitate repair, another strategy is to direct macrophages to perform an anti-inflammatory and pro-reparative role. It is thus of interest that, in addition to regulating the growth, differentiation, and survival of macrophages, CSF-1 appears to promote the anti-inflammatory and wound healing capabilities of macrophages in mice and human beings.<sup>19,74</sup> CSF-1 has been linked to angiogenesis *in vivo*<sup>75</sup> with these effects likely to result from the production of VEGF and matrix metalloproteinases (MMPs) from CSF-1-activated macrophages.<sup>76,77</sup> Tumor studies show that increased CSF-1 levels correspond with angiogenesis and subsequent tumor growth and metastasis.<sup>78</sup> The role of CSF-1 in these models has been shown via the use of blocking antibodies, antisense oligonucleotides, or small interfering RNAs, which reduces human mammary tumor xenografts in mice.<sup>79,80</sup> The depletion of phagocytic macrophages using liposomal clodronate also inhibits tumor development.<sup>81</sup> A further study compared CSF-1 inhibition with VEGF inhibition, another proposed method to block pathogenic angiogenesis associated with tumor development and retinal neovascular disease.<sup>82</sup> Interestingly, the macrophages associated with retinal neovascular development did not express VEGF but had high levels of the collagenases MMP-2 and MMP-9, which contributed to vascular remodeling as a result of ECM degradation.<sup>83,84</sup> Although CSF-1-deficient *CSF-1<sup>op</sup>/CSF-1<sup>op</sup>* mice develop a normal vasculature, CSF-1 and macrophages are involved in the retinal neovascularization present in a mouse model of diabetic retinopathy in which hyperoxia results in ischemic vascular damage.<sup>82</sup> Also, tumors in MMP-9 knockout mice show disorganized and irregular ECM deposits similar to inhibition of CSF-1 in

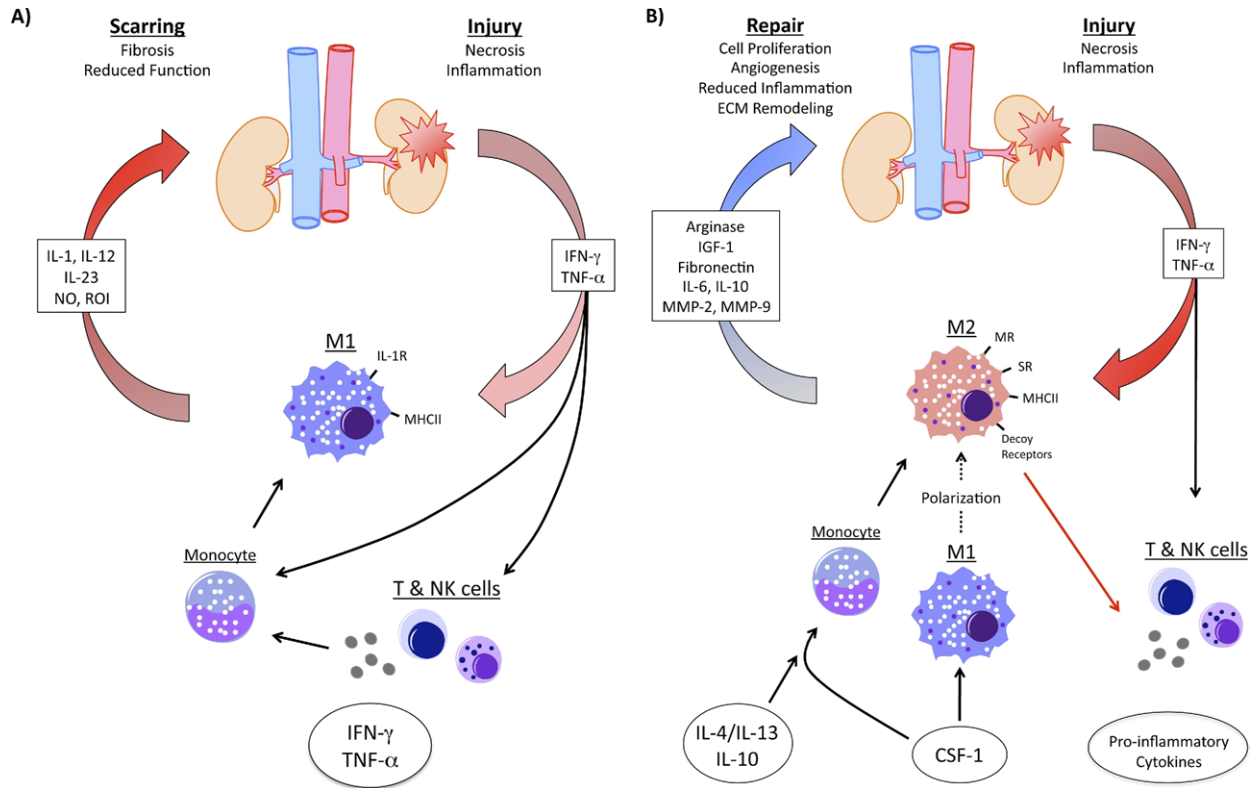


**Figure 2.** Different types of macrophages can contribute to both the damage and tissue repair processes after kidney injury. (A) After damage, necrosis and apoptosis result in Th1-type inflammatory responses, primarily mediated by IFN- $\gamma$  and TNF- $\alpha$ . This recruits M1 or classically activated macrophages and Th1-associated T and natural killer (NK) cells, which produce additional proinflammatory cytokines to enhance the inflammatory response but that also perpetuate damage, resulting in fibrosis, scarring, and reduced organ function. Proinflammatory factors act on both resident macrophages and circulating peripheral monocytes and macrophages, driving M1 polarization. (B) M2, or alternatively activated macrophages, can mediate cellular repair processes by clearing cellular debris, reducing inflammation, promoting angiogenesis, stimulating cellular proliferation, and contributing to matrix remodeling. Targeting specific macrophage-related receptors or cell products may rapidly accelerate tissue repair and organ regeneration. The production of cytokines IL-4, IL-13, and IL-10 can facilitate M2 polarization, and growth factors including CSF-1, arginase, insulin-like growth factor (IGF-1), fibronectin, certain interleukins, and MMPs may further contribute to accelerated renal repair. (B) The descending red arrow from the M2 macrophage indicates that decoupled proinflammatory chemokine receptors act as decoy receptors, eliminating particular proinflammatory mediators. IL-4, IL-13, IL-10, and CSF-1 may produce alternatively activated macrophages from monocytes as well as drive polarization of M2 from M1 macrophages.

wild-type mice, suggesting an important role for macrophage-derived MMPs in ECM remodeling.<sup>82</sup> MMPs also are involved in chemokine and growth factor production, cell receptor expression, and cell migration such that targeting MMPs also may aid the wound repair process<sup>85,86</sup> (Fig. 2). CSF-1 also has been shown to elicit a direct autocrine/paracrine effect on renal tubular epithelial cells after ischemic injury, in which they transiently express the CSF-1R in conjunction with the endogenous production of CSF-1.<sup>65</sup> However, a macrophage-dependent repair process also was shown after depletion

of CD11b-expressing cells although the impairment of repair was less than that evident after antibody-mediated blocking of CSF-1R on both epithelial cells and macrophages.

## HARNESSING MACROPHAGE BIOLOGY FOR THERAPY

Although macrophages are recruited to the injured kidney, they alternatively can be activated to play a pro-reparative role via the production of anti-inflammatory cytokines (IL-4, IL-10) and this raises the possibility of therapeutically

enhancing this reparative capacity *in vivo*. Potential therapeutic approaches include reducing macrophage infiltration, altering the response of the tissue to the presence of macrophages, delivering reparative factors directly to the kidney via genetic manipulation of macrophages, or the induction of a M2 alternative activation phenotype *in situ* to directly promote repair.

Modulation of macrophage infiltration via the delivery of decoy receptors or antibodies has been discussed previously. For example, deficiency of selectins reduced macrophage infiltration and fibrosis in obstructive nephropathy.<sup>55</sup> In contrast, blockade of either intercellular adhesion molecule-1 or vascular cell adhesion molecule did not reduce macrophage numbers in nephrotoxic nephritis although disease still was less severe.<sup>87</sup> Manipulation of a wide variety of chemoattractants, including monocyte chemoattractant protein-1, monocyte inflammatory proteins-1 $\alpha$ , CCL5, and fractalkine, also reduce glomerular macrophage accumulation.<sup>88</sup> Inhibition of classic activating cytokines including TNF- $\alpha$  or IL-1 $\beta$  is anti-inflammatory whereas the genetic deletion of anti-inflammatory cytokines such as IL-4, IL-10, and IL-13 that induce M2 macrophage activation result in more severe macrophage infiltration of glomeruli. In Alport syndrome, in which there is a genetic defect in the gene for type IV collagen, the GBM irregularities are mediated, at least in part, by glomerular macrophage production of MMP-12 because specific inhibition of MMP-12 greatly improves GBM ultrastructure.<sup>89</sup> This study implicates macrophages in the GBM damage of a genetic disease and indicates that modification of macrophage activity can improve outcome. Various methods of suppressing macrophage function have been reported to attenuate injury and fibrosis in experimental models of renal disease, including glomerulonephritis,<sup>90</sup> allograft rejection,<sup>91</sup> and obstructive nephropathy.<sup>92</sup>

Modification of the response of the tissue itself to macrophage accumulation has been attempted via the delivery of specific genes directly into the kidney itself. For example, the gene for 15-lipoxygenase, the enzyme responsible for the production of lipoxins, which re-

duce macrophage activation, was delivered virally into the glomeruli in a rat model of experimental glomerulonephritis via viral injection into the renal artery.<sup>93</sup> Interestingly, this manipulation reduced proteinuria without reducing macrophage accumulation. An alternative strategy has been to use the efficient macrophage homing mechanism to deliver the gene product to the inflamed kidney. In these studies, macrophages that have been transduced virally to overexpress anti-inflammatory mediators such as IL-1 $\alpha$ , IL-4, and IL-10 were administered with a beneficial effect on outcome evident.<sup>90,94,95</sup> Also, the administration of macrophages transduced with a dominant-negative inhibitor of nuclear factor  $\kappa$ B reduced glomerular expression of inducible nitric oxide synthase and MHC class II expression in rats with nephrotoxic nephritis.<sup>96</sup> Advances in this area have focused on longer-term gene expression using lentiviruses and the modification of the bone marrow to produce a continuous supply of anti-inflammatory cells; an approach successfully used in a model of Goodpasture syndrome.<sup>97</sup>

An extension of the approach of genetic manipulation of macrophages to overexpress a single anti-inflammatory molecule is to capitalize on our increasing understanding of macrophage heterogeneity to stimulate the appropriate alternative activation response. Such a manipulation would involve shifting the balance between M1 and M2 activation, with this tipping of the M1/M2 balance predicted to bias the macrophage response to repair rather than inflammation. Direct evidence that this approach can be effective was shown after the adoptive transfer of murine splenic macrophages programmed *ex vivo* with IL-4/IL-13 to adopt an alternative activation state before systemic administration to a mouse model of chronic inflammatory renal disease. The macrophages trafficked to the inflamed kidneys and maintained their phenotype for up to 4 weeks.<sup>98</sup> Furthermore, the adoptively transferred macrophages modulated the host macrophages toward an M2 phenotype as has been suggested to occur in models of glomerular inflammation.<sup>95,96</sup>

## CONCLUSIONS

In conclusion, there is considerable renewed interest in macrophages in both kidney development and disease with a focus on their reparative functions. However, given the clear capacity for macrophages to play distinct roles at different times of the disease process, it will be important to better understand the nature of the interrelationships between the various states of macrophage activation. It also will be critical to gain a better understanding of the distinction between embryonic and postnatal resident tissue macrophages and the kinetics of turnover of resident macrophages. It is likely that future insights into the complexity of macrophage biology will lead to novel therapies to promote renal development, diminish injury, and promote repair of the diseased kidney.

## REFERENCES

1. van Furth R, Cohn ZA, Hirsch JG, Humphrey JH, Spector WG, Langevoort HL. Mononuclear phagocytic system: new classification of macrophages, monocytes and of their cell line. *Bull World Health Organ.* 1972;47:651-8.
2. Takahashi K, Naito M. Development, differentiation, and proliferation of macrophages in the rat yolk sac. *Tissue Cell.* 1993;25:351-62.
3. Hume DA. The mononuclear phagocyte system. *Curr Opin Immunol.* 2006;18:49-53.
4. Lichanska AM, Browne CM, Henkel GW, Murphy KM, Ostrowski MC, McKercher SR, et al. Differentiation of the mononuclear phagocyte system during mouse embryogenesis: the role of transcription factor PU.1. *Blood.* 1999;94:127-38.
5. Ovchinnikov DA. Macrophages in the embryo and beyond: much more than just giant phagocytes. *Genesis.* 2008;46:447-62.
6. Takeya M, Takahashi K. Ontogenic development of macrophage subpopulations and Ia-positive dendritic cells in fetal and neonatal rat spleen. *J Leukoc Biol.* 1992;52:516-23.
7. Izumi S, Takeya M, Takagi K, Takahashi K. Ontogenetic development of synovial A cells in fetal and neonatal rat knee joints. *Cell Tissue Res.* 1990;262:1-8.
8. Henson PM, Hume DA. Apoptotic cell removal in development and tissue homeostasis. *Trends Immunol.* 2006;27:244-50.
9. Cohen PE, Chisholm O, Arceci RJ, Stanley ER, Pollard JW. Absence of colony-stimulating factor-1 in osteopetrotic (csf1op/csf1op) mice results in male fertility defects. *Biol Reprod.* 1996;55:310-7.
10. Dai X-M, Ryan GR, Hapel AJ, Dominguez MG, Russell RG, Kapp S, et al. Targeted disruption of the mouse colony-stimulating factor 1 receptor gene results in osteopetrosis, mononuclear phagocyte deficiency, increased primitive progenitor cell frequencies, and reproductive defects. *Blood.* 2002;99:111-20.
11. Michaelson MD, Bieri PL, Mehler MF, Xu H, Arezzo JC, Pollard JW, et al. CSF-1 deficiency in mice results in abnormal brain development. *Development.* 1996;122:2661-72.
12. Van Nguyen A, Pollard JW. Colony stimulating factor-1 is required to recruit macrophages into the mammary gland to facilitate mammary ductal outgrowth. *Dev Biol.* 2002;247:11-25.
13. Banaei-Bouchareb L, Gouon-Evans V, Samara-Boustani D, Castellotti MC, Czernichow P, Pollard JW, et al. Insulin cell mass is altered in Csf1op/Csf1op macrophage-deficient mice. *J Leukoc Biol.* 2004;76:359-67.
14. Shepard JL, Zon LI. Developmental derivation of embryonic and adult macrophages. *Curr Opin Hematol.* 2000;7:3-8.
15. Lichanska AM, Hume DA. Origins and functions of phagocytes in the embryo. *Exp Hematol.* 2000;28:601-11.
16. Mantovani A, Sica A, Sozzani S, Allavena P, Vecchi A, Locati M. The chemokine system in diverse forms of macrophage activation and polarization. *Trends Immunol.* 2004;25:677-86.
17. Martinez FO, Helming L, Gordon S. Alternative activation of macrophages: an immunologic functional perspective. *Annu Rev Immunol.* 2009;27:451-83.
18. Cassol E, Cassetta L, Rizzi C, Alfano M, Poli G. M1 and M2a Polarization of human monocyte-derived macrophages inhibits HIV-1 replication by distinct mechanisms. *J Immunol.* 2009;182:6237-46.
19. Verreck FAW, de Boer T, Langenberg DML, Hoeve MA, Kramer M, Vaisberg E, et al. Human IL-23-producing type 1 macrophages promote but IL-10-producing type 2 macrophages subvert immunity to (myco)bacteria. *Proc Natl Acad Sci U S A.* 2004;101:4560-5.
20. MacMicking J, Xie Q-W, Nathan C. Nitric oxide and macrophage function. *Annu Rev Immunol.* 1997;15:323-50.
21. Nathan C, Shiloh MU. Reactive oxygen and nitrogen intermediates in the relationship between mammalian hosts and microbial pathogens. *Proc Natl Acad Sci U S A.* 2000;97:8841-8.
22. Kito T, Kuroda E, Yokota A, Yamashita U. Cytotoxicity in glioma cells due to interleukin-12 and interleukin-18 stimulated macrophages mediated by interferon- $\gamma$  regulated by nitric oxide. *J Neurosurg.* 2003;98:385-92.
23. Ricardo SD, van Goor H, Eddy AA. Macrophage diversity in renal injury and repair. *J Clin Invest.* 2008;118:3522-30.
24. Martinez FO, Sica A, Mantovani A, Locati M. Macrophage activation and polarization. *Front Biosci.* 2008;13:453-61.
25. Watanabe K, Jose PJ, Rankin SM. Eotaxin-2 generation is differentially regulated by lipopolysaccharide and

- IL-4 in monocytes and macrophages. *J Immunol.* 2002;168:1911-8.
26. Gratchev A, Guillot P, Hakiy N, Politz O, Orfanos C, Schledzewski K, et al. Alternatively activated macrophages differentially express fibronectin and its splice variants and the extracellular matrix protein betaG-H3. *Scand J Immunol.* 2001;53:386-92.
27. Gibson MA, Kumaratilake JS, Cleary EG. Immunohistochemical and ultrastructural localization of MP78/70 (big-h3) in extracellular matrix of developing and mature bovine tissues. *J Histochem Cytochem.* 1997;45:1683-96.
28. Tsuboi R, Shi C-M, Sato C, Cox GN, Ogawa H. Co-administration of insulin-like growth factor (IGF)-I and IGF-binding protein-1 stimulates wound healing in animal models. *J Invest Dermatol.* 1995;104:199-203.
29. Kratz G, Lake M, Gidlund M. Insulin like growth factor-1 and -2 and their role in the re-epithelialisation of wounds; interactions with insulin like growth factor binding protein type 1. *Scand J Plast Reconstr Surg Hand Surg.* 1994;28:107-12.
30. Elsner J, Escher SE, Forssmann U. Chemokine receptor antagonists: a novel therapeutic approach in allergic diseases. *Allergy.* 2004;59:1243-58.
31. Gerber JS, Mosser DM. Reversing lipopolysaccharide toxicity by ligating the macrophage Fc gamma receptors. *J Immunol.* 2001;166:6861-8.
32. Anderson CF, Mosser DM. Cutting edge: biasing immune responses by directing antigen to macrophage Fc{gamma} receptors. *J Immunol.* 2002;168:3697-701.
33. Anderson CF, Mosser DM. A novel phenotype for an activated macrophage: the type 2 activated macrophage. *J Leukoc Biol.* 2002;72:101-6.
34. Sozzani S, Ghezzi S, Iannolo G, Luini W, Borsatti A, Polentarutti N, et al. Interleukin 10 increases CCR5 expression and HIV infection in human monocytes. *J Exp Med.* 1998;187:439-44.
35. Bleharski JR, Niazi KR, Sieling PA, Cheng G, Modlin RL. Signaling lymphocytic activation molecule is expressed on CD40 ligand-activated dendritic cells and directly augments production of inflammatory cytokines. *J Immunol.* 2001;167:3174-81.
36. Punnonen J, Cocks BG, Carballido JM, Bennett B, Peterson D, Aversa G, et al. Soluble and membrane-bound forms of signaling lymphocytic activation molecule (SLAM) induce proliferation and Ig synthesis by activated human B lymphocytes. *J Exp Med.* 1997;185:993-1004.
37. Mosser DM, Edwards JP. Exploring the full spectrum of macrophage activation. *Nat Rev Immunol.* 2008;8:958-69.
38. Rae F, Woods K, Sasmono T, Campanale N, Taylor D, Ovchinnikov DA, et al. Characterisation and trophic functions of murine embryonic macrophages based upon the use of a Csf1r-EGFP transgene reporter. *Dev Biol.* 2007;308:232-46.
39. Martinez FO, Gordon S, Locati M, Mantovani A. Transcriptional profiling of the human monocyte-to-macrophage differentiation and polarization: new molecules and patterns of gene expression. *J Immunol.* 2006;177:7303-11.
40. Greaves DR, Gordon S. Macrophage-specific gene expression: current paradigms and future challenges. *Int J Hematol.* 2002;76:6-15.
41. Sica A, Bronte V. Altered macrophage differentiation and immune dysfunction in tumor development. *J Clin Invest.* 2007;117:1155-66.
42. Lamagna C, Aurrand-Lions M, Imhof BA. Dual role of macrophages in tumor growth and angiogenesis. *J Leukoc Biol.* 2006;80:705-13.
43. Mantovani A, Sica A, Locati M. Macrophage polarization comes of age. *Immunity.* 2005;23:344-6.
44. Biswas SK, Gangi L, Paul S, Schioppa T, Saccani A, Sironi M, et al. A distinct and unique transcriptional program expressed by tumor-associated macrophages (defective NF-kappaB and enhanced IRF-3/STAT1 activation). *Blood.* 2006;107:2112-22.
45. Tsuda Y, Takahashi H, Kobayashi M, Hanafusa T, Herndon DN, Suzuki F. Three different neutrophil subsets exhibited in mice with different susceptibilities to infection by methicillin-resistant *Staphylococcus aureus*. *Immunity.* 2004;21:215-26.
46. Gordon S, Taylor PR. Monocyte and macrophage heterogeneity. *Nat Rev Immunol.* 2005;5:953-64.
47. Kelly J, Ali Khan A, Yin J, Ferguson TA, Apte RS. Senescence regulates macrophage activation and angiogenic fate at sites of tissue injury in mice. *J Clin Invest.* 2007;117:3421-6.
48. Luo Y, Zhou H, Krueger J, Kaplan C, Lee SH, Dolman C, et al. Targeting tumor-associated macrophages as a novel strategy against breast cancer. *J Clin Invest.* 2006;116:2132-41.
49. Gouon-Evans V, Lin E, Pollard J. Requirement of macrophages and eosinophils and their cytokines/chemokines for mammary gland development. *Breast Cancer Res.* 2002;4:155-64.
50. Roth P, Dominguez MG, Stanley ER. The effects of colony-stimulating factor-1 on the distribution of mononuclear phagocytes in the developing osteopetrotic mouse. *Blood.* 1998;91:3773-83.
51. Humphreys BD, Bonventre JV. The contribution of adult stem cells to renal repair. *Nephrol Ther.* 2007;3:3-10.
52. Shikata K, Makino H. Role of macrophages in the pathogenesis of diabetic nephropathy. *Contrib Nephrol.* 2001;134:46-54.
53. Huang XR, Tipping PG, Apostolopoulos J, Oettinger C, D'Souza M, Milton G, et al. Mechanisms of T cell-induced glomerular injury in anti-glomerular basement membrane (GBM) glomerulonephritis in rats. *Clin Exp Immunol.* 1997;109:134-42.
54. Tesch GH, Maifert S, Schwarting A, Rollins BJ, Kelley VR. Monocyte chemoattractant protein 1-dependent leukocytic infiltrates are responsible for autoimmune

- disease in MRL-Fas(lpr) mice. *J Exp Med.* 1999;190:1813-24.
55. Lange-Sperandio B, Cachat F, Thornhill BA, Chevalier RL. Selectins mediate macrophage infiltration in obstructive nephropathy in newborn mice. *Kidney Int.* 2002;61:516-24.
  56. Khan S, Cleveland RP, Koch CJ, Schelling JR. Hypoxia induces renal tubular epithelial cell apoptosis in chronic renal disease. *Lab Invest.* 1999;79:1089-99.
  57. Kang D-H, Joly AH, Oh S-W, Hugo C, Kerjaschki D, Gordon KL, et al. Impaired angiogenesis in the remnant kidney model: I. Potential role of vascular endothelial growth factor and thrombospondin-1. *J Am Soc Nephrol.* 2001;12:1434-47.
  58. Mori T, Bartocci A, Satriano J, Zuckerman A, Stanley R, Santiago A, et al. Mouse mesangial cells produce colony-stimulating factor-1 (CSF-1) and express the CSF-1 receptor. *J Immunol.* 1990;144:4697-702.
  59. Gerharz C-D, Reinecke P, Schneider EM, Schmitz M, Gabbert HE. Secretion of GM-CSF and M-CSF by human renal cell carcinomas of different histologic types. *Urology.* 2001;58:821-7.
  60. Isbel NM, Hill PA, Foti R, Mu W, Hurst LA, Stambe C, et al. Tubules are the major site of M-CSF production in experimental kidney disease: correlation with local macrophage proliferation. *Kidney Int.* 2001;60:614-25.
  61. Isbel NM, Nikolic-Paterson DJ, Hill PA, Dowling J, Atkins RC. Local macrophage proliferation correlates with increased renal M-CSF expression in human glomerulonephritis. *Nephrol Dial Transplant.* 2001;16:1638-47.
  62. Lenda DM, Kikawada E, Stanley ER, Kelley VR. Reduced macrophage recruitment, proliferation, and activation in colony-stimulating factor-1-deficient mice results in decreased tubular apoptosis during renal inflammation. *J Immunol.* 2003;170:3254-62.
  63. Le Meur Y, Leprivey-Logeot V, Mons S, Jose M, Dantal J, Lemauff B, et al. Serum levels of macrophage-colony stimulating factor (M-CSF): a marker of kidney allograft rejection. *Nephrol Dial Transplant.* 2004;19:1862-5.
  64. Jose MD, Le Meur Y, Atkins RC, Chadban SJ. Blockade of macrophage colony-stimulating factor reduces macrophage proliferation and accumulation in renal allograft rejection. *Am J Transplant.* 2003;3:294-300.
  65. Menke J. CSF-1 signals directly to renal tubular epithelial cells to mediate repair in mice. *J Clin Invest.* 2009;119:2330-42.
  66. Nguyen D, Ping F, Mu W, Hill P, Atkins RC, Chadban SJ. Macrophage accumulation in human progressive diabetic nephropathy. *Nephrology.* 2006;11:226-31.
  67. Lim A, Ma F, Nikolic-Paterson D, Thomas M, Hurst L, Tesch G. Antibody blockade of c-fms suppresses the progression of inflammation and injury in early diabetic nephropathy in obese db/db mice. *Diabetologia.* 2009;52:1669-79.
  68. Naito T, Yokoyama H, Moore KJ, Dranoff G, Mulligan RC, Kelley VR. Macrophage growth factors introduced into the kidney initiate renal injury. *Mol Med.* 1996;2:297-312.
  69. Pull SL, Doherty JM, Mills JC, Gordon JI, Stappenbeck TS. Activated macrophages are an adaptive element of the colonic epithelial progenitor niche necessary for regenerative responses to injury. *Proc Natl Acad Sci U S A.* 2005;102:99-104.
  70. Rice EK, Nikolic-Paterson DJ, David JR, Bucala R, Metz CN, Atkins RC, et al. Macrophage accumulation and renal fibrosis are independent of macrophage migration inhibitory factor in mouse obstructive nephropathy. *Nephrology.* 2004;9:278-87.
  71. Ophascharoensuk V, Giachelli CM, Gordon K, Hughes J, Pichler R, Brown P, et al. Obstructive uropathy in the mouse: Role of osteopontin in interstitial fibrosis and apoptosis. *Kidney Int.* 1999;56:571-80.
  72. Nony PA, Schnellmann RG. Mechanisms of renal cell repair and regeneration after acute renal failure. *J Pharmacol Exp Ther.* 2003;304:905-12.
  73. Jo S-K, Sung S-A, Cho W-Y, Go K-J, Kim H-K. Macrophages contribute to the initiation of ischaemic acute renal failure in rats. *Nephrol Dial Transplant.* 2006;21:1231-9.
  74. Otero K, Turnbull IR, Poliani PL, Vermi W, Cerutti E, Aoshi T, et al. Macrophage colony-stimulating factor induces the proliferation and survival of macrophages via a pathway involving DAP12 and [beta]-catenin. *Nat Immunol.* 2009;10:734-43.
  75. Aharinejad S, Marks SC, Bck P, Mason-Savas A, MacKay CA, Larson EK, et al. CSF-1 treatment promotes angiogenesis in the metaphysis of osteopetrotic (toothless, *tl*) rats. *Bone.* 1995;16:315-24.
  76. Eubank TD, Galloway M, Montague CM, Waldman WJ, Marsh CB. M-CSF induces vascular endothelial growth factor production and angiogenic activity from human monocytes. *J Immunol.* 2003;171:2637-43.
  77. Johnson C, Sung H-J, Lessner SM, Fini ME, Galis ZS. Matrix metalloproteinase-9 is required for adequate angiogenic revascularization of ischemic tissues: potential role in capillary branching. *Circ Res.* 2004;94:262-8.
  78. Lin EY, Nguyen AV, Russell RG, Pollard JW. Colony-stimulating factor 1 promotes progression of mammary tumors to malignancy. *J Exp Med.* 2001;193:727-40.
  79. Aharinejad S, Paulus P, Sioud M, Hofmann M, Zins K, Schafer R, et al. Colony-stimulating factor-1 blockade by antisense oligonucleotides and small interfering RNAs suppresses growth of human mammary tumor xenografts in mice. *Cancer Res.* 2004;64:5378-84.
  80. Paulus P, Stanley ER, Schafer R, Abraham D, Aharinejad S. Colony-stimulating factor-1 antibody reverses chemoresistance in human MCF-7 breast cancer xenografts. *Cancer Res.* 2006;66:4349-56.
  81. Zeisberger SM, Odermatt B, Marty C, Zehnder-Fjallman AHM, Ballmer-Hofer K, Schwendener RA. Clodronate-liposome-mediated depletion of tumour-associated macrophages: a new and highly effective

- antiangiogenic therapy approach. *Br J Cancer*. 2006; 95:272-81.
82. Kubota Y, Takubo K, Shimizu T, Ohno H, Kishi K, Shibuya M, et al. M-CSF inhibition selectively targets pathological angiogenesis and lymphangiogenesis. *J Exp Med*. 2009;206:1089-102.
  83. Murphy G, Nguyen Q, Cockett MI, Atkinson SJ, Allan JA, Knight CG, et al. Assessment of the role of the fibronectin-like domain of gelatinase A by analysis of a deletion mutant. *J Biol Chem*. 1994;269:6632-6.
  84. Ashworth JL, Murphy G, Rock MJ, Sherratt MJ, Shapiro SD, Shuttleworth CA, et al. Fibrillin degradation by matrix metalloproteinases: implications for connective tissue remodelling. *Biochem J*. 1999;340:171-81.
  85. Sternlicht MD, Werb Z. How matrix metalloproteinases regulate cell behavior. *Annu Rev Cell Dev Biol*. 2001;17:463-516.
  86. Somerville R, Oblander S, Apte S. Matrix metalloproteinases: old dogs with new tricks. *Genome Biol*. 2003;4:216.
  87. Allen AR, McHale J, Smith J, Cook HT, Karkar A, Haskard DO, et al. Endothelial expression of VCAM-1 in experimental crescentic nephritis and effect of antibodies to very late antigen-4 or VCAM-1 on glomerular injury. *J Immunol*. 1999;162:5519-27.
  88. Erwig L-P, Kluth DC, Rees AJ. Macrophages in renal inflammation. *Curr Opin Nephrol Hypertens*. 2001; 10:341-7.
  89. Rao VH, Meehan DT, Delimont D, Nakajima M, Wada T, Gratton MA, et al. Role for macrophage metalloelastase in glomerular basement membrane damage associated with Alport syndrome. *Am J Pathol*. 2006; 169:32-46.
  90. Yokoo T, Ohashi T, Utsunomiya Y, Kojima H, Imasawa T, Kogure T, et al. Prophylaxis of antibody-induced acute glomerulonephritis with genetically modified bone marrow-derived vehicle cells. *Hum Gene Ther*. 1999;10:2673-8.
  91. Yang J, Reutzel-Selke A, Steier C, Jurisch A, Tullius SG, Sawitzki B, et al. Targeting of macrophage activity by adenovirus-mediated intragraft overexpression of TNFRp55-Ig, IL-12p40, and vIL-10 ameliorates adenovirus-mediated chronic graft injury, whereas stimulation of macrophages by overexpression of IFN-gamma accelerates chronic graft injury in a rat renal allograft model. *J Am Soc Nephrol*. 2003;14:214-25.
  92. Nishida M, Okumura Y, Fujimoto S, Shiraishi I, Itoi T, Hamaoka K. Adoptive transfer of macrophages ameliorates renal fibrosis in mice. *Biochem Biophys Res Commun*. 2005;332:11-6.
  93. Munger KA, Montero A, Fukunaga M, Uda S, Yura T, Imai E, et al. Transfection of rat kidney with human 15-lipoxygenase suppresses inflammation and preserves function in experimental glomerulonephritis. *Proc Natl Acad Sci U S A*. 1999;96:13375-80.
  94. Kluth DC, Ainslie CV, Pearce WP, Finlay S, Clarke D, Anegon I, et al. Macrophages transfected with adenovirus to express IL-4 reduce inflammation in experimental glomerulonephritis. *J Immunol*. 2001;166:4728-36.
  95. Wilson HM, Chettibi S, Jobin C, Walbaum D, Rees AJ, Kluth DC. Inhibition of macrophage nuclear factor-kappaB leads to a dominant anti-inflammatory phenotype that attenuates glomerular inflammation in vivo. *Am J Pathol*. 2005;167:27-37.
  96. Wilson HM, Chettibi S, Jobin C, Walbaum D, Rees AJ, Kluth DC. Inhibition of macrophage nuclear factor-kappaB leads to a dominant anti-inflammatory phenotype that attenuates glomerular inflammation in vivo. *Am J Pathol*. 2005;167:27-37.
  97. Yokoo T, Ohashi T, Utsunomiya Y, Shen JS, Hisada Y, Eto Y, et al. Genetically modified bone marrow continuously supplies anti-inflammatory cells and suppresses renal injury in mouse Goodpasture syndrome. *Blood*. 2001;98:57-64.
  98. Wang Y, Wang YP, Zheng G, Lee VW, Ouyang L, Chang DH, et al. Ex vivo programmed macrophages ameliorate experimental chronic inflammatory renal disease. *Kidney Int*. 2007;72:290-9.



# Establishing the Flow Cytometric Assessment of Myeloid Cells in Kidney Ischemia/Reperfusion Injury

Timothy M. Williams,<sup>1</sup> Andrea F. Wise,<sup>1</sup> Maliha A. Alikhan,<sup>2</sup> Daniel S. Layton,<sup>3</sup> Sharon D. Ricardo<sup>1\*</sup>

<sup>1</sup>Department of Anatomy and Developmental Biology, Monash University, Victoria, Australia

<sup>2</sup>Monash Centre for Inflammatory Diseases, Monash University, Victoria, Australia

<sup>3</sup>Monash Antibody Technologies Facility, Monash University, Victoria, Australia

Received 13 June 2013; Revised 1 November 2013; Accepted 6 November 2013

Grant sponsor: National Health and Medical Research Council (NHMRC); Grant number: 1003806; Grant sponsor: the Alport Foundation of Australia.

Additional Supporting Information may be found in the online version of this article.

\*Correspondence to: Sharon D. Ricardo; Department of Anatomy and Developmental Biology, Level 3, Building 75, Monash University, Clayton, Victoria 3800, Australia.

Published online 00 Month 2013 in Wiley Online Library (wileyonlinelibrary.com)

DOI: 10.1002/cyto.a.22420

© 2013 International Society for Advancement of Cytometry

## • Abstract

Polychromatic flow cytometry is a powerful tool for assessing populations of cells in the kidney through times of homeostasis, disease and tissue remodeling. In particular, macrophages have been identified as having central roles in these three settings. However, because of the plasticity of myeloid cells it has been difficult to define a specific immunophenotype for these cells in the kidney. This study developed a gating strategy for identifying and assessing monocyte and macrophage subpopulations, along with neutrophils and epithelial cells in the healthy kidney and following ischemia/reperfusion (IR) injury in mice, using antibodies against CD45, CD11b, CD11c, Ly6C, Ly6G, F4/80, CSF-1R (CD115), MHC class II, mannose receptor (MR or CD206), an alternatively activated macrophage marker, and the epithelial cell adhesion marker (EpcAM or CD326). Backgating analysis and assessment of autofluorescence was used to extend the knowledge of various cell types and the changes that occur in the kidney at various time-points post-IR injury. In addition, the impact of enzymatic digestion of kidneys on cell surface markers and cell viability was assessed. Comparisons of kidney myeloid populations were also made with those in the spleen. These results provide a useful reference for future analyses of therapies aimed at modulating inflammation and enhancing endogenous remodeling following kidney injury. © 2013 International Society for Advancement of Cytometry

## • Key terms

monocyte; macrophage; kidney; ischemia/reperfusion injury

## INTRODUCTION

A common feature of the progression of immune and nonimmune kidney disease of diverse aetiology is the infiltration of inflammatory macrophages (1). Macrophage numbers have shown to correlate with disease progression, making them a useful tool in predicting disease outcome (1–3). More recently, macrophage heterogeneity has been shown to correspond to the diverse roles that these cells play in both the initiation of tissue fibrosis and the positive role in wound healing and tissue remodeling (4,5). Monocytes recruited in response to inflammatory cues can undergo differentiation into two broad macrophage subsets based on phenotype, function, and polarization state. The classically activated or M1 macrophage is the pro-inflammatory cell type closely associated with the innate immune response, whereas the alternatively activated or M2 macrophage possesses a range of anti-inflammatory and wound healing capabilities (6–8). In part, achieving wound repair and tissue remodeling requires an appropriate balance between the M1 and M2 polarization states.

Traditionally, studies investigating the number of infiltrating macrophages in damaged kidneys have relied on immunohistochemistry (IHC) and immunofluores-

cence (IF) techniques to assess kidney histopathology, cell morphology, and receptor expression. However, flow cytometry is becoming an increasingly important tool, particularly because of the ability to evaluate a panel of cell surface and intracellular markers on individual cells at a rate of over 10,000 cells/second. Eight-color polychromatic flow cytometry in conjunction with two nonfluorescent parameters, forward and side light scattering, is now common and with the latest flow cytometers measuring up to 20 parameters, the information obtainable from each experiment is destined to grow, and with it the need for more rigorous methods of data analysis (9). However, even with improving technology, there remain a number of key challenges related to the preparation of kidney samples for flow cytometry, the selection of appropriate target markers and the informative analysis of the resulting data, which need to be addressed.

The aim of this study was to assess the impact of enzymes (used to produce a kidney single cell suspension) and ischemia/reperfusion (IR) injury on cell yield, viability, surface marker expression, and autofluorescence. Gating strategies were created that best characterize various myeloid cell types, especially where particular receptors were expressed at low levels. The panel of monocyte-, macrophage-, dendritic cell (DC)- and granulocyte-associated markers used included CD11b, CD11c, Ly6C, Ly6G, major histocompatibility complex class II (MHCII), colony stimulating factor-1 receptor (CSF-1R or CD115), mannose receptor (MR or CD206), and F4/80. Particular emphasis of the study was on the assessment of kidney myeloid cell analysis in the inflammatory phase of IR injury, which is characterized by widespread epithelial cell death, an influx of pro-inflammatory cells and heightened inflammatory cytokine production.

In addition, the apoptotic and necrotic epithelial cells of the damaged kidney tubular epithelium, related to the reduced glomerular filtration that follows injury, leads to the accumulation of tubular casts (10). This hallmark of acute kidney injury results in autofluorescence and nonspecific background signals, which leads to difficulties in interpretation of flow cytometric data that is unique to the kidney. Unless addressed, this can lead to erroneous analysis. The intrinsic autofluorescent properties of kidney cells also apply to macrophages because of their propensity to phagocytose cellular debris.

Finally, backgating analysis was used to define and extend the knowledge of myeloid subpopulations in terms of their co-expression of multiple markers and for their spatial location on parent dot plots. This study clarifies and addresses the anomalies encountered when assessing myeloid cells in the kidney, as compared to the more commonly assessed primary and secondary lymphoid organs, while forming a comparative base for which various therapies aimed at manipulating cell numbers and function can be referenced.

## MATERIALS AND METHODS

### Animals and Surgery

Male 6–8 week old (20–25 g) C57BL/6J mice obtained from Monash Animal Services (Melbourne, Australia) were

used. All studies were approved by the Monash University Animal Ethics Committee and were performed in accordance with the *Australian Code of Practice for the Care and Use of Animals for Scientific Purposes*. Mice were anesthetized with 2.0% inhaled isoflurane (Abbott Australasia, Sydney, Australia) before the left renal pedicle was occluded using a vascular clamp (0.4–1.0 mm; Fine Science Tools, Heidelberg, Germany) for 40 min via a flank incision to induce unilateral IR injury ( $n = 5$  mice/group/time-point). Following removal of the clamp, reperfusion was visually confirmed prior to wound closure using silk suture (size 5-0, Ethicon, NJ, USA). An additional group of mice served as a sham-operated control group where the animals were anaesthetized and a flank incision was performed without renal pedicle clamping.

### Digestion and Preparation of the Kidney and Spleen for Flow Cytometry

Mice were culled using a CO<sub>2</sub> cull chamber at 6 hours, 1 day or 7 days after IR injury. The spleen and left kidney were removed and placed in cold FACS buffer (PBS supplemented with 0.2% BSA, 0.02% NaN<sub>3</sub> and 5 mM EDTA).

Spleens were cleaned of any connective tissue and mechanically digested in cold FACS buffer to produce a single cell suspension. Mechanical digestion (MD) was achieved by making small incisions in the side of the spleen before gently pressing the organ between two frosted glass slides.

Kidneys were decapsulated and finely chopped with surgical scissors before enzymatic digestion (ED) in 1 mL of dissociation media consisting of HBSS (Sigma-Aldrich, St. Louis, MO, USA) supplemented with 3 mg/mL collagenase/dispase (Roche Applied Science, Penzberg, Germany), 0.2 mg/mL DNase type 1 (Roche Applied Science), 50  $\mu$ M CaCl<sub>2</sub>, preheated to 37°C. The samples were mixed on a rotary tube suspension mixer (20 RPM; Ratek Instruments, Melbourne, Australia) at 37°C for 20 min and then mechanically digested using a 1000  $\mu$ L pipette tip. The samples were mixed for two further 5 min periods (20 RPM) with mechanical dissociation in between. After 30 min, mechanical dissociation with an 18-gauge needle resulted in a single cell suspension. Nine mL of cold FACS buffer was added in order to inhibit enzyme activity.

ED for kidneys and MD for spleens were used for all aspects of this study except for the comparison between ED and MD (Section “Using Enzymes to Aid in the Digestion of the Kidney is more Suitable than MD Alone” and Fig. 1) where both ED and MD were performed on each of the organs.

All single cell suspensions were incubated for 1 min with 1 mL of red blood cell lysis buffer (8.3 g/L Na<sub>4</sub>Cl, 10 mM Tris-HCl, pH7.5) to remove red blood cells. All samples were filtered with a 40  $\mu$ m nylon cell strainer (BD Bioscience, San Jose, USA) prior to antibody labeling.

### Cell Counts and Viability

For flow cytometry cell preparation, cell counts and viability determination were performed using a Z2 Coulter Counter (Beckman Coulter, USA). In addition, for the ED

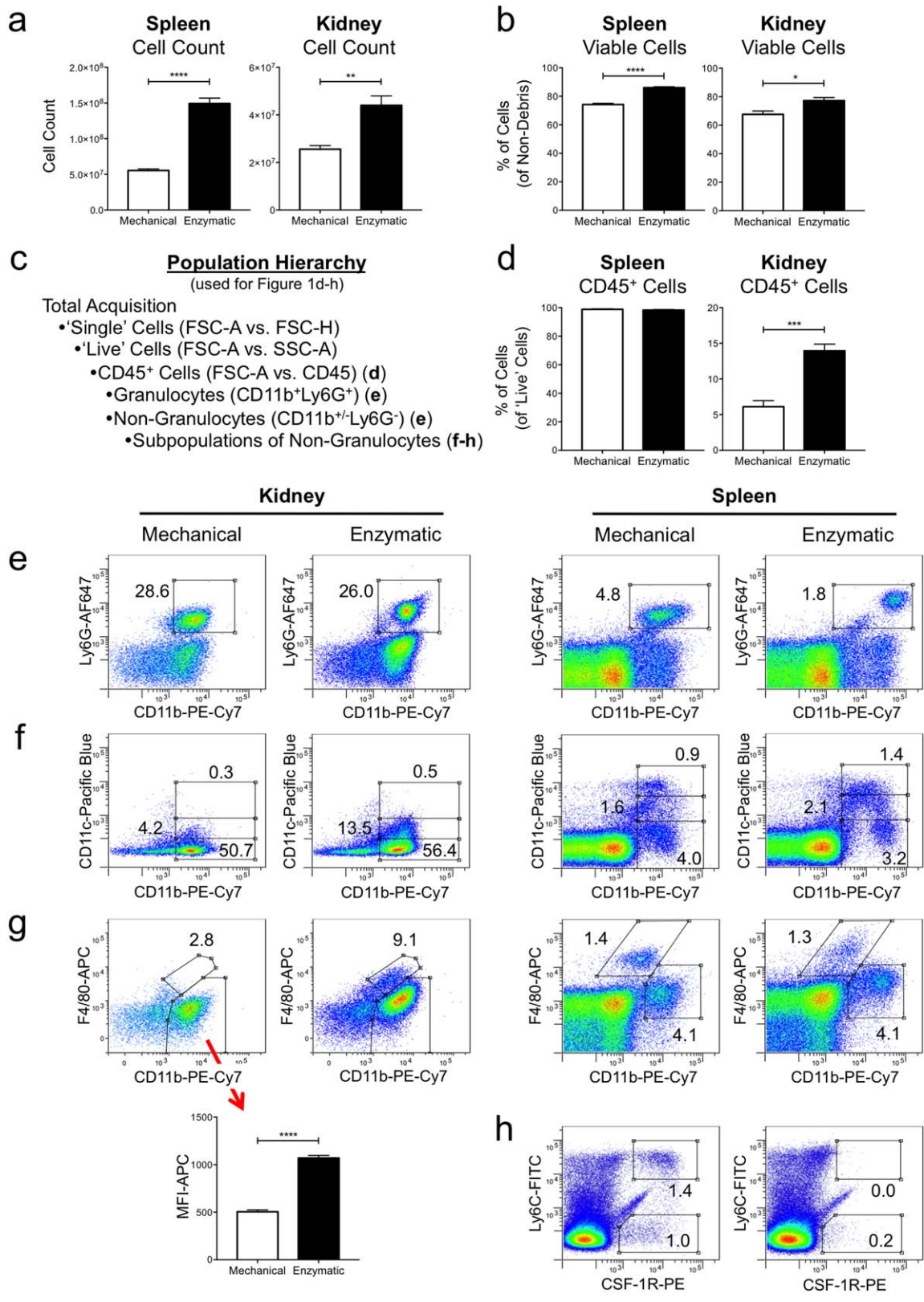


Figure 1.

ROO

versus MD study, propidium iodide (PI) was also used to determine cell viability.

### Antibody Labeling

Three million cells from kidney or spleen single cell suspensions were incubated for 20 min at 4°C in the dark with the following fluorochrome-conjugated antimouse antibodies: anti-CD45 APC-Cy7 (clone 30-F11; Biolegend, San Diego, USA) and PE-Cy5 (clone 30-F11; BD Biosciences), anti-CD11b PE-Cy7 (clone M1/70; BD Biosciences), anti-CD11c Pacific Blue (clone N418; Biolegend), anti-I-A/I-E (MHCII) PE-Cy5 (clone M5/114.15.2; Biolegend), anti-CSF-1R (CD115) PE (clone AFS98; eBioscience, San Diego, USA), anti-F4/80 APC (clone BM8; eBioscience), anti-Ly6G Alexa Fluor 647 (clone 1A8; Biolegend), anti-Ly6C FITC (clone HK1.4; Biolegend), anti-CD206 (mannose receptor) Alexa Fluor 488 (clone C068C2; Biolegend), and anti-EpCAM (CD326) PE-Cy7 (clone G8.8; Biolegend). Fc receptor block (anti-CD16/32 antibody) was added to all antibody cocktails. Intracellular MR labeling involved the use of a CytoFix/CytoPerm kit (BD Biosciences). Following surface receptor labeling, cells were permeabilized and incubated with antibody for 30 min at 4°C in the dark before being washed twice in 1× Perm/Wash buffer (BD Biosciences) and resuspend in FACS buffer. Isotype matched controls were used for each antibody in a fluorescence minus one (FMO) manner.

### Flow Cytometric Acquisition and Analysis

Data were acquired on a BD FACS Canto II flow cytometer (BD Biosciences) equipped with 405, 488, and 633 nm excitation lasers in conjunction with FACS Diva acquisition software (BD Biosciences). Compensation was performed with single color controls for each organ using the same conjugated antibodies used in the study. Data analysis was performed using FlowLogic FCS analysis software (Inivai Technologies, Melbourne, Australia).

### Statistical Analysis

Statistical analysis was performed using GraphPad Prism software version 6.0c (GraphPad Software, San Diego, USA). A Student's *t*-test (unpaired, two-tailed, with Welch's correction) was used to analyze data between two groups. A one-way analysis of variance with a Tukey's multiple comparisons

test was used to analyze data contained in three groups. Data are displayed as means ± SEM.  $P < 0.05$  was considered statistically significant.

## RESULTS

### Using Enzymes to Aid in the Digestion of the Kidney is more Suitable than MD Alone

Using enzymes (collagenase/dispase, DNase type I) to aid in the digestion of kidney tissue risks cleaving particular cell surface receptors. In addition, optimal primary and secondary lymphoid organ cell preparations are often achieved with MD alone. It was therefore necessary to test whether ED is indeed required for kidney dissociation. Ten mice received 40 min unilateral IR injury and 24 hours later the spleen and injured kidney were removed. One group of 5 mice had both organs digested with the aid of enzymes, whereas the remaining mice had their organs digested purely by mechanical means. Once digested, cells from each organ were labeled with antibodies against CD45, CD11b, CD11c, Ly6G, Ly6C, MHCII, F4/80, and CSF-1R, and assessed using flow cytometry. Our data show that in both the spleen and the kidney, ED yielded a higher viable cell count compared to MD (spleen MD:  $5.54 \times 10^7$ , spleen ED:  $1.49 \times 10^8$ ,  $P < 0.0001$ ; kidney MD:  $2.56 \times 10^7$ , kidney ED:  $4.40 \times 10^7$ ,  $P = 0.0025$ ) (Fig. 1a). Furthermore, propidium iodide staining revealed that ED yielded greater viability for both spleen and kidney cells (spleen MD: 74.2%, spleen ED: 86.1%,  $P < 0.0001$ ; kidney MD: 67.7%, kidney ED: 77.3%,  $P = 0.0153$ ) (Fig. 1b). In assessing hematopoietic cells (as per the gating hierarchy described in Fig. 1c), we found no difference in the proportion of CD45<sup>+</sup> leukocytes in the spleen with the different digestion methods (MD: 98.8%, ED: 98.3%). However, ED of the kidney resulted in a significantly greater proportion of CD45<sup>+</sup> cells compared to MD (MD: 6.1%, ED: 13.9%,  $P = 0.0003$ ) (Fig. 1d). Within the CD45<sup>+</sup> cell pool in the kidney, the digestion method caused no difference in the proportion of Ly6G<sup>+</sup> granulocytes (MD: 28.6%, ED: 26.0%). However, in the spleen, ED significantly reduced the proportion of this cell type (MD: 4.8%, ED: 1.8%,  $P = 0.0241$ ) (Fig. 1e). In both organs, ED significantly increased the expression (mean fluorescence intensity) of both

**Figure 1.** Using enzymes to aid in the digestion of the kidney is more suitable than mechanical digestion alone. To compare the effects of two different organ digestion methods, spleens and kidneys from mice at 24 hours post-IR injury were subjected to either mechanical digestion (MD) or enzymatic digestion (ED). For both organs, ED yielded a higher cell count (a). ED also resulted in a greater proportion of viable cells as assessed using propidium iodide (b). The gating hierarchy used to assess viable cells, CD45<sup>+</sup> cells, Ly6G<sup>+</sup> granulocytes, and subpopulations of CD11b<sup>+</sup>Ly6G<sup>+</sup> cells is shown (c). There was no difference in the proportion of CD45<sup>+</sup> cells in the spleen between ED and MD. However, ED yielded a greater proportion of CD45<sup>+</sup> cells in the kidney compared to MD (d). The digestion method had no impact on the proportion of CD11b<sup>+</sup>Ly6G<sup>+</sup> granulocytes in the kidney but significantly reduced the proportion of granulocytes in the spleen (e). In the spleen ED resulted in a greater proportion of CD11b<sup>+</sup>CD11c<sup>high</sup> and CD11b<sup>+</sup>CD11c<sup>low</sup> cells compared to MD (f). However, ED increased CD11b expression and resulted in less well-defined CD11c populations (f). The CD11b<sup>+</sup>CD11c<sup>high</sup> group was largely absent in the kidney, while ED greatly increased the proportion of the CD11b<sup>+</sup>CD11c<sup>low</sup> population (f). There was no significant difference in the proportions between the CD11b<sup>+</sup>CD11c populations in either organ with regards to the digestion method (f). The proportion of F4/80<sup>+</sup> cells was significantly greater in the kidney following ED compared to MD (g). No difference was observed in this population in the spleen between MD and ED (g). The MFI of the CD11b<sup>+</sup>F4/80<sup>low</sup> population in the kidney (depicted graphically) was significantly increased following ED compared to MD (g). CSF-1R expression was dramatically reduced in the spleen following ED compared to MD for both Ly6C<sup>high</sup> and Ly6C<sup>+</sup> populations (h). Numbers on dot plots represent proportions of parent populations. Statistical analysis was performed using a Student's *t*-test (unpaired, two-tailed, with Welch's correction); \*\* $P < 0.01$ , \*\*\* $P < 0.001$ , \*\*\*\* $P < 0.0001$ . Data are displayed as means ± SEM ( $n = 5$ /group).

Ly6G and CD11b on this population, as seen in the dot plots (Fig. 1e) (data not shown).

After excluding the granulocytes, three populations of CD11b<sup>+</sup> cells were assessed in conjunction with CD11c expression (Fig. 1f). In the spleen, ED resulted in a greater proportion of CD11b<sup>+</sup>CD11c<sup>high</sup> DCs (MD: 0.9%, ED: 1.4%,  $P = 0.0034$ ), although the populations were less well defined compared to those acquired following MD (Fig. 1f). There were very few cells that shared this phenotype in the kidney, regardless of the digestion method.

The proportion of a second population, which expressed low levels of CD11c, was statistically higher following ED in both the kidney (MD: 4.2%, ED: 13.5%,  $P = 0.0003$ ) and spleen (MD: 1.6%, ED: 2.1%,  $P = 0.0084$ ) (Fig. 1f).

There was no significant difference in the proportion of CD11b<sup>+</sup>CD11c<sup>-</sup>(Ly6G<sup>-</sup>) cells between the two groups in either the kidney (MD: 50.7%, ED: 56.4%) or spleen (MD: 4.0%, ED: 3.2%) (Fig. 1f).

F4/80 expression was assessed on the same CD11b<sup>+</sup>Ly6G<sup>-</sup> population with a notable difference identified between the two digestion methods in the kidney. With MD, the F4/80<sup>+</sup> cells were barely detectable but made up over 9% of CD11b<sup>+</sup>Ly6G<sup>-</sup> cells following ED (MD: 2.8%, ED: 9.1%,  $P < 0.0001$ ) (Fig. 1g). In the spleen there was no difference in the proportion of F4/80<sup>+</sup> cells (MD: 1.4%, ED: 1.3%) although the population appeared more dispersed following ED (Fig. 1g). In addition, the two digestion methods resulted in substantial differences in the CD11b<sup>+</sup>F4/80<sup>low/-</sup> populations in the kidney. Once gated, the MFI for the F4/80-APC parameter was assessed and shown to be significantly greater following ED (MD: 505 MFI, ED: 1070 MFI,  $P < 0.0001$ ) (Fig. 1g).

In the spleen, ED reduced the expression of two CSF-1R<sup>+</sup> populations: a Ly6C<sup>high</sup>CSF-1R<sup>+</sup> (MD: 1.38%, ED: 0.03%,  $P = 0.0073$ ) and a Ly6C<sup>-</sup>CSF-1R<sup>+</sup> population (MD: 1.0%, ED: 0.2%,  $P < 0.0001$ ) (Fig. 1h). Very few CSF-1R<sup>+</sup> cells were detected in either group in the kidney (data not shown). It must be noted that a change in the proportion of one population can affect the proportion of other populations. However, ED does appear important for assessing F4/80 expression in the kidney, while dramatically reducing surface CSF-1R expression, as demonstrated in the spleen. With this knowledge, a suitable gating strategy was created to clearly identify subpopulations of CD11b<sup>+</sup> cells in the kidney, both in the steady state and in the inflammatory phase following IR injury.

### Gating Strategy for Myeloid Cells in the Kidney

With up to eight-color flow cytometry commonly employed to assess cell phenotypes, there are inevitably many different theoretical subsets that can be defined in any experiment. Here we describe a gating procedure designed to clearly identify important myeloid cell populations in the kidney, accounting for the high potential for autofluorescence, particularly following injury. Figure 2a outlines the population hierarchy used to distinguish between CD11b<sup>+</sup>Ly6G<sup>+</sup> granulocytes and CD11b<sup>+</sup>Ly6G<sup>-</sup> nongranulocytes. Initially, a

polygon gate was created on the FSC-A vs. FSC-H plot to select the ‘Single’ cells that passed by the lasers individually (Fig. 2b). CD45<sup>+</sup> cells from the resulting daughter population were subsequently viewed against FSC-A. These cells represent a viable CD45<sup>+</sup> population as compared with a similar population identified using propidium iodide to exclude dead cells (data not shown). These CD45<sup>+</sup> cells were colored red and viewed on a FSC-A vs. SCA-A plot. The coloring of this population enabled a ‘Live’ gate to be drawn on the FSC-A vs. SCA-A plot, to select viable hematopoietic cells and exclude debris (Fig. 2b). This is otherwise difficult to achieve when assessing cells in the kidney as compared to those from lymphoid organs because of the low proportion of CD45<sup>+</sup> cells. This same technique can also be employed to aid in the creation of the initial ‘Single’ cells gate. A population of CD45<sup>+</sup>CD11b<sup>+</sup> cells (encompassing resident and infiltrating myeloid cells) was selected from the ‘Live’ cell pool (Fig. 2b). The plots in Figure 2b represent the cells in the kidney 6 hours post-IR surgery, which is characterized by an influx of CD45<sup>+</sup> cells. Granulocytes were identified in the resulting daughter population based on the positive expression of Ly6G (also Ly6C<sup>low</sup>) (Fig. 2c) with their proportion being significantly higher at 6 hrs post-IR injury (sham-IR: 23.0%, IR: 28.3%,  $P = 0.0222$ ). An inverse gate effectively excluded the granulocytes for further analysis of myeloid cell subpopulations. Examples from sham-IR and IR kidneys at 6 hours post-surgery are shown (Fig. 2c).

### Gating Strategy for Myeloid Cell Subpopulations in the Kidney

The gating strategy used to interrogate CD11b<sup>+</sup>Ly6G<sup>-</sup> subsets shown in Figure 3a extends from the gating procedure described in Section “Gating Strategy for Myeloid Cells in the Kidney”. Expression of the antigen-presenting molecule MHCII was compared to other markers to identify subpopulations of monocytes and macrophages. An intracellular antibody against MR was used to identify M2 macrophages (Fig. 3b). A quadrant gate was used to identify two MR<sup>+</sup> populations based on a combination of MR and MHCII expression. While most mature M2 macrophages co-express MHCII (16.9% of CD45<sup>+</sup>CD11b<sup>+</sup>Ly6G<sup>-</sup> cells at 24 hrs post-IR injury), there was a population of MHCII<sup>-</sup> cells in which MR was detected (8.5%). The example shown is from a kidney assessed 24 hours following IR injury, prior to the recognized tissue remodeling phase, where M2 macrophages are the predominant macrophage population (11).

CD11b<sup>+</sup>Ly6G<sup>-</sup> cells were also examined for their expression of the monocyte-associated marker Ly6C (Fig. 3c), the historical mature macrophage marker F4/80 (Fig. 3d) and the DC-associated marker CD11c (Fig. 3e). These markers were all compared to the expression of MHCII. Both a Ly6C<sup>high</sup> (sham-IR: 3.8%, IR: 27.9%,  $P = 0.0004$ ) and a Ly6C<sup>low</sup> (sham-IR: 1.4%, IR: 4.5%,  $P = 0.0257$ ) population not expressing MHCII were identified with a much greater proportion in the IR injured kidney. Ly6C is a marker of monocyte immaturity and expression is lost as monocytes transition into macrophages. A general population of Ly6C<sup>+</sup> cells expressing MHCII was seen (sham-IR: 3.3%, IR: 11.0%,  $P = 0.0066$ ),

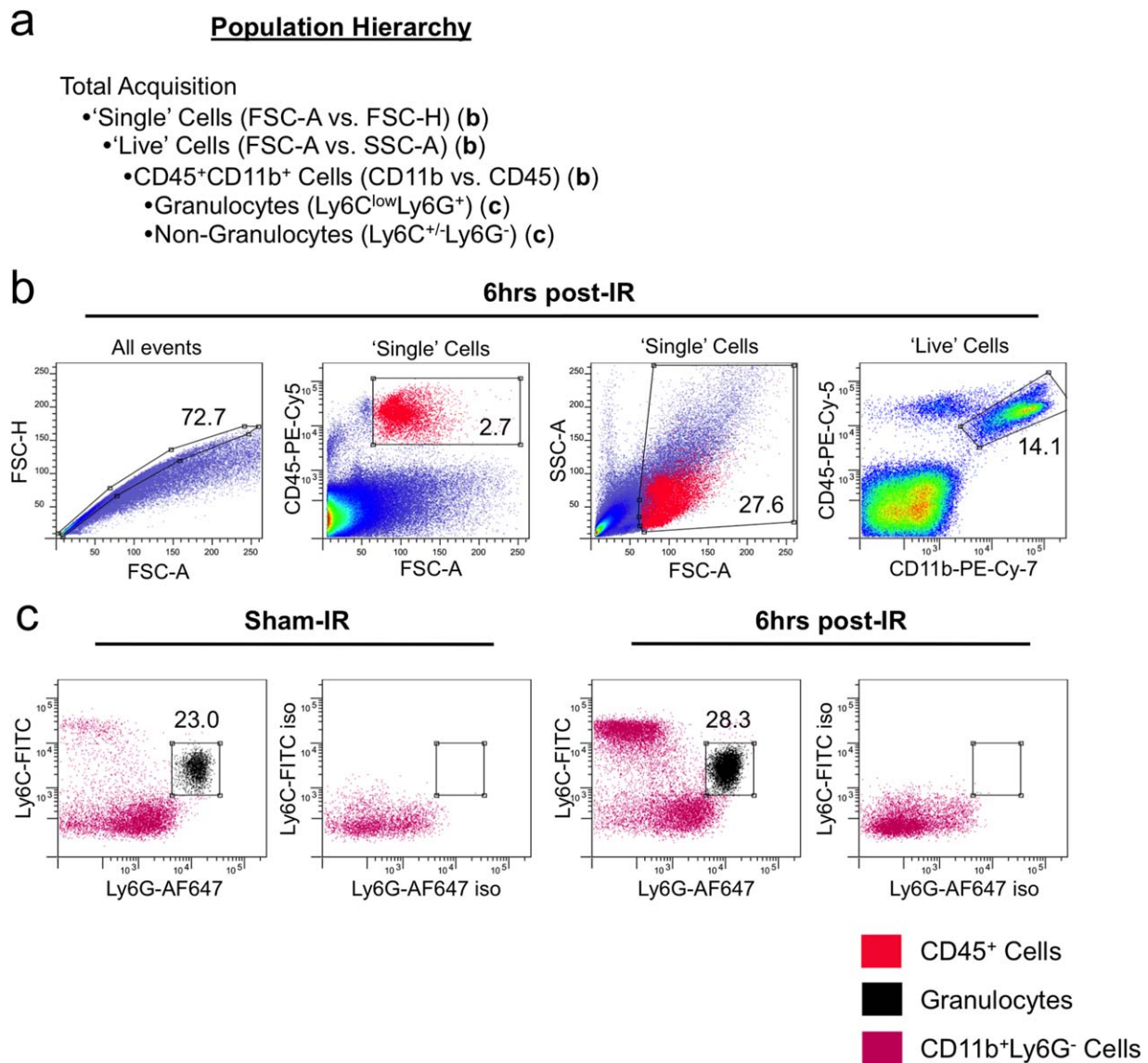


**Figure 2.** Gating strategy for assessing myeloid cells in the kidney. The population hierarchy shows the CD11b<sup>+</sup> gating strategy (a). 'Single' cells (excluding doublets and triplets) were selected with a polygon gate on a FSC-A vs. FSC-H dot plot (b). CD45<sup>+</sup> cells were gated on the resulting daughter population on a FSC-A vs. CD45 dot plot. These cells were colored (red) and viewed on a FSC-A vs. SSC-A dot plot (b). A 'Live' cell gate (which excludes debris) was created with the aid of the colored CD45<sup>+</sup> cells (b). CD45<sup>+</sup>CD11b<sup>+</sup> cells were selected with a polygon gate (b). Granulocytes were selected by gating on Ly6C<sup>low</sup>Ly6G<sup>+</sup> cells (c). An inverse gate to select CD11b<sup>+</sup>Ly6C<sup>+/−</sup>Ly6G<sup>−</sup> cells (pink) was used to gate out granulocytes (black) for further analysis of myeloid cell subsets (c). Plots in b are from a kidney taken 6 hours post-IR injury. Plots in c are from kidneys taken 6 hours post-IR surgery from IR and sham-IR animals. Numbers on dot plots represent proportions of parent populations.

indicating a population of maturing monocytes, which appear to down-regulate their expression of Ly6C and up-regulate MHCII concomitantly (Fig. 3c). F4/80 has historically been regarded as a mature macrophage marker (12). However, more recent reports have shown that it is not expressed on all macrophage populations and has been identified on some Ly6C<sup>+</sup> monocytes along with a range of other myeloid cells, revoking its status as a sole identifier of macrophages (13–16). When viewed against MHCII, three F4/80<sup>+</sup> populations were identified (Fig. 3d). The classical F4/80<sup>+</sup>MHCII<sup>high</sup> mature macrophage was prominent in both sham-IR and IR groups

(gated population) (sham-IR: 59.0%, IR: 30.5%,  $P = 0.0001$ ). When viewed as an overlay containing F4/80 stained cells and an isotype control antibody, an F4/80<sup>+</sup>MHCII<sup>low</sup> and an F4/80<sup>+</sup>MHCII<sup>high</sup> population were made evident, particularly following IR-injury (Fig. 3d). The latter population also corresponded with the Ly6C<sup>high</sup> monocyte population when these cells were gated on a MHCII vs. Ly6C plot and colored (green) (Fig. 3d).

There is much discussion surrounding the similarities and differences between macrophages and DCs. In this model, a clearly defined CD11b<sup>+</sup>CD11c<sup>high</sup> population, generally

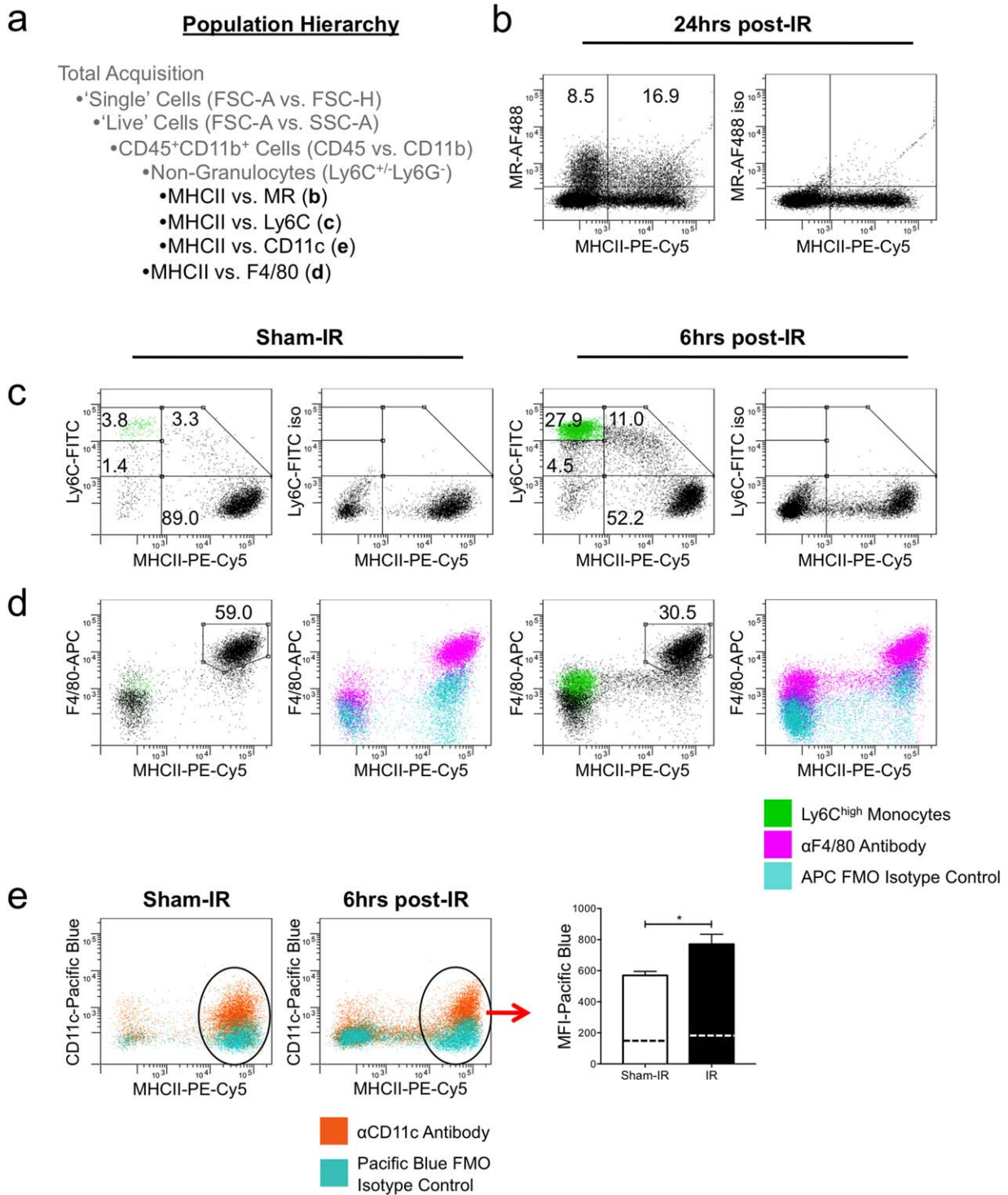


Figure 3.

recognized as DCs, was not observed in the kidney (Fig. 3e). There were cells that expressed a low level of CD11c but this population differs from the distinct CD11c<sup>high</sup> DCs seen in other organs, such as the spleen. For this reason, CD11c expression was viewed on the CD45<sup>+</sup>CD11b<sup>+</sup> population, rather than as an initial differentiating marker for macro-

phages and DCs. To further investigate the changes to these cells following IR injury, the entire MHCII<sup>high</sup> population was gated and the change in the MFI of the anti-CD11c antibody analyzed. As seen in the overlay plots for both the sham-IR and the IR groups at 6 hours postsurgery, antibody labeling exists at levels above the isotype control. There is also a

significant increase in the MFI of this parameter following IR injury (sham-IR: 570 MFI, IR: 770 MFI,  $P = 0.031$ ) (Fig. 3e).

### Kidney and Spleen Ly6C<sup>+</sup>, Ly6G<sup>+</sup>, and MHCII<sup>+</sup> Cell Population Comparison

Backgating analysis was used to further characterize various myeloid subpopulations in the kidney. Comparisons were also made between these cells and their counterparts in the spleen. Figure 4a shows Ly6G<sup>+</sup> (Ly6C<sup>low</sup>) granulocytes (dark blue). These cells are also displayed on the grandparent FSC-A vs. SSC-A plot (Figure 4b). Granulocytes in the spleen appear similar to those in the sham-IR and IR kidneys 6 hours post-surgery. However, they compose a greater proportion of the CD45<sup>+</sup>CD11b<sup>+</sup> pool (spleen: 72.5%, sham-IR kidney: 23.0%, IR kidney: 28.3%).

In a similar fashion, MHCII<sup>+</sup>Ly6C<sup>-</sup> cells (red) (Fig. 4a) were backgated and overlaid onto the same FSC-A vs. SSC-A plots (Fig. 4b) (spleen: 34.2%, sham-IR kidney: 89.0%, IR kidney: 52.2% of the CD45<sup>+</sup>CD11b<sup>+</sup>Ly6G<sup>-</sup> pool). A far greater proportion and number of Ly6C<sup>high</sup> cells (green) were present in the IR kidney compared to the sham-IR kidneys (spleen: 31.2%, sham-IR kidney: 3.8%, IR kidney: 27.9% of the CD45<sup>+</sup>CD11b<sup>+</sup>Ly6G<sup>-</sup> pool) (Fig. 4a). There were distinctly fewer MHCII<sup>-</sup>Ly6C<sup>low</sup> cells (purple) compared to the Ly6C<sup>high</sup> population (spleen: 9.2%, sham-IR kidney: 1.4%, IR kidney: 4.5% of the CD45<sup>+</sup>CD11b<sup>+</sup>Ly6G<sup>-</sup> pool) (Fig. 4a). The maturing or transitioning monocytes (MHCII<sup>low</sup>Ly6C<sup>+</sup>, light blue) are also most prevalent in the IR compared to the sham-IR kidneys (spleen: 12.4%, sham-IR kidney: 3.3%, IR kidney: 11.0% of the CD45<sup>+</sup>CD11b<sup>+</sup>Ly6G<sup>-</sup> pool) (Fig. 4a). All of the Ly6C expressing cells from both organs present in a similar fashion on the FSC-A vs. SCA-A plots, as do the MHCII<sup>+</sup> populations. The granulocyte population in the spleen appears to be composed of cells with a greater range of size and granularity compared to that in the kidney (Fig. 4b).

### Assessing Epithelial Cells and Autofluorescence in the Post-Ischemic Kidney

Epithelial proliferation leading to regeneration and repair is central to processes of healing following various forms of kidney disease, including IR injury (17). As such, the pan epithelial marker EpCAM was used to assess the impact of IR injury on epithelial cell populations. To assess EpCAM<sup>+</sup> cells,

'Single' cells were gated, followed by 'Live' cells (to exclude debris), as depicted in the population hierarchy (Fig. 5a). EpCAM expression was then compared to CD45 expression, with a gate placed around the CD45<sup>+</sup>EpCAM<sup>+</sup> population (Fig. 5b). The proportion of EpCAM<sup>+</sup> cells had already significantly decreased at 6 hours post-IR injury (sham-IR: 16.3%, IR: 9.6%,  $P=0.0001$ ) and fell further as seen at day 7 postinjury (sham-IR: 14.3%, IR: 5.9%,  $P=0.0001$ ). Autofluorescence can pose a problem, as is evident when the kidneys taken 6 hours post-IR are displayed alongside those taken 7 days postinjury, where prominent autofluorescence is visible in the IR anti-EpCAM antibody and isotype control groups (Fig. 5b). The autofluorescence was not present in the IR group 6 hours postinjury. For the day 7 time-point, a modified EpCAM<sup>+</sup> gate was created in order to exclude the autofluorescence from the EpCAM<sup>+</sup> population. This method can also be employed for clearly distinguishing CD45<sup>+</sup> cells from the rest of the kidney cells. Backgating analysis of the EpCAM<sup>+</sup>, autofluorescent and CD45<sup>+</sup> cells was performed to view their location on the parent FSC-A vs. SSC-A dot plot (Fig. 5c). The difference between the different cell types is clear, with the CD45<sup>+</sup> cells forming a tighter group further along the forward scatter axis compared to the EpCAM<sup>+</sup> cells and autofluorescent events.

Autofluorescence increases progressively with time after IR injury. Figure 5d shows autofluorescent cells, after gating on CD45<sup>+</sup>CD11b<sup>+</sup> cells, on a Ly6C vs. MHCII plot from a sham-IR kidney along with injured kidneys at 24 hours and 7 days post-IR. The autofluorescent populations were backgated and shown in pink on the CD11b vs. CD45 parent plot. At 7 days post-IR the autofluorescence is very difficult to distinguish from nonautofluorescent CD11b<sup>+</sup> cells. Empty channels may be useful for gating out autofluorescence that is associated with IR-induced damage. The increase in the autofluorescence increased almost threefold between 24 hours and 7 days post-IR injury (sham-IR: 1.3%, 24 hrs post-IR: 7.8%, 7 days post-IR: 21.2%) (Fig. 5e).

### DISCUSSION

Identifying and characterizing macrophage functional/polarization states is necessary to understand processes of disease progression and healing. Here, we have described a polychromatic flow cytometry analysis strategy, taking into

**Figure 3.** Gating strategy for CD11b<sup>+</sup> cell subpopulations in the kidney. The gating hierarchy (continued from Figure 2) shows the procedure used to assess CD11b<sup>+</sup> cells following the exclusion of Ly6G<sup>+</sup> granulocytes (a). M2 macrophages, defined as being MR<sup>+</sup>, were assessed in conjunction with the expression of MHCII (b). Subsequent monocyte/macrophage subsets were defined based on the cellular expression of MHCII, Ly6C, F4/80 and CD11c (c–e). Ly6C was used to distinguish monocytes at various maturation stages. Ly6C<sup>high</sup> cells (MHCII<sup>-</sup>) are immature monocytes. The marker is down regulated as the cells mature. A prominent Ly6C<sup>high</sup> (MHCII<sup>-</sup>) population is present at 6hrs post-IR injury (green) (c), along with a smaller Ly6C<sup>low</sup>MHCII<sup>-</sup> population (c). A maturing or transitioning population of MHCII<sup>low</sup>Ly6C<sup>+</sup> cells exist, particularly following IR-injury (c). A prominent Ly6C<sup>high</sup>MHCII<sup>high</sup> population exists in kidneys following both sham-IR and IR-surgery (c). MHCII can also be used to distinguish between three F4/80<sup>+</sup> populations. A prominent F4/80<sup>+</sup>MHCII<sup>high</sup> population was identified (gated cells) (d). The dot plot overlay shows this population (pink) compared with an isotype control antibody (light blue) (d). The overlay also helped identify populations of F4/80<sup>+</sup>MHCII<sup>low</sup> and F4/80<sup>+</sup>MHCII<sup>-</sup> cells. The latter corresponds to the Ly6C<sup>high</sup> population (green) (d). Low levels of CD11c expression can make it difficult to distinctly categorize CD11c<sup>+</sup> cells in the kidney, as opposed to its expression when examined in lymphoid organs or the blood. Here the CD11c labeled cells (orange) were overlaid with an isotype control (light blue) (e). In addition, the MFI of the CD11c-Pacific Blue antibody was assessed for the MHCII<sup>high</sup> population. These data are displayed graphically with the MFI for the isotype controls indicated using a broken line (e). Appropriate isotype controls (iso) are displayed. Numbers on dot plots represent proportions of parent populations. Statistical analysis was performed using a Student's *t*-test (unpaired, two-tailed, with Welch's correction); \* $P < 0.05$ . Data are displayed as means  $\pm$  SEM ( $n = 5$ /group).

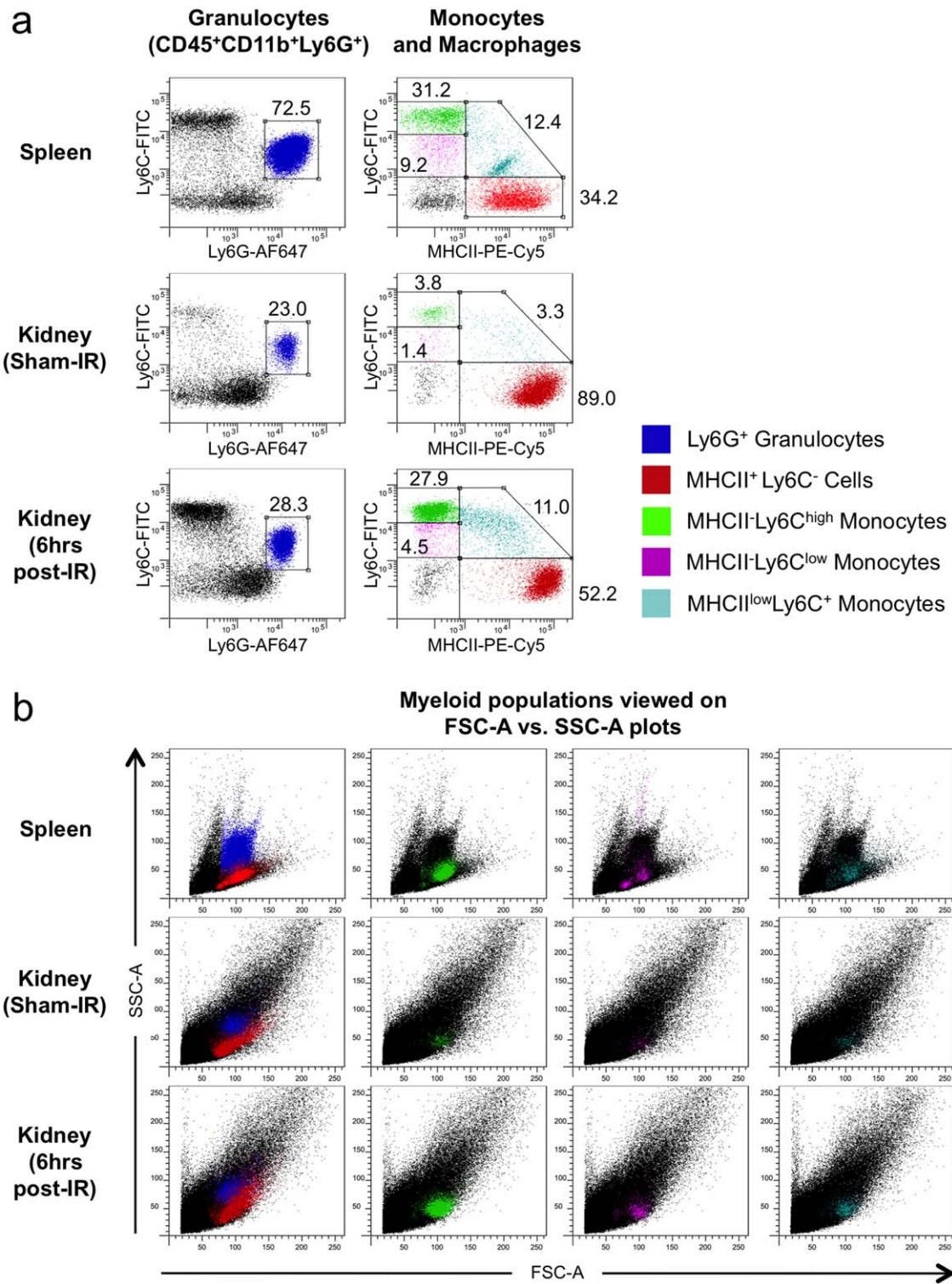


**Figure 4.** Kidney and spleen Ly6C<sup>+</sup>, Ly6G<sup>+</sup> and MHCII<sup>+</sup> cell population comparison. Backgating analysis of flow cytometry data was used to compare the relative positioning of Ly6G<sup>+</sup> granulocytes (dark blue), MHCII<sup>+</sup> Ly6C<sup>-</sup> cells (red), MHCII<sup>+</sup> Ly6C<sup>high</sup> cells (green), MHCII<sup>+</sup> Ly6C<sup>low</sup> cells (purple) and maturing or transitioning monocytes (MHCII<sup>low</sup> Ly6C<sup>+</sup>) (light blue) (a). Backgating analysis of these populations shows their profiles on FSC-A vs. SSC-A dot plots (b). Examples from spleen and kidneys at 6 hours post-sham-IR and IR surgery. Numbers on dot plots represent proportions of parent populations.

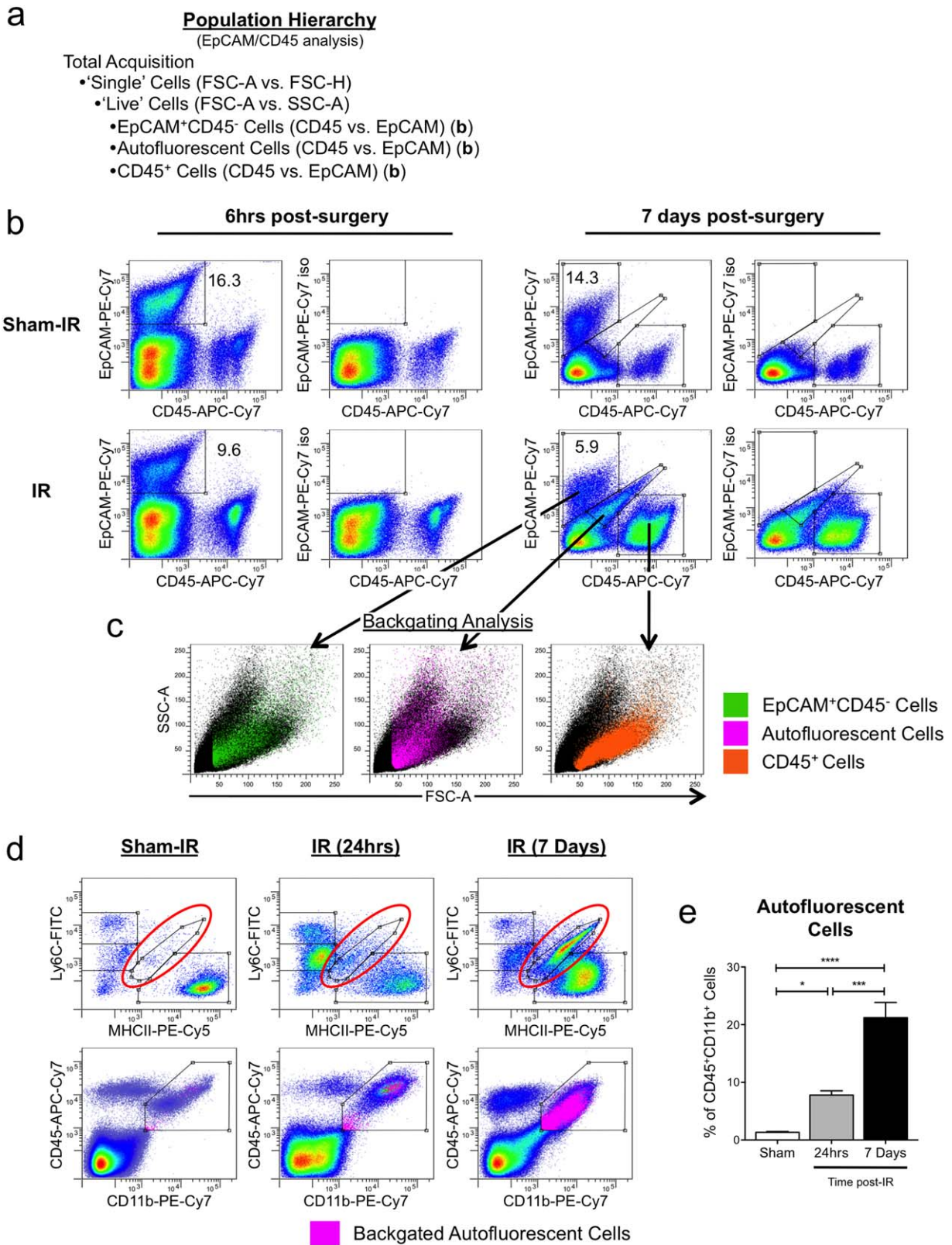


Figure 5.

account light scattering and autofluorescent characteristics, to assess infiltrating and resident cells in the uninjured kidney and in the inflammatory phase following IR injury. Performing backgating analysis along with coloring populations and viewing them against multiple parameters will lead to more detailed phenotypic and functional descriptions. This includes information regarding the maturation state of the cell, its autofluorescent properties and functional capacity, which can be linked to other data, such as cytokine production and enzyme activity. This is particularly relevant to tissue macrophages because of their heterogeneity, especially in the disease setting where they play central roles in inflammation and tissue remodeling.

One marker that we focused on was Ly6C, as its expression can be used to define monocyte maturation and function, with Ly6C<sup>high</sup> pro-inflammatory cells down regulating the marker as they mature into Ly6C<sup>low</sup> macrophages (18). In addition, the activation of monocytes at various maturation stages leads to mature macrophages of distinct functional states (18). Following unilateral ureteral obstruction, Ly6C<sup>high</sup> cells have been shown to home to kidneys where they differentiate into monocytes/macrophages of distinct functional states, indeed identified by the level of Ly6C expression (19). Our data showed that the initial inflammatory phase of the IR model involves a dramatic increase in the proportion and number of Ly6C<sup>high</sup> monocytes. As such, assessing changes in this population with various treatments or in fact targeting this cell type directly may impact the degree of injury or provide increased potential for regeneration. A number of studies have used antibodies against Gr-1, a complex formed by both Ly6C and Ly6G, to separate monocytes from granulocytes (20). Confirmed here in the kidney, using separate antibodies against Ly6C and Ly6G allows for an easier delineation of monocytes and granulocytes, and where applicable allows for further separation of the granulocyte pool into neutrophils and eosinophils (21). Monocyte populations have also been defined by their expression of the chemokine receptors, CX<sub>3</sub>CR1 and CCR2 (22,23). CD11b<sup>+</sup>CCR2<sup>low</sup>Gr1<sup>int</sup>Ly6C<sup>high</sup>CX<sub>3</sub>CR1<sup>high</sup> monocytes migrate to normal tissues, whereas inflammatory monocytes with a CD11b<sup>+</sup>CCR2<sup>high</sup>Gr1<sup>int</sup>Ly6C<sup>high</sup>CX<sub>3</sub>CR1<sup>low</sup> phenotype home to injured tissues (24).

We also chose to assess MR expression as it is a useful identifier of M2 macrophages (4,25). Indeed, mannose receptor 2 has been shown to be upregulated on macrophages following unilateral ureteral obstruction and is believed to play a role in modulating fibrosis through binding and internalizing

collagen via an extracellular fibronectin type II domain (26,27). Interestingly, this study showed that two populations of MR<sup>+</sup> cells (MHCII<sup>-</sup> and MHCII<sup>+</sup>) exist in the kidney at 24 hours post-IR injury. Again, targeting or manipulating this cell type may help promote kidney remodeling and regeneration. When considering assessing MR expression with flow cytometry, it should be noted that MR is expressed weakly on the cell surface (28). Membrane permeabilization may result in more effective labeling, although this does not allow for isolation of a potential viable M2 population via FACS.

Autofluorescence is another characteristic of kidney IR injury that needs to be considered carefully. Myeloid cells, particularly those expressing CD11b, CD11c and high levels of F4/80, exhibit autofluorescence at a range of excitation and emission wavelengths (14). Certain myeloid populations can even be defined based on their autofluorescence signature. However, if a full panel of fluorochromes is being used then there is a risk of erroneous emission signals. Using an FMO approach for antibody controls is useful for identifying and minimizing the effects of autofluorescence (29). This study showed that autofluorescence increases over time in kidney IR injury and can be potentially problematic when assessing both hematopoietic and nonhematopoietic populations. Measuring autofluorescence may also prove to be a useful indicator of injury and repair, especially if assessed over a longer time-course and correlated with other injury biomarkers.

The subtle differential expression of markers such as MHCII may also prove to be important in characterizing macrophage subsets and determining functional capabilities. Even the notion of a DC has been challenged in recent times with some evidence suggesting that they might be more closely associated with macrophages than previously thought. This study highlights the difference in the expression of the classical DC marker, CD11c, between the spleen and the kidney, and that the lack of a clear CD11c population may mean that examining CD11c on subpopulations may be more useful than trying to, for example, separate the CD45<sup>+</sup> population into macrophages and DCs. The assessment of CD11c expression in this study also demonstrates the usefulness of measuring MFI for a particular antibody in lieu of, or in addition to, population proportions, especially when the expression is low or when shifts in expression levels are subtle.

Part of the challenge in using flow cytometry to assess subpopulations of cells in the kidney is choosing an appropriate panel of markers to investigate. This is further complicated knowing that different digestion methods may enhance

**Figure 5.** Assessing epithelial cells and autofluorescence in the post-ischemic kidney. The population hierarchy resulting from the EpCAM<sup>+</sup> epithelial gating analysis is shown (a). Following the gating of 'Single' cells (FSC-A vs. FSC-H) and 'Live' cells (FSC-A vs. SSC-A) (data not shown), EpCAM<sup>+</sup> epithelial cells were selected for their expression of EpCAM and for a lack of expression of the hematopoietic marker CD45 (b). With the progression of time in the IR model, autofluorescence becomes increasingly prominent. In this example, at 7 days post-IR, the EpCAM<sup>+</sup> gate was altered so as not to include autofluorescent cells (b). Backgating analysis shows the difference in the FSC-A vs. SSC-A profile of CD45<sup>-</sup>EpCAM<sup>+</sup>, autofluorescent and CD45<sup>+</sup> populations (c). An autofluorescent population appeared when examining the CD45<sup>+</sup>CD11b<sup>+</sup> cell pool in the kidney following IR injury (d). On the MHCII vs. Ly6C dot plots, autofluorescence became more prominent with time after injury (d). This autofluorescent population was backgated and displayed in pink on the parent CD11b vs. CD45 plot (d). The increase in the proportion of this autofluorescent population with time (after injury) is shown graphically (e). Numbers on dot plots represent proportions of parent populations. Statistical analysis was performed using a one-way analysis of variance with a Tukey's multiple comparisons test; \*\**P* < 0.01, \*\*\**P* < 0.001, \*\*\*\**P* < 0.0001. Data are displayed as means ± SEM (*n* = 5/group).

detection of a particular cell type or negatively impact individual markers or receptors. The ED protocol described in this paper was optimized for the combination of enzymes used (collagenase/dispase, DNase type 1). The enzyme concentrations and incubation times, along with the method of mechanical dissociation (size of pipette tip and timing of the dissociations), were all methodically tested to achieve an optimal digestion as determined by cell counts, viability and flow cytometric profiles. This study demonstrated that ED is indeed required to achieve greater viable and CD45<sup>+</sup> cells yields and to most effectively study cells expressing markers such as F4/80. However, variations in dissociation media may be required for different disease models, as some are characterized by inflammation, cell infiltrate, and cell death, whilst others may centre on fibrosis and collagen deposition. The combination of collagenase/dispase and DNase type 1 appeared to impact negatively on CSF-1R expression, as seen on Ly6C<sup>high</sup> and Ly6C<sup>+</sup> cells in the spleen, again highlighting the need to optimize digestion methods for each specific study.

Equally as rapid as the advancements in flow cytometer technology, is the development of new fluorochromes and viability dyes. These are providing narrower emission spectra allowing for greater clarity in population identification. There is also now a range of viability dyes available for a large variety of excitation and emission wavelengths. The interactive tools available online, such as spectra viewers and panel builders are also very useful in creating optimal antibody cocktails.

## CONCLUSION

This study has highlighted some of the advantages and limitations associated with assessing kidney cells using flow cytometry, particularly in the IR injury model. This can be an incredibly powerful tool but requires a tested and systematic approach, including the method for organ digestion, antibody selection (target antigen and fluorochrome) and specific gating strategies. Other analytical techniques, including IHC, IF, and PCR should be used in conjunction with flow cytometry data to provide a complete depiction of cell types present together with localization in the tissue in which they reside. The obvious extension of the use of flow cytometry to analyze cell populations is the sorting of live populations for further investigations *in vitro* or in adoptive transfer experiments.

## ACKNOWLEDGMENTS

Timothy M. Williams and Daniel S. Layton have been involved in the development of FlowLogic FCS analysis software.

## REFERENCES

- Duffield JS. Macrophages and immunologic inflammation of the kidney. *Semin Nephrol* 2010;30:234–254. Available at: <http://eutils.ncbi.nlm.nih.gov/entrez/eutils/efetch.fcgi?dbfrom=pubmed&id=20620669&retmode=ref&cmd=prlinks>.
- Nguyen D, Ping F, Mu W, Hill P, Atkins RC, Chadban SJ. Macrophage accumulation in human progressive diabetic nephropathy. *Nephrology (Carlton, Vic)* 2006;11:226–231.
- Chow F, Ozols E, Nikolic-Paterson DJ, Atkins RC, Tesch GH. Macrophages in mouse type 2 diabetic nephropathy: correlation with diabetic state and progressive renal injury. *Kidney Int* 2004;65:116–128.
- Ricardo SD, van Gooor H, Eddy AA. Macrophage diversity in renal injury and repair. *J Clin Invest* 2008;118:3522–3530.
- Williams TM, Little MH, Ricardo SD. Macrophages in renal development, injury, and repair. *Semin Nephrol* 2010;30:255–267.
- Mantovani A, Sica A, Sozzani S, Allavena P, Vecchi A, Locati M. The chemokine system in diverse forms of macrophage activation and polarization. *Trends Immunol* 2004;25:677–686.
- Martinez FO, Helming L, Gordon S. Alternative activation of macrophages: An immunologic functional perspective. *Annu Rev Immunol* 2009;27:451–483.
- Mosser DM, Edwards JP. Exploring the full spectrum of macrophage activation. *Nat Rev Immunol* 2008;8:958–969.
- Chattopadhyay PK, Roederer M. Cytometry: Today's technology and tomorrow's horizons. *Methods* 2012;57:251–258.
- Zuk AA, Bonventre JV, Brown DD, Matlin KSK. Polarity, integrin, and extracellular matrix dynamics in the posts ischemic rat kidney. *Am J Physiol* 1998;275:C711–C731.
- Lee S, Huen S, Nishio H, Nishio S, Lee HK, Choi B-S, Ruhrberg C, Cantley LG. Distinct macrophage phenotypes contribute to kidney injury and repair. *J Am Soc Nephrol* 2011;22:317–326.
- Austyn JM, Gordon SS. F4/80, a monoclonal antibody directed specifically against the mouse macrophage. *Eur J Immunol* 1981;11:805–815.
- Taylor PRP, Brown GDG, Geldhof ABA, Martinez-Pomares LL, Gordon SS. Pattern recognition receptors and differentiation antigens define murine myeloid cell heterogeneity *ex vivo*. *Eur J Immunol* 2003;33:2090–2097.
- Mitchell AJ, Pradel LC, Chasson L, Van Rooijen N, Grau GE, Hunt NH, Chimini G. Technical advance: Autofluorescence as a tool for myeloid cell analysis. *J Leukoc Biol* 2010;88:597–603.
- Nonaka K, Saio M, Suwa T, Frey AB, Umemura N, Imai H, Ouyang G-F, Osada S, Balazs M, Adany R, Kawaguchi Y, Yoshida K, Takami T. Skewing the Th cell phenotype toward Th1 alters the maturation of tumor-infiltrating mononuclear phagocytes. *J Leukoc Biol* 2008;84:679–688.
- Stables MJ, Shah S, Camon EB, Lovering RC, Newson J, Byström J, Farrow S, Gilroy DW. Transcriptomic analyses of murine resolution-phase macrophages. *Blood* 2011;118:e192–208.
- Alikhan MA, Jones CV, Williams TM, Beckhouse AG, Fletcher AL, Kett MM, Sakkal S, Samuel CS, Ramsay RG, Deane JA, Wells CA, Little MH, Hume DA, Ricardo SD. Colony-stimulating factor-1 promotes kidney growth and repair via alteration of macrophage responses. *Am J Pathol* 2011;179:1243–1256.
- Sunderkötter C, Nikolic T, Dillon MJ, van Rooijen N, Stehling M, Drevets DA, Leenen PJM. Subpopulations of mouse blood monocytes differ in maturation stage and inflammatory response. *J Immunol* 2004;172:4410–4417.
- Lin SL, Castaño AP, Nowlin BT, Lupher ML, Duffield JS. Bone marrow Ly6Chigh monocytes are selectively recruited to injured kidney and differentiate into functionally distinct populations. *J Immunol* 2009;183:6733–6743.
- Fleming TJT, Fleming MLM, Malek TRT. Selective expression of Ly-6G on myeloid lineage cells in mouse bone marrow. RB6–8C5 mAb to granulocyte-differentiation antigen (Gr-1) detects members of the Ly-6 family. *J Immunol* 1993;151:2399–2408.
- Rose S, Misharin A, Perlman H. A novel Ly6C/Ly6G-based strategy to analyze the mouse splenic myeloid compartment. *Cytometry Part A* 2012;81A:343–350.
- Geissmann F, Jung S, Littman DR. Blood monocytes consist of two principal subsets with distinct migratory properties. *Immunity* 2003;19:71–82.
- Li L, Huang L, Sung S-SJ, Vergis AL, Rosin DL, Rose CE, Lobo PI, Okusa MD. The chemokine receptors CCR2 and CX3CR1 mediate monocyte/macrophage trafficking in kidney ischemia–reperfusion injury. *Kidney Int* 2008;74:1526–1537.
- Tacke F, Randolph GJ. Migratory fate and differentiation of blood monocyte subsets. *Immunobiology* 2006;211:609–618.
- Gordon S. Alternative activation of macrophages. *Nat Rev Immunol* 2003;3:23–35.
- Kushiyama T, Oda T, Yamada M, Higashi K, Yamamoto K, Sakurai Y, Miura S, Kumagai H. Alteration in the phenotype of macrophages in the repair of renal interstitial fibrosis in mice. *Nephrology (Carlton, Vic)* 2011;16:522–535.
- Lopez-Guisa JM, Cai X, Collins SJ, Yamaguchi I, Okamura DM, Bugge TH, Isacke CM, Emson CL, Turner SM, Shankland SJ, Eddy AA. Mannose receptor 2 attenuates renal fibrosis. *J Am Soc Nephrol* 2012;23:236–251.
- Martinez-Pomares LL, Reid DMD, Brown GDG, Taylor PRP, Stillion RJR, Linehan SAS, Zamze SS, Gordon SS, Wong SYCS. Analysis of mannose receptor regulation by IL-4, IL-10, and proteolytic processing using novel monoclonal antibodies. *J Leukoc Biol* 2003;73:604–613.
- Perfetto SP, Chattopadhyay PK, Roederer M. Seventeen-colour flow cytometry: unravelling the immune system. *Nat Rev Immunol* 2004;4:648–655.

RESEARCH

Open Access

# M2 macrophage polarisation is associated with alveolar formation during postnatal lung development

Christina V Jones<sup>1</sup>, Timothy M Williams<sup>1</sup>, Kenneth A Walker<sup>1</sup>, Hayley Dickinson<sup>2</sup>, Samy Sakkal<sup>1</sup>, Bree A Rumballe<sup>3</sup>, Melissa H Little<sup>3</sup>, Graham Jenkin<sup>2</sup> and Sharon D Ricardo<sup>1\*</sup>

## Abstract

**Background:** Macrophages are traditionally associated with inflammation and host defence, however a greater understanding of macrophage heterogeneity is revealing their essential roles in non-immune functions such as development, homeostasis and regeneration. In organs including the brain, kidney, mammary gland and pancreas, macrophages reside in large numbers and provide essential regulatory functions that shape organ development and maturation. However, the role of macrophages in lung development and the potential implications of macrophage modulation in the promotion of lung maturation have not yet been ascertained.

**Methods:** Embryonic day (E)12.5 mouse lungs were cultured as explants and macrophages associated with branching morphogenesis were visualised by wholemount immunofluorescence microscopy. Postnatal lung development and the correlation with macrophage number and phenotype were examined using Colony-stimulating factor-1 receptor-enhanced green fluorescent protein (*Csf1r*-EGFP) reporter mice. Structural histological examination was complemented with whole-body plethysmography assessment of postnatal lung functional maturation over time.

Flow cytometry, real-time (q)PCR and immunofluorescence microscopy were performed to characterise macrophage number, phenotype and localisation in the lung during postnatal development. To assess the impact of developmental macrophage modulation, CSF-1 was administered to neonatal mice at postnatal day (P)1, 2 and 3, and lung macrophage number and phenotype were assessed at P5. EGFP transgene expression and *in situ* hybridisation was performed to assess CSF-1R location in the developing lung.

**Results:** Macrophages in embryonic lungs were abundant and densely located within branch points during branching morphogenesis. During postnatal development, structural and functional maturation of the lung was associated with an increase in lung macrophage number. In particular, the period of alveolarisation from P14-21 was associated with increased number of *Csf1r*-EGFP+ macrophages and upregulated expression of *Arginase 1* (*Arg1*), *Mannose receptor 1* (*Mrc1*) and *Chemokine C-C motif ligand 17* (*Ccl17*), indicative of an M2 or tissue remodelling macrophage phenotype. Administration of CSF-1 to neonatal mice increased trophic macrophages during development and was associated with increased expression of the M2-associated gene *Found in inflammatory zone* (*Fizz1*) and the growth regulator *Insulin-like growth factor* (*Igf*)1. The effects of CSF-1 were identified as macrophage-mediated, as the CSF-1R was found to be exclusively expressed on interstitial myeloid cells.

(Continued on next page)

\* Correspondence: [REDACTED]

<sup>1</sup>Department of Anatomy and Developmental Biology, Monash University, Clayton, Victoria, Australia

Full list of author information is available at the end of the article

(Continued from previous page)

**Conclusions:** This study identifies the presence of CSF-1R+ M2-polarised macrophages localising to sites of branching morphogenesis and increasing in number during the alveolarisation stage of normal lung development. Improved understanding of the role of macrophages in lung developmental regulation has clinical relevance for addressing neonatal inflammatory perturbation of development and highlights macrophage modulation as a potential intervention to promote lung development.

**Keywords:** Macrophage, CSF-1, Lung development, M2, Alveolarisation

## Background

A diverse network of regulators govern the developmental transformation from multipotent progenitors in the post-induction lung buds to the complex architecture and highly specialised terminal cell types that make up the mature lung. These include a range of growth factors, signalling pathways and transcriptional regulators that arise from epithelial, mesodermal and mesothelial origins [Reviewed in [1]]. Another important component of the lung organogenic milieu is the tissue macrophage. Traditionally associated with host defence, inflammation and scavenging functions, a greater appreciation of macrophage diversity has revealed broader functions of macrophages including vital roles in tissue repair [2-6] and organ development [7-11].

Macrophages first arise in the yolk sac around embryonic day (E)8 in the mouse, and migrate into the developing head before colonising the entire embryo [12-14]. Large numbers of macrophages are present in virtually all developing organs, with maximum numbers correlating with key periods of organogenesis [15]. Macrophages contribute to development through apoptosis, phagocytic clearance of cellular debris associated with tissue remodeling, and as potent effector cells producing a range of trophic factors that stimulate growth, regulate cellular differentiation and promote angiogenesis [Reviewed in [16]]. Furthermore, mice deficient in tissue macrophages display a range of developmental abnormalities including skeletal and neurological deficiencies and impaired growth and fertility [17-19].

Macrophages are essential in the normal development of the mammary gland, pancreas and kidney; organs which, similar to the lung, develop through branching morphogenesis. Normally, macrophages are located surrounding developing terminal buds but, in their absence, branching is impaired resulting in atrophic, poorly-branched terminal buds in the mammary gland [9,20], and abnormal islet cell morphology and reduced insulin production in the pancreas [21,22]. Furthermore, the addition of the key macrophage regulatory cytokine colony-stimulating factor (CSF)-1 to embryonic organ cultures was shown to enhance development of the pancreas [8] and kidney [11], which was associated with increased number of tissue macrophages. While the organogenic

contribution of macrophages to these organs is well described, less has been investigated regarding their roles in the development of the lung.

Macrophages are present in the lung from the initiation of development, and at E10 are located abundantly in the mesenchyme and in association with elongating lung buds [23,24]. Fetal lung macrophages likely contribute to lung development through the regulation of apoptosis and clearance of cellular debris. Defective pulmonary phagocytosis in the phosphatidylerine receptor (*psr*)<sup>-/-</sup> mutant mouse is associated with impaired removal of apoptotic cells during development, which in turn results in solid lungs devoid of alveoli [25]. Macrophages in the lung are also sources of trophic factors such as insulin-like growth factor (IGF)-1 [26] and wingless-type MMTV integration site (Wnt)7b [27], both of which are important regulators in lung development.

To date, the understanding of lung macrophage function has focussed on pathological implications in settings associated with neonatal inflammation with little insight regarding their contribution to normal developmental regulation. In this study, we provide the first report characterising macrophages during the alveolarisation stage of lung development in the mouse. Macrophages in the postnatal lung displayed a phenotype indicative of an M2 or alternatively activated macrophage polarisation state, which is characteristic of macrophages involved in trophic and tissue remodeling functions. Furthermore, the number of CSF-1 receptor (CSF-1R)+F4/80+ macrophages was increased during alveolarisation and, together with the expression of M2-associated genes, indicates the importance of trophic macrophages during this period of significant tissue remodelling.

## Methods

### Animals

All animal experiments were approved in advance by the Monash University Animal Ethics Committee and conducted in accordance with the "Australian Code of Practice for the Care and Use of Animals for Scientific Purposes" (7<sup>th</sup> Edition, 2004). For embryonic lung culture, time-mated C57BL/6J females were humanely euthanised by cervical dislocation at 12.5 days postcoitum, with 0.5 defined as noon on the day a

plug was detected. Embryos were collected, development was assessed using the Theiler Staging (TS) criteria (TS 15–16/27–31 somites) and the lungs were dissected. Postnatal lung analyses were performed on *Csf1r*-EGFP mice, which directs enhanced green fluorescent protein (EGFP) expression to cells of the myeloid lineage under the control of the *Csf1r* promoter [14]. Neonatal mice were administered mouse recombinant CSF-1 (1 µg/g bodyweight; University of Queensland Protein Facility, Brisbane, Australia) in phosphate buffered saline (PBS) via intraperitoneal (i.p.) injection at a final volume of 50 µl at postnatal day (P)1, 2 and 3, with P1 defined as day of birth [2]. Littermate controls received vehicle PBS at the equivalent final volume.

#### **Embryonic lung culture and wholemount immunofluorescence labelling**

Embryonic lungs were transferred onto polycarbonate membranes (3 µm pore size; GE Water and Processing Technologies, Oakville, Canada), floating on serum-free media in a 24 well plate (BD Biosciences). Culture media was composed of Dulbecco's Modified Eagle Medium F/12 (Gibco/Invitrogen, Mulgrave, VIC, Australia), supplemented with 2.5 mM L-glutamine (Gibco/Invitrogen), 5 µg/ml insulin transferrin selenium (Gibco/Invitrogen) and 100 µg/ml penicillin streptomycin (Gibco/Invitrogen). Organs were incubated for 48 hours at 37°C in 5% CO<sub>2</sub>. Explants were fixed in ice-cold methanol (for 30 min at -20°C) and wholemount immunolabelled to visualise macrophages in development. Explants were permeabilised in 0.1% Triton X (in PBS for 10 min) and non-specific binding was blocked by incubation with 10% goat serum and 2% bovine serum albumin (BSA; in PBS for 30 min). Explants were incubated with rat anti-F4/80 (1:100; Serotec, Kidlington, UK; Clone Cl:A3-1) and rabbit anti-E-cadherin (1:100; Cell Signalling Technologies, Danvers, MA, USA; Clone 24E10) primary antibodies (at 37°C for 2 hrs) to demarcate macrophages and lung epithelium, respectively. Explants were washed in PBS (3 × 5 min at room temperature), incubated with Alexa Fluor<sup>®</sup> goat anti-rat 555 and goat anti-rabbit 488 (Invitrogen; 1:500) secondary antibodies (at 37°C for 1 hr). Membrane-bound explants were placed on glass slides with PBS and coverslipped.

#### **Postnatal lung histology and macrophage immunofluorescence labelling**

Lungs were reinflated and fixed *in situ* through intratracheal instillation of 10% buffered formalin at a pressure of 20 cmH<sub>2</sub>O. After ligating the trachea, the entire thorax was immersion fixed for 24 hr before lungs were dissected. To assess histology, lungs were processed, embedded in paraffin wax, sectioned at 5 µm, mounted on Polylysine™ slides (Menzel-Glaser, Braunschweig, Germany) and stained with haematoxylin and eosin. For immunofluorescence labelling, excised lungs were placed in 30% sucrose solution (in PBS)

and allowed to infiltrate overnight at 4°C. Organs were immersed in OCT compound (Sakura, Torrance, CA, USA) in Tissue-Tek<sup>®</sup> cryomoulds (Sakura) and frozen by floating moulds on chilled isopentane on dry ice. Lungs were cryosectioned at 5 µm and mounted on SuperFrost<sup>®</sup> Plus slides (Menzel-Glaser). For macrophage visualisation, sections were blocked in 10% goat serum, incubated with rat anti-F4/80 primary antibody (1:100; Serotec), washed and incubated with AlexaFluor<sup>®</sup> goat anti-rat 488 secondary antibody (1:500; Invitrogen). Sections were counterstained with DAPI nuclear stain (1:10,000 in PBS; Invitrogen) for 5 - minutes, washed, mounted with DAKO fluorescent mounting medium (DAKO Cytomation, Botany, NSW, Australia) and coverslipped.

#### **Flow cytometry**

Whole lungs underwent enzymatic and mechanical digestion to yield a single cell suspension as described previously [2]. In brief, organs were finely minced and incubated in 1ml digestion buffer; comprising 1 mg/ml collagenase/dispase (Roche Diagnostics, Indianapolis, IN, USA), 0.1% DNase I (Roche Diagnostics) and 5 mM CaCl<sub>2</sub> in Hank's Balanced Salt Solution (Invitrogen) at 37°C for 20 minutes. Lungs were mechanically disrupted using a 1000 µl pipette, before cells were gently passed through a 25-gauge needle to yield a single cell suspension. Cell suspensions were washed in fluorescence-activated cell sorting (FACS) buffer; comprising PBS supplemented with 0.2% BSA, 0.5 M ethylenediaminetetraacetic acid (EDTA) and 0.02% sodium azide, and centrifuged at 485 relative centrifugal force (rcf; for 5 minutes at 4°C). Red blood cells were lysed by resuspending samples in 1 ml of red blood cell lysis buffer (at 37°C for 1 min; 8.3 g/L ammonium chloride; pH 7.5;) and cell suspensions were filtered through a 40 µm cell strainer (BD Biosciences, North Ryde, NSW, Australia). Cell counts were performed using a Coulter<sup>®</sup> Particle Count and Size Analyzer (Beckman Coulter Australia Pty Ltd, Gladesville, NSW, Australia). To assess macrophages across postnatal development, 1 × 10<sup>6</sup> cells were immunolabelled with anti-CD45 PE Cy5-conjugated antibody (1:1000; BD Biosciences; Clone 30-F11) at a final volume of 20 µl for 20 minutes at 4°C in a 96 well plate. Cells were washed in FACS buffer and centrifuged, repeated twice, before being resuspended in 200 µl FACS buffer and run on a BD FACSCalibur cytometer (BD Biosciences). To assess macrophages at P5 following CSF-1 administration, cells were immunolabelled with anti-CD45 APC Cy7-conjugated (1:800; BioLegend, San Diego, CA, USA; Clone 30-F11) and rat anti-F4/80 APC-conjugated (1:200; eBioscience, San Diego, CA, USA; Clone BM8) antibodies. Samples were run on a BD FACSCanto II cytometer (BD Biosciences). Data analysis was performed using Flow Jo FCS analysis software (Tree Star Inc., Ashland, OR, USA).

### Plethysmography

Respiratory physiology across a time course of postnatal development was assessed using unrestrained barometric whole-body plethysmography, as described previously [28,29]. In brief, mice were placed in a sealed cylindrical Perspex chamber (Neonate; 75 mm × 50 mm, Adolescent/Adult; 150 mm × 50 mm), where changes in pressure caused by breath tidal movements were measured using a volumetric pressure transducer (model PT5A; Grass Instrument Co., Quincy, MA, USA), amplified (Octal Bridge Amp model ML228 and Powerlab 8/30 model ML870; ADInstruments, Bella Vista, NSW, Australia) and the respiratory trace patterns recorded using Chart™ software (v5.1; ADInstruments). At the beginning of each session the plethysmograph was calibrated by measuring the pressure deflection caused by the injection of a known volume (300 µl) of air into the chamber. The temperature and relative humidity within the chamber were noted at the beginning and end of recordings (model HM34; Vaisala, Hawthorn, VIC, Australia). Waveform analysis (Chart™; ADInstruments) of respiratory traces was used to directly derive the pressure deflection per tidal breath ( $P_T$ ), total breath cycle time ( $T_{tot}$ ; sec), breath frequency ( $f$ ; breaths/min), inspiration time ( $T_i$ ; sec) and expiration time ( $T_e$ ; sec). To calculate tidal volume ( $V_T$ ; mL), the  $P_T$  value obtained from the respiratory trace was inputted into the equation of Drorbaugh and Fenn [30], which was subsequently used to determine minute volume ( $V_E$ ; mL/min;  $V_T \times f$ ) and inspiratory flow rate ( $V_T/T_i$ ; mL/sec).

### QPCR

Semi-quantitative real-time (qPCR) was used to assess gene expression in whole lungs across postnatal development and in response to CSF-1. Lungs were dissected and snap frozen in RNeasy RNA stabilisation reagent (Qiagen, Doncaster, VIC, Australia). Total RNA was extracted from organs using an RNeasy Mini Kit (Qiagen) and concentration and purity were analysed using a Nanodrop® Spectrometer (Nanodrop® Technologies, Wilmington, DE, USA). RNA was converted to cDNA using a High Capacity cDNA Reverse Transcription Kit (Applied Biosystems, Mulgrave, VIC, Australia). qPCR was performed using Taqman® Gene Expression Assays (Applied Biosystems) which provided pre-designed primer and probes to assess the genes  $\beta$ -actin (*Actb*; Assay ID: Mm00607939\_s1), Chemokine C-C motif ligand (*Ccl2*) (Mm00441242\_m1), Inducible nitric oxide synthase (*Nos2*; Mm00440485\_m1), Tumor necrosis factor- $\alpha$  (*Tnf*; Mm00443258\_m1), *Ccl17* (Mm00516136\_m1), Arginase 1 (*Arg1*; Mm00475988\_m1), *Igf1* (Mm00439561\_m1) and Found in Inflammatory Zone 1 (*Fizz1*; Mm00445109\_m1). Reactions were performed in triplicate and run on a 7500 Real-Time PCR machine using SDS Software (v1.3; Applied Biosystems). Threshold cycle (Ct) values were normalised

against endogenous *Actb* expression and presented as relative quantification (RQ).

### In situ hybridisation and microscopy

Section *in situ* hybridisation for the *Csflr* gene was performed on paraffin-embedded, 5 µm sections of E12.5 embryonic lungs, as described previously [31] (Probe ID: MGI:50000914; http://www.gudmap.org). Sections were counterstained with haematoxylin. Light and fluorescence microscopy were performed using an Olympus Provis AX70 microscope (Olympus, Mt Waverley, VIC, Australia) and AnalysisB software (Soft Imaging Systems GmbH, Muenster, Germany). Bright field images were captured using a DP70 colour camera (Olympus). Fluorescence images were captured using an F-View black and white camera (Olympus). Image preparation and compilation was performed using AnalysisB software (Soft Imaging Systems) and Microsoft Power Point (Microsoft Corporation, Redmond, WA, USA).

### Statistical analysis

Data is presented as mean ± standard error of the mean (SEM). Statistical analysis was performed using GraphPad Prism™ (Version 5 for Windows; GraphPad Software Inc, La Jolla, CA, USA). Significance was assessed using a one-way ANOVA and Tukey's post hoc test for comparisons across multiple time points or unpaired Student's *t*-test for comparisons between two experimental groups. A *p* value <0.05 was considered statistically significant.

## Results

### Macrophages are abundant in embryonic lungs and localise within branch points

To assess macrophages and their involvement in lung branching morphogenesis, E12.5 lungs were cultured as embryonic explants, with a continuation of branching morphogenesis observed over 48 hours of culture (Figure 1A-C). In this model system, flattening of the organ facilitated wholemount visualisation and the examination of macrophage localisation within the embryonic lung. Immunofluorescence labelling demonstrates that embryonic macrophages express the mature macrophage marker F4/80 and are found abundantly within embryonic lungs undergoing branching morphogenesis (Figure 1D&E). In particular, the dense concentration of macrophages localised within branch points is prominent (Figure 1E). Such abundance, branch-specific location and intimate epithelial interaction support the relevance of macrophages in the regulation of lung development. Furthermore, this system indicates the importance of early fetal macrophages in colonising organs undergoing development. With the explant system eliminating the contribution of infiltrating cells at later stages of development, it also indicates that the large numbers of macrophages

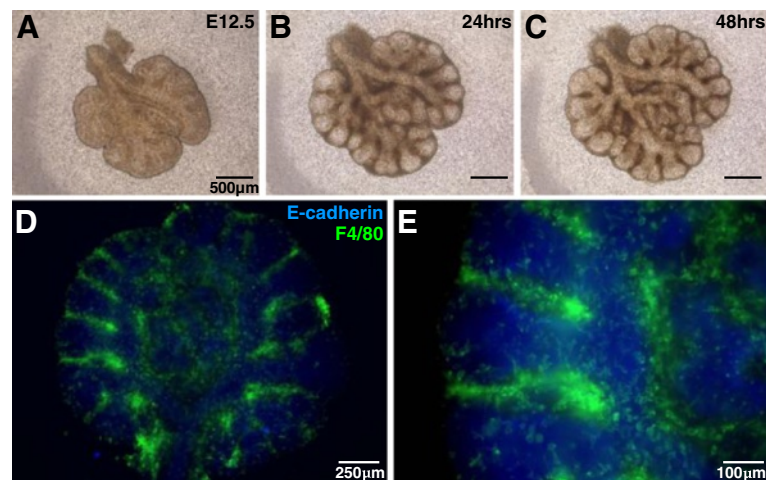


**Figure 1 Macrophages are abundant in developing embryonic lungs.** *Ex vivo* culture of E12.5 embryonic lungs, maintained for 48 hours on floating polycarbonate membranes at the air-liquid interface, supported continuation of branching morphogenesis (A-C). Wholemount immunofluorescence labelling of the lung epithelium (anti-E-cadherin; blue) and macrophages (anti-F4/80; green) revealed extensive macrophage accumulation within developing lungs (D), and in particular within branch points (E).

observed are seeded within the lung before E12.5, and are then maintained through local mechanisms to support ongoing branching morphogenesis.

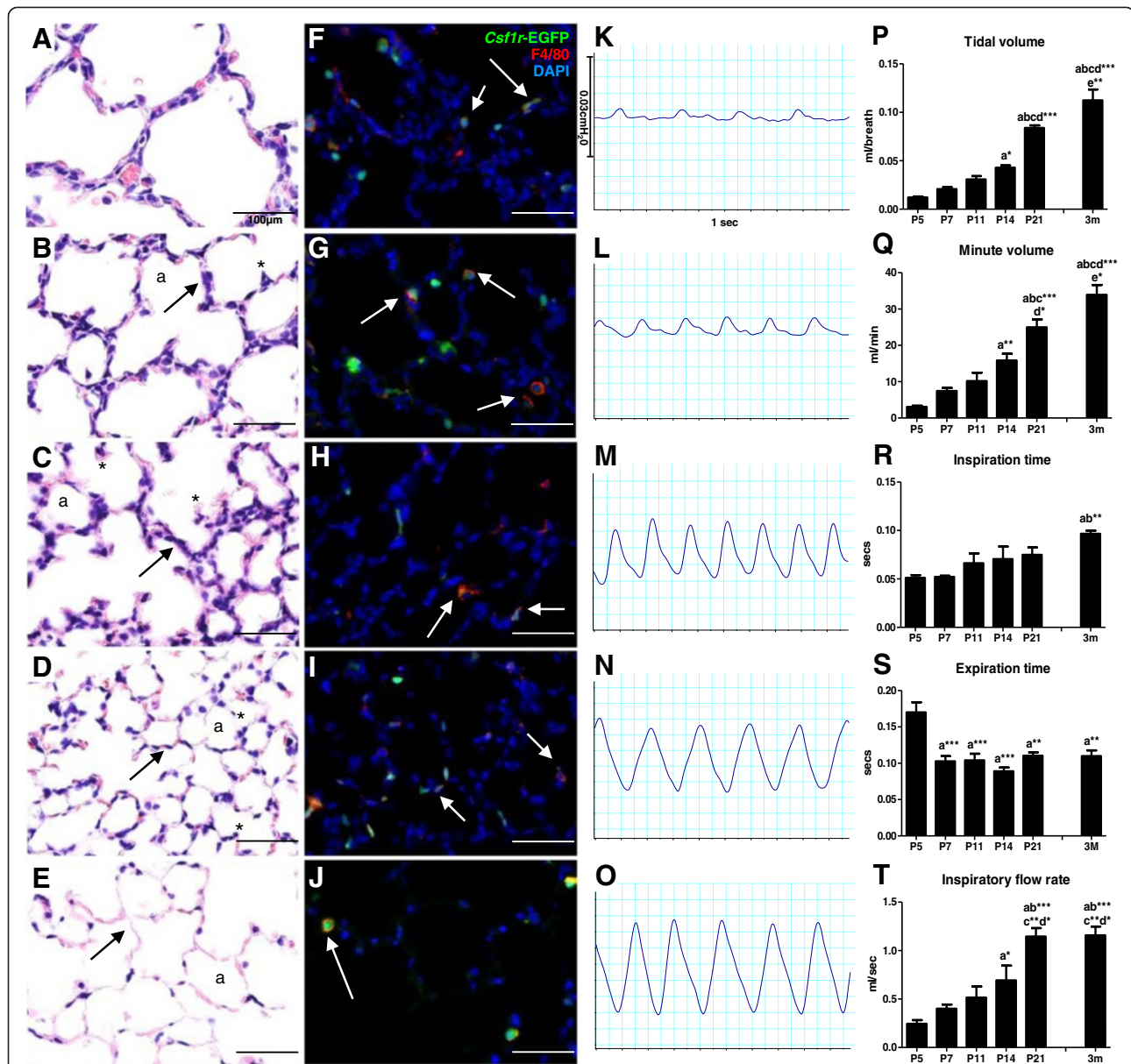
#### Macrophages are associated with the structural and functional postnatal maturation in the mouse

In the mouse, the lung undergoes a significant period of postnatal development comprising both the closing stages of the saccular phase (E18.5–P5) and the alveolarisation phase (P5–P36) [1,32], and thereby provides an important animal species for investigating aspects of developmental regulation. The structural and functional maturation across the time course of postnatal lung development was characterised in *Csf1r*-EGFP mice.

Structural maturation facilitates the progressive gain in gas exchange efficiency; from large, thick-walled terminal sacs to smaller, thin-walled alveoli with a large surface area (Figure 2A-E). Histologically at P5, the lung parenchyma consisted of large terminal sacs (Figure 2A), and with continuing alveolarisation the subdivision into smaller alveoli through the process of secondary septation was evidenced by the formation of ridges on sac walls invading into the alveolar space (Figure 2B&C). Continued secondary septation was evident at P14, with significant numbers of smaller alveoli present (Figure 2C). By P21 there was considerable thinning of alveolar walls bringing blood vessels into close association with the epithelium lining the alveolar space (Figure 2D). In these later stages of the alveolarisation phase, much of the secondary septation was complete and maturation involved thinning of the alveolar wall interstitium (Figure 2D). The adult lung at 3M showed all the structural hallmarks of an efficient gas exchange organ; large number of alveoli

providing a large surface area and extremely thin walls to allow for efficient gas exchange (Figure 2E). Postnatal development was accompanied by the identification of macrophages in the lung parenchyma. Visualised by *Csf1r*-EGFP expression, these myeloid cells were predominantly macrophages, evident by their consistent co-expression of F4/80 (Figure 2F-J). The large numbers of macrophages within the lung from P5–P21 correlates with the key period of alveolar development.

These structural changes were mirrored by the functional improvements observed during postnatal development. Trace recordings from unrestrained barometric whole-body plethysmography illustrated the breath patterns and functional maturation of the lungs of mice during postnatal development through measurement of tidal pressure changes within the chamber due to respiration (Figure 2K-0). At P5, before alveolarisation, the respiratory capacity was limited, evidenced by trace recordings where breaths were shallow, uneven and dispersed (Figure 2K). With maturation and the formation of increasing numbers of alveoli from P7–P14 (Figure 2L&M), breaths became deeper, more frequent and more even. At P21, a breath pattern comparable to the adult was observed (Figure 2N), however as lung growth continued tidal volume increased, as evidenced by the increased amplitude of the trace pattern of the 3M lung (Figure 2O). Waveform analysis provided a quantitative assessment of lung function parameters to provide a functional correlation with the structural maturation of the postnatal lung. Progressive increases in tidal and minute volume were evident during postnatal lung development, increasing 8-fold ( $0.012 \pm 0.001$  vs.  $0.113 \pm 0.011$ ,  $p < 0.001$ ; Figure 2P) and 10-fold ( $3.09 \pm 0.30$  vs.



33.93 ± 2.70,  $p < 0.001$ ; Figure 2Q) from P5 to 3M, respectively, as the number of alveoli and overall size of the gas exchange compartment of the lung increased. As observed in the respiratory trace, breath patterns in immature lungs were quite uneven with short inhalations and slow dribbled exhalations at P5 and P7. This

was also demonstrated in the waveform measurements, where expiration time decreased with the onset of alveolarisation (Figure 2S) and inspiration time progressively increased (Figure 2R) as a more even breath pattern emerged. A progressive increase in inspiratory flow rate was also observed, increasing approximately 4-fold

from P5-P21 ( $0.24 \pm 0.04$  vs.  $1.15 \pm 0.09$ ,  $p < 0.001$ ) when a maximum flow rate was then reached and maintained in the adult lung at 3M (Figure 2T).

### Lung macrophage number is increased during alveolarisation

To more comprehensively assess the correlation between macrophages and alveolarisation, flow cytometry was performed to quantitatively examine the proportion and number of macrophages in the lung during postnatal development and into adulthood (Figure 3A-C). Again EGFP transgene expression facilitated the quantification of *Csf1r*+ myeloid cells (Figure 3D), which were confirmed as predominantly macrophages by consistent co-expression of F4/80 (Figure 2F-J) evident in both alveolar and interstitial macrophage subpopulations (Figure 3E&F). Lungs were analysed at P1 in the sacular stage, at P5 when the lung transitions from the sacular to alveolarisation stage, at P7, P14 and P21 during alveolarisation, and at 3M in the

mature lung. During postnatal life the overall cellularity of the lung gradually increased peaking at P14 during alveolarisation with an approximately 5-fold increase compared to P1 ( $7.78 \pm 0.14 \times 10^6$  vs.  $35.50 \pm 5.01 \times 10^6$ ,  $p < 0.001$ ; Figure 3A). From P14 onwards, as alveoli continued to develop and mature the total cellularity of the lung decreased. At 3M, despite the overall size difference, cellularity was comparable between the mature lung composed primarily of air sacs and the dense lung at P1 ( $7.78 \pm 0.14 \times 10^6$  vs.  $12.24 \pm 2.23 \times 10^6$ ,  $p = \text{ns}$ ). Similarly, the number of macrophages followed a parallel trend, and increased 9-fold from P1 to P14 ( $5.65 \pm 0.87 \times 10^5$  vs.  $50.68 \pm 4.95 \times 10^5$ ,  $p < 0.001$ ), before a  $\sim 2.5$ -fold reduction by 3M ( $50.68 \pm 4.95 \times 10^5$  vs.  $19.93 \pm 1.39 \times 10^5$ ,  $p > 0.05$ ; Figure 3B). In contrast to number, the proportion of macrophages in the lung steadily increased throughout postnatal life (Figure 3C). During the sacular stage at P1 and P5, macrophages represented approximately 8% of cells in the lung. This is significantly

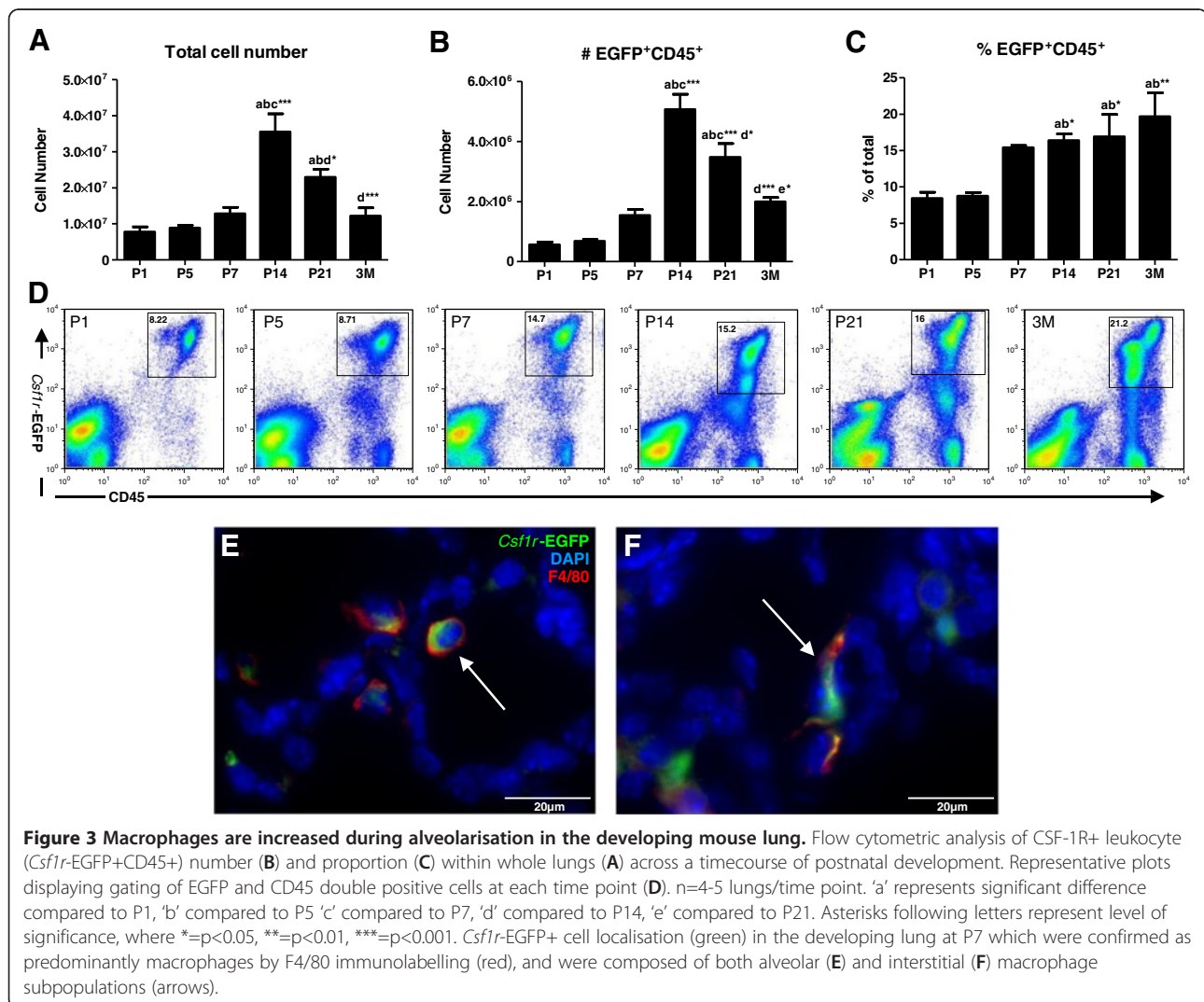


**Figure 3 Macrophages are increased during alveolarisation in the developing mouse lung.** Flow cytometric analysis of CSF-1R+ leukocyte (*Csf1r*-EGFP+CD45+) number (B) and proportion (C) within whole lungs (A) across a timecourse of postnatal development. Representative plots displaying gating of EGFP and CD45 double positive cells at each time point (D). n=4-5 lungs/time point. 'a' represents significant difference compared to P1, 'b' compared to P5 'c' compared to P7, 'd' compared to P14, 'e' compared to P21. Asterisks following letters represent level of significance, where \*= $p < 0.05$ , \*\*= $p < 0.01$ , \*\*\*= $p < 0.001$ . *Csf1r*-EGFP+ cell localisation (green) in the developing lung at P7 which were confirmed as predominantly macrophages by F4/80 immunolabelling (red), and were composed of both alveolar (E) and interstitial (F) macrophage subpopulations (arrows).

increased at P14 and P21 during alveolarisation to approximately 16% ( $p < 0.05$ ), and at 3M a significant resident macrophage population was maintained in the adult lung (Figure 3C).

#### Macrophages are polarised to an M2 phenotype during alveolarisation

Correlations between macrophage phenotype and stages of lung development were investigated by analysing expression of genes indicative of different macrophage activation states (Figure 4). An upregulated expression of *Ccl2*, *Nos2* and *Tnf* is associated with an M1 or classical phenotype where macrophages contribute to host defence. M2 or alternatively activated macrophages are important in tissue remodelling, immunoregulatory and trophic functions, and are characterised by upregulation of genes including *Arg1*, *Ccl17*, *Mrc1*. A limited correlation between M1 gene expression and postnatal lung development was observed, although *Ccl2* expression was highest after birth (Figure 4A) and *Nos2* decreased in later life at P21 and 3M (Figure 4B). In contrast, significant upregulation of M2 genes showed a distinct correlation with the key period of alveolar development. *Arg1* expression was low in early postnatal life and began to increase at P14 (Figure 4D). At P21, *Arg1* expression peaked and was 48-fold higher than at P1 ( $p < 0.01$ ), before returning to a low level of expression in the adult lung. *Ccl17* was also shown to increase during the alveolarisation stage (Figure 4E). After low expression from birth to P7, *Ccl17* expression increased 9-fold at P14 ( $p < 0.001$ ) before decreasing by P21. The resident population of macrophages in the mature lung at 3M also maintained significant *Ccl17* expression. Similarly, *Mrc1* expression remained unchanged throughout early postnatal lung development but peaked at P14 with a 3-fold increase compared to P7 ( $p < 0.01$ ; Figure 4F). Expression was decreased at P21 before high levels of *Mrc1* expression were maintained in the resident lung macrophage population at 3M. When all the genes analysed are presented on the same graph, the increase in the three genes indicative of an M2 macrophage phenotype is particularly evident (Figure 4G). This demonstrates a clear correlation between M2 macrophage phenotype and the key period of alveolarisation.

#### CSF-1 administration increases developmental macrophages in the lung and is associated with increased *Igf1* expression

CSF-1 is the primary regulator of macrophage differentiation, survival and proliferation, and during development it plays an essential and non-redundant role in regulating organogenic macrophage functions [17,18,33,34]. Administration of CSF-1 to neonatal mice was shown to increase the number and proportion of developmental macrophages

within the lung at P5. Flow cytometric analysis was performed on whole lungs, with populations of *Csf1r*-EGFP+ leukocytes (Figure 5C) further gated on F4/80 expression to investigate macrophages (Figure 5D&E). There was a trend towards an increase in total cellularity in CSF-1-treated lungs (Figure 5A). CSF-1 treatment resulted in a 6% increase in macrophage number ( $58.10 \pm 2.49 \times 10^4$  vs.  $69.32 \pm 2.56 \times 10^4$ ,  $p < 0.05$ ), and a 19% increase in macrophage proportion ( $57.77 \pm 1.15\%$  vs.  $63.88 \pm 1.78\%$ ,  $p < 0.05$ ), compared to PBS-treated littermates (Figure 5B). Analysis of gene expression also indicated that the CSF-1-mediated increase in macrophages was associated with upregulation of the Th2-associated molecule *Fizz1* ( $1.05 \pm 0.18$  vs.  $1.56 \pm 0.05$ ,  $p < 0.05$ ; Figure 5F) and the important growth regulator *Igf1* ( $1.01 \pm 0.11$  vs.  $2.55 \pm 0.41$ ,  $p < 0.05$ ; Figure 5G).

These effects of CSF-1 administration were confirmed to be via a macrophage-mediated mechanism as the CSF-1R was expressed exclusively on interstitial myeloid cells and not other cells of the developing lung. *In situ* hybridisation for the CSF-1R at E12.5 (Figure 5H) and *Csf1r* driven EGFP transgene expression at P7 (Figure 5I) confirmed that the trophic activity of CSF-1 during lung development is through macrophage regulation. Furthermore, the finding that CSF-1 supplementation promoted a trophic M2 macrophage phenotype highlights CSF-1 and the manipulation of CSF-1-responsive cells as a potential intervention for rescuing or promoting organ development and maturation.

#### Discussion

The renewed interest in macrophages has stemmed from an increased understanding of monocyte/macrophage heterogeneity and how it relates to functional diversity [35-38]. Differential activation states have been broadly classified as M1, which encompasses macrophages involved in host defence and inflammation, and M2, which represent a more wound healing or tissue remodelling phenotype. Despite the M1/M2 activation dichotomy arising from studies of tissue disease and repair, understanding macrophage phenotype and function has implications for discerning and potentially enhancing their contribution to organ development. Functions of M2 macrophages, such as extracellular matrix (ECM) production, release of trophic factors and promotion of angiogenesis, are fundamental to organogenesis. Furthermore, our microarray expression profiling has revealed that embryonic macrophages in developing lungs, kidneys and brains show a comparable gene expression profile consistent with an M2 activation state [11]. In addition, CSF-1 can also promote an 'M2' macrophage activation state, which is increasingly being linked to tissue repair and regeneration [2,39,40].

During embryonic development, macrophages are located abundantly within the embryo and are present in

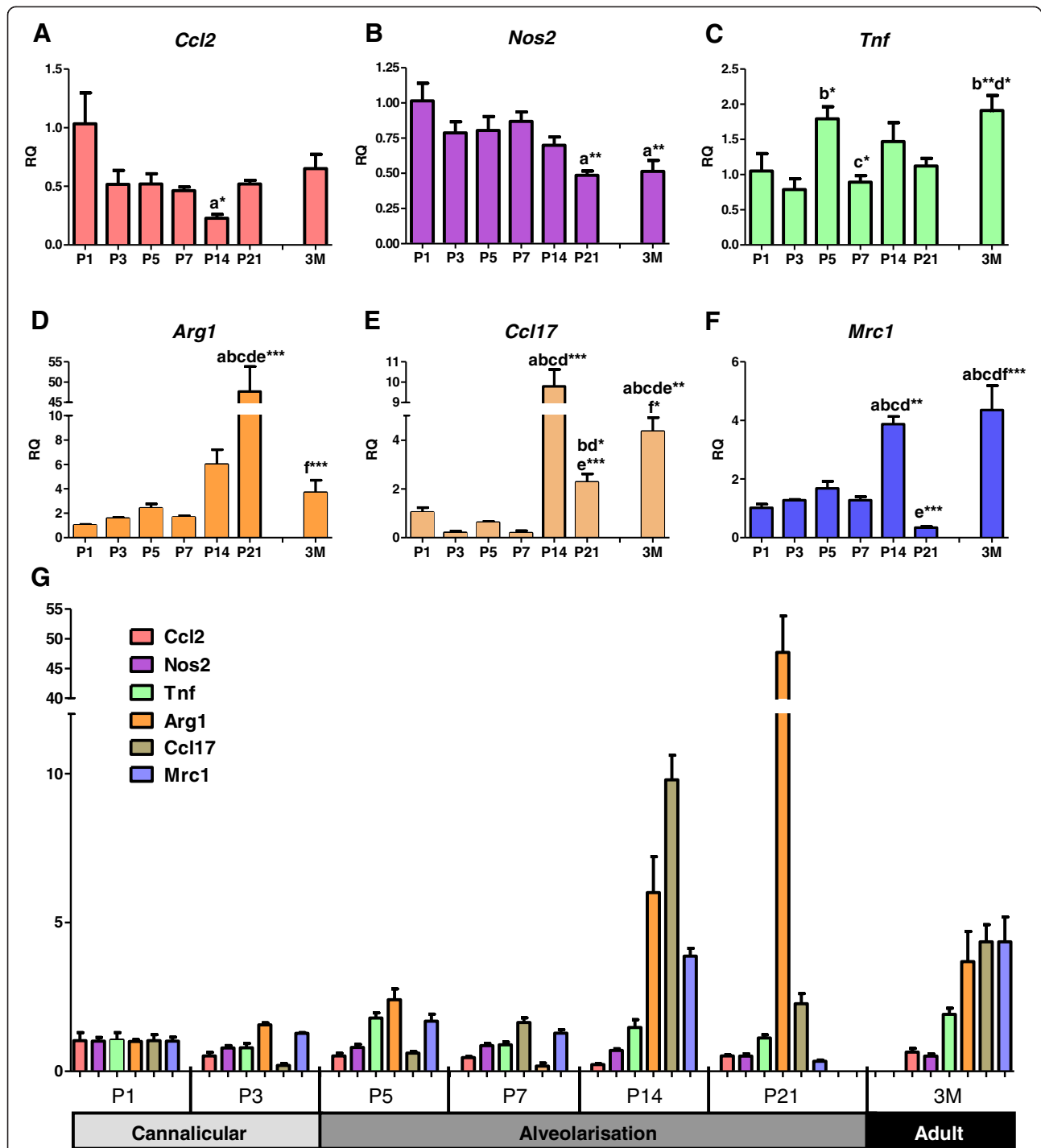


**Figure 4 Alveolar development is associated with M2 macrophage polarisation.** qPCR assessment of gene expression indicative of different macrophage polarisation states. Expression of pro-inflammatory M1 (A-C) and remodelling M2 (D-F) genes were normalised against  $\beta$ -actin expression and presented as relative quantification (RQ) compared to P1. All genes displayed on the same axis demonstrate the upregulation in M2 markers during alveolarisation (G). n=4 littermate lungs/time point. 'a' represents significant difference compared to P1, 'b' compared to P3, 'c' compared to P5, 'd' compared to P7. 'e' compared to P14, 'f' compared to P21. Asterisks following letters represent level of significance, where \*= $p < 0.05$ , \*\*= $p < 0.01$ , \*\*\*= $p < 0.001$ .

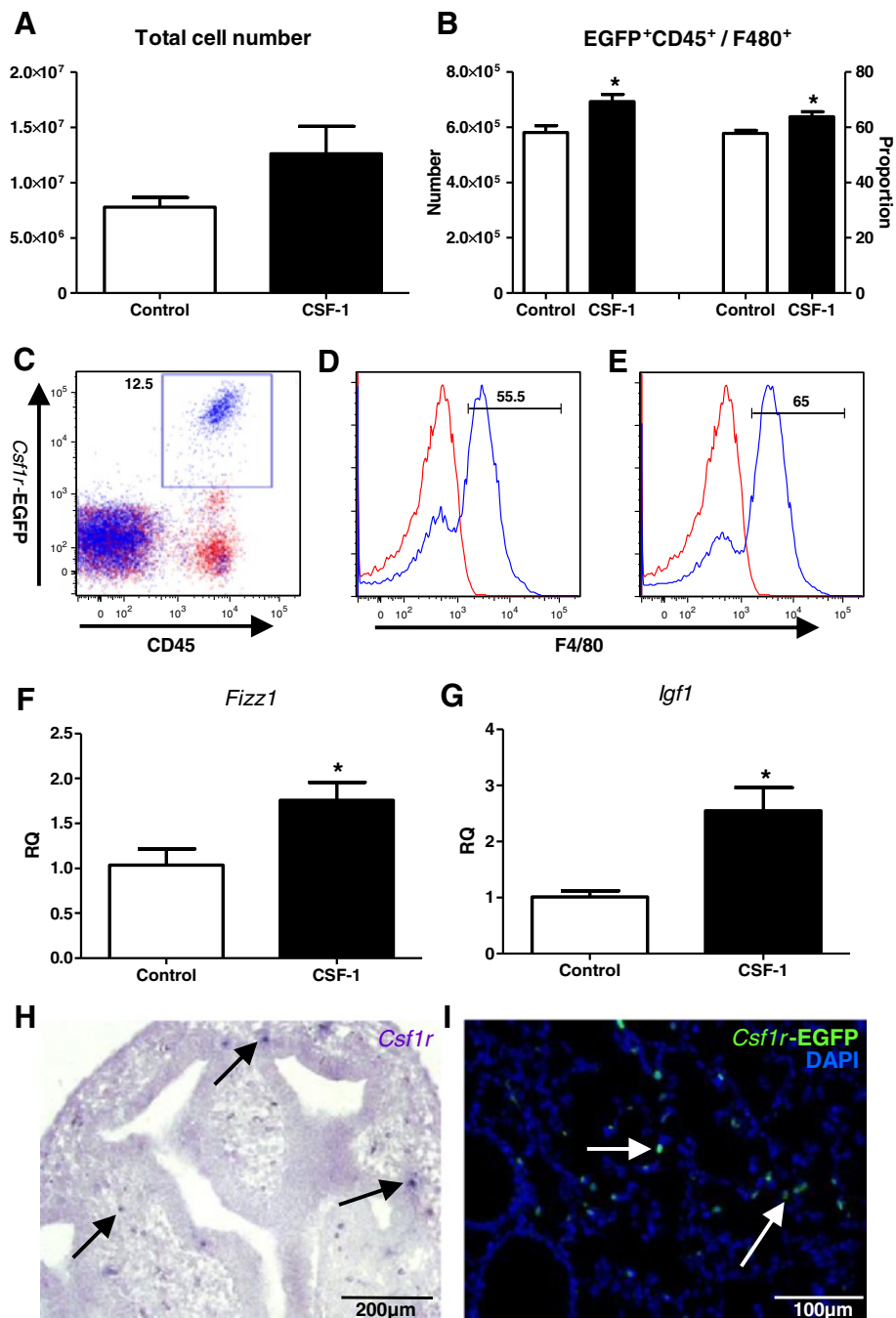


**Figure 5 CSF-1 increases developmental macrophages and promotes M2 gene and IGF-1 upregulation.** Flow cytometric analysis of macrophages (A-E) and qPCR analysis of gene expression in whole lungs (F&G) at P5, following administration of mrCSF-1 (1 μg/g i.p. at final volume of 50 μl; black bars) or PBS vehicle control (white bars) to littermate neonatal *Csfr-EGFP* mice at P1, 2 and 3. Cells from whole lungs (A) were gated on *Csfr-EGFP*+CD45<sup>+</sup> myeloid cells (C) and further gated on F4/80 expression to assess macrophage number and proportion (B), as displayed in representative histograms from control (D) and CSF-1-treated mice (E). Staining (blue) is overlaid with an isotype control (red). *Igf1* (G) and M2 gene *Fizz1* (F) expression was normalised against  $\beta$ -actin expression and presented as RQ compared to controls. n=3-4 littermate lungs/treatment. \*= $p < 0.05$ . Photomicrographs of *in situ* hybridisation for a *Csfr* riboprobe at E12.5 (H; purple) and fluorescence *Csfr-EGFP* transgene expression at P5 (I; green) demonstrated that during development the CSF-1R is expressed on interstitial myeloid cells (arrows), and not on the developing lung epithelium.

virtually all developing organs [7]. Macrophage functions that support organogenesis include clearance of apoptotic cellular debris associated with tissue remodelling [41] and the provision of trophic support by producing a range of regulatory mediators [5,42]. Macrophages also contribute to appropriate cellular differentiation [8,21,22] and angiogenic regulation [43], through both the production of angiogenic factors [44] and by physically directing angiogenic positioning [10]. As the lung buds form, macrophages surround the elongating primary bronchi [24]. The use of the *Csf1r*-EGFP reporter mice has been an important tool in demarcating the developmental role of macrophages in the embryo and has demonstrated a significant population of CSF-1R-expressing macrophages within the lungs at E13.5 [14]. Eliciting its effect through binding with the CSF-1R [45], CSF-1 is a pleiotropic growth factor also important in the regulation of pregnancy, fetal development and tissue regeneration [Reviewed in [33,34,40]].

Macrophages in the lung have been well described for their functions in host defence and inflammatory diseases, however the importance of CSF-1R+ macrophages in contributing to lung development has not been elucidated. The present study demonstrates the localisation of CSF-1R+EGFP+ alveolar and interstitial macrophages, which co-express the mature macrophage marker F4/80, in developing lungs during postnatal development. In addition, CSF-1R+ macrophages were identified in embryonic lung explants using wholemount immunofluorescence microscopy, where they were found to accumulate at branch points during lung branching morphogenesis.

The proposal that key organogenic periods are accompanied by an M2 macrophage phenotype was examined in the postnatal lung. During alveolarisation from P14 to P21, the expression of the M2 markers examined (*Arg1*, *Ccl17* and *Mrc1*) showed a significantly increased expression. The remodelling functions of M2 macrophages are in accordance with the structural changes occurring within the lung at this time. *Mrc1* provides an important mechanism for cellular clearance associated with homeostasis and tissue reorganisation [46]. *Arg1* is associated with collagen formation and ECM production [47]. This study thus highlights the importance of macrophages in the alveolarisation stage of lung development, and in particular the association with an M2 activation state. Furthermore in the adult lung, an upregulation of M2 genes was also observed, supporting the homeostatic and immunomodulatory functions of resident pulmonary macrophages.

We have previously reported that CSF-1-responsive developmental macrophages are associated with growth and organ development, with delivery of recombinant protein to neonatal mice resulting in increased body and organ weight [2]. The present study showed that

administration of CSF-1 to neonatal mice was also increased the number of macrophages in the developing lung and promoted an increase in *Fizz1* (*Retnla*) and *Igf1* expression. *Fizz1* is an important mediator of lung development and maturation, and is upregulated during the saccular and alveolar stages, where its angiogenic and proliferative functions are suggested to promote alveolar development [48]. *Fizz1* is also reported to participate in lung maturation by modulating surfactant production [49]. Expressed on lung cells such as mesenchymal and alveolar type II cells, the function of macrophage-derived *Fizz1* is under-examined in previous reports, and its upregulation with CSF-1 supplementation indicates it may provide beneficial effects in regulating lung development.

The increase in the key growth regulator IGF-1 in response to CSF-1 administration provides insight regarding the potential mechanism of trophic macrophage function in organogenesis, and also supports an emerging link between CSF-1, macrophages and the IGF-1 growth axis [34]. Interestingly, many of the growth and developmental deficiencies observed in CSF-1-deficient mice are common to IGF-1-deficient animals [50]. Moreover, an interaction between CSF-1 and the IGF-1 growth axis is supported by the finding that CSF-1-deficient rats fail to produce the postnatal spike in IGF-1 [34]. Furthermore, IGF-1 production as a key mechanism of trophic macrophage function is supported by a previous study which demonstrated that kidney regeneration in an experimental model of acute kidney disease is mediated by CSF-1-responsive macrophages and an upregulation of IGF-1 [2]. This has important parallels for normal lung development as IGF-1 increases during alveolarisation, and the promotion of lung maturation using retinoic acid and dexamethasone has been shown to correlate positively with increased levels of IGF-1 [51].

Identification of M2-polarised macrophages as an important component of the organogenic milieu during alveolar development has important potential clinical implications, not only for understanding normal developmental processes, but also for addressing lung immaturity and the impact of neonatal inflammation of developmental perturbation. Inflammatory activation of macrophages not only contributes to tissue damage and perturbation of organ development through pro-inflammatory injury, but also disrupts morphogenesis in the lung and alters the expression of key genes important in lung development [23,52]. Nuclear factor kappa-light-chain-enhancer of activated B cells (NF- $\kappa$ B) signalling in fetal macrophages upregulates pro-inflammatory mediators such as interleukin-1 $\beta$  and alters expression of *Wnt7b*, bone morphogenic protein-4 [23] and fibroblast growth factor-10 [52]. Given the correlation between the

timing of lung structural establishment and lung immunological maturity [53], it is plausible that the developmental deficits associated with inflammation may also result from skewing of macrophages prematurely away from their organogenic activities toward pro-inflammatory mediation roles.

Understanding the regulation of alveolar development has particular relevance with regard to clinical implications of developmental perturbation, and especially in the setting of preterm birth. The neonatal mouse provides an excellent model for studying these aspects of lung development as mice are born at a stage where earlier aspects of organ development are still ongoing. The period of postnatal development in the mouse was characterised; correlating structural and functional maturation with macrophage localisation. The histological time course of postnatal lung development demonstrates the processes of structural maturation, whereby large saccules evident at the end of the saccular stage at P5 begin to subdivide through secondary septation to form definitive alveoli clearly evident at P21. This period of alveolarisation is critical in establishment of the gas exchange units required for proper function of the lung. This is evidenced by the chronic lung dysfunction associated with disruptions of alveolar development that often result from preterm birth and injurious therapeutic interventions that are required to keep the neonate alive [54,55]. Indeed, Mund et al. reported that murine alveolarisation occurs in two stages; phase 1 from P4-21 where alveoli arise from immature septae, and phase 2 from P21-36 where alveoli lift off from existing mature alveoli [32].

The histological time course of postnatal lung development was complemented by analysis of functional maturation over this time. Changes in breath cycle parameters were examined throughout postnatal lung development using unrestrained barometric whole-body plethysmography. This technique has been utilised in adult models of lung injury [28,29] and was optimised for use in neonatal mice in our study. Modifications including the adjustment of the Perspex chamber size and increased sensitivity settings for pressure transduction recording enabled the measurement of lung function from as early as P5. Trace recordings showed discernable changes in breath patterns from P5 to adulthood, which when analysed provided quantitative changes in lung function. As the number of alveoli increased and the gas exchange compartment expanded, there was a correlation with changes in lung function parameters including an 8- and 10-fold increase in tidal and minute volume from the beginning of alveolarisation at P5 to adulthood. Normalisation of inspiratory flow rate and expiratory time were also observed over this time period of postnatal development as the chest wall and diaphragm mature.

The unique saccular architecture of the mature lung is associated with a different developmental cellularity pattern than that of solid organs. Overall cellularity increases rapidly in the alveolarisation phase and peaks at P14. From this stage, development is associated with significant remodelling and apoptosis as alveolar sacs form and mature, resulting in a decrease in cellularity in the adult mature lung. By digesting whole lungs, both interstitial as well as alveolar macrophages were able to be included for analysis, as opposed to the commonly used bronchoalveolar lavage-based collection method which restricts analysis to alveolar macrophages only. The proportion of macrophages in the lung is highest during the alveolarisation stage of lung development. A significant resident population is also maintained in the adult lung post completion of development, indicative of the unique air-exposed environment and the importance of pulmonary macrophages in clearing inhaled debris and modulating immune responses. The increased proportion of macrophages observed during alveolarisation – a time that lacks immunological relevance in this normal setting – therefore suggests that macrophages are associated with developmental functions.

## Conclusion

This study has demonstrated that macrophages provide a valuable contribution to normal lung development, and in particular that macrophages are increased and display an M2 polarisation phenotype during alveolarisation. An improved understanding of the organogenic environment important in regulating alveolar development has significant clinical relevance. The impact of inflammation and therapeutics on organogenic macrophage populations should be considered when studying the dysregulation and damage of the neonatal lung associated with preterm birth. It also supports research into modulation of macrophages in lung development to provide a novel intervention for enhancing lung maturation.

## Competing interests

CVJ & SDR hold a patent relating to the content of this manuscript

## Authors' contributions

CVJ contributed to study design, performed the acquisition and analysis of data, and wrote the manuscript. TMW and SS assisted with flow cytometry, KAW participated in embryonic explant culture, HD assisted with plethysmography and lung histology, BAR performed *in situ* hybridisation under the supervision of MHL, GJ provided intellectual input and critical drafting of the manuscript and SDR oversaw study design and coordination, data interpretation and writing of the manuscript. All authors read and approved the final manuscript.

## Acknowledgments

This work was supported by the National Health and Medical Research Council Project Grant # 1003806 and Development Grant # 1000615. HD is funded by an ARC Australian Post-Doctoral Research Fellowship. The authors wish to acknowledge Monash Micro Imaging, Monash University for technical support.

#### Author details

<sup>1</sup>Department of Anatomy and Developmental Biology, Monash University, Clayton, Victoria, Australia. <sup>2</sup>The Ritchie Centre, Monash Institute of Medical Research, Monash University, Clayton, Victoria, Australia. <sup>3</sup>Institute for Molecular Bioscience, The University of Queensland, St Lucia, Brisbane, Australia.

Received: 8 January 2013 Accepted: 28 March 2013

Published: 5 April 2013

#### References

- Morrissey EE, Hogan BL: Preparing for the first breath: genetic and cellular mechanisms in lung development. *Dev Cell* 2010, **18**:8–23.
- Alikhan MA, Jones CV, Williams TM, Beckhouse AG, Fletcher AL, Kett MM, Sakkal S, Samuel CS, Ramsay RG, Deane JA, et al: Colony-stimulating factor-1 promotes kidney growth and repair via alteration of macrophage responses. *Am J Pathol* 2011, **179**:1243–1256.
- Duffield JS, Forbes SJ, Constandinou CM, Clay S, Partolina M, Vuthoori S, Wu S, Lang R, Iredale JP: Selective depletion of macrophages reveals distinct, opposing roles during liver injury and repair. *J Clin Invest* 2005, **115**:56–65.
- Boulter L, Govaere O, Bird TG, Radulescu S, Ramachandran P, Pellicoro A, Ridgway RA, Seo SS, Spee B, Van Rooijen N, et al: Macrophage-derived Wnt opposes notch signaling to specify hepatic progenitor cell fate in chronic liver disease. *Nat Med* 2012, **18**:572–579.
- Lin SL, Li B, Rao S, Yeo EJ, Hudson TE, Nowlin BT, Pei H, Chen L, Zheng JJ, Carroll TJ, et al: Macrophage Wnt7b is critical for kidney repair and regeneration. *Proc Natl Acad Sci U S A* 2010, **107**:4194–4199.
- London A, Itskovich E, Benhar I, Kalchenko V, Mack M, Jung S, Schwartz M: Neuroprotection and progenitor cell renewal in the injured adult murine retina requires healing Monocyte-derived macrophages. *J Exp Med* 2011, **208**:23–39.
- Ovchinnikov DA: Macrophages in the embryo and beyond: much more than just giant phagocytes. *Genesis* 2008, **46**:447–462.
- Geutskens SB, Otonkoski T, Pulkkinen MA, Drexhage HA, Leenen PJ: Macrophages in the murine pancreas and their involvement in fetal endocrine development in vitro. *J Leukoc Biol* 2005, **78**:845–852.
- Ingman WW, Wyckoff J, Gouon-Evans V, Condeelis J, Pollard JW: Macrophages promote collagen fibrillogenesis around terminal end buds of the developing mammary gland. *Dev Dyn* 2006, **235**:3222–3229.
- Fantin A, Vieira JM, Gestri G, Denti L, Schwarz Q, Prykhodzij S, Peri F, Wilson SW, Ruhrberg C: Tissue macrophages act as cellular chaperones for vascular anastomosis downstream of VEGF-mediated endothelial tip cell induction. *Blood* 2010, **116**:829–840.
- Rae F, Woods K, Sasmono T, Campanale N, Taylor D, Ovchinnikov DA, Grimmond SM, Hume DA, Ricardo SD, Little MH: Characterisation and trophic functions of murine embryonic macrophages based upon the use of a Csf1r-EGFP transgene reporter. *Dev Biol* 2007, **308**:232–246.
- Lichanska AM, Hume DA: Origins and functions of phagocytes in the embryo. *Exp Hematol* 2000, **28**:601–611.
- Ovchinnikov DA, van Zuylen WJ, DeBats CE, Alexander KA, Kellie S, Hume DA: Expression of Gal4-dependent transgenes in cells of the mononuclear phagocyte system labeled with enhanced cyan fluorescent protein using Csf1r-Gal4VP16/UAS-ECFP double-transgenic mice. *J Leukoc Biol* 2008, **83**:430–433.
- Sasmono RT, Oceandy D, Pollard JW, Tong W, Pavli P, Wainwright BJ, Ostrowski MC, Himes SR, Hume DA: A macrophage colony-stimulating factor receptor-green fluorescent protein transgene is expressed throughout the mononuclear phagocyte system of the mouse. *Blood* 2003, **101**:1155–1163.
- Cecchini MG, Dominguez MG, Mocci S, Wetterwald A, Felix R, Fleisch H, Chisholm O, Hofstetter W, Pollard JW, Stanley ER: Role of colony stimulating factor-1 in the establishment and regulation of tissue macrophages during postnatal development of the mouse. *Development* 1994, **120**:1357–1372.
- Stefater JA 3rd, Ren S, Lang RA, Duffield JS: Metchnikoff's Policemen: macrophages in development, homeostasis and regeneration. *Trends Mol Med* 2011, **17**:743–752.
- Wiktor-Jedrzejczak W, Bartocci A, Ferrante AW Jr, Ahmed-Ansari A, Sell KW, Pollard JW, Stanley ER: Total absence of colony-stimulating factor 1 in the macrophage-deficient osteopetrotic (op/op) mouse. *Proc Natl Acad Sci U S A* 1990, **87**:4828–4832.
- Yoshida H, Hayashi S, Kunisada T, Ogawa M, Nishikawa S, Okamura H, Sudo T, Shultz LD: The murine mutation osteopetrosis is in the coding region of the macrophage colony stimulating factor gene. *Nature* 1990, **345**:442–444.
- Dai X, Ryan G, Hapel A, Dominguez M, Russell R, Kapp S, Sylvestre V, Stanley E: Targeted disruption of the mouse colony-stimulating factor 1 receptor gene results in osteopetrosis, mononuclear phagocyte deficiency, increased primitive progenitor cell frequencies, and reproductive defects. *Blood* 2002, **99**:111–120.
- Gouon-Evans V, Rothenberg ME, Pollard JW: Postnatal mammary gland development requires macrophages and eosinophils. *Development* 2000, **127**:2269–2282.
- Banaei-Bouchareb L, Gouon-Evans V, Samara-Boustani D, Castellotti MC, Czernichow P, Pollard JW, Polak M: Insulin cell mass is altered in Csf1op/Csf1op macrophage-deficient mice. *J Leukoc Biol* 2004, **76**:359–367.
- Banaei-Bouchareb L, Peuchmaur M, Czernichow P, Polak M: A transient microenvironment loaded mainly with macrophages in the early developing human pancreas. *J Endocrinol* 2006, **188**:467–480.
- Blackwell TS, Hippos AN, Yamamoto Y, Han W, Barham WJ, Ostrowski MC, Yull FE, Prince LS: NF-kappaB signaling in fetal lung macrophages disrupts airway morphogenesis. *J Immunol* 2011, **187**:2740–2747.
- Higashi K, Naito M, Takeya M, Ando M, Araki S, Takahashi K: Ontogenetic development, differentiation, and phenotypic expression of macrophages in fetal rat lungs. *J Leukoc Biol* 1992, **51**:444–454.
- Li MO, Sarkisian MR, Mehal WZ, Rakic P, Flavell RA: Phosphatidylserine receptor is required for clearance of apoptotic cells. *Science* 2003, **302**:1560–1563.
- Wynes MW, Frankel SK, Riches DW: IL-4-induced macrophage-derived IGF-1 protects myofibroblasts from apoptosis following growth factor withdrawal. *J Leukoc Biol* 2004, **76**:1019–1027.
- Rajagopal J, Carroll TJ, Guseh JS, Bores SA, Blank LJ, Anderson WJ, Yu J, Zhou Q, McMahon AP, Melton DA: Wnt7b Stimulates embryonic lung growth by coordinately increasing the replication of epithelium and mesenchyme. *Development* 2008, **135**:1625–1634.
- Milton PL, Dickinson H, Jenkin G, Lim R: Assessment of respiratory physiology of C57BL/6 mice following bleomycin administration using barometric plethysmography. *Respiration* 2011, **83**:253–266.
- Murphy S, Lim R, Dickinson H, Acharya R, Rosli S, Jenkin G, Wallace E: Human amnion epithelial cells prevent bleomycin-induced lung injury and preserve lung function. *Cell Transplant* 2010, **20**:2010.
- Drorbaugh JE, Fenn WO: A barometric method for measuring ventilation in newborn infants. *Pediatrics* 1955, **16**:81–87.
- Rumballe B, Georgas K, Little MH: High-throughput paraffin section *in situ* hybridization and dual immunohistochemistry on mouse tissues. *CSH Protoc* 2008, **2008**:pdb prot5030.
- Mund SI, Stamparoni M, Schittny JC: Developmental alveolarization of the mouse lung. *Dev Dyn* 2008, **237**:2108–2116.
- Douglass TG, Driggers L, Zhang JG, Hoa N, Delgado C, Williams CC, Dan Q, Sanchez R, Jeffes EW, Wepsic HT, et al: Macrophage colony stimulating factor: not just for macrophages anymore! a gateway into complex biologies. *Int Immunopharmacol* 2008, **8**:1354–1376.
- Gow DJ, Sester DP, Hume DA: CSF-1, IGF-1, and the control of postnatal growth and development. *J Leukoc Biol* 2010, **88**:475–481.
- Martinez FO, Sica A, Mantovani A, Locati M: Macrophage activation and polarization. *Front Biosci* 2008, **13**:453–461.
- Mosser DM, Edwards JP: Exploring the full spectrum of macrophage activation. *Nat Rev Immunol* 2008, **8**:958–969.
- Williams TM, Little MH, Ricardo SD: Macrophages in renal development, injury, and repair. *Semin Nephrol* 2010, **30**:255–267.
- Pollard JW: Trophic macrophages in development and disease. *Nat Rev Immunol* 2009, **9**:259–270.
- Zhang MZ, Yao B, Yang S, Jiang L, Wang S, Fan X, Yin H, Wong K, Miyazawa T, Chen J, et al: CSF-1 signaling mediates recovery from acute kidney injury. *J Clin Invest* 2012, **122**:4519–4532.
- Hamilton JA: Colony-stimulating factors in inflammation and autoimmunity. *Nat Rev Immunol* 2008, **8**:533–544.
- Lang RA, Bishop JM: Macrophages are required for cell death and tissue remodeling in the developing mouse eye. *Cell* 1993, **74**:453–462.
- Nacu N, Luzina IG, Highsmith K, Lockatell V, Pochetuhin K, Cooper ZA, Gillmeister MP, Todd NW, Atamas SP: Macrophages produce TGF-beta-induced (beta-ig-h3) following ingestion of apoptotic cells and regulate MMP14 levels and collagen turnover in fibroblasts. *J Immunol* 2008, **180**:5036–5044.

43. Nucera S, Bizziato D, De Palma M: **The interplay between macrophages and angiogenesis in development, tissue injury and regeneration.** *Int J Dev Biol* 2011, **55**:495–503.
44. Stefater JA 3rd, Lewkowich I, Rao S, Mariggi G, Carpenter AC, Burr AR, Fan J, Ajima R, Molkenin JD, Williams BO, *et al*: **Regulation of angiogenesis by a non-canonical Wnt-Flt1 pathway in myeloid cells.** *Nature* 2011, **474**:511–515.
45. Sherr CJ: **Colony-stimulating factor-1 receptor.** *Blood* 1990, **75**:1–12.
46. Allavena P, Chieppa M, Monti P, Piemonti L: **From pattern recognition receptor to regulator of homeostasis: the double-faced macrophage mannose receptor.** *Crit Rev Immunol* 2004, **24**:179–192.
47. Durante W, Johnson FK, Johnson RA: **Arginase: a critical regulator of nitric oxide synthesis and vascular function.** *Clin Exp Pharmacol Physiol* 2007, **34**:906–911.
48. Wagner KF, Hellberg AK, Balenger S, Depping R, Dodd OJ, Johns RA, Li D: **Hypoxia-induced mitogenic factor has antiapoptotic action and is upregulated in the developing lung: coexpression with hypoxia-inducible factor-2alpha.** *Am J Respir Cell Mol Biol* 2004, **31**:276–282.
49. Tong Q, Zheng L, Dodd-o J, Langer J, Wang D, Li D: **Hypoxia-induced mitogenic factor modulates surfactant protein B and C expression in mouse lung.** *Am J Resp Cell Mol* 2006, **34**:28–38.
50. Liu JL, Yakar S, LeRoith D: **Conditional knockout of mouse insulin-like growth factor-1 gene using the Cre/loxP system.** *Proc Soc Exp Biol Med* 2000, **223**:344–351.
51. Liu H, Chang L, Rong Z, Zhu H, Zhang Q, Chen H, Li W: **Association of insulin-like growth factors with lung development in neonatal rats.** *J Huazhong Univ Sci Technolog Med Sci* 2004, **24**:162–165.
52. Benjamin JT, Carver BJ, Plosa EJ, Yamamoto Y, Miller JD, Liu JH, van der Meer R, Blackwell TS, Prince LS: **NF-kappaB activation limits airway branching through inhibition of Sp1-mediated fibroblast growth factor-10 expression.** *J Immunol* 2010, **185**:4896–4903.
53. Dickie R, Tasat DR, Alanis EF, Delfosse V, Tsuda A: **Age-dependent changes in porcine alveolar macrophage function during the postnatal period of alveolarization.** *Dev Comp Immunol* 2009, **33**:145–151.
54. Moss TJ: **Respiratory consequences of preterm birth.** *Clin Exp Pharmacol Physiol* 2006, **33**:280–284.
55. Kinsella JP, Greenough A, Abman SH: **Bronchopulmonary dysplasia.** *Lancet* 2006, **367**:1421–1431.

doi:10.1186/1465-9921-14-41

**Cite this article as:** Jones *et al.*: M2 macrophage polarisation is associated with alveolar formation during postnatal lung development. *Respiratory Research* 2013 **14**:41.

**Submit your next manuscript to BioMed Central and take full advantage of:**

- Convenient online submission
- Thorough peer review
- No space constraints or color figure charges
- Immediate publication on acceptance
- Inclusion in PubMed, CAS, Scopus and Google Scholar
- Research which is freely available for redistribution

Submit your manuscript at  
[www.biomedcentral.com/submit](http://www.biomedcentral.com/submit)



# Human mesenchymal stem cells alter macrophage phenotype and promote regeneration via homing to the kidney following ischemia-reperfusion injury

Andrea F. Wise,<sup>1</sup> Timothy M. Williams,<sup>1</sup> Mensiena B. G. Kiewiet,<sup>1</sup> Natalie L. Payne,<sup>2</sup>  
Christopher Siatskas,<sup>1</sup> Chrishan S. Samuel,<sup>3</sup> and Sharon D. Ricardo<sup>1</sup>

<sup>1</sup>Department of Anatomy and Developmental Biology, Monash University, Clayton, Victoria, Australia; <sup>2</sup>Australian Regenerative Medicine Institute, Monash University, Clayton, Victoria, Australia; and <sup>3</sup>Department of Pharmacology, Monash University, Clayton, Victoria, Australia

Submitted 19 December 2013; accepted in final form 6 March 2014

**Wise AF, Williams TM, Kiewiet MB, Payne NL, Siatskas C, Samuel CS, Ricardo SD.** Human mesenchymal stem cells alter macrophage phenotype and promote regeneration via homing to the kidney following ischemia-reperfusion injury. *Am J Physiol Renal Physiol* 306: F1222–F1235, 2014. First published March 12, 2014; doi:10.1152/ajprenal.00675.2013.—Mesenchymal stem cells (MSCs) ameliorate injury and accelerate repair in many organs, including the kidney, although the reparative mechanisms and interaction with macrophages have not been elucidated. This study investigated the reparative potential of human bone marrow-derived MSCs and traced their homing patterns following administration to mice with ischemia-reperfusion (IR) injury using whole body bioluminescence imaging. The effect of MSCs on macrophage phenotype following direct and indirect coculture was assessed using qPCR. Human cytokine production was measured using multiplex arrays. After IR, MSCs homed to injured kidneys where they afforded protection indicated by decreased proximal tubule kidney injury molecule-1 expression, blood urea nitrogen, and serum creatinine levels. SDS-PAGE and immunofluorescence labeling revealed MSCs reduced collagen  $\alpha_1(I)$  and IV by day 7 post-IR. Gelatin zymography confirmed that MSC treatment significantly increased matrix metalloproteinase-9 activity in IR kidneys, which contributed to a reduction in total collagen. Following direct and indirect coculture, macrophages expressed genes indicative of an anti-inflammatory “M2” phenotype. MSC-derived human GM-CSF, EGF, CXCL1, IL-6, IL-8, MCP-1, PDGF-AA, and CCL5 were identified in culture supernatants. In conclusion, MSCs home to injured kidneys and promote repair, which may be mediated by their ability to promote M2 macrophage polarization.

ischemia-reperfusion injury; mesenchymal stem cells; macrophage

SINCE THE INITIAL EXCITEMENT surrounding the multilineage potential and self-renewal properties of mesenchymal stem (stromal) cells (MSCs), their therapeutic potential to elicit tissue regeneration has been explored experimentally and in a wide range of clinical applications (45). MSCs are capable of modulating inflammation through interacting with a variety of immune cells (53, 68). These immunomodulatory properties, in combination with their tissue-regenerative capabilities, have created great enthusiasm for these cells to be used as a treatment for a wide variety of pathological conditions ranging from autoimmune to chronic inflammatory diseases (for a review, see Refs. 45, 62, and 68). MSCs reside in most postnatal organs and tissues and can be isolated and expanded in culture (13). Unlike embryonic stem (ES) cells and induced pluripotent stem (iPS) cells, MSCs typically do not form

tumors following transplantation in rodents and are free of the ethical limitations associated with ES cell research.

Human MSCs have been shown to ameliorate the symptoms of inflammatory diseases in rodent models (4, 9, 24, 27, 41, 70); however, the mechanisms responsible for their protective and regenerative effects are not completely understood. The interaction of MSCs with macrophages may play a vital role in their downstream anti-inflammatory and immunomodulatory effects, yet the specific cell cross talk MSCs have with infiltrating macrophages and damaged kidney cells, along with the cytokines that contribute to their unique immunomodulatory properties, remains poorly defined.

MSCs secrete a broad range of cytokines, including macrophage chemoattractants, as well as a variety of factors with renoprotective and reparative capabilities. These include anti-inflammatory, antiapoptotic, mitogenic, antifibrotic, and proangiogenic agents, which most likely govern repair via paracrine and endocrine pathways (5, 19, 21, 67). In a setting of acute kidney injury (AKI), transplanted MSCs localized within peritubular capillaries, adjacent to the renal tubules, and glomeruli (56). However, the survival of MSCs and timing of administration leading to the interplay between MSCs and macrophages, along with their ability to modify the tissue microenvironment in a setting where aberrant wound healing-induced collagen accumulation leads to fibrosis, have yet to be elucidated.

Macrophages comprise a heterogeneous population that is governed by the inflammatory cues in the surrounding microenvironment (54). Although initially recognized as contributing to the pathogenesis of kidney injury, macrophages may also play a vital role in the remodeling phase of kidney regeneration following acute damage (30, 61, 63). Subsequently, macrophages have been broadly classified into one of two opposing polarization states: classically activated “M1” and alternatively activated “M2” populations (38). M1 macrophages secrete numerous proinflammatory cytokines and are involved in pathogen clearance whereas M2 macrophages secrete anti-inflammatory cytokines that mediate wound healing and tissue remodeling (38).

This study investigated the therapeutic potential of human bone marrow (BM)-derived MSCs in conjunction with their homing patterns following intravenous (iv) administration to mice with ischemia-reperfusion (IR) injury using whole body bioluminescence imaging. In addition, the effect of MSCs on macrophage phenotype and the soluble factors produced following direct and indirect coculture experiments were assessed.

Address for reprint requests and other correspondence: S. D. Ricardo, Dept. of Anatomy and Developmental Biology, Level 3, Bldg. 75, Monash Univ., Clayton, Victoria 3800, Australia.

## MATERIALS AND METHODS

**Mesenchymal stem cell culture.** Human BM-derived MSCs purchased from the Tulane Center for Stem Cell Research and Regenerative Medicine (Tulane University, New Orleans, LA) and enhanced green fluorescent protein (eGFP) and firefly luciferase (fluc) eGFP<sup>+</sup>fluc<sup>+</sup> MSCs were cultured as previously described (47). Karyotype analysis was performed on MSCs at passage 3 (Southern Cross Pathology, Clayton, Australia). The clonogenic potential of MSCs was tested using a colony-forming unit-fibroblast (CFU-F) assay, and colonies were stained with 3% (wt/vol) crystal violet (Sigma-Aldrich, St. Louis, MO).

**Multilineage differentiation.** To demonstrate multilineage differentiation potential, MSCs were differentiated toward osteogenic, adipogenic, and chondrogenic lineages using a human functional identification kit (R&D Systems, Minneapolis, MN). Following differentiation, osteocytes were stained with Alizarin red S (Sigma-Aldrich), adipocytes with fatty acid binding protein-4 (FABP-4; R&D Systems), and chondrocytes with aggrecan (R&D Systems).

**Flow cytometry.** Immunophenotypic analysis of MSCs by flow cytometry was performed using the following fluorochrome-conjugated anti-human antibodies: CD73-PE, CD90-PerCP-Cy5.5, CD105-Alexa Fluor 647, CD14-APC (eBioscience), CD19-FITC, CD34-APC, CD45-APC, and HLA-DR-FITC. All antibodies were purchased from BD Biosciences (San Jose, CA) unless otherwise indicated. Cell population data was acquired using a FACSCanto II flow cytometer (BD Biosciences) and analyzed using Flowlogic Software (Invivo Technologies, Mentone, Australia).

**Experimental design.** All animal studies were approved by the Monash University Animal Ethics Committee, which adheres to the Australian Code of Practice for the Care and Use of Animals for Scientific Purposes. For IR injury, male 6- to 8-wk-old C57BL/6J mice (Monash Animal Services, Clayton, Australia) were anesthetized with 2.5% (vol/vol) inhaled isoflurane (Abbott Australasia Pty, Kurnell, Australia), and injury was induced by clamping the left renal pedicle for 40 min (unilateral) or both renal pedicles for 25 min (bilateral) with a microvascular clamp (0.4–0.1 mm; S&T Fine Science Tools, Foster City, CA) through a flank incision. Following reperfusion, mice were injected iv with  $1 \times 10^6$  MSCs resuspended in 120  $\mu$ l PBS or a vehicle control (120  $\mu$ l PBS alone). A third group of mice served as a sham-operated control group, whereby the animals were anesthetized and a flank incision made without clamping the renal pedicle. Mice that received bilateral IR injury were placed in metabolic cages to obtain 24-h urine samples. Urinary kidney injury molecule (Kim)-1 was measured with a Kim-1 mouse ELISA (Abcam, Cambridge, UK). Concentrations of blood urea nitrogen (BUN) and serum creatinine were measured 3 days post-IR using the i-STAT CHEM8+ cartridges and the i-STAT system ( $n = 8$ ; Abbott, Ontario, Canada).

**Bioluminescence imaging.** Mice ( $n = 5$ ) were anesthetized with 2.5% (vol/vol) isoflurane, injected intraperitoneally (ip) with 200  $\mu$ l D-luciferin (15 mg/ml in PBS; VivoGlo Luciferin, Promega, San Luis Obispo, CA) and imaged 10 min after injection using the Xenogen IVIS 200 system (Xenogen, Alameda, CA) on days 0 (1-h post-MS-C injection), 1, and 3 post-IR. Regions of interest (ROI) were drawn, and fluc luminescent signal intensities were analyzed using Living Image 3.2 software (Xenogen).

**Histology and immunofluorescence labeling.** Histopathology was assessed on formalin-fixed, 4- $\mu$ m-thick paraffin sections stained with hematoxylin and eosin (H&E). Semiquantification of histopathology was performed after taking five fields of view/kidney section within the corticomedullary region ( $n = 3$ ; 3 sections/mouse;  $\times 400$ ). Proximal tubular damage and protein cast formation were assessed, and the percentage of kidney damage was graded on a scale of 0 to 4 (refer to Table 1).

To assess proliferation, kidney sections were stained with mouse anti-PCNA (DakoCytomation, Glostrup, Denmark) and rabbit anti-mouse Ki67 (Abcam) primary antibodies followed by Alexa Fluor

Table 1. Injury scale used to grade kidney damage following IR injury

Scale	Percentage of Kidney Damage
0	Normal tubules and no protein casts
0.5	Minor tubular damage and protein cast formation
1.0	Involvement of <10% corticomedullary region
2.0	Involvement of 10% to 25% of corticomedullary region
2.5	Involvement of 26% to 50% of corticomedullary region
3.0	Involvement of 51% to 75% of corticomedullary region
4.0	Widespread damage >75% of corticomedullary region

IR, ischemia-reperfusion.

488 donkey anti-mouse (Molecular Probes, Eugene, OR) and Alexa Fluor 555 goat anti-rabbit (Molecular Probes) secondary antibodies. For proximal tubule Kim-1 expression, immunohistochemical staining was performed with rat anti-mouse Kim-1 (R&D Systems) using the avidin-biotin complex (ABC) method as described previously (43). The area of 3,3'-diaminobenzidine staining per unit area of tissue was measured using a custom macro from the image-analysis software ImageJ/FIJI, version 1.48d. Areas of positive staining were quantified in five nonoverlapping, randomly selected fields of view ( $n = 3$ , 3 sections/mouse;  $\times 400$  magnification).

For the visualization of type IV collagen, kidney sections were stained with a goat anti-human collagen type IV primary antibody (Southern Biotech, Birmingham, AL) followed by an Alexa Fluor 647 chicken anti-goat antibody (Molecular Probes) and for macrophage staining, a rat anti-mouse F4/80 antibody (AbD Serotec, Oxford, UK) followed by an Alexa Fluor 555 goat anti-rat antibody (Molecular Probes). Sections were counterstained with 4,6-diamidino-2-phenylindole (Molecular Probes) and viewed with a Provis AX70 fluorescence microscope (Olympus, Tokyo, Japan). Fluorescence images were captured with an F-view II digital camera (Soft Imaging System, Munster, Germany).

**Hydroxyproline, SDS-PAGE, and zymographic analyses.** A kidney from each animal was divided into portions containing both cortex and medulla for use in each assay. The total collagen content (% collagen content/dry weight tissue) in the kidney ( $n = 3$ /group) was measured using a hydroxyproline assay as previously described (49). In brief, kidneys were lyophilized to measure dry weight, hydrolyzed in 6 M hydrochloric acid, and hydroxyproline levels were determined by measuring the absorbance of hydrolyzed samples at 558 nm, using a Digital Spectrophotometer (Varian, Palo Alto, CA) (50). Total collagen content was determined by multiplying the hydroxyproline measurements by a factor of 6.94.

SDS-PAGE analysis was used to detect changes in interstitial collagen subtypes within the kidney (50). The supernatants from pepsin-digested kidneys were analyzed on 5% (wt/vol) acrylamide gels with 3.5% (wt/vol) acrylamide stacking gels. The  $\alpha_1$ (III) chains were separated from the  $\alpha_1$ (I) collagen chains with interrupted electrophoresis with delayed reduction of type III collagen. The gels were stained with 0.1% Coomassie blue R-250 overnight at 4°C and then destained with 30% (vol/vol) methanol containing 7% (vol/vol) acetic acid. Densitometry was performed with a calibrated imaging densitometer (Gel Scan-710, Bio-Rad, Hercules, CA), and data were analyzed using Quantity-One software (Bio-Rad).

Matrix metalloproteinase (MMP)-2 and MMP-9 activity was assessed by gelatin zymography (65). Zymographs consisted of 7.5% (wt/vol) acrylamide gels containing 1 mg/ml gelatin. The gels were stained with 0.1% (wt/vol) Coomassie blue R-250 overnight at 37°C and then destained with 7% (vol/vol) acetic acid. Clear bands indicated gelatinolytic activity, where the enzymes had digested the substrate. Densitometry of these MMP bands was performed, and data were analyzed using Quantity-One software.

**MSC and macrophage coculture.** BM was isolated from male 6- to 8-wk-old C57BL/6J mice and cultured in DMEM/F12 (Invitrogen,

Camarillo, CA) supplemented with 10% FBS, 10 mM L-glutamine, 100  $\mu\text{g}/\text{ml}$  penicillin/streptomycin, and 100 U/ml mouse recombinant colony-stimulating factor (CSF)-1 (Chiron) to generate macrophages. On *day 7*, the purity of the BM-derived macrophages was  $>95\%$  when checked by flow cytometry.

For coculture experiments, macrophages were primed with 120 ng/ml of IFN- $\gamma$  (R&D Systems) and 10 ng/ml LPS (Sigma-Aldrich) to induce an M1 phenotype or with 20 ng/ml IL-4 (Invitrogen) to induce an M2 phenotype. The macrophages were then washed with PBS before MSCs were plated indirectly, on a 0.4- $\mu\text{m}$  pore size Transwell (Corning Life Sciences, Pittsford, PA), or directly and cultured for 48 h. Following 24 h of coculture, 1 ml of the coculture supernatant was collected and screened for human MSC-derived cytokines, using a MILLIPLEX<sub>MAP</sub> Human Cytokine/Chemokine Panel (Millipore).

**Real-time quantification PCR gene expression analysis.** Macrophages were sorted by fluorescence-activated cell sorting (FACS) from the cocultures using the conjugated anti-mouse antibodies CD45-FITC (BD Biosciences) and F4/80-APC (BD Biosciences). RNA was extracted using an RNeasy Micro Kit (Qiagen, Hilden, Germany) according to the manufacturer's guidelines. RNA samples were reverse transcribed using a High Capacity cDNA Reverse Transcription Kit (Applied Biosystems, Foster City, CA), and real-time quantitative PCR (qPCR) for each target gene was performed in duplicate on cDNA samples using TaqMan Universal PCR Master Mix (Applied Biosystems) and TaqMan Gene Expression Assays (Applied Biosystems; see Table 2). The threshold cycle (Ct) values were normalized against endogenous control  $\beta$ -actin to determine  $\Delta\text{Ct}$ .

**Statistical analyses.** Statistical analyses of the data were performed using GraphPad Prism software version 5.0 (GraphPad Software, San Diego, CA). An unpaired *t*-test was used to analyze data between two groups. Comparisons among three groups were performed by one-way ANOVA followed by Tukey's multiple comparison tests. All data were expressed as means  $\pm$  SE.  $P < 0.05$  was considered statistically significant.

## RESULTS

**Characterization of MSCs.** Human MSCs were initially characterized to confirm their cellular identity using the minimal criteria established by Dominici et al. (14). In vitro, cultured MSCs adhered to plastic, had a spindle-shaped morphology (Fig. 1A), displayed a normal karyotype (Fig. 1B), and formed CFU-F (Fig. 1C). Functionally, MSCs differentiated into osteocytes, adipocytes, and chondrocytes as evidenced by positive staining with Alizarin red (Fig. 1D), FABP-4 (Fig. 1E), and aggrecan (Fig. 1F), respectively. Finally, MSCs were uniformly positive for the canonical MSC markers CD73, CD90, and CD105 and lacked the expression of the hematopoietic markers CD14, CD19, CD34, CD45, and HLA-DR (Fig. 1G).

**MSCs home to the injured kidney following unilateral and bilateral IR injury.** eGFP<sup>+</sup>fluc<sup>+</sup> MSCs were FACS sorted to enrich for the number of eGFP<sup>+</sup>fluc<sup>+</sup> MSCs (Fig. 2A), with the purity of the postsorted cells also determined by flow cytometry (Fig. 2A). eGFP expression was confirmed visually using fluorescence microscopy (Fig. 2B). Using a noninvasive bioluminescent imaging technique, eGFP<sup>+</sup>fluc<sup>+</sup> MSCs were tracked in vivo following iv administration immediately following surgery in mice with unilateral or bilateral IR injury and in sham-operated control mice (see diagram in Fig. 2C).

Following sham surgery, MSCs accumulated only in the lungs, likely the result of being trapped in the pulmonary capillaries (Fig. 3A). Bioluminescence measurements in the sham-operated control mice decreased over the 3-day time

Table 2. Real-time PCR TaqMan gene expression assays

Gene Symbol	Assay ID
<i>Actb</i>	Mm00607939_s1
<i>Arg1</i>	Mm00475988_m1
<i>Chi3l3</i>	Mm00657889_m1
<i>Fizz1 (Retnla)</i>	Mm00445108_m1
<i>Ccl2</i>	Mm00441242_m1
<i>Mrc1</i>	Mm00485148_m1

course ( $2.038 \times 10^7$  photons $\cdot\text{s}^{-1}\cdot\text{cm}^{-2}\cdot\text{sr}^{-1}$  on *day 0* to  $3.362 \times 10^6$  photons $\cdot\text{s}^{-1}\cdot\text{cm}^{-2}\cdot\text{sr}^{-1}$  on *day 1* as per mouse in Fig. 3A). No signal was detected at *day 3*. In contrast, following unilateral and bilateral IR injury, MSCs homed to the site of damage via two routes: directly to the kidney(s), as detected at the *day 0* imaging time point (Fig. 3, B and D, respectively), or to the kidney(s) via the lungs (Fig. 3, C and E, respectively). The localization of the MSCs in the kidney was confirmed by imaging the lateral aspect of the mouse (images not shown) before the kidneys were excised and imaged *ex vivo*. Examples of each of the MSC homing patterns with detected fluc signals in sham and IR mice are shown in Fig. 3. The fluc signal following direct homing to the kidney with unilateral IR injury was marginally decreased from *day 0* to *day 1* ( $4.436 \times 10^7$  to  $3.828 \times 10^7$  photons $\cdot\text{s}^{-1}\cdot\text{cm}^{-2}\cdot\text{sr}^{-1}$ ) and further by *day 3* ( $1.953 \times 10^7$  photons $\cdot\text{s}^{-1}\cdot\text{cm}^{-2}\cdot\text{sr}^{-1}$ ; Fig. 3B). In contrast to the unilateral model, the fluc signal with bilateral IR injury gradually increased from  $5.109 \times 10^7$  photons $\cdot\text{s}^{-1}\cdot\text{cm}^{-2}\cdot\text{sr}^{-1}$  on *day 1* to  $1.706 \times 10^8$  photons $\cdot\text{s}^{-1}\cdot\text{cm}^{-2}\cdot\text{sr}^{-1}$  on *day 3*. At 7 days post-IR, the fluc signal was no longer detected in either the unilateral or bilateral models. In the mice where MSCs were observed to accumulate in the lungs before migrating to the damaged kidney(s) following unilateral or bilateral IR injury (Fig. 3, C and E), the majority of injected cells had localized in the lungs at 1 h postadministration. However, the MSCs further migrated from the lungs to the injured kidney(s) (imaged on *days 1* and *3*), with the majority of cells being present in the kidney(s) at *day 3*. Again, at *day 7*, no cells were detected.

**MSCs promote structural and functional regeneration.** Compared to sham-operated mice, at 7 days following IR injury there was widespread tubular epithelial cell damage within the kidney, evidenced by numerous protein casts, interstitial matrix expansion, and extracellular matrix deposition along with a marked infiltration of inflammatory cells (Fig. 4A). In contrast, the administration of MSCs to mice with IR injury promoted structural regeneration, including reduced inflammation and reestablishment of the tubular epithelium. Semiquantitative examination of kidney sections revealed a significant reduction in the number of protein casts ( $P < 0.001$ ) and proximal tubule epithelial cell damage ( $P < 0.001$ ; Fig. 4B) by 5 days following MSC injection. Structural regeneration of the MSC-treated kidneys was associated with a significant increase in tubular epithelial cell proliferation demonstrated at the *day 3* time point, as assessed with Ki67 and PCNA immunostaining (Fig. 4, C and D). This MSC-mediated repair was further evidenced by functional recovery. BUN and serum creatinine concentrations were measured 3 days post-MS administration (Fig. 5, A and B). At 3 days after bilateral IR surgery, BUN levels had increased over twofold compared with sham-operated controls ( $18.1 \pm 1.9$  vs.  $8.4 \pm 0.4$  mmol/l;  $P < 0.001$ ) and serum creatinine

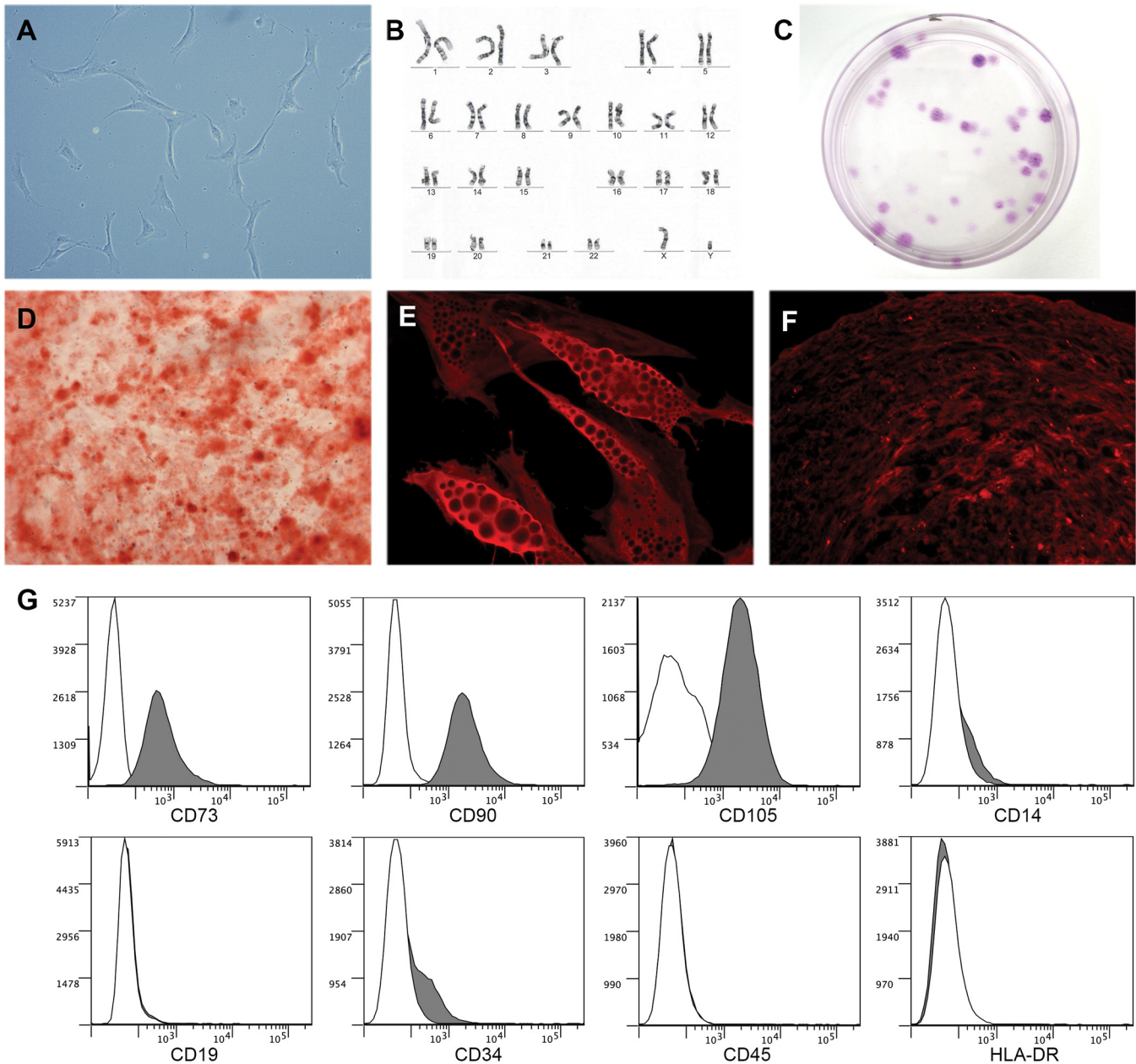


Fig. 1. In vitro characterization of human mesenchymal stem cells (MSCs). MSCs adhered to plastic in standard tissue culture conditions (magnification  $\times 200$ ; A), displayed a normal 46XY karyotype (B), and formed colony-forming unit-fibroblasts (CFU-F), demonstrated by crystal violet staining, following 14 days in vitro culture (C). MSCs possessed multilineage differentiation potential in vitro, differentiating into osteocytes, indicated by the formation of calcium-rich deposits detected with alizarin red staining (magnification  $\times 50$ ; D), adipocytes, identified by the presence of lipid vacuoles and fatty acid binding protein-4 staining (magnification  $\times 400$ ; E), and chondrocytes, visualized by the presence of aggrecan staining (magnification  $\times 200$ ; F). MSCs expressed the cell surface antigens CD73, CD90, and CD105, however, and lacked the expression of CD14, CD19, CD34, CD45, and HLA-DR (G).

1.5-fold higher than sham levels ( $34.7 \pm 3.1$  vs.  $22.4 \pm 2.1$   $\mu\text{mol/l}$ ;  $P < 0.05$ ). In MSC-treated mice, both the BUN and serum creatinine concentrations were comparable to baseline measurements and were significantly lower than the vehicle-treated controls (Fig. 5, A and B). In addition, immunohistochemical staining revealed increased expression of Kim-1, a marker of proximal tubular injury, on the apical membrane of proximal tubule cells 3 days after IR injury, compared with sham-operated kidneys (Fig. 5C), while Kim-1 expression was markedly reduced in MSC-treated mice. Notably, urinary Kim-1, assessed by an ELISA, was significantly increased at 7

days post-IR compared with sham-operated control mice ( $P < 0.001$ ) but returned to baseline levels in MSC-treated mice ( $P < 0.01$ ; Fig. 5D).

*MSCs reduce collagen accumulation in the injured kidney.* MSC therapy following IR injury reduced interstitial collagen accumulation as assessed by hydroxyproline assay, SDS-PAGE, and type IV collagen immunofluorescence labeling. IR injury resulted in a gradual but significant increase in the total collagen concentration at 3 ( $P < 0.05$ ), 5 ( $P < 0.001$ ), and 7 ( $P < 0.001$ ) days postinjury compared with sham-operated controls (Fig. 6A). At 5 days post-IR injury, MSC treatment

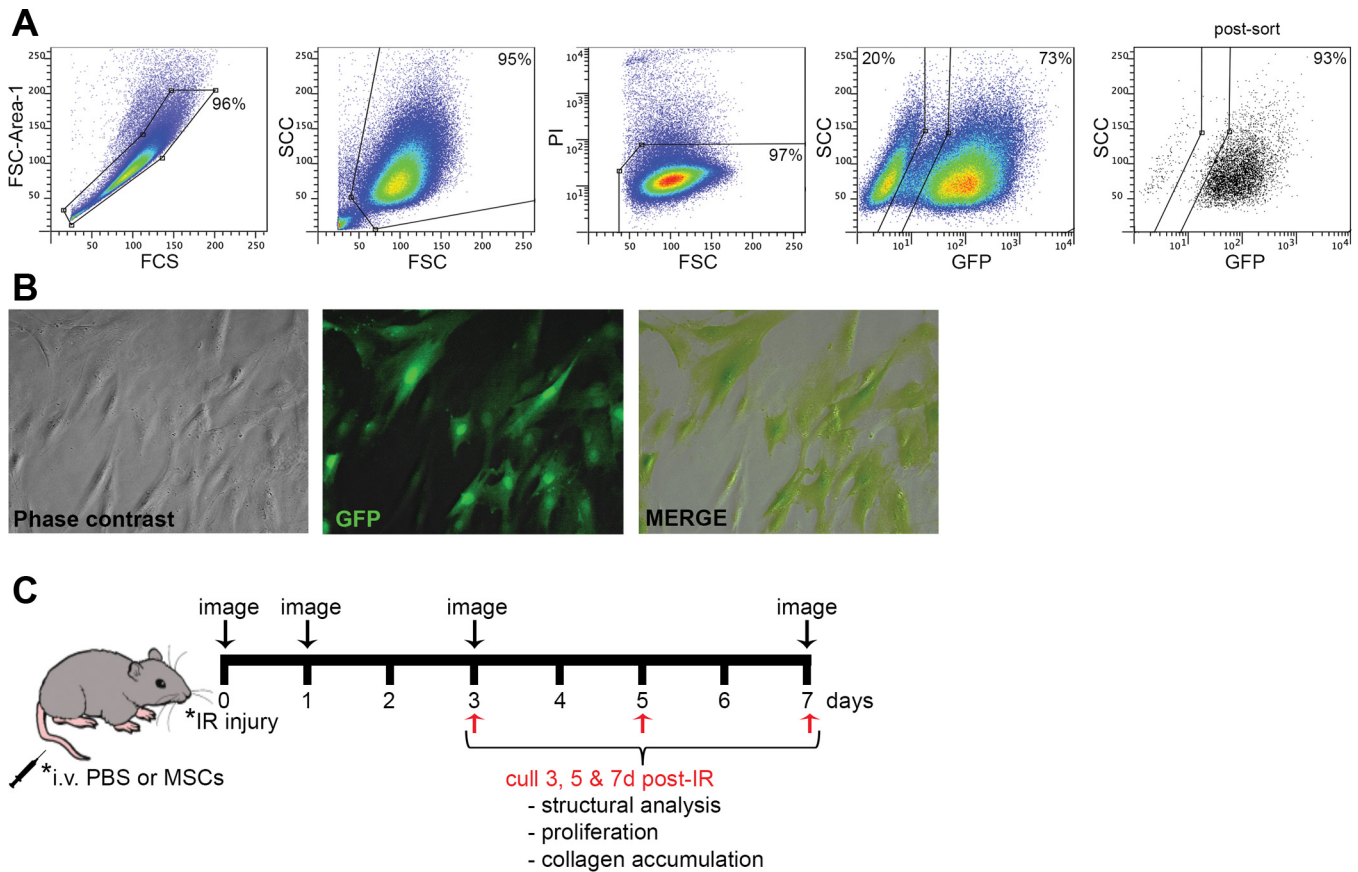


Fig. 2. Isolation of enhanced green fluorescent protein+ firefly luciferase+ (eGFP+fluc+) MSCs and experimental design for in vivo bioluminescence tracing. eGFP+fluc+ MSCs were FACS sorted based on their forward and side light-scattering properties, viability using propidium iodide (PI), and eGFP expression (A). Representative micrographs are shown of the MSCs demonstrating eGFP expression (magnification  $\times 200$ ; B) and a schematic diagram of the experimental timeline following the induction of unilateral (40 min) or bilateral (25 min) ischemia-reperfusion (IR) injury with and without MSC treatment (C).

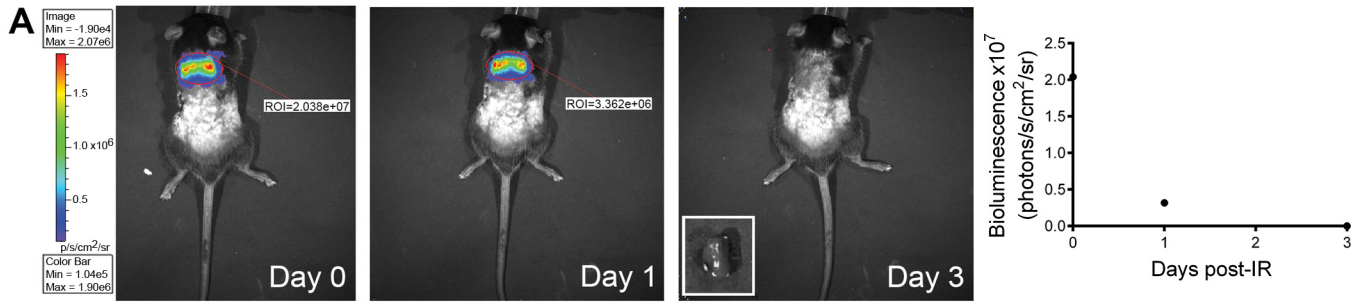
significantly decreased the total renal collagen concentration ( $P < 0.05$ ) compared with vehicle-treated mice. SDS-PAGE revealed the predominant interstitial collagen subtypes within the kidney were type 1 collagen [ $\alpha_1(I)$  and  $\alpha_2(I)$  monomers and dimers of two  $\alpha_1(I)$  chains ( $\beta 11$ ) or  $\alpha_1(I)$  and  $\alpha_2(I)$  monomers ( $\beta 12$ )], and a small amount of type V collagen (Fig. 6B). Scanning densitometry further revealed a decrease in the accumulation of the collagen subtype  $\alpha_1(I)$  in MSC-treated kidneys compared with the vehicle-treated controls at 5 and 7 days postinjury (Fig. 6B), which reached significance ( $P < 0.05$ ) at day 7. Immunofluorescence microscopy was utilized to visualize type IV collagen and macrophage (F4/80) localization within the kidney (Fig. 6D). At day 7, an accumulation of interstitial collagen was evident in vehicle-treated kidneys. In comparison, type IV collagen appeared as a delicate framework surrounding the glomeruli and reepithelialized tubules of MSC-treated kidneys, with a pattern of expression comparable to kidneys from sham-operated control mice.

Gelatin zymography revealed that IR injury resulted in a significant increase in latent and active MMP-2 levels compared with sham-operated control kidneys at both 5 ( $P < 0.001$ ) and 7 ( $P < 0.001$ ) days postinjury (Fig. 6C). In comparison, the latent and active forms of MMP-2 in the MSC-treated kidneys remained significantly lower than in the vehicle-treated kidneys at both days 5 and 7. Active MMP-9 was also significantly increased in vehicle-treated kidneys at 3 ( $P < 0.001$ ), 5 ( $P < 0.01$ ), and 7 ( $P < 0.05$ ) days postinjury compared with the sham-operated kidneys (Fig. 6C). Notably, MSC treatment resulted in a significant increase in active MMP-9 at 3 days postinjury ( $P < 0.05$ ) compared with its vehicle-treated counterpart.

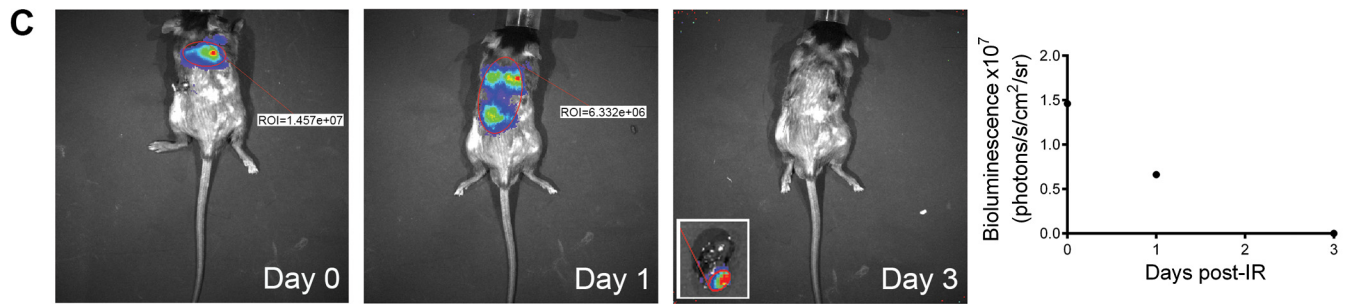
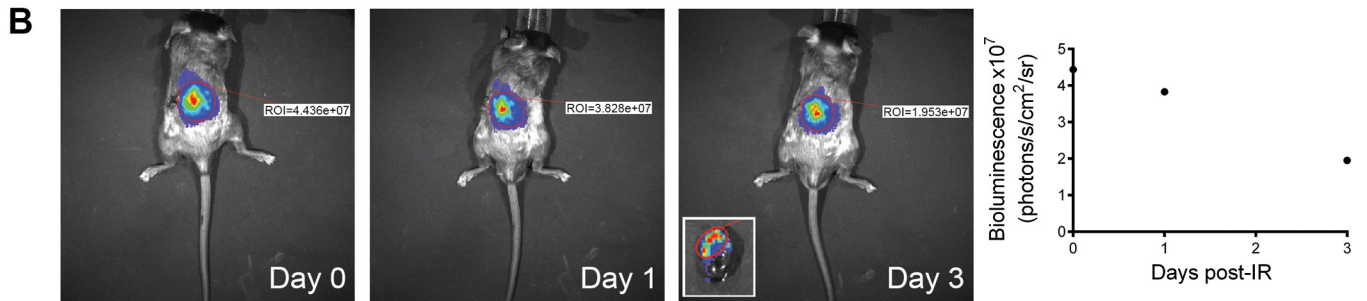
*MSCs alter macrophage phenotype following in vitro coculture.* Direct and indirect coculture of MSCs with macrophages resulted in an MSC-dependent polarization of macrophages toward an M2 phenotype. BM-derived murine macrophages that had been stimulated to display an M1 or M2 phenotype in vitro were cocultured

Fig. 3. MSCs traffic to the injured kidney(s) following unilateral and bilateral IR injury. Representative images of the distribution of MSCs 0, 1, and 3 days post-intravenous injection in sham-operated control mice, showing the accumulation of these cells in the lungs (A) and in mice with unilateral or bilateral IR injury, where the cells homed directly to the injured kidney (B and D, respectively) or to the injured kidney via the lungs (C and E, respectively). The region of interest (ROI) indicates photon emission within the red-circled area. Red indicates areas with the highest photon emission density, and blue indicates the areas with the lowest. The in vivo ROIs for each animal on days 0, 1, and 3 are displayed in each corresponding graph.

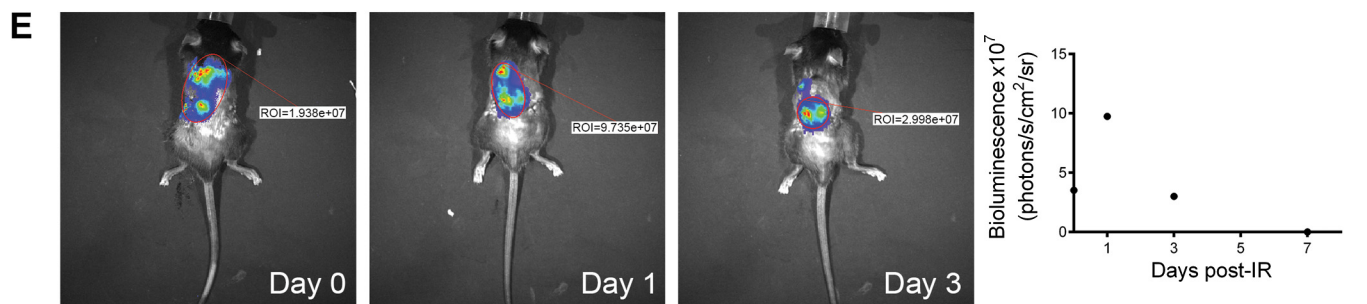
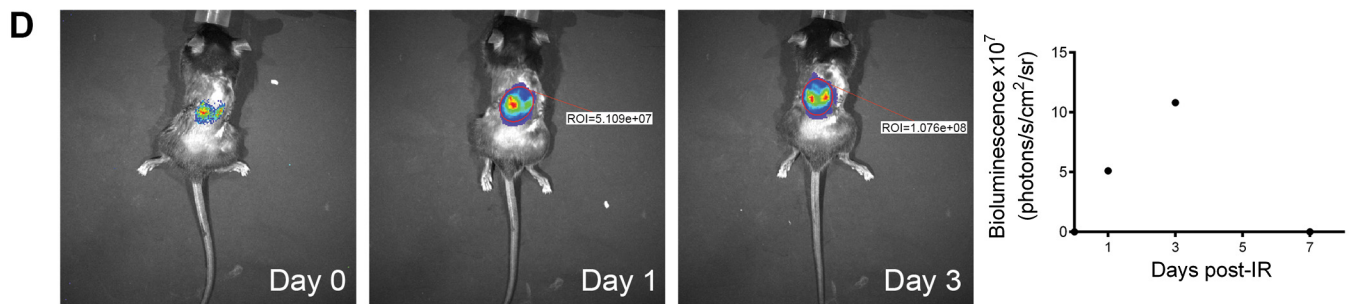
Sham



Unilateral IR injury



Bilateral IR injury



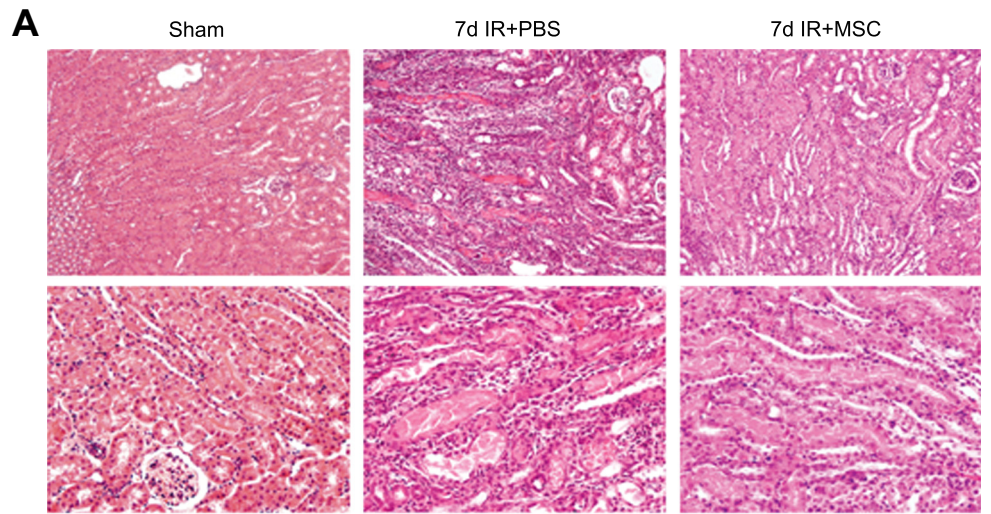
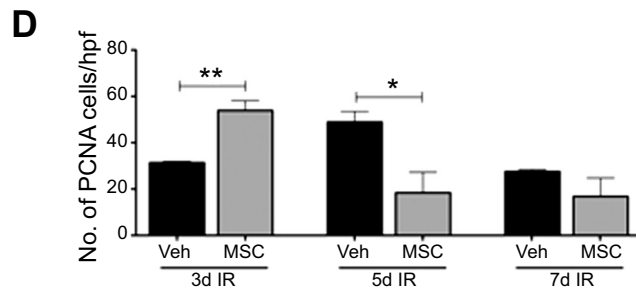
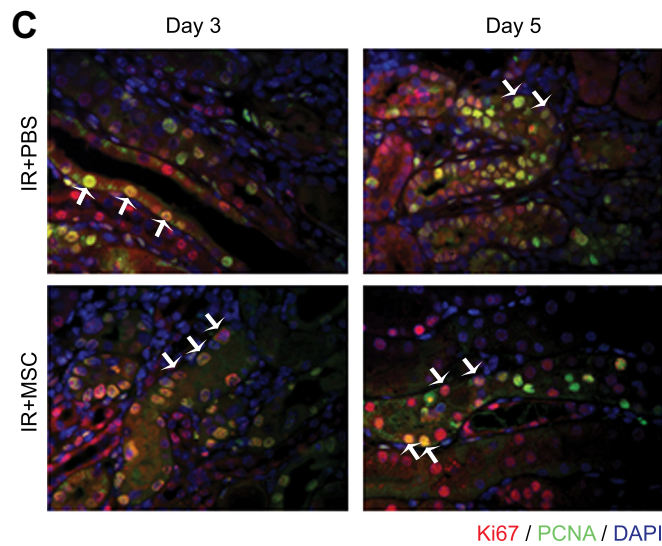
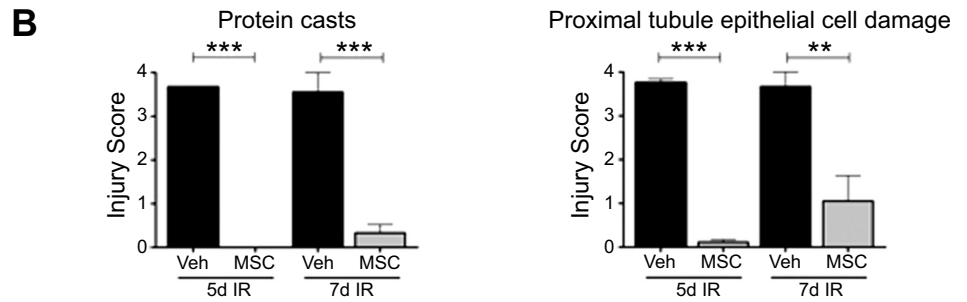


Fig. 4. MSC treatment following IR injury accelerates structural repair in adult mice. Representative micrographs of hematoxylin and eosin (H&E)-stained sections show the histoarchitecture of the corticomedullary region from sham and unilateral IR kidneys with and without MSC treatment, 7 days postinjury (magnification  $\times 200$  and  $\times 400$ ; A). Semiquantitative analysis of kidney injury from IR kidneys with and without MSC treatment 5 and 7 days post-IR is displayed graphically (B). Tubular epithelial cell proliferation was demonstrated with Ki67 (red) and PCNA (green) immunofluorescence labeling in kidneys with and without MSC treatment (C). PCNA expression was quantified at 3, 5, and 7 days following IR injury (magnification  $\times 400$ ; D). Veh, vehicle; cells/hpf, cells per high-power field. Values are means  $\pm$  SE;  $n = 3$ . \* $P < 0.05$ . \*\* $P < 0.01$ . \*\*\* $P < 0.001$ .



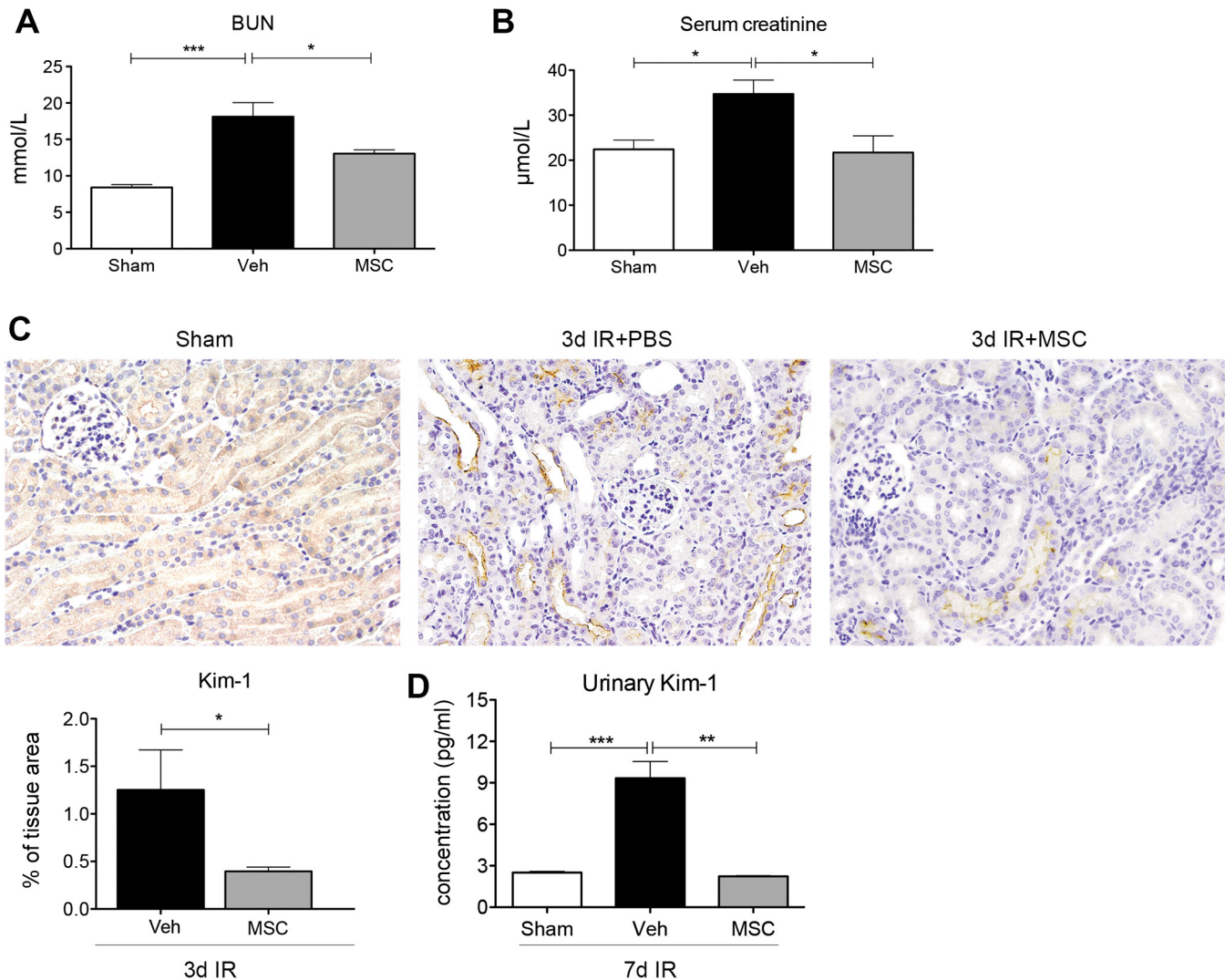


Fig. 5. MSCs improve kidney function and reduce the expression and excretion of Kim-1 in the kidney following IR injury. Functional analysis is shown measuring blood urea nitrogen (BUN; *A*) and serum creatinine (*B*) in sham and bilateral IR mice with and without MSC treatment 3 days postinjury. Representative micrographs and semiquantification of Kim-1 expression in sham and IR kidneys 3 days following MSC treatment are shown (magnification  $\times 400$ ; *C*). Urinary Kim-1 levels from days 6–7 was significantly increased in mice with IR but returned to baseline levels following MSC treatment (*D*). Values are means  $\pm$  SE. \*\* $P < 0.01$ . \*\*\*  $P < 0.001$ .

with MSCs for 48 h either directly or indirectly using a Transwell coculture system (see diagram in Fig. 7*A*). qPCR analysis of macrophage gene expression showed that the direct coculture of M1 macrophages with MSCs caused an upregulation of the M2-associated gene, *Arg1* (Fig. 7*B*). Another M2-associated gene, *Ccl2*, was also upregulated following the indirect coculture of M1 macrophages with MSCs (Fig. 7*B*). Furthermore, an enhanced expression of the M2-associated genes, *Arg1*, *Chi3l3*, *Ccl2*, and *Fizz1* (also known as *Retnla*), was observed following both the direct and indirect coculture of M2 macrophages with MSCs (Fig. 7*B*).

The MSC-macrophage coculture medium was then screened using a panel of human cytokines and chemokines (Table 3). The human soluble factors EGF, granulocyte macrophage colony-stimulating factor (GM-CSF), CXCL1, IL-6, IL-8, monocyte chemoattractant protein (MCP)-1, PDGF-AA, and CCL5 were detected in the coculture supernatants, suggesting these factors may play a role in the MSC-mediated shift in macrophage polarization.

## DISCUSSION

The therapeutic efficacy of MSCs derived from various sources including BM (41), adipose (11), umbilical cord (7), embryos (69), and Wharton's jelly (15) to treat cisplatin- (5, 17, 41)-, glycerol (18, 42)-, unilateral ureteral obstruction (UUO) (2, 34, 35, 46)-, and IR (28, 51, 56, 57)-induced experimental models of AKI have been investigated (for a review, see Ref. 64). However, the mechanisms by which MSCs elicit repair remain largely unknown. Following injury, MSCs have the capacity to migrate along an inflammatory cytokine gradient, governed largely by chemokines and their receptors, to the site of damage (18, 23, 33, 58). The present study demonstrated that MSCs administered to sham-operated mice migrated directly to the lungs, where they remained and were cleared within 3 days. In comparison, MSCs administered to mice following IR had the potential to home directly to the injured kidney(s), where they remained for up to 3 days postadministration and exerted beneficial effects over the lon-

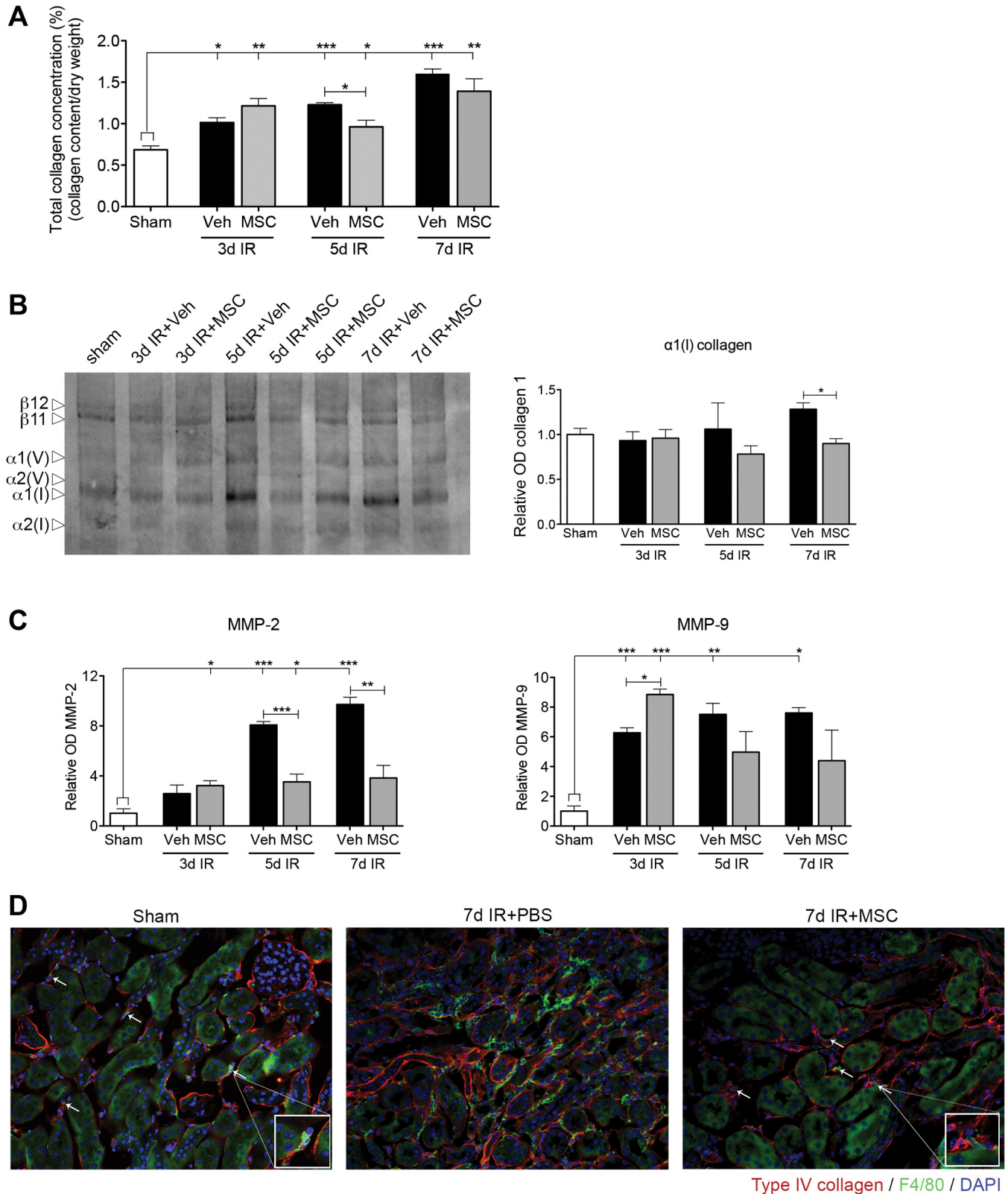


Fig. 6. MSCs reduce collagen accumulation in the kidney following IR injury. *A*: total kidney collagen concentration (% collagen content/dry weight tissue) in sham and IR kidneys with and without MSC treatment. *B*: SDS-PAGE analysis and densitometry of sham and IR kidneys 3, 5, and 7 days after vehicle or MSC treatment. *C*: densitometry of matrix metalloproteinase (MMP)-2 and MMP-9 in sham and IR kidneys 3, 5, and 7 days following IR injury with vehicle or MSC treatment. *D*: representative fluorescence micrographs showing type IV collagen (red) and F4/80 (green) staining in sham and IR kidneys 7 days after vehicle or MSC treatment (magnification  $\times 200$ ). OD, optical density. Values are means  $\pm$  SE;  $n = 3$ . \* $P < 0.05$ . \*\* $P < 0.01$ . \*\*\* $P < 0.001$ .

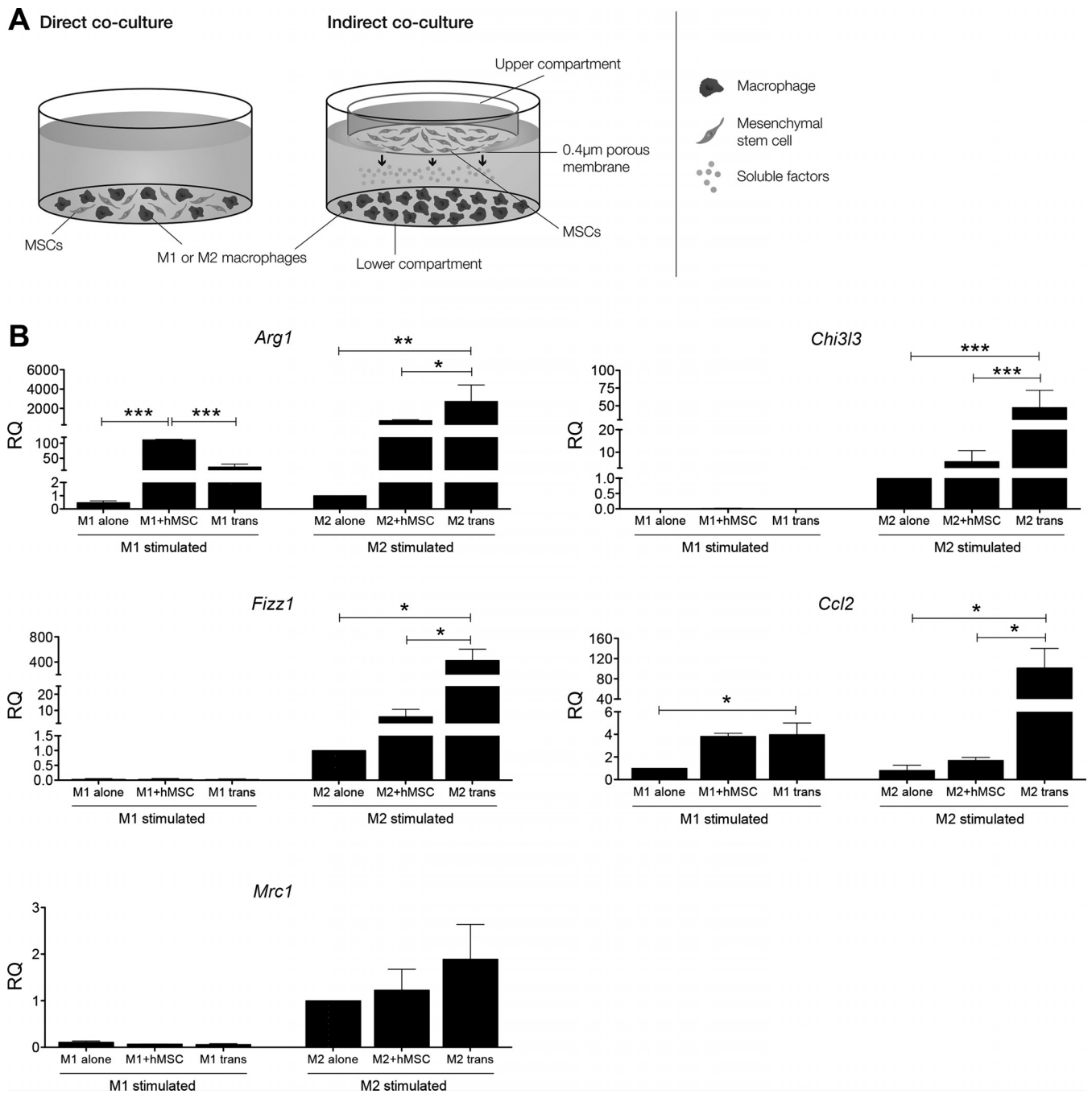


Fig. 7. MSCs can alter macrophage phenotype following in vitro coculture. *A*: schematic diagram of the coculture system used to culture macrophages and MSCs. *B*: qPCR analysis of anti-inflammatory “M2” gene expression in mouse bone marrow-derived M1- and M2-stimulated macrophages cocultured for 48 h either directly (M1 or M2+MSC) or indirectly (M1 or M2 trans) with MSCs. RQ, relative quantification; trans, Transwell. Values are means  $\pm$  SE;  $n = 3$ . \* $P < 0.05$ . \*\* $P < 0.01$ . \*\*\* $P < 0.001$ .

ger term. These findings are consistent with previously published work (59). While some MSCs still traveled to the lung, these cells retained the ability to migrate to the injured kidney(s) within the first 3 days following IR injury. The localization of the MSCs in the lungs of mice has been confirmed in previous studies in other experimental models (29, 44). Cell size is believed to contribute to the initial entrapment of the MSCs within the pulmonary capillaries, due to the small diameter of the vessels. In addition, adhesion molecules ex-

pressed by MSCs and the corresponding receptors expressed on the lung endothelia may also contribute to the MSC lung entrapment and dislodgment (44). Although tissue-specific homing has been demonstrated in a number of different conditions, long-term engraftment of the MSCs has rarely been shown. Consequently, several studies have investigated strategies aimed at enhancing the MSC migratory properties, survival, and consequently regenerative capacity through preconditioning with various growth factors such as IGF-1 (66), glial

Table 3. Human cytokines secreted following 24 h of MSC and mouse bone marrow-derived macrophage coculture in vitro

Cytokine, pg/ml	Coculture Conditions					
	M1+MSC direct	M1+MSC Transwell	Significance	M2+MSC direct	M2+MSC Transwell	Significance
EGF	8.3 ± 5.0	16.6 ± 3.2	NS	2.57 ± 2.6	0	NS
Eotaxin	0	0	NS	0	0	NS
FGF2	0	0	NS	0	0	NS
Flt-3L	0	0	NS	0	0	NS
Fractalkine	0	0	NS	0	0	NS
G-CSF	0	0	NS	0	0	NS
GM-CSF	3.5 ± 0.2	0	†	0	0	NS
GRO (CXCL1)	67.8 ± 3.6	0	†	30.8 ± 5.1	0	†
IFN-α2	0	0	NS	0	0	NS
IFN-γ	0	0	NS	0	0	NS
IL-1α	0	0	NS	0	0	NS
IL-1β	0	0	NS	0	0	NS
IL-1Rα	0	0	NS	0	0	NS
IL-2	0	0	NS	0	0	NS
IL-3	0	0	NS	0	0	NS
IL-4	0	0	NS	0	0	NS
IL-5	0	0	NS	0	0	NS
IL-6	732.6 ± 22.6	193.9 ± 10.7	†	423.2 ± 38.3	88.7 ± 3.7	†
IL-7	0	0	NS	0	0	NS
IL-8	133.5 ± 7.7	23.2 ± 4.0	†	68.3 ± 11.9	6.8 ± 0.4	*
IL-9	0	0	NS	0	0	NS
IL-10	0	0	NS	0	0	NS
IL12p40	0	0	NS	0	0	NS
IL12p70	0	0	NS	0	0	NS
IL-13	0	0	NS	0	0	NS
IL-15	0	0	NS	0	0	NS
IL-17A	0	0	NS	0	0	NS
IP10 (CXCL10)	0	0	NS	0	0	NS
MCP-1 (CCL2)	433.1 ± 16.1	103.9 ± 8.7	†	86.1 ± 11.8	51.3 ± 2.7	†
MCP-3 (CCL7)	0	0	NS	0	0	NS
MDC (CCL22)	0	0	NS	0	0	NS
MIP-1α (CCL3)	0	0	NS	0	0	NS
MIP-1β (CCL4)	0	0	NS	0	0	NS
PDGF-AA	38.1 ± 2.5	13.5 ± 1.0	†	35.2 ± 1.0	15.5 ± 0.2	†
PDGF-BB	0	0	NS	0	0	NS
RANTES (CCL5)	0	16.2 ± 1.0	†	0	3.58 ± 0.9	*
sCD40Lα	0	0	NS	0	0	NS
sIL-2Rα	0	0	NS	0	0	NS
TGF-α	0	0	NS	0	0	NS
TNF-α	0	0	NS	0	0	NS
TNF-β	0	0	NS	0	0	NS

Values are means ± SE; *n* = 3. MSC, mesenchymal stem cell; G-CSF, granulocyte colony-stimulating factor; GM-CSF, granulocyte macrophage colony-stimulating factor; IL-1RA, IL-1 receptor antagonist; IP-10, IFN-γ-induced protein; MCP-1, monocyte chemotactic protein; MDC, macrophage-derived chemokine; MIP, monocyte inflammatory protein; RANTES, regulated and normal T cell expressed and secreted; sCD40L, soluble CD40 ligand; sIL-2Rα, soluble IL-2 receptor-α; TGF, transforming growth factor; NS, not significant. \**P* < 0.01. †*P* < 0.001.

cell-derived neurotrophic factor (GDNF) (52), melatonin (40), exposure to hypoxia (20), or genetic modification (10, 12, 16, 69, 71).

The current study utilized the xenogeneic transplantation of MSCs into immunocompetent mice without the use of immunosuppressant agents. Although there are extensive data demonstrating the immunomodulatory properties of MSCs in vitro, it is unclear why these cells remain tolerated by the host's immune system following xenogeneic transplantation (3). In the current study, the possibility that the host's immune system cleared the transplanted MSCs by the *day 7* time point cannot be discounted. Nevertheless, numerous studies have demonstrated extraordinary regenerative efficacy following successful transplantation of human MSCs into mice in several disease models (31). However, the type of MSC transplantation (allogeneic vs. autologous), tissue of origin (BM, adipose, umbilical cord), isolation method (enzymatic vs. mechanical), delivery

route (systemic vs. local), dose, and timing of administration are also key factors that may influence the renoprotective effect of MSC therapy and need to be carefully considered before clinical application. For example, in an experimental model of glomerulonephritis, the administration of MSCs improved renal function but resulted in long-term maldifferentiation into glomerular adipocytes (26). These findings raise considerable concerns surrounding the safety of MSC-based therapies, and so it is imperative that studies looking into their long-term safety and unwanted differentiation are performed.

In this study, we demonstrate that following migration to the kidney in response to IR injury, MSCs promoted tubular epithelial cell proliferation, resulting in structural repair and tissue remodeling concurrent with a reduction in collagen. MMPs are enzymes that are involved in extracellular matrix remodeling via collagen degradation (8). The identification of an MSC-induced increase in MMP-9 at *day 3* and decrease in

MMP-2 at days 5 and 7 provides insight into the temporal pattern of MSC-mediated tissue remodeling. In addition to structural improvement, proximal tubular Kim-1 expression and urinary Kim-1 levels were assessed, as a direct measure of kidney injury. Both demonstrated significant improvements in the severity of injury at 3 and 7 days post-MSC treatment. Kim-1 is a sensitive AKI biomarker useful for detecting early disease onset and can provide useful insight into the state of injury before the production of classic indicators of nephrotoxicity, such as serum creatinine levels (22, 60).

MSCs have unique immunomodulatory properties and their trophic effects on T, B, natural killer, and dendritic cells have been thoroughly investigated (53, 68). However, the effect of MSCs on macrophage polarization and the consequences of this cell-cell interaction in altering the proinflammatory course of injury remains largely unknown. Our findings are consistent with other studies that have demonstrated the ability of MSCs to polarize macrophages toward an M2 phenotype in vitro (1, 25, 32, 36, 37). However, the influence MSCs have on the phenotypic and functional characteristics of macrophages is often variable. For example, MSCs have been shown to both upregulate and inhibit the expression of IL-6. Similarly, macrophage phagocytic activity has been both enhanced and suppressed by MSCs (1, 25, 32, 37).

Li et al. (32) demonstrated that MSC repair requires the infiltration of macrophages after the induction of IR injury. Given this important observation, we show herein that MSCs significantly enhanced the expression of M2-associated macrophage genes in both M1 and M2 macrophage subsets in vitro. Furthermore, MSC-induced M2 polarization was evident in both direct and indirect coculture systems, indicating that the alteration of macrophage phenotype was mediated through paracrine mechanisms. Screening of the coculture supernatants detected the presence of MSC-derived EGF, GM-CSF, CXCL1, IL-6, IL-8, MCP-1/CCL2, PDGF-AA, and RANTES/CCL5, all of which, except for EGF, GM-CSF, CXCL1, and PDGF-AA, have previously been shown to promote M2 polarization (1, 6, 39, 48, 55). Interestingly, CXCL1 was only detected in the direct coculture system, indicating that its production required direct cell-to-cell contact. Conversely, RANTES/CCL5 was only detected in the Transwell coculture system, signifying that the direct cell-to-cell contact inhibited the release of this chemokine. Although the enhancement of an M2 phenotype was facilitated through paracrine mechanisms, with the exception of EGF and RANTES/CCL5, direct coculture did result in increased levels of MSC-secreted soluble factors.

In summary, whole body bioluminescence imaging to trace MSCs delivered to mice with unilateral or bilateral IR injury demonstrated a unique pattern of infiltration where MSCs either homed directly to the injured kidney(s) or mobilized from the lungs to the injured kidney(s). MSC therapy was renoprotective and promoted kidney repair, as indicated by decreased proximal tubule Kim-1 expression and urinary Kim-1 levels. In addition, MSC therapy stimulated somatic tubular epithelial cell proliferation and significantly reduced aberrant collagen accumulation, resulting in improved kidney function. This highlights the therapeutic potential of MSCs in ameliorating the progression of kidney disease, of which established fibrosis is a common characteristic. MSCs are thought to elicit repair through paracrine and/or endocrine

mechanisms that modulate the immune response, leading to tissue repair and cellular replacement. Our results provide important insights into the production of various cytokines, chemokines, and enzymes resulting from macrophage-MSC interactions and how these govern the inflammatory and remodeling phases of AKI. However, determining the optimal delivery methods for engraftment, testing long-term safety, and understanding their ability to modify the tissue microenvironment in a setting of progressive fibrosis require further consideration.

#### ACKNOWLEDGMENTS

We thank Professor Claude Bernard for intellectual input and Keith Schulze from Monash Micro Imaging, Monash University, for technical support.

#### GRANTS

This study was funded by a Project Grant (1003806) from the National Health and Medical Research Council (NHMRC) of Australia. C. S. Samuel is supported by Monash University Mid-Career and NHMRC Senior Research Fellowships.

#### DISCLOSURES

No conflicts of interest, financial or otherwise, are declared by the authors.

#### AUTHOR CONTRIBUTIONS

Author contributions: A.F.W., C.S.S., and S.D.R. provided conception and design of research; A.F.W., T.M.W., M.B.G.K., N.L.P., and C.S. performed experiments; A.F.W., T.M.W., M.B.G.K., and C.S.S. analyzed data; A.F.W., T.M.W., M.B.G.K., and S.D.R. interpreted results of experiments; A.F.W. prepared figures; A.F.W. drafted manuscript; A.F.W., T.M.W., C.S.S., and S.D.R. edited and revised manuscript; A.F.W., T.M.W., M.B.G.K., N.L.P., C.S., C.S.S., and S.D.R. approved final version of manuscript.

#### REFERENCES

1. Adutler-Lieber S, Ben-Mordechai T, Naftali-Shani N, Asher E, Loberman D, Raanani E, Leor J. Human macrophage regulation via interaction with cardiac adipose tissue-derived mesenchymal stromal cells. *J Cardiovasc Pharmacol Ther* 18: 78–86, 2012.
2. Asanuma H, Vanderbrink BA, Campbell MT, Hile KL, Zhang H, Meldrum DR, Meldrum KK. Arterially delivered mesenchymal stem cells prevent obstruction-induced renal fibrosis. *J Surg Res* 168: e51–e59, 2011.
3. Atoui R, Chiu RC. Concise review: immunomodulatory properties of mesenchymal stem cells in cellular transplantation: update, controversies, and unknowns. *Stem Cells Transl Med* 1: 200–205, 2012.
4. Bai L, Lennon DP, Eaton V, Maier K, Caplan AI, Miller SD, Miller RH. Human bone marrow-derived mesenchymal stem cells induce Th2-polarized immune response and promote endogenous repair in animal models of multiple sclerosis. *Glia* 57: 1192–1203, 2009.
5. Bi B, Schmitt R, Israilova M, Nishio H, Cantley LG. Stromal cells protect against acute tubular injury via an endocrine effect. *J Am Soc Nephrol* 18: 2486–2496, 2007.
6. Bögels M, Braster R, Nijland PG, Gül N, van de Luitgaarden W, Fijneman RJ, Meijer GA, Jimenez CR, Beelen RH, van Egmond M. Carcinoma origin dictates differential skewing of monocyte function. *Oncimmunology* 1: 798–809, 2012.
7. Cao H, Qian H, Xu W, Zhu W, Zhang X, Chen Y, Wang M, Yan Y, Xie Y. Mesenchymal stem cells derived from human umbilical cord ameliorate ischemia/reperfusion-induced acute renal failure in rats. *Bio-technol Lett* 32: 725–732, 2010.
8. Catania JM, Chen G, Parrish AR. Role of matrix metalloproteinases in renal pathophysiology. *Am J Physiol Renal Physiol* 292: F905–F911, 2007.
9. Chang YS, Oh W, Choi SJ, Sung DK, Kim SY, Choi EY, Kang S, Jin HJ, Yang YS, Park WS. Human umbilical cord blood-derived mesenchymal stem cells attenuate hyperoxia-induced lung injury in neonatal rats. *Cell Transplant* 18: 869–886, 2009.
10. Chen Y, Qian H, Zhu W, Zhang X, Yan Y, Ye S, Peng X, Li W, Xu W. Hepatocyte growth factor modification promotes the amelioration

- effects of human umbilical cord mesenchymal stem cells on rat acute kidney injury. *Stem Cells Dev* 20: 103–113, 2011.
11. **Chen YT, Sun CK, Lin YC, Chang LT, Chen YL, Tsai TH, Chung SY, Chua S, Kao YH, Yen CH, Shao PL, Chang KC, Leu S, Yip HK.** Adipose-derived mesenchymal stem cell protects kidneys against ischemia-reperfusion injury through suppressing oxidative stress and inflammatory reaction. *J Transl Med* 9: 51, 2011.
  12. **Cheng Z, Ou L, Zhou X, Li F, Jia X, Zhang Y, Liu X, Li Y, Ward CA, Melo LG, Kong D.** Targeted migration of mesenchymal stem cells modified with CXCR4 gene to infarcted myocardium improves cardiac performance. *Mol Ther* 16: 571–579, 2008.
  13. **da Silva Meirelles L, Chagastelles PC, Nardi NB.** Mesenchymal stem cells reside in virtually all post-natal organs and tissues. *J Cell Sci* 119: 2204–2213, 2006.
  14. **Dominici M, Le Blanc K, Mueller I, Slaper-Cortenbach I, Marini F, Krause D, Deans R, Keating A, Prockop D, Horwitz E.** Minimal criteria for defining multipotent mesenchymal stromal cells. The International Society for Cellular Therapy position statement. *Cytotherapy* 8: 315–317, 2006.
  15. **Du T, Cheng J, Zhong L, Zhao XF, Zhu J, Zhu YJ, Liu GH.** The alleviation of acute and chronic kidney injury by human Wharton's jelly-derived mesenchymal stromal cells triggered by ischemia-reperfusion injury via an endocrine mechanism. *Cytotherapy* 14: 1215–1227, 2012.
  16. **Hagiwara M, Shen B, Chao L, Chao J.** Kallikrein-modified mesenchymal stem cell implantation provides enhanced protection against acute ischemic kidney injury by inhibiting apoptosis and inflammation. *Hum Gene Ther* 19: 807–819, 2008.
  17. **Herrera MB, Bussolati B, Bruno S, Fonsato V, Romanazzi GM, Camussi G.** Mesenchymal stem cells contribute to the renal repair of acute tubular epithelial injury. *Int J Mol Med* 14: 1035–1041, 2004.
  18. **Herrera MB, Bussolati B, Bruno S, Morando L, Mauriello-Romanazzi G, Sanavio F, Stamenkovic I, Biancone L, Camussi G.** Exogenous mesenchymal stem cells localize to the kidney by means of CD44 following acute tubular injury. *Kidney Int* 72: 430–441, 2007.
  19. **Humphreys BD, Bonventre JV.** Mesenchymal stem cells in acute kidney injury. *Annu Rev Med* 59: 311–325, 2008.
  20. **Hung SC, Pochampally RR, Hsu SC, Sanchez C, Chen SC, Spees J, Prockop DJ.** Short-term exposure of multipotent stromal cells to low oxygen increases their expression of CX3CR1 and CXCR4 and their engraftment in vivo. *PLoS One* 2: e416, 2007.
  21. **Hung SC, Pochampally RR, Chen SC, Hsu SC, Prockop DJ.** Angiogenic effects of human multipotent stromal cell conditioned medium activate the PI3K-Akt pathway in hypoxic endothelial cells to inhibit apoptosis, increase survival, and stimulate angiogenesis. *Stem Cells* 25: 2363–2370, 2007.
  22. **Ichimura T, Hung CC, Yang SA, Stevens JL, Bonventre JV.** Kidney injury molecule-1: a tissue and urinary biomarker for nephrotoxicant-induced renal injury. *Am J Physiol Renal Physiol* 286: F552–F563, 2004.
  23. **Kang SK, Shin IS, Ko MS, Jo JY, Ra JC.** Journey of mesenchymal stem cells for homing: strategies to enhance efficacy and safety of stem cell therapy. *Stem Cells Int* 2012: 1–11, 2012.
  24. **Khakoo AY, Pati S, Anderson SA, Reid W, Elshal MF, Rovira II, Nguyen AT, Malide D, Combs CA, Hall G, Zhang J, Raffeld M, Rogers TB, Stetler-Stevenson W, Frank JA, Reitz M, Finkel T.** Human mesenchymal stem cells exert potent antitumorigenic effects in a model of Kaposi's sarcoma. *J Exp Med* 203: 1235–1247, 2006.
  25. **Kim J, Hematti P.** Mesenchymal stem cell-educated macrophages: a novel type of alternatively activated macrophages. *Exp Hematol* 37: 1445–1453, 2009.
  26. **Kunter U, Rong S, Boor P, Eitner F, Müller-Newen G, Djuric Z, van Roeyen CR, Konieczny A, Ostendorf T, Villa L, Milovanceva-Popovska M, Kerjaschki D, Floege J.** Mesenchymal stem cells prevent progressive experimental renal failure but maldifferentiate into glomerular adipocytes. *J Am Soc Nephrol* 18: 1754–1764, 2007.
  27. **Lange C, Cakiroglu F, Spiess AN, Cappallo-Obermann H, Dierlamm J, Zander AR.** Accelerated and safe expansion of human mesenchymal stromal cells in animal serum-free medium for transplantation and regenerative medicine. *J Cell Physiol* 213: 18–26, 2007.
  28. **Lange C, Tögel F, Itrich H, Clayton F, Nolte-Ernsting C, Zander AR, Westenfelder C.** Administered mesenchymal stem cells enhance recovery from ischemia/reperfusion-induced acute renal failure in rats. *Kidney Int* 68: 1613–1617, 2005.
  29. **Lee RH, Pulin AA, Seo MJ, Kota DJ, Ylostalo J, Larson BL, Semprun-Prieto L, Delafontaine P, Prockop DJ.** Intravenous hMSCs improve myocardial infarction in mice because cells embolized in lung are activated to secrete the anti-inflammatory protein TSG-6. *Cell Stem Cell* 5: 54–63, 2009.
  30. **Lee S, Huen S, Nishio H, Nishio S, Lee HK, Choi BS, Ruhrberg C, Cantley LG.** Distinct macrophage phenotypes contribute to kidney injury and repair. *J Am Soc Nephrol* 22: 317–326, 2011.
  31. **Li J, Ezzelarab MB, Cooper DK.** Do mesenchymal stem cells function across species barriers? Relevance for xenotransplantation. *Xenotransplantation* 19: 273–285, 2012.
  32. **Li W, Zhang Q, Wang M, Wu H, Mao F, Zhang B, Ji R, Gao S, Sun Z, Zhu W, Qian H, Chen Y, Xu W.** Macrophages are involved in the protective role of human umbilical cord-derived stromal cells in renal ischemia-reperfusion injury. *Stem Cell Res* 10: 405–416, 2013.
  33. **Liu H, Liu S, Li Y, Wang X, Xue W, Ge G, Luo X.** The role of SDF-1-CXCR4/CXCR7 axis in the therapeutic effects of hypoxia-preconditioned mesenchymal stem cells for renal ischemia/reperfusion injury. *PLoS One* 7: e34608, 2011.
  34. **Liu X, Shen W, Yang Y, Liu G.** Therapeutic implications of mesenchymal stem cells transfected with hepatocyte growth factor transplanted in rat kidney with unilateral ureteral obstruction. *J Pediatr Surg* 46: 9–9, 2011.
  35. **Liu YL, Wang YD, Zhuang F, Xian SL, Fang JY, Su W, Zhang W.** Immunosuppression effects of bone marrow mesenchymal stem cells on renal interstitial injury in rats with unilateral ureteral obstruction. *Cell Immunol* 276: 144–152, 2012.
  36. **Lu W, Fu C, Song L, Yao Y, Zhang X, Chen Z, Li Y, Ma G, Shen C.** Exposure to supernatants of macrophages that phagocytized dead mesenchymal stem cells improves hypoxic cardiomyocytes survival. *Int J Cardiol* 165: 330–340, 2013.
  37. **Maggini J, Mirkin G, Bognanni I, Holmberg J, Piazzón IM, Nepomnaschy I, Costa H, Cañones C, Raiden S, Vermeulen M, Geffner JR.** Mouse bone marrow-derived mesenchymal stromal cells turn activated macrophages into a regulatory-like profile. *PLoS One* 5: e9252, 2010.
  38. **Mantovani A, Sica A, Sozzani S, Allavena P, Vecchi A, Locati M.** The chemokine system in diverse forms of macrophage activation and polarization. *Trends Immunol* 25: 677–686, 2004.
  39. **Medina RJ, O'Neill CL, O'Doherty TM, Knott H, Guduric-Fuchs J, Gardiner TA, Stitt AW.** Myeloid angiogenic cells act as alternative M2 macrophages and modulate angiogenesis through interleukin-8. *Mol Med* 17: 1045–1055, 2011.
  40. **Mias C, Trouche E, Seguelas MH, Calcagno F, Dignat-George F, Sabatier F, Piercecchi-Marti MD, Daniel L, Bianchi P, Calise D, Bourin P, Parini A, Cussac D.** Ex vivo pretreatment with melatonin improves survival, proangiogenic/mitogenic activity, and efficiency of mesenchymal stem cells injected into ischemic kidney. *Stem Cells* 26: 1749–1757, 2008.
  41. **Morigi M, Inrona M, Imberti B, Corna D, Abbate M, Rota C, Rottoli D, Benigni A, Perico N, Zoja C, Rambaldi A, Remuzzi A, Remuzzi G.** Human bone marrow mesenchymal stem cells accelerate recovery of acute renal injury and prolong survival in mice. *Stem Cells* 26: 2075–2082, 2008.
  42. **Morigi M, Imberti B, Zoja C, Corna D, Tomasoni S, Rottoli D, Angioletti S, Benigni A, Perico N, Alison M, Remuzzi G.** Mesenchymal stem cells are renoprotective, helping to repair the kidney and improve function in acute renal failure. *J Am Soc Nephrol* 15: 1794–1804, 2004.
  43. **Nozaki Y, Nikolic-Paterson DJ, Yagita H, Akiba H, Holdsworth SR, Kitching AR.** Tim-1 promotes cisplatin nephrotoxicity. *Am J Physiol Renal Physiol* 301: F1098–F1104, 2011.
  44. **Nystedt J, Anderson H, Tikkanen J, Pietilä M, Hirvonen T, Takalo R, Heiskanen A, Satomaa T, Natunen S, Lehtonen S, Hakkarainen T, Korhonen M, Laitinen S, Valmu L, Lehenkari P.** Cell surface structures influence lung clearance rate of systemically infused mesenchymal stromal cells. *Stem Cells* 31: 317–326, 2013.
  45. **Otto WR, Wright NA.** Mesenchymal stem cells: from experiment to clinic. *Fibrogenesis Tissue Repair* 4: 1–14, 2011.
  46. **Park HC, Yasuda K, Ratliff B, Stoessel A, Sharkovska Y, Yamamoto I, Jasmin JF, Bachmann S, Lisanti MP, Chander P, Goligorsky MS.** Postobstructive regeneration of kidney is derailed when surge in renal stem cells during course of unilateral ureteral obstruction is halted. *Am J Physiol Renal Physiol* 298: F357–F364, 2010.
  47. **Payne NL, Sun G, McDonald C, Layton D, Moussa L, Emerson-Webber A, Veron N, Siatskas C, Herszfeld D, Price J, Bernard CC.**

- Distinct immunomodulatory and migratory mechanisms underpin the therapeutic potential of human mesenchymal stem cells in autoimmune demyelination. *Cell Transplant* 22: 1409–1425, 2013.
48. **Roca H, Varsos ZS, Sud S, Craig MJ, Ying C, Pienta KJ.** CCL2 and interleukin-6 promote survival of human CD11b+ peripheral blood mononuclear cells and induce M2-type macrophage polarization. *J Biol Chem* 284: 34342–34354, 2009.
  49. **Samuel CS, Butkus A, Coghlan JP, Bateman JF.** The effect of relaxin on collagen metabolism in the nonpregnant rat pubic symphysis: the influence of estrogen and progesterone in regulating relaxin activity. *Endocrinology* 137: 3884–3890, 1996.
  50. **Samuel CS.** Determination of collagen content, concentration, and subtypes in kidney tissue. *Methods Mol Biol* 466: 223–235, 2009.
  51. **Semedo P, Palasio CG, Oliveira CD, Feitoza CQ, Gonçalves GM, Cenedeze MA, Wang PM, Teixeira VP, Reis MA, Pacheco-Silva A, Câmara NO.** Early modulation of inflammation by mesenchymal stem cell after acute kidney injury. *Int Immunopharmacol* 9: 677–682, 2009.
  52. **Shi H, Patschan D, Dietz GP, Bähr M, Plotkin M, Goligorsky MS.** Glial cell line-derived neurotrophic growth factor increases motility and survival of cultured mesenchymal stem cells and ameliorates acute kidney injury. *Am J Physiol Renal Physiol* 294: F229–F235, 2008.
  53. **Spaggiari GM, Moretta L.** Cellular and molecular interactions of mesenchymal stem cells in innate immunity. *Immunol Cell Biol* 91: 27–31, 2013.
  54. **Stefater JA III, Ren S, Lang RA, Duffield JS.** Metchnikoff's policemen: macrophages in development, homeostasis and regeneration. *Trends Mol Med* 17: 743–752, 2011.
  55. **Takai H, Ashihara M, Ishiguro T, Terashima H, Watanabe T, Kato A, Suzuki M.** Involvement of glypican-3 in the recruitment of M2-polarized tumor-associated macrophages in hepatocellular carcinoma. *Cancer Biol Ther* 8: 2329–2338, 2009.
  56. **Tögel F, Hu Z, Weiss K, Isaac J, Lange C, Westenfelder C.** Administered mesenchymal stem cells protect against ischemic acute renal failure through differentiation-independent mechanisms. *Am J Physiol Renal Physiol* 289: F31–F42, 2005.
  57. **Tögel F, Cohen A, Zhang P, Yang Y, Hu Z, Westenfelder C.** Autologous and allogeneic marrow stromal cells are safe and effective for the treatment of acute kidney injury. *Stem Cells Dev* 18: 475–486, 2009.
  58. **Tögel F, Isaac J, Hu Z, Weiss K, Westenfelder C.** Renal SDF-1 signals mobilization and homing of CXCR4-positive cells to the kidney after ischemic injury. *Kidney Int* 67: 1772–1784, 2005.
  59. **Tögel F, Yang Y, Zhang P, Hu Z, Westenfelder C.** Bioluminescence imaging to monitor the in vivo distribution of administered mesenchymal stem cells in acute kidney injury. *Am J Physiol Renal Physiol* 295: F315–F321, 2008.
  60. **Vaidya VS, Ramirez V, Ichimura T, Bobadilla NA, Bonventre JV.** Urinary kidney injury molecule-1: a sensitive quantitative biomarker for early detection of kidney tubular injury. *Am J Physiol Renal Physiol* 290: F517–F529, 2006.
  61. **Vinuesa E, Hotter G, Jung M, Herrero-Fresneda I, Torras J, Sola A.** Macrophage involvement in the kidney repair phase after ischaemia/reperfusion injury. *J Pathol* 214: 104–113, 2007.
  62. **Wang S, Qu X, Zhao RC.** Clinical applications of mesenchymal stem cells. *J Hematol Oncol* 5: 1–9, 2012.
  63. **Williams TM, Little MH, Ricardo SD.** Macrophages in renal development, injury, and repair. *Semin Nephrol* 30: 255–267, 2010.
  64. **Wise AF, Ricardo SD.** Mesenchymal stem cells in kidney inflammation and repair. *Nephrology (Carlton)* 17: 1–10, 2011.
  65. **Woessner JF Jr.** Quantification of matrix metalloproteinases in tissue samples. *Methods Enzymol* 248: 510–528, 1995.
  66. **Xinaris C, Morigi M, Benedetti V, Imberti B, Fabricio AS, Squarcina E, Benigni A, Gagliardini E, Remuzzi G.** A novel strategy to enhance mesenchymal stem cell migration capacity and promote tissue repair in an injury specific fashion. *Cell Transplant* 22: 423–436, 2013.
  67. **Yagi H, Soto-Gutierrez A, Kitagawa Y, Tilles AW, Tompkins RG, Yarmush ML.** Bone marrow mesenchymal stromal cells attenuate organ injury induced by LPS and burn. *Cell Transplant* 19: 823–830, 2009.
  68. **Yi T, Song SU.** Immunomodulatory properties of mesenchymal stem cells and their therapeutic applications. *Arch Pharm Res* 35: 213–221, 2012.
  69. **Yuan L, Wu MJ, Sun HY, Xiong J, Zhang Y, Liu CY, Fu LL, Liu DM, Liu HQ, Mei CL.** VEGF-modified human embryonic mesenchymal stem cell implantation enhances protection against cisplatin-induced acute kidney injury. *Am J Physiol Renal Physiol* 300: F207–F218, 2011.
  70. **Zhang S, Jia Z, Ge J, Gong L, Ma Y, Li T, Guo J, Chen P, Hu Q, Zhang P, Liu Y, Li Z, Ma K, Li L, Zhou C.** Purified human bone marrow multipotent mesenchymal stem cells regenerate infarcted myocardium in experimental rats. *Cell Transplant* 14: 787–798, 2005.
  71. **Zhen-Qiang F, Bing-Wei Y, Yong-Liang L, Xiang-Wei W, Shan-Hong Y, Yuan-Ning Z, Wei-Sheng J, Wei C, Ye G.** Localized expression of human BMP-7 by BM-MSCs enhances renal repair in an in vivo model of ischemia-reperfusion injury. *Genes Cells* 17: 53–64, 2011.

# Colony-Stimulating Factor-1 Promotes Kidney Growth and Repair via Alteration of Macrophage Responses

Maliha A. Alikhan,\* Christina V. Jones,\*  
Timothy M. Williams,\* Anthony G. Beckhouse,†  
Anne L. Fletcher,\* Michelle M. Kett,‡  
Samy Sakkal,\* Chrishan S. Samuel,§¶  
Robert G. Ramsay,|| James A. Deane,\*  
Christine A. Wells,† Melissa H. Little,\*\*  
David A. Hume,†† and Sharon D. Ricardo\*

From the Monash Immunology and Stem Cell Laboratories (MISCL)\* and the Department of Physiology,‡ Monash University, Melbourne, Australia; the Australian Institute for Bioengineering and Nanotechnology (AIBN)† and the Institute for Molecular Bioscience,\*\* University of Queensland, Brisbane, Australia; the Howard Florey Institute<sup>§</sup> and the Department of Biochemistry and Molecular Biology,<sup>¶</sup> University of Melbourne, Melbourne, Australia; the Peter MacCallum Cancer Institute,<sup>||</sup> Melbourne, Australia; and The Roslin Institute and Royal (Dick) School of Veterinary Studies,<sup>††</sup> The University of Edinburgh, Scotland, United Kingdom

**Colony-stimulating factor (CSF)-1 controls the survival, proliferation, and differentiation of macrophages, which are recognized as scavengers and agents of the innate and the acquired immune systems. Because of their plasticity, macrophages are endowed with many other essential roles during development and tissue homeostasis. We present evidence that CSF-1 plays an important trophic role in postnatal organ growth and kidney repair. Notably, the injection of CSF-1 postnatally enhanced kidney weight and volume and was associated with increased numbers of tissue macrophages. Moreover, CSF-1 promotes postnatal renal repair in mice after ischemia-reperfusion injury by recruiting and influencing macrophages toward a reparative state. CSF-1 treatment rapidly accelerated renal repair with tubular epithelial cell replacement, attenuation of interstitial fibrosis, and functional recovery. Analysis of macrophages from CSF-1-treated kidneys showed increased expression of insulin-like growth factor-1 and anti-inflammatory genes that are known CSF-1 targets. Taken together, these data suggest that CSF-1 is important in kidney growth and the promotion of endogenous repair and reso-**

**lution of inflammatory injury. (Am J Pathol 2011, 179: 1243–1256; DOI: 10.1016/j.ajpath.2011.05.037)**

Macrophages are versatile cells that have been long recognized as immune effectors where their recruitment to sites of injury is a fundamental feature of inflammation. Although their role in host defense has been well documented, macrophages and their precursors are also important during embryogenesis, normal tissue maintenance, and postnatal organ repair.<sup>1,2</sup> Almost all developing organs contain a population of resident monocytes that infiltrate very early during organogenesis and persist throughout adult life.<sup>3–6</sup> In addition to their phagocytic capabilities during tissue remodeling-associated apoptosis,<sup>5,7</sup> fetal macrophages have many trophic effects that promote tissue and organ growth.<sup>6,8,9</sup>

Colony-stimulating factor (CSF)-1 controls the differentiation, proliferation, and survival of macrophages by binding to a high-affinity cell-surface tyrosine kinase receptor (CSF-1R), encoded by the *c-fms* proto-oncogene that is expressed on macrophages and their progenitors.<sup>6</sup> CSF-1 is critical for both adult and embryonic macrophage development. This is manifested by multiple organ growth deficiencies observed in osteopetrotic (*Csf1<sup>OP</sup>/Csf1<sup>OP</sup>*) mice that have a spontaneous mutation in the *csf-1* gene. These mice show growth restriction and developmental abnormalities of the bones, brain, and reproductive and endocrine organs,<sup>10–13</sup> a phenotype that can be rescued by injection of exogenous CSF-1 or insertion of a *csf-1* transgene.<sup>14–16</sup>

In adult organs, there is considerable heterogeneity of monocytes and macrophages with distinct subsets defined by phenotype, function, and the differential expression of cell surface markers.<sup>17–19</sup> Subpopula-

Supported by the Kidney Health Australia and the Australian Stem Cell Centre.

Accepted for publication May 23, 2011.

Supplemental material for this article can be found at <http://ajp.amjpathol.org> or at doi: 10.1016/j.ajpath.2011.05.037.

Address reprint requests to Sharon D. Ricardo, Ph.D., Monash Immunology and Stem Cell Laboratories (MISCL), Monash University, Clayton VIC 3800, Australia. [REDACTED]

tions of macrophages directly contribute to wound healing and tissue repair, supporting the concept that some macrophage phenotypes can promote organ regeneration after a pro-inflammatory state of injury.<sup>20</sup> The concept of macrophage polarization states has emerged; the M1 "classically activated" pro-inflammatory cell type apparently opposed by an M2 "alternatively activated" immune regulatory macrophage.<sup>18</sup> In general, these two states are thought to be analogous to the opposing T helper 1 and T helper 2 immune responses, although in both cases this model is probably too simplistic. Functionally, it is more likely that distinct subpopulations of macrophages may exist in the same tissue and play critical roles in both the injury and recovery phases of inflammatory scarring.<sup>20</sup>

Our previous study provided evidence that the addition of CSF-1 to a developing murine kidney promotes a growth and differentiation response that is accompanied by increased numbers of macrophages.<sup>3</sup> Furthermore, with the use of expression profiling we demonstrated that fetal kidney, lung, and brain macrophages share a characteristic gene expression profile that includes the production of factors important in the suppression of inflammation and the promotion of proliferation.<sup>3</sup> Embryonic macrophages appear to play a positive trophic role that may have parallel reparative functions in many adult tissues undergoing repair and cellular replacement.<sup>1,20</sup> A number of studies have suggested that infiltrating macrophages along with the trophic factors they release participate in tissue repair of the kidney,<sup>20–22</sup> brain,<sup>23</sup> skin,<sup>24,25</sup> lung,<sup>26</sup> liver,<sup>27</sup> heart,<sup>28</sup> gastrointestinal tract,<sup>29,30</sup> and skeletal muscle.<sup>31,32</sup> Indeed, the pleiotrophic roles for CSF-1 in reproduction, development of multiple organ systems, and maternal-fetal interactions during pregnancy by macrophage-mediated processes have also been well defined.<sup>2,33,34</sup>

To determine the physiological relevance of CSF-1 as a component of the mammalian growth regulatory axis, CSF-1 was administered to neonatal mice. We report that CSF-1 administration to newborn mice increased body weight and kidney weight and volume and was associated with increased numbers of macrophages. Our results also establish that CSF-1 injection into mice after ischemia-reperfusion (IR) injury promoted endogenous repair with characteristic rapid re-epithelialization of the damaged tubular epithelium, leading to functional recovery. Flow cytometric and gene expression analyses were used to delineate the macrophage profile present in the kidneys during the early and resolution phase of IR injury with and without CSF-1 therapy. We thus provide evidence that CSF-1 recruits macrophages to the reparative site and influences their phenotype, partly through an insulin-like growth factor (IGF)-1 signaling response. Therefore, macrophages under the stimulus of CSF-1 in an acute setting of renal disease markedly accelerate renal cell replacement and tissue remodeling while attenuating downstream interstitial extracellular matrix accumulation.

## Materials and Methods

### Mice

*Csf1r*-enhanced green fluorescent protein (EGFP) transgenic or C57BL/6J mice were obtained from Monash University Animal House, Melbourne, Australia. The *csf1r*-EGFP transgenic mice express EGFP under the control of the CSF-1R (*c-fms*) promoter and first intron.<sup>6</sup> These mice were backcrossed onto the C57BL/6J background for 10 generations. All experiments were approved by the Monash University Animal Ethics Committee, which adheres to the Australian Code of Practice for the Care and Use of Animals for Scientific Purposes.

### Newborn Mouse Analysis

Newborn *csf1r*-EGFP transgenic mice received treatment by i.p. injection at postnatal day (P) 0.5, P1.5, and P2.5. Littermate newborn mice were injected with either mouse recombinant CSF-1 protein (1  $\mu$ g/g of body weight; Chiron Corporation, Emeryville, CA) or vehicle (PBS). Mice were sacrificed at P30 for unbiased stereologic approaches to estimate kidney and glomerular volumes. The kidneys from *csf1r*-null mutant mice<sup>10</sup> and wild-type kidneys were collected at P19, and the body and organ weights were assessed.

CSF-1 and vehicle-injected littermate pups were sacrificed at P5 to investigate kidney macrophage number. The number of *csf1r*-EGFP macrophages was quantified from three sections at  $\times 1000$  magnification, with a minimum of three medullary and five cortical fields of view per section.

### Stereologic Estimation of Total Kidney and Glomerular Volumes

Unbiased estimation was performed on the kidneys from littermate mice injected with CSF-1 and vehicle at P30. Kidneys were immersion fixed in 10% formalin for 48 hours and embedded in Technovit 7100 glycol methacrylate resin (Electron Microscopy Sciences, Hatfield, PA). Tissue was then serial sectioned at 20  $\mu$ m, and every 10th and 11th sections were collected, beginning at a random number, and stained with periodic acid-Schiff reagent. To determine total kidney volume, every 10th section was viewed on a RF3A microfiche reader (Fugi, Tokyo, Japan) overlaid with a 2  $\times$  2-cm grid at a final magnification of  $\times 24.25$ . Total volume was calculated with the Cavalieri Principle.<sup>35,36</sup> Glomerular volume was estimated with the physical dissector/fractionator principle as previously described<sup>37,38</sup> where sections were projected on an unbiased 2  $\times$  2-cm grid at a final magnification of  $\times 298$ .

### Unilateral IR Injury in Adult Mice

Male mice (20 to 25 g) were anesthetized with 2% inhaled isoflurane (Abbott Australasia Pty Ltd, Kurnell, Australia), and IR injury was induced by 40 minutes of left renal artery clamping with a vascular clamp (0.4 to 1.0 mm;

S&T Fine Science Tools, Foster City, CA) through a flank incision. After IR injury, mice either received mouse recombinant CSF-1 protein (Chiron Corporation) or vehicle (PBS), starting at 3 days after the induction of injury and continuing daily for 3 consecutive days. A third group of mice served as a sham-operated control group in which the animals were anesthetized, and a flank incision was performed without renal artery clamping.

### *Functional Assessment*

*Csf1r*-EGFP mice (20 to 25 g) were used for functional assessment and placed in metabolic cages to obtain 24-hour urine samples. Mice underwent bilateral IR injury for 25 minutes on both kidneys by flank incisions. After IR surgery, mice were injected with CSF-1 (Chiron Corporation) or vehicle (PBS) at 3, 4, and 5 days. Twenty-four-hour urinary albumin excretion was measured with a murine-specific albumin ELISA (Exocell Inc., Philadelphia, PA).

### *Histology and Immunofluorescence Microscopy*

For structural analysis, *csf1r*-EGFP or C57BL/6J mice were perfusion-fixed with 4% paraformaldehyde at 100 mmHg for 10 minutes. Mid-coronal kidney sections were immersion fixed in 4% paraformaldehyde embedded in paraffin wax and sectioned at 5  $\mu$ m and processed for H&E staining for histopathologic analysis or deparaffinized and rehydrated for quantification of tubular epithelial cell proliferation. For quantification of renal pathology five fields of view per section at a magnification of  $\times 400$  were assessed within the outer stripe of the outer medulla (OSOM) of the kidney for proximal tubular damage and protein cast formation in modification to a previously reported method.<sup>21</sup> The percentage of renal damage was graded on a scale of 0 to 4.0, with 0 representing normal tubules and no protein casts; 0.5, minor tubular damage and protein cast formation; 1, involvement of  $<10\%$  of OSOM; 2, involvement of  $<25\%$  of OSOM; 2.5, involvement of 26% to 50% of OSOM; 3, involvement of 51% to 75% of OSOM; and 4, widespread damage  $>75\%$  of OSOM.

For proliferating cell nuclear antigen (PCNA) quantification, kidney sections were antigen retrieved in boiling 10 mmol/L sodium citrate buffer, followed by blocking nonspecific binding with the use of the MOM blocking kit (Vector Laboratories, Burlingame, CA). Sections were stained with mouse anti-PCNA primary Ab (1:100; DakoCytomation, Glostrup, Denmark) for 30 minutes, followed by donkey anti-mouse Alexa Fluor 555 (1:1000; Molecular Probes, Eugene, OR) for 30 minutes. PCNA-positive tubular epithelial cells were quantified in five randomly selected fields of view per section at a magnification of  $\times 400$  within the OSOM.

For fluorescence visualization of *csf1r*-EGFP macrophages, after perfusion-fixation of adult and P5 kidneys, tissue was postfixed in 4% paraformaldehyde for 24 hours, transferred to PBS containing 30% sucrose for overnight incubation at 4°C, embedded in OCT (TissueTek, Tokyo, Japan), and stored at  $-80^{\circ}\text{C}$ . Frozen sections were cut at 5  $\mu$ m, washed in PBS, and

blocked with 1% bovine serum albumin. For determination of collagen type IV localization, a goat anti-human collagen type IV primary Ab (1:400; Southern Biotech, Birmingham, AL) was added for 1 hour, followed by a chicken anti-goat Alexa Fluor 488 (1:1000; Molecular Probes) for 30 minutes. For macrophage staining, sections were incubated with rat anti-mouse F4/80 (1:100; AbD Serotec, Oxford, UK) for 1 hour, followed by a goat anti-rat Alexa Fluor 594 (1:1000; Molecular Probes) for 30 minutes. After staining, sections were counterstained with DAPI (1:10,000; Molecular Probes) and then mounted with Fluorescent Mounting Medium (DakoCytomation). Sections were analyzed with a Provis AX70 fluorescent microscope (Olympus, Tokyo, Japan), and fluorescent images were captured with the F-view II digital camera (Soft Imaging System, Munster, Germany).

### *Hydroxyproline and SDS-PAGE Analyses of Kidney Collagen Content*

Hydroxyproline content was measured from one-half of each kidney (cross-sectioning the same region of cortex, medulla, and papilla for analysis) of sham control and treated adult C57BL/6J mice (20 to 25 g) as previously described.<sup>39,40</sup> Hydroxyproline values were then multiplied by a factor of 6.94 to extrapolate collagen content from each sample (because hydroxyproline represents  $\sim 14.4\%$  of the amino acid composition of collagen).<sup>41</sup> Collagen concentration was then determined by dividing collagen content as a percentage of the dry weight tissue. The other half of each kidney was digested for the detection of changes in interstitial collagen subtypes by SDS-PAGE analysis.<sup>39,40</sup> The pepsin-digested supernatant fluids were then analyzed on 5% (w/v) acrylamide gels with stacking gels of 3.5% (w/v) acrylamide. The  $\alpha 1(\text{I})$  collagen chains were separated from the  $\alpha 1(\text{III})$  chains by interrupted electrophoresis with delayed reduction of the disulfide bonds of type III collagen. The gels were stained with 0.1% Coomassie Blue R-250 overnight at 4°C and destained with 30% methanol supplemented with 7% acetic acid.<sup>42</sup> Densitometry of the  $\alpha 1(\text{I})$  and  $\alpha 2(\text{I})$  chains (representing type I collagen monomers) was then performed with a calibrated imaging densitometer and Quantity-One software version 4.1 (Bio-Rad, Hercules, CA).

### *Flow Cytometry of the CSF-1 Inflammatory Profile*

The left kidneys of neonatal *csf1r*-EGFP mice at P5 and adult C57BL/6J mice (20 to 25 g) were removed and prepared for single-cell suspensions. Kidneys were placed in cold fluorescent-activated cell sorting (FACS) buffer containing PBS supplemented with 0.2% bovine serum albumin, 0.5 mol/L EDTA, and 0.02% NaAz. Kidneys were finely minced and incubated in HBSS containing 1 mg/mL Collagenase/Dispase (Roche Diagnostics, Indianapolis, IN), 0.1% DNase I (Roche Diagnostics), and 5 mmol/L  $\text{CaCl}_2$  at 37°C for 30 minutes on a rotating board. Cells were manually digested into a single-cell suspension with a 1000- $\mu$ L pipette and further incubated

for 5 minutes. The cell suspensions were washed in FACS buffer and recovered by centrifugation at 400 g for 5 minutes at 4°C. Cells were filtered through a 40- $\mu$ m cell strainer (BD Biosciences, North Ryde, Australia), washed, centrifuged, and lysed with red blood cell lysis buffer (8.3 g/L ammonium chloride, pH 7.5). Cells were adjusted to  $3 \times 10^6$  cells/test in 96-well trays and stained with the following mAb cocktail for 15 minutes at 4°C: CD45-APC Cy7 (clone 30-F11), CD11c-Pacific Blue, (clone N418), mannose receptor (MR) CD206-Alexa Fluor 488 (clone MR5D3; BioLegend, San Diego, CA); CD11b-PE Cy7 (clone M1/70) MHCII/1-A/1-E-PE (Clone M5/114.15.2; BD Biosciences); and F4/80-APC (clone BM8; eBioscience, San Diego, CA). For intracellular MR staining, surface-labeled cells were fixed, permeabilized, and stained for 30 minutes at 4°C with the use of the CytoFix/CytoPerm kit (BD Biosciences) according to the manufacturer's instructions. Cells were washed twice in  $1 \times$  Perm/Wash buffer (BD Biosciences) and finally resuspended in FACS buffer. Labeled kidney cells were then analyzed with the FACSCanto II (BD Biosciences), and flow cytometric data were analyzed with FlowJo software version 8.8.6 (TreeStar, Palo Alto, CA).

### Real-Time Quantitative PCR Gene Expression Analysis

Total RNA was extracted from whole kidneys with the use of the RNeasy Mini Kit (Qiagen, Doncaster, Australia), and kidney macrophages were sorted on the expression of CD45-APC (Clone 30-F11; BD Biosciences) and CD11b-FITC (Clone M1/70; BD Biosciences) and the absence of CD11c-PE (Clone HL3; BD Biosciences) with the use of the RNAqueous-Micro Kit (Ambion, Austin, TX) according to the manufacturer's instructions. RNA samples were reverse transcribed into cDNA with the use of the High Capacity cDNA Reverse Transcription Kit (Applied Biosystems, Foster City, CA). Real-time quantitative PCR (qPCR) of target mRNA expression was performed with the TaqMan Universal PCR Master Mix (Applied Biosystems) and the TaqMan Gene Expression Assays (Applied Biosystems). Reactions were measured on the 7500 Real Time PCR System (Applied Biosystems), and relative quantification PCR analysis was analyzed with the SDS software version 1.3 (Applied Biosystems). The threshold cycle (Ct) values were measured in triplicate and normalized against the endogenous control  $\beta$ -actin to determine the  $\Delta$ Ct value. The  $\Delta$ Ct value of the different treatment groups was standardized against the control group to yield the  $\Delta\Delta$ Ct for each gene. The relative quantification was then calculated as  $2^{-\Delta\Delta Ct}$  and graphed. The primers were as follows: *Actb*, Mm00607939\_s1; *Ccl2*, Mm00441242\_m1; *Nos2*, Mm00440485\_m1; *Tnf*, Mm00443258\_m1; *Cxcl2*, Mm00436450\_m1; *Ccl17*, Mm00516136\_m1; *Mrc1*, Mm00485148\_m1; *Msr2*, Mm00472833\_m1; *Arg1*, Mm00475988; *Igf1*, Mm00439561\_m1; *Wnt7b*, Mm01301717\_m1; *Tgfb1*, Mm01178820\_m1; *Acta2*, Mm01546133\_m1; and *Mmp9*, Mm00442991\_m1. All primers were purchased from Applied Biosystems.

### Microarray and Data Analyses

Microarray experiments were undertaken with the use of Illumina Mouse Ref8 V2 gene expression arrays (San Diego, CA). RNA was extracted from sorted macrophage cells as described above with the use of the RNeasy Micro Kit (Qiagen). Two technical replicates were included to determine whether the RNA extraction and labeling procedure and the hybridization procedure were reproducible. RNA quantity was measured with a Nanodrop ND1000 spectrophotometer (Rockland, DE), quality was determined with a Bioanalyzer 2100 (Agilent, Santa Clara, CA), and an RNA integrity number threshold of  $>8$  was used for all samples. The procedures for amplifying RNA, labeling, hybridization, scanning, and data extraction were performed exactly as outlined previously with the following exception: The quantity of total RNA used in the initial amplification process was 150 ng and the *in vitro* transcription reaction was incubated for 14 hours.<sup>43</sup> All microarray data have been submitted to the ArrayExpress database (<http://www.ebi.ac.uk/arrayexpress>) under the accession number E-MTAB-557. Data were normalized with the

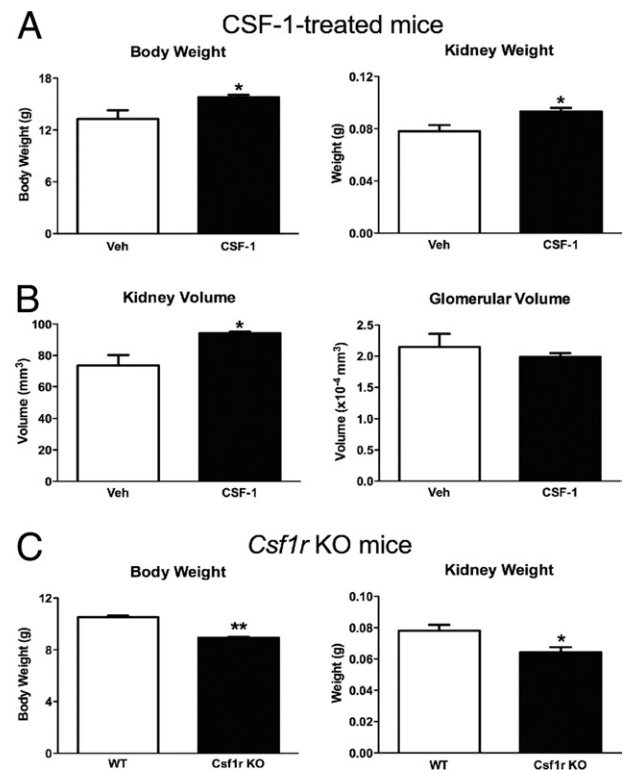


**Figure 1.** CSF-1 administration to newborn mice increased body and kidney weights and kidney volume, and in comparison *csf1r* knockout mice exhibit decreased body and kidney weights. **A:** Mean body and kidney weights of CSF-1 or vehicle control mice at P30, after injection at P0.5, P1.5, and P2.5 ( $n = 8$  per group). CSF-1-treated mice had a 19% increase in body weight ( $P = 0.02$ ) and a 19% increase in kidney weight ( $P = 0.04$ ) compared with vehicle-injected controls. **B:** Unbiased stereologic estimation of kidney and glomerular volumes at P30 after littermates received either CSF-1 or vehicle control ( $n = 3$  per group). Kidney volume was increased by 28% ( $P = 0.04$ ), whereas no significant change in glomerular volume was observed. **C:** *Csf1r* knockout mice had significantly decreased body and kidney weights compared with wild-type animals ( $n = 3$  per group). Body weight was decreased by 15% ( $P = 0.0002$ ) and kidney weight by 28% ( $P = 0.048$ ). Data were analyzed with a Student's *t*-test (unpaired, 2-tailed); \* $P < 0.05$ , \*\* $P < 0.005$ . Data are mean  $\pm$  SEMs. KO, knockout; Veh, vehicle; WT, wild type.

Lumi R/Bioconductor package and Log2 transformed. Samples were grouped on the basis of treatment regime, and genes were filtered on detection score whereby genes had to be detected in  $\geq 75\%$  of the samples in each group. Welch's *t*-test was applied to determine genes that were significantly different ( $P < 0.05$ ) between the two groups. The lists of differentially expressed genes were then subjected to pathway analyses within the Ingenuity Pathway Analysis software version 8.8 (Ingenuity Systems, Redwood City, CA).

### Cell Culture in Vitro

Bone marrow-derived macrophages (BMMs) were isolated and cultured with an established protocol.<sup>44</sup> Cells were initially grown for 24 hours in serum medium with CSF-1 protein (100 ng/mL; Chiron Corporation). Once BMMs were plated, medium was replaced with serum-free medium, and cells were synchronized for 24 hours. BMMs were stimulated with CSF-1 protein (100 ng/mL; Chiron Corporation) in the presence of anti-IGF-1 mAb (3  $\mu$ g/mL; R&D Systems, Minneapolis, MN) for 72 hours in serum-free medium. Cell proliferation was measured with the 3-(4,5-dimethylthiazol-2-yl)-5-(3-carboxymethoxyphenyl)-2-(4-sulfophenyl)-2H-tetrazolium (MTS) assay, CellTiter 96 Aqueous One Solution Cell Proliferation Assay (Promega, Madison, WI) according to the manufacturer's instructions.

### Statistical Analysis

Statistic analysis was performed with GraphPad Prism software version 5.0 (GraphPad Software Inc., San Di-

ego, CA). A *P* value  $< 0.05$  was considered statistically significant. All data were expressed as means  $\pm$  SEMs.

## Results

### CSF-1 Treatment Increases Body Weight and Kidney Weight

The murine kidney undergoes significant postnatal maturation. CSF-1 increases in the circulation and tissues, including kidney, liver, and lung, in the immediate postnatal period. To determine whether the availability of CSF-1 is limiting in this period and to investigate the role(s) that CSF-1 may play in postnatal renal development, CSF-1 was administered to newborn *csf1r*-EGFP mice at P0.5, P1.5, and P2.5.<sup>45</sup> CSF-1 treatment resulted in a significant 19% increase in body weight at P30 ( $P = 0.02$ ) compared with littermate vehicle-injected controls (Figure 1A). At day 30, a significant increase in kidney weight ( $P = 0.04$ ) of 19% was also observed (Figure 1A). Conversely, mice lacking CSF-1 signaling experienced retarded growth. The kidneys from *csf1r*-null mutant mice were assessed at P19 because of the shortened lifespan of the animals.<sup>10</sup> Overall body weight was significantly decreased in knockout compared with wild-type mice of the same age (Figure 1C;  $10.53 \pm 0.11$  versus  $8.94 \pm 0.06$  g;  $P < 0.0002$ ). Furthermore, *csf1r* knockout mice had a significant decrease in kidney weight compared with their wild-type counterparts (Figure 1C;  $0.078 \pm 0.004$  versus  $0.064 \pm 0.003$  g;  $P < 0.05$ ).

Unbiased stereology was used to estimate kidney and glomerular volumes in CSF-1-injected kidneys compared with littermate control-injected mice to determine whether

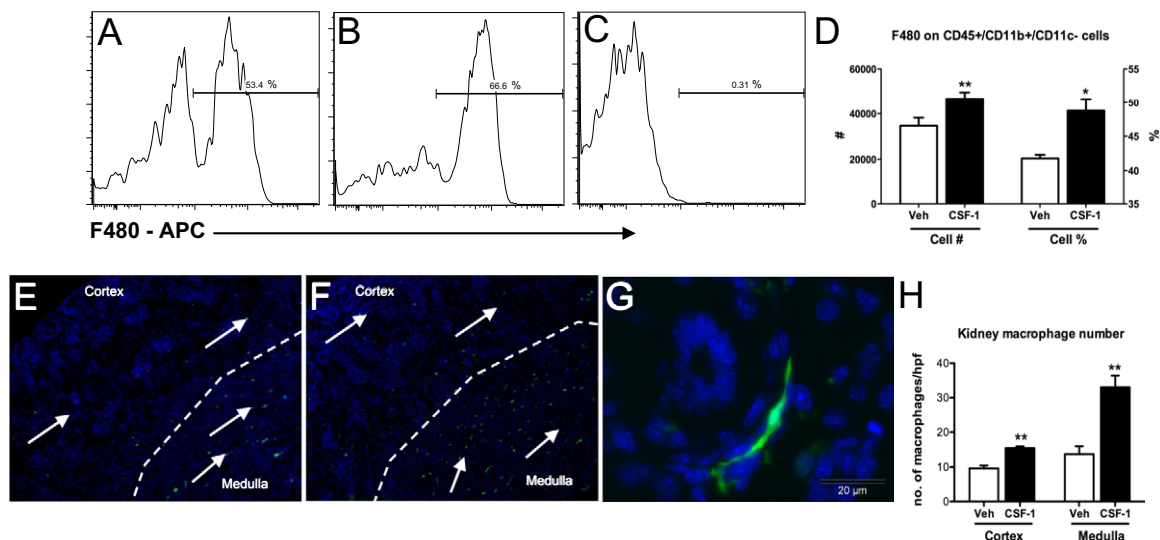


**Figure 2.** Macrophage infiltration is increased in kidneys at P5 after treatment with CSF-1. **A–D:** Flow cytometric analysis of whole kidneys indicates CD45<sup>+</sup>CD11b<sup>+</sup>CD11c<sup>-</sup>/F4/80<sup>+</sup> renal macrophages are increased in CSF-1-treated mice at P5. Representative histograms show an increase in CD45<sup>+</sup>CD11b<sup>+</sup>CD11c<sup>-</sup> cells expressing the macrophage marker F4/80 with CSF-1 treatment (**B**) compared with littermate vehicle-injected controls (**A**). **C:** Positive staining was confirmed with appropriate isotype controls. **E–G:** Representative images with the use of fluorescent microscopy show *csf1r*-EGFP macrophage infiltration (arrows) in kidneys at P5 after treatment with either CSF-1 or vehicle control at P1, P2, and P3 ( $n = 4$  per group). Nuclei are stained with DAPI (blue). Low magnification ( $\times 100$ ) shows that kidneys treated with CSF-1 (**F**) had increased numbers of macrophages in the renal medulla and cortex, compared with vehicle controls (**E**). **G:** *csf1r*-EGFP macrophages show a spindle-shaped structure, wrapping around newly developed structures. **H:** Estimation of the number of renal *csf1r*-EGFP macrophages showed a 42% ( $P = 0.004$ ) increase in macrophages within the cortex and a 157% ( $P = 0.003$ ) increase within the medulla after treatment with CSF-1, compared with vehicles ( $n = 3$  to 4 per group). Data were analyzed with a Student's *t*-test (unpaired, 2-tailed); \* $P < 0.05$ , \*\* $P < 0.01$ . Data are means  $\pm$  SEMs. Veh, vehicle.

increased kidney weight was associated with overall renal volume or glomerular changes. At P30 the increase in kidney weight in CSF-1-treated mice correlated with a 28% increase in total kidney volume compared with littermate controls (Figure 1B). This increased volume was not associated with glomerular hypertrophy with no alteration in glomerular volume (Figure 1B). At P5, flow cytometric analysis of kidney macrophages after CSF-1 treatment showed an increase in both cell number ( $53.5 \pm 0.8$  versus  $67.5 \pm 2.2$ ;  $P = 0.003$ ) and proportion ( $34,633 \pm 3561$  versus  $46,750 \pm 2864$ ;  $P = 0.04$ ) of  $CD45^+CD11b^+CD11c^-$  cells expressing the macrophage marker F4/80 (Figure 2, A–D). Semiquantitative analysis of the number of interstitial *csf1r*-EGFP cells showed significant increases in both the medulla (157%;  $P = 0.003$ ) and cortex (42%;  $P = 0.004$ ; Figure 2, E–H). Furthermore, the *csf1r*-EGFP cells displayed a more elongated, spindle-like structure and were regularly found to wrap around tubules (Figure 2G).

### Structural Regeneration and Functional Recovery in Response to CSF-1

On the basis of the observations of the role of CSF-1 in growth and development of the kidney in newborn mice, we tested the effect of CSF-1 in promoting kidney repair after IR injury (see diagram in Figure 3A). IR injury of the kidney leads to tubular epithelial cell damage within the OSOM, the area most susceptible to hypoxic damage. Compared with sham-operated kidneys, at 5 days after IR injury widespread tubular epithelial cell damage was evident with a prominent inflammatory cell infiltrate, interstitial matrix expansion, and tubular cast formation (Figure 3B). By contrast, when mice with IR injury were administered CSF-1, there was an acceleration of renal repair and reduced tubular damage (Figure 3, B and C), also characterized by increased tubular epithelial cell proliferation as measured by quantification of PCNA immunostaining in proximal tubules (Figure 3D). At 7 days after IR in mice with vehicle injection, renal damage was evident with numerous proteinaceous casts present and a marked inflammatory cell infiltrate associated with the accumulation of extracellular matrix proteins and interstitial matrix expansion (Figure 3B). Quantification of the histopathologic analysis of kidneys from IR mice with and without CSF-1 treatment showed that CSF-1 treatment rescued tubular damage as confirmed by the reduction in the number and size of tubular casts and restoration of the tubular epithelial cell layer (Figure 3C) that was associated with reduced tubular epithelial cell proliferation (Figure 3D).

This reparative effect of CSF-1 therapy in IR mice was further supported by evidence of functional recovery and the expression of Wnt7b in sorted macrophage populations. Urinary albumin excretion was measured in 24-hour urine samples from 7-day bilateral IR mice (Figure 3E). Baseline urinary albumin levels were determined in both vehicle- and CSF-1-treated groups before IR surgery (Figure 3E). At 7 days after bilateral IR surgery urinary albumin levels of vehicle-treated mice were twice that of baseline

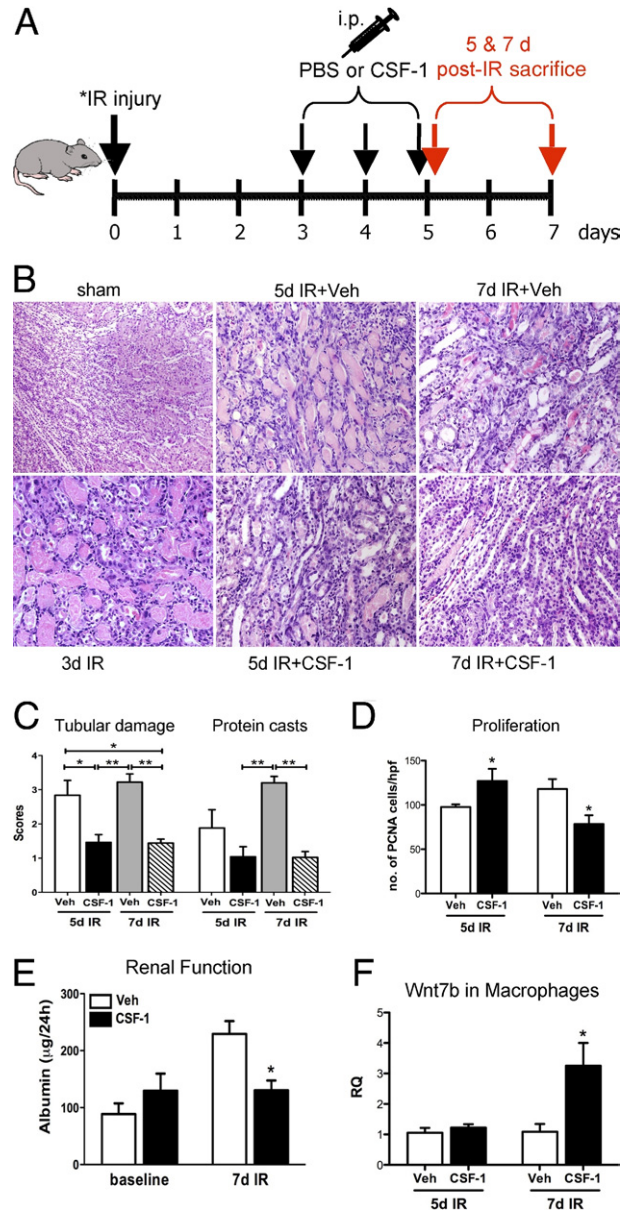


**Figure 3.** CSF-1 treatment, starting at 3 days after IR injury, accelerates endogenous cellular repair and improves renal function in adult mice after IR injury. **A:** Schematic diagram of the dosing regimen for CSF-1 therapy, beginning at 3 days after unilateral (40 minutes) or bilateral (25 minutes) renal artery clamping. **B:** Representative H&E-stained sections showing the histoarchitecture of the OSOM from sham control (original magnification,  $\times 200$ ), 3 days after unilateral IR kidney, 5 and 7 days after unilateral IR kidneys with vehicle or CSF-1 injections (original magnification,  $\times 400$ ). **C:** Semiquantitative analysis of kidney injury from kidneys 5 and 7 days after IR with vehicle or CSF-1 treatment. Data were analyzed by a one-way analysis of variance with an accompanying Tukey's post hoc test for multiple comparisons;  $*P < 0.05$ ,  $**P < 0.01$ , and  $***P < 0.001$ . **D:** Tubular epithelial cell proliferation measured by immunostaining with PCNA in kidneys 5 and 7 days after IR treated with CSF-1 or vehicle injections. Data were analyzed with a Student's *t*-test (unpaired, 2-tailed);  $*P < 0.05$ . **E:** Functional analysis measuring 24-hour urinary albumin excretion at baseline and in kidneys 7 days after bilateral IR. Albumin data were analyzed with a two-way analysis of variance;  $*P < 0.05$ . **F:** qPCR analysis of Wnt7b expression in sorted macrophage populations at 5 and 7 days after IR in kidneys treated with CSF-1 or vehicle injections. Data were analyzed with a Student's *t*-test (unpaired, 2-tailed);  $*P = 0.03$ . Data are means  $\pm$  SEMs ( $n = 5$  to 6 per group). RQ, relative quantification; Veh, vehicle.

measurements (Figure 3E;  $88.69 \pm 18.59$  versus  $229.46 \pm 22.52 \mu\text{g}/24$  hours). However, 24-hour urinary albumin excretion of IR mice treated with CSF-1 was not different from baseline measurements and approximately one-half that of

vehicle-injected controls (Figure 3E;  $130.47 \pm 17.14$  versus  $229.46 \pm 22.52 \mu\text{g}/24$  hours;  $P < 0.05$ ).

Recently, it was shown that Wnt7b ligand production from in sorted macrophage populations in mouse IR kidneys is critical for repair of the kidney tubule basal lamina and the proliferation and migration of epithelial cells.<sup>46</sup> With the use of qPCR, the expression of Wnt7b in sorted kidney macrophages was investigated with and without CSF-1 therapy after IR injury. A significant increase in Wnt7b expression was found in sorted kidney macrophages (CD45<sup>+</sup>CD11b<sup>+</sup>CD11c<sup>-</sup>) at day 7 after IR, a time corresponding to both structural and functional recovery, compared with vehicle-treated kidneys (Figure 3F;  $1.091 \pm 0.25$  versus  $3.25 \pm 0.75$  relative quantification;  $P = 0.03$ ).

### Assessment of Collagen Accumulation

CSF-1 treatment of mice with IR injury reduced the accumulation of interstitial collagen as assessed by hydroxyproline assay, SDS-PAGE analysis, and immunostaining for type IV collagen. In IR kidneys a significant increase was observed in total renal collagen concentration by hydroxyproline assay at both 5 and 7 days, compared with sham-operated kidneys (both  $P < 0.01$  versus sham controls; Figure 4A). At 7 days after IR a significant decrease in total kidney collagen concentration ( $P < 0.05$ ) was evident in CSF-1-treated mice than in kidneys from

vehicle-treated mice (Figure 4A). In addition, most of the interstitial collagen in the kidney as assessed by SDS-PAGE was type 1 collagen [ $\alpha 1(I)$  and  $\alpha 2(I)$  monomers and dimers of two  $\alpha 1(I)$  chains ( $\beta 11$ ) or  $\alpha 1(I)$  and  $\alpha 2(I)$  monomers ( $\beta 12$ )], with a smaller amount of type V collagen also being present. At 7 days after IR, a significant decrease was observed in collagen, particularly type 1 collagen, after CSF-1 treatment compared with vehicle-injected IR mice as determined by scanning densitometry (Figure 4A). Furthermore, immunofluorescence microscopy was used to visualize type IV collagen localization (Figure 4B). At 7 days, type IV collagen was present as a fine framework within the glomerular and tubulointerstitium without evidence of interstitial collagen accumulation in IR kidneys after CSF-1 treatment, compared with IR kidneys without treatment. These findings suggest that CSF-1-dependent macrophages prevent fibrosis during tissue remodeling. At day 5, qPCR showed a decreased expression of TGF- $\beta$  and  $\alpha$ -SMA in CSF-1-treated animals compared with vehicle-injected IR mice, with an up-regulation of MMP9 by day 7 (Figure 4C).

### Alteration of Macrophage Phenotype after IR Injury with CSF-1 Treatment

With the use of fluorescence microscopy at 7 days after IR injury, a marked interstitial inflammatory response was observed with an infiltration of *csf1r*-EGFP macrophages

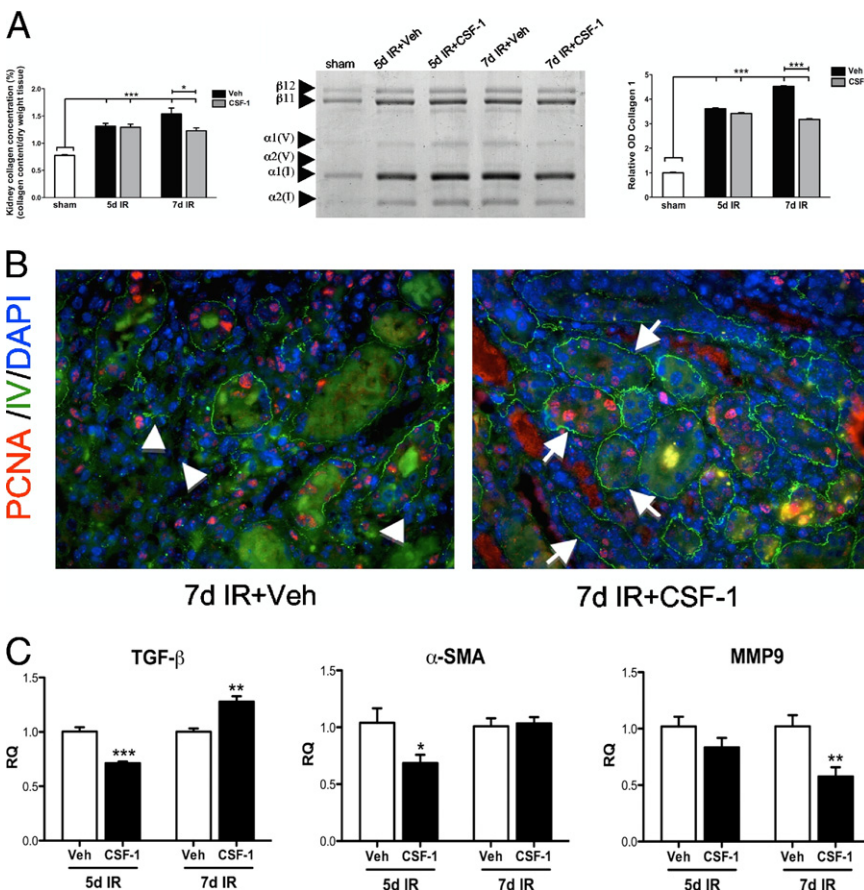


**Figure 4.** CSF-1 reduces renal fibrosis by 7 days after IR injury. **A:** Kidney collagen concentration, SDS-PAGE analysis, and densitometry of sham, and kidneys 5 and 7 days after IR treated with CSF-1 or vehicle. Type 1 collagen monomers are represented by  $\alpha 1(I)$  and  $\alpha 2(I)$  chains,  $\beta 11$  represents dimers of two  $\alpha 1(I)$  chains, whereas  $\beta 12$  represents dimers of  $\alpha 1(I)$  and  $\alpha 2(I)$  chains. Type V collagen is represented by  $\alpha 1(V)$  and  $\alpha 2(V)$  chains. **B:** Representative fluorescent micrographs showing type IV collagen (green) and PCNA (red) staining at 7 days after IR injury with and without CSF-1 treatment. Original magnification,  $\times 400$ . Type IV collagen in the CSF-1-treated IR kidneys displays a fine supportive network around re-epithelialized tubules (arrows) compared with interstitial collagen accumulation (arrowheads) and disruption of the tissue architecture evidence in vehicle-injected controls. **C:** qPCR analysis of TGF- $\beta$ ,  $\alpha$ -SMA, and MMP9 expression in sorted macrophage populations of kidneys at 5 and 7 days after IR treated with CSF-1 or vehicle injections. Hydroxyproline and densitometry data were analyzed with a one-way analysis of variance with an accompanying Tukey's post hoc test. qPCR analysis was analyzed with a Student's *t*-test (unpaired, 2-tailed); \* $P < 0.05$ , \*\* $P < 0.005$ , and \*\*\* $P < 0.0001$ . Data are means  $\pm$  SEMs ( $n = 5$  to 6 per group). RQ, relative quantification; Veh, vehicle.

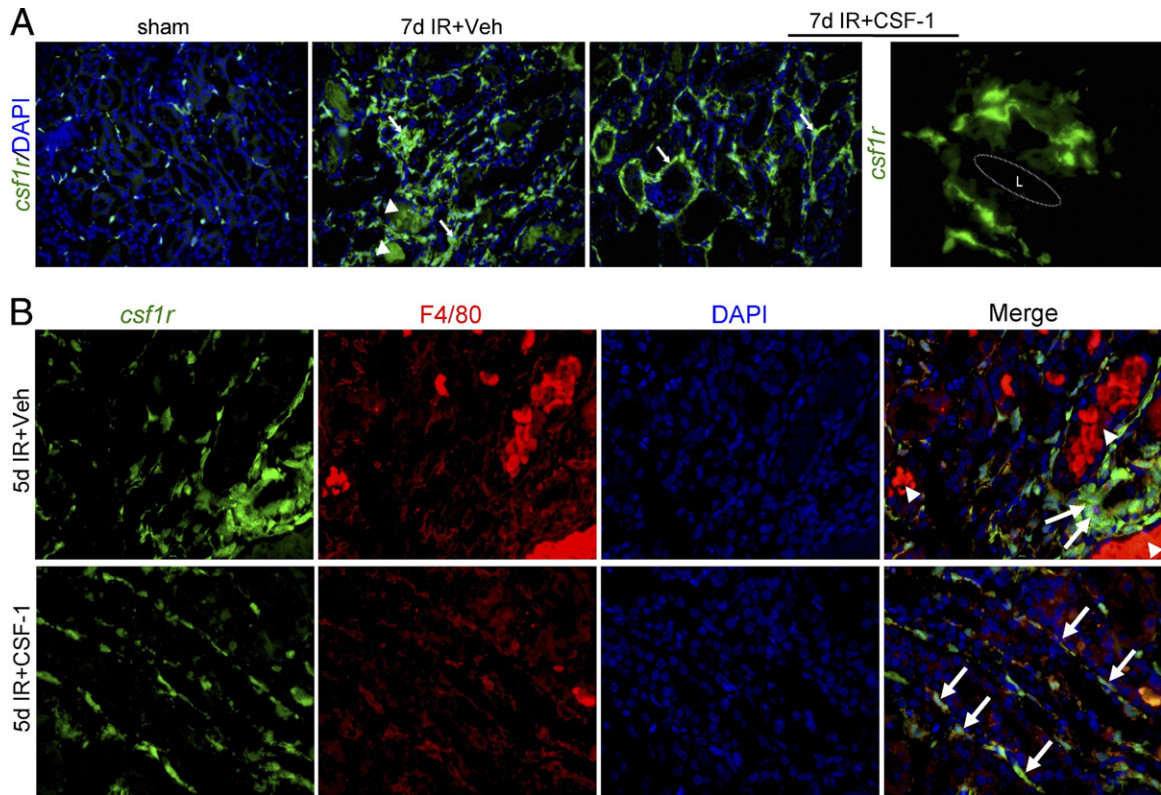


**Figure 5.** CSF-1 alters macrophage phenotype after IR injury. **A:** Representative fluorescent micrographs depicting the phenotypic changes of *csf1r*-EGFP (green) interstitial macrophages from sham control (original magnification,  $\times 200$ ) and kidneys 7 days after IR with and without CSF-1 treatment (original magnification,  $\times 400$ ). In vehicle-injected IR kidneys there is a marked infiltrate of interstitial macrophages (**arrows**) with autofluorescent tubular casts also evident (**arrowheads**). In comparison, kidneys from the CSF-1-treated mice had a prominent interstitial macrophage infiltrate that displayed a spindle-shaped structure (**arrows**). At high power the *csf1r*-EGFP macrophages in CSF-1-treated IR kidneys envelop the tubules with connecting cytoplasmic projections closely adjacent to the tubular basement membrane. Original magnification,  $\times 1000$ . **B:** Representative immunofluorescence microscopy showing co-expression of F4/80 (red) with *csf1r*-EGFP macrophages (green) 5 days after IR injury with vehicle or CSF-1 injection. Original magnification,  $\times 400$ . L, tubular lumen.

in the tubulointerstitium associated with the presence of tubular casts. In response to CSF-1, *csf1r*-EGFP macrophages were also observed in large numbers in the tubulointerstitium (Figure 5A), however, without evidence of collagen accumulation or interstitial expansion. CSF-1-responsive *csf1r*-EGFP macrophages manifested a spindle-shaped structure such that the cells surrounded tubules with interconnecting projections surrounding the tubular basement membrane (Figure 5A).

Immunofluorescence staining was then used to determine the maturation status of the macrophage with the use of the F4/80 antigen on *csf1r*-EGFP macrophages in kidneys 5 and 7 days after IR with and without CSF-1 treatment. At 5 and 7 days (data not shown) after IR, expression of F4/80 completely localized with *csf1r*-EGFP in presumptive macrophages in the interstitium surrounding damaged tubules (Figure 5B). In CSF-1-treated kidneys, mature F4/80/*csf1r*-EGFP macrophages adopted a flattened spindle-shaped structure that lined the basement membrane of repaired tubules (Figure 5B).

#### Characterization of Macrophage Phenotype after IR Injury in Response to CSF-1

The inflammatory profile and functional phenotype of macrophages in response to CSF-1 was further exam-

ined by flow cytometry, qPCR, and expression profiling with the use of the Illumina Mouse Ref8 V2 gene expression arrays (Illumina) in C57BL/6J mice. At 5 days after IR surgery, there was a large influx of macrophages ( $CD45^+CD11b^+CD11c^-$ ), which increased further in response to CSF-1, compared with vehicle- ( $P < 0.05$ ) and sham-treated ( $P < 0.001$ ) kidneys (Figure 6A). The number of macrophages remained consistent between 5 and 7 days after IR in vehicle-treated animals, whereas the inflammatory infiltrate declined in the CSF-1-treated animals, suggesting an accelerated recovery (Figure 6A). These inflammatory cells predominantly expressed F4/80 and major histocompatibility complex (MHC) class II, and CSF-1 treatment did not change the relative proportions of cells expressing these markers (Figure 6A). However, CSF-1 administration did increase the level of MHC class II expression on F4/80<sup>+</sup> macrophages at 5 days after IR compared with vehicle-treated animals, as shown by a positive shift in the mean fluorescent intensity ( $P < 0.01$ ; Figure 6B).

The accelerated resolution of the lesions in response to CSF-1 suggested the presence of an anti-inflammatory response. The macrophage MR has been associated with an anti-inflammatory phenotype in macrophages.<sup>47,48</sup> The number of macrophages expressing

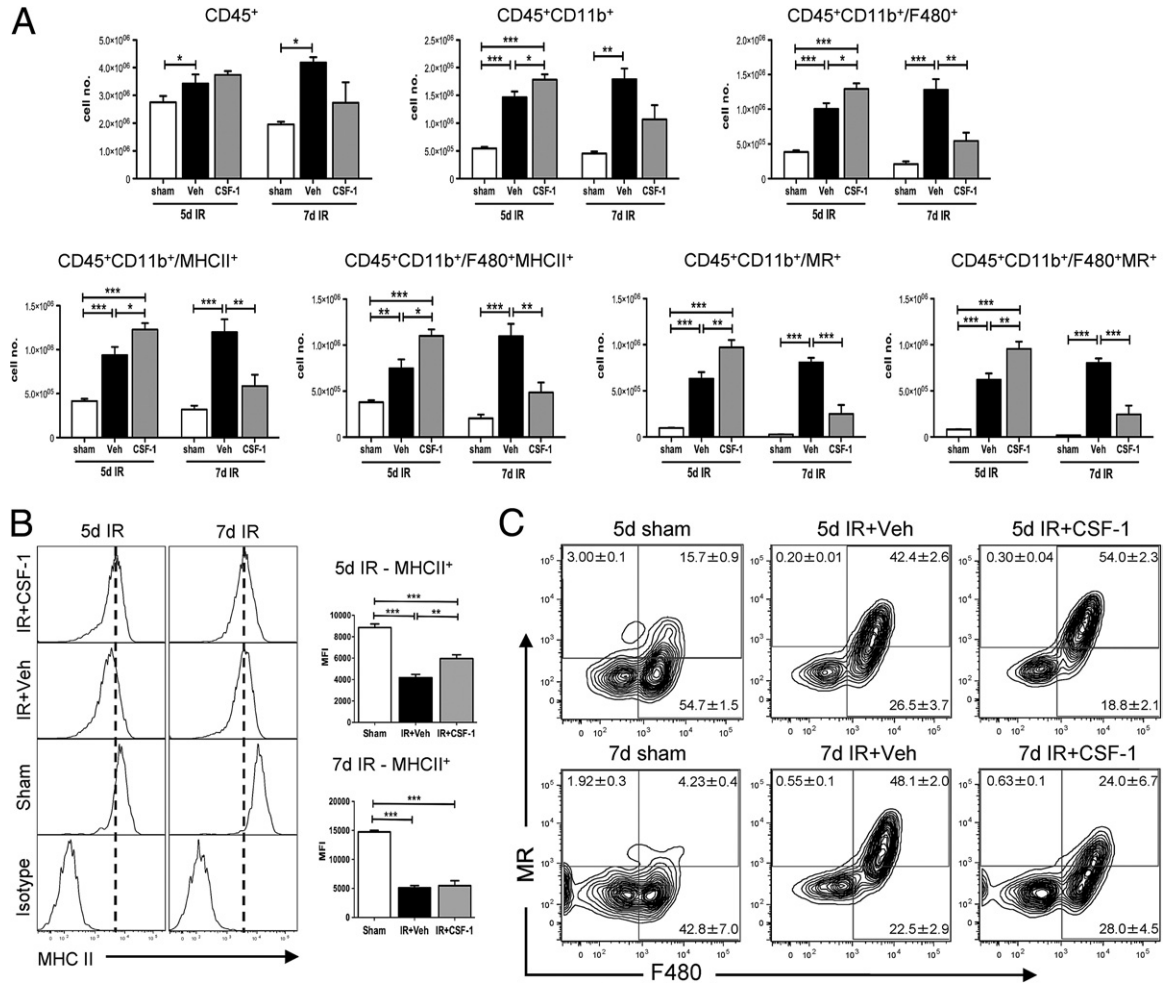


**Figure 6.** CD45<sup>+</sup>CD11b<sup>+</sup>CD11c<sup>-</sup> renal macrophages in CSF-1-treated mice display an altered phenotype and cell number compared with vehicle-treated mice at 5 and 7 days after IR injury. Flow cytometric analysis was performed on sham-operated kidneys and kidneys 5 and 7 days after IR treated with vehicle or CSF-1. **A:** Flow cytometric quantification of leukocytes stained for F480, MR, and MHC class II on CD45<sup>+</sup>CD11b<sup>+</sup>CD11c<sup>-</sup> renal macrophages. **B:** Representative histograms displaying the shift in mean fluorescent intensity of MHC class II<sup>+</sup> cells gated on CD45<sup>+</sup>CD11b<sup>+</sup>CD11c<sup>-</sup>/F480<sup>+</sup> macrophages. **C:** Representative contour plots of F480 and MR co-expression on CD45<sup>+</sup>CD11b<sup>+</sup>CD11c<sup>-</sup> macrophages. Positive staining was confirmed with appropriate isotype controls. Percentages of cells in each quadrant represent mean ± SEM. Statistical analysis was performed with a one-way analysis of variance with an accompanying Tukey's post hoc test for multiple comparisons; \**P* < 0.05, \*\**P* < 0.01, and \*\*\**P* < 0.001. Data are means ± SEMs (*n* = 5 per group). MFI, mean fluorescent intensity; Veh, vehicle.

MR at 5 days after IR with CSF-1 therapy was significantly increased than with vehicle- (*P* < 0.01) and sham-treated (*P* < 0.001) mice (Figure 6A). These MR cells were also positive for F4/80 (Figure 6A) with a shift from F4/80<sup>+</sup>MR<sup>hi</sup> population at 5 days after IR to a F4/80<sup>+</sup>MR<sup>lo</sup> population at 7 days after IR in response to CSF-1 (Figure 6C). In vehicle-treated mice, this phenotypic shift was mostly reversed with a F4/80<sup>+</sup>MR<sup>lo</sup> population at 5 days after IR to a F4/80<sup>+</sup>MR<sup>hi</sup> population at 7 days after IR injury (Figure 6C). These results suggest that CSF-1 accelerates macrophage maturation, leading to a more rapid resolution of injury.

The numbers of CD45<sup>+</sup>CD11b<sup>+</sup>CD11c<sup>-</sup> macrophages in the inflamed kidney are sufficient to allow detection of relevant macrophage-expressed genes with the use of qPCR analysis. At 5 days after IR, CSF-1 therapy increased the initial inflammatory response, as evidenced by TNF- $\alpha$  and CCL2 expressions (Figure 7A) but did not alter iNOS and Cxcl2 expressions (Fig-

ure 7A). By 7 days, these effects of CSF-1 were no longer evident (Figure 7A). Conversely, at 5 days after IR, CSF-1 therapy also induced the expression of arginase and CCL17 more often associated with an anti-inflammatory phenotype, and by 7 days after IR macrophage scavenger receptor 2 (MSR2) and MR were also induced further by CSF-1 (Figure 7B).

Gene expression profiling was performed to further examine the differentially expressed genes and altered signaling pathways in sorted kidney macrophages at both 5 and 7 days after IR injury with CSF-1 therapy compared with untreated mice. Hierarchical clustering of genes in each group showed distinct patterns of gene expression because of time and treatment with CSF-1. The largest difference in transcript expression between vehicle and CSF-1 treatment samples was seen at day 5 after IR; this was less obvious at day 7 after IR between treatment groups (Figure 8A). The lists of differentially expressed genes were then sub-

**A** pro-inflammatory phenotype    **B** anti-inflammatory phenotype

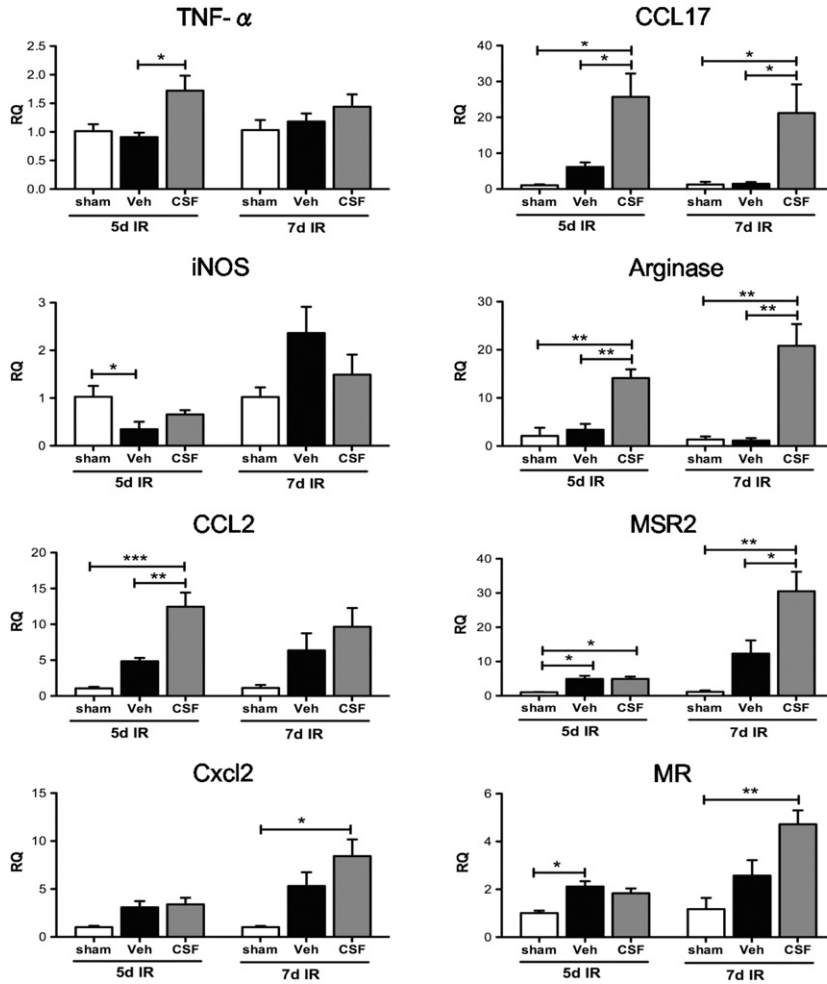


**Figure 7.** qPCR analysis of pro-inflammatory and anti-inflammatory gene expression in sorted CD45<sup>+</sup>CD11b<sup>+</sup>CD11c<sup>-</sup> macrophages from sham-operated kidneys and kidneys 5 and 7 days after IR treated with CSF-1 or vehicle injections. Pro-inflammatory (INOS, TNF- $\alpha$ , CCL2, and Cxcl2) (A) and anti-inflammatory (CCL17, arginase, MSR2, and MR) (B) gene expression in response to CSF-1 treatment. Sham-operated kidneys were used as the baseline control. Statistical analysis was performed with a one-way analysis of variance with an accompanying Tukey's post hoc test for multiple comparisons; \* $P < 0.05$ , \*\* $P < 0.01$ , and \*\*\* $P < 0.001$ . Data are means  $\pm$  SEMs ( $n = 5$  per group). RQ, relative quantification; Veh, vehicle.

jected to pathway overrepresentation analyses with the use of Ingenuity Pathway Analysis software version 8.8 (Ingenuity Systems). Overrepresentation analyses are a measure of probability that the gene lists at both 5 and 7 days after IR with CSF-1 treatment compared with vehicle contains more members of the biochemical pathway than because of chance alone (Figure 8B). Interestingly, in the day-5 CSF-1-treated macrophage populations, the glucocorticoid receptor, IL-10, and IGF-1 signaling pathways were identified, all are associated with a M2 macrophage response (Figure 8B). Networks of differentially expressed genes were also generated with Ingenuity Pathway Analysis version 8.8 (Ingenuity Systems), and network hubs were identified around IL-1 receptor antagonist, arginase, and mice STAT3 molecules, all associated with an M2 macrophage response (see Supplemental Figures S1 and S2 at <http://ajp.amjpathol.org>). The pathways significantly overrepresented in the day-7 CSF-1-treated macrophages included platelet-derived growth factor (PDGF), granulocyte macrophage (GM)-CSF-1, and apoptosis signaling (Figure 8B).

*IGF-1 Expression in IR Kidneys*

IGF-1 has been shown to play an important role in the reparative process of postischemic rat kidneys,<sup>49–51</sup> and CSF-1 is known to control the expression of IGF-1.<sup>52,53</sup> We therefore investigated IGF-1 expression by qPCR at 5 and 7 days after IR injury following CSF-1 therapy (Figure 9). In whole kidneys, at 5 days after IR no difference in IGF-1 expression was observed between vehicle- and CSF-1-treated mice. However, by 7 days after IR, IGF-1 expression was significantly increased in CSF-1 mice compared with vehicle-treated animals ( $P < 0.01$ ; Figure 9A), which correlated with the structural and functional recovery evident at the same time point. To confirm that macrophages were the source of IGF-1, we assessed the expression in sorted CD45<sup>+</sup>CD11b<sup>+</sup>CD11c<sup>-</sup> macrophage cells after IR injury. IGF-1 was significantly up-regulated in CSF-1-treated mice at both 5 ( $P < 0.001$ ) and 7 ( $P < 0.01$ ) days after IR injury compared with vehicle-treated animals (Figure 9A). In addition, BMMs cultured with CSF-1 protein in the presence of IGF-1-neutralizing antibody inhibited CSF-1-stimulated BMM cell prolifer-

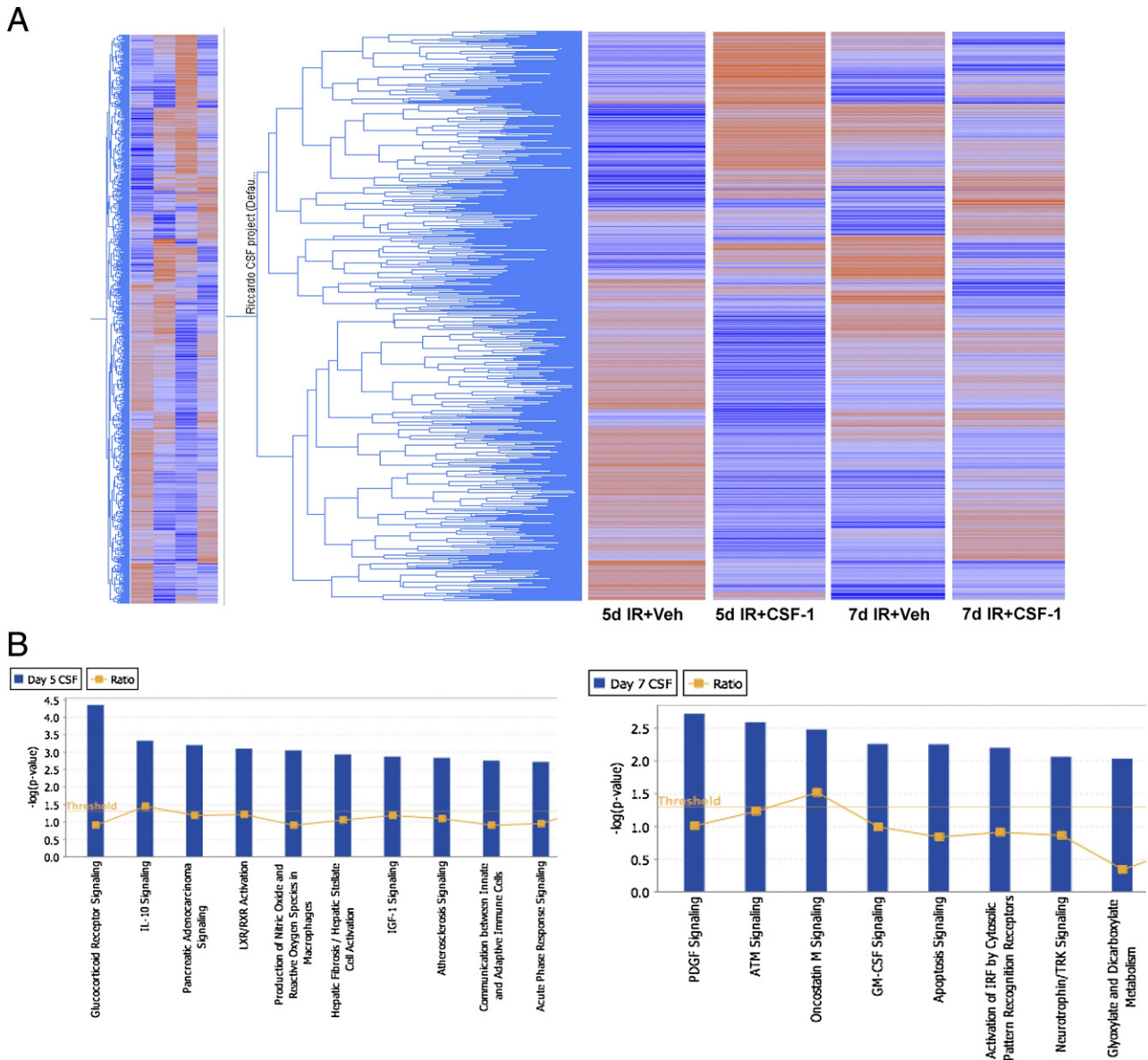


**Figure 8.** Microarray analysis of sorted macrophage populations from kidneys 5 and 7 days after IR with or without CSF-1 therapy. **A:** Hierarchical cluster of expressed genes in each group, where blue represents low gene expression and red represents high gene expression. **B:** Canonical signaling pathways significantly overrepresented in sorted macrophages from kidneys 5 and 7 days after IR with CSF-1 therapy compared with vehicle treatment. The threshold line indicates the cutoff probability ( $P < 0.05$ ) calculated from a right-tailed Fisher's exact test within the Ingenuity Pathway Analysis software version 8.8 (Ingenuity Systems). The ratio line indicates the number of genes from the gene list that pass cutoff criteria in the pathway divided by the total number of genes in the pathway. ATM, ataxia telangiectasia mutated; LXR/RXR, liver X receptor/retinoid X receptor; TRK, tyrosine kinase receptor; Veh, vehicle.

ation, suggesting that CSF-1 can promote macrophage growth by IGF-1 signaling (Figure 9B).

### Discussion

The pleiotropic role for CSF-1 in reproduction, including mammary branching morphogenesis and placental growth, suggest that CSF-1 exerts many of its actions through the trophic activities of cells of the mononuclear phagocytic lineage.<sup>54</sup> Fetal macrophages are among the first hematopoietic cells found in the kidney, entering the murine kidney at embryonic day 12.<sup>3</sup> Furthermore, the numbers of macrophages in most major organs of the

mouse undergo a substantial numerical increase in response to a postnatal surge of CSF-1.<sup>2,14</sup> In the current study, we report that CSF-1 increases overall body weight and kidney weight and volume when administered during the final week of development, and we provide evidence that this is accompanied by an increase in macrophage numbers in the kidneys with the use of a *csf1r*-EGFP reporter mouse described previously.<sup>6</sup>

Osteopetrotic (*csf1<sup>op</sup>/csf1<sup>op</sup>*) mice that have a spontaneous mutation in the *csf1* gene, show growth restriction and developmental abnormalities<sup>11,12,23</sup> that can be partially reversed by the exogenous administration of CSF-1.<sup>16</sup> Targeted disruption of the *csf1r* gene results in

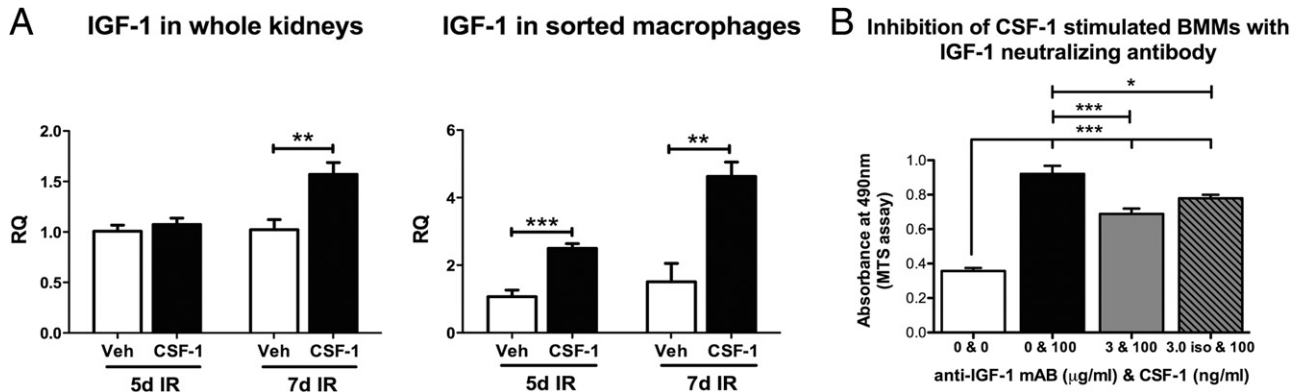


**Figure 9.** CSF-1 can promote macrophage growth and cell proliferation by IGF-1 signaling. **A:** qPCR analysis of IGF-1 expression in adult kidneys and sorted macrophages 5 and 7 days after IR injury with and without CSF-1 treatment. **B:** MTS proliferation assay of BMMs cultured with CSF-1 (100 ng/mL) in the presence of IGF-1 neutralizing antibody (3 μg/mL). qPCR data were analyzed with a Student's *t*-test (unpaired, 2-tailed), and MTS proliferation data were analyzed with a one-way analysis of variance with an accompanying Tukey's post hoc test for multiple comparisons; \**P* < 0.01, \*\**P* < 0.01, and \*\*\**P* < 0.001. Data are means ± SEMs (*n* = 5 per group). RQ, relative quantification; Veh, vehicle.

growth deficiencies, reduced macrophage numbers, and reproductive defects similar to *csf1<sup>op</sup>/csf1<sup>op</sup>* mice yet more severely.<sup>10</sup> Here, we further show that *csf1r*-null mice have decreased kidney weight. The CSF-1-deficient *csf1<sup>op</sup>/csf1<sup>op</sup>* mouse has many developmental deficiencies in common with the IGF-1-deficient mouse, including a failure to produce insulin-producing cells in the islets, neurologic defects, deficiencies in male and female reproductive systems, and failure of mammary gland development.<sup>55</sup> Our previous report showing that CSF-1 can promote nephrogenesis in kidney explants<sup>3</sup> is analogous to the growth-promoting role of IGF-1 in human fetal kidney explants that supports the induction and differentiation of the nephrogenic zone.<sup>56</sup> The production of IGF-1 by CSF-1-stimulated macrophages has been recognized previously,<sup>52,57,58</sup> but no comparative abundance data have previously been presented.

The present data suggest that macrophages respond to CSF-1 signaling by the production of IGF-1, an essential growth factor that regulates postnatal growth and development.<sup>55</sup> In fact, the biology we observe is consistent with a study of muscle regeneration, in which IGF-1 not only promotes repair but also dampens expression of inflammatory cytokines.<sup>59</sup> The other possibility is that there is another cell type able to transduce the CSF-1 signal. Indeed, Menke et al<sup>60</sup> have also reported that CSF-1 can promote kidney repair but conclude that the renal epithelium itself expresses the CSF-1R, suggesting a direct signaling mechanism for this outcome. They report the detection of CSF-1R mRNA and protein on mouse primary tubular epithelial cells *in vitro*, although at a very low level in comparison to macrophage lines.<sup>60</sup>

Local microenvironmental cues play an important role in macrophage heterogeneity. Therefore, CSF-1 activation of tissue macrophages may influence the growth, proliferation, and maturation of the kidney during organogenesis, a phenomenon that may be mirrored in repairing kidneys after CSF-1 therapy. We report that the administration of CSF-1 to mice with established IR injury resulted in tubular epithelial proliferation, attenuation of interstitial fibrosis, and functional recovery. In many settings regeneration of the kidney is macrophage dependent, evi-

denced by the switch of macrophage phenotype from a pro-inflammatory to an anti-inflammatory phenotype,<sup>21</sup> which is followed by the production of angiogenic and anti-inflammatory factors in addition to phagocytic tissue remodeling.<sup>22,61</sup> The precise phenotype of the macrophages seen in the repairing kidney in our study does not strictly conform to the M1/M2 dichotomy, because we see expression of genes associated with both extremes and the profile changes with time. Mosser and Edwards<sup>48</sup> have suggested a third macrophage classification, associated with wound healing, that is distinct from the M2 category. In reality, the repairing kidney should be considered as a unique environment. Induction of genes such as IGF-1, and the MSR<sup>62</sup> are probably direct responses to CSF-1. The macrophage MR is also highly expressed in CSF-1-stimulated BMMs (see data at <http://www.bioGPS.org>) and in macrophages of the embryo.<sup>48</sup> Urokinase plasminogen activator is another relevant gene that is inducible by CSF-1.<sup>63</sup> Previous reports implicate urokinase plasminogen activator in the prevention of fibrosis in kidney and other tissues.<sup>64,65</sup> Other genes expressed by macrophages that we observed may be in response to the presence of apoptotic cells. Our microarray profiling of differentially expressed genes and signaling pathways showed distinct patterns that correspond to macrophage phenotypes that showed genes in common with *csf1r*-EGFP-expressing macrophages during embryonic development.<sup>3</sup>

Original studies of CSF-1 administration to adult mice showed that it can increase circulating monocytes and tissue macrophages.<sup>66</sup> Notwithstanding the surge in availability in the postnatal period, injected CSF-1 can additionally promote postnatal growth in newborn mice. We have recently reported that the administration of CSF-1R blocking antibody selectively reduced monocyte precursors of resident tissue macrophages.<sup>67</sup> The current study suggests that CSF-1 acts, at least in part, through production of IGF-1 by kidney macrophages. We further propose that an activation of CSF-1 by tissue macrophages creates a microenvironment that influences the growth, proliferation, and differentiation of renal epithelial cells and promotes matrix remodeling and

cellular replacement in an inflammatory setting. CSF-1 thus may bias the macrophage response to one of mediating tissue repair rather than driving inflammation. An understanding of the factors that control differentiation and activation of regenerative macrophages and the environmental cues that govern the outcome of inflammation is vital to the successful development of cellular-based therapies that may prevent or retard the progression of renal disease.

## References

- Ovchinnikov DA: Macrophages in the embryo and beyond: much more than just giant phagocytes. *Genesis* 2008, 46:447–462
- Pollard JW: Trophic macrophages in development and disease. *Nat Rev Immunol* 2009, 9:259–270
- Rae F, Woods K, Sasmono T, Campanale N, Taylor D, Ovchinnikov DA, Grimmond SM, Hume DA, Ricardo SD, Little MH: Characterisation and trophic functions of murine embryonic macrophages based upon the use of a Csf1r-EGFP transgene reporter. *Dev Biol* 2007, 308:232–246
- Hume DA, Ross IL, Himes SR, Sasmono RT, Wells CA, Ravasi T: The mononuclear phagocyte system revisited. *J Leukoc Biol* 2002, 72:621–627
- Lichanska AM, Hume DA: Origins and functions of phagocytes in the embryo. *Exp Hematol* 2000, 28:601–611
- Sasmono RT, Oceandy D, Pollard JW, Tong W, Pavli P, Wainwright BJ, Ostrowski MC, Himes SR, Hume DA: A macrophage colony-stimulating factor receptor-green fluorescent protein transgene is expressed throughout the mononuclear phagocyte system of the mouse. *Blood* 2003, 101:1155–1163
- Penalzo C, Orlanski S, Ye Y, Entezari-Zaher T, Javdan M, Zakeri Z: Cell death in mammalian development. *Curr Pharm Des* 2008, 14:184–196
- Henson PM, Hume DA: Apoptotic cell removal in development and tissue homeostasis. *Trends Immunol* 2006, 27:244–250
- Smith SJ, Kotecha S, Towers N, Latinkic BV, Mohun TJ: XPOX2-peroxidase expression and the XLRP-1 promoter reveal the site of embryonic myeloid cell development in *Xenopus*. *Mech Dev* 2002, 117:173–186
- Dai XM, Ryan GR, Hapel AJ, Dominguez MG, Russell RG, Kapp S, Sylvestre V, Stanley ER: Targeted disruption of the mouse colony-stimulating factor 1 receptor gene results in osteopetrosis, mononuclear phagocyte deficiency, increased primitive progenitor cell frequencies, and reproductive defects. *Blood* 2002, 99:111–120
- Cohen PE, Chisholm O, Arcenci RJ, Stanley ER, Pollard JW: Absence of colony-stimulating factor-1 in osteopetrotic (csfmp/op) mice results in male fertility defects. *Biol Reprod* 1996, 55:310–317
- Van Nguyen A, Pollard JW: Colony stimulating factor-1 is required to recruit macrophages into the mammary gland to facilitate mammary ductal outgrowth. *Dev Biol* 2002, 247:11–25
- Banaei-Bouchareb L, Gouon-Evans V, Samara-Boustani D, Castellotti MC, Czernichow P, Pollard JW, Polak M: Insulin cell mass is altered in Csf1op/Csf1op macrophage-deficient mice. *J Leukoc Biol* 2004, 76:359–367
- Cecchini MG, Dominguez MG, Mocci S, Wetterwald A, Felix R, Fleisch H, Chisholm O, Hofstetter W, Pollard JW, Stanley ER: Role of colony stimulating factor-1 in the establishment and regulation of tissue macrophages during postnatal development of the mouse. *Development* 1994, 120:1357–1372
- Ryan GR, Dai XM, Dominguez MG, Tong W, Chuan F, Chisholm O, Russell RG, Pollard JW, Stanley ER: Rescue of the colony-stimulating factor 1 (CSF-1)-nullizygous mouse (Csf1(op)/Csf1(op)) phenotype with a CSF-1 transgene and identification of sites of local CSF-1 synthesis. *Blood* 2001, 98:74–84
- Wiktor-Jedrzejczak W, Urbanowska E, Aukerman SL, Pollard JW, Stanley ER, Ralph P, Ansari AA, Sell KW, Szperl M: Correction by CSF-1 of defects in the osteopetrotic op/op mouse suggests local, developmental, and humoral requirements for this growth factor. *Exp Hematol* 1991, 19:1049–1054
- Martinez FO, Gordon S, Locati M, Mantovani A: Transcriptional profiling of the human monocyte-to-macrophage differentiation and polarization: new molecules and patterns of gene expression. *J Immunol* 2006, 177:7303–7311
- Mantovani A, Sica A, Sozzani S, Allavena P, Vecchi A, Locati M: The chemokine system in diverse forms of macrophage activation and polarization. *Trends Immunol* 2004, 25:677–686
- Martinez FO, Helming L, Gordon S: Alternative activation of macrophages: an immunologic functional perspective. *Annu Rev Immunol* 2009, 27:451–483
- Ricardo SD, van Goor H, Eddy AA: Macrophage diversity in renal injury and repair. *J Clin Invest* 2008, 118:3522–3530
- Wang Y, Wang YP, Zheng G, Lee VW, Ouyang L, Chang DH, Mahajan D, Coombs J, Wang YM, Alexander SI, Harris DC: Ex vivo programmed macrophages ameliorate experimental chronic inflammatory renal disease. *Kidney Int* 2007, 72:290–299
- Vinuesa E, Hotter G, Jung M, Herrero-Fresneda I, Torras J, Sola A: Macrophage involvement in the kidney repair phase after ischaemia/reperfusion injury. *J Pathol* 2008, 214:104–113
- Michaelson MD, Bieri PL, Mehler MF, Xu H, Arezzo JC, Pollard JW, Kessler JA: CSF-1 deficiency in mice results in abnormal brain development. *Development* 1996, 122:2661–2672
- Ishida Y, Gao JL, Murphy PM: Chemokine receptor CX3CR1 mediates skin wound healing by promoting macrophage and fibroblast accumulation and function. *J Immunol* 2008, 180:569–579
- Wang H, Peters T, Kess D, Sindrilaru A, Oreshkova T, Van Rooijen N, Stratis A, Renkl AC, Sunderkotter C, Wlaschek M, Haase I, Scharffetter-Kochanek K: Activated macrophages are essential in a murine model for T cell-mediated chronic psoriasiform skin inflammation. *J Clin Invest* 2006, 116:2105–2114
- Nakamura T, Abu-Dahab R, D. Menger M, Schafer U, Vollmar B, Wada H, Lehr CM, Schafers HJ: Depletion of alveolar macrophages by clodronate-liposomes aggravates ischemia-reperfusion injury of the lung. *J Heart Lung Transplant* 2005, 24:38–45
- Duffield JS, Forbes SJ, Constadinou CM, Clay SA, Partolina MA, Vuthoori SA, Wu SA, Lang RA, Iredale JP: Selective depletion of macrophages reveals distinct, opposing roles during liver injury and repair. *J Clin Invest* 2005, 115:56–65
- Leor J, Rozen L, Zulloff-Shani A, Feinberg MS, Amsalem Y, Barbash IM, Kachel E, Holbova R, Mardor Y, Daniels D, Ocherashvili A, Orenstein A, Danon D: Ex vivo activated human macrophages improve healing, remodeling, and function of the infarcted heart. *Circulation* 2006, 114(1 Suppl):I94–I100
- Pull SL, Doherty JM, Mills JC, Gordon JI, Stappenbeck TS: Activated macrophages are an adaptive element of the colonic epithelial progenitor niche necessary for regenerative responses to injury. *Proc Natl Acad Sci U S A* 2005, 102:99–104
- Ramsay RG, Micallef SJ, Williams B, Lightowler S, Vincan E, Heath JK, Mantamadiotis T, Bertoncello I: Colony-stimulating factor-1 promotes clonogenic growth of normal murine colonic crypt epithelial cells in vitro. *J Interferon Cytokine Res* 2004, 24:416–427
- Bryer SC, Fantuzzi G, Van Rooijen N, Koh TJ: Urokinase-type plasminogen activator plays essential roles in macrophage chemotaxis and skeletal muscle regeneration. *J Immunol* 2008, 180:1179–1188
- Arnold L, Henry A, Poron F, Baba-Am Y, van Rooijen N, Plonquet A, Gherardi RK, Chazaud B: Inflammatory monocytes recruited after skeletal muscle injury switch into antiinflammatory macrophages to support myogenesis. *J Exp Med* 2007, 204:1057–1069
- Arcenci RJ, Shanahan F, Stanley ER, Pollard JW: Temporal expression and location of colony-stimulating factor 1 (CSF-1) and its receptor in the female reproductive tract are consistent with CSF-1-regulated placental development. *Proc Natl Acad Sci U S A* 1989, 86:8818–8822
- Pollard JW, Bartocci A, Arcenci R, Orlofsky A, Ladner MB, Stanley ER: Apparent role of the macrophage growth factor, CSF-1, in placental development. *Nature* 1987, 330:484–486
- Pakkenberg B, Gundersen HJ: Total number of neurons and glial cells in human brain nuclei estimated by the dissector and the fractionator. *J Microsc* 1988, 150:1–20
- Kett MM, Alcorn D, Bertram JF, Anderson WP: Glomerular dimensions in spontaneously hypertensive rats: effects of AT1 antagonism. *J Hypertens* 1996, 4:107–113
- Betram J: Analyzing renal glomeruli with the new stereology. *Int Rev Cytol* 1995, 161:111–172

38. Sims-Lucas S, Caruana G, Dowling J, Kett MM, Bertram JF: Augmented and accelerated nephrogenesis in TGF-beta2 heterozygous mutant mice. *Pediatr Res* 2008, 63:607–612
39. Cochrane AL, Kett MM, Samuel CS, Campanale NV, Anderson WP, Hume DA, Little MH, Bertram JF, Ricardo SD: Renal structural and functional repair in a mouse model of reversal of ureteral obstruction. *J Am Soc Nephrol* 2005, 16:3623–3630
40. Samuel C, Butkus A, Coghlan J, Bateman J: The effect of relaxin on collagen metabolism in the nonpregnant rat pubic symphysis: the influence of estrogen and progesterone in regulating relaxin activity. *Endocrinology* 1996, 137:3884–3890
41. Gallop PM, Paz MA: Posttranslational protein modifications, with special attention to collagen and elastin. *Physiol Rev* 1975, 55:418–487
42. Sykes B, Puddle B, Francis M, Smith R: The estimation of two collagens from human dermis by interrupted gel electrophoresis. *Biochem Biophys Res Commun* 1976, 72:1472–1480
43. Matigian N, Abrahamsen G, Sutharsan R, Cook AL, Vitale AM, Nouwens A, Bellette B, An J, Anderson M, Beckhouse AG, Bennebroek M, Cecil R, Chalk AM, Cochrane J, Fan Y, Feron F, McCurdy R, McGrath JJ, Murrell W, Perry C, Raju J, Ravishankar S, Silburn PA, Sutherland GT, Mahler S, Mellick GD, Wood SA, Sue CM, Wells CA, Mackay-Sim A: Disease-specific, neurosphere-derived cells as models for brain disorders. *Dis Model Mech* 2010, 3:785–798
44. Zhang X, Goncalves R, Mosser DM: The isolation and characterization of murine macrophages. *Curr Protoc Immunol* 2008, Chapter 14:Unit 14.1
45. Roth P, Stanley ER: Colony stimulating factor-1 expression is developmentally regulated in the mouse. *J Leukoc Biol* 1996, 59:817–823
46. Lin SL, Li B, Rao S, Yeo EJ, Hudson TE, Nowlin BT, Pei H, Chen L, Zheng JJ, Carroll TJ, Pollard JW, McMahon AP, Lang RA, Duffield JS: Macrophage Wnt7b is critical for kidney repair and regeneration. *Proc Natl Acad Sci U S A* 2010, 107:4194–4199
47. Stein M, Keshav S, Harris N, Gordon S: Interleukin 4 potently enhances murine macrophage mannose receptor activity: a marker of alternative immunologic macrophage activation. *J Exp Med* 1992, 176:287–292
48. Mosser DM, Edwards JP: Exploring the full spectrum of macrophage activation. *Nat Rev Immunol* 2008, 8:958–969
49. Ding H, Kopple JD, Cohen A, Hirschberg R: Recombinant human insulin-like growth factor-I accelerates recovery and reduces catabolism in rats with ischemic acute renal failure. *J Clin Invest* 1993, 91:2281–2287
50. Hirschberg R, Ding H: Mechanisms of insulin-like growth factor-I-induced accelerated recovery in experimental ischemic acute renal failure. *Miner Electrolyte Metab* 1998, 24:211–219
51. Miller SB, Martin DR, Kissane J, Hammerman MR: Insulin-like growth factor I accelerates recovery from ischemic acute tubular necrosis in the rat. *Proc Natl Acad Sci U S A* 1992, 89:11876–11880
52. Arkins S, Rebeiz N, Brunke-Reese D, Minshall C, Kelley K: The colony-stimulating factors induce expression of insulin-like growth factor-I messenger ribonucleic acid during hematopoiesis. *Endocrinology* 1995, 136:1153–1160
53. Gow DJ, Sester DP, Hume DA: CSF-1, IGF-1, and the control of postnatal growth and development. *J Leukoc Biol* 2010, 88:475–481
54. Pollard JW: Role of colony-stimulating factor-1 in reproduction and development. *Mol Reprod Dev* 1997, 46:54–61
55. Liu JL, Yakar S, LeRoith D: Conditional knockout of mouse insulin-like growth factor-1 gene using the Cre/loxP system. *Proc Soc Exp Biol Med* 2000, 223:344–351
56. Matsell DG, Bennett T: Evaluation of metanephric maturation in a human fetal kidney explant model. *In Vitro Cell Dev Biol Anim* 1998, 34:138–148
57. Long E, Huynh HT, Zhao X: Involvement of insulin-like growth factor-1 and its binding proteins in proliferation and differentiation of murine bone marrow-derived macrophage precursors. *Endocrine* 1998, 9:185–192
58. Kelley KW, Arkins S, Minshall C, Liu Q, Dantzer R: Growth hormone, growth factors and hematopoiesis. *Horm Res* 1996, 45:38–45
59. Pelosi L, Giacinti C, Nardis C, Borsellino G, Rizzuto E, Nicoletti C, Wannenes F, Battistini L, Rosenthal N, Molinaro M, Musaro A: Local expression of IGF-1 accelerates muscle regeneration by rapidly modulating inflammatory cytokines and chemokines. *FASEB J* 2007, 21:1393–1402
60. Menke J, Iwata Y, Rabacal WA, Basu R, Yeung YG, Humphreys BD, Wada T, Schwarting A, Stanley ER, Kelley VR: CSF-1 signals directly to renal tubular epithelial cells to mediate repair in mice. *J Clin Invest* 2009, 119:2330–2342
61. Ferenbach D, Kluth DC, Hughes J: Inflammatory cells in renal injury and repair. *Semin Nephrol* 2007, 27:250–259
62. de Villiers WJ, Fraser IP, Hughes DA, Doyle AG, Gordon S: Macrophage-colony-stimulating factor selectively enhances macrophage scavenger receptor expression and function. *J Exp Med* 1994, 180:705–709
63. Stacey KJ, Fowles LF, Colman MS, Ostrowski MC, Hume DA: Regulation of urokinase-type plasminogen activator gene transcription by macrophage colony-stimulating factor. *Mol Cell Biol* 1995, 15:3430–3441
64. Yamaguchi I, Lopez-Guisa JM, Cai X, Collins SJ, Okamura DM, Eddy AA: Endogenous urokinase lacks antifibrotic activity during progressive renal injury. *Am J Physiol Renal Physiol* 2007, 293:F12–F19
65. Zhang G, Kim H, Cai X, Lopez-Guisa JM, Carmeliet P, Eddy AA: Urokinase receptor modulates cellular and angiogenic responses in obstructive nephropathy. *J Am Soc Nephrol* 2003, 14:1234–1253
66. Hume DA, Pavli P, Donahue RE, Fidler IJ: The effect of human recombinant macrophage colony-stimulating factor (CSF-1) on the murine mononuclear phagocyte system in vivo. *J Immunol* 1988, 141:3405–3409
67. Macdonald KP, Palmer JS, Cronau S, Seppanen E, Olver S, Raffelt NC, Kuns R, Pettit AR, Clouston A, Wainwright B, Branstetter D, Smith J, Paxton RJ, Cerretti DP, Bonham L, Hill GR, Hume DA: An antibody against the colony-stimulating factor 1 receptor (CSF1R) depletes the resident subset of monocytes and tissue and tumor-associated macrophages but does not inhibit inflammation. *Blood* 2010, 116:3955–3963

RESEARCH

Open Access

# The effect of CSF-1 administration on lung maturation in a mouse model of neonatal hyperoxia exposure

Christina V Jones<sup>1</sup>, Maliha A Alikhan<sup>1</sup>, Megan O'Reilly<sup>1</sup>, Foula Sozo<sup>1</sup>, Timothy M Williams<sup>1</sup>, Richard Harding<sup>1</sup>, Graham Jenkin<sup>2</sup> and Sharon D Ricardo<sup>1\*</sup>

## Abstract

**Background:** Lung immaturity due to preterm birth is a significant complication affecting neonatal health. Despite the detrimental effects of supplemental oxygen on alveolar formation, it remains an important treatment for infants with respiratory distress. Macrophages are traditionally associated with the propagation of inflammatory insults, however increased appreciation of their diversity has revealed essential functions in development and regeneration.

**Methods:** Macrophage regulatory cytokine Colony-Stimulating Factor-1 (CSF-1) was investigated in a model of neonatal hyperoxia exposure, with the aim of promoting macrophages associated with alveologeneses to protect/rescue lung development and function. Neonatal mice were exposed to normoxia (21% oxygen) or hyperoxia (Hyp; 65% oxygen); and administered CSF-1 (0.5 µg/g, daily × 5) or vehicle (PBS) in two treatment regimes; 1) after hyperoxia from postnatal day (P)7-11, or 2) concurrently with five days of hyperoxia from P1-5. Lung structure, function and macrophages were assessed using alveolar morphometry, barometric whole-body plethysmography and flow cytometry.

**Results and discussion:** Seven days of hyperoxia resulted in an 18% decrease in body weight and perturbation of lung structure and function. In regime 1, growth restriction persisted in the Hyp + PBS and Hyp + CSF-1 groups, although perturbations in respiratory function were resolved by P35. CSF-1 increased CSF-1R+/F4/80+ macrophage number by 34% at P11 compared to Hyp + PBS, but was not associated with growth or lung structural rescue. In regime 2, five days of hyperoxia did not cause initial growth restriction in the Hyp + PBS and Hyp + CSF-1 groups, although body weight was decreased at P35 with CSF-1. CSF-1 was not associated with increased macrophages, or with functional perturbation in the adult. Overall, CSF-1 did not rescue the growth and lung defects associated with hyperoxia in this model; however, an increase in CSF-1R+ macrophages was not associated with an exacerbation of lung injury. The trophic functions of macrophages in lung development requires further elucidation in order to explore macrophage modulation as a strategy for promoting lung maturation.

## Introduction

Immaturity of the lungs due to preterm birth is one of the most significant complications affecting neonatal mortality. As preterm infants with respiratory distress are born with lungs at an anatomical stage not yet conducive to gas exchange, routine care practices include mechanical ventilation and oxygen supplementation. However, these lifesaving interventions can also cause permanent damage to the developing lung, resulting in a chronic lung disease termed

bronchopulmonary dysplasia (BPD) [1,2]. Modern therapeutic improvements such as the administration of surfactant and corticosteroids have seen a transformation in BPD pathology away from the fibrotic injury of the past. Instead today, with many extremely preterm babies now surviving, 'new' BPD pathology is characterised by a disruption of alveolar formation [3,4].

Delivery of high concentrations of oxygen to neonatal animals is widely used to investigate the basis of arrested alveolar development associated with BPD in preterm infants [5,6]. In humans, alveolarisation begins *in utero* at around 36 weeks gestation, with 85% of alveoli formed after birth [7]. In the mouse, alveolar formation occurs

\* Correspondence: [REDACTED]

<sup>1</sup>Department of Anatomy and Developmental Biology, Monash University, Clayton, Victoria, Australia

Full list of author information is available at the end of the article

entirely postnatally, beginning approximately 4 days after birth and proceeding until P36 [8]. Exposure of the developing lung to high levels of oxygen results in inflammation and oxidant damage, and dysregulation of alveolar development [9-11]. Understanding the mechanisms of alveolar formation has clinical relevance for the development of therapeutic strategies to improve lung maturation in preterm infants.

Macrophages are key immune cells commonly associated with inflammation and the propagation of tissue injury associated with oxygen toxicity in hyperoxia exposure. However, a greater appreciation of macrophage diversity is revealing that this heterogeneous cell type is also essential in regulating organ development and regeneration [12-15]. In particular, diversity in macrophage subpopulation activation in the lung has been shown to be important in both the induction and resolution of lung injury [16].

Colony-Stimulating Factor-1 (CSF-1) is a key regulator of macrophage differentiation, proliferation, survival and activation, and acts as a pleiotropic growth factor essential in reproduction and organogenesis [17]. During pregnancy, uterine production of CSF-1 increases 1000-fold [18], and macrophages colonise the embryo and are present in large numbers in virtually all developing organs [19]. The absence of CSF-1 results in severe developmental impairment including reduced growth, neurological and reproductive defects, as well as altered development of the mammary gland, bone and pancreas [20-22]. We have previously reported that lung CSF-1R<sup>+</sup> macrophages increase during normal lung development and peak during the alveolarisation stage [23]. In the absence of CSF-1, alveolar macrophage populations are severely depleted during postnatal development [24-26], and in adulthood mice develop spontaneous emphysema associated with deregulated matrix metalloproteinases (MMPs) and abnormal elastin deposition [26].

CSF-1 administration has been shown to enhance organogenesis. Increased branching morphogenesis was observed in embryonic kidney explants following the addition of CSF-1 [27], and in embryonic pancreas explants  $\beta$ -cell proliferation and insulin production were increased [28]. Furthermore, CSF-1 is suggested to preferentially regulate macrophage populations associated with trophic functions such as development [29]. While abnormalities seen in CSF-1-deficient animals are associated with a virtual absence of tissue macrophages, organogenic enhancement with CSF-1 administration is correlated with increased macrophage numbers [20-22,27,28].

CSF-1-responsive macrophages in developing embryonic kidneys and lungs exhibit a gene expression profile characteristic of an M2 or tissue remodelling-type macrophage [27]. Similarly we have demonstrated the importance of

trophic macrophages in alveolarisation, with an upregulation of M2 genes observed during this developmental stage in the mouse [23]. Furthermore, CSF-1 has important immunomodulatory properties, and in a murine model of neonatal hyperoxia, mesenchymal stem cell (MSC)-mediated amelioration of injury was associated with increased CSF-1 levels [30]. We hypothesise that the administration of CSF-1 to promote augmentation of developmental macrophages associated with alveolarisation may reduce the need for damaging long-term oxygen therapy in preterm newborns and attenuate the developmental arrest of the lung associated with BPD.

The aim of this study was to determine the impact of CSF-1 administration on lung maturation in a model of hyperoxia-associated lung developmental perturbation, when delivered either as a treatment after hyperoxia or when administered prophylactically with concurrent hyperoxia exposure. In particular, we assessed lung functional maturation and the impact of a CSF-1-mediated increase in macrophages. We found that CSF-1 did not rescue the growth and pulmonary defects associated with hyperoxia in this model; however the concomitant increased infiltration of CSF-1-responsive macrophages was not associated with exacerbation of lung injury.

## Methods

### Hyperoxia exposure

All animal experiments were approved by the Monash University Animal Ethics Committee and conducted in accordance with the "Australian Code of Practice for the Care and Use of Animals for Scientific Purposes". This study utilised *csf1r*-EGFP mice, which express enhanced green fluorescent protein (EGFP) in cells of the myeloid lineage via the insertion of an EGFP transgene under the control of the *Csf1r* promoter [31]. Pregnant *csf1r*-EGFP mice were allowed to litter-down naturally in individually ventilated cages (Green Line IVC Sealsafe; Techniplast, Buguggiate, Italy). Litters were randomly assigned to receive either normoxia (ambient room air; 21% oxygen) or hyperoxia (65% oxygen). Hyperoxia was achieved by mixing 100% medical grade oxygen and medical grade dry air, delivered to cages via Perspex(R) tubing into ventilation ports. Oxygen and carbon dioxide concentrations were continuously monitored by a gas analyser (Servoflex MiniMP 5200, Servomex, Valley Point, Singapore). Dams remained with their own pups for the entire experiment. Boxes were briefly disconnected from hyperoxia gases for a maximum of 15 minutes when injections were performed. Following hyperoxia exposure (regime 1: 7 days; regime 2: 5 days), mice were maintained in room air until experimental endpoints at P11 and P35.

### CSF-1 administration

Hyperoxia-exposed littermate pups received either mouse recombinant CSF-1 (0.5  $\mu$ g/g body weight; University of

Queensland Protein Facility, Brisbane, Australia) or vehicle (PBS), administered via intraperitoneal (i.p.) injection at a final volume of 25  $\mu$ l. Biological activity was confirmed with *in vitro* culture assays demonstrating CSF-1-mediated proliferation of bone-marrow derived macrophages (data not shown). In treatment regime 1, neonatal pups were continuously exposed to hyperoxia from birth for 7 days with subsequent injections performed once daily for 5 days from P7-11. In treatment regime 2, newborn pups were exposed to hyperoxia and were administered CSF-1 concurrently, and therefore a shorter exposure of 5 days was used to facilitate 5 concurrent daily injections. At experimental endpoints (regime 1: P11 and P35; regime 2: P5 and P35) mice were humanely euthanised via cervical dislocation for morphometric or flow cytometric analysis.

### Plethysmography

Respiratory function was assessed using unrestrained barometric whole-body plethysmography, as described previously [23,32,33]. In brief, mice were placed in a sealed cylindrical Perspex chamber (Neonate; 75 mm  $\times$  50 mm, Adolescent/Adult; 150 mm  $\times$  50 mm), and changes in pressure caused by tidal breathing movements were measured using a volumetric pressure transducer (model PT5A; Grass Instrument Co., Quincy, MA, USA) and amplified (Octal Bridge Amp model ML228 and Powerlab 8/30 model ML870; ADInstruments, Bella Vista, NSW, Australia). Pressure fluctuations were recorded using Chart™ software (v5.1; ADInstruments). At the beginning of each session the plethysmograph was calibrated by measuring the pressure deflection caused by the injection of a known volume (300  $\mu$ l) of air into the chamber. The temperature and relative humidity within the chamber were noted at the beginning and end of recordings (model HM34; Vaisala, Hawthorn, VIC, Australia). Waveform analysis (Chart™; ADInstruments) was used to derive breath frequency (breaths/min), total breath cycle time (ms), inspiration time (ms), expiration time (ms), tidal volume ( $\mu$ L), minute volume (mL/min), inspiratory duty cycle (%) and inspiratory flow rate ( $\mu$ L/sec). Measurements were performed at P5 or P7 at the end of hyperoxia, following CSF-1 administration at P11 and then at P14, P21, P28 and P35.

### Morphometry

For morphometric assessments, the trachea was cannulated immediately after euthanasia and the lungs inflation-fixed *in situ* via intratracheal instillation of 10% buffered formalin at a pressure of 20 cmH<sub>2</sub>O. The entire thorax was subsequently immersion fixed for 24 hr before lungs were dissected. The left lobe was processed, embedded in paraffin wax, sectioned at 5  $\mu$ m, mounted

on Polysine™ slides (Menzel-Glaser, Braunschweig, Germany) and stained with haematoxylin and eosin. Images from 15 non-overlapping fields of view were captured at  $\times$  400 magnification and ImagePro Plus software (Media Cybernetics, Bethesda, MA, USA) was used to assess mean linear intercept (MLI), as an estimate of alveolar diameter, and tissue/airspace percentage, as described previously [34]. In brief, MLI was calculated by superimposing two transverse lines over lung images and counting intersecting points. The percentage airspace and tissue was estimated by superimposing 21 equidistant line segments over lung images and counting line termini intersections with either tissue or airspace, respectively. Fields of view containing parenchyma only were analysed, with care taken to exclude areas with airways or extensive vasculature. Measurements were conducted in a blinded manner by the same individual (CV) to reduce bias.

### Flow cytometry

To assess macrophage populations in hyperoxic lungs and their response to CSF-1 treatment, whole lungs of littermate mice underwent flow cytometric analysis at the end of treatment at P11 or P5, with the final injection being administered 3 hours before lungs were collected. Whole lungs underwent enzymatic and mechanical digestion to yield a single cell suspension as described previously [12]. Red blood cells were lysed and cell suspensions were filtered through a 40  $\mu$ m cell strainer (BD Biosciences, North Ryde, NSW, Australia). Cell counts were performed using a Coulter® Particle Count and Size Analyzer (Beckman Coulter Australia Pty Ltd, Gladesville, NSW, Australia).  $3 \times 10^6$  cells were immunolabelled with anti-CD45 APC Cy7-conjugated (1:800; BioLegend, San Diego, CA, USA; Clone 30-F11) and anti-F4/80 APC-conjugated (1:200; eBioscience, San Diego, CA, USA; Clone BM8) antibodies. Samples were run on a BD FACSCanto II cytometer (BD Biosciences) and data analysis was performed using FlowJo FCS analysis software (Tree Star Inc., Ashland, OR, USA).

### Statistical analysis

This study included 17 litters of mice, ranging between 4 and 8 pups per litter. The N numbers for bodyweight and lung function analysis outlined in appropriate figure legends are a cumulative of a minimum two repeated experiments. Flow cytometric analysis was performed on one representative litter for inter-litter comparison. Data are presented as mean  $\pm$  standard error of the mean (SEM). Graphing and statistical analyses were performed using GraphPad Prism™ (GraphPad Software; Section 3.14). Specific statistical tests used are outlined in figure legends. A p value of less than 0.05 was considered statistically significant.

## Results

### Neonatal hyperoxia exposure for 7 days results in decreased body weight and perturbations in lung structure and function

Neonatal murine hyperoxia is a model of impaired alveologenesis and a clinically relevant model of preterm lung damage. In our hyperoxia model, neonatal mice were exposed to 65% oxygen from birth for 7 days. Hyperoxia significantly decreased growth of neonatal mice. At birth there

was no significant difference in body weight between groups ( $p = 0.09$ ); however after 7 days of hyperoxia exposure body weight was decreased by 18% compared to normoxia-exposed offspring ( $4.37 \pm 0.12$  g vs.  $3.57 \pm 0.01$  g,  $p < 0.001$ ; Figure 1A). Lung structural alterations were assessed via morphometric analyses. Compared to normoxia, hyperoxia resulted in a 17% increase in MLI ( $80.9 \pm 2.1$   $\mu\text{m}$  vs.  $94.6 \pm 2.4$   $\mu\text{m}$ ,  $p < 0.05$ ; Figure 1B), a 6% decrease in percentage tissue ( $44.3 \pm 0.5\%$  vs.  $38.6 \pm 1.1\%$ ,  $p < 0.05$ ;

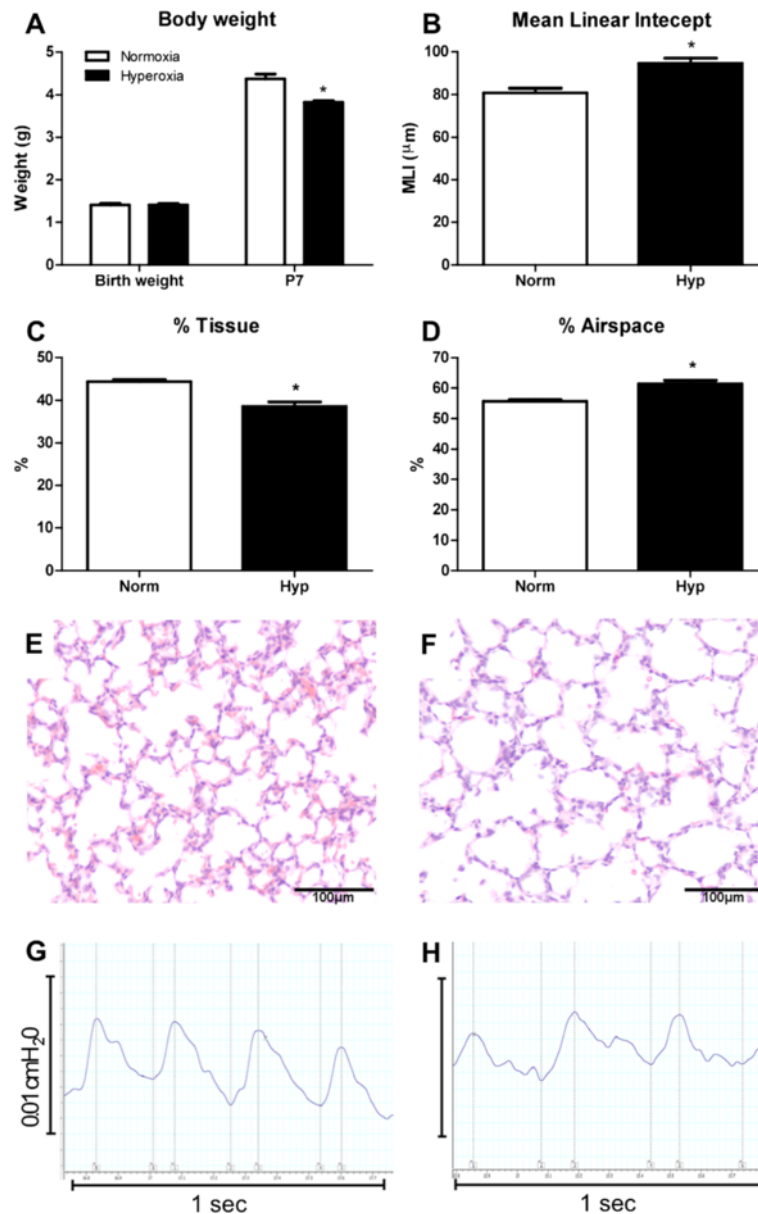


**Figure 1 Neonatal hyperoxia exposure resulted in decreased growth and lung structural and functional alterations.** Body weights of mice exposed to hyperoxia for 7 days from birth compared to neonates exposed to normoxia (A).  $n = 9$  &  $13$  mice/treatment. Morphometric estimation of mean linear intercept (B), percentage tissue (C) and percentage airspace (D) in lungs exposed to hyperoxia and normoxia.  $n = 4$  &  $5$  lungs/treatment. Data were analysed using two-tailed unpaired t-tests.  $*p < 0.05$ . Normoxia (E) and hyperoxia-exposed (F) lungs at P7 demonstrated the decrease in tissue percentage and increase in alveolar size due to hyperoxia. Respiratory trace recordings revealed that mice exposed to hyperoxia (H) display abnormal breath patterns compared to normoxic mice (G).

Figure 1C) and a corresponding 6% increase in percentage airspace ( $55.7 \pm 0.5\%$  vs.  $61.4 \pm 1.1\%$ ,  $p < 0.05$ ; Figure 1D). These quantitative measurements reflect the histological changes observed in hyperoxic lungs, where alveoli appeared larger and secondary septation appeared to be impaired (Figure 1F), in comparison to the lungs of normoxic mice which had smaller alveoli and evidence of extensive secondary septation (Figure 1E). These structural perturbations associated with hyperoxia exposure were reflected in functional alterations (Table 1). Unrestrained barometric whole-body plethysmography assessment of respiratory function after 7 days of hyperoxia indicated that these mice exhibited abnormal breathing patterns compared to normoxic mice (Figure 1G&H). Quantification revealed significant reductions in tidal volume (21%  $p < 0.0001$ ), minute volume (29%  $p < 0.01$ ), breath frequency (9%  $p < 0.05$ ) and inspiratory flow rate (30%  $p < 0.001$ ; Table 1). Functional alterations also included significant increases in total cycle time (9%  $p < 0.05$ ), expiration time (50%  $p < 0.001$ ) and a trend towards increased inspiration time (14%  $p = 0.08$ ).

**CSF-1 treatment after hyperoxia did not rescue body weight, but increased macrophage numbers were not associated with exacerbation of lung structural or functional perturbation**

In the first treatment regime, CSF-1 was administered after 7 days of hyperoxia-induced lung injury to assess the ability of CSF-1 therapy to rescue growth and promote alveolar development. Comparing hyperoxia and normoxia groups, a significant reduction in body weight was observed in Hyp + PBS mice, which persisted from P11 ( $6.43 \pm 0.34$  g vs.  $5.07 \pm 0.13$  g,  $p < 0.001$ ) to adulthood at P35 ( $21.17 \pm 0.47$  g vs.  $17.70 \pm 0.76$  g,  $p < 0.001$ ; Figure 2A). While both groups exposed to hyperoxia weighed significantly less than the Norm group, there was no significant

difference in growth between the Hyp + PBS and Hyp + CSF-1 groups (Figure 2A). From P11 at the end of treatment ( $5.07 \pm 0.13$  g vs.  $5.05 \pm 0.16$  g) to adulthood at P35 ( $17.70 \pm 0.76$  g vs.  $17.35 \pm 0.70$  g), CSF-1 treatment did not rescue body weight when compared to mice exposed to hyperoxia and administered PBS (Figure 2A).

Removal of mice from hyperoxia resulted in a marked improvement in lung structure. At the end of treatment at P11, there was no significant difference in MLI, percentage tissue or percentage airspace amongst any of the three groups (Table 2). However, there was a trend towards increased MLI in the Hyp + PBS group compared to Norm, and this increase was not observed in the CSF-1 treated group. In adulthood at P35, no significant differences were observed in any of the lung structure parameters investigated in any group. However, of note is that all Hyp + CSF-1 values were more similar to Norm values than Hyp + PBS, indicating that structural abnormalities had not been exacerbated with CSF-1 treatment.

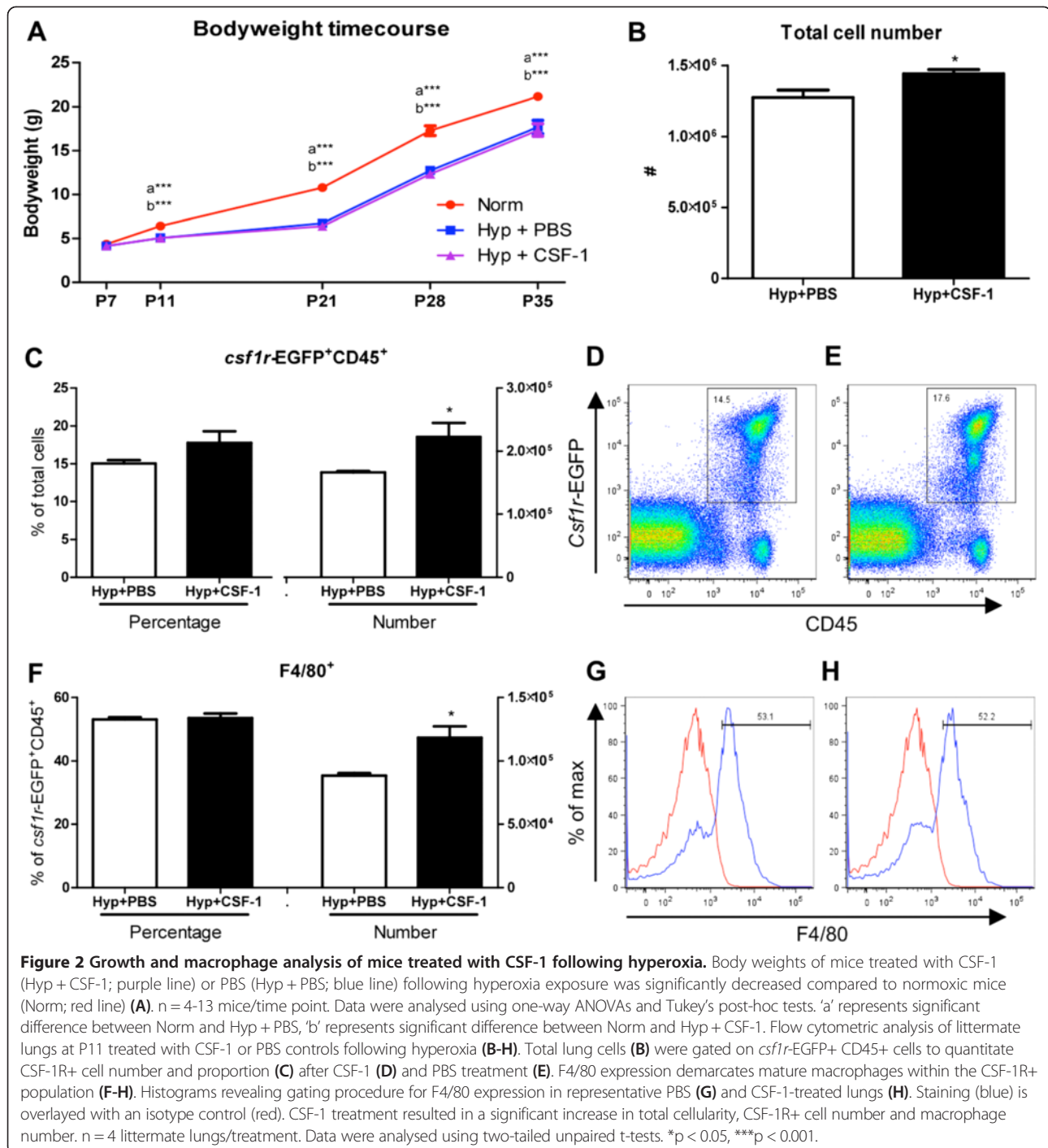
A time course analysis of lung function was performed from the conclusion of hyperoxia exposure at P7, at the end of treatment at P11, and weekly throughout development from P14 to adulthood at P35 (Figure 3). Tidal volume (Figure 3A), minute volume (Figure 3B), tidal volume/body weight ratio (Figure 3G) and inspiratory flow rate (Figure 3I) all increased during postnatal development, with all three groups following a similar trajectory. No significant differences were observed at any time point, with the exception of P21 when a significant reduction in tidal volume ( $79.5 \pm 6.0$   $\mu$ l vs.  $53.0 \pm 5.0$   $\mu$ l,  $p < 0.01$ ; Figure 3A), minute volume ( $23.2 \pm 1.3$  ml vs.  $15.9 \pm 0.8$  ml,  $p < 0.05$ ; Figure 3B) and tidal volume/body weight ( $7.4 \pm 0.6$   $\mu$ l/g vs.  $6.3 \pm 0.4$   $\mu$ l/g,  $p < 0.05$ ; Figure 3G) was observed in the Hyp + CSF-1 group compared to Norm. Some early alterations were observed in parameters

**Table 1 Effect of neonatal hyperoxia exposure on lung function**

	Normoxia	Hyperoxia	Significance	p value
Tidal volume ( $\mu$ l)	$13.64 \pm 0.76$	$10.74 \pm 0.34$	***	0.0008
Minute volume (ml/min)	$3.28 \pm 0.25$	$2.34 \pm 0.13$	**	0.0014
Frequency (breaths/min)	$238.0 \pm 6.63$	$216.4 \pm 6.18$	*	0.031
Total cycle time (ms)	$254.2 \pm 7.32$	$276.9 \pm 7.07$	*	0.044
Inspiration time (ms)	$72.51 \pm 3.85$	$82.75 \pm 3.64$		0.076
Expiration time (ms)	$137.7 \pm 22.11$	$206.4 \pm 10.76$	**	0.005
Inspiratory flow rate ( $\mu$ l/sec)	$191.6 \pm 12.93$	$133.5 \pm 8.06$	***	0.0006
Inspiratory duty cycle (%)	$28.73 \pm 1.66$	$29.99 \pm 1.29$		0.55
Tidal volume ( $\mu$ l)/bw (g)	$3.11 \pm 0.11$	$2.98 \pm 0.17$		0.56
Minute volume (ml/min)/bw (g)	$744.0 \pm 42.11$	$650.8 \pm 48.17$		0.19

\* $p < 0.05$ , \*\* $p < 0.01$ , \*\*\* $p < 0.001$ .

Plethysmographic analysis of respiratory parameters in neonates exposed to normoxia or hyperoxia for 7 days following birth. Hyperoxia exposure resulted in significant perturbation of lung function at P7, compared to normoxia controls,  $n = 9/16$  per group. Data were analysed using two-tailed unpaired t-tests. Bw – body weight.



including frequency (Figure 3C), total cycle time (Figure 3D), inspiration time (Figure 3E) and minute volume/body weight (Figure 3H), where at P11 CSF-1-treated mice had significant alterations in breathing patterns compared to Norm or Hyp + PBS mice. Furthermore, only in frequency (Figure 3C), expiration time (Figure 3F) and minute volume/body weight (Figure 3H) was there an alteration with CSF-1 treatment that was significantly different compared

to PBS administration at P11. However, any earlier perturbations associated with hyperoxia exposure and/or CSF-1 administration resolved and at P35 no significant difference was observed amongst the three treatment groups in the breathing parameters examined.

To investigate the impact of CSF-1 treatment on lung macrophages, flow cytometry was performed on littermate hyperoxic lungs after treatment with either PBS or

**Table 2 Morphometric analysis of lungs from CSF-1-treated mice after 7 days of neonatal hyperoxia exposure**

		Normoxia	Hyp + PBS	Hyp + CSF-1
P11	% Tissue	50.66 ± 1.61	53.62 ± 2.99	52.98 ± 1.90
	% Airspace	49.34 ± 1.61	46.38 ± 2.99	47.02 ± 1.90
	MLI	88.59 ± 2.42	94.33 ± 2.37	87.42 ± 0.99
P35	% Tissue	36.97 ± 1.29	39.15 ± 2.01	35.92 ± 0.87
	% Airspace	63.03 ± 1.29	60.85 ± 2.01	64.08 ± 0.87
	MLI	64.99 ± 1.78	68.67 ± 1.64	67.34 ± 1.63

Morphometric estimation of percentage tissue, percentage airspace and mean linear intercept (MLI) at P11 (n = 4 lungs/treatment) and P35 (n = 6-7 lungs/treatment) in newborn mice exposed to normoxia or hyperoxia for 7 days followed by either CSF-1 or PBS treatment for 5 consecutive days. No significant changes were observed in the morphometric parameters examined amongst the three treatment groups. Data were analysed using one-way ANOVAs and Tukey's post-hoc tests.

CSF-1 at P11 (Figure 2). The total lung cell number was significantly increased by 13% in mice treated with CSF-1 ( $128 \pm 5.3 \times 10^5$  vs.  $144 \pm 3.1 \times 10^5$ ,  $p < 0.05$ ; Figure 2B). Transgenic *csflr*-EGFP mice, which express EGFP under control of the *csflr* promoter, identified CSF-1-responsive cells. The number of CSF-1R+ cells significantly increased by 34% with CSF-1 treatment compared to PBS ( $16.7 \pm 0.2 \times 10^4$  vs.  $22.2 \pm 2.2 \times 10^4$ ,  $p < 0.05$ ; Figure 2C). CSF-1R was not expressed outside the leukocyte population, with no CD45- lung cells found to express the EGFP transgene (Figure 2D&E). F4/80 expression was used to identify mature macrophages (Figure 2F-H). The number of F4/80+ macrophages significantly increased by 34% with CSF-1 treatment at P11 ( $88 \pm 2.0 \times 10^3$  vs.  $118 \pm 9.0 \times 10^3$ ,  $p < 0.05$ ; Figure 2F).

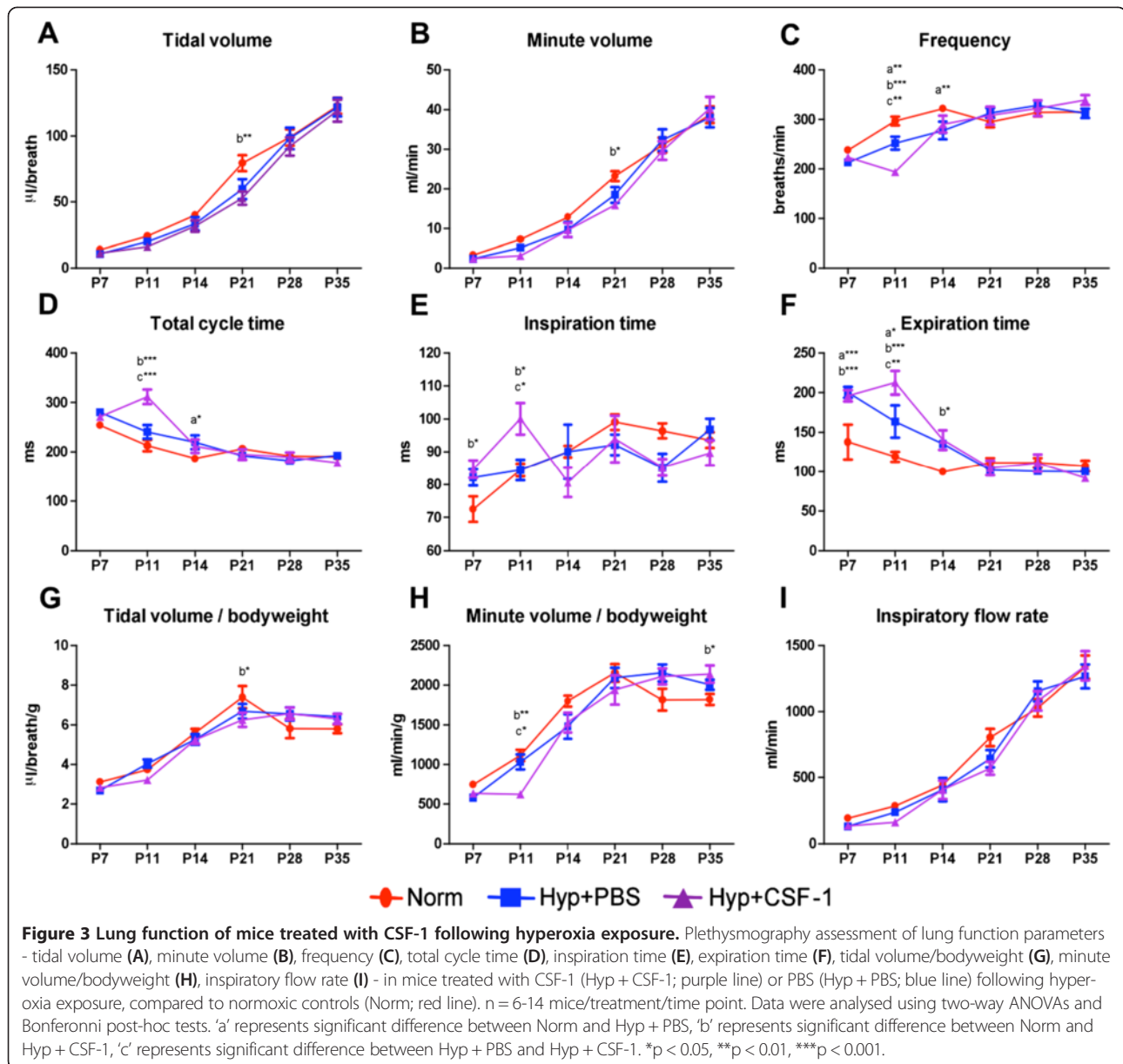
**Delivery of CSF-1 in conjunction with hyperoxia exposure resulted in reduced body weight; however structural alterations were not exacerbated and pulmonary macrophages were not increased**

In the second treatment regime, CSF-1 was administered in conjunction with high oxygen exposure to assess the potential of CSF-1 to mitigate lung damage and promote alveolar formation. In this more clinically relevant regime, neonatal mice were exposed to hyperoxia for 5 days to allow for 5 concurrent daily injections of CSF-1 or PBS. Body weight was measured to assess growth over the time course of development, from the end of treatment at P5, and weekly throughout postnatal development from P14 to adulthood at P35 (Figure 4A). Body weight was not significantly altered in the Hyp + PBS group compared to Norm. These two treatment groups followed a similar growth trajectory and no significant changes were observed at any of the time points examined. However, Hyp + CSF-1 was found to negatively affect body weight, although this emerged only at later time points. By P28, the growth trajectory was decreased in the Hyp +

CSF-1 group and body weight was significantly lower than in the Norm group ( $17.27 \pm 0.54$  g vs.  $15.20 \pm 0.42$  g,  $p < 0.001$ ). Also, at P35, body weight was significantly lower in the Hyp + CSF-1 group compared to both the Norm ( $21.47 \pm 0.51$  g vs.  $18.50 \pm 0.53$  g,  $p < 0.001$ ) and Hyp + PBS groups ( $20.89 \pm 0.61$  g vs.  $18.50 \pm 0.53$  g,  $p < 0.001$ ; Figure 4A).

The effect of hyperoxia and concurrent CSF-1 treatment on structural development of the lung was assessed at P5 (Table 3). No significant differences were observed in the structural parameters examined between the three groups. A trend of altered structural measurements was observed in the Hyp + PBS group compared to Norm, although it did not reach significance. In the Hyp + CSF-1 group, all parameters measured approached the values of the Norm group and structural alterations were not exacerbated with CSF-1 administration. In the adult at P35, percentage tissue and airspace were unaltered in the Hyp + PBS or Hyp + CSF-1 groups compared to Norm. However, MLI was affected by hyperoxia exposure. Compared to Norm, a significant increase in MLI was observed in the Hyp + PBS ( $65.0 \pm 1.8$   $\mu$ m vs.  $72.7 \pm 1.2$   $\mu$ m,  $p < 0.05$ ) and the Hyp + CSF-1 groups ( $65.0 \pm 1.8$   $\mu$ m vs.  $75.3 \pm 2.8$   $\mu$ m,  $p < 0.01$ ; Table 3). CSF-1 treatment did not significantly affect the outcome of hyperoxia on the lung, as no significant difference in MLI compared to PBS was observed. Histologically, there were fewer and larger alveoli in the lungs of mice exposed to both Hyp + PBS (Figure 4J) and Hyp + CSF-1 (Figure 4K) as compared to Norm controls (Figure 4I).

Plethysmographic analysis of breath parameters (Figure 5) indicated that initial perturbations at P5 were present in breath frequency (Figure 5C), total cycle time (Figure 5D), inspiration time (Figure 5E), expiration time (Figure 5F) and minute volume/body weight ratio (Figure 5H). However, these alterations were observed in both hyperoxia groups compared to Norm, and were thus not a result of CSF-1 delivery. After initial perturbation at P5, breathing frequency, total cycle time and expiration time were subsequently comparable amongst all treatment groups. Inspiration time was altered in the hyperoxia groups compared to Norm, with a significant decrease at P21 (Norm vs. Hyp + PBS 15%,  $p < 0.05$ ; Norm vs. Hyp + CSF-1 23%,  $p < 0.01$ ) and P28 (Norm vs. Hyp + PBS 17%,  $p < 0.01$ ; Norm vs. Hyp + CSF-1 16%,  $p < 0.05$ ; Figure 5E). Tidal volume (Figure 5A), minute volume (Figure 5B) and inspiratory flow rate (Figure 5I) increased during postnatal life and followed a similar trajectory in all three treatment groups. No significant differences were observed in inspiratory flow rate at any time points. However, at P35 in the Hyp + CSF-1 group there was a significant decrease in tidal volume ( $122.84 \pm 5.98$   $\mu$ l vs.  $98.36 \pm 4.26$   $\mu$ l,  $p < 0.001$ ; Figure 5A) and minute volume ( $38.7 \pm 2.1$  ml vs.  $32.0 \pm 1.9$  ml,  $p < 0.01$ ; Figure 5B) compared to Norm.



To investigate the impact of CSF-1 treatment on lung macrophages, flow cytometry was performed on littermate lungs at P5, after either PBS or CSF-1 treatment was delivered concurrently with hyperoxia. Total lung cell number was not altered with CSF-1 treatment, with no significant change compared to PBS was observed (Figure 4B). *Csf1r*-EGFP transgene expression on CD45+ leukocytes revealed that the number and percentage of CSF-1R+ cells within the lung was comparable amongst both PBS and CSF-1-treated mice (Figure 4C-E). Similarly, when cells were further gated on F4/80 expression to identify macrophages (Figure 4G&H), no change in the number or percentage of macrophages in the lung was observed as a result of CSF-1 treatment (Figure 4F).

## Discussion

Oxygen supplementation remains a critical and lifesaving intervention for infants with respiratory distress; however, it can result in detrimental alterations to the developing lung. Exposing neonatal mice to high concentrations of oxygen mimics the damage to the lung associated with BPD, providing a relevant model to assess the function of CSF-1 in rescuing and enhancing alveolar formation. This study employed a hyperoxia regime of 65% oxygen for 1 week after birth, providing a milder, more clinically-relevant exposure that more closely resembles the oxygen therapy regime of ventilated premature infants than other previous studies [5,35]. It was also selected to minimize maternal oxygen toxicity and avoid stress and abandonment

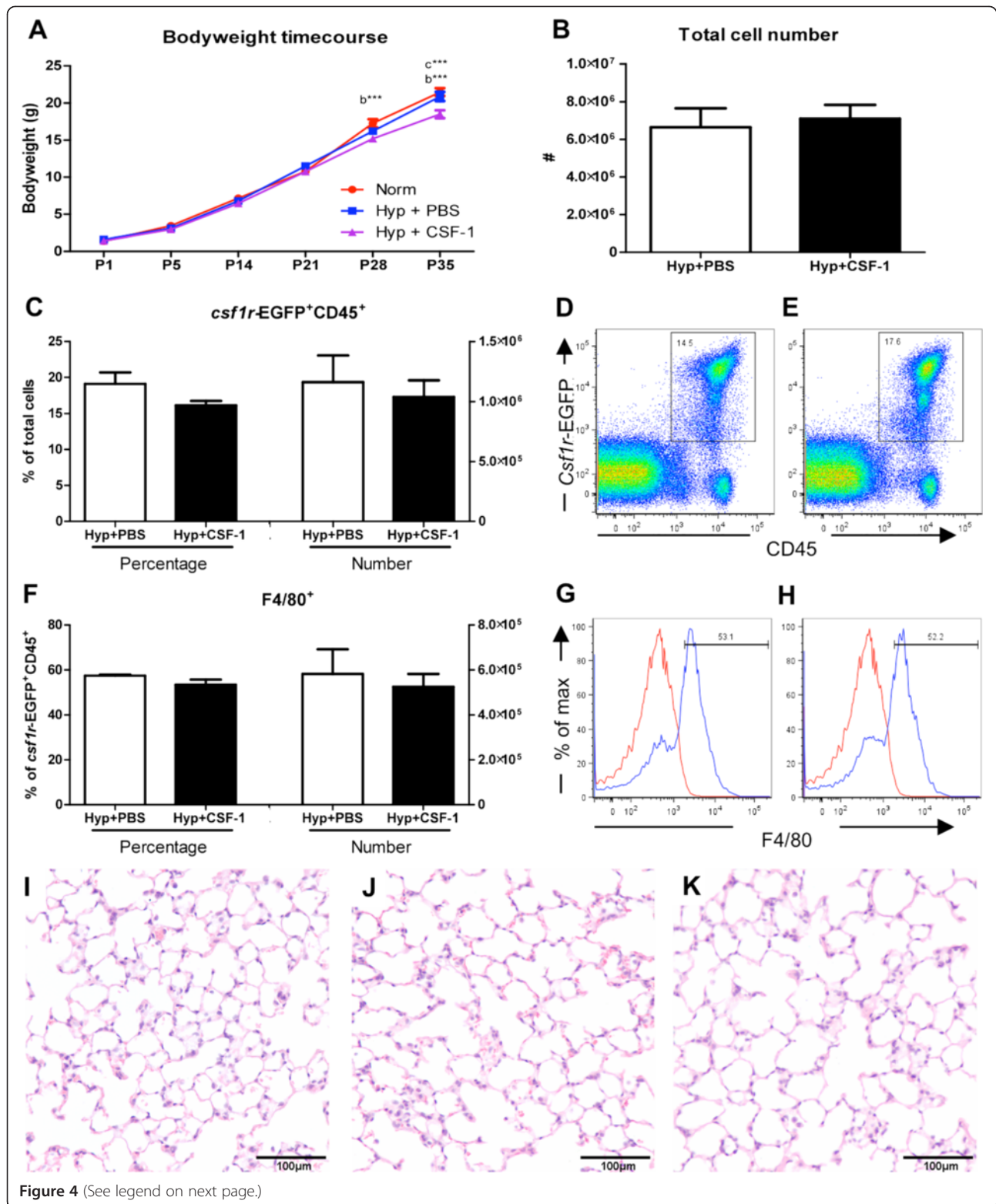


Figure 4 (See legend on next page.)

(See figure on previous page.)

**Figure 4 Growth and macrophage analysis in mice treated with CSF-1 during concurrent hyperoxia exposure.** Body weights of mice treated with CSF-1 (Hyp + CSF-1; purple line) or PBS (Hyp + PBS; blue line) during hyperoxia exposure compared to normoxic mice (Norm; red line) (A). n = 4-13 mice/time point. Data were analysed using a two-way ANOVA and Bonferonni post-hoc test. 'b' represents significant difference between Norm and Hyp + CSF-1, 'c' represents significant difference between Hyp + PBS and Hyp + CSF-1. \*\*\*p < 0.001. Flow cytometric analysis of littermate lungs at P5 following treatment with CSF-1 or PBS during hyperoxia. Total lung cells (B) were gated on *csf1r*-EGFP+ CD45+ cells to quantitate CSF-1R+ cell number and proportion (C) after CSF-1 (E) and PBS treatment (D). F4/80 expression demarcates mature macrophages within the CSF-1R+ population (F-H). Histograms revealing gating procedure for F4/80 expression in representative PBS (G) and CSF-1-treated lungs (H). Staining (blue) is overlaid with an isotype control (red). n = 3 littermate lungs/treatment. Data were analysed using two-tailed unpaired t-tests. Photomicrographs of Norm (I), Hyp + PBS (J) and Hyp + CSF-1 (K) lungs at P35 stained with H&E demonstrated fewer, larger alveoli with hyperoxia exposure (J & K).

issues associated with dam rotation. Hallmarks of this hyperoxia model included growth restriction, impaired lung structural development indicative of reduced alveolarisation, and as a consequence measurable perturbations of respiratory function. While body weight was comparable at birth, hyperoxia impacted negatively on neonatal growth as evidenced by the reduction in body weight in the hyperoxia group by the end of exposure. Although there is potential for maternal oxygen toxicity to impact on the growth restriction observed, such growth restriction associated with this model is important to examine the growth promoting functions of CSF-1 as observed previously [23]. Lung structural alterations characteristic of oxygen toxicity and BPD were also observed. MLI and percentage airspace were increased, while percentage tissue was decreased. This is in agreement with other hyperoxia studies, where oxygen supplementation caused BPD-like pathological changes to the lung parenchyma and impaired alveolarisation resulting in fewer, larger alveoli [5,6].

Functional perturbations were also revealed following hyperoxia. Unrestrained barometric whole-body plethysmography proved a beneficial analytical technique sensitive enough to reveal measurable differences in neonates at 7 days of age. While the accuracy of absolute quantitation in small animals is debatable [36], this technique provides a qualitative comparative assessment applicable to this study. Furthermore, the non-invasive nature of this technique makes it invaluable for these experiments

in assessing the effects of CSF-1 and the rescue of lung function over time. Abnormal breathing patterns were associated with hyperoxia exposure after 7 days. In agreement with previously reported effects of hyperoxia on pulmonary activity [37], changes included an increase in total cycle time primarily due to lengthened expiratory time. Furthermore, hyperoxia resulted in a reduction in tidal volume, supporting the structural observation of impaired alveolar formation. However, effects on tidal and minute volumes were mitigated when normalised to body weight, suggesting that the overall growth restriction contributes to the reduced lung volumes.

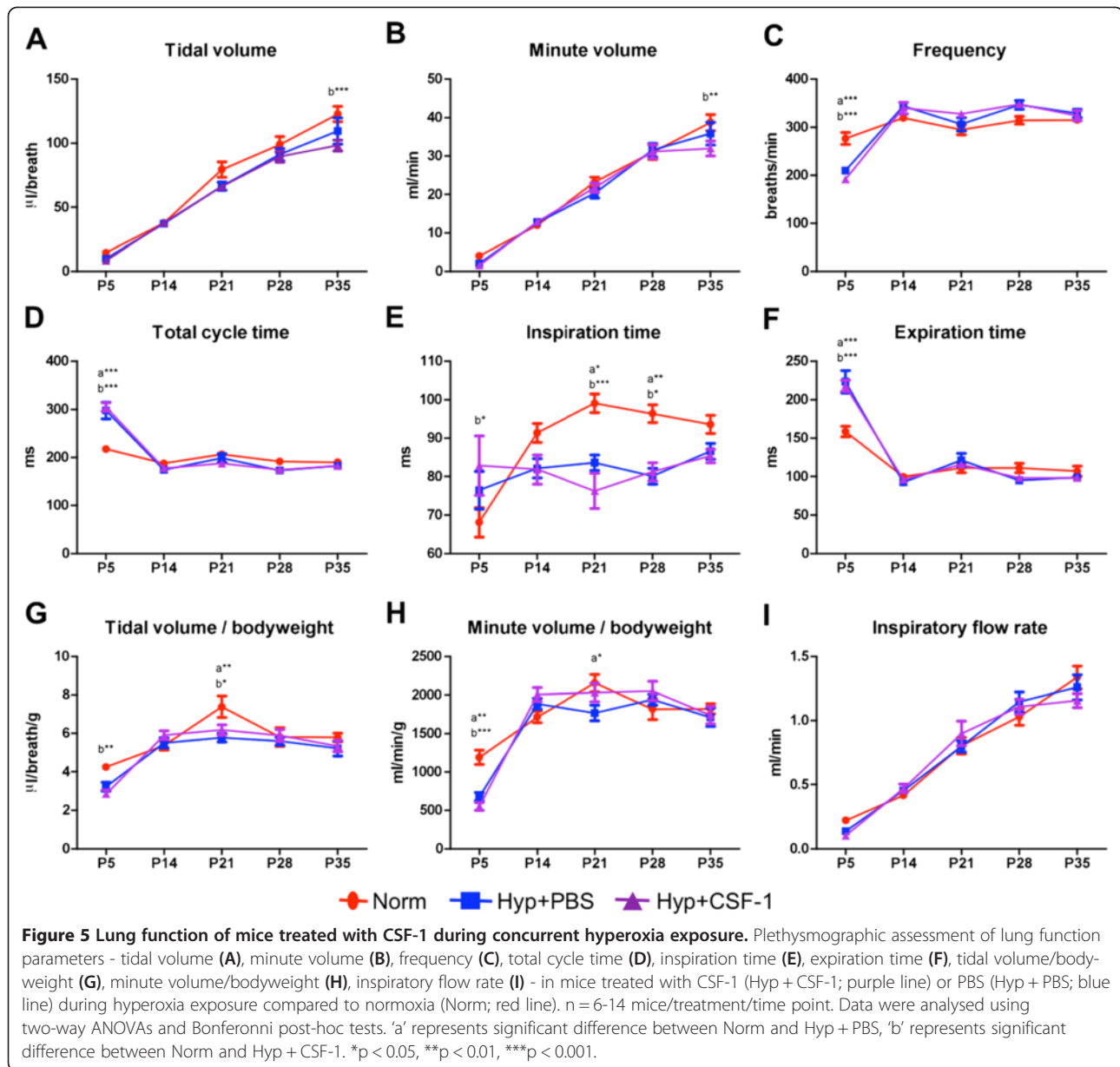
Harnessing the organogenic importance of growth factors involved in alveolar formation has been a fundamental strategy for promoting lung maturation. Factors such as keratinocyte growth factor [38], hepatocyte growth factor [39], retinoic acid [40] and vascular endothelial growth factor [41] are important in alveolarisation and have shown positive effects in rescuing alveolar development in hyperoxic animal studies. The injury-induced perturbation of development associated with BPD is also being tackled by using anti-inflammatory approaches, such as interleukin (IL)-10 [42] or inflammatory chemokine blockade [43], and by optimising ventilation strategies [44] to mitigate damage and protect alveolar formation.

CSF-1 provides a particularly attractive candidate for use in this setting because it is a growth factor with proven organogenic [27,28], anti-inflammatory [29,45] and regenerative capabilities [12,46]. During development, endogenous CSF-1 preferentially regulates trophic macrophages associated with organogenesis, as evidenced by the widespread developmental defects observed in CSF-1-deficient mice [20-22]. Functions of trophic macrophages that support organogenesis include apoptotic clearance of cellular debris associated with tissue remodelling [47], regulation of angiogenesis through the production of angiogenic factors [48,49] and by physically directing vascular development [50]. Macrophages act as potent effector cells producing a range of important trophic mediators such as insulin-like growth factor-1 (IGF-1) [51], wingless-type MMTV integration site family, member 7b (Wnt7b) [52], transforming growth factor- $\beta$  (TGF- $\beta$ ) [53] and MMP9 [54], which are involved in epithelial proliferation and matrix reorganisation. These processes are all essential in lung development,

**Table 3 Morphometric analysis of lungs from mice administered CSF-1 during concurrent hyperoxia exposure**

		Normoxia	Hyp + PBS	Hyp + CSF-1
P5	% Tissue	34.92 ± 1.83	28.31 ± 1.83	32.15 ± 1.74
	% Airspace	65.08 ± 1.83	71.69 ± 1.83	67.85 ± 1.74
	MLI	113.00 ± 3.22	121.70 ± 7.97	116.40 ± 3.45
P35	% Tissue	36.97 ± 1.29	38.48 ± 2.01	36.92 ± 0.88
	% Airspace	63.03 ± 1.29	61.52 ± 2.01	63.08 ± 0.88
	MLI	64.99 ± 1.78	72.66 ± 1.22 a*	75.27 ± 2.79 b**

Morphometric estimation of percentage tissue, percentage airspace and mean linear intercept at P5 at the cessation of treatment (n = 4-5/group), and at P35 (n = 6-7/group). Data were analysed by one-way ANOVA and Tukey's post-hoc test. 'a' represents significant difference between Norm and Hyp + PBS, 'b' represents significant difference between Norm and Hyp + CSF-1. \*p < 0.05, \*\*p < 0.01.



particularly in alveolarisation. Macrophages in both the embryonic lung and the postnatal lung undergoing alveolarisation demonstrate a gene expression profile, indicative of a trophic M2 macrophage activation state [23,27].

The role of CSF-1 in polarising macrophages towards an M2 phenotype may also provide beneficial effects in hyperoxia through its involvement in immune dampening [29]. Inflammation has a negative impact on lung development [55,56]. Inflammatory cell influx and release of pro-inflammatory mediators promotes apoptotic and necrotic cell death that disrupts lung morphogenesis and impairs function. Furthermore, inflammatory activation disrupts organogenic signalling pathways by altering expression of

key genes important in lung development [57,58]. While inflammatory challenges such as lipopolysaccharide (LPS) or IL-1 $\beta$  administration in animal models of chorioamnionitis promote lung maturation, the mechanism is distinct from alveolarisation and is instead a survival adaptation that comes at the expense of proper alveolar formation resulting in a lung pathology associated with BPD [59].

The infiltration of inflammatory macrophages is associated with the progression of lung injury and pathology [60,61]. However macrophage diversity is revealing the importance of lung macrophages in both the injury and repair stages [16], and differential activation suggests

that a GM-CSF driven M1 pro-inflammatory response may be distinct from CSF-1-mediated stimulation of macrophages to take on a remodelling/anti-inflammatory M2 phenotype [29]. In a recent study, CSF-1 was associated with repair and rescue of alveolar formation following hyperoxia in the mouse [30]. It was reported that the administration of MSC-conditioned media into a neonatal murine hyperoxia model reduced inflammation and prevented alveolar and vascular damage [30]. Interestingly, this correlated with high levels of CSF-1, indicating that the developmentally protective effect of MSCs may be indirectly mediated by the immunomodulatory effect of CSF-1 [30].

In the present study, CSF-1 was administered to a neonatal murine hyperoxia model and growth, lung structure and respiratory function were assessed. In the first treatment regime, CSF-1 was administered post-hyperoxic injury to investigate whether CSF-1 could rescue developmental perturbation and promote alveolar formation. Results demonstrated limited success of CSF-1 in the mitigation of hyperoxia-induced injury. Deficits in growth were not improved, with the body weights of CSF-1-treated mice comparable to the Hyp + PBS group. With regard to lung function, a negative impact was revealed at P11 at the end of treatment. In parameters such as total cycle time, expiration time and minute volume/body weight ratio the detrimental effect of hyperoxia was exacerbated with CSF-1. Interestingly, these initial defects did normalise over time and by P35 no differences between treatment groups were observed. This normalisation was also seen in the Hyp + PBS group, and therefore CSF-1 treatment did not accelerate or enhance functional recovery, although increased numbers of CSF-1R+ macrophages were evident. Nevertheless, it is noteworthy that CSF-1 did not have a negative impact on the parameters measured in the adult. It is interesting that earlier perturbations observed with hyperoxia resolved by adulthood. Whether this impacts on the lungs capacity to cope with challenges and aging in later life is unknown. Furthermore questions remain about potential negative effects associated with catch up growth. Indeed CSF-1R+ macrophages have been shown to be increased in the alveolarisation stage of lung development [23], however whether in this setting the increase in CSF-1R+/F4/80+ macrophages is retained and whether it is associated with positive or negative outcomes in lung physiology is also of ongoing interest.

Oxygen supplementation is a critical life saving intervention for babies with respiratory distress, and clinically any maturation-based therapies would need to be delivered concurrently. Therefore, in the second part of this study, CSF-1 was administered from birth in conjunction with hyperoxic exposure, in a setting where a prophylactic effect of CSF-1 treatment was aimed at preventing damage and alveolar loss and enhancing alveolarisation. A

shortened exposure time was utilised to enable the 5 daily doses to be administered in conjunction with hyperoxia. The lack of growth restriction is likely due to the decreased oxygen exposure, as pup litters size was consistent amongst regimes. Structurally and functionally, the lungs of both hyperoxia groups were impacted negatively. Morphometric analysis in the adult revealed significant increases in MLL, with fewer, larger alveoli in both the Hyp + PBS and Hyp + CSF-1 groups compared to Norm. Although CSF-1 was not found to improve the structural alterations caused by hyperoxia, this treatment did not exacerbate the negative impact of hyperoxia and no significant difference between PBS and CSF-1-treated mice was observed. There were no differences between any groups at P5, although this time coincides with the beginning of the alveolarisation phase. Of note is that Hyp + CSF-1 values began to approach Norm values in all parameters. Functionally in the adult, CSF-1 did not exacerbate the adverse effects on lung function that were characteristic of hyperoxia exposure, as represented by the Hyp + PBS group. Although no negative effect of CSF-1 was identified, it must be noted that no functionally beneficial effects with regard to preventing hyperoxic damage or further enhancing lung development were observed. The only changes with CSF-1 at P35 were in tidal volume and minute volume. However, these were normalised when body weight was accounted for and, relative to their size, there were no changes in these parameters as a result of CSF-1 treatment.

Overall, CSF-1 treatment showed little effect in promoting alveolar formation in the hyperoxic settings employed in this study. Ongoing studies examining the role of M2 polarisation in the protection and rescue of hyperoxic injury will be important before a definitive statement that CSF-1-responsive macrophages are not effective can be made. Also further experiments utilizing a premature birth model – where animals are prematurely removed from their high uterine CSF-1 environment – will be important to better model this aspect of the clinical situation. However, in this study the finding that CSF-1 treatment did not exacerbate the pathological response to high oxygen levels was encouraging in that macrophage-mediation may provide a novel strategy for the immunomodulation and trophic promotion of alveolar development. In particular in the second regime where potential negative outcomes were a legitimate concern, CSF-1 did not exacerbate damage with concurrent oxygen supplementation. This is a significant finding that is important for any potential clinical use of CSF-1, and supports ongoing studies to improve understanding of the role of CSF-1 in alveolar formation.

#### Competing interests

CVJ and SDR hold patents relating to CSF-1 and organ growth.

#### Authors' contributions

CVJ contributed to study design, performed the experiments and analysis of data, and wrote the manuscript. MAA assisted with plethysmography, TMW performed flow cytometry, MoR and FS assisted with the hyperoxia model, equipment and provided critical drafting of the manuscript under the direction of RH, GJ provided intellectual input and critical drafting of the manuscript, and SDR oversaw study design and coordination, data interpretation and writing of the manuscript. All authors read and approved the final manuscript.

#### Author details

<sup>1</sup>Department of Anatomy and Developmental Biology, Monash University, Clayton, Victoria, Australia. <sup>2</sup>The Ritchie Centre, Monash Institute of Medical Research and Department of Obstetrics Gynaecology, Monash University, Clayton, Victoria, Australia.

Received: 7 March 2014 Accepted: 28 August 2014

Published: 6 September 2014

#### References

- Gien J, Kinsella JP: Pathogenesis and treatment of bronchopulmonary dysplasia. *Curr Opin Pediatr* 2011, **23**:305–313. 310.1097/MOP.1090b1013e328346577f.
- Kinsella JP, Greenough A, Abman SH: Bronchopulmonary dysplasia. *Lancet* 2006, **367**:1421–1431.
- Jobe AJ: The new BPD: an arrest of lung development. *Pediatr Res* 1999, **46**:641–643.
- Merritt TA, Deming DD, Boynton BR: The 'new' bronchopulmonary dysplasia: challenges and commentary. *Semin Fetal Neonat M* 2009, **14**:345–357.
- Warner BB, Stuart LA, Papes RA, Wispe JR: Functional and pathological effects of prolonged hyperoxia in neonatal mice. *Am J Physiol* 1998, **275**:L110–L117.
- Dauger S, Ferdjadjji L, Saumon G, Vardon G, Peuchmaur M, Gaultier C, Gallego J: Neonatal exposure to 65% oxygen durably impairs lung architecture and breathing pattern in adult mice. *Chest* 2003, **123**:530–538.
- Burri PH: Structural aspects of postnatal lung development - alveolar formation and growth. *Biol Neonate* 2006, **89**:313–322.
- Schittny JC, Burri H: Development and Growth of the Lung. In *Fishman's Pulmonary Diseases and Disorders*. 4th edition. Edited by Fishman AP. New York: The McGraw Hill Companies, Inc; 2008:91–114.
- Coalson JJ: Pathology of new bronchopulmonary dysplasia. *Semin Neonatol* 2003, **8**:73–81.
- Bourbon J, Boucherat O, Chailley-Heu B, Delacourt C: Control mechanisms of lung alveolar development and their disorders in bronchopulmonary dysplasia. *Pediatr Res* 2005, **57**:38R–46R.
- Bhandari V: Hyperoxia-derived lung damage in preterm infants. *Semin Fetal Neonatal Med* 2010, **15**:223–229.
- Alikhan MA, Jones CV, Williams TM, Beckhouse AG, Fletcher AL, Kett MM, Sakkal S, Samuel CS, Ramsay RG, Deane JA, Wells CA, Little MH, Hume DA, Ricardo SD: Colony-stimulating factor-1 promotes kidney growth and repair via alteration of macrophage responses. *Am J Pathol* 2011, **179**:1243–1256.
- Stefater JA 3rd, Ren S, Lang RA, Duffield JS: Metchnikoff's policemen: macrophages in development, homeostasis and regeneration. *Trends Mol Med* 2011, **7**:743–752.
- Pollard JW: Trophic macrophages in development and disease. *Nat Rev Immunol* 2009, **9**:259–270.
- Mosser DM, Edwards JP: Exploring the full spectrum of macrophage activation. *Nat Rev Immunol* 2008, **8**:958–969.
- Johnston LK, Rims CR, Gill SE, McGuire JK, Manicone AM: Pulmonary macrophage subpopulations in the induction and resolution of acute lung injury. *Am J Respir Cell Mol Biol* 2012, **47**:417–426.
- Pixley FJ, Stanley ER: CSF-1 regulation of the wandering macrophage: complexity in action. *Trends Cell Biol* 2004, **14**:628–638.
- Bartocci A, Pollard JW, Stanley ER: Regulation of colony-stimulating factor 1 during pregnancy. *J Exp Med* 1986, **164**:956–961.
- Ovchinnikov DA: Macrophages in the embryo and beyond: much more than just giant phagocytes. *Genesis* 2008, **46**:447–462.
- Wiktor-Jedrzejczak W, Bartocci A, Ferrante AW Jr, Ahmed-Ansari A, Sell KW, Pollard JW, Stanley ER: Total absence of colony-stimulating factor 1 in the macrophage-deficient osteopetrotic (op/op) mouse. *Proc Natl Acad Sci U S A* 1990, **87**:4828–4832.
- Yoshida H, Hayashi S, Kunisada T, Ogawa M, Nishikawa S, Okamura H, Sudo T, Shultz LD, Nishikawa S: The murine mutation osteopetrosis is in the coding region of the macrophage colony stimulating factor gene. *Nature* 1990, **345**:442–444.
- Pollard JW, Stanley ER: Pleiotropic roles for CSF-1 in development defined by the mouse mutant osteopetrotic (op). *Adv Dev Biochem* 1996, **4**:153–193.
- Jones CV, Williams TM, Walker KA, Dickinson H, Sakkal S, Rumballe BA, Little MH, Jenkin G, Ricardo SD: M2 macrophage polarisation is associated with alveolar formation during postnatal lung development. *Respir Res* 2013, **14**:41.
- Wiktor-Jedrzejczak W, Ratajczak MZ, Ptasznik A, Sell KW, Ahmed-Ansari A, Ostertag W: CSF-1 deficiency in the op/op mouse has differential effects on macrophage populations and differentiation stages. *Exp Hematol* 1992, **20**:1004–1010.
- Roth P, Dominguez MG, Stanley ER: The effects of colony-stimulating factor-1 on the distribution of mononuclear phagocytes in the developing osteopetrotic mouse. *Blood* 1998, **91**:3773–3783.
- Shibata Y, Zsengeller Z, Otake K, Palaniyar N, Trapnell BC: Alveolar macrophage deficiency in osteopetrotic mice deficient in macrophage colony-stimulating factor is spontaneously corrected with age and associated with matrix metalloproteinase expression and emphysema. *Blood* 2001, **98**:2845–2852.
- Rae F, Woods K, Sasmono T, Campanale N, Taylor D, Ovchinnikov DA, Grimmond SM, Hume DA, Ricardo SD, Little MH: Characterisation and trophic functions of murine embryonic macrophages based upon the use of a Csf1r-EGFP transgene reporter. *Dev Biol* 2007, **308**:232–246.
- Geutskens SB, Otonkoski T, Pulkkinen MA, Drexhage HA, Leenen PJ: Macrophages in the murine pancreas and their involvement in fetal endocrine development in vitro. *J Leukoc Biol* 2005, **78**:845–852.
- Hamilton JA: Colony-stimulating factors in inflammation and autoimmunity. *Nat Rev Immunol* 2008, **8**:533–544.
- Aslam M, Baveja R, Liang OD, Fernandez-Gonzalez A, Lee C, Mitsialis SA, Kourembanas S: Bone marrow stromal cells attenuate lung injury in a murine model of neonatal chronic lung disease. *Am J Respir Crit Care Med* 2009, **180**:1122–1130.
- Sasmono RT, Oceandy D, Pollard JW, Tong W, Pavli P, Wainwright BJ, Ostrowski MC, Himes SR, Hume DA: A macrophage colony-stimulating factor receptor-green fluorescent protein transgene is expressed throughout the mononuclear phagocyte system of the mouse. *Blood* 2003, **101**:1155–1163.
- Milton PL, Dickinson H, Jenkin G, Lim R: Assessment of respiratory physiology of C57BL/6 mice following bleomycin administration using barometric plethysmography. *Respiration* 2012, **83**:253–266.
- Murphy S, Lim R, Dickinson H, Acharya R, Rosli S, Jenkin G, Wallace E: Human amnion epithelial cells prevent bleomycin-induced lung injury and preserve lung function. *Cell Transplant* 2011, **20**:909–923.
- Dunnill MS: Quantitative methods in the study of pulmonary pathology. *Thorax* 1962, **17**:320–328.
- Rogers LK, Valentine CJ, Pennell M, Velten M, Britt RD, Dingess K, Zhao X, Welty SE, Tipple TE: Maternal docosahexaenoic acid supplementation decreases lung inflammation in hyperoxia-exposed newborn mice. *J Nutr* 2011, **141**:214–222.
- Enhorning G, Sv S, Lundgren C, Vargas I: Whole-body plethysmography, does it measure tidal volume of small animals? *Can J Physiol Pharm* 1998, **76**:945–951.
- Mortola JP, Tenney SM: Effects of hyperoxia on ventilatory and metabolic rates of newborn mice. *Respir Physiol* 1986, **63**:267–274.
- Franco-Montoya ML, Bourbon JR, Durmeyer X, Lorotte S, Jarreau PH, Delacourt C: Pulmonary effects of keratinocyte growth factor in newborn rats exposed to hyperoxia. *Am J Physiol Lung Cell Mol Physiol* 2009, **297**:L965–L976.
- Ohki Y, Mayuzumi H, Tokuyama K, Yoshizawa Y, Arakawa H, Mochizuki H, Morikawa A: Hepatocyte growth factor treatment improves alveolarization in a newborn murine model of bronchopulmonary dysplasia. *Neonatology* 2009, **95**:332–338.
- Zimova-Herknerova M, Myslivecek J, Potmesil P: Retinoic acid attenuates the mild hyperoxic lung injury in newborn mice. *Physiol Res* 2008, **57**:33–40.
- Kunig AM, Balasubramaniam V, Markham NE, Morgan D, Montgomery G, Grover TR, Abman SH: Recombinant human VEGF treatment enhances alveolarization after hyperoxic lung injury in neonatal rats. *Am J Physiol Lung Cell Mol Physiol* 2005, **289**:L529–L535.
- Hoegl S, Boost KA, Czerwonka H, Dolfen A, Scheiermann P, Muhl H, Zwissler B, Hofstetter C: Inhaled IL-10 reduces biotrauma and mortality in a model of ventilator-induced lung injury. *Respir Med* 2009, **103**:463–470.

43. Liao L, Ning Q, Li Y, Wang W, Wang A, Wei W, Liu X, Auten RL, Tanswell AK, Luo X: **CXCR2 blockade reduces radical formation in hyperoxia-exposed newborn rat lung.** *Pediatr Res* 2006, **60**:299–303.
44. Ramanathan R, Sardesai S: **Lung protective ventilatory strategies in very low birth weight infants.** *J Perinatol* 2008, **28**:S41–S46.
45. Fleetwood AJ, Lawrence T, Hamilton JA, Cook AD: **Granulocyte-macrophage colony-stimulating factor (CSF) and macrophage CSF-dependent macrophage phenotypes display differences in cytokine profiles and transcription factor activities: implications for CSF blockade in inflammation.** *J Immunol* 2007, **178**:5245–5252.
46. Yano T, Miura T, Whittaker P, Miki T, Sakamoto J, Nakamura Y, Ichikawa Y, Ikeda Y, Kobayashi H, Ohori K, Shimamoto K: **Macrophage colony-stimulating factor treatment after myocardial infarction attenuates left ventricular dysfunction by accelerating infarct repair.** *J Am Coll Cardiol* 2006, **47**:626–634.
47. Lang RA, Bishop JM: **Macrophages are required for cell death and tissue remodeling in the developing mouse eye.** *Cell* 1993, **74**:453–462.
48. Stefater JA 3rd, Lewkowich I, Rao S, Mariggi G, Carpenter AC, Burr AR, Fan J, Ajima R, Molkentin JD, Williams BO, Wills-Karp M, Pollard JW, Yamaguchi T, Ferrara N, Gerhardt H, Lang RA: **Regulation of angiogenesis by a non-canonical Wnt-Flt1 pathway in myeloid cells.** *Nature* 2011, **474**:511–515.
49. Nucera S, Bizziato D, De Palma M: **The interplay between macrophages and angiogenesis in development, tissue injury and regeneration.** *Int J Dev Biol* 2011, **55**:495–503.
50. Fantin A, Vieira JM, Gestri G, Denti L, Schwarz Q, Prykholzhij S, Peri F, Wilson SW, Ruhrberg C: **Tissue macrophages act as cellular chaperones for vascular anastomosis downstream of VEGF-mediated endothelial tip cell induction.** *Blood* 2010, **116**:829–840.
51. Wynes MW, Riches DW: **Induction of macrophage insulin-like growth factor-I expression by the Th2 cytokines IL-4 and IL-13.** *J Immunol* 2003, **171**:3550–3559.
52. Rajagopal J, Carroll TJ, Guseh JS, Bores SA, Blank LJ, Anderson WJ, Yu J, Zhou Q, McMahon AP, Melton DA: **Wnt7b stimulates embryonic lung growth by coordinately increasing the replication of epithelium and mesenchyme.** *Development* 2008, **135**:1625–1634.
53. Nacu N, Luzina IG, Highsmith K, Lockett V, Pochetuhin K, Cooper ZA, Gillmeister MP, Todd NW, Atamas SP: **Macrophages produce TGF-beta-induced (beta-ig-h3) following ingestion of apoptotic cells and regulate MMP14 levels and collagen turnover in fibroblasts.** *J Immunol* 2008, **180**:5036–5044.
54. Gibbs DF, Warner RL, Weiss SJ, Johnson KJ, Varani J: **Characterization of matrix metalloproteinases produced by rat alveolar macrophages.** *Am J Respir Cell Mol Biol* 1999, **20**:1136–1144.
55. Speer CP: **Pulmonary inflammation and bronchopulmonary dysplasia.** *J Perinatol* 2006, **26**:S57–S62.
56. Speer CP: **Chorioamnionitis, postnatal factors and proinflammatory response in the pathogenetic sequence of bronchopulmonary dysplasia.** *Neonatology* 2009, **95**:353–361.
57. Blackwell TS, Hipps AN, Yamamoto Y, Han W, Barham WJ, Ostrowski MC, Yull FE, Prince LS: **NF-kappaB signaling in fetal lung macrophages disrupts airway morphogenesis.** *J Immunol* 2011, **187**:2740–2747.
58. Benjamin JT, Carver BJ, Plosa EJ, Yamamoto Y, Miller JD, Liu JH, van der Meer R, Blackwell TS, Prince LS: **NF-kappaB activation limits airway branching through inhibition of Sp1-mediated fibroblast growth factor-10 expression.** *J Immunol* 2010, **185**:4896–4903.
59. Kramer BW, Kallapur S, Newnham J, Jobe AH: **Prenatal inflammation and lung development.** *Semin Fetal Neonatal Med* 2009, **14**:2–7.
60. Frank JA, Wray CM, McAuley DF, Schwendener R, Matthay MA: **Alveolar macrophages contribute to alveolar barrier dysfunction in ventilator-induced lung injury.** *Am J Physiol Lung Cell Mol Physiol* 2006, **291**:L1191–L1198.
61. Laskin DL, Sunil VR, Gardner CR, Laskin JD: **Macrophages and tissue injury: agents of defense or destruction?** *Annu Rev Pharmacol Toxicol* 2011, **51**:267–288.

doi:10.1186/s12931-014-0110-5

**Cite this article as:** Jones *et al.*: The effect of CSF-1 administration on lung maturation in a mouse model of neonatal hyperoxia exposure. *Respiratory Research* 2014 **15**:110.

**Submit your next manuscript to BioMed Central and take full advantage of:**

- Convenient online submission
- Thorough peer review
- No space constraints or color figure charges
- Immediate publication on acceptance
- Inclusion in PubMed, CAS, Scopus and Google Scholar
- Research which is freely available for redistribution

Submit your manuscript at  
www.biomedcentral.com/submit

